# Cenozoic potassic magmatism and uplift of the Western United States

## Thesis

# Cenozoic Potassic Magmatism and Uplift of the Western United States

Thesis presented for the degree of

Doctor of Philosophy

By

Geoffrey Mark Nowell

BSc (Hons.) *Leicester.* 1989

The Department of Earth Sciences

OPEN UNIVERSITY



Submitted 20th September 1993

Date of award: 18th April 1994

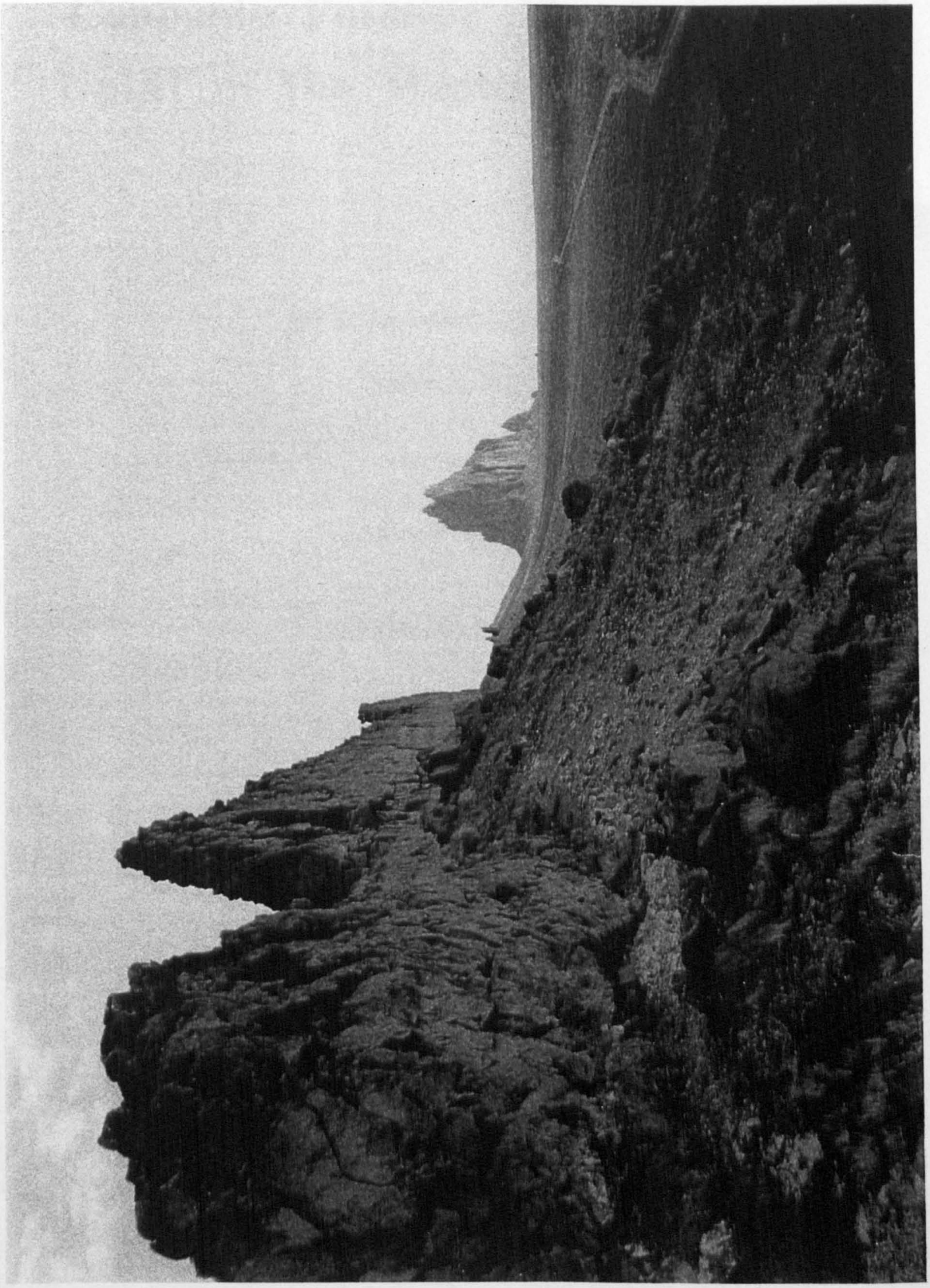

Ship Rock minette diatreme and associated radial dyke of the Oligo-Miocene Navajo Volcanic Field, Four Corners, Colorado Pateau.

# ABSTRACT

The geochemistry and temporal evolution of small volume potassium-rich mafic volcanics within the non-extensional, uplifted central Colorado Plateau and Sierra Nevada have been studied in detail and a general model is proposed for non-extensional, uplift-related, magmatism within the Western Cordillera.

The Oligo-Miocene potassic-ultrapotassic lamprophyres of the Navajo Volcanic Field, Colorado Plateau, and the late Miocene-Pliocene shoshonites of the San Joaquin-Kings Volcanic Field, Sierra Nevada, represent primary or near primary mantle-derived melts that have experienced limited crystal fractionation and/or crustal contamination. Yet despite this each suite of samples is characterised by a significant range of trace element and isotope ratios. The variation in LIL/HFS ratios (Ba/Nb=11-77) and isotopic ratios ($^{87}Sr/^{86}Sr$=0.7044-0.7071) of the Navajo lamprophyres are attributed to small degrees of melting of a compositionally and mineralogically heterogeneous lithospheric mantle source. By contrast a similar, though slightly more extreme, variation in trace element and isotope ratios of shoshonites from the Sierra Nevada (Ba/Nb=70-325, $^{87}Sr/^{86}Sr$=0.7050-0.7069) are attributed to mixing of magmas derived from incompatible element enriched lithospheric mantle and depleted asthenospheric mantle.

Despite the differences in petrogenetic model for the magmatism within the each study area, the magmatic evolution of both the Colorado Plateau as a whole and the Sierra Nevada are similar. Initial magmatism within each province is dominated by a comparatively long history of incompatible element-enriched lithosphere-derived potassic magmatism. After a period of volcanic quiescence, lasting approximately 11 and 5Ma within the Colorado Plateau and Sierra Nevada respectively, the final, relatively short period of volcanism is characterised by compositions more typical of asthenosphere-derived magmas.

New Ar-Ar ages for the Navajo lamprophyres and existing K-Ar ages for the Sierran shoshonites suggest that the onset of lithosphere-dominated magmatism within both the central Colorado Plateau and Sierra Nevada was coeval with the onset of major uplift during the late Cenozoic.

The temporal evolution of magmatism and the degree of uplift, combined with geophysical and xenolith evidence, are consistent with a model in which uplift and pre-extensional magmatism of the Colorado plateau and Sierra Nevada resulted from the convective removal of the lower lithosphere. In the case of the Colorado Plateau convective thinning of the lithosphere is in response to its previous thickening during the Laramide orogeny whereas in the Sierra Nevada it is related to the cessation of subduction and the development of the San Andreas transform margin during the late Cenozoic. Uplift resulting from convective thinning of the lithosphere increases the gravitational potential of the orogen and the likelihood for later collapse and provides an explanation for the close temporal relationship of mafic mantle-derived magmatism, uplift and major crustal extension typical of the Western Cordillera of the United States.

# Acknowledgements

The delights of geology and igneous petrology were first introduced to me by Mr Lambert back in 1984 when he convinced me that it had more long term prospects than 'O' level technical drawing. Little did I know at the time that, as a result of geology, I would still be poor ten years later while my friends who did not take his advice are probably bored but rich. Cheers mate!

Once it became clear that the original nitrogen isotope based project was not to be Nick Rogers took on the unenviable task of keeping me in line for the next four years and in which he occasionally seemed to take great sadistic pleasure. Nevertheless I am especially grateful to Nick for always being available for a chat, his considerable patience and help throughout this research, and for his honest comments on *numerous* earlier versions of this thesis. Simon Turner who arrived at the O.U. as I began writing helped me develop some of the ideas of lithospheric thinning discussed in chapters five and six whilst we and others, notably Kathy Stewart and Shaggers, consumed many an ale at the 'conference table' in the Cellar Bar

Nick along with Janet, to whom I am also grateful for lifts from Leicester to MK, and Paul were great company during the 'Yorkshire lads' tour of the States and helped keep me alive on the Plateau. Ren Thompson of the USGS, Denver, provided invaluable financial assistance in transporting the huge quantity of rock back to the UK. Bill Laughlin of the Los Alomos National Laboratory kindly supplied a number of katungite samples from the Navajo volcanic field which proved so important to the Navajo story. Samples from the Navajo volcanic field and the Sierra National Forest were collected with the permission and assistance of the Navajo Indian Nation and the US Forestry Service respectively. Also in the States two of my greatest friends, Greg and Pam Townley, showed me considerable hospitality and I was lucky enough to share their company in Yosemite for two great weeks.

Brian 'Happy' Ellis and Kay 'Agony Aunt' Chambers are thanked for all their work (and advice) preparing samples and thin sections respectively. Thanks also to Tim Brewer, Peter Webb and John Watson for XRF data; Nick for INAA; Simon Kelley for Ar-Ar ages on the Navajo samples; and, Mabs and Peter van Calsteren for an entertaining time in the radiogenic lab. John Holbrook worked miracles with travel advances and, although occasionally unknowingly, provided other means of transport on a regular basis.

In the transline thanks must go to Shaggers, Samlet, Kate, Ben and Frank who had to put up with me, my habits and my muddy bike. Three pleasurable years were spent living with Marcey, Phil W., Steve Reddy, and Mark S., the latter two and Mike A.providing much inspiration on the garage climbing wall (Sorry about the holes Mrs Agar). Life in Milton Keynes would not nearly have been the fun it was without May whose wit and sarcasm will be missed. Many an entertaining night was spent in the

company of May, Steve, Graham P., Sam P., Paul Casey and Justine in the Swan mainly getting all the answers wrong with the help of quiz master Graham. All of the above along with Mark G, Tim B., Phil G., Ashley 'Fester' M, Penny, Bill R, Fran, always provided an all too easy distraction from writing in the final months and the occasional Port party. Ben provided much entertainment with his Captain Sensible and Twenty Stomps from the Swamps whilst we were writing up during the unsociable early morning hours and also proved an excellent frisby partner although occasional shots were just a little wide!

Thanks must go to my parents and family who have always supported my decision to continue in geology and provided much needed moral and financial support throughout the last seven years. Thanks to also to John, Jerry, Phil and Paul of the Outdoor Shop, Stony Stratford, for additional financial help in the form of a job, even if it did mean no free Saturdays and never any grant left! Finally I would like to thank Justine not only for her considerable help in finally putting this thesis together but also for putting up with my unsociable hours, moods, and insanity during perhaps the most stressful 8 months of my life writing up and doing Nick's corrections.

# Contents

# LIST OF FIGURES.

## Chapter 1: Introduction.



## Chapter 2: Composition and Age of Potassic and Ultrapotassic Magmatism from the Navajo Volcanic Field, Central Colorado Plateau.

## Chapter 3: Petrogenesis and Evolution of the Oligo-Miocene Ultrapotassic Navajo Intrusives: Constraints on the Composition of the Lithosphere Beneath the Colorado Plateau.

## Chapter 5: Magmatism and uplift of the Colorado Plateau and Central Sierra Nevada Provinces: A Case for Oligo-Miocene Convective Thinning of the Lithospheric Mantle Beneath the Western United States

## Chapter 6: Summary and Conclusions.

# List of Tables

==========

## Chapter 2: Composition and Age of Potassic and Ultrapotassic Magmatism from the Navajo Volcanic Field, Central Colorado Plateau.



## Chapter 3: Petrogenesis and Evolution of the Oligo-Miocene Ultrapotassic Navajo Intrusives: Constraints on the Composition of the Lithosphere Beneath the Colorado Plateau.

## Chapter 4: Geochemistry and Petrogenesis of late Cenozoic, Potassis and Alkali-rich Volcanics of the Central Sierra Nevada, California.

# List of Plates

# Chapter 1

## Introduction

West of the Rocky Mtns the United States can be divided into several physiographic and tectonic provinces, as illustrated in Fig 1.1 (Bayer, 1983; Eaton, 1986), each of which is also characterised by a distinct style of mafic volcanism. The Basin & Range extensional province is associated with voluminous silicic and basaltic volcanics which tend to be concentrated around the margins referred to as the Western Great Basin and Tranzition Zone (Fig 1.1). In stark contrast the stable peripheral highlands, such as the Colorado Plateau and Sierra Nevada, are associated with only minor small volume, and predominantly potassic and ultrapotassic, magmatism.

In general the tectonomagmatic evolution of the western United States in the 40Ma period since the end of the Laramide orogeny has been dominated by large scale crustal extension and voluminous outpourings of initially silicic, and later more bimodal basaltic-rhyolitic volcanic rocks most spectacularly illustrated in the Basin & Range province (Fig 1.1). It is therefore not surprising that so much literature addresses the nature and relationship of extension and basaltic volcanism and whether extension drives the magmatism or the magmatism thermally weakens the crust allowing extension.

In addition to crustal extension however, much of the western United States has also undergone regional uplift during the Cenozoic, producing the Western Cordillera as illustrated in the cross section of Fig 1.1. Indeed even the Basin & Range, with an average elevation of 1.5-1.8km (Harry & Sawyer, 1993), is anomalously high given that, as a result of extension, its present crustal thickness is only in the order of 25-35km (Catchings & Mooney, 1991). The scale of uplift within the western United States, illustrated in the cross section of Fig 1.1, and the presence of asthenosphere-derived magmas was interpreted by Fitton et al (1991) to be consistent with the presence of a mantle plume beneath this region. However Hawkesworth & Gallagher (1994) have demonstrated how the temporal evolution of magmatism within a given area can be used to constrain the likely cause of melt generation.

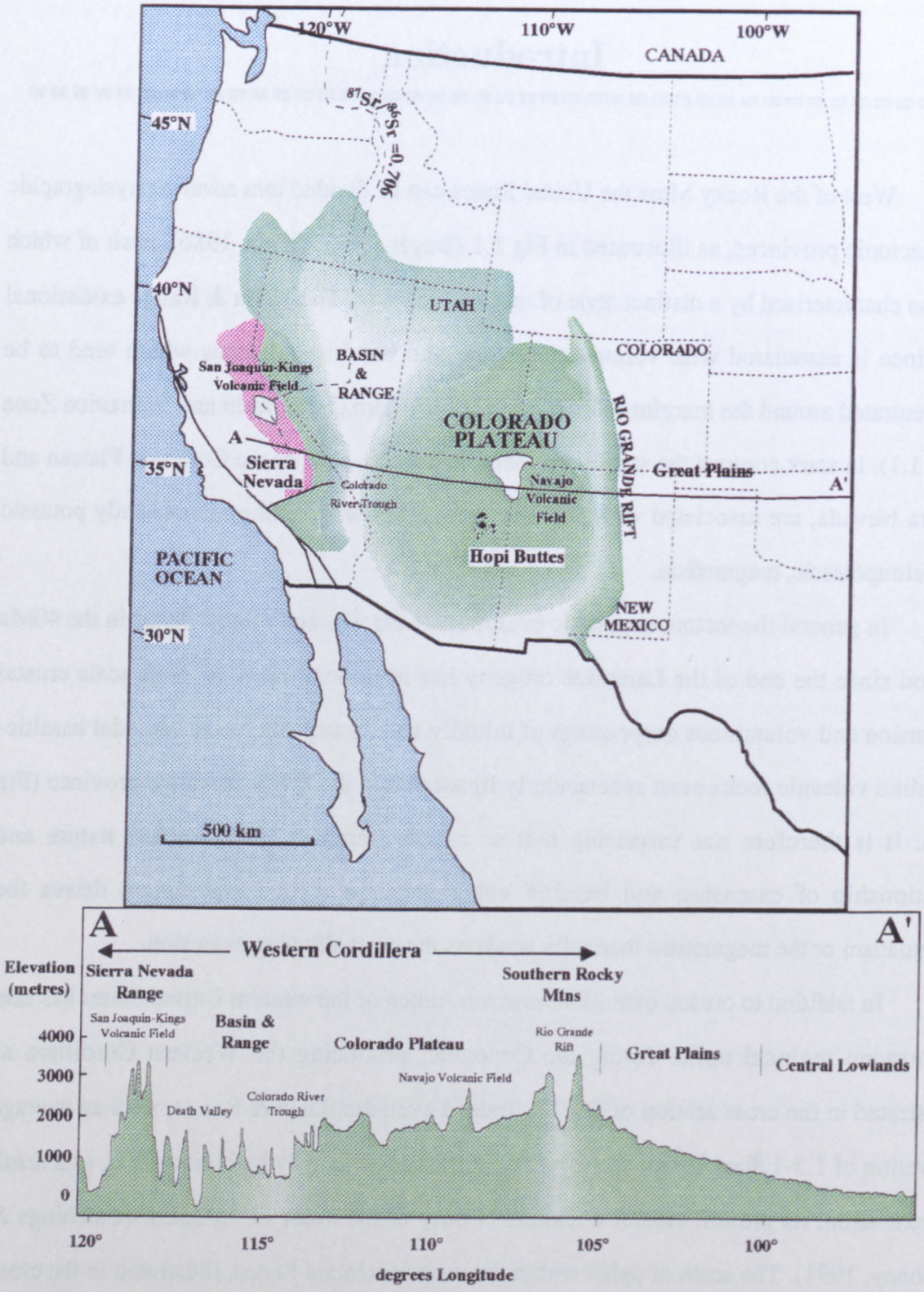


**Figure 1.1.** Map of the western United States showing the main physiographic and tectonic provinces and locations of the Navajo and San Joaquin-Kings volcanic fields within the central Colorado Plateau and Sierra Nevada respectively. Variation in shading between the Rio Grande Rift - Basin & Range and Colorado Plateau - Sierra Nevada diagramatically illustrates the variation in extension where regions of extension are lighter. The topographic cross-section (adapted after Eaton, 1987) runs from the Great Valley, California (A) to Tulsa Oklahoma (B) as shown on the map. Vertical exaggeration approximately 100x. Note that despite extension within the Basin & Range and Rio Grande Rift the whole region west of the southern Rocky Mtns has anomalously high elevations.

In the case of the Colorado River Trough (Fig 1.1) they illustrated how the shift from lithospheric to asthenospheric characteristics reflected melt generation in response to extension and not to the effect of a mantle plume. In the absence of a mantle plume therefore the question of the cause of uplift, and indeed the driving force for extension remains.

Those regions which have not experienced extension and have thus retained a considerable elevation, such as the Colorado Plateau and the central Sierra Nevada, are spatially associated with small volume potassic and ultrapotassic magmas. Although these potassic volcanics are perhaps volumetrically insignificant when compared to their basaltic counterparts in the Basin & Range, they represent the most trace element enriched melts in the whole region and are possibly derived from volatile-rich regions within the lithospheric mantle. They therefore provide the first magmatic evidence for a thermal perturbation within the lithosphere.

It has become apparent that the close spatial and temporal association between mantle-derived volcanics, crustal extension and uplift in many regions of the world, including Tibet (England & Houseman, 1988; Turmer et al., 1993) and the western United States, can be reconciled by a single geodynamic process that involves the convective removal of thickened mantle lithosphere (Houseman et al., 1981; Sandiford & Powell, 1990). Determining whether such a process occurred beneath the western United States, resulting in uplift and thus providing the driving force for extension is hampered in the Basin & Range by the extension itself. Although extension may ultimately result from convective thinning of the lithosphere, it has a tendency to overprint the evidence for the amount and timing of uplift. Furthermore extensional driven magmatism may also obscure the small volume volcanics expected with convective thinning of the lithosphere. As extension has not yet encroached upon either the central Colorado Plateau or Sierra Nevada, these two regions provide ideal locations to determine the role for convective thinning of the lithosphere in the tectonic and physiographic development of the western United States.

This study takes a similar approach to that of Hawkesworth & Gallagher (1994) and initially examines the temporal variation in composition of potassic volcanics from the central Colorado Plateau and Sierra Nevada. The aim is to use the temporal evolution of magmatism to determine the cause of melt generation within these two non-extensional regions of the

western United States.

The potassic lamprophyres of the Navajo volcanic field (NVF) are initially focussed upon in Chapters 2 and 3 as a type example of nonextensional magmatism within an uplifted region of the western United States. These initial chapters also address the compositional evolution of other potassic and non-potassic magmatism within the central Colorado Plateau. In Chapter 2 the petrology and geochemistry (major, trace and isotope) of the NVF are described and endmember compositions identified. New Ar-Ar age determinations are also presented for 14 phlogopite separates and used to determine any temporal variations in magma composition. Chapter 3 examines the petrogenesis of the Navajo intrusives and, as it is variations in the mantle signature which provide constraints on the cause of melt generation, initially establishes to what extent fractionation and/or crustal contamination have modified the composition of the minettes and to identify primary or near primary magmas. The remainder of chapter 3 uses the compositional variation of the primitive magmas from the Navajo volcanic field and other regions of the Colorado Plateau, namely the Hopi Buttes, to address the nature of mantle processes operating beneath the plateau during the Oligo-Miocene.

Chapter 4 presents compositional data for shoshonitic basalts from the San Joaquin-Kings volcanic field (SKVF), central Sierra Nevada. Determining the temporal evolution of magmatism within the SKVF was undertaken primarily as a control study to establish the wider relevance of the results from the Colorado Plateau to other uplifted regions of the western United States. For this reason alone the petrogenesis of the SKVF shoshonites is examined in the framework of the model proposed for NVF intrusives so as to draw comparisons where appropriate.

Chapter 5 attempts to constrain the timing of uplift of both the Colorado Plateau and Sierra Nevada and to assess the relationship between uplift and potassic magmatism in each province. The temporal evolution of magmatism within the Colorado Plateau and Sierra Nevada is then used, in conjunction with pressure and temperature estimates for xenoliths (where available) and geophysical data, to constrain the likely cause of melt generation in these nonextensional uplifted provinces of the western United States and finally examines the link between potassic magmatism and geodynamic models of uplift.

Chapter 6 initially provides a brief summary of the temporal variation in magmatism within both the Colorado Plateau and Sierra Nevada. This is then used to propose a model for the compositional evolution of uplift-related magmatism within the western United States and to show that this also has more worldwide relevance. Finally the role for convective removal of thickened lithosphere in the evolution of magmatism and extension in the Basin & Range is examined in light of the model proposed for magmatism associated with convective thinning of the lithosphere.

# Chapter 2

## Composition and Age of Ultrapotassic Magmatism from the Navajo Volcanic Field, Central Colorado Plateau.

## 2.1 Introduction:

The Colorado Plateau, despite acting as an independent crustal unit throughout much of the Proterozoic and Phanerozoic, is nevertheless important in the understanding of the Cenozoic evolution of the western United States. It is presently being encroached upon by the extensional provinces of the Basin and Range and Rio Grande Rift and therefore arguably represents a remnant of a larger plateau already destroyed by large-scale crustal extension (Oldow et al., 1989). In the Basin & Range magmatism frequently predates extension (Gans et al., 1989) and was therefore not necessarily driven by extension. Magmatism on the Colorado Plateau is clearly unrelated to extension but was initially contemporaneous with subduction of the Farallon plate and later with extension in the peripheral Basin & Range and Rio Grande provinces. An understanding of the composition and temporal evolution of this magmatism provides an insight into melt generation in nonextensional provinces and consequentley may have important implications for pre-extensional magmatism in other areas of the western U.S. now affected by extensional tectonism and magmatism.

Magmatism on the stable central Colorado Plateau was both volumetrically limited and sporadic throughout the Cenozoic and was restricted to small-volume ultrapotassic dykes [eg. Wasatch Plateau, Tingey et al (1991)] and diatremes [Navajo Volcanic Field, Roden (1980); Laughlin et al (1986)] active from the early Oligocene to middle Miocene and finally the nephelinitic lava-flows of the Hopi Buttes erupted in the late Miocene-early Pliocene. This chapter examines the geochemistry of the earliest phase of volcanism on the Colorado Plateau; namely the Oligo-Miocene ultrapotassic intrusives of the Navajo Volcanic Field (NVF) and presents new comprehensive data on 71 samples. The initial aims are to distinguish any geochemically distinct magmatic groups within the NVF and with the aid of $^{40}Ar$-$^{39}Ar$ dating on phlogopite separates from selected samples attempt to identify any

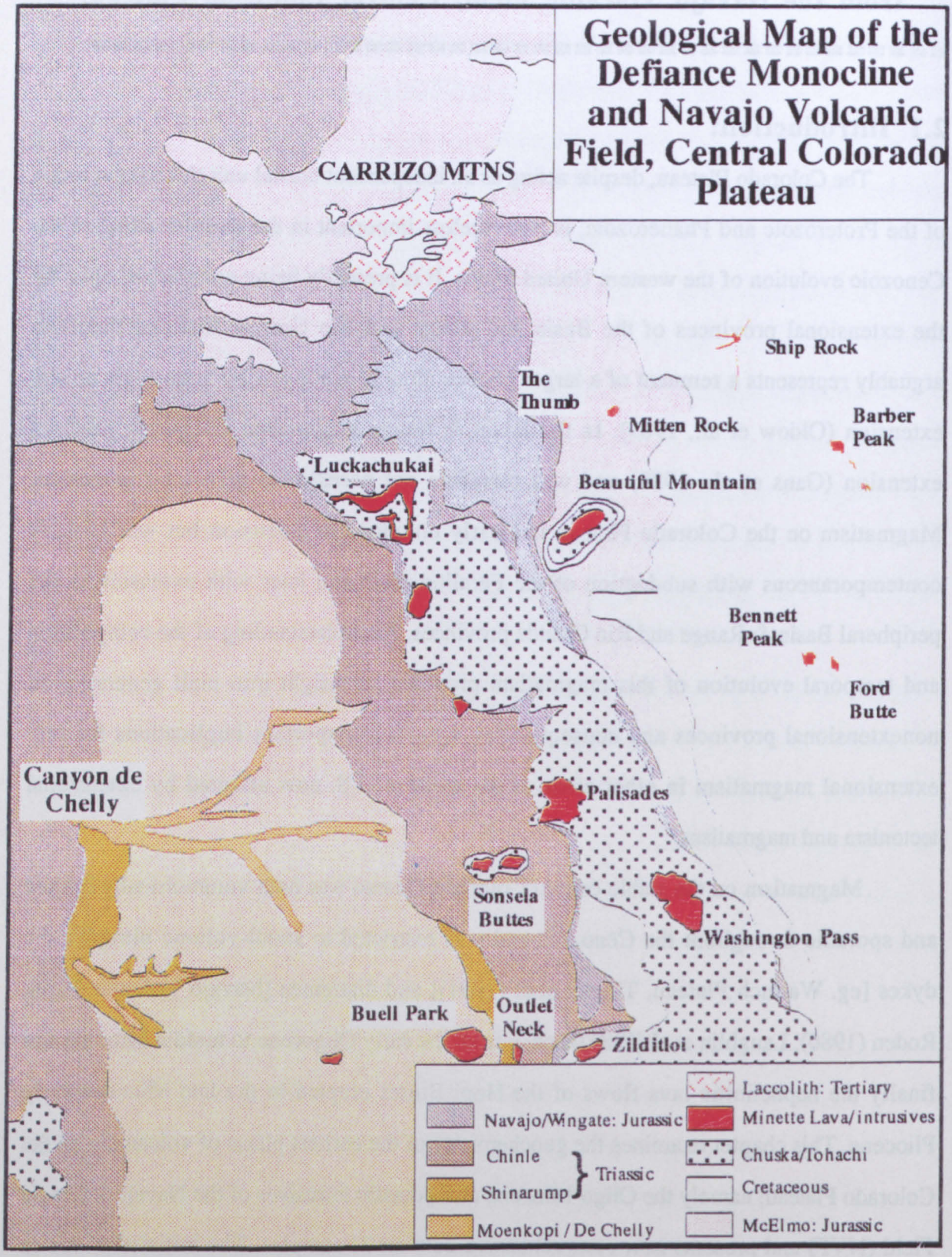


**Figure 2.1.** Simplified geological map of the Defiance Monocline and Oligo-Miocene Navajo Volcanic Field of the central Colorado Plateau. Adapted from Williams (1936).

temporal variations in magma composition which may reflect the changing tectonic regime of the western United States.

## 2.2: Background Geology of the Central Colorado Plateau:

Figure 2.1 is a generalised geological map of the Navajo region of the central Colorado Plateau (Gregory, 1917) which shows the relatively undeformed Mesozoic sediments that overly Precambrian basement.

### 2.2.1: Precambrian basement:

Little is known regarding the age and nature of the basement of the Colorado Plateau, other than that obtained from deep crustal xenoliths contained in host minette and ultramafic diatremes of the Navajo volcanic field (Section 2.3) and, by extrapolation from peripheral regions, due to the 3-5km thick veneer of Phanerozoic sediments that cover much of the area (Fig 2.1).

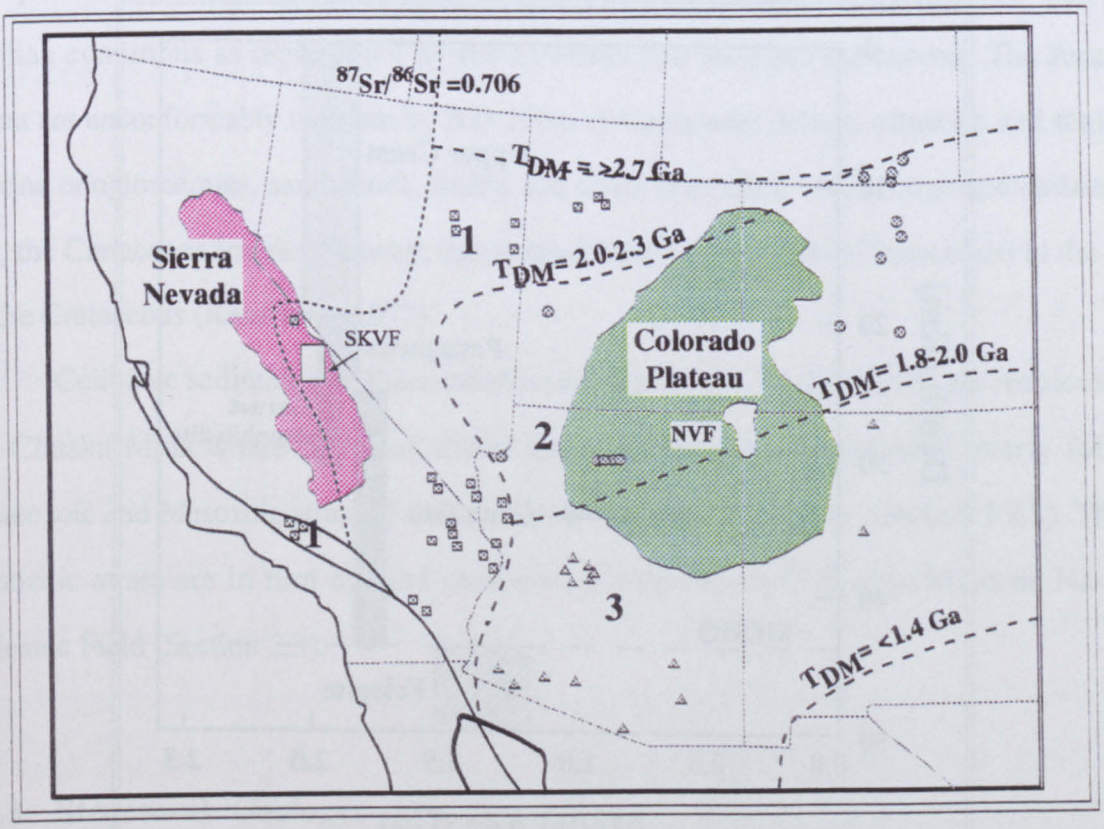


**Figure 2.2.** Crust-formation provinces of the western United States adapted from Bennett & DePaolo (1987). Provinces are distinguished on the basis of regional differences in Nd isotopic evolution paths as determined by measurements of crustal samples of different ages. Squares=province 1 ($T_{DM}$=2.0-2.3Ga), circles=province 2 ($T_{DM}$=1.8-2.0Ga), triangles=province 3 ($T_{DM}$=1.71.8Ga).

Despite the lack of exposure of basement or Mesozoic-Tertiary plutonics, Bennett & DePaolo (1987), by extrapolation of Nd model ages from the southern Rocky Mtns and Colorado River Trough, proposed a gradual increase in neodymium, depleted mantle, model ages ($T_{DM}$) from 1.7 Ga in the south of the Colorado Plateau to 2Ga in the north (Fig 2.2). Such a variation in model ages is consistent with growth of this segment of crust by the continuous incorporation of island-arc material during the Proterozoic and suggests that no Archean lithosphere is present beneath the Colorado Plateau (Condie, 1986; Bennett & DePaolo, 1987).

Wendlandt et al (1993) confirm the 1.7 - 2.0 Ga crustal formation age of the Colorado Plateau, suggested by Bennett & DePaolo (1987), with their Sr-Nd isotope study of lower and upper crustal xenoliths carried in the diatremes of the Navajo Volcanic Field (Section 2.3.2). Their results of lower and upper crustal xenoliths indicate that old, 1.8 - 2.0 Ga material is present at all levels of the Colorado Plateau crust (Fig 2.3).

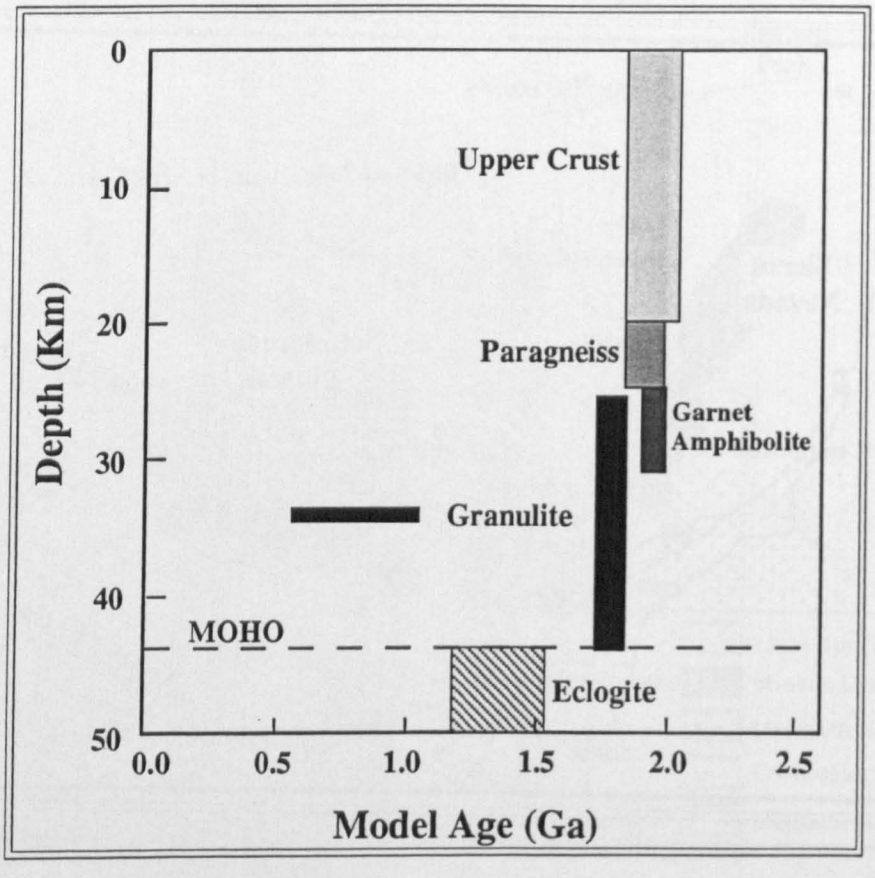


**Figure 2.3.** Nd model ages for crustal xenoliths derived from various depths within the Colorado Plateau. Depth estimates are based on thermobarometry from Wendlandt et al (1993) and seismic velocities of different xenolith types. The range in model ages is equal to one standard deviation of the data for that particular group.

The uniformity of $T_{DM}$ model ages throughout the crust are inconsistent with growth of this portion of crust by underplating of magmas derived from the depleted mantle since the main crust-formation event at 1.85Ga (Wendlandt et al., 1993) but are consistent with the lateral accretion model of Bennett and DePaolo (1987).

### 2.2.2: Palaeozoic-Cenozoic Sedimentary Veneer:

A detailed account of the Palaeozoic-Cenozoic sedimentary stratigraphy of the Navajo region of the Colorado Plateau is provided by Gregory (1917). In brief the sedimentary stratigraphy consists of 350-450m of Carboniferous shallow-marine limestones, shales and sandstones overlain by Permian lacustrine shales, sandstones and limestones and the Permian aeolian De Chelly sandstone. Unconformably overlying the Palaeozoic strata are Triassic coastal conglomerates and the Chinle formation, a sequence of laccustrine shales, marls, sandstones and limestones with abundant vertebrate, invertebrate and plant remains. Jurassic strata also record laccustrine conditions interspersed with arid aeolian conditions as represented by the La Platta and McElmo sandstones. The Jurassic strata are unconformably overlain by 300-700m of Cretaceous deltaic, estuarine and shallow marine conglomerates, sandstones, shales and coals associated with a large epicontinental sea, the Cretaceous Interior Seaway, that existed from L.Albian (mid-Cretaceous) to the end of the Cretaceous (Kauffman, 1977).

Cenozoic sediments of Paleocene/Eocene age in the Navajo region are restricted to the Chuska Mtns where 300m of shales and sandstones unconformably overly folded Palaeozoic and Mesozoic strata of the Laramide, Defiance Monocline (Section 2.2.3). These Cenozoic strata are in turn cut and overlain by lavas of the Oligocene/Miocene Navajo Volcanic Field (Section 2.3).

### 2.2.3: Structural Geology:

The central Colorado Plateau has essentially remained an independent tectonic block and retained its structural integrity since crustal formation in the Proterozoic (Condie, 1986) despite other regions of the Foreland Fold Belt recording three compressional orogenic

episodes during the Phanerozoic and the Cenozoic extensional orogeny (Dickinson et al., 1989).

The Late Cretaceous to Early Tertiary Sevier/Laramide orogeny resulted in crustal thickening of much of the western United States including the Colorado Plateau, hitherto undeformed (Bird, 1984). The Sevier orogeny of the intermountain region (Coney, 1976) was one of thin-skinned thrusting that predated Laramide, basement-involved, deformation of the central and southern Rocky Mtns and Colorado Plateau regions (Dickinson et al., 1988). By the end of the Laramide orogeny, in the late Eocene, the crustal thickness of the Colorado Plateau was approximately 50Km (Bird, 1984; Hauser & Lundy, 1989) a thickening factor of 1.4, assuming an initial crustal thickness of 35Km. Despite this degree of crustal thickening during the Laramide, contractional deformation of the Colorado Plateau was limited to broad basement-cored uplifts, blind thrust monoclines, evident as the Comb Ridge and Defiance monoclines of the Navajo region and intervening basins resulting from flexural effects along the flanks of adjacent uplifts (Hagen et al., 1985; Dickinson et al., 1988; Oldow et al., 1989). Nevertheless internal deformation and development of contractional features in the Colorado Plateau was limited and not sufficient to nucleate later extensional collapse (Oldow et al., 1989).

### 2.2.4: Cenozoic-Recent Uplift:

Both the timing and cause of uplift of the Colorado Plateau remain controversial issues (McGetchin et al., 1980) and are addressed more fully in Chapter 5. The controversy arises in part due to the intimate relationship of the plateau and surrounding Basin & Range and Rio Grande Rift extensional provinces throughout the Mesozoic and Cenozoic (Oldow et al., 1989). It is difficult to attribute the elevation of the plateau to uplift when it can only be made with reference to provinces that have experienced concomitant extensional collapse and hence a decrease in elevation. Frequently quoted methods for determining the age of onset of uplift include reversals in drainage patterns, the movement, distribution and relative thicknesses of ash-flow tuffs that blanket both the Colorado Plateau and peripheral extensional provinces (Nielson et al., 1990). However such methods can only place temporal constraints on the age of structural differentiation between the 'Colorado Plateau'

and Basin & Range, ***not*** the initial onset of uplift. Hamblin (1984) argues, on the basis of palaeo-stream profiles preserved beneath Cenozoic basalt flows, that the absolute motion between the two provinces during the Cenozoic did indeed involve uplift of the Colorado Plateau alongside a 'stable' Basin and Range. However similar evidence for relative motions of the Colorado Plateau and Basin & Range evidence is lacking from the majority of the plateau-rim.

During the mid to late Cretaceous the region was submerged beneath the Cretaceous Interior Seaway, receiving shallow marine and coastal deposits (Gregory,1917; Kauffman, 1977). By late Eocene the post-Laramide topography was one of basement-cored uplifts and basins with a palaeotopographic relief of ≥1000m (Hansen,1984). Floral evidence however suggests the uplifts were generally <1000m (Epis & Chapin,1975) while mammalian and freshwater fish faunas from the Green River Formation, S.W. Wyoming, suggest much lower average Eocene elevations of ≤300m (Hansen, 1985). However it must be stated that estimates of absolute elevation based upon the climate regimes of flora and fauna can be misleading as global-scale climate changes can have much greater effects than localised elevational control, and as such there is no reliable evidence for variations in absolute elevation of the Colorado Plateau throughout the mid Cenozoic to the present. Despite this lack of evidence Oldow et al (1989) suggest that during the mid-late Oligocene the 'Colorado Plateau - Basin & Range' province experienced uplift of perhaps 2-3Km. Between 18 and 10 Ma differential elevation between the Colorado Plateau and Basin & Range province was ≈1Km on the basis of distribution of the Peach Springs Tuff (Young & Brennan, 1974) though again the absolute elevations are impossible to determine. Uplift of the Colorado Plateau on the western flank of a broad continental rise, centred on the southern Rocky Mtns has continued throughout the late Cenozoic (Chapter 5).

### 2.2.5: Cenozoic-Recent Extension:

Regional uplift of the Western Cordillera during the Paleogene was followed by crustal extension within the Basin & Range and Rio Grande, the onset of which was apparently diachronous, initiating in the south (≈32°) in the Oligocene (Gans et al., 1989; Oldow et al., 1989). However due to the lack of contractional structures in the lithosphere,

which could later nucleate extensional faults, the Colorado Plateau retained its structural integrity while the surrounding provinces, where Laramide crustal compression was accommodated by major thrusting, underwent large-scale crustal extension.

In detail the Colorado Plateau can be divided into two subprovinces. The stable central plateau has been characterised by an isotropic stress regime since uplift during the Oligocene (Laughlin et al., 1986) whereas the 100-150km wide transition zone between the stable interior plateau and peripheral extensional provinces experienced limited extension during the Oigo-Miocene resulting in the development of normal block faulting. Extension is gradually encroaching upon the stable central plateau as shown by the northeastward migration of the locus of extension-related magmatism in the San Fransisco volcanic field of the southwest transition zone (Tanaka et al., 1986).

### 2.2.6: Cenozoic Magmatism:

From 1.4Ga, the last major episode of granitic magmatism that occurred within the southwestern United States in the vicinity of the Colorado Plateau (Bennett & DePaolo, 1987), to the Eocene the Colorado Plateau remained amagmatic (Oldow et al., 1989).

By late-Oligocene early-Miocene, extension of the periphery of the plateau was accompanied by small volume basaltic to bimodal volcanism which evolved toward predominantly basaltic compositions with continuing extension. During the same period magmatism in the central plateau was very sparse and may be divided into two periods. The middle Oligocene to middle Miocene was characterised by the emplacement of the S.E. Utah diorite-syenite laccoliths (Sullivan et al., 1991; Nelson et al., 1992) and small-volume ultrapotassic lamprophyres of the Navajo Volcanic Field (section 2.3) and the Wasatch Plateau (Tingey et al., 1991). A state of magmatic quiescence returned to the southern plateau until the late Miocene-early Pliocene and the eruption of small volume nephelinite lavas of the Hopi Buttes Volcanic Field 60Km southwest of the Navajo volcanic field.

## 2.3: The Navajo Volcanic Field (NVF):

The Navajo Volcanic Field (NVF) (Gregory, 1917; Williams, 1936) comprises numerous dykes, diatremes and rare volcanic centres (Fig 2.4) scattered over some 30,000km$^2$ of the Four Corners region of the central Colorado Plateau. Although the intrusions are scattered there is a greater density along the Defiance and Comb Ridge monoclines (Ehrenberg, 1978), as illustrated in Fig 2.4, which may reflect magma migration along pre-existing fault zones (Smith & Levy, 1976). Compositionally the intrusions are heterogeneous (Sections 2.6) and include serpentinised ultramafic breccias (Roden, 1980, 1981), Katungites (Laughlin et al., 1986, 1989) and melanephelinites (Alibert et al., 1986; Section 2.6). The dominant lithology, however, is an ultrapotassic lamprophyre, with phlogopite and diopside phenocrysts set in a matrix of sanidine, referred to as minette (Williams, 1936; Rock, 1984).

Based on K-Ar (Roden et al., 1978; Laughlin et al., 1985) and Ar-Ar (This study, section 2.7) geochronological studies on phlogopite separates, volcanism in the Navajo region occurred from middle Oligocene through to late upper Miocene (28.5 to 19.4 Ma).

### 2.3.1: Diatreme Structure and Style of Volcanism:

Erosion of the Colorado Plateau since the emplacement of the Navajo intrusions during the Oligo-Miocene has resulted in the present day exposures of the volcanic centres at various structural levels down to as low as 900m below the original palaeo-surface (McGetchin, 1968). In the high Chuska Mtns (Fig 2.4), the highest region within the NVF, maar-type craters and lava flows are preserved as erosional remnants unconformably overlying the Chuska Sandstone (Appledorn and Wright, 1957) and hence this level can be interpreted as the Oligocene paleaosurface. Comparing Washington Pass volcanic centre with more deeply exposed diatremes such as West Sonsela Buttes and Ship Rock (Fig 2.4) a model for a typical Navajo minette diatreme can be constructed (Ehrenberg, 1977).

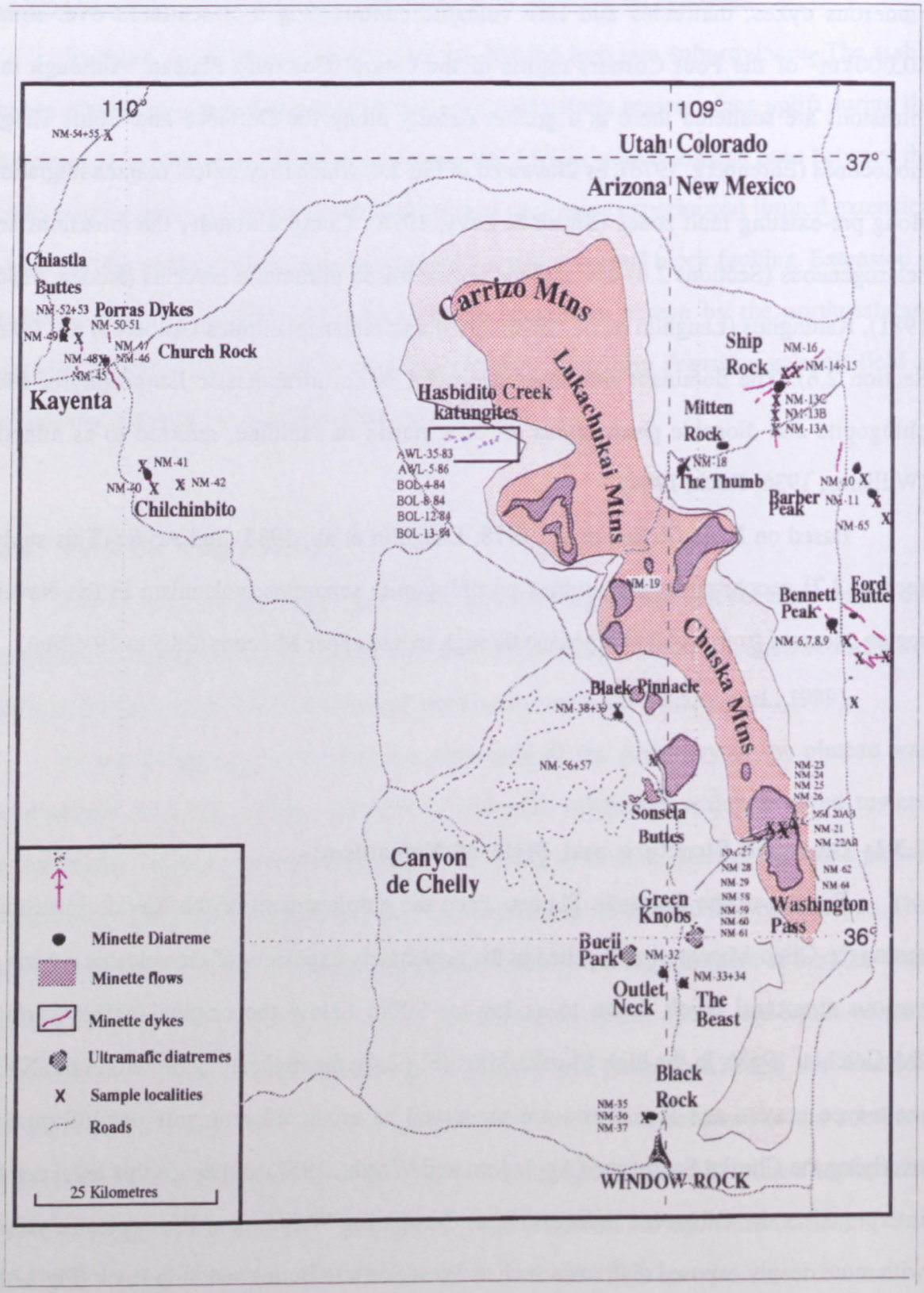


**Figure 2.4.** Minette sampling locations within in the Navajo Volcanic Field. Also show is the approximate location of the katungite samples provided by A.W. Laughlin.

Figure 2.5 is a diagrammatical representation of a minette diatreme where the profiles of Washington Pass, Sonsela Buttes and Ship Rock are superimposed at their actual elevations. Although individual minette centres exhibit wide morphological diversity, a typical diatreme may have been characterised by a shallow, open maar-like crater several kilometres in diameter and perhaps 100-200m deep which rapidly steepened to a narrow conduit approximately 0.5 Km in diameter.

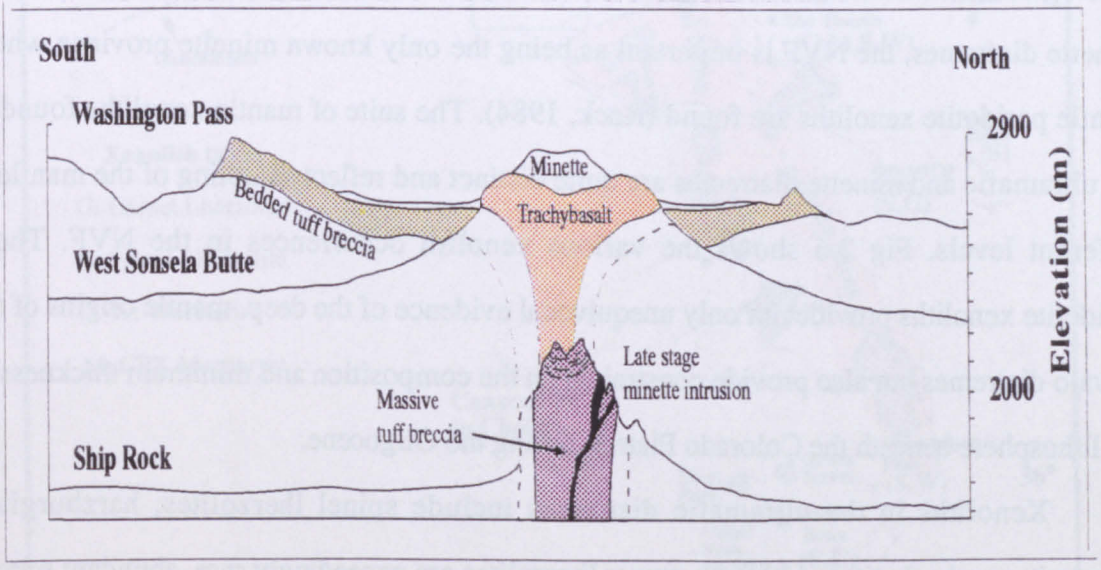


**Figure 2.5.** Diagrammatic representation of the structure of a typical Navajo minette-diatreme based on north-south cross-sections of the Washington Pass, West Sonsela Buttes and Ship Rock diatremes from Ehrenberg (1978). Vertical exaggeration 1.5x

A typical eruption sequence of a Navajo minette diatreme consisted of an initial, explosive, diatreme emplacement associated with pyroclastic activity. The initial pyroclastic phase was followed by the subsequent intrusion and eruption of minette magma. The Serpentinised ultramafic breccia (SUM) diatremes differ from the minette diatremes in that they were emplaced as a non-magmatic, subsolidus, gas-peridotite mixture, perhaps triggered by the injection of minette magma into hydrated and carbonated peridotite in the shallow mantle (Smith, 1977).

The source of volatiles responsible for the explosive pyroclastic activity associated with emplacement of both minette and ultramafic diatremes may have originated from the breakdown of hydrous and carbonate phases within the mantle for which there is good

evidence (Hunter & Smith, 1981), exsolution of $H_2O$ and $CO_2$ from the ascending volatile-rich magma or, by the vaporization of groundwater contained within the porous sandstone aquifers common in the Navajo Volcanic Field. Ehrenberg (1978) concludes that the major component of pyroclastic activity is the result of phreatic groundwater-magma interaction.

### 2.3.2: Occurrence of Xenoliths:

Although crustal xenoliths, including granites, granitic gneisses and sedimentary lithologies are common (McGetchin & Silver, 1970; Wendlandt et al,.1993) in many of the minette diatremes, the NVF is important as being the only known minette province where mantle peridotite xenoliths are found (Rock, 1984). The suite of mantle xenoliths found in the ultramafic and minette diatremes are quite distinct and reflect sampling of the mantle at different levels. Fig 2.6 shows the various xenolith occurrences in the NVF. These peridotite xenoliths provide not only unequivocal evidence of the deep, mantle origins of the Navajo diatremes but also provide constraints on the composition and minimum thickness of the lithosphere beneath the Colorado Plateau during the Oligocene.

Xenoliths in the ultramafic diatremes include spinel lherzolites, harzburgites, websterites and eclogites. Although garnet lherzolites are exceedingly rare, abundant pyrope xenocrysts and low-Al diopsides are interpreted as remnants from disaggregated garnet lherzolite. Spinel lherzolites and mineral inclusions in garnet xenocrysts yield equilibration conditions of <700°C at ≈60km and 500-700°C at 60-75km respectively, implying derivation of these diatreme eruptions from relatively shallow levels of the upper mantle (Hunter & Smith, 1981). The garnet xenocrysts are notable for the inclusions of hydrous and carbonate phases (McGetchin & Silver, 1970; McGetchin and Besancon, 1973; Hunter and Smith, 1981; Smith, 1987) such as amphibole, dolomite, calcite and magnesite. These carbonate phases are preserved only in xenocrysts from the ultramafic intrusions, presumably as a consequence of the eruption of the ultramafic breccias as sub-solidus gas-solid mixtures. The presence of primary-textured hydrous and carbonate phases within mantle xenoliths supports the hypothesis that hydrous and carbonate phases were primary parts of the garnet-lherzolite lithosphere beneath the Colorado Plateau (McGetchin & Silver, 1970 ; Chapter 3)

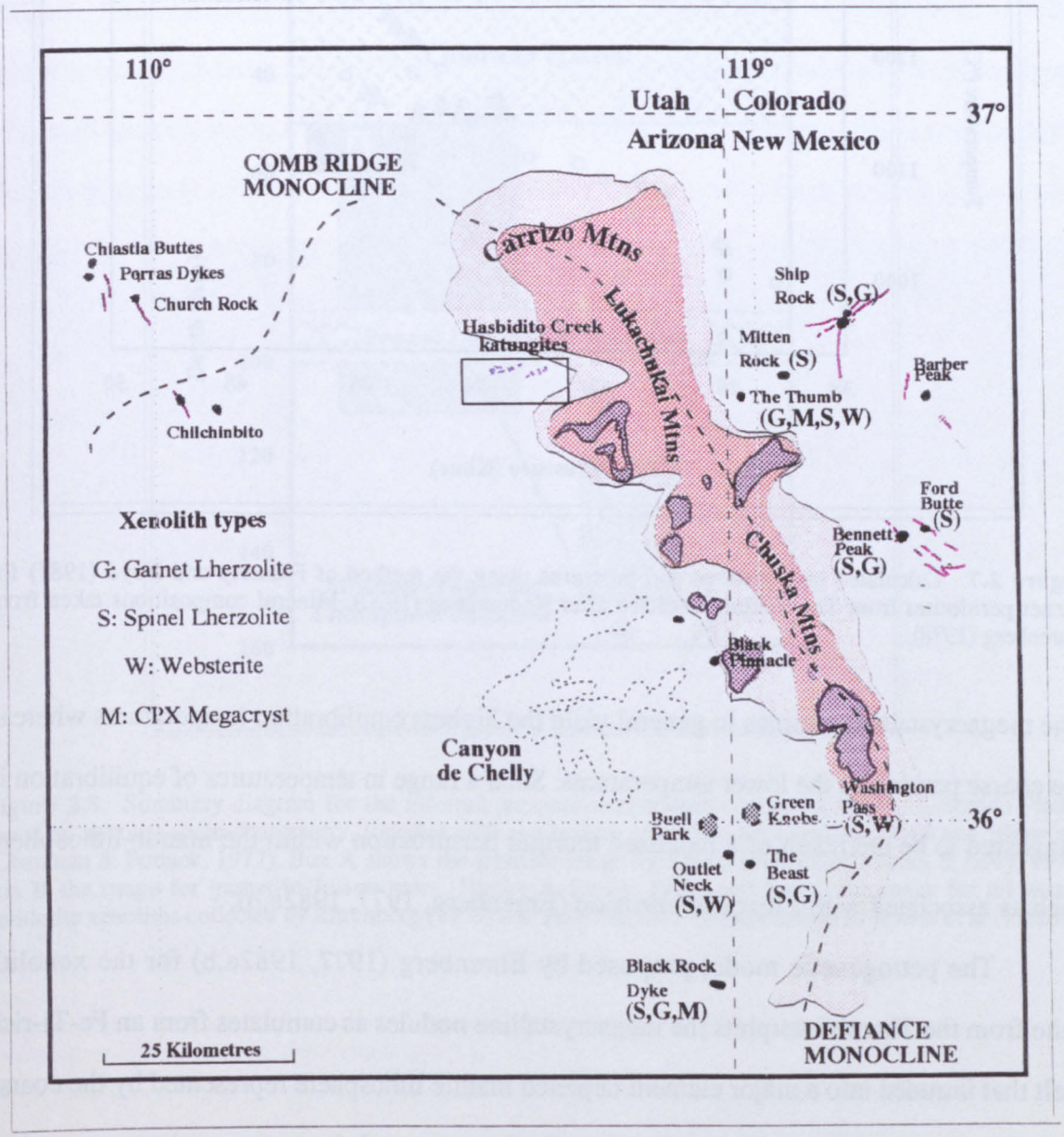


**Figure 2.6**. Xenolith localities of the Navajo Volcanic Field of the central Colorado Plateau, western United States. Taken from Ehrenberg (1982a).

Although minette diatremes contain abundant spinel lherzolites similar to those of the ultramafic diatremes, they also contain rare garnet lherzolites (Ehrenberg, 1977, 1982a, b) and therefore may have sampled deeper levels of the lithosphere. Ehrenberg (1977, 1982a, b) divides the garnet peridotites into three groups on the basis of texture and composition: coarse garnet peridotites with minerals low in Fe and Ti, sheared garnet peridotites with minerals high in Fe and Ti and medium to ultracoarse or, "megacrystalline", peridotites. The various xenolith groups equilibrated over a range of temperatures and pressures summarised in Fig 2.7, from 1000-1250°C and 40-48 Kbar (Roden et al., 1990).

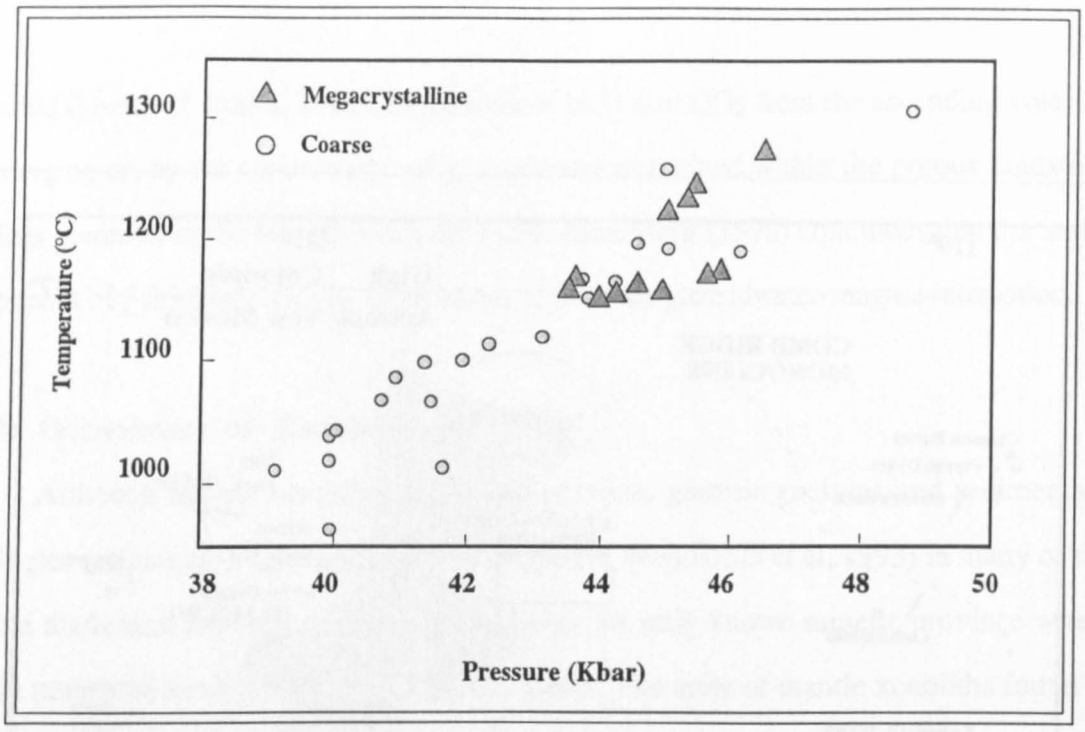


**Figure 2.7.** Calculated temperatures and pressures using the method of Finnerty and Boyd (1987) for garnet peridotites from The Thumb modified after Roden et al (1990). Mineral compositions taken from Ehrenberg (1978).

The megacrystalline samples in general yield the highest equilibration temperatures whereas the coarse peridotites the lower temperatures. Such a range in temperatures of equilibration is suggested to be the result of a localised thermal perturbation within the mantle lithosphere such as associated with a diapiric intrusion (Ehrenberg, 1977, 1982a,b).

The petrogenetic model proposed by Ehrenberg (1977, 1982a,b) for the xenolith suite from the Thumb interprets the megacrystalline nodules as cumulates from an Fe-Ti-rich melt that intruded into a major element depleted mantle lithosphere represented by the coarse garnet peridotites. The same Fe-Ti-rich melt also caused deformation and metasomatism around its periphery resulting in the Fe-Ti-rich sheared garnet lherzolites. On the basis of the short life expectancy of olivine neoblasts and Fe-Mg gradients in garnets of the sheared lherzolite group at 1200°C, the period between introduction of the thermal perturbation, here an intrusion; the metasomatism and deformation of the garnet lherzolite and the final incorporation into the minette host magmas must have been short (less than 10,000 thousand years [Ehrenberg, 1979, 1982a,b; Smith and Ehrenberg, 1984]). Fig 2.8 summarises the inferred P-T equilibrium conditions of xenoliths from the Navajo Volcanic Field (Hunter & Smith, 1981).

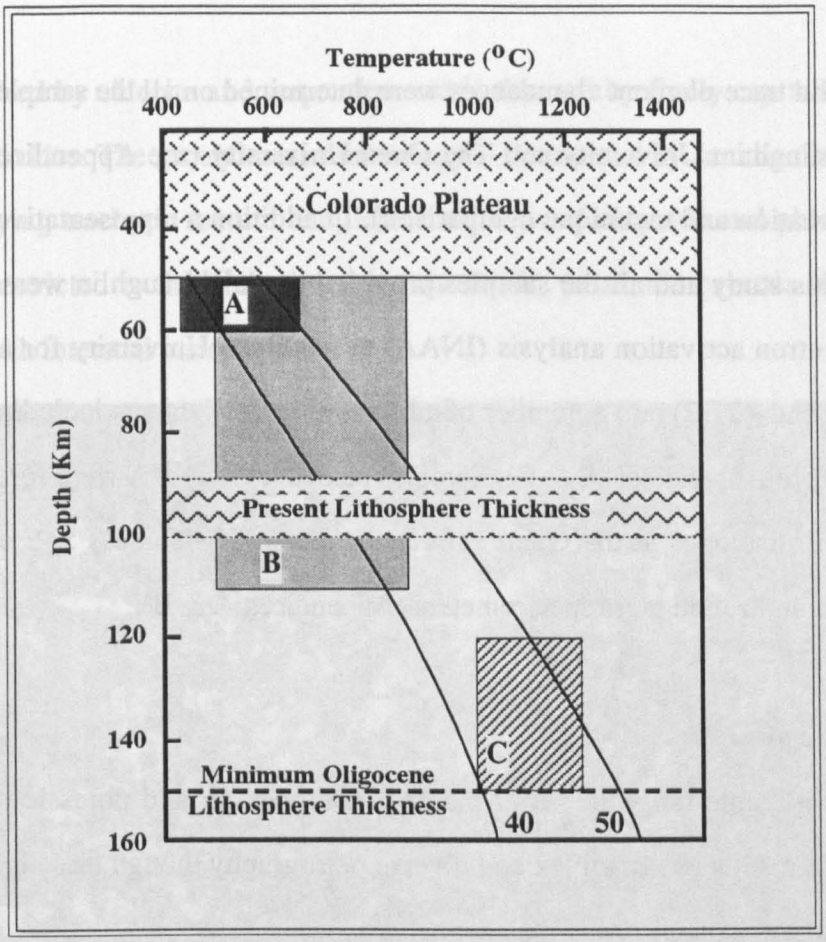


**Figure 2.8**. Summary diagram for the inferred pressure-temperature conditions for the Colorado Plateau based on xenolith thermobarometry, together with continental geotherms for heatflows of 40 and 50mw m-2 (Chapman & Pollack, 1977). Box **A** shows the possible range for Spinel Lherzolites (Smith & Levy, 1976), box **B** the range for garnet-inclusion pairs (Hunter & Smith, 1981) and box **C** the range for all garnet-peridotite xenoliths collected by Ehrenberg (1979) and based on the P-T calculations of Roden et al (1990).

## 2.4: Petrography and Geochemistry:

A total of 65 samples were collected from across the Navajo Volcanic Field and a further 5 samples of Katungite from the Hasbidito Creek were kindly made available for re-analysis by Dr. A.W.Laughlin. Fig 2.4 shows the sample locations and identification numbers for material collected during 1990

Sampling was generally restricted to the numerous volcanic necks and/or dykes as these provided the greatest chance of collecting fresh material with primitive compositions. Samples from the Washington Pass volcanic centre were collected so as to identify any possible role for fractionation processes in the petrogenesis of the comparatively rare lavas of the NVF.

Major and trace-element abundances were determined on all the samples using XRF facilities at Nottingham University and The Open University (see Appendices A & B for analytical information and technique comparison). In addition a representative selection of samples from this study and all the samples provided by A.W.Laughlin were analysed by instrumental neutron activation analysis (INAA) at the Open University for a selection of Rare Earth elements (REE) and a number of additional trace elements including Th, U, Hf, Ta, Sc, and Co (see Appendices A & B). Samples selected for INAA were further analysed for Sr, Nd and Pb isotopes at the Open University using VG-Isomass 54E and Finnigan MAT261 thermal ionization mass spectrometers (Appendices A & B).

### 2.4.1: Petrography:

The considerable range in major element composition and potassic nature of the Navajo intrusions results in a complex and diverse petrography though three lithologies can be discerned: minette, katungite, and melanephelinite.

#### 2.4.1a: Minettes:

Minettes exhibit a wide range in silica content (48-60 wt%), recognised in the field by a change in colour from black to pale grey. The range of mafic to felsic minettes is accompanied by changes in petrography, mainly in mineral modes, though it possible to identify characteristics common to the entire range.

Typically minettes are characterised by seriate-textured diopside and phlogopite, with or without olivine in a glassy to microcrystalline, commonly trachytic, groundmass of sanidine+diopside+phlogopite+oxides+apatite±glass. Diopside crystals vary from <0.01-3mm, the larger crystals being euhedral, very rarely embayed and, commonly exhibiting spongy or sieve-textured cores unlike the anhedral groundmass crystals (Plate 2.1). Phlogopite crystals vary from <0.01-2mm, occasionally exhibiting a trachytic texture where the crystal orientations are parallel to the dyke margins. Zoning within phlogopite phenocrysts is common with pale brown cores rimmed by a dark phlogopite overgrowth. The groundmass phlogopite typically has the same dark colour of the phenocryst rims. Olivine is rare (0-2%) and is present only in the silica-poor minettes as phenocrysts (up to 2mm) and very occasionally as groundmass. The majority of the olivine is partially or totally

pseudomorphed by chlorite and serpentine and is rimmed by finely crystalline phlogopite and opaque oxides. The groundmass mineralogy is dominated by sanidine laths (0.1-5mm) often displaying trachytic texture and, lesser amounts of diopside and phlogopite. Opaqe oxides are restricted to the groundmass as are stubby prismatic crystals of apatite, often associated with interstial residual glass.

**Plate 2.1.** NM-46 showing seriate-textured diopside and phlogopite phenocrysts set in a groundmass of predominantely sanidine feldspar laths phlogopite and diopside. Note the spongy-cored diopside phenocrysts in the lower right. Scale bar approximately 1mm.

A comparison of silica-poor through to silica-rich minettes reveals several petrological differences. Olivine, though rare is more abundant in the silica-poor minettes where it is often associated with a feldspathoid (Gregory, 1917; Roden & Smith, 1979) and very occasionally accessory perovskite («1%). The clinopyroxene:phlogopite ratio decreases from mafic to felsic minettes. Quartz is absent in the mafic minettes and rare in the felsic minettes where it forms interstitial patches.

Extrusive minettes, equivalent to trachybasalts, present at Washington Pass and Sonsela Buttes, are compositionally similar to their intrusive counterparts though they differ mineralogically and lack the seriate-porphyritic texture typical of lamprophyres. Within the Washington Pass volcanic centre three trachybasalt units can be recognised (Ehrenberg, 1978).

Units A and B (terminology from Ehrenberg, 1978) are porphyritic, < 10% phenocrysts of diopside, phlogopite, and olivine, usually altered to chlorite. The lower, unit A, has an aphanitic-microcrystalline groundmass of sanidine laths (70%), diopside (10%), phlogopite (10%), opaque oxides, quartz and apatite (Plate 2.2). The overlying unit B has large sanidine oikocrysts, commonly showing Carlsbad twinning, poikilitically enclosing crystals of diopside, phlogopite, oxides and apatite (Plate 2.3).

Unit C is a porphyritic, leucocratic trachybasalt consisting of phenocrysts of diopside (15%) and phlogopite up to 5mm in a trachytic microcrystalline matrix of sanidine, diopside, phlogopite, oxides and apatite. In contrast to units A and B, altered spinel peridotite xenoliths are abundant ≤ 5% (Plate 2.4) which indicates a mantle origin for even the felsic minettes.

**Plate 2.2.** NM-60 from Unit A of Washington Pass (Ehrenberg, 1978) showing spongy-cored diopside phenocrysts set in microcrystalline matrix of sanidine, diopside and phlogopite laths. Scale bar approximately 1mm.

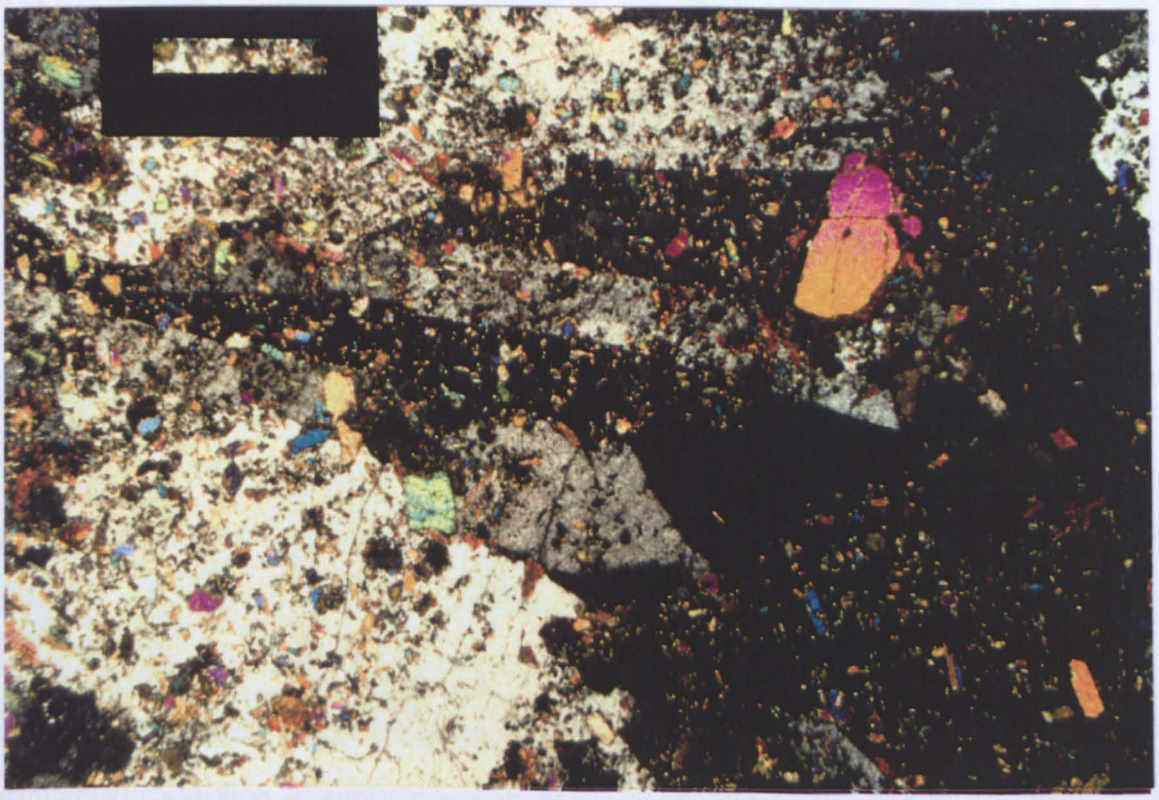

**Plate 2.3.** NM-26 from Unit B of Washington Pass (Ehrenberg, 1978) showing large sanidine oikocrysts with Carlsbad twinning poikilitically enclosing mainly diopside and phlogopite crystals but also opaque oxides and small quantities of apatite. Scale bar approximately 1mm.

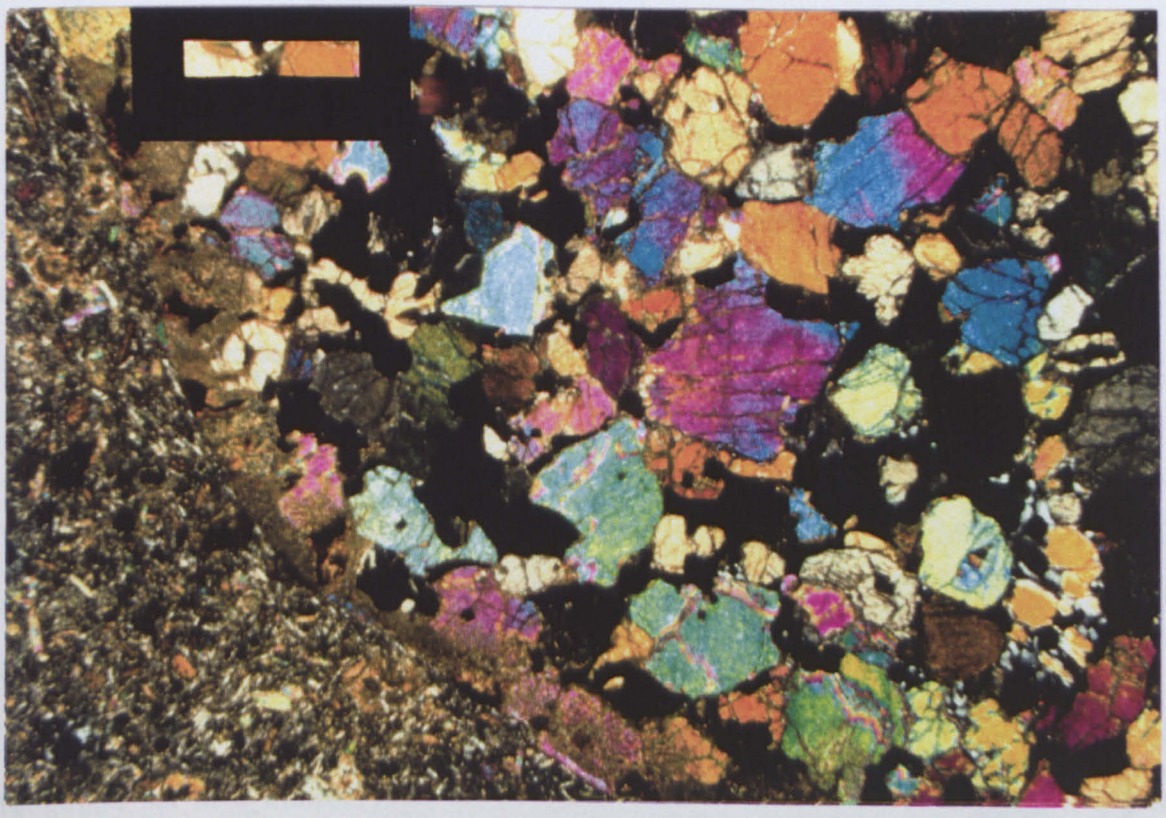

**Plate 2.4.** NM-20 shows a slightly altered spinel peridotite xenolith enclosed within a microcrystalline trachytic assemblage of sanidine, diopside, phlogopite, opaque oxides and apatite characteristic of Unit C of the Washington Pass volcanic centre (Ehrenberg, 1978). Scale bar approximately 1mm.

**2.4.1b: Katungites:**

Only the salient features of the Navajo katungites and olivine melilitite are discussed below as detailed petrographic descriptions are presented in Laughlin et al (1989). The most striking feature of these highly silica-undersaturated magmas is the large number of phases observed, 20 in all and up to 18 in a single sample (Laughlin et al., 1989). A summary of the modal mineralogical compositions is presented in Table 2.1

There is considerable heteromorphism within the katungites (Laughlin et al, 1989; Table 2.2). All the samples exhibit seriate-textured olivine and phlogopite, up to 8mm and 3mm long respectively, set in a matrix of anhedral olivine, phlogopite, melilite, perovskite, glass, apatite ± clinopyroxene (Plate 2.5). Olivine abundance varies between 5 and 20% and it exhibits alteration along fractures as in samples BOL-4-84 and BOL-13-84, or more pervasive alteration to serpentine as in BOL-8-84 and BOL-12-84. Phlogopite abundance varies between 16 and 30% and occurs as phenocrysts, occasionally poikilitically enclosing olivine and clinopyroxene crystals. The abundance of essential melilite is variable and is restricted to the groundmass as small lath-shaped crystals.

| *SAMPLE #* | AWL-35-83 | BOL-4-84 | BOL-12-84 | BOL-13-84 | BOL-8-84 | AWL-5-86 |
|---|---|---|---|---|---|---|
| *Olivine* | 12 | 18 | 2 | 16 | 6 | 22 |
| *Phlogopite* | 30 | 29 | 16 | 31 | 25 | 6 |
| *Perovskite* | 7 | 5 | 3 | 4 | 4 | 2 |
| *Early CPX* | tr | tr | – | – | tr | tr |
| *Melilitite* | 23 | 18 | tr | 3 | – | 3 |
| *Late CPX* | – | – | 20 | – | 22 | – |
| *Opaque Oxides* | 7 | 7 | 8 | 9 | 5 | 14 |
| *Nepheline* | – | – | – | tr | 4 | – |
| *Wollastonite* | 2 | tr | – | ? | – | – |
| *K-Feldspar* | – | – | tr | – | – | – |
| *Pectolite* | 3 | – | – | 2 | – | tr |
| *Thomsonite* | 1 | – | – | 1 | – | – |
| *Natrolite* | – | – | tr | – | – | – |
| *Andradite* | 1 | tr | – | tr | tr | – |
| *Na-Amphibole* | – | – | – | tr | – | – |
| *Pyrite* | tr | tr | – | – | – | – |
| *Serpentine* | tr | – | 17 | tr | tr | 14 |
| *Chlorite* | tr | – | – | – | – | – |
| *Haematite* | tr | – | – | – | – | – |
| *Tobermorite* | tr | – | – | – | – | – |
| *Calcite* | 2 | – | – | tr | – | – |
| *Aenigmatite* | tr? | – | – | – | – | – |
| *Apatite* | tr | tr | 1 | tr | tr | – |
| *Dolomite* | – | – | – | – | – | – |
| *Groundmass (unidentified)* | 10 | 22 | 33 | 33 | 18 | 39 |

**Table 2.1.** Modal mineralogical compositions of Arizona katungites. AWL-35-83 and BOL-4-84 were collected from the same dike. (taken from Laughlin et al., 1989)

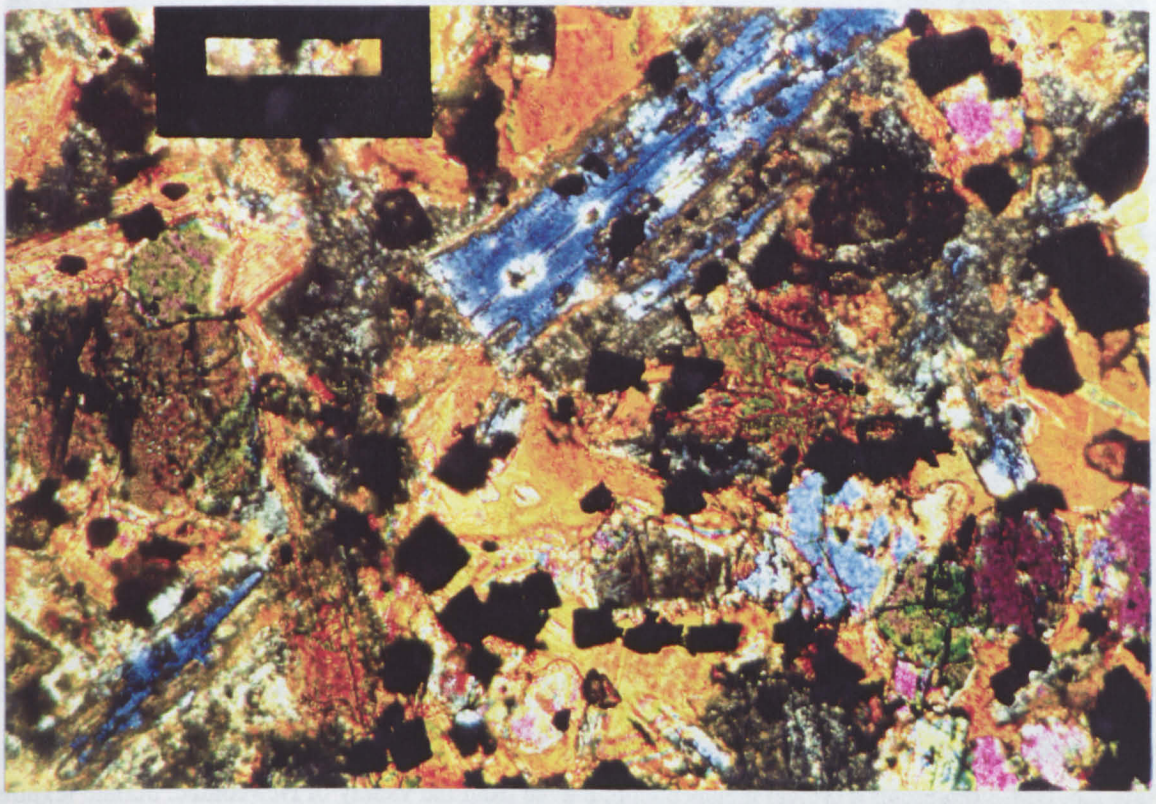

**Plate 2.5.** BOL-13-84 is a katungite sample from Hasbidito Creek provided by A.W.Laughlin. Lath shaped crystal (top centre) with anomalous blue birefringence is melilite. Dark brown, almost opaque crystals are perovskite. Diopside exhibits bright green and pink birefringence colours whereas phlogopite, masked by its browm body colour appears greeny yellow. Scale bar approximately 0.25mm.

AWL-5-86 lacks the seriate-porphyritic texture typical of the minettes and katungites and consists of up to 22% olivine phenocrysts (0.5mm diam) in a microcrystalline matrix of anhedral olivine, phlogopite, melilite, oxides and perovskite. Olivines are commonly altered to and, a few are completely psuedomorphed by serpentine. Clinopyroxene is rare, <2% of the matrix, and is present only as small anhedral masses.

**2.4.1c: Melanephelinites:**

Two petrographic varieties of dyke represented by only three samples which appear mineralogically transitional to the minettes and katungites are recognised from the region of Newcombe.

Samples NM-3 and NM-4 are characterised by seriate-textured olivine, diopside and phlogopite set in a microcrystalline to glassy matrix of olivine+diopside+phlogopite +nepheline+minor quantities of perovskite, melilite and opaque Fe oxides (Plate 2.6).

**Plate 2.6.** NM-3 represents a typical melanephelinite dyke from the vicinty of Newcombe. Seriate textured diopside, phlogopite and olivine, usually showing pervasive alteration, is enclosed by a microcrystalline to glassy matrix of a similar assemblage. Note altered olivine just to the lower right of centre. Scale bar approximately 0.5mm.

Both phenocryst and groundmass olivine is extensively though not completely altered to chlorite and serpentinite and is commonly rimmed by phlogopite. Olivine originally comprised approximately 20% of the rock. Euhedral diopside laths show a weak preferred orientation in NM-4 but are random in NM-3. In neither sample are sieve textured diopside cores, so typical of the minettes, observed. Phlogopite occurs as both microphenocrysts which poikilitically enclose clinopyroxene and anhedral overgrowths to some olivine crystals and comprises approximately 10% of the rock. Essential nepheline, though present as microphenocrysts <0.5mm length, is generally restricted to the groundmass, interstitial to diopside and phlogopite, and comprises <10% of the rock. The presence of nepheline in these dykes along with the high abundance of the mafic minerals and original olivine contents in excess of 20% are typical of Olivine Melanephelinites.

NM-1 is generally similar to the olivine melanephelinite dykes though it has more similarities to minettes. Perovskite and melilite are absent and although nepheline is present it is subordinate to feldspar. The most striking difference is in the modal abundance of phlogopite which reaches approximately 25% in NM-1. NM-1 is very similar to the mica-melanephelinites of the Wasatch Plateau in Utah (Tingey et al., 1991)

### 2.4.2: Classification:

The Navajo volcanic field has long been regarded as a classic continental ultrapotassic province and indeed the majority of samples analysed in this study are potassic. Although the rocks from the NVF are hypabyssal intrusives it is useful to compare the total alkali-silica (TAS: $Na_2O+K_2O$ vs. $SiO_2$) variation of the Navajo samples with the fields for extrusive volcanic rocks from Le Bas (1986) as shown in Figure 2.9. Group I samples maybe regarded as the intrusive equivalents to basanites through potassic trachybasalts and shoshonites to latites whereas Group II samples, with $SiO_2$ «40wt%, do not have any reasonable extrusive equivalents and are therefore cannot easily be classified using the TAS diagram. Finally the Group III, comprised of just three samples, are the intrusive equivalents of basanites.

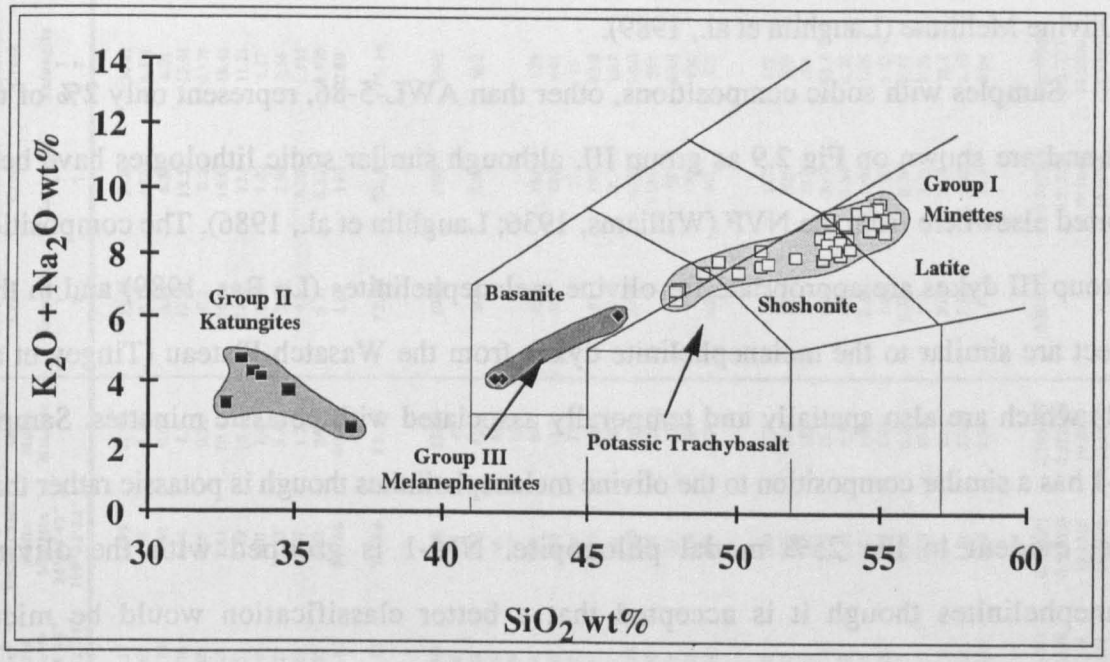


**Figure 2.9.** Total alkalis versus $SiO_2$ wt% for intrusives of the Navajo Volcanic Field. Fields are labelled for rocks with K>Na and are taken from Le Bas (1986).

All the intrusives of the Navajo volcanic field have compositions combined with mineralogies and seriate-textures appropriate for lamprophyres. However the compositional and mineralogical variability of lamprophyres has lead to a confusion in nomenclature and classification. This section merely offers a simple classification to aid in later discussion and where appropriate retains previous terminology for purposes of continuity.

The dominant lithology, Group I, is referred to as minette, a potassic to ultrapotassic calc-alkaline lamprophyre equivalent to extrusive potassic trachybasalt (Rock, 1984; Le Maitre, 1989). Typically a minette has diopside and phlogopite ± olivine phenocrysts set in a matrix containing the same phases plus sanidine (section 2.4.1a). The minettes of the NVF exhibit a considerable compositional and mineralogical range and can be further subdivided into mafic and felsic minette varieties (Roden, 1981; Section 2.4.3a).

The highly silica-undersaturated, potassic lamprophyre samples (group II, Fig 2.9) from the Hasbidito Creek region of the NVF (fig 2.4: Laughlin et al., 1986, 1989). are classified as Katungites (Laughlin et al., 1989) on the basis of their compositional similarity to the Ugandan katungites described by Holmes (1937). One sample however, AWL-5-86 has $K_2O/Na_2O<1$, contains abundant olivine and as a result has higher MgO than the more typical katungites and although included with the group II katungites it is best classified as an Olivine Melilitite (Laughlin et al., 1989).

Samples with sodic compositions, other than AWL-5-86, represent only 2% of the total and are shown on Fig 2.9 as group III, although similar sodic lithologies have been reported elsewhere from the NVF (Williams, 1936; Laughlin et al., 1986). The composition of group III dykes are appropriate for olivine melanephelinites (Le Bas, 1989) and in this respect are similar to the melanephelinite dykes from the Wasatch Plateau (Tingey et al, 1991) which are also spatially and temporally associated with potassic minettes. Sample NM-1 has a similar composition to the olivine melanephelinites though is potassic rather than sodic, evident in the 25% modal phlogopite. NM-1 is grouped with the olivine melanephelinites though it is accepted that a better classification would be mica-melanephelinite (Tingey et al., 1991).

### 2.4.3: Major Element variations:

Geochemical data for a selection of representative samples from the three petrographic groups discussed above are presented in Table 2.2 and the complete database presented in Appendix A. In an attempt to exclude the effects of secondary alteration in the assessment of geochemical variations, samples with LOI >4wt% and showing visible signs of alteration have been excluded from geochemical modelling except the Katungites, with LOI from 3.6 - 10wt%, as fresher samples were not available.

| Sample Location | 90-NM-11 Dyke SE Barber Peak | 90-NM-28 Washington Pass | 90-NM-32 | 90-NM-55 S. Mexican Hat | AWL-35-83 Hasbidito Creek | BOL-4-84 Hasbidito Creek | BOL-8-84 Hasbidito Creek | BOL-12-84 Hasbidito Creek | BOL-13-84 Hasbidito Creek | AWL-5-86 Hasbidito Creek Olivine | 90-NM-1 Newcombe | 90-NM-3 Newcombe | 90-NM-4 Newcombe |
|---|---|---|---|---|---|---|---|---|---|---|---|---|---|
| Rock Type | Mafic Minette | Mafic Minette | Outlet Neck Mafic Minette | Mafic Minette | Katungite ? ? | Katungite ? ? | Katungite ? ? | Katungite ? ? | Katungite ? ? | Melilitite ? ? | Melanephelinite | Melanephelinite | Melanephelinite |
| Lat | 36°34'13" | 36°05'18" | 35°54'47" | | | | | | | | 36°16'49" | 36°20'43" | 36°20'43" |
| Long | 108°41'17" | 108°52'29" | 109°02'32" | | | | | | | | 108°42'10" | 108°38'29" | 108°41'21" |
| $SiO_2$ | 48.89 | 55.17 | 54.95 | 47.99 | 33.58 | 33.82 | 34.81 | 32.66 | 33.16 | 36.94 | 45.97 | 42.02 | 41.83 |
| $TiO_2$ | 2.28 | 1.67 | 1.33 | 2.38 | 4.74 | 4.267 | 4.338 | 4.124 | 4.283 | 3.295 | 3.23 | 3.65 | 3.41 |
| $Al_2O_3$ | 9.25 | 10.72 | 10.58 | 9.01 | 6.84 | 6.85 | 6.01 | 6.34 | 6.76 | 5.45 | 8.02 | 8.33 | 7.48 |
| $Fe_2O_3$ | 8.74 | 7.06 | 6.44 | 8.9 | 12.96 | 13.57 | 12.91 | 12.91 | 14.06 | 13.22 | 9.57 | 11.94 | 11.68 |
| MnO | 0.13 | 0.09 | 0.09 | 0.11 | 0.2 | 0.2 | 0.178 | 0.186 | 0.211 | 0.185 | 0.1 | 0.15 | 0.18 |
| MgO | 10.28 | 8.28 | 7.84 | 10.52 | 16.14 | 16.61 | 18.45 | 16.09 | 15.72 | 22.59 | 13.22 | 12.62 | 13.99 |
| CaO | 9.21 | 6.53 | 7.19 | 10.12 | 14.25 | 13.5 | 11.21 | 12.42 | 14.37 | 9.28 | 9.32 | 12.31 | 12.44 |
| $Na_2O$ | 2.31 | 2.41 | 2.01 | 1.45 | 1.45 | 1.22 | 1.17 | 1.49 | 1.57 | 1.33 | 0.87 | 2.51 | 2.42 |
| $K_2O$ | 5.09 | 6.22 | 7.53 | 5.43 | 2.87 | 2.95 | 2.56 | 1.85 | 3.13 | 1.26 | 5.26 | 1.59 | 1.65 |
| $P_2O_5$ | 1.2 | 0.83 | 1.07 | 1.27 | 1.6 | 1.701 | 1.185 | 1.478 | 1.918 | 1.103 | 1.16 | 1.41 | 1.33 |
| LOI | 2.18 | 0.85 | 0.63 | 2.73 | 5.37 | 5.312 | 7.179 | 10.452 | 4.818 | 5.347 | 2.81 | 3.36 | 3.5 |
| Total | **99.56** | **99.83** | **99.66** | **99.91** | **100** | **100** | **100** | **100** | **100** | **100** | **99.53** | **99.89** | **99.91** |
| Mg# | **71.15** | **71.09** | **71.86** | **71.26** | **72.31** | **72.53** | **75.14** | **72.96** | **72.09** | **79.53** | **74.34** | **68.91** | **71.53** |
| XRF | | | | | | | | | | | | | |
| Ba | 2690 | 2209 | 2526 | 2229 | 1960 | 2197 | 1607 | 2504 | 1928 | 1221 | 1537 | 2437 | 2040 |
| Co | 48 | 36 | 33 | 42 | | | | | | | 55 | 63 | 57 |
| Cr | 354 | 247 | 232 | 435 | 560 | 526 | 602 | 548 | 487 | 806 | 339 | 454 | 489 |
| Cu | 56 | 49 | 46 | 61 | | | | | | | 75 | 83 | 77 |
| Ga | 19 | 19 | 17 | 15 | | | | | | | 18 | 14 | 12 |
| Nb | 73 | 38 | 33 | 94 | 155 | 152 | 128 | 139 | 161 | 110 | 77 | 122 | 115 |
| Ni | 306 | 240 | 238 | 312 | 510 | 481 | 641 | 501 | 405 | 834 | 381 | 263 | 382 |
| Pb | 23 | 42 | 30 | 25 | | 21 | 15 | 15 | 22 | 12 | 14 | 21 | 15 |
| Rb | 133 | 168 | 210 | 142 | 95 | 105 | 82.8 | 65.1 | 103 | 62.6 | 129 | 73 | 63 |
| Sc | 10 | 3 | 10 | 16 | 24.6 | 25.7 | 19.8 | 21.9 | 25 | 19.2 | 9 | 12 | 19 |
| Sr | 1696 | 1273 | 1380 | 1742 | 2090 | 4373 | 1492 | 1598 | 2958 | 1118 | 1040 | 1660 | 1513 |
| V | 208 | 157 | 137 | 226 | | 314 | 293 | 277 | 302 | 276 | 258 | 354 | 287 |
| Y | 30 | 23 | 35 | 33 | | 36 | 25.8 | 32.7 | 40.1 | 26.2 | 26 | 28 | 26 |
| Zn | 99 | 89 | 100 | 109 | | 130 | 106 | 117 | 136 | 115 | 75 | 114 | 100 |
| Zr | 417 | 381 | 459 | 430 | 450 | 441 | 376 | 387 | 497 | 376 | 438 | 435 | 384 |
| INAA | | | | | | | | | | | | | |
| La | 147 | 132 | 189 | 172 | 164 | 157 | 117 | 142 | 180 | 107 | 114 | 140 | 135 |
| Ce | 285 | 243 | 335 | 316 | 335 | 301 | 226 | 278 | 346 | 206 | 236 | 277 | 267 |
| Nd | 130 | 113 | 166 | 152 | 151 | 131 | 101 | 125 | 154 | 95.9 | 113 | 124 | 121 |
| Sm | 21.6 | 17.4 | 27.6 | 25.6 | 15.6 | 20.2 | 15.4 | 19 | 23.2 | 15.9 | 20.4 | 21.2 | 20.9 |
| Eu | 5.34 | 4.2 | 6.45 | 6.1 | 4.99 | 5.64 | 4.24 | 5.31 | 6.38 | 4.27 | 5.08 | 5.58 | 5.46 |
| Tb | 1.72 | 1.4 | 2.02 | 1.91 | 2.28 | 1.69 | 1.26 | 1.58 | 1.92 | 1.31 | 1.5 | 1.69 | 1.68 |
| Yb | 1.51 | 1.29 | 1.77 | 1.63 | 2.66 | 1.95 | 1.23 | 1.5 | 2 | 1.22 | 1.22 | 1.45 | 1.4 |
| Lu | 0.21 | 0.2 | 0.26 | 0.25 | 0.282 | 0.26 | 0.15 | 0.19 | 0.25 | 0.16 | 0.14 | 0.21 | 0.2 |
| Th | 28.2 | 57.1 | 57.9 | 49.6 | 9.2 | 9.21 | 8.38 | 8.91 | 9.79 | 7.03 | 23.8 | 28.8 | 27.3 |
| U | 6.47 | 12.6 | 13 | 10.1 | 20.2 | 20.9 | 16.4 | 19.9 | 22.6 | 14.6 | 7.38 | 8.44 | 7.49 |
| Ta | 4.2 | 2.23 | 1.82 | 5.02 | 5.56 | 5.58 | 4.42 | 5.46 | 5.87 | 4.49 | 5.37 | 7.2 | 6.97 |
| Hf | 10.1 | 9.24 | 10.8 | 9.83 | 11 | 10.5 | 8.94 | 9.09 | 11.3 | 8.36 | 11.1 | 10.1 | 9 |
| ISOTOPES | | | | | | | | | | | | | |
| $^{87}Sr/^{86}Sr$ | 0.705619 | | 0.706303 | 0.707051 | 0.705693 | 0.704676 | 0.705768 | 0.704966 | 0.704427 | 0.705623 | 0.70494 | 0.705377 | 0.705203 | 0.70514 |
| $^{143}Nd/^{144}Nd$ | | 0.512628 | 0.512538 | 0.512674 | | | 0.512728 | 0.51273 | 0.51272 | | 0.512794 | 0.512791 | 0.512804 | |
| $^{206}Pb/^{204}Pb$ | | 19.0399 | 19.1328 | 19.2401 | | | 19.1860 | 19.2020 | 19.1640 | 19.0960 | 19.2520 | 19.192 | 19.183 | |
| $^{207}Pb/^{204}Pb$ | | 15.6173 | 15.6678 | 15.6437 | | | 15.6260 | 15.5790 | 15.6090 | 15.5610 | 15.5840 | 15.651 | 15.656 | |
| $^{208}Pb/^{204}Pb$ | | 38.7656 | 39.0014 | 38.9758 | | | 38.9350 | 38.7640 | 38.7980 | 38.6720 | 38.8720 | 39.009 | 39.039 | |

**Table 2.2.** Major and trace element and isotopic compositions of representative samples of the three magmatic groups of the Navajo Volcanic Field, central Colorado Plateau.

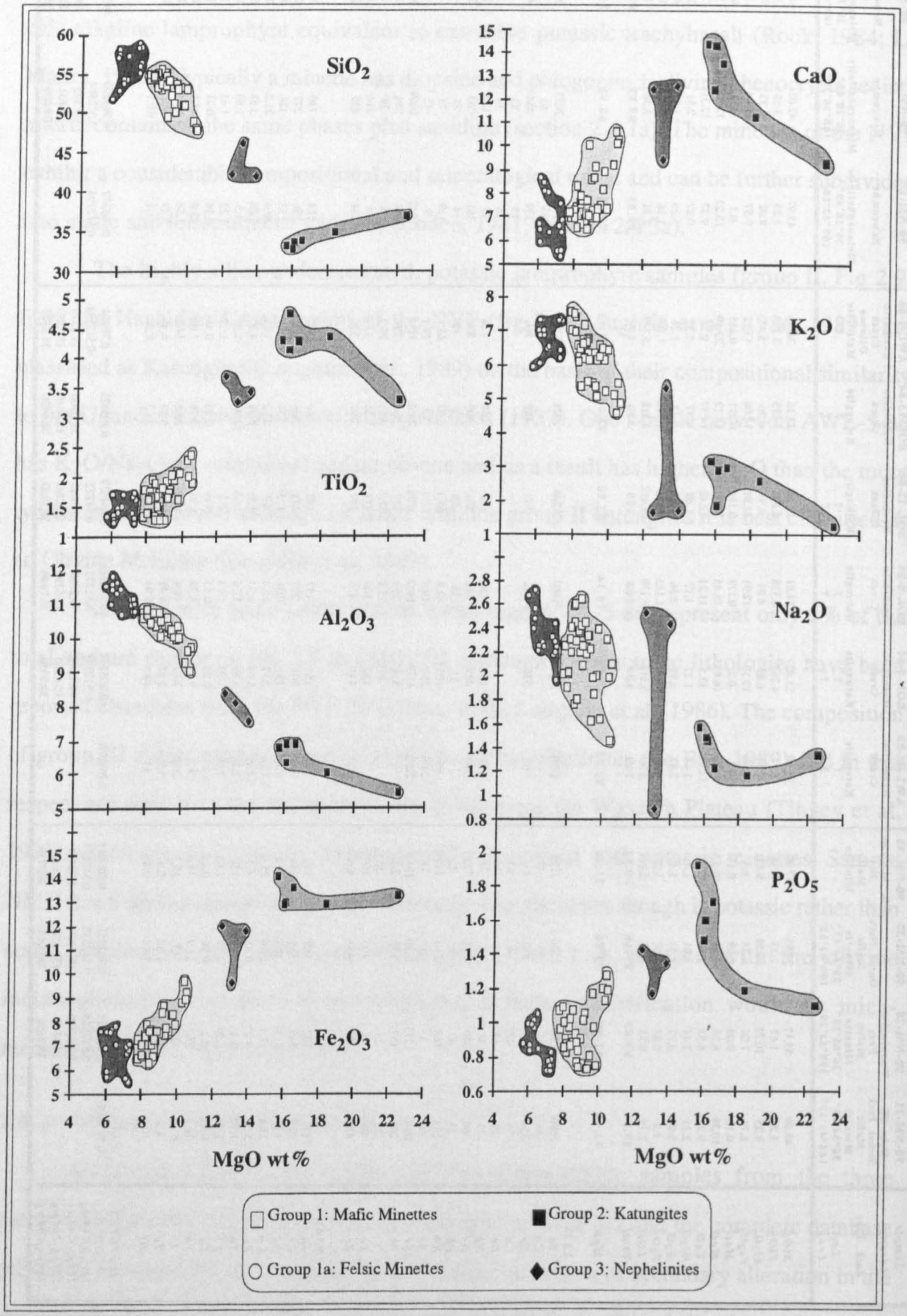


**Figure 2.10**. Major element variations with MgO for the four main groups of the Navajo Volcanic Field, central Colorado Plateau, USA. Total iron expressed as $Fe_2O_3$.

Fig 2.10 shows the variations in major element composition of Navajo magmas plotted against MgO abundance. Despite a wide variation in major element abundances three, compositionally distinct, groups can be identified and are described below:

#### 2.4.3a: Group 1 Minettes:

Minettes, the most dominant magma type in the NVF, exhibit a wide variation in MgO from ≈5.8 to 11 %. Despite such a range, samples with MgO ≥7.8% exhibit a narrow range in $Mg^{\#}$≈70-73 reflecting their primitive nature (Frey et al., 1978). The remaining samples with MgO <7.8% have more fractionated $Mg^{\#}$'s of 55-68 suggesting they have experienced limited closed system fractionation (Chapter 3). Samples from the Washington Pass volcanic centre have $Mg^{\#}$'s ≈75 which may reflect accumulation of spinel peridotite (Chapter 3). The point of inflexion of Mg# at MgO≈7.8% is used as a more logical basis for dividing the minettes into two subgroups, group I mafic minettes and group Ia felsic minettes, than selecting an arbitrary $SiO_2$ value of 53 wt% (Roden, 1981). The oxides $SiO_2$, $Al_2O_3$, and to a lesser extent $K_2O$ and $Na_2O$ all exhibit negative correlations with MgO, while $TiO_2$, $Fe_2O_3t$, CaO and $P_2O_5$ all correlate positively with MgO (Fig 2.10). All the minettes are ultrapotassic with $K_2O/Na_2O$ ≈2-4 and exhibit a bimodality in $K_2O$ abundances with a potassium gap at 5.5 - 6 wt%.

#### 2.4.3b: Group 2 Katungites:

Katungites are notable in having very high abundances of MgO from 15.72 to 22.59wt% (Fig 2.10) with correspondingly high $Mg^{\#}$'s ≈72-79 which, as with group1, suggest a primitive nature. However the petrography of sample AWL-5-86, with $Mg^{\#}$=79 (Table 2.2), suggests it has experienced olivine accumulation (Laughlin et al., 1989). Katungites are also characterised by high abundances of CaO, $TiO_2$ and $Fe_2O_3$ and while having extremely low abundances of $Al_2O_3$ and $SiO_2$. Indeed the katungites represent the most silica-undersaturated magmas found on the Colorado Plateau and the southwestern United States. The largest overall variations in elemental abundances are observed for MgO (≈15.7-22.6wt%), CaO (≈9.3-14.4wt%) and $P_2O_5$ (≈1.1-1.9wt%), while the remaining elements vary little in abundance. All katungite samples, except AWL-5-86, are potassic with $K_2O/Na_2O$ ≈1-2.

**Group 3 Melanephelinites:**

As the nephelinites are only represented by three samples with a limited range in MgO (12-14 wt%) correlations within the group cannot be clearly identified. However relative to the above two groups, the nephelinites show intermediate abundances of all the major elements though there is some scatter most notably in the abundance of $K_2O$ and $Na_2O$ and to some degree in $Fe_2O_3t$ and CaO. Samples NM-3 and NM-4 are sodic, $K_2O/Na_2O \approx 0.12$, whereas NM-1, despite its similarity in other major elements has very low $Na_2O$ and high $K_2O$ (table 2.3) and is hence potassic, $K_2O/Na_2O=5.5$.

Although on plots of $SiO_2$, $TiO_2$, CaO and $P_2O_5$ the katungite group define a trend oblique to that of the Navajo magmas, as a whole the three Navajo magmatic groups considered together do define distinct linear major-element correlations, illustrated in Fig 2.10. The elements $SiO_2$, $Al_2O_3$, and to a lesser degree $K_2O$ and $Na_2O$ are all negatively correlated with MgO abundance whereas TiO2, Fe2O3, CaO and P2O5 are all positively correlated with MgO. Although Laughlin et al (1986) conclude a genetic relationship between the minettes and katungites is untenable such coherent correlations both within and between groups identified in the present study strongly suggests that the three magma groups are petrogenetically related and this is explored in detail in Chapter 3.

### 2.4.4: Trace Element variations:

Compatible trace elements such as Ni and Cr show wide variations in abundance, up to 312 and 435 ppm respectively in the minettes and 834 and 806 ppm in the Katungites. Although this may suggest the minettes are more evolved than the katungites the majority of minettes are characterised by Mg#'s of approximately 70 which suggests they could be primary or near-primary melts derived directly from their mantle source regions without experiencing subsequent fractionation and/or crustal contamination (see section 3.2.1).

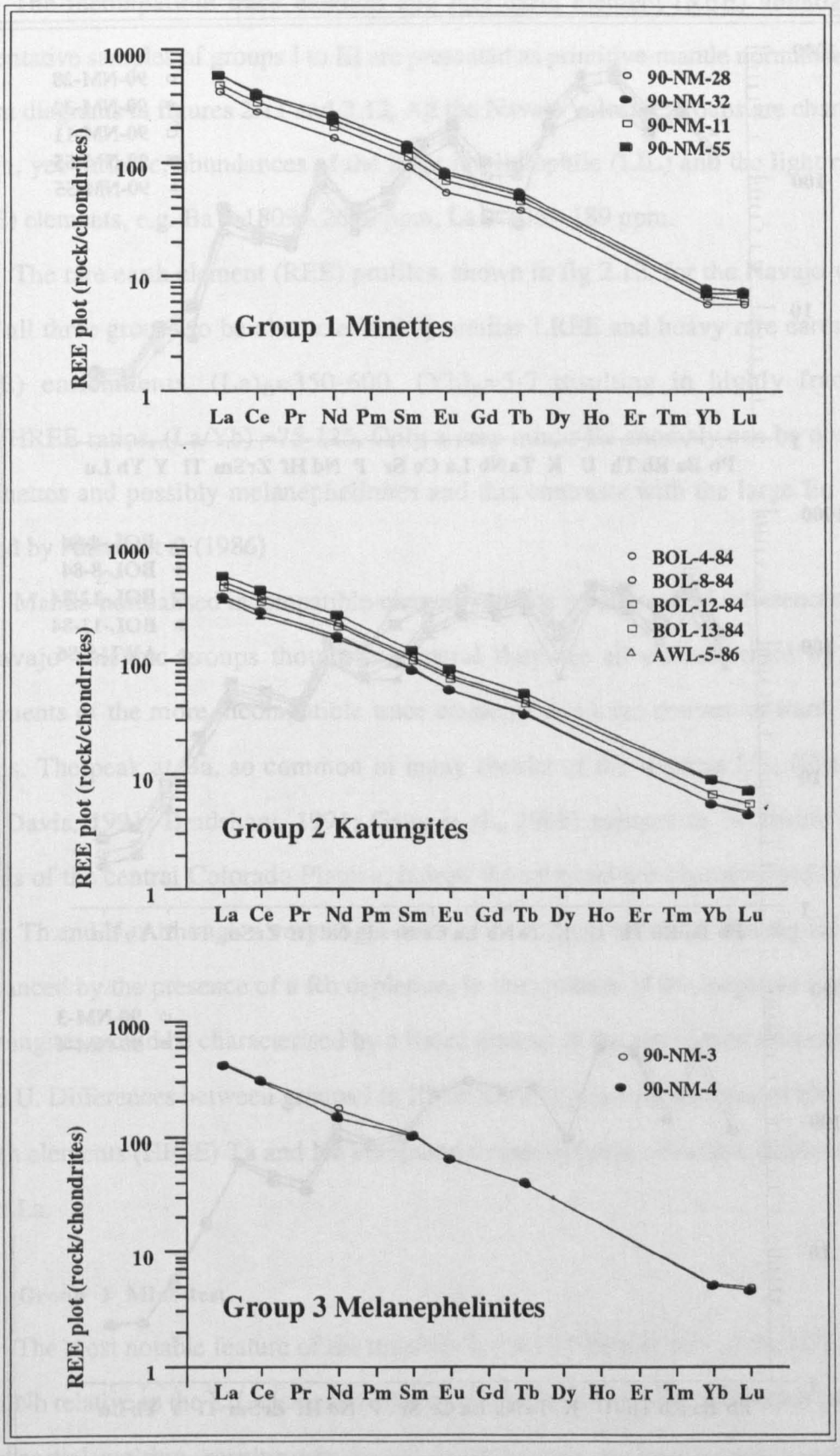


**Figure 2.11**. Rare earth element abundances for representative samples of the three magmatic groups of the Navajo Volcanic Field normalised to the chondrite composition of Sun & McDonough (1989).

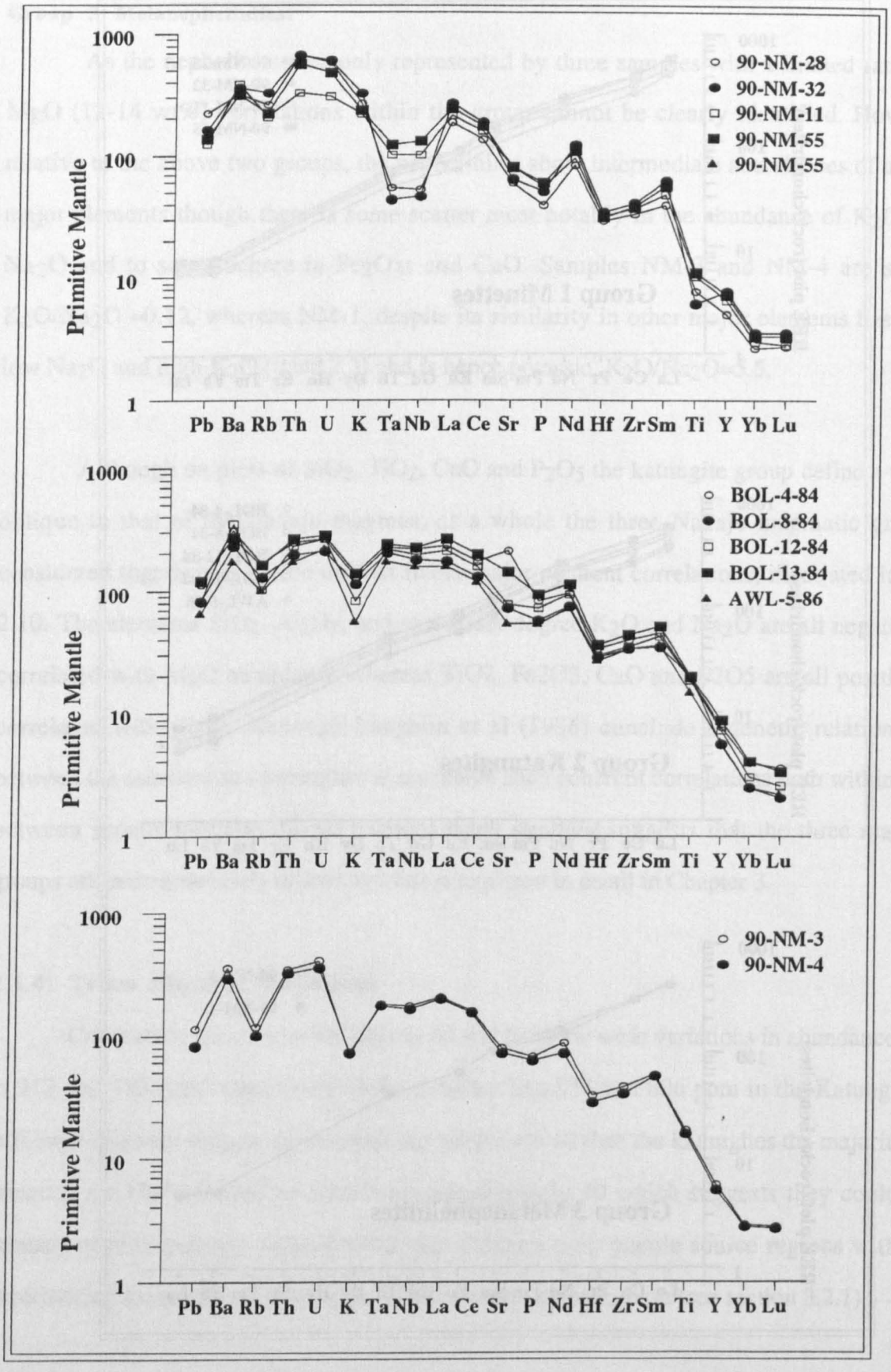


**Figure 2.12**. Primitive-mantle normalised trace element profiles for representative samples of the three main magmatic groups of the Navajo Volcanic Field, central Colorado Plateau. Primitive mantle abundances from Sun & McDonough (1989).

The incompatible trace element and rare earth element (REE) abundances for representative samples of groups I to III are presented as primitive-mantle normalised, multi-element diagrams in figures 2.11 and 2.12. All the Navajo volcanic groups are characterised by high, yet variable, abundances of the large ion lithophile (LIL) and the light rare earth (LREE) elements, e.g. Ba = 1809 - 2690 ppm, La = 105 - 189 ppm.

The rare earth element (REE) profiles, shown in fig 2.12, for the Navajo volcanics reveal all three groups to be characterised by similar LREE and heavy rare earth element (HREE) enrichments, $(La)_n$=350-600, $(Yb)_n$=5-7 resulting in highly fractionated LREE/HREE ratios, (La/Yb) ≈75-125. Only a very minor Eu anomaly can be observed in the minettes and possibly melanephelinites and this contrasts with the large Eu anomaly reported by Alibert et al (1986)

Mantle-normalised incompatible-element profiles reveal several differences between the Navajo volcanic groups though in general they are all characterised by extreme enrichments of the more incompatible trace elements and have convex-upward, irregular patterns. The peak at Ba, so common in many basalts of the western US, (Fitton et al., 1991; Davis, 1991; Bradshaw, 1991; Gans et al., 1989) appears to be absent from the magmas of the central Colorado Plateau, indeed the minettes are characterised by a broad peak in Th and U. Although a very slight peak in Ba is apparent in the Katungites this may be enhanced by the presence of a Rb depletion. In the absence of this negative Rb anomaly the katungites would be characterised by a broad plateau in the abundance elements Ba, Rb, Th and U. Differences between groups I to III lie in the relative abundances of the high field strength elements (HFSE) Ta and Nb compared to similarly incompatible elements such as Ba and La.

#### 2.4.4a: Group I Minettes:

The most notable feature of the minettes is the low abundances of the HFS elements Ta and Nb relative to the LIL elements, inferred to have similar bulk distribution coefficients during partial melting, resulting in Ta-Nb troughs, such as are commonly observed in subduction-related magmatism (Gill. 1981). The magnitude of the Ta-Nb depletion in the minettes varies considerably as shown by K/Yb vs Ta/Yb (fig 2.13) where K/Ta is taken as a measure of Ta-Nb depletion.

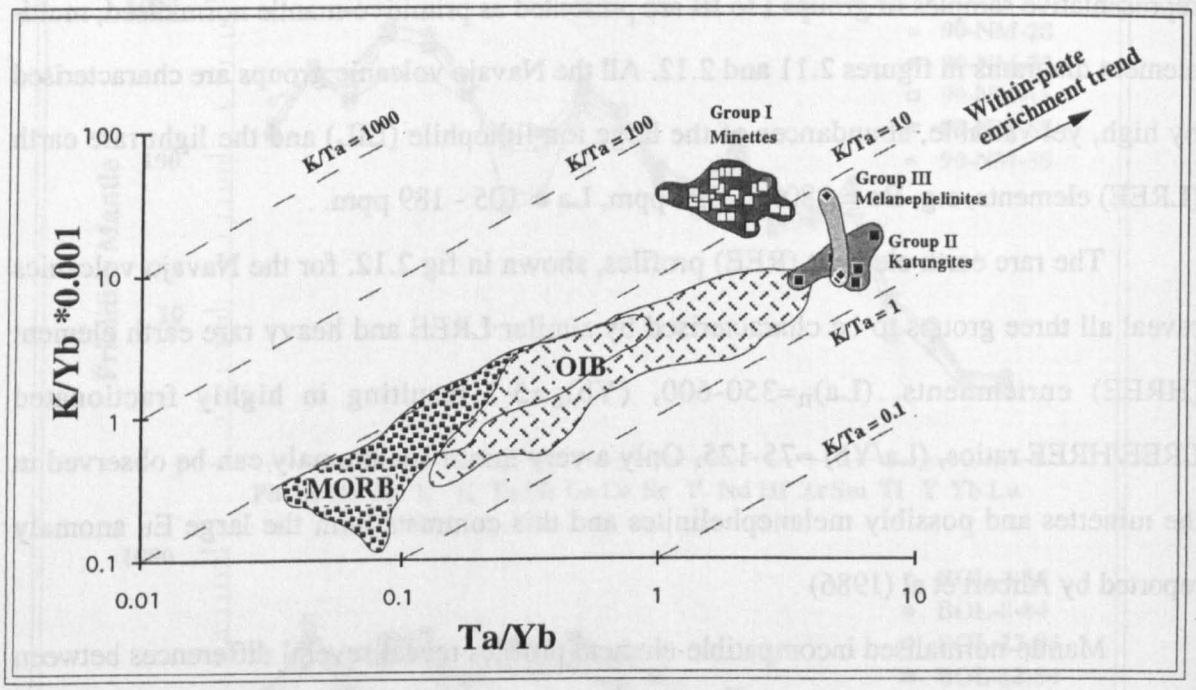


**Figure 2.13.** Variation of K/Yb with Ta/Yb in the magmas of the Navajo Volcanic Field, MORB and OIB.

**2.4.4b: Group II Katungites:**

The katungites are distinct from the minettes in that they lack a depletion in Ta-Nb (Fig 2.12), indeed the trace element profiles reveal a maxima in these elements. The LIL/HFS element ratios are more similar to ocean island basalt (OIB) trace element compositions, albeit at higher overall abundances, as shown by figure 2.13, where they plot on the MORB-OIB within-plate trend, distinct from the minettes. Figure 2.12 shows that despite the potassic nature of katungites the LIL elements K and Rb are depleted relative to similarly incompatible trace elements such as Ba, Th and U. Negative $K_2O$ and Rb anomalies have been observed in similarly silica undersaturated small-degree melts such as melilitites (Rogers et al., 1992) where they have been attributed to melt generation in equilibrium with a phlogopite-bearing restite.

**2.4.4c: Group III Melanephelinites:**

The nephelinites have trace-element abundances and LIL/HFS ratios very similar to the katungites despite their dissimilar major element compositions. The only slight differences with the nephelinites are the higher Th and U and lower Ta and Nb concentrations.

### 2.4.5: Radiogenic Isotopes:

A total of 34 group I minettes were analysed for Sr isotopes, 23 for both Sr and Nd, along with all katungite and nephelinite samples. Figure 2.14 shows the variation of $^{143}Nd/^{144}Nd$ with $^{87}Sr/^{86}Sr$ of the Navajo intrusives along with additional isotopic data for Colorado Plateau volcanics (Data for Hopi Butte nephelinites and San Francisco basalts from Alibert et al .,1986) and Geronimo alkali basalts from the southern Basin & Range (Fitton & Kempton unpubl data) representative of post 5Ma asthenosphere-derived average alkali basalts from the Basin & Range

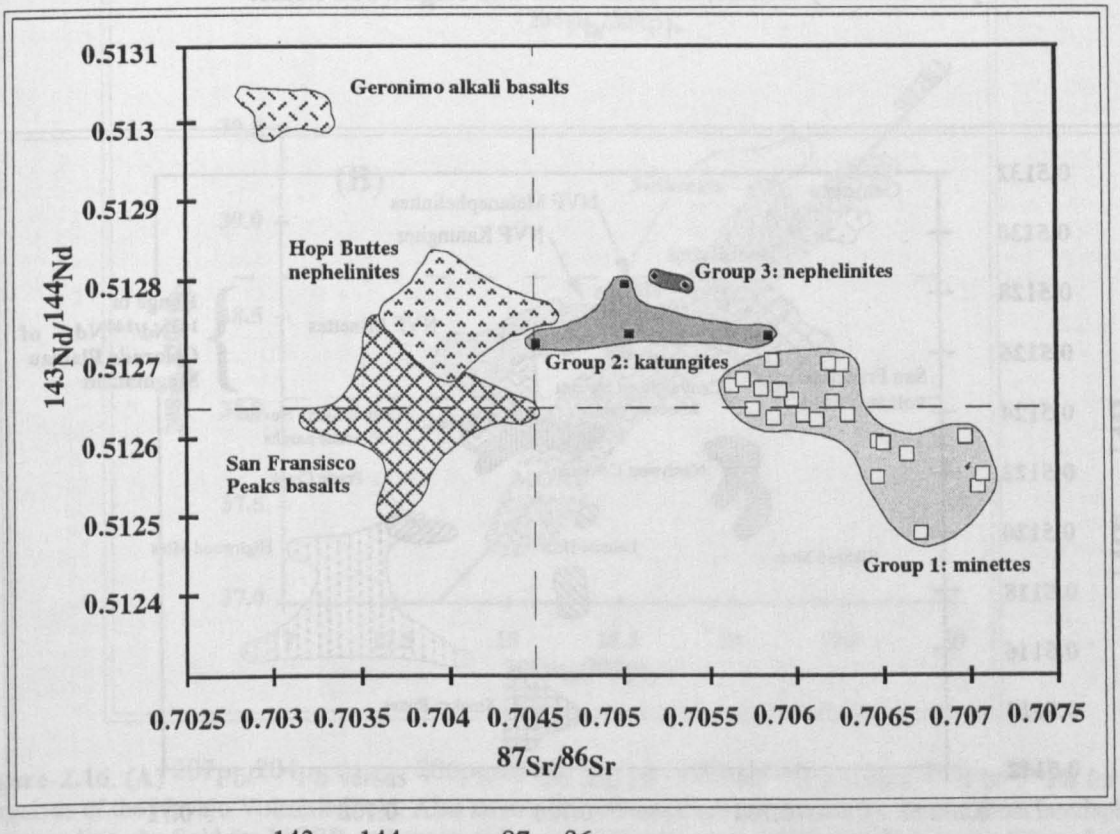


**Figure 2.14.** Variation of $^{143}Nd/^{144}Nd$ with $^{87}Sr/^{86}Sr$ in magmas from the Colorado Plateau. Data for Hopi Buttes and San Francisco Peaks from Alibert et al (1986).

Group I minettes plot to the right of the mantle-array, within the enriched quadrant and display a broad negative correlation between Sr and Nd isotopes which vary between 0.70563-0.70705 and 0.51247-0.5127. The field for Group II katungites is flat-lying and plots within and to the right of the low $^{143}Nd/^{144}Nd$ end of the mantle-array with $^{87}Sr/^{86}Sr$ =0.70443-0.70577 and $^{143}Nd/^{144}Nd$ =0.51272-0.51279. Isotopically they appear broadly similar to OIB.

The nephelinites have intermediate Sr isotope ratios $^{87}Sr/^{86}Sr$ =0.70514-0.70538 although slightly higher $^{143}Nd/^{144}Nd$ ratios = 0.51280-0.51281 than the minettes and katungites.

The most striking feature of the isotopic composition of magmas from the Colorado Plateau (Navajo, Hopi Buttes and San Francisco volcanic fields) is the restricted range in $^{143}Nd/^{144}Nd$ of 0.5124-0.5128 associated with a more significant variation in $^{87}Sr/^{86}Sr$ of ≈0.703-0.707 resulting in a sub-horizontal trend. This variation is clearly illustrated in fig 2.15 where the Sr-Nd isotope variation of the Colorado Plateau volcanics are compared to other similarly enriched ultrapotassic magmas of the western United States. Other potassic magmas from the western United States plot at lower $^{143}Nd/^{144}Nd$ ratios clearly demonstrated by the Smokey Buttes, Leucite Hills and Highwood Mtns.

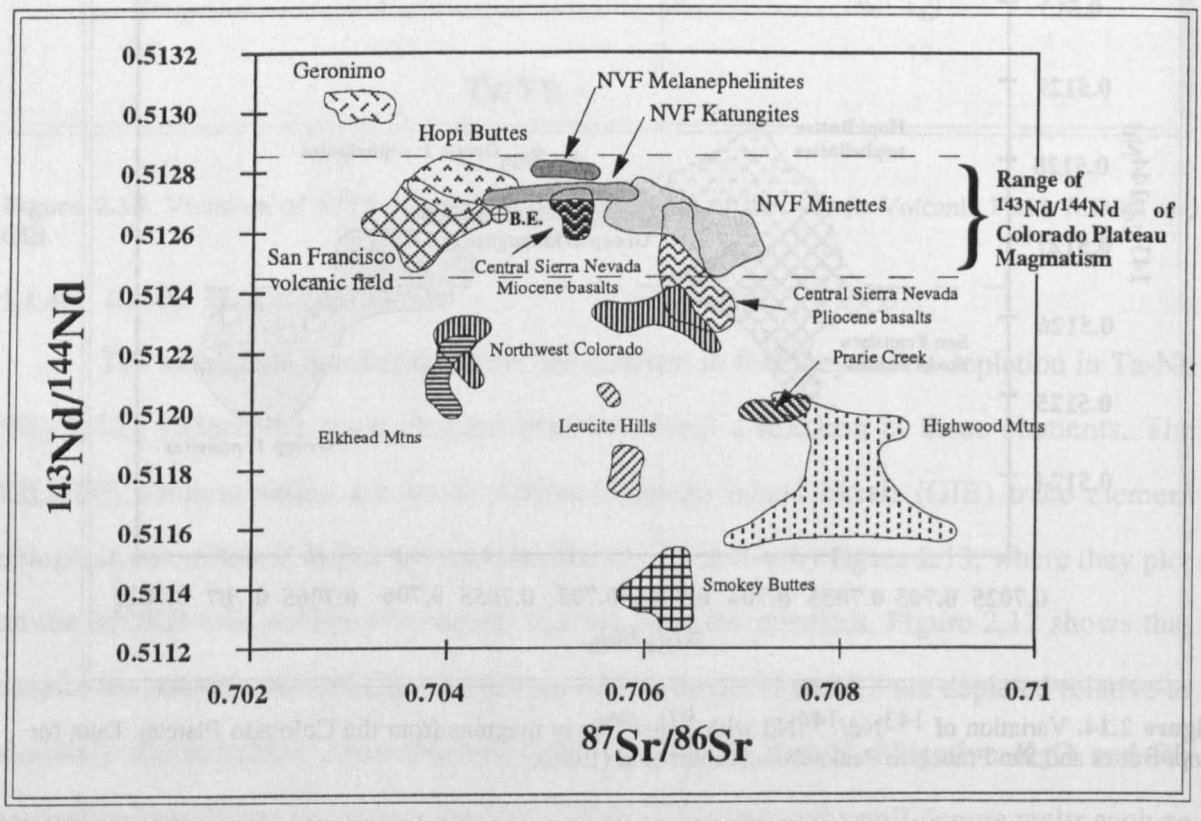


**Figure 2.15**. Variation of $^{143}Nd/^{144}Nd$ with $^{87}Sr/^{86}Sr$ in magmas from the NVF, Hopi Buttes and San Francisco volcanic fields (Alibert et al., 1986) of the central Colorado Plateau compared to mafic potassic volcanics from the western United States, Leucite Hills, Smokey Buttes and Prarie Creek from Fraser (1987).

Pb isotopic compositions for the Navajo intrusives are shown in fig 2.16 relative to the geochron and the Northern Hemisphere Reference Line (NHRL) for ocean basalts (Hart, 1984). Also shown are available data for additional Colorado Plateau volcanics (Hopi Buttes and San Francisco from Alibert et al., 1986) and Geronimo alkali basalts (Fitton & Kempton unpubl data) and, ocean sediments (Othman et al., 1989).

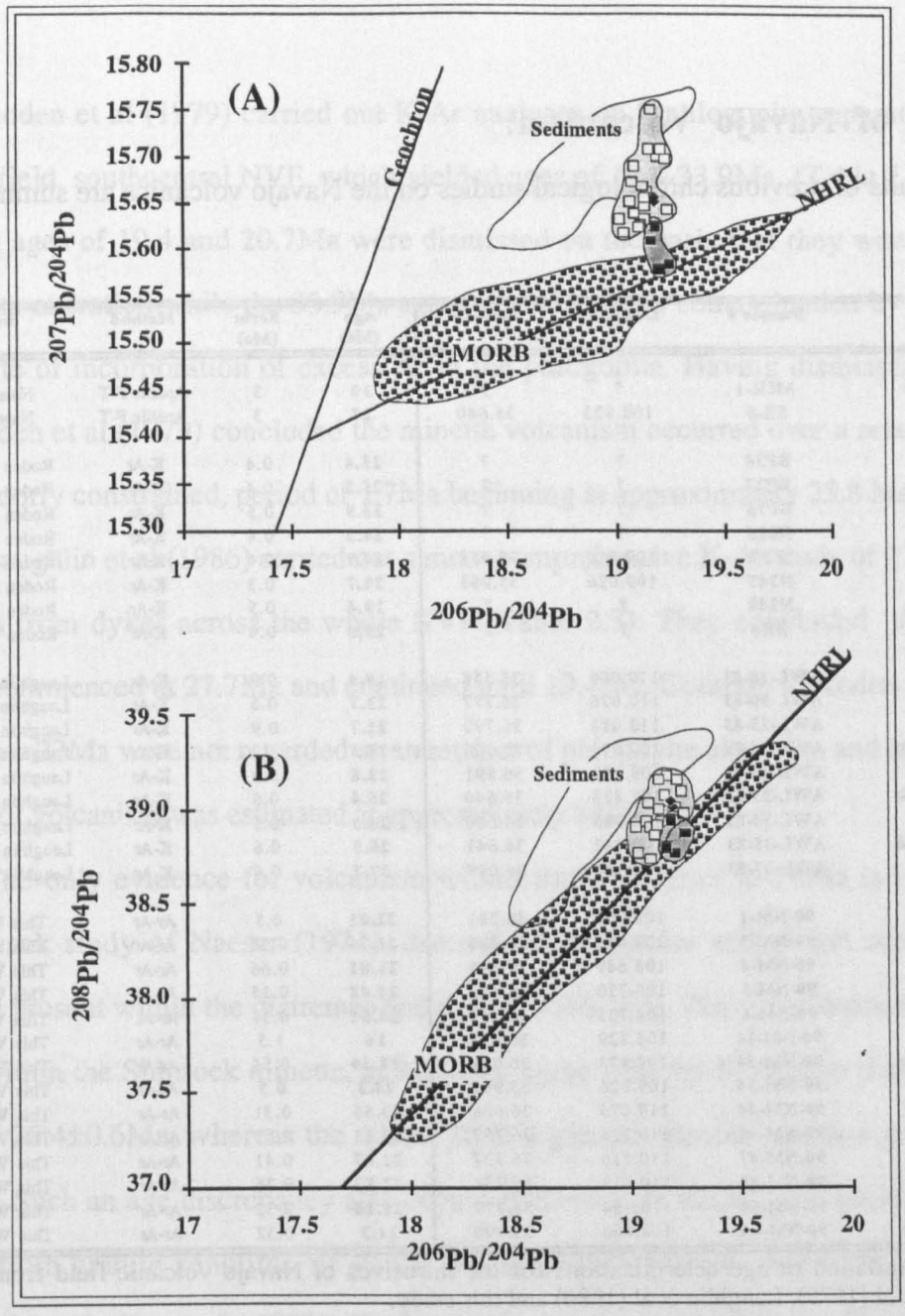


**Figure 2.16.** (A) $^{207}Pb/^{204}Pb$ versus $^{206}Pb/^{204}Pb$ and (B) $^{208}Pb/^{204}Pb$ versus $^{206}Pb/^{204}Pb$ for the intrusives of the Navajo Volcanic Field. Also shown for reference are the Geochron, the northern hemisphere reference line, the field for MORB and ocean sediments (Othman et al., 1989). Symbols as for Figure 2.10.

The most obvious feature of the Pb isotope composition of Navajo volcanics is a limited, almost constant, $^{206}Pb/^{204}Pb$ ratio of 19.0-19.18 and $^{208}Pb/^{204}Pb$ (≈38.86-39.18) ratios similar to radiogenic MORB, or OIB such as the Canary Islands (Sun,1980). The variation of $^{207}Pb/^{206}Pb$ (15.57 -15.75) is considerably greater than $^{206}Pb/^{204}Pb$ $^{208}Pb/^{204}Pb$ variations and implies a complex evolution. The Navajo volcanics as a whole plot as a vertical linear array on Fig 2.16a anchored to the NHRL by the katungites and extending to high $^{207}Pb/^{204}Pb$ appropriate for ocean sediments (Othman et al., 1989). The age represented by the trend at »4.5Ga. obviously has no significance and as such the trend may well reflect mixing.

## 2.5: Age of Navajo Volcanism:

Results of previous chronological studies on the Navajo volcanics are summarised in Table 2.3.

| Locality | Sample # | Longitude | Latitude | Age (Ma) | Error (Ma) | Method | Source |
|---|---|---|---|---|---|---|---|
| *Mitten Rock* | MtR-1 | ? | ? | 30 | 3 | Apatite F-T | Naeser '71 |
| *Ship Rock* | SR-6 | 108.823 | 36.640 | 27 | 3 | Apatite F-T | Naeser '71 |
| *Buell Park* | BP34 | ? | ? | 25.4 | 0.4 | K-Ar | Roden et al '79 |
| *Buell Park* | BP37 | ? | ? | 25.2 | 0.4 | K-Ar | Roden et al '79 |
| *Buell Park* | BP75 | ? | ? | 33.9 | 0.5 | K-Ar | Roden et al '79 |
| *Buell Park* | N255 | ? | ? | 24.3 | 0.4 | K-Ar | Roden et al '79 |
| *The Beast* | TB7 | 109.026 | 35.968 | 24.9 | 0.4 | K-Ar | Roden et al '79 |
| *The Beast* | N247 | 109.026 | 35.968 | 20.7 | 0.3 | K-Ar | Roden et al '79 |
| *Outlet Neck* | N240 | ? | ? | 19.4 | 0.5 | K-Ar | Roden et al '79 |
| *Black Rock* | BR4 | ? | ? | 25.8 | 0.4 | K-Ar | Roden et al '79 |
| *Chilchinbito* | AWL-18-83 | 110.066 | 36.558 | 19.4 | 0.9 | K-Ar | Laughlin et al '86 |
| *Comb Ridge* | AWL-19-83 | 110.076 | 36.777 | 23.7 | 0.6 | K-Ar | Laughlin et al '86 |
| *Comb Ridge* | AWL-23-83 | 110.088 | 36.792 | 21.7 | 0.9 | K-Ar | Laughlin et al '86 |
| *Nakaito Bench* | AWL-24-83 | 109.500 | 37.966 | 24.3 | 1 | K-Ar | Laughlin et al '86 |
| *Teec Nos Pos* | AWL-25-83 | 109.100 | 36.891 | 22.8 | 0.9 | K-Ar | Laughlin et al '86 |
| *SSE Ship Rock* | AWL-33-83 | 108.823 | 36.640 | 26.4 | 0.6 | K-Ar | Laughlin et al '86 |
| *Red Rock* | AWL-34-83 | 108.985 | 36.620 | 24.3 | 0.5 | K-Ar | Laughlin et al '86 |
| *Hasbidito Creek* | AWL-35-83 | 109.342 | 36.641 | 25.5 | 0.6 | K-Ar | Laughlin et al '86 |
| *Sonsela Butte* | AWL-37-83 | 109.120 | 36.097 | 27.7 | 0.6 | K-Ar | Laughlin et al '86 |
| *Newcombe* | 90-NM-1 | 108.702 | 36.281 | 22.01 | 0.5 | Ar-Ar | This Work |
| *Newcombe* | 90-NM-3 | 108.641 | 36.345 | 21.74 | 0.35 | Ar-Ar | This Work |
| *Newcombe* | 90-NM-4 | 108.689 | 36.345 | 21.81 | 0.66 | Ar-Ar | This Work |
| *Bennet Peak* | 90-NM-5 | 108.720 | 36.355 | 24.48 | 0.35 | Ar-Ar | This Work |
| *Bennet Peak* | 90-NM-6 | 108.735 | 36.374 | 24.51 | 0.38 | Ar-Ar | This Work |
| *Ship Rock* | 90-NM-14 | 108.829 | 36.692 | 16 | 1.5 | Ar-Ar | This Work |
| *Washington Pass* | 90-NM-24 | 108.873 | 36.088 | 27.49 | 0.56 | Ar-Ar | This Work |
| *The Beast* | 90-NM-34 | 109.026 | 35.968 | 24.2 | 0.5 | Ar-Ar | This Work |
| *Chiastala Butte* | 90-NM-44 | 110.076 | 36.608 | 20.55 | 0.31 | Ar-Ar | This Work |
| *Chiastala Butte* | 90-NM-46 | 110.114 | 36.737 | 23.11 | 0.61 | Ar-Ar | This Work |
| *Chiastala Butte* | 90-NM-47 | 110.116 | 36.737 | 22.47 | 0.41 | Ar-Ar | This Work |
| *Chiastala Butte* | 90-NM-48 | 110.118 | 36.738 | 22.52 | 0.36 | Ar-Ar | This Work |
| *Chilchinbito* | 90-NM-50 | 110.164 | 36.777 | 21.14 | 0.32 | Ar-Ar | This Work |
| *Washington Pass* | 90-NM-64 | 108.856 | 36.096 | 24.3 | 0.32 | Ar-Ar | This Work |

**Table 2.3.** Compilation of age determinations for the intrusives of Navajo volcanic field from Naeser (1971), Roden et al (1979), Laughlin et al (1986) and this study.

The first attempt to constrain the age of volcanism in the Navajo Indian Reservation was based on stratigraphic and palaeontological evidence within the Hopi Buttes region, to the southwest of the Navajo volcanic field. The evidence suggested the Hopi diatremes were emplaced during the middle or upper Pliocene. Although no palaeontological evidence exists in the Navajo region, Williams (1936) believed there to be no reason to doubt that the Navajo volcanics were not emplaced at the same time as the Hopi Buttes. Evernden et al (1964) measured a K/Ar age of 4.1Ma for a basalt flow from the Hopi Butte volcanic field thereby confirming the Pliocene age of volcanic activity. However the first reported K-Ar analysis of a Navajo sample (Ziony,1966) yielded an age of 27Ma which contradicted the belief of Williams (1936) and Shoemaker (1956) that the Navajo diatremes were of a similar age to the Hopi diatremes.

Roden et al (1979) carried out K-Ar analyses on 9 phlogopite separates from the Zilditloi field, southcentral NVF, which yielded ages of 19.4-33.9Ma. (Table 2.3). The two youngest ages of 19.4 and 20.7Ma were dismissed on the basis that they were a result of phlogopite alteration while the 33.9Ma age was attributed to contamination by xenocrystic phlogopite or incorporation of excess Ar in the phlogopite. Having dismissed unreliable dates Roden et al (1979) concluded the minette volcanism occurred over a relatively short, though poorly constrained, period of 1.7Ma beginning at approximately 25.8 Ma.

Laughlin et al (1986) carried out a more comprehensive K-Ar study of 13 phlogopite separates from dykes across the whole NVF (Table 2.3). They concluded that volcanic activity commenced at 27.7Ma and continued until 19.4Ma. Contrary to Roden et al (1979), ages below 23Ma were not regarded as an artifact of phlogopite alteration and as a result the duration of volcanism was estimated at approximately 8Ma.

The only evidence for volcanism within the NVF prior to 28Ma is based on the fission-track study of Naeser (1971), determined on apatite and zircon separates from xenoliths present within the diatremes and dykes (Table 2.3). The fision-track results for an apatite within the Shiprock minette, at 27±3Ma. agree with the K-Ar date (Laughlin et al., 1986) of 26.4±0.6Ma, whereas the apatite from a granite xenolith yields a greater age of 32±3Ma. Such an age discrepancy also occurs at Buell Park where the fission-track age of apatites from granite xenoliths, at 30±7.8Ma, is greater than the phlogopite K-Ar age of 24.3-25.4Ma (Roden et al., 1979). Fission-track ages determined on apatites from granite xenoliths may be misleading in that the apparently greater ages may simply reflect incomplete annealing of previous fission tracks.

### 2.5.1: $^{40}Ar$-$^{39}Ar$ Dating of the Navajo Volcanics:

During the present study 15 phlogopite separates from mafic minette dykes, selected to cover the whole area of Navajo volcanism, were analysed using a laser ablation $^{40}Ar/^{39}Ar$ dating technique. The advantage of this technique is the determination of both potassium and argon on the same sample, overcoming the problem of sample heterogeneity and allowing the dating of small samples. The analytical procedure is outlined in Appendix B

The argon isotopic composition of an igneous rock or mineral is considered to be a two component mixture. The initial, or inherited argon component, incorporated at the time of crystallisation, is assumed to be atmospheric argon with $^{36}Ar/^{40}Ar=0.003384$. The radiogenic component consists of $^{40}Ar$ produced by the decay of $^{40}K$ in the sample. Provided the rock has remained closed to argon since crystallisation, the $^{40}Ar/^{39}Ar$ of the radiogenic component can be corrected for the presence of atmospheric $^{40}Ar$ and the age of the sample calculated. If the $^{36}Ar/^{40}Ar$ of the inherited argon is *less* than the value for atmospheric argon the sample has an apparent excess of $^{40}Ar$, whereas if the $^{36}Ar/^{40}Ar$ of the inherited argon is greater than atmosphere the sample has an apparent loss of radiogenic argon. These effects can be recognised and an age obtained by use of the inverse argon-isotope correlation diagram.

**Results:**

The weighted mean age with errors for each sample is presented in Table 2.3. and calculated assuming assuming *all* $^{36}Ar$ is atmospheric argon with a $^{36}Ar/^{40}Ar$ ratio of 0.003384. Figure 2.17 is an inverse argon isotope correlation diagram (Merrihue & Turner,1966) for the individual phlogopite analyses where samples are joined by tie-lines.

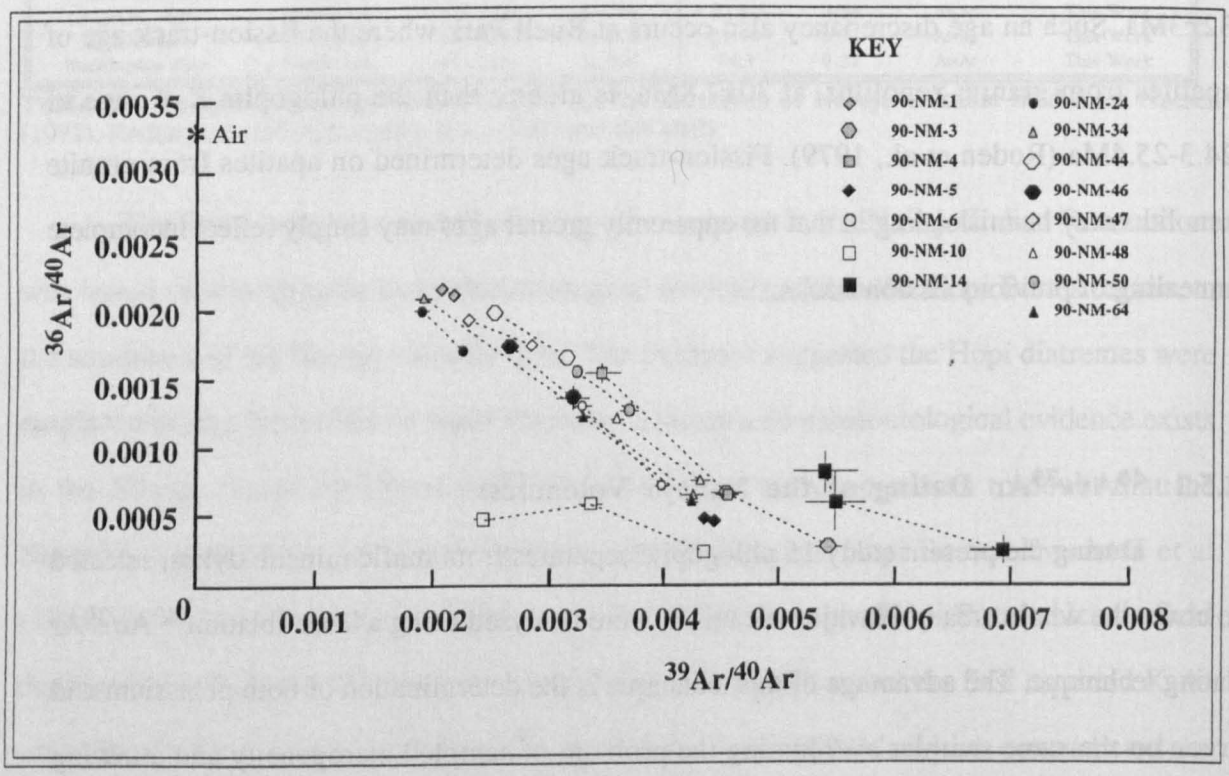


**Figure 2.17**. Inverse Ar-Ar isochron plot for individual analyses for phlogopite separates from minettes from the Navajo Volcanic Field. Analyses on the same sample are joined by tie lines. Most samples define mixing lines between air (*) and a radiogenic component.

Clearly the two Ar-Ar measurements for each sample (3 analyses on samples NM-10 and NM-14) in the majority of cases lie on mixing lines between a radiogenic component and an inherited argon component with a $^{36}Ar/^{40}Ar$ ratio very close to that of atmosphere (Fig 2.17). It would therefore appear that most of the minette phlogopites do not contain appreciable excesses of $^{40}Ar$ and have not experienced Ar loss due to alteration and hence the ages are reliable.

Model ages were calculated for each individual phlogopite analysis assuming that the argon within the sample was a mixture between atmospheric argon, with a $^{36}Ar/^{40}Ar=0.003384$, and a radiogenic component, and that $^{40}Ar$ was niether gained or lost since the time of crystallisation. On the basis that most samples lie on mixing curves between atmosphere and a radiogenic component in Fig 2.17 these assumptions appear reasonable for samples other than NM-10 and NM-14. The age of the sample is related to its measured $^{40}Ar^*/^{39}Ar_K$ (where $^{40}Ar^*$ is the amount of radiogenic $^{40}Ar$, and $^{39}Ar_K$ is the amount of $^{39}Ar$ derived from $^{39}K$) by the standard age equation:

$$t=(1/\lambda)\ln(1+J(^{40}Ar^*/^{39}Ar_K))$$

where 1 is the decay constant of 40K, and J is a dimensionless irradiation paramter. The value for J used in the present study was 0.00007±0.0000007 and was measured by irradiating the standard BERN 4B (age=17.3±0.2Ma).

A weighted average for the two individual phlogopite analyses was calculated and it is these weighted model ages that are presented in Table 2.3

The mafic minettes from this study yield model ages of 27.5±0.5Ma to 20.5±0.31Ma (although NM-14 yields an isochron age of 16±1.5Ma) whereas the nephelinites yield ages of 22±0.5Ma to 21.7±0.35Ma. The only locality for which a comparison of the Ar-Ar ages from this study and previous K-Ar ages can be made for fresh unaltered samples is the Beast, Zilditloi field, where the $^{40}Ar/^{39}Ar$ age at 24.2±0.5Ma is within error of the K-Ar age of 24.9±0.4 Ma (Roden et al., 1979). Although Laughlin et al (1986) quote an age for a Chilchinbito dyke of 19.4±0.9Ma this is not the same dyke as that quoted in the present study at 21.14Ma±0.32Ma although they are within error of each other.

Two samples, NM-10 and NM-14, do not lie on a simple two component mixing array between atmosphere and a radiogenic component as do the other samples. The age of these samples was calculated using a least squares fit to an inverse isochron plot. The individual analyses for NM-10, a dyke near Barber Peak, yielded a range in model ages from 26.75±0.4 to 43.9±1.2Ma with a weighted mean of 28.9±0.37Ma which suggests an excess of 40Ar. Figure 2.19 shows that the least squares fit to NM-10 yields a $^{36}Ar/^{40}Ar$ intercept below the atmospheric value and is hence consistent with the presence of excess 40Ar. Despite the large errors the isochron age of NM-10 at 21.1±1.2 Ma is similar to those ages determined on the other samples in this study although because of the large errors it is not included in any further discussion.

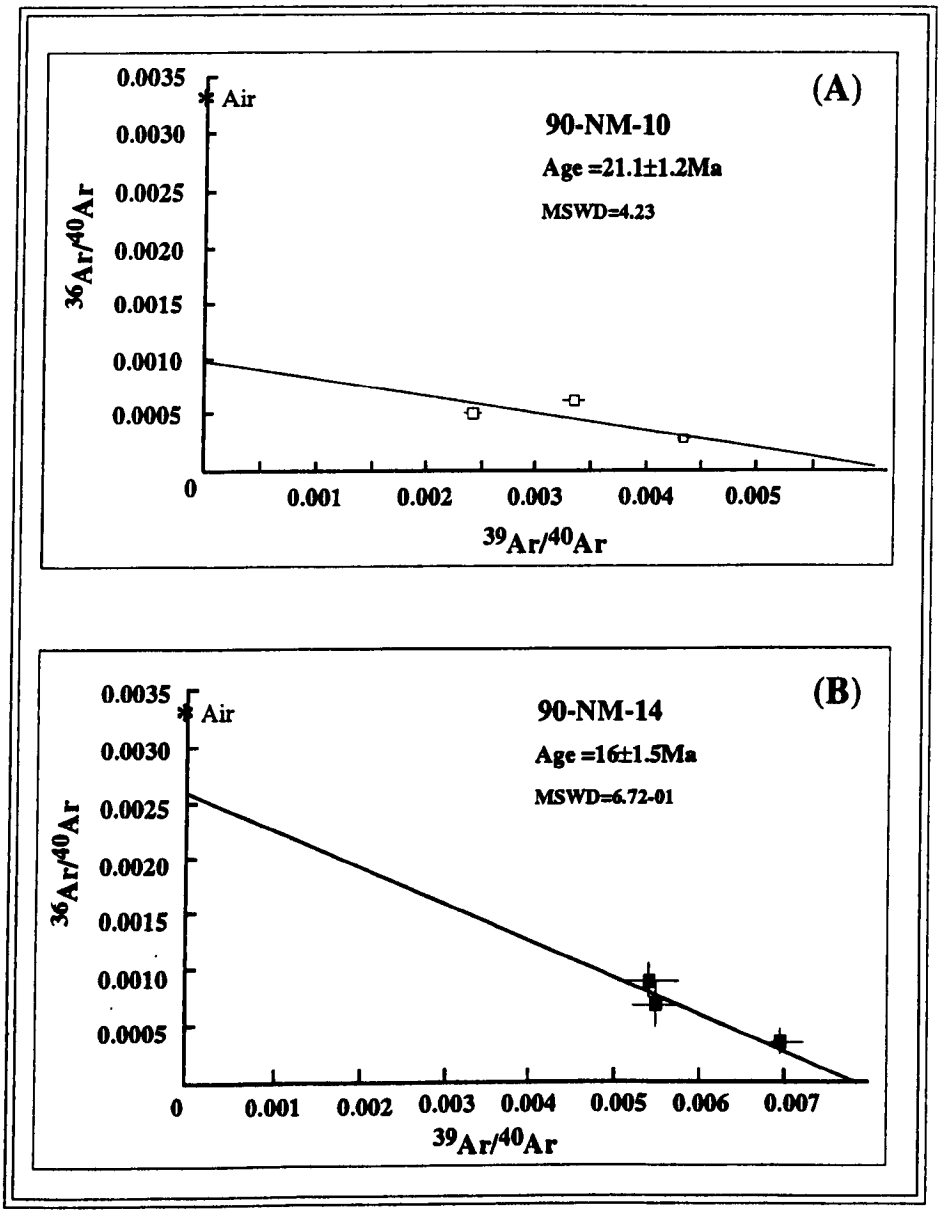


**Figure 2.18.** Ar-Ar isochron plot for (A) 90-NM-10, Bennet Peak and (B) 90-NM-14, from a Ship Rock satellite intrusion.

Sample NM-14, a small satellite plug associated with Ship Rock, yields model ages of 16.5±0.8Ma to 18.5±1.5Ma (weighted mean from 3 analyses =17.06±0.68Ma) and these are lower than ages determined on other minettes in this study, the study of Roden et al (1979) and Laughlin et al (1985) which may suggest loss of radiogenic $^{40}Ar$ through alteration. The isochron age of sample NM-14 is 16.0±1.5Ma (MSWD =0.67), the large errors reflecting the small sample size and hence the small quantities of Ar released. This age is much lower than the 26.4±0.6Ma K-Ar age for the SSE radial Ship Rock dyke quoted by Laughlin et al (1986) although as a satellite intrusion it does not necessarily have to be of a similar age. The LOI for sample NM-14 however is 6.7wt%, considerably higher than the minette average of 1.1wt% and this is associated with the occurrence of phlogopite microphenocrysts that appear cloudy and have ill-defined cleavage traces which may suggest slight alteration. As such the age derived from NM-14 is not regarded as wholly reliable and may be an artifact of alteration. Therefore NM-14 is not included in any subsequent discussions.

### 2.5.2: Duration of Navajo Volcanism:

$^{40}Ar/^{39}Ar$ ages obtained on phlogopite separates from minettes collected from the NVF during present study suggest that volcanism within the Navajo volcanic field of the central Colorado Plateau commenced at 27.5±0.5Ma and continued until 20.5±0.31Ma, a duration of 7Ma. The K/Ar results of Laughlin et al (1986) suggest that the onset of Navajo volcanism began at 27.7±0.6 Ma, in good agreement with the Ar-Ar dates of this study. However Laughlin et al (1986) quote the lower age limit of volcanism at 19.4±0.9 Ma based on a sample which shows no signs of alteration and this implies that the duration of volcanism in the Navajo volcanic field may have been approximately 8Ma.

An 8Ma duration of volcanism in the NVF is in stark contrast to that proposed by McDowell et al (1986) and Roden et al (1979) who dismiss young ages as an artifact of alteration and loss of radiogenic 40Ar, and conclude that the period of volcanism was only 2-2.5Ma. The rationale, in addition to alteration, behind the dismissal of ages <23Ma is the observation that potassic rocks elsewhere are apparently emplaced over short intervals of time (McDowell et al., 1986 & Roden et al., 1979). For example the lamproites of West

Kimberly, Australia, were emplaced over a 4 Ma period (Jaques et al., 1984).

On the basis of the present Ar-Ar study there appears to be no valid reason for dismissing ages of <23 Ma and restricting the duration of Navajo volcanism to <5Ma and it is concluded, in agreement with Laughlin et al (1986), that volcanism commenced at 27.5±0.5 Ma ending possibly as late as 19.4±0.9 Ma a period of approximately 8Ma.

## 2.6: Temporal variation in magma composition:

The preceding discussions highlighted the compositional variation and identified three distinct intrusive groups within the Navajo volcanic field.

| Composition | Group I Minettes | Group II Katungites | Group III Melanephelinites |
|---|---|---|---|
| **Major Elements** | | | |
| $SiO_2$ | 48.0-58.4 | 33.2-36.9 | 41.8-46.0 |
| Mg# | 62.0-75.0 | 72.0-80.0 | 69-74.0 |
| $K_2O/Na_2O$ | 2.0-3.9 | 0.9-2.4 | 0.6-6.0 |
| **Trace elements** | | | |
| La/Yb | 76-122 | 61.95 | 93-97 |
| Ba ppm | 1809-2690 | 1221-2504 | 1537-2437 |
| Nb ppm | 29-94 | 110-161 | 77-122 |
| Ba/Nb | 24-77 | 11-18 | 18-20 |
| **Isotopes** | | | |
| $^{87}Sr/^{86}Sr$ | 0.70562-0.70710 | 0.70443-0.70577 | 0.70495-0.70538 |
| $^{143}Nd/^{144}Nd$ | 0.51247-0.51270 | 0.51272-0.51279 | ≈0.51280 |
| $^{206}Pb/^{207}Pb$ | 19.03-19.24 | 19.16-19.25 | 19.18-19.19 |
| $^{207}Pb/^{204}Pb$ | 15.62-15.74 | 15.57-15.62 | ≈15.65 |
| $^{208}Pb/^{204}Pb$ | 38.73-39.18 | 38.76-38.93 | ≈39.00 |

**Table 2.4.** Summary of some of the main major and trace element and isotopic characteristics of the minettes, katungites and melanephelinites of the Navajo Volcanic Field, central Colorado Plateau.

Table 2.4 summarises the main compositional characteristics of these magmatic groups. The most notable variations are in LIL/HFS element and isotope ratios. Minettes are characterised by the highest Ba/Nb ratios of 24-77 and $^{87}Sr/^{86}Sr$ ratios of 0.70562-0.70705 while the katungites have the lowest ratios, Ba/Nb ≈11-18 and $^{87}Sr/^{86}Sr$ =0.70443-0.70577 and appear very OIB-like. Between these extreme endmembers there is an almost continuous variation as illustrated in Fig 2.19. Furthermore both trace element and isotope ratios correlate with major elements such as $SiO_2$ and $Al_2O_3$.

Similar LIL/HFS element and isotope ratios to those of the NVF have been identified in mid-late Tertiary basalts of the Rio Grande Rift (Perry et al., 1987), Basin & Range (Bradshaw, 1991; Fitton et al., 1991; Gans et al., 1989) and its peripheries (Ormerod, 1988; Davis, 1991). In each case a temporal evolution in magma composition has been identified

from early high LIL/HFS and $^{87}Sr/^{86}Sr$ magmas to low LIL/HFS and $^{87}Sr/^{86}Sr$ OIB-like magmas. This temporal evolution in magma composition has been attributed to an increasing dominance of asthenosphere-derived melts in the mid to late-Tertiary magmatism of the Basin & Range and its peripheries.

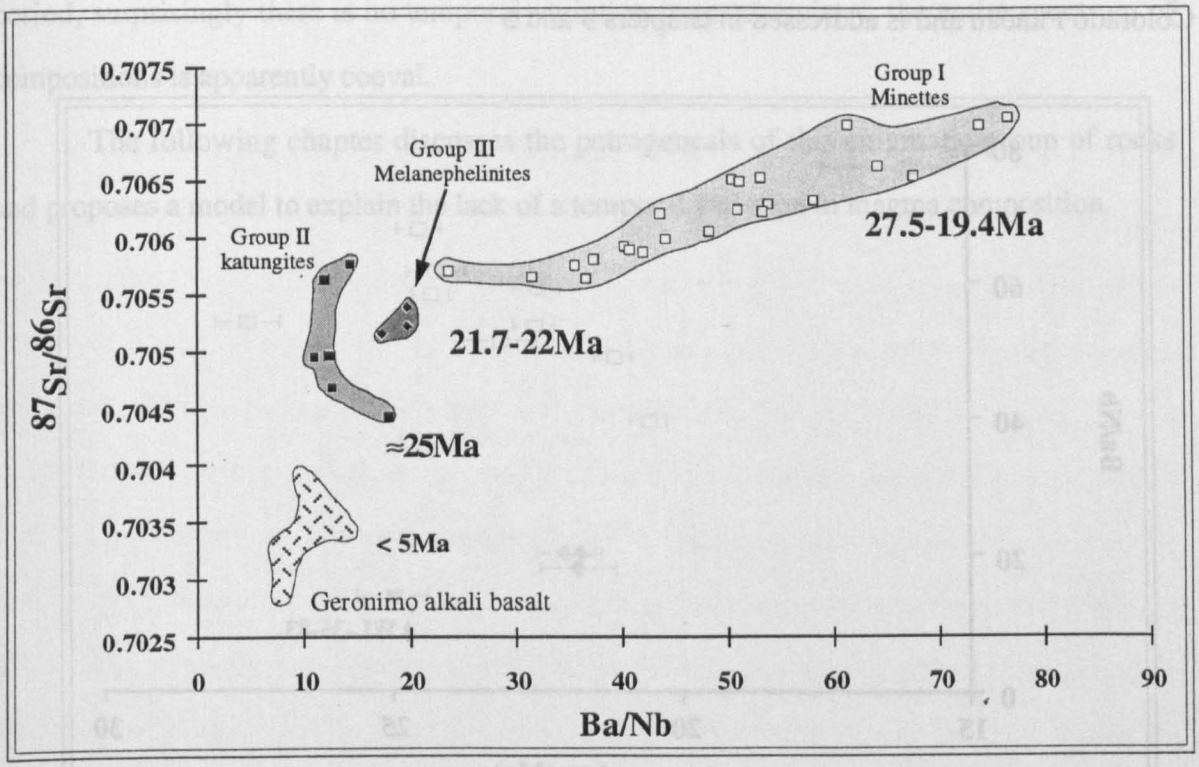


**Figure 2.19**. Variation of $^{87}Sr/^{86}Sr$ with Ba/Nb in magmas from the Navajo Volcanic Field illustrating the wide variation in both trace element and isotope ratios. Also shown is the approximate range in age for each group which demonstrates the lack of a temporal variation in composition.

To allow an evaluation of temporal variations in magma composition the K-Ar (Laughlin et al., 1986) and Ar-Ar ages (this study) for the three intrusive groups of Navajo volcanic field are plotted against Ba/Nb in Fig 2.20 and are also shown in Fig 2.19.

It is evident from these figures that, despite the 8Ma duration of magmatism and the considerable range in trace element compositions, there is no temporal variation in magma composition in the NVF. Although the Navajo magmas have a similar range in trace element and isotopic compositions to basalts from other volcanic provinces in the western United States (Bradshaw, 1991; Fitton et al., 1991; Ormerod, 1988; Davis, 1991) a simple model whereby the range of LIL/HFS and $^{87}Sr/^{86}Sr$ ratios reflect a temporal increase in the contribution from asthenosphere-derived low LIL/HFS and $^{87}S/^{86}Sr$ magmas is not applicable to the intrusives of the Navajo volcanic field. The composition of Navajo magmas

suggest either a variable contribution from the asthenosphere throughout the period of volcanic activity or melting of a heterogeneous source. The onset and duration of Navajo volcanism with the apparent lack of any temporal variation in magma composition clearly has important implications for the cause and evolution of Oligo-Miocene magmatism on the Colorado Plateau and is addressed in chapters 3 and 5

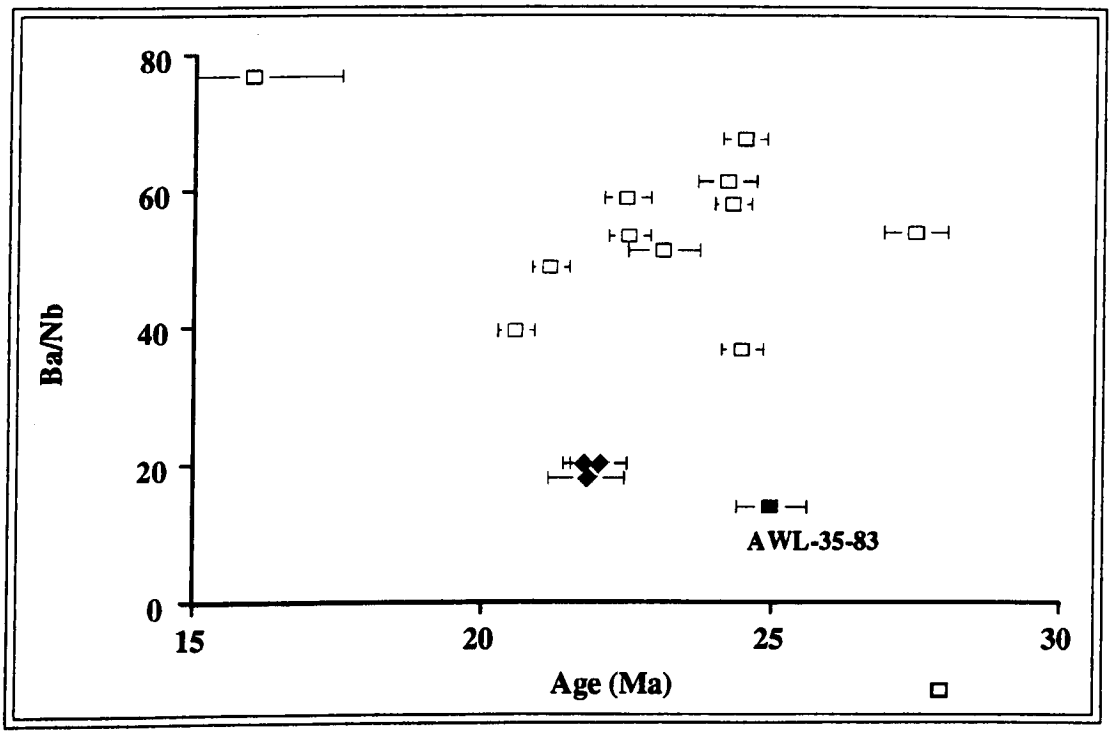


**Figure 2.20.** Variation of Ba/Nb with age for intrusives from the Navajo Volcanic Field. Data for AWL-35-83 from Laughlin et al (1986). Symbols as for Figure 2.10.

## 2.7: Summary and Conclusions:

The intrusives of the Navajo volcanic field have a wide, semi-continuous, variation in composition. Rare, highly silica-undersaturated, potassic katungites have trace element and isotopic compositions within the range of OIB magmas, whereas the comparatively common mildly silica-undersaturated ultrapotassic minette lamprophyres have distinct Ta and Nb depletions, more typical of subduction-related volcanics than within-plate magmas. Despite this wide range in composition the majority of samples have primitive characteristics with high Mg numbers of ≥70 and high abundances of the compatible trace elements, suggesting they represent primitive magmas whose compositions are inherited from their mantle sources. Those minettes with <7.8% MgO are grouped as felsic minettes on the basis of their lower Mg#'s and may represent the products of fractionation.

Published K-Ar dates and $^{40}Ar$-$^{39}Ar$ dating conducted during the present study show that volcanic activity within the Navajo region of the central Colorado Plateau commenced at approximately 27.5 Ma (Laughlin et al., 1986; this study) and continued for approximately 8Ma. Although magmas with a wide range in compositions were erupted throughout this period, surprisingly there is no temporal variation in geochemistry, the entire spectrum of compositions is apparently coeval.

The following chapter discusses the petrogenesis of this enigmatic group of rocks and proposes a model to explain the lack of a temporal variation in magma composition.

# CHAPTER 3

## Petrogenesis and Evolution of the Oligo-Miocene Ultrapotassic Navajo Intrusives: Constraints on the Composition of the Lithosphere Beneath the Colorado Plateau.

---

## 3.1: Introduction:

The volcanic and hypabyssal rocks of the Navajo Volcanic Field (NVF) cover a wide compositional range (e.g. $SiO_2$= 32.6-58.4wt%), a wide geographical area and a large span of geological time. Yet, unlike the more volumetrically significant volcanic fields of the Basin & Range and Rio Grande provinces, they are not associated with contemporary extension. The purpose of this chapter is to integrate the data presented in chapter 2 into a coherent petrogenetic model that accounts for the observed major compositional variations, identifies contributions from asthenospheric and lithospheric sources, both crust and mantle, and temporal changes in magma source regions. The latter in particular are critical for placing constraints on geodynamic models for magma generation that are the subject of chapter 5. In addition, the evolution of the magma source regions will be examined in the light of recently proposed models to describe the possible evolution of the mantle lithosphere beneath the Colorado Plateau .

## 3.2: Petrogenesis:

Chapter 2 highlighted the compositional variation, both within and between the three magmatic groups identified in the Navajo Volcanic Field viz. the minettes, katungites and melanephelinites. These variations have been variously attributed to fractional crystallisation (Roden, 1979,1981; Alibert et al.,1986), crustal contamination (Williams, 1936) and to mixing of magmas from distinct mantle sources (Alibert et al.,1986). This section aims to identify the effects of these processes on major and trace element and isotope variations, and in particular to identify primary magmas that reflect the composition of the mantle source regions beneath the Colorado Plateau. In order to achieve this it is first necessary to identify and account for those variations related to processes that have affected the magma since it

segregated from its source region, such as fractional crystallisation and/or crustal contamination that may have overprinted mantle-derived geochemical signatures.

### 3.2.1: Primary or Evolved Magmas:

Despite the considerable range in composition, many of the intrusives of the NVF have primitive compositions, with high MgO, high Mg#'s (70-80) and high abundances of the compatible elements Ni and Cr. These characteristics indicate that they represent primitive, perhaps primary melts that were derived directly from their mantle source regions, without experiencing significant crystal fractionation prior to emplacement. The minettes however can be subdivided into two groups (see chapter 2), a primitive group with MgO≥7.8%, Mg#≥70 and high Ni and Cr (217-322 and 231-502 respectively) and a felsic or evolved group with MgO<7.8%, lower Mg#'s and lower Ni and Cr concentrations.

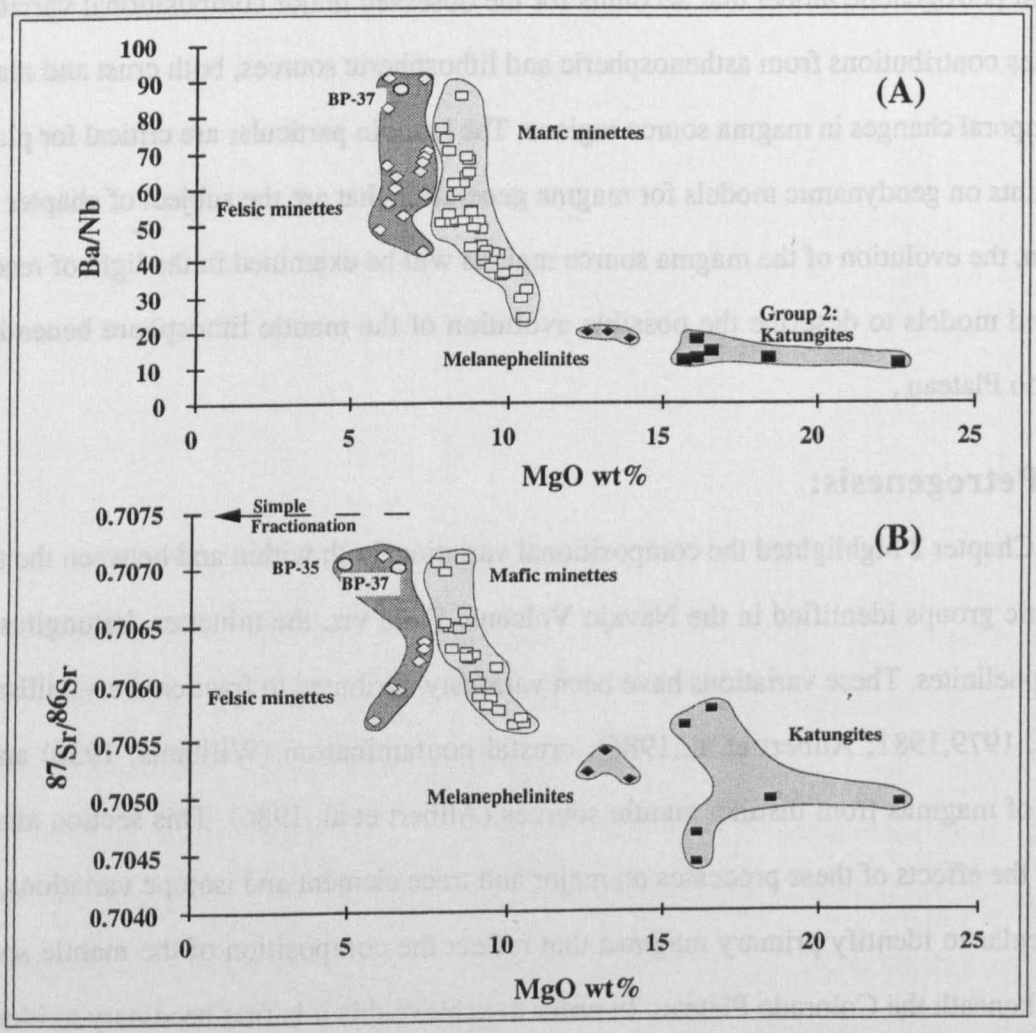


**Figure 3.1.** Variation of trace element and isotope ratios with major elements as represented by MgO,highlighting the inadequacy of simple fractionation processes in establishing the compositional variations within, and between, the Navajo intrusive groups. Minettes with <7.8% MgO show no correlation between trace elements or isotope ratios with major elements. Expected trends for simple fractionation are represented by dashed arrows in top left of each plot. Data for BP-37 and BP-35 from Roden & Smith (1979) and Roden (1981). A) Ba/Nb versus MgO. B) $^{87}Sr/^{86}Sr$ versus

Fig 3.1 shows the variation of $^{87}Sr/^{86}Sr$ and Ba/Nb with MgO for intrusives and volcanics of the NVF, with the minettes subdivided into the mafic and felsic subgroups, along with the expected vector for simple closed-system fractionation. Two features are apparent from this diagram; firstly the felsic minettes, which have lower MgO contents, cover a similar range in both $^{87}Sr/^{86}Sr$ and Ba/Nb to the mafic minettes and secondly both parameters are lower in the more mafic melanephelinites and katungites. There is no systematic increase in isotope or trace element ratios with closed-system fractionation and therefore if felsic minettes evolved from the mafic minettes it is likely that the parent had similar isotope and incompatible element ratios. By contrast, variations both within and between the mafic minettes and katungite groups, both of which have primary characteristics, imply large source variations.

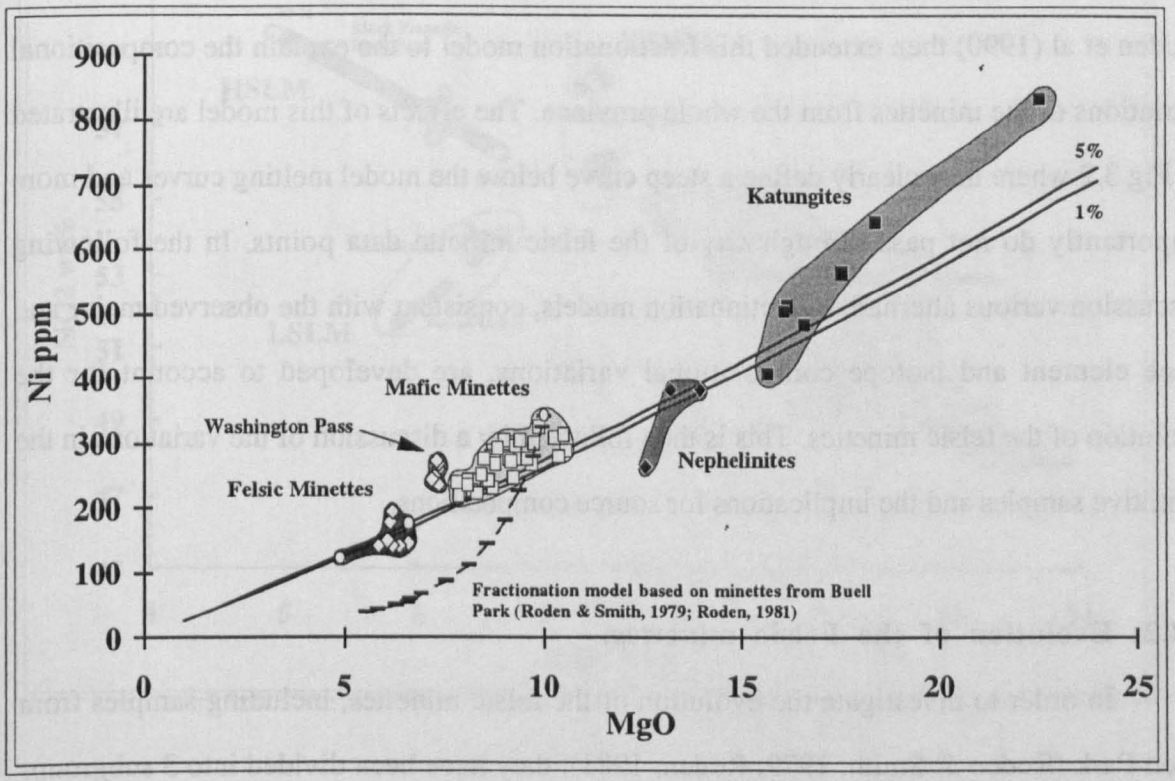


**Figure 3.2.** Variation of Ni with MgO for the Navajo mafic and felsic minettes, melanephelinites and katungites. Fractionation curve based on major and trace element modelling of mafic and felsic minettes from Buell Park (Roden & Smith, 1979; Roden, 1981). Melting curves are for 1 and 5% melting of a spinel lherzolite, calculated according to the method of Hart & Davis (1978). Open circles represent Buell Park data from Roden and Smith (1979) and Roden (1981).

Melting and fractionation vectors are generally distinct on Ni-MgO variation diagrams and on Fig 3.2 the Navajo magmatic groups are compared with model partial melt curves of a mantle lherzolite (Hart & Davis, 1978). The primitive group of minettes, the melanephelinites and the katungites all lie close to these curves emphasising their primary nature. However the felsic minettes also lie close to the modelled melt curves except in the case of the Washington Pass volcanic centre where samples plot above them (Fig 3.2) suggesting that the felsic minettes may not be evolved.

The difference between mafic and felsic minettes have been the subject of previous investigations notably Ehrenberg (1978) and Roden and co-workers. The results of Roden & Smith (1979) and Roden et al (1990) have been based largely upon a small number of minettes from the the Buell Park diatreme, which encompasses the major element compositional range of minettes from the entire province. Roden's favoured model for the petrogenesis of the Buell Park minettes invokes up to 50% fractionation of an assemblage dominated by phlogopite and diopside with minor amounts of spinel, apatite ± olivine. Roden et al (1990) then extended this fractionation model to the explain the compositional variations of the minettes from the whole province. The effects of this model are illustrated in Fig 3.2 where they clearly define a steep curve below the model melting curves and more importantly do not pass through *any* of the felsic minette data points. In the following discussion various alternative fractionation models, consistent with the observed major and trace element and isotope compositional variations, are developed to account for the evolution of the felsic minettes. This is then followed by a discussion of the variations in the primitive samples and the implications for source compositions.

### 3.2.2: Evolution of the Felsic minettes:

In order to investigate the evolution of the felsic minettes, including samples from Buell Park (Roden & Smith, 1979; Roden, 1981), they have been divided into 3 subgroups on the basis of MgO and $SiO_2$ contents, as shown in Fig 3.3 and outlined in Table 3.1 below.

| Group 1 (HSLM): Buell Park/ Black Pinnacle | Group 2 (HSHM): Washington Pass | Group 3 (LSLM): Chilchinbito/Porras Dykes |
|---|---|---|
| High $SiO_2$ ≈ 56.2 - 59.5% | High $SiO_2$ ≈ 55.5 - 58.4% | Low $SiO_2$ ≈51.5 -54.2% |
| Low MgO ≈4.8 - 6.8 % | High MgO ≈7.2 - 7.4 % | Low MgO ≈ 5.9 - 6.6% |
| Ni ≈ 120 - 180 ppm | Ni ≈ 233 - 272 ppm | Ni ≈.136 - 146 ppm |
| Constant $^{87}Sr/^{86}Sr$ | Low $^{87}Sr/^{86}Sr$ | Low $^{87}Sr/^{86}Sr$ |
| ≈0.70705 - 0.70715 | ≈ 0.70604 - 0.70679 | ≈0.70568 - 0.70594 |

**Table 3.1** Compositional characteristics for individual felsic minette subgroups.Group 1: high Si, low MgO (HSLM); Group 2: high Si, high MgO (HSHM); Group 3, low Si, low MgO (LSLM).

High silica-low magnesium (HSLM) minettes are characteristic of the Buell Park-Black Pinnacle volcanic centres, whereas high silica-high magnesium (HSHM) are found at the Washington Pass volcanic centre and the low silica-low magnesium (LSLM) minettes characteristic of the Chilchinbito and Porass Dykes.

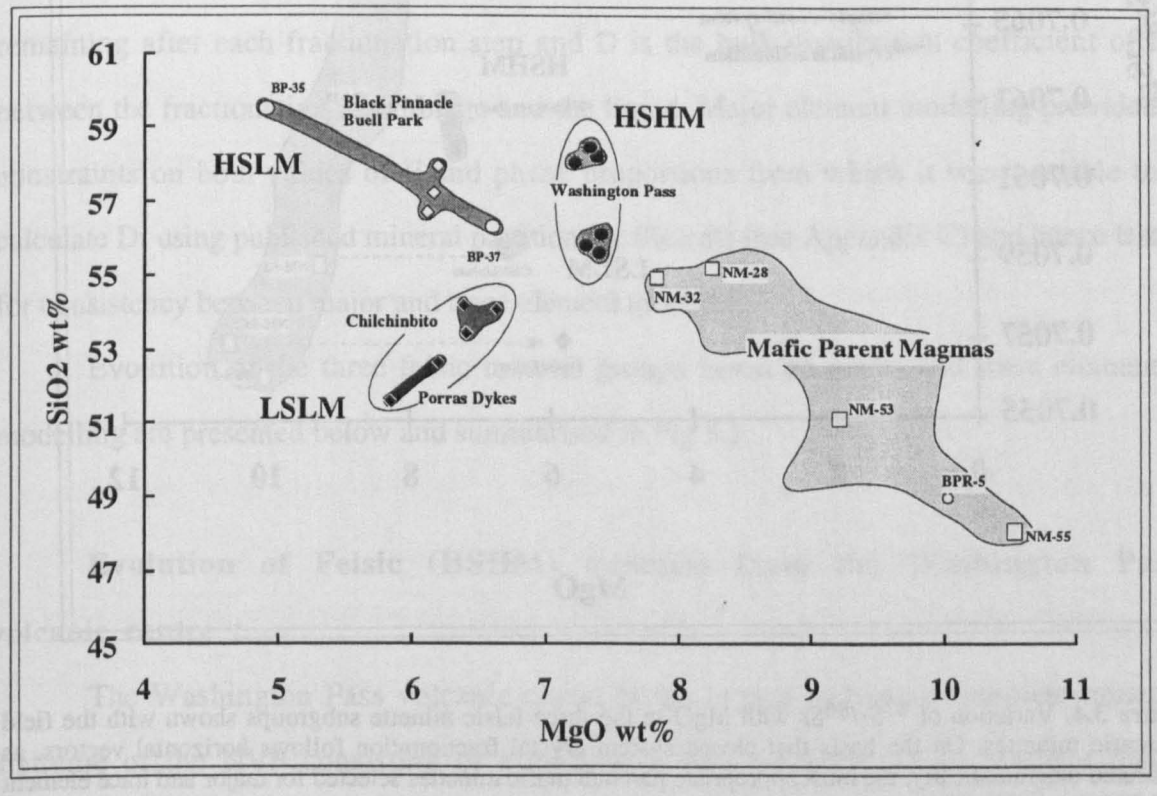


**Figure 3.3.** Variation of $SiO_2$ with MgO in the minettes of the NVF [including data for Buell park from Roden & Smith (1979) and Roden (1981)]. Felsic minettes with MgO <7.8% are divided into high-silica-high-magnesium (HSHN), high-silica-low-magnesium (HSLM) and low-silica-low-magnesium (LSLM) minette subgroups

Each felsic minette group has a restricted and distinct range of $^{87}Sr/^{86}Sr$ ratios as illustrated in Fig 3.4 and can be modelled in terms of simple closed-system fractional crystallisation of four isotopically distinct mafic parents. The mafic parent minettes used in fractionation modelling, selected for their isotopic similarity and close geographic proximity to the felsic minettes in question, are also illustrated in Fig 3.4 and presented in Table 3.2.

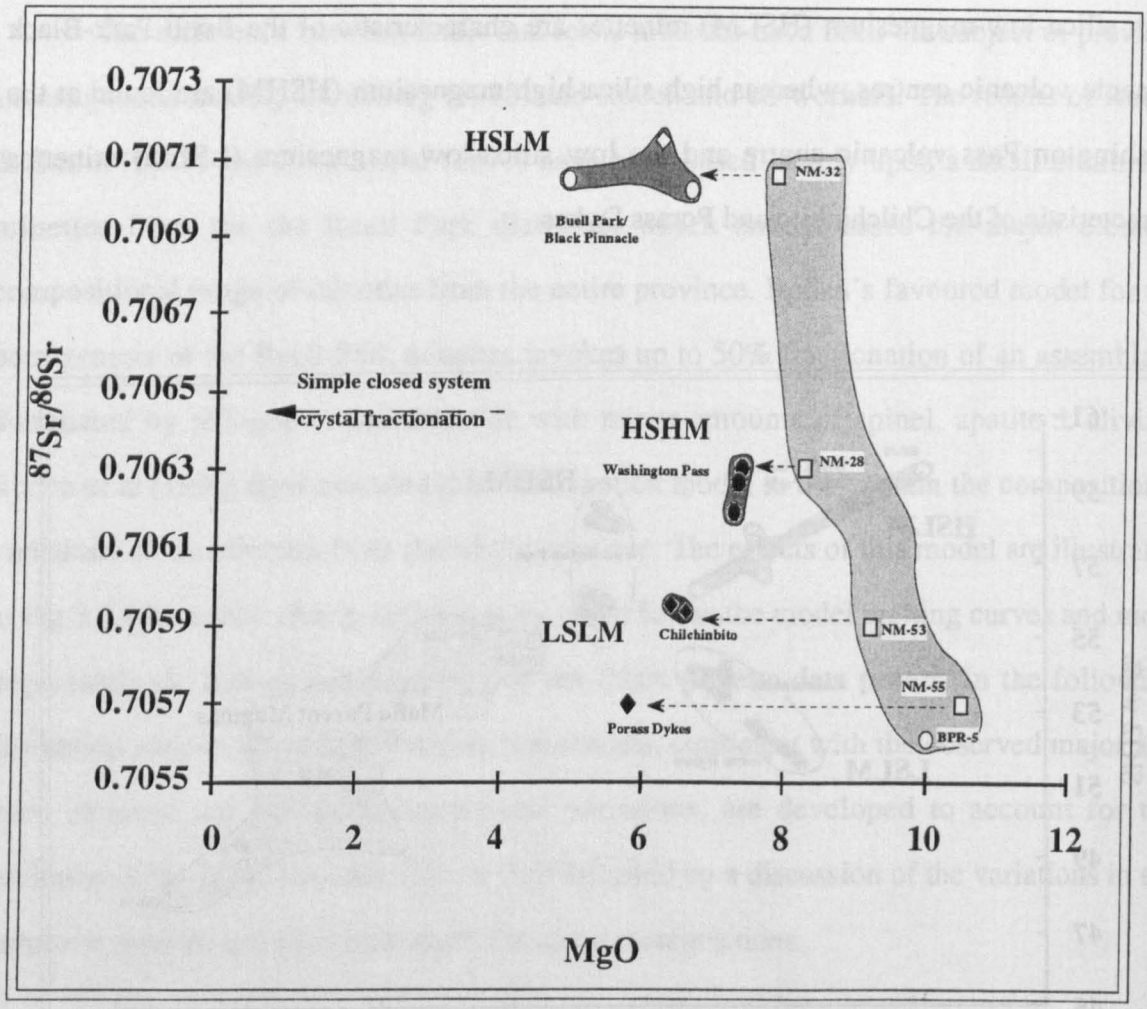


**Figure 3.4.** Variation of $^{87}Sr/^{86}Sr$ with MgO in the three felsic minette subgroups shown with the field for mafic minettes. On the basis that closed system crystal fractionation follows horizontal vectors, as illustrated diagramatically, the most appropriate parental mafic minettes selected for major and trace element modelling are indicated.

The major element variations of the felsic minettes were modelled using a combined linear programming and least squares analysis approach (Wright & Doherty, 1970) and mineral compositions appropriate for the minettes, taken from Nicholls (1969), Ehrenberg (1977), Roden (1979) and a spinel peridotite xenolith composition from Smith & Levy (1976), are presented in Table 3.2

| | Parent Magmas | | | | Mineral Phases | | | | | |
|---|---|---|---|---|---|---|---|---|---|---|
| | NM-32 | NM-28 | NM-53 | NM-55 | Diopside | Phlogopite | Olivine | Magnatite | Apatite | Peridotite |
| | | | | | 1 | 2 | 1 | 3 | 1 | 4 |
| $SiO_2$ | 54.95 | 54.95 | 51.14 | 47.99 | 54.50 | 37.80 | 39.40 | 0.00 | 0.00 | 44.40 |
| $TiO_2$ | 1.33 | 1.33 | 1.63 | 2.38 | 0.25 | 3.50 | 0.00 | 14.60 | 0.00 | 0.80 |
| $Al_2O_3$ | 10.58 | 10.58 | 10.55 | 9.01 | 0.64 | 12.40 | 0.00 | 0.32 | 0.00 | 2.10 |
| $Fe_2O_{3(T)}$ | 6.44 | 6.44 | 8.36 | 8.90 | 3.37 | 6.80 | 13.42 | 75.20 | 0.00 | 8.30 |
| MnO | 0.09 | 0.09 | 0.14 | 0.11 | 0.14 | 0.02 | 0.18 | 0.00 | 0.00 | 0.00 |
| MgO | 7.84 | 7.84 | 9.21 | 10.52 | 18.20 | 23.00 | 46.80 | 1.24 | 0.00 | 41.10 |
| CaO | 7.19 | 7.19 | 8.65 | 10.12 | 22.50 | 0.00 | 0.16 | 0.00 | 56.00 | 2.30 |
| $Na_2O$ | 2.01 | 2.01 | 2.33 | 1.45 | 0.37 | 0.54 | 0.00 | 0.00 | 0.00 | 0.25 |
| $K_2O$ | 7.53 | 7.53 | 5.33 | 5.43 | 0.02 | 9.30 | 0.00 | 0.00 | 0.00 | 0.00 |
| $P_2O_5$ | 1.07 | 1.07 | 1.01 | 1.27 | 0.00 | 0.00 | 0.00 | 0.00 | 44.00 | 0.00 |

**Table 3.2:** Parental magma and mineral compositions used in the major element combined linear programming and least squares analysis. 1. Data from Roden (1979). 2. Average of 6 analyses of phlogopite phenocryst cores (Nicholls, 1969). 3. Average of magnetite analyses from Washington Pass and The Thumb (Ehrenberg, 1977). 4. Average of 3 analyses of spinel peridotite from Green Knobs diatreme (Smith and Levy, 1976).

The effects of fractionation on trace elements were calculated using the Rayleigh Fractionation equation, $C_l i/C_o i = F^{(Di-1)}$: where $C_o i$ is the initial concentration of element $i$ in the parent liquid, $C_l i$ the concentration of $i$ after fractionation, F the proportion of liquid remaining after each fractionation step and D is the bulk distribution coefficient of $i$ between the fractionating assemblage and the liquid. Major element modelling provided constraints on both values of F and phase proportions from which it was possible to calculate Di using published mineral partition coefficients (see Appendix C) and hence test for consistency between major and trace element models.

Evolution of the three felsic minette groups based on major and trace element modelling are presented below and summarised in Fig 3.5.

**Evolution of Felsic (HSHM) minettes from the Washington Pass volcanic centre :**

The Washington Pass volcanic centre is the largest and most complete minette diatreme of the NVF consisting of a circular 3.4km diameter crater, remnant felsic trachybasalt flows and a number of more mafic minette dykes and plugs (Ehrenberg, 1978). As felsic minettes are spatially and temporally associated with more mafic minettes this volcanic centre provides an excellent opportunity to examine the evolution of these more evolved rocks.

Felsic minettes from Washington Pass can be further divided into two subgroups, as illustrated in Fig 3.3, one characterised by greater abundances of $SiO_2$ than the other, yet in other respects, notably Sr isotopic composition, they are very similar. The isotopic composition of mafic minettes from Washington Pass is variable though sample NM-28 is similar to the felsic minettes (Fig 3.3) and therefore interpreted as a suitable parent magma. The results of least squares and trace element modelling of the Washington Pass felsic minettes are presented in Table 3.3.

| Model Pair | NM-28⇒NM-59 | | NM-28⇒NM-61 | | NM-28⇒NM-64 | | NM-28⇒NM-20A | | NM-20A⇒NM-22B | |
|---|---|---|---|---|---|---|---|---|---|---|
| **Results** | | | | | | | | | | |
| **Major element modelling** | Parent Obs | Calc | Parent Obs | Calc | Parent Obs | Calc | Parent Obs | Calc | Parent Obs | Calc |
| $SiO_2$ | 55.17 | 55.17 | 55.17 | 55.16 | 55.17 | 54.97 | 55.17 | 55.22 | 58.02 | 58.01 |
| $TiO_2$ | 1.67 | 1.68 | 1.67 | 1.71 | 1.67 | 1.77 | 1.67 | 1.68 | 1.36 | 1.32 |
| $Al_2O_3$ | 10.72 | 10.54 | 10.72 | 10.75 | 10.72 | 10.69 | 10.72 | 10.22 | 11.04 | 11.02 |
| $Fe_2O_3t$ | 7.06 | 7.01 | 7.06 | 7.05 | 7.06 | 6.35 | 7.06 | 7.06 | 5.57 | 5.58 |
| MnO | 0.09 | 0.11 | 0.09 | 0.13 | 0.09 | 0.06 | 0.09 | 0.06 | 0.06 | 0.07 |
| MgO | 8.28 | 8.21 | 8.28 | 8.25 | 8.28 | 7.83 | 8.28 | 8.26 | 7.24 | 7.25 |
| CaO | 6.53 | 6.59 | 6.53 | 6.61 | 6.53 | 7.17 | 6.53 | 6.44 | 5.52 | 5.53 |
| $Na_2O$ | 2.41 | 1.87 | 2.41 | 2.1 | 2.41 | 1.99 | 2.41 | 2.05 | 2.3 | 2.37 |
| $K_2O$ | 6.22 | 6.64 | 6.22 | 6.29 | 6.22 | 7.25 | 6.22 | 6.75 | 7.27 | 7.32 |
| $P_2O_5$ | 0.83 | 0.75 | 0.83 | 0.72 | 0.83 | 1.1 | 0.83 | 0.94 | 0.71 | 0.7 |
| $\Sigma r^2$ | 0.5 | | 0.12 | | 0.15 | | 0.68 | | 0.01 | |
| **Trace element modelling** | Daughter Obs | Calc | Daughter Obs | Calc | Daughter Obs | Calc | Daughter Obs | Calc | Daughter Obs | Calc |
| Ni | 257 | 230 | 244 | 241 | 233 | 248 | 243 | 230 | 272 | 265 |
| Cr | 269 | 200 | 271 | 230 | 254 | 235 | | | | |
| Ba | 2297 | 2203 | 2419 | 2174 | 2205 | 2116 | | | | |
| **% Fractionation** | 7% | | 7.3% | | 5.5% | | 12.5% | | 2.5% | |
| **Fractionating Assemblage** | | | | | | | | | | |
| Diopside | 46 | | 43 | | 22 | | 43 | | 39 | |
| Phlogopite | 44 | | 52 | | 73 | | 33 | | 49 | |
| Apatite | ~1 | | <1 | | 2 | | 6 | | 1 | |
| Magnetite | 9 | | 4 | | 3 | | 18 | | 11 | |
| **% Peridotite Accumulation** | 0 | | 0 | | 0 | | 0.5 | | 2 | |

**Table 3.3.** Results of major and trace element fractionation and spinel peridotite assimilation modelling for the derivation of the Washington Pass HSHM minettes.

Evolution of the low silica subgroup (samples NM-59,61,64) involves 5 to 7% fractionation of predominantly diopside and phlogopite with minor quantities of apatite and magnetite. Field observations reveal the high silica subgroup (NM-20A, 22A, 22B) to contain abundant altered spinel lherzolite and websterite xenoliths (Ehrenberg, 1978) and major and trace element modelling which allows for accumulation of spinel peridotite (composition based on the average of six spinel peridotites from Green Knobs: Smith & Levy, 1976) yields close agreement between the calculated and observed magma

compositions (Table 3.3 and Fig 3.5). The high silica subgroup can be modelled in two stages (NM-28⇒NM-20A and NM-20A⇒NM-22B) involving 12.5 and 2.5% fractionation of a diopside-phlogopite-magnetite-apatite assemblage, associated with accumulation of between 0.5-2% spinel peridotite.

An important implication of the inclusion of mantle xenoliths within the HSHM felsic minettes of Washington Pass is that the geochemical diversity resulting from fractionation was established prior to incorporation of these xenoliths in the upper mantle and therefore represents a high pressure process.

**Evolution of Felsic (HSLM) minettes from the Buell Park volcanic centre :**

The evolution of the Buell Park diatreme has been extensively studied by Roden & Smith (1979) and Roden (1981). They attribute the felsic minettes, included in the HSLM group of this study, to fractionation from the mafic minette BPR-5. However, as illustrated in figs 3.1 and 3.4, simple closed-system crystal fractionation of Roden's BPR-5 is unable to reproduce the compatible element variations of the Buell Park felsic minettes as the parent and daughter magmas are isotopically different. The implication of this, and the conclusion reached by Roden et al (1990), is that the felsic minettes are not related to BPR-5 via simple closed system fractionation crystallisation processes. Roden et al (1990) propose an alternative model whereby the "isotopic heterogeneity at Buell Park could be a primary feature and may be decoupled from the bulk chemical variation, which is adequately explained by crystal fractionation." Such decoupling of isotopes from major and trace elements is regarded as both unsatisfactory and unnecessary as discussed below.

NM-32, on the basis that it has an $^{87}Sr/^{86}Sr$ identical to the Buell Park felsic minettes (Fig 3.4) and was collected from Outlet Neck, a small intrusion only 3km east of Buell Park, may represent a more appropriate parent magma composition for the HSLM minettes. The results of least squares and trace element modelling are presented in Table 3.4 and Fig 3.5. The Buell Park felsic minettes can be modelled in two stages, NM-32⇒BP-37 and BP-37⇒BP-35, requiring 11 and 14% fractionation respectively of an assemblage composed of variable proportions of diopside-phlogopite-apatite and magnetite. Felsic minettes from Black Pinnacle can also be modelled in a similar manner.

| Model Pair | NM-32⇒NM-39 | | NM-32⇒BP-37 | | BP-37⇒BP-35 | |
|---|---|---|---|---|---|---|
| **Results** | | | | | | |
| **Major element modelling** | **Parent** | | **Parent** | | **Parent** | |
| | Obs | Calc | Obs | Calc | Obs | Calc |
| $SiO_2$ | 54.95 | 54.98 | 54.95 | 54.86 | 56.23 | 56.3 |
| $TiO_2$ | 1.33 | 1.49 | 1.33 | 1.3 | 1.08 | 1.24 |
| $Al_2O_3$ | 10.58 | 10.96 | 10.58 | 11.42 | 12.14 | 11.93 |
| $Fe_2O_3t$ | 6.44 | 6.4 | 6.44 | 6.44 | 5.74 | 5.71 |
| MnO | 0.09 | 0.08 | 0.09 | 0.08 | 0.08 | 0.06 |
| MgO | 7.84 | 7.98 | 7.84 | 7.97 | 6.63 | 6.61 |
| CaO | 7.19 | 6.98 | 7.19 | 7.28 | 6.37 | 6.23 |
| $Na_2O$ | 2.01 | 2.35 | 2.01 | 2.36 | 2.6 | 2.23 |
| $K_2O$ | 7.53 | 6.49 | 7.53 | 6.45 | 6.76 | 6.78 |
| $P_2O_5$ | 1.07 | 1.33 | 1.07 | 0.96 | 0.77 | 0.95 |
| $\Sigma r^2$ | 1.5 | | 2 | | 0.27 | |
| **Trace element modelling** | **Daughter** | | **Daughter** | | **Daughter** | |
| | Obs | Calc | Obs | Calc | Obs | Calc |
| Ni | 194 | .174 | 176 | 177 | 123 | 114 |
| Sc | NA | 11.5 | 12 | 11.75 | 9.8 | 10.1 |
| Cr | 186 | 162 | 234 | 186 | 154 | 105 |
| Ba | 2354 | 2472 | 2270 | 2494 | 2280 | 2475 |
| **% Fractionation** | **15%** | | **11%** | | **14%** | |
| **Fractionating assemblage** | | | | | | |
| Diopside | 36 | | 47 | | 37 | |
| Phlogopite | 48 | | 39 | | 45 | |
| Apatite | 9 | | 5 | | 7 | |
| Magnetite | 7 | | 9 | | 11 | |

**Table 3.4.** Results of major and trace element fractionation modelling for derivation of the Buell Park (samples BP-37 and BP-35 from Roden & Smith, 1979; Roden, 1981) and Black Pinnacle HSLM minettes. (NA: Not available)

The results of the modelling presented here demonstrate how the HSLM minettes of Buell Park, and Black Pinnacle, can be related to an appropriate mafic minette by simple closed-system fractionation and do not require complex models involving the decoupling of isotopes from major and trace elements.

**Evolution of Felsic (LSLM) minettes of the Chilchinbito and Porass Dykes intrusions :**

Unfortunately the LSLM felsic minettes of the Chilchinbito and Porass Dykes intrusions are not spatially associated with parental mafic minettes. However as the preceding discussions have shown that the HSHM and HSLM felsic minettes can be attributed to simple, generally closed system, fractionation a similar model may also be invoked for the LSLM minettes. The mafic minettes NM-53 and NM-55 are isotopically similar to the Chilchinbito and Porass Dykes intrusions respectively, as illustrated in Fig 3.4, are located less than 15km away in each case, and therefore may represent suitable parental compositions to the LSLM felsic minettes. The results of least squares and trace

element modelling of the Chilchinbito and Porass Dykes LSLM felsic minettes from NM-53 and NM-55 respectively are presented in Table 3.5 and Fig 3.5.

| Model Pair | NM-53⇒NM-40 | | NM-53⇒NM-41 | | NM-55⇒NM-50 | | NM-55⇒NM-51 | |
|---|---|---|---|---|---|---|---|---|
| **Results** | | | | | | | | |
| **Major element modelling** | **Parent** Obs | Calc | **Parent** Obs | Calc | **Parent** Obs | Calc | **Parent** Obs | Calc |
| $SiO_2$ | 51.14 | 52.05 | 51.14 | 52.01 | 47.99 | 47.85 | 47.99 | 47.95 |
| $TiO_2$ | 1.63 | 1.79 | 1.63 | 1.77 | 2.38 | 1.95 | 2.38 | 1.93 |
| $Al_2O_3$ | 10.55 | 10.31 | 10.55 | 10.32 | 9.01 | 9.4 | 9.01 | 9.21 |
| $Fe_2O_3t$ | 8.36 | 8.48 | 8.36 | 8.48 | 8.9 | 8.98 | 8.9 | 8.98 |
| MnO | 0.14 | 0.17 | 0.14 | 0.14 | 0.11 | 0.1 | 0.11 | 0.1 |
| MgO | 9.21 | 9.26 | 9.21 | 9.24 | 10.52 | 10.63 | 10.52 | 10.62 |
| CaO | 8.65 | 8.78 | 8.65 | 8.89 | 10.12 | 10.34 | 10.12 | 10.11 |
| $Na_2O$ | 2.33 | 1.9 | 2.33 | 1.85 | 1.45 | 1.82 | 1.45 | 1.73 |
| $K_2O$ | 5.53 | 6.0 | 5.53 | 6.23 | 5.43 | 5.26 | 5.43 | 5.16 |
| $P_2O_5$ | 1.01 | 1.05 | 1.01 | 0.96 | 1.27 | 0.99 | 1.27 | 0.28 |
| $\Sigma r^2$ | 0.78 | | 1.2 | | 0.66 | | 0.4 | |
| **Trace element modelling** | **Daughter** Obs | Calc | **Daughter** Obs | Calc | **Daughter** Obs | Calc | **Daughter** Obs | Calc |
| Ni | 146 | 148 | 136 | 133 | 141 | 90 | 142 | 80 |
| Sc | 9 | 13.3 | 9 | 12.7 | 9 | 10.4 | 9 | 10 |
| Cr | 161 | 171 | 143 | 146 | 167 | 100 | 159 | 93 |
| Ba | 2312 | 2166 | 2641 | 2196 | 1995 | 2181 | 2173 | 2266 |
| **% Fractionation** | 20.5% | | 11% | | 37% | | 37% | |
| **Fractionating assemblage** | | | | | | | | |
| Diopside | 47 | | 47 | | 44 | | 45 | |
| Phlogopite | 43 | | 39 | | 45 | | 41 | |
| Apatite | 2 | | 5 | | 3 | | 5 | |
| Magnetite | 8 | | 9 | | 8 | | 9 | |

**Table 3.5.** Major and trace element fractionation modelling for derivation of the Chilchinbito and Porass Dykes LSLM felsic minettes from mafic parents NM-53 and NM-55.

The composition of the Chilchinbito felsic minettes is consistent with a model that invokes 11-20.5% fractionation of diopside-phlogopite-apatite-magnetite whereas the Porass Dykes felsic minettes require 37% fractionation of the same assemblage but with different phase proportions.

The conclusion based on the preceding modelling is that all the felsic minettes can be simply related to local mafic parents with similar Ba/Nb and $^{87}Sr/^{86}Sr$ ratios by simple closed-system fractionation. There is no need to appeal to decoupling between major elements, trace elements and isotopes as proposed by Roden et al (1990). The presence of mantle peridotite xenoliths in the felsic minettes suggests fractionation occurred in the mantle and therefore the composition of the mafic minettes probably reflect mantle source compositions.

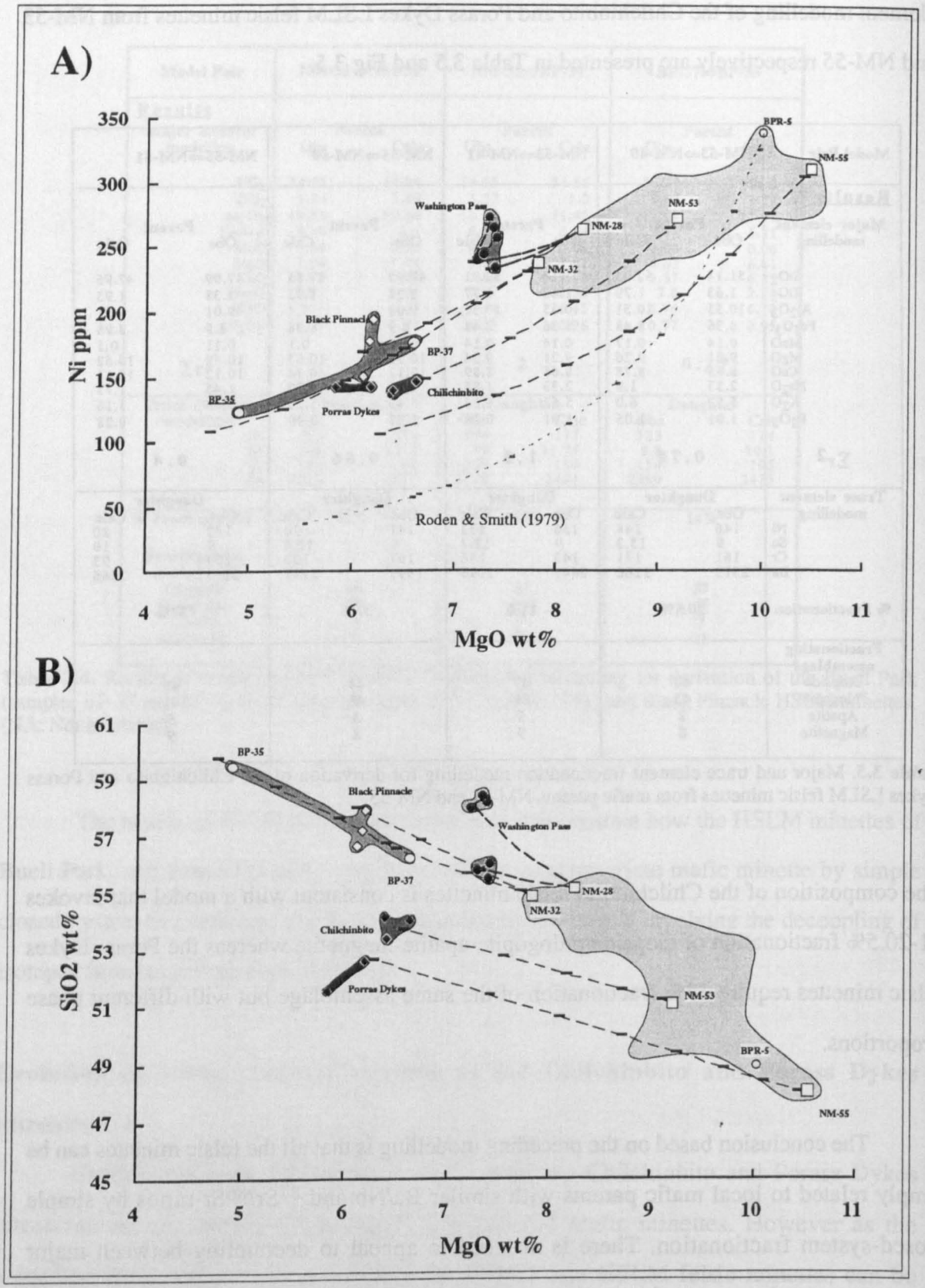


**Figure 3.5.** Fractionation (±spinel peridotite accumulation) curves for the derivation of the Buell Park-Black Pinnacle HSLM, Washington Pass HSHM and Porass Dykes-Chilchinbito LSLM minattes from their respective parental magmas based on the major and trace element modelling presented in Tables 3.3 to 3.5. The fractionation model proposed by Roden & Smith (1979) and Roden (1981) and shown on Ni vs. MgO clearly cannot reproduce the range of Ni abundances observed in either the felsic or mafic minettes. Note the two Washington Pass subgroups; low $SiO_2$ subgroup equates to unit B whereas the high $SiO_2$ subgroup equates unit C of Ehrenberg (1978). A) Ni versus MgO. B) $SiO_2$ versus MgO.

### 3.2.3: Role of Crustal Contamination:

The high LIL and LREE abundances, coupled with depletions in Nb and Ta, high $^{87}Sr/^{86}Sr$ and low $^{143}Nd/^{144}Nd$ that are typical of the mafic Navajo minettes are characteristics observed in many western US mid-late Tertiary basaltic magmas (Fitton et al.,1991; Ormerod, 1988; Davis, 1991; Bradshaw, 1991) and often attributed to crustal or mantle lithospheric contributions. This section addresses the possibility that the comparatively silica-rich Navajo minettes are the products of crustal contamination of less silica-saturated magmas such as katungites or OIB-like mantle-derived melts.

Roden (1981) suggested the $^{87}Sr/^{86}Sr$ isotopic heterogeneity of mafic and felsic minettes from Buell Park might result from crustal contamination of a mafic parent magma and in support cited the presence of abundant crustal xenoliths in certain minette diatremes (Wendlandt et al.,1993). Section 3.2.2 has shown that the Navajo *felsic* minettes can be derived by simple fractionation of an isotopically similar mafic parent and that it is unnecessary to appeal to combined crustal assimilation and fractionation (AFC) to explain the high $^{87}Sr/^{86}Sr$ ratios. Furthermore as the heat required to melt wall rocks is largely derived from the latent heat of crystallisation (Taylor, 1980) and the felsic minettes of Washington Pass and Buell Park (Roden & Smith, 1979; Ehrenberg, 1977) are interpreted as having fractionated in the upper mantle, it is unlikely that during their traverse of the crust sufficient heat was available to allow crustal assimilation. Thus although crustal contamination is not required to explain the compositional range of felsic minettes, arguably it may explain the range of LIL/HFS and isotope ratios of the mafic magmas with >7.8% MgO. However there are several observations that are inconsistent with this model.

Although a wide range of crustal endmembers, characterised by low HFS element abundances and high LIL/HFS and $^{87}Sr/^{86}Sr$ ratios, were considered in the present study as potential contaminants, *all* have $K_2O$ abundances similar to the katungites but less than the majority of the minettes (Table 3.6, Fig 3.6).

| Crustal Endmember | C1 | C2 | C3 | C4 |
|---|---|---|---|---|
| $SiO_2$ | 69.17 | 57.5 | 59.06 | 73.8 |
| $TiO_2$ | 0.54 | 0.84 | 0.4 | 0.24 |
| $Al_2O_3$ | 14.24 | 17.4 | 22.59 | 13.59 |
| $Fe_2O_3$ | 3.31 | 6.9 | 1.68 | 2.15 |
| MnO | 0.07 | 0.11 | 0.027 | 0.05 |
| MgO | 1.29 | 3.8 | 0.9 | 0.95 |
| CaO | 2.7 | 6.6 | 9.11 | 2.63 |
| $Na_2O$ | 3.91 | 4 | 4.46 | 3.18 |
| $K_2O$ | 3.71 | 2 | 0.81 | 3.14 |
| $P_2O_5$ | 0.16 | 0.24 | 0.57 | 0.03 |
| Ba | 991 | 690 | 6876 | 1070 |
| Cr | 13 | 56 | 7 | <4 |
| Nb | 15 | 9 | 1 | 8.9 |
| Ni | 17 | 35 | 5 | <1 |
| Rb | 83 | 37 | 6 | 54 |
| Sr | 562 | 563 | 823 | 220 |
| Ta | 1.07 | | 0.03 | 0.4 |
| Th | 8 | 0.23 | 0.3 | 7.6 |
| V | 41 | | 29 | |
| Y | 16 | 25 | 3 | 18 |
| Zr | 151 | 147 | 84 | 189 |
| La | 35 | 23 | 3 | 36 |
| Ce | 74 | 48 | 5 | 87 |
| Nd | 25 | 25 | 2.4 | 32 |
| Sm | | 5 | 0.53 | 5.8 |
| Eu | | 1.4 | 0.35 | 1.07 |
| Tb | | 0.66 | 0.11 | 0.77 |
| Yb | | 2.22 | 0.3 | 2.43 |
| Lu | | 0.36 | 0.04 | 0.39 |
| $^{87}Sr/^{86}Sr$ | 0.712767 | 0.71012 | 0.704782 | |
| $^{143}Nd/^{144}Nd$ | | 0.51225 | 0.511759 | |

**Table 3.6.** Major and trace element and isotope data for potential contaminants: C1, granitic crustal xenolith from the NVF; C2, Average lower crustal meta-diorite xenolith from the Geronimo volcanic field, Kempton et al (1990); C3, mid-crustal xenolith 5LT276 (Thompson et al., 1993); C4, Proterozoic gneiss, sample 5LT321, from Elhead Mtns, Colorado (Leat et al.,1988).

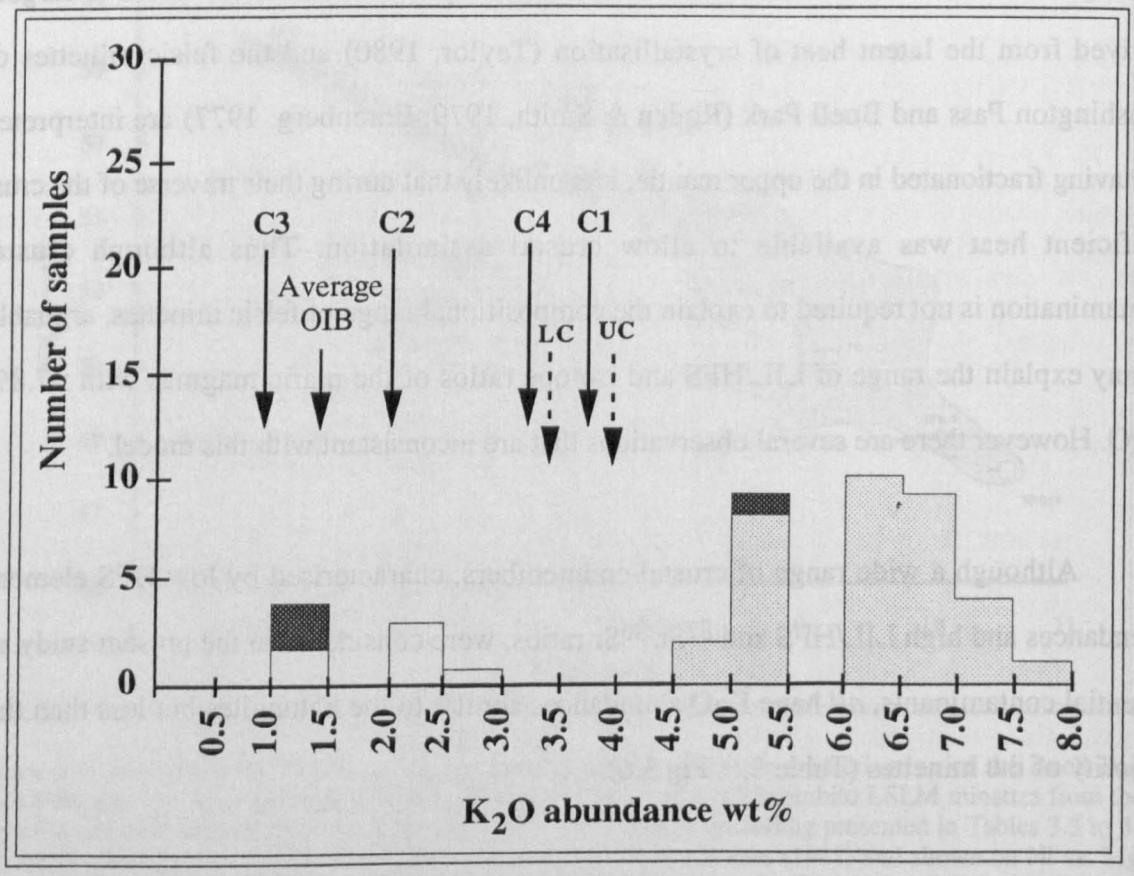


**Figure 3.6.** $K_2O$ abundances of the Navajo intrusives: light grey, minettes; dark grey, melanephelinites; white, katungites. Also shown are the $K_2O$ abundances for the various crustal lithologies C1-C4 (see Table 3.6), the value for average OIB (Sun & McDonough, 1989) and both lower and upper crust (LC, UC; Taylor & McLennan, 1985).

Therefore bulk contamination of katungite with crustal endmembers C1-C4 in any proportions would be unable to generate the high $K_2O$ characteristics of the minettes. Furthermore as both katungites and minettes are highly enriched in trace elements relative to most crustal lithologies, they are insensitive to the effects of crustal contamination. Although crustal contamination of katungite by C1-C4 is unable to reproduce the *entire* geochemical variation of the minettes, those variations that can be generated require between 75 and 95% addition of the crustal endmember to produce the most enriched mafic minette, NM-32. Ormerod et al (1988), Thompson et al (1989), and Leat et al (1991) have also demonstrated that crustal contamination of OIB-type basaltic, mantle-derived, magmas require ≥80% contribution from the crustal endmember to generate similarly enriched magmas. Clearly the resultant magma would no longer retain primitive characteristics such as high Ni, Cr and Mg# as are characteristic of the Navajo minettes (Section 3.2.1). Finally the Navajo intrusives represent small volume volatile-rich magmas which on the basis of the structure of their diatremes (Roden & Smith, 1979; Ehrenberg, 1979) are interpreted to have ascended very rapidly from mantle depths to the surface, perhaps too rapidly to experience significant crustal assimilation. It is concluded that neither the mafic or felsic minette compositional characteristics can be adequately explained by crustal contamination of katungite or OIB-like mantle-derived magmas.

### 3.2.4: Geochemical Variation within the Primitive Magmas:

Those Navajo samples with ≥7.8% MgO have been shown to represent primitive magmas in the preceding discussion and it must be concluded therefore that the range of major and trace element and isotope compositions of these samples are inherited from the mantle and reflect either variations in source composition or processes operating in the mantle. The following sections use only these primitive magmas to identify the processes operating in the mantle beneath the Colorado Plateau. Additional data for the Hopi Buttes nephelinites and San Francisco Peaks basalts from the central Colorado Plateau and its periphery respectively (Alibert et al.,1986; Fitton & Kempton unpub data) and the Geronimo alkali basalts, southern Basin & Range (Kempton, 1987), assumed to be typical of young asthenosphere-derived Basin & Range basalts, are incorporated into the discussion. These

extend the magmatic record of the Colorado Plateau from the Oligo-Miocene, represented by the NVF, to the late Miocene-early Pliocene and allow long-term temporal variations in magma composition to be identified.

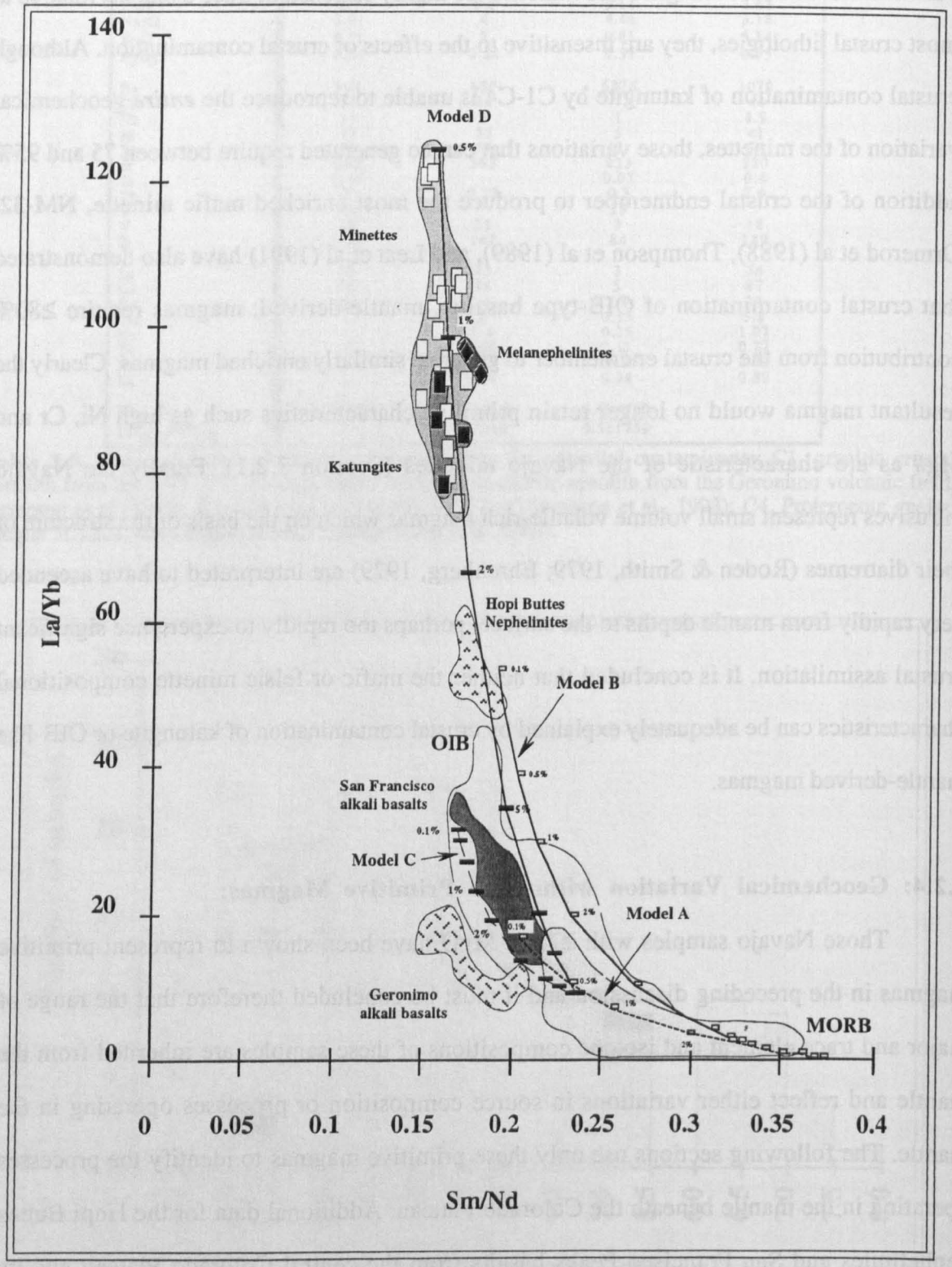


**Figure 3.7.** Variation of La/Yb with Sm/Nd for the Navajo intrusives and representative samples from the Hopi Buttes and San Francisco volcanic fields (Alibert et al., 1986)of the central Colorado Plateau, the Geronimo volcanic field of the southern Basin & Range (Kempton et al., 1987) and the fields for MORB and OIB. Model curves are for melting of the appropriate source by the melt mode given in Table 3.7 and above. Model A & B REE compositions are for depleted and primitive mantle source regions respectively (McKenzie & O'Nions, 1991), while the source mineralogy and melt modes are adapted from Bradshaw (1991). Models C & D taken from Bradshaw (1991). The variation of La/Yb within the Navajo intrusives would be consistent with between 0.5-1.5% melting of a LREE enriched source in the presence of residual garnet.

Figure 3.7 illustrates the variation of La/Yb with Sm/Nd for the Colorado Plateau volcanics with the fields for both MORB and OIB shown for reference. This plot clearly shows the great range in La/Yb, from 15-125, in magmas of the central Colorado Plateau with the NVF showing both the highest values and the greatest range. Superimposed on this diagram are four melting models based on the batch partial melting equation of Allegre & Minster (1978). The source composition, mineralogy and the melt modes used in the calculation of the melt curves are presented in Table 3.7.

| Source Composition | | | | | Source Mineralogy | | | | | Melt Mode | | | |
|---|---|---|---|---|---|---|---|---|---|---|---|---|---|
| Model | A | B | C | D | | A | B | C | D | A | B | C | D |
| La | 0.206 | 0.55 | 1.70 | 2.2 | Ol | 0.6 | 0.6 | 0.6 | 0.6 | 0.1 | 0.1 | 0.1 | 0.1 |
| Nd | 0.815 | 1.08 | 1.55 | 4.6 | OPX | 0.23 | 0.23 | 0.2 | 0.23 | 0.3 | 0.3 | 0.1 | 0.3 |
| Sm | 0.299 | 0.35 | 0.37 | 1.1 | CPX | 0.12 | 0.12 | 0.15 | 0.12 | 0.55 | 0.55 | 0.5 | 0.55 |
| Yb | 0.347 | 0.372 | 1.55 | 2.2 | GT | 0.05 | 0.05 | | 0.05 | 0.05 | 0.05 | | 0.05 |
| | | | | | SP | | | 0.05 | | | | 0.3 | |

**Table 3.7.** Source REE composition (ppm), mineralogy and melt modes for modelling presented in Fig 3.7. Models A and B are the depleted and primitive mantle compositions of McKenzie & O'Nions (1991) while source mineralogy and melt modes are adapted from Bradshaw (1991) and McKenzie & O'Nions (1991). Models C and D are for melting of LRE element enriched spinel amd garnet-bearing sources taken from Bradshaw (1991).

Model A involves melting a depleted source (McKenzie & O'Nions, 1991) in the garnet stability field and clearly this is incapable of reproducing either the La/Yb or Sm/Nd fractionation in the NVF intrusives, even at very low degrees of partial melting. Varying the mineral melting mode or the inclusion phlogopite in the model has a minimal effect on the degree of REE fractionation. Similarly even very small degree melts derived from a primitive source (McKenzie & O'Nions, 1991) in the garnet stability field, model B in fig 3.7, do not reproduce the extreme REE fractionation of the NVF intrusives. It is clear from both models that the Navajo intrusives cannot be derived from either a depleted or primitive mantle source region.

Model C involves the melting of a spinel-bearing, mildly LREE enriched mantle source calculated from the inversion of Colorado River Trough basalts (Bradshaw, 1991). This adequately reproduces the La/Yb and Sm/Nd variations of the San Francisco Peaks basalts by 0.1-5% melting, implying that they may be derived from an enriched spinel-

bearing mantle source. However it cannot generate the very high La/Yb ratios of either the Hopi Buttes nephelinites or the intrusives of the NVF. Finally, model D represents melting of enriched garnet-bearing lherzolite taken from Bradshaw (1991). In this model the range of La/Yb ratios of the NVF intrusives can be reproduced by 0.5-1.5% melting of the source given in Table 3.7.

The melting calculations presented in Fig 3.7 illustrate the degree of REE fractionation in the Navajo intrusives can only be generated by small and variable degrees of partial melting (0.5-1.5% assuming a source with 5% garnet) of a trace element-enriched mantle source region with garnet as a residual phase. However within the minettes and the NVF in general there is considerable isotopic and trace element variation, as illustrated in Fig 3.1, inconsistent with a homogenous mantle source for the NVF magmas. This isotopic and trace element variation is most effectively illustrated in Fig 3.8 where the decrease in $^{87}Sr/^{86}Sr$ with Ba/Nb, characteristic of the Navajo minettes and katungites, is compared with Geronimo alkali basalts, typical of post 5Ma Basin & Range basalts.

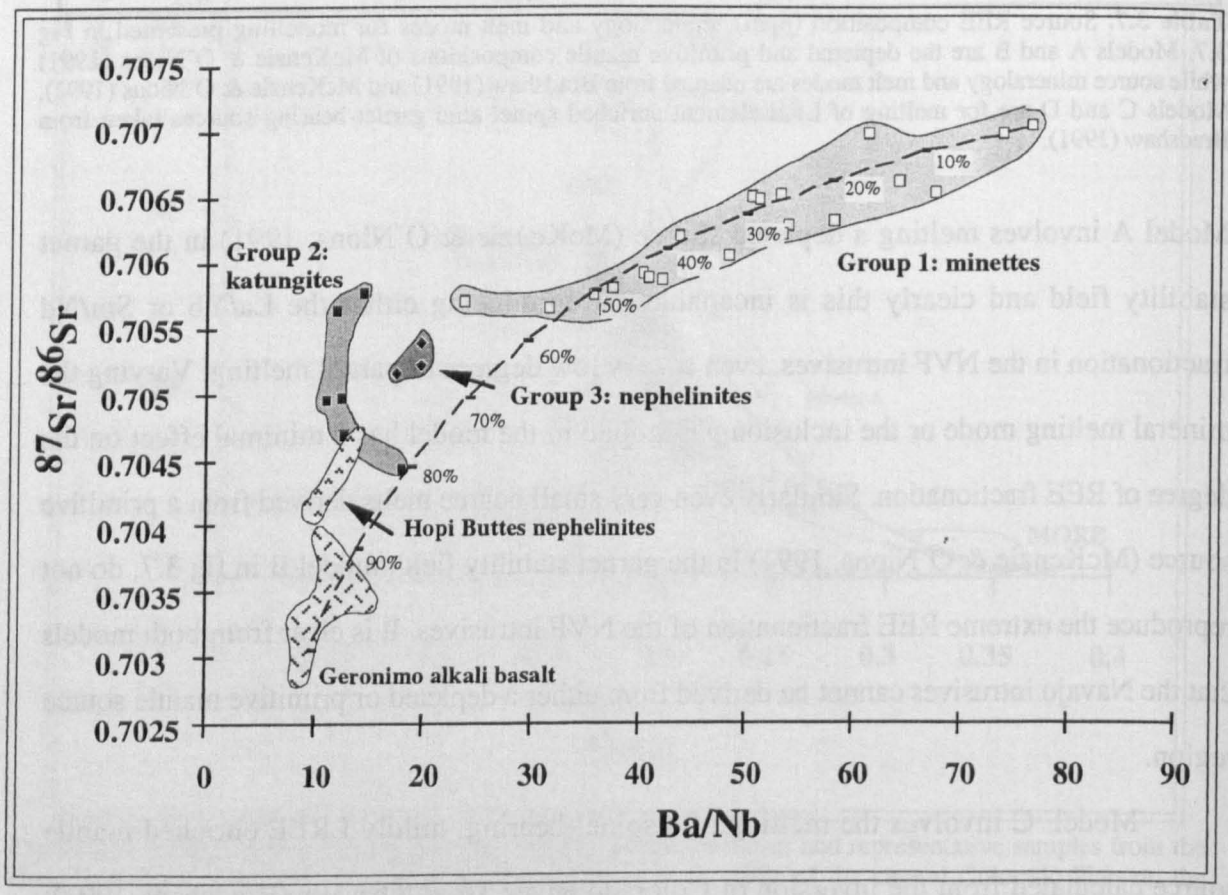


**Figure 3.8.** $^{87}Sr/^{86}Sr$ verus Ba/Nb. Calculated mixing curve between high $^{87}Sr/^{87}Sr$ minette endmember NM-32 and low $^{87}Sr/^{86}Sr$ post 5Ma Basin & Range basalt shows that 50% addition of the low $^{87}Sr/^{86}Sr$ magmas to NM-32 is required to reproduce the variations in both trace element and isotope ***ratios*** of the latter. Greater degrees of contamination of NM-32 is required to reproduce the Navajo nephelinites and katungites. Data for Geronimo and Hopi Buttes from Kempton & Fitton (unpubl data) and Alibert et al., (1986).

Previous investigations (Perry et al.,1987; Davis, 1991; Fitton et al.,1991; Thompson et al 1989; 1990) have identified similar trends in mid to late-Cenozoic basalts of the western United States and attributed them to an increasing contribution from asthenosphere-derived melts to magmatism. A possible mixing curve based on this model, with Geronimo alkali basalts representing post 5Ma asthenosphere-derived magmas, is also illustrated in Fig 3.8. Superficially this diagram suggests that the compositional range of Navajo magmas may be explained by an increasing contribution from asthenosphere-derived melts to a minette-like magma. However such a model cannot account for the elemental abundances of the Navajo samples. This is illustrated in Fig 3.9, a plot of Ba/Nb vs. Nb abundance.

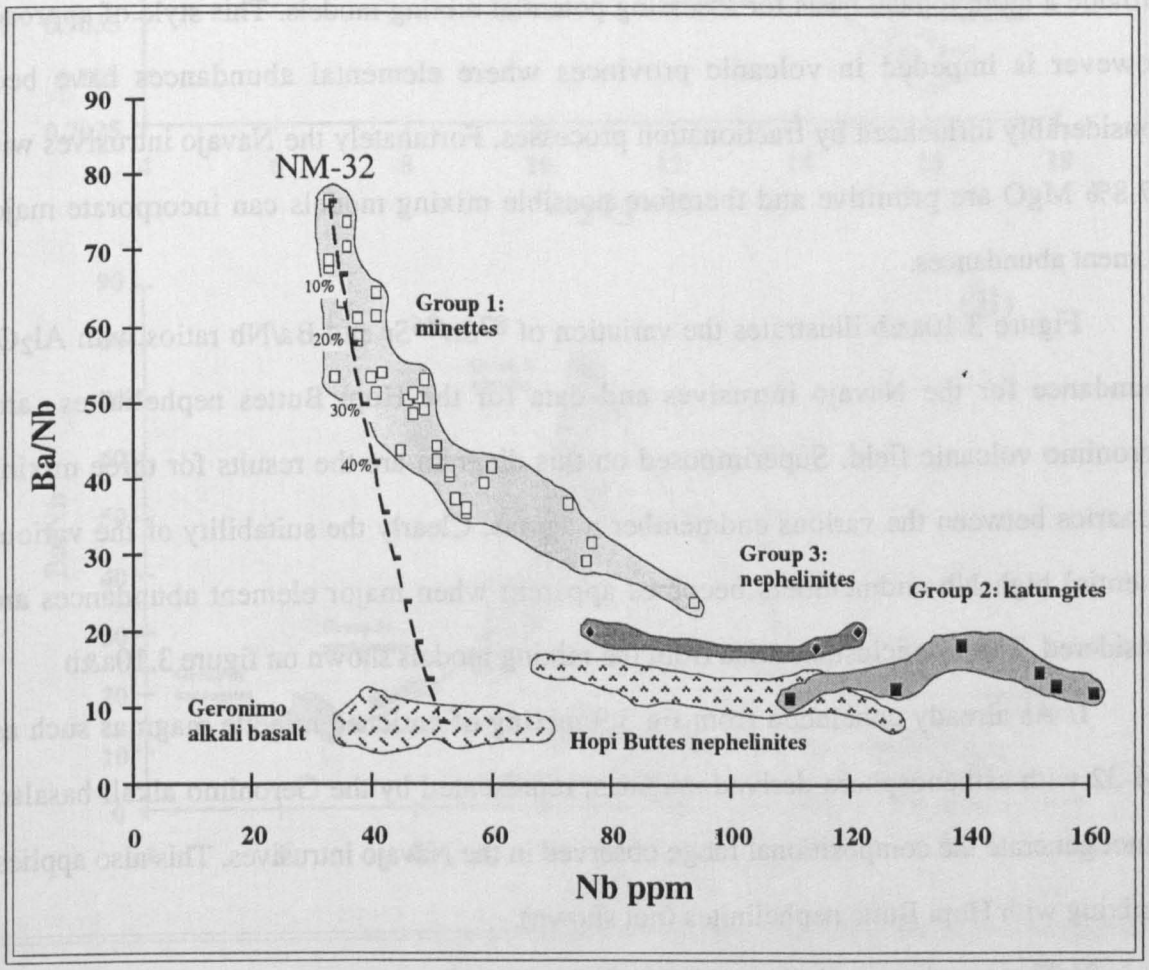


**Figure 3.9.** Ba/Nb versus Nb ppm for Navajo and Hopi Buttes magmas. Mixing curve between low-Nb minette (NM-32) and average post 5Ma Basin & Range average basalt highlights the inability of such mixing, as proposed by Alibert et al (1986), to generate the trace element abundances of the Navajo intrusives. Data for Geronimo and Hopi Buttes from Kempton & Fitton (unpubl data) and Alibert et al (1986).

Here data for the same samples are plotted and compared to the same mixing model illustrated in Fig 3.8. It is quite clear that the minettes trend toward much higher Nb

abundances at low Ba/Nb ratios, that part of the diagram occupied by the katungites and the Hopi Buttes nephelinites. Thus a simple model involving mixing between asthenosphere-derived melts, as represented by the Geronimo alkali basalts, and enriched minette magmas is inapplicable.

If the range of minette compositions does result from mixing of primary magmas then ratio-ratio plots such as Fig 3.8 do not clearly differentiate between the various high-Nb and low $^{87}Sr/^{86}Sr$ magmas, as all the potential high-Nb end-members can reproduce the range of minette trace element and isotope *ratios* . It is the failure to reproduce major and trace element abundances where individual models fail and as such, ratio-abundance plots provide a more logical basis for assessing potential mixing models. This style of approach however is impeded in volcanic provinces where elemental abundances have been considerably influenced by fractionation processes. Fortunately the Navajo intrusives with >7.8% MgO are primitive and therefore possible mixing models can incorporate major element abundances.

Figure 3.10a&b illustrates the variation of $^{87}Sr/^{86}Sr$ and Ba/Nb ratios with $Al_2O_3$ abundance for the Navajo intrusives and data for the Hopi Buttes nephelinites and Geronimo volcanic field. Superimposed on this diagram are the results for three mixing scenarios between the various endmember magmas. Clearly the suitability of the various potential high Nb endmembers becomes apparent when major element abundances are considered. Three conclusions arise from the mixing models shown on figure 3.10a&b

1/ As already concluded from fig 3.9 mixing of enriched minette magmas such as NM-32 with asthenosphere-derived magmas, represented by the Geronimo alkali basalts, cannot generate the compositional range observed in the Navajo intrusives. This also applies to mixing with Hopi Butte nephelinites (not shown).

2/ The trend towards low $Al_2O_3$ defined by the minettes implies the high Nb endmember must also be characterised by low concentrations of $Al_2O_3$ and on the Colorado Plateau such magmas are represented by the Navajo katungite magmas. Indeed the major and trace element and isotope compositions of the minettes are consistent with up to 50% addition of a katungite magma to the minette NM-32.

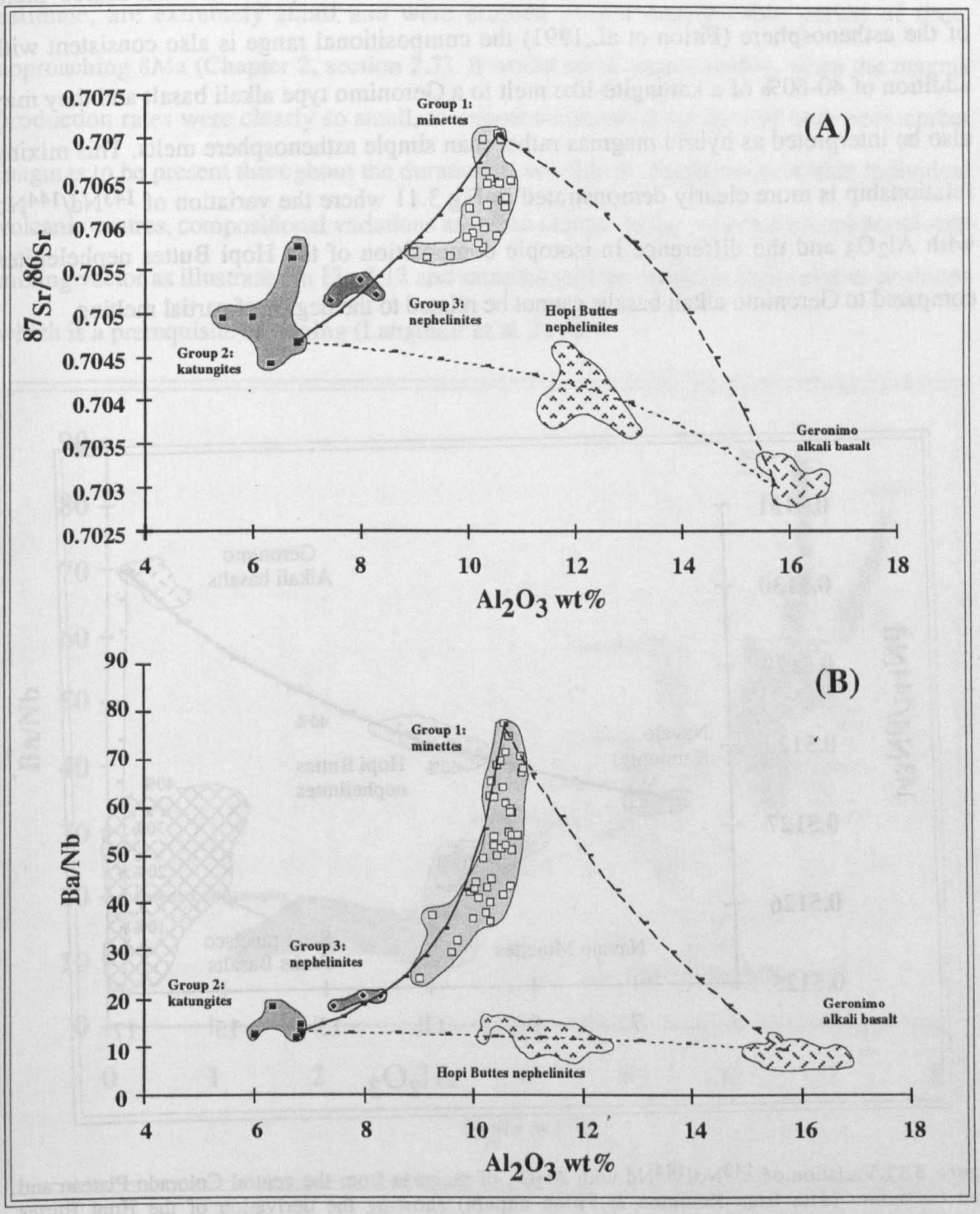


**Figure 3.10.** Calculated mixing arrays for the low-Nb minette NM-32 with average High-Nb post 5Ma Basin & Range basalt(long dashes) and Navajo katungite AWL-5-86 (solid line) showing the inability of minette-'OIB' mixing to reproduce the range of minette elemental abundances and the possibility minette-katungite magma interaction. Also shown is a mixing array for average post 5Ma Basin & Range OIB-like alkali basalt with a Navajo katungite AWL-5-86 (short dashes) demonstrating the ability to reproduce the Hopi Butte nephelinites by contamination of the katungite endmember with 40-60% of the post 5Ma Basin & Range OIB-like basalt. Fields for Geronimo, representative of post 5Ma Basin & Range basalts, and Hopi Buttes based on data from Kempton & Fitton (unpubl data) and Alibert et al (1986). **A)** $^{87}Sr/^{86}Sr$ versus $Al_2O_3$. **B)** Ba/Nb verus $Al_2O_3$.

3/ Although the Hopi Buttes have previously been interpreted as small degree melts of the asthenosphere (Fitton et al.,1991) the compositional range is also consistent with addition of 40-60% of a katungite-like melt to a Geronimo type alkali basalt and they may also be interpreted as hybrid magmas rather than simple asthenosphere melts. This mixing relationship is more clearly demonstrated in Fig 3.11 where the variation of $^{143}Nd/^{144}Nd$ with $Al_2O_3$ and the difference in isotopic composition of the Hopi Buttes nephelenites compared to Geronimo alkali basalts cannot be related to the degree of partial melting.

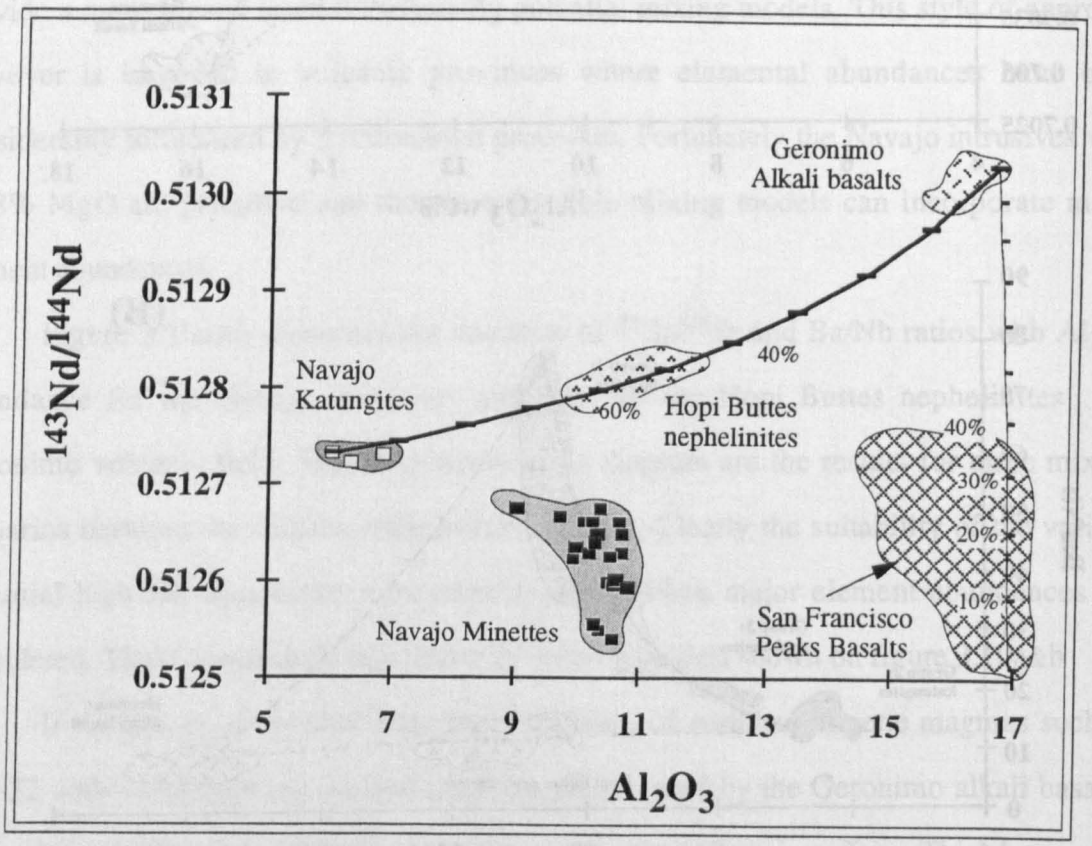


**Figure 3.11.** Variation of $^{143}Nd/^{144}Nd$ with $Al_2O_3$ of magmas from the central Colorado Plateau and from Geronimo (data from Kempton & Fitton unpubl) showing the derivation of the Hopi Buttes nephelinites by mixing of isotopically distinct katungite and Geronimo endmember magmas, the latter representing western United States asthenosphere-derived basalt. Basalts from the San Frnacisco Peaks, although having major element abundances influenced by fractionation processes, can be modelled as small volume melts derived from an enriched spinel-bearing lithosphere contaminated by up to 40% of an asthenosphere-derived alkali basalt.

Although Figs 3.10 & 11 suggest the range of Navajo magmas may result from mixing of katungite and minette endmember magmas there are several observations which are inconsistent with such a hypothesis.

The relative volumes of the minette and katungite magmas, although difficult to estimate, are extremely small and were erupted over a considerable period of time, approaching 8Ma (Chapter 2, section 2.7). It would seem unreasonable, when the magma production rates were clearly so small, to expect sufficient quantities of both endmember magmas to be present throughout the duration of volcanism. Furthermore within individual volcanic centres, compositional variations are often oblique to the expected katungite-minette mixing vector as illustrated in Fig 3.12 and samples seldom maintain their relative positions which is a prerequisite of mixing (Langmuir et al.,1978).

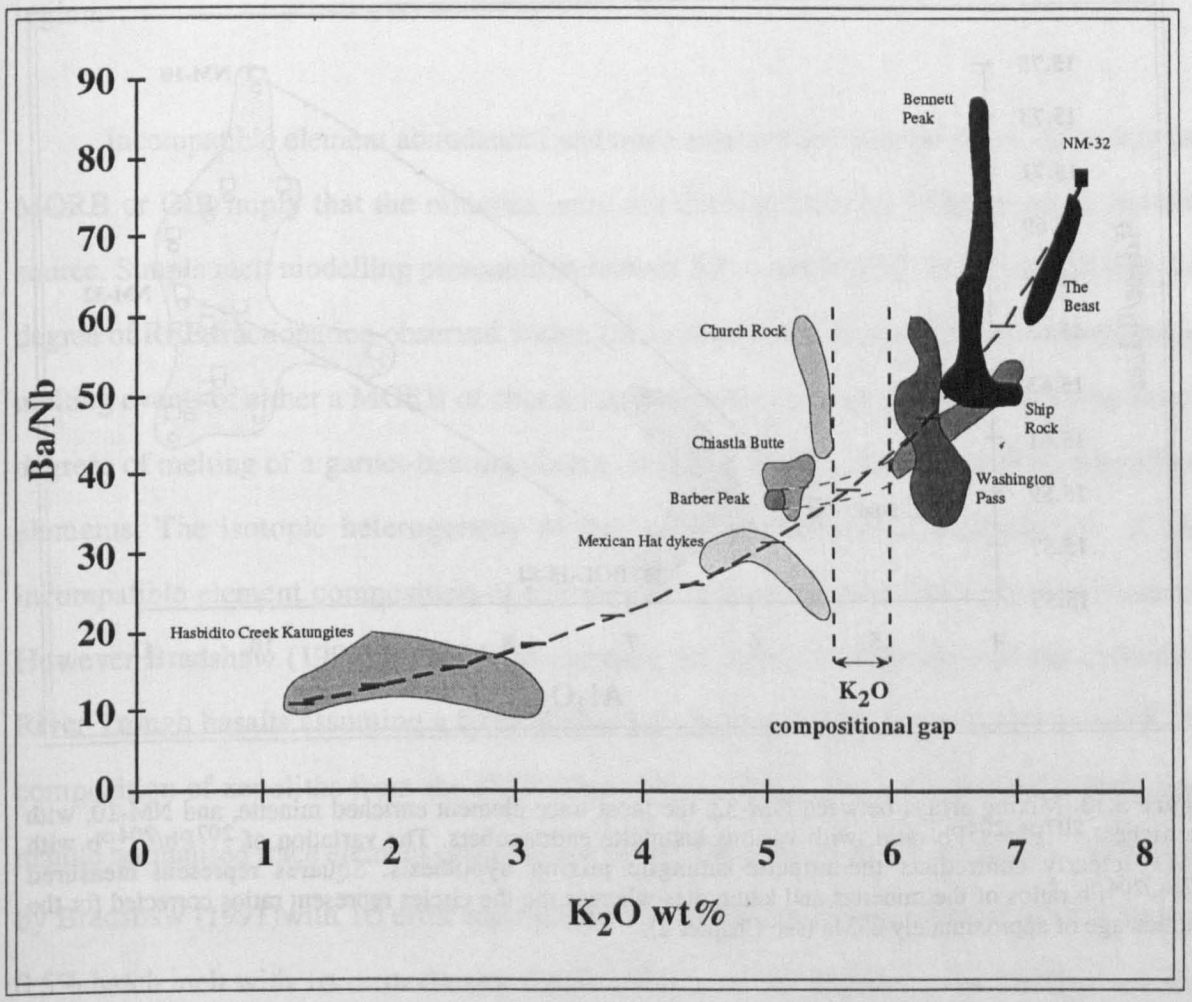


**Figure 3.12.** Variation of Ba/Nb with $K_2O$ illustrates how the majority of volcanic centres within the NVF show variations oblique to the calculated mixing array between NM-32 and AWL-5-86. Furthermore although there is a complete range in Ba/Nb there is a small but distinct compositional gap in $K_2O$ between 5.5-6%. Both these observations are inconsistent with simple mixing.

In addition although most elements show continuous variations, within the minettes there is a compositional gap in $K_2O$, clearly shown in Figs 3.6 and 3.12, again inconsistent with

simple magma mixing. However perhaps the most conclusive evidence against magma mixing is shown in Fig 3.13 where the variation of $^{207}Pb/^{204}Pb$ with $Al_2O_3$ abundance is illustrated for the minette and katungite groups. Not only does NM-32, normally the most enriched minette, have a relatively low $^{207}Pb/^{204}Pb$ ratio but the field for minettes is vertical, quite different from the almost subhorizontal arrays calculated for mixing between katungite and minette.

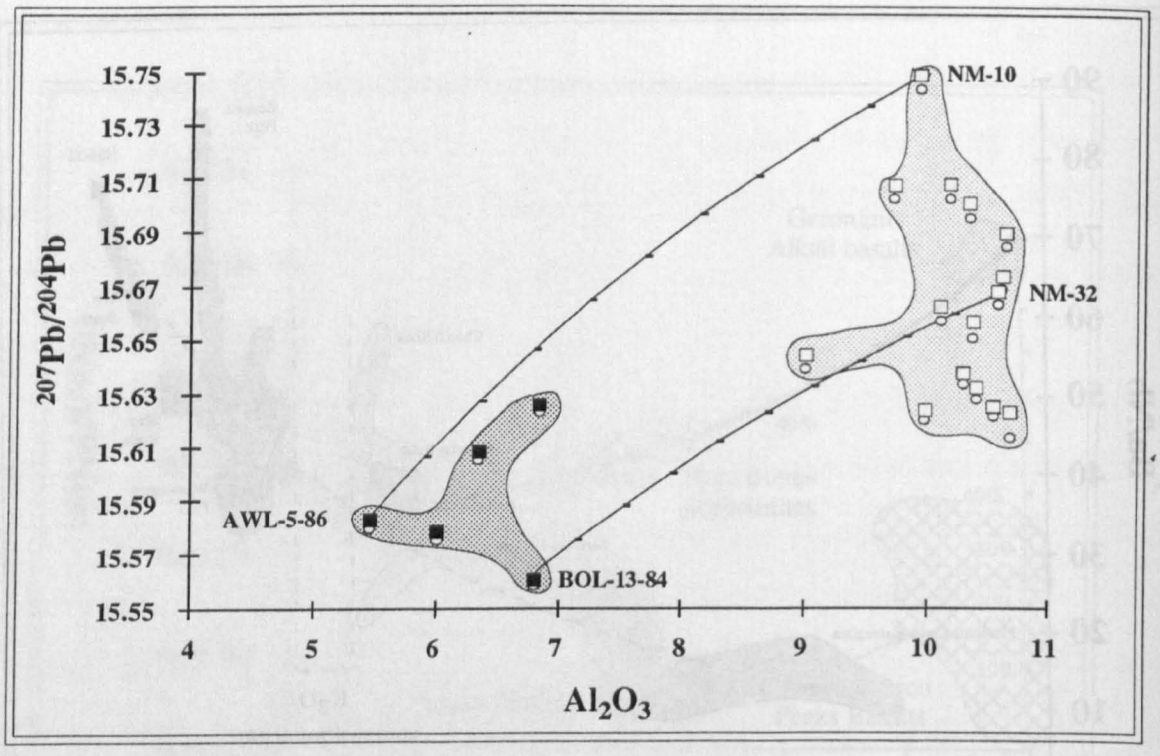


**Figure 3.13.** Mixing arrays between NM-32, the most trace element enriched minette, and NM-10, with the highest $^{207}Pb/^{204}Pb$ ratio, with various katungite endmembers. The variation of $^{207}Pb/^{204}Pb$ with $Al_2O_3$ clearly contradicts the minette-katungite mixing hypothesis. Squares represent measured $^{207}Pb/^{204}Pb$ ratios of the minettes and katungites whereas the the circles represent ratios corrected for the eruption age of approximately 25Ma (see Chapter 2).

As simple mixing of katungite and minette magmas cannot reproduce the range of Navajo intrusives an alternative model whereby the range of Navajo intrusives were derived from a heterogeneous mantle source region is explored in the following discussions.

### 3.2.5: Nature and location of Minette and Katungite Mantle Source Regions: Asthenosphere versus Lithosphere:

Recognition of two distinct endmember magma types within the NVF might initially suggest melt generation within two discrete mantle source regions. However there is an almost complete range in compositions between minette and katungite which cannot be related to mixing of hypothetical 'endmembers' and may reflect melting of a compositionally heterogeneous source. Before discussing the process that might result in a compositionally heterogeneous source it is first pertinent to address the nature and location of that source region.

Incompatible element abundances and trace element and isotope ratios distinct from MORB or OIB imply that the minettes were not derived from an asthenospheric mantle source. Simple melt modelling presented in section 3.2.4. and Fig 3.7 demonstrated that the degree of REE fractionation observed within the minettes was inconsistent with single stage melting events of either a MORB or chondritic source and can only be reproduced by small degrees of melting of a garnet-bearing source enriched in the LRE and other incompatible elements. The isotopic heterogeneity of the minettes prevents a determination of the incompatible element composition of the minette source by inversion of trace elements. However Bradshaw (1991) was able to estimate the source composition of the Colorado River Trough basalts assuming a fixed source La abundance of 2.2ppm based on the REE composition of xenoliths from the NVF (Ehrenberg, 1982a). Fig 3.14 shows the primitive mantle normalised trace element composition of the Colorado River Trough source estimated by Bradshaw (1991)with $1\sigma$ error represented by the dark shading. Also shown is a simple 0.5% batch melt with $1\sigma$ error (heavy stipple) of this source. Close agreement between the calculated melt and minette endmember NM-32 suggests the source of the Colorado River Trough basalts and Navajo minettes may be very similar, characterised by enrichments in the incompatible elements and relative depletions in Nb and Ta. The elevated $^{87}Sr/^{86}Sr$ and low $^{143}Nd/^{144}Nd$ ratios require time integrated high Rb/Sr and low Sm/Nd and therefore a stable source, isolated from the convecting asthenosphere, such as the lithosphere, and the minette source is therefore interpreted as lying within sub-continental mantle lithosphere.

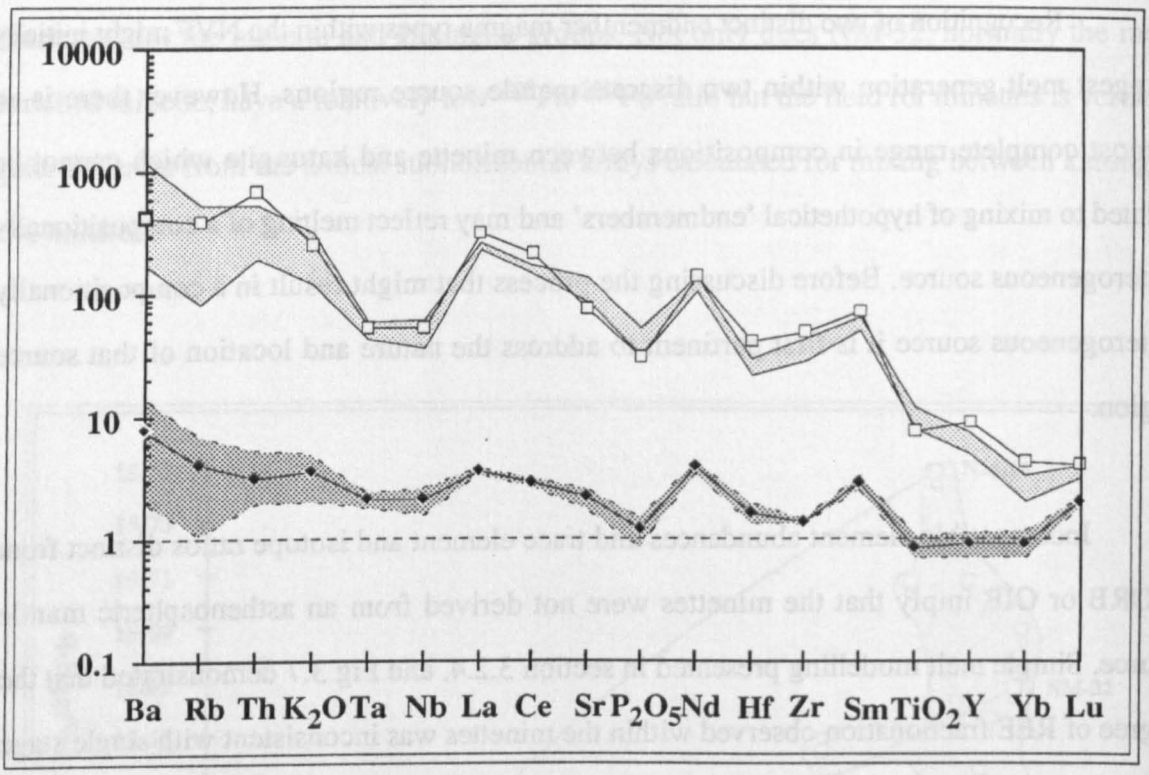


**Figure 3.14.** Mantle-normalised composition of minette endmember NM-32, open squares, compared to the calculated composition of a 0.5% melt, light shading, derived from the group 3 Colorado River Trough basalt lithospheric mantle source region calculated by Bradshaw (1991). Filled diamonds represent the mean composition of the source with 1s errors represented by the dark shading. Abundances of La, Nd, Sm and Yb taken from the 'initial model' of Bradshaw (1991). Source mineralogy and melt mode as for Fig 3.7.

The major and trace element composition of the minettes provide further constraints on the nature of their mantle source region. The minettes represent small degree melts derived from considerable depths, and pressure estimates on entrained xenoliths suggesting depths in excess of 140km. However they are only mildly silica-undersaturated, with $SiO_2$ ≈55%, despite $Mg^{\#}$'s of 70-80. Duncan & Green (1987) showed melts derived from a major element depleted mantle source would be more $SiO_2$-rich and have lower abundances of CaO and $Al_2O_3$ than those from more fertile source regions. High $K_2O$ concentrations of the minettes in conjunction with high Rb/Sr ratios suggest the existence of the hydrous mineral phlogopite in the source region and it is known that $K_2O$ and $H_2O$ also increase the degree of silica saturation of melts (Kushiro, 1975). The geochemical characteristics of the minettes, notably the degree of REE fractionation, have been shown to be inconsistent with melts derived from asthenospheric mantle and they are therefore interpreted as small degree (≈0.5%) melts of a trace element-enriched phlogopite-bearing garnet-lherzolite lithosphere

The location of the katungite source region is more ambiguous. Occurrences of such highly silica-undersaturated potassic katungites are restricted to ancient, Proterozoic or Archean, continental cratonic settings, suggesting their source lies within old subcontinental mantle lithosphere. However the trace element and isotope ratios of at least the NVF katungites bear a number of similarities to asthenosphere-derived OIB magmas (Chapter 2; section 2.6). Yet despite OIB-like trace element ratios, the degree of LRE element enrichment in the NVF katungites is similar to that of the minettes, implying that they too represent small melt fractions of a garnet-bearing source region enriched in the LRE and incompatible trace elements. Furthermore it is important to note that the Navajo katungites are isotopically *enriched* in comparison to the uniform post 5Ma alkali basalts of the western United States (Figs 3.10, 3.11), representative of the asthenosphere beneath this region (Leat et al., 1990; Fitton et al.,1991). Thus, the katungites are clearly derived from a source with time integrated enrichments in the LIL and LRE elements compared to the asthenosphere. The conclusion based on this evidence is that katungites, like the minettes, are also derived from an incompatible element enriched source region located within the sub-continental lithospheric mantle and their apparent similarity to OIB magmas may be related to the style of metasomatism of the lithospheric source region.

Although the katungites are interpreted as products of melting of enriched mantle lithosphere they are unlike the minettes in that they are highly silica-undersaturated ($SiO_2$ 33-36%). At pressures >21kb and subsolidus temperatures, $CO_2$ reacts with olivine and clinopyroxene to form dolomite and orthopyroxene, while at pressures ≥28kb dolomite reacts with orthopyroxene to form magnesite and clinopyroxene (Falloon & Green, 1989; Olafsson & Eggler, 1983; Brey & Green, 1975, 1977). Initial melts of a carbonated mantle are dominated by the breakdown of carbonate phases and are therefore highly silica-undersaturated while rich in MgO, CaO, Sr and as Sr is more compatible than Rb in carbonate, melts will also be characterised by low Rb/Sr ratios. Furthermore melting of a carbonate-rich source in equilibrium with a garnet-bearing restite will also yield $Al_2O_3$-poor magmas with highly fractionated mantle-normalised REE profiles. The composition of katungites from the Colorado Plateau (Chapter 2, section 2.6) are consistent with being

derived from a carbonated source and thus different conditions during melting compared with the minettes.

Melilitites from Namaqualand, although non potassic, are similar in composition to the katungites and have pronounced negative anomalies in $K_2O$ on mantle-normalised trace element profiles (Rogers et al.,1992). The $K_2O$ anomalies in these rocks are attributed to melt generation from a carbonated source in the presence of residual phlogopite. Similar negative $K_2O$ anomalies are observed in the katungites (Chapter 2, section 2.6) along with a Rb anomaly, and these could have similar origins to the Namaqualand melilitites. However the potassic nature of the NVF katungites and the presence of phlogopite phenocrysts in some samples implies that unlike in the generation of melilitite magmas, phlogopite was not entirely residual during their generation. It is proposed therefore that the Navajo katungites are the products of 0.5-1% melting of a carbonated phlogopite-garnet peridotite source located within the sub-continental mantle lithosphere and that melting involved the complete breakdown of carbonate phases and partial breakdown of phlogopite in the presence of a phlogopite and garnet-bearing restite. The presence of carbonate within the mantle lithosphere of the Colorado Plateau is supported from the identification of the carbonate phases dolomite and magnesite, often associated with amphibole and/or phlogopite, within pyrope xenocrysts contained the Garnet Ridge and Red Mesa ultramafic diatremes (McGetchin & Besancon, 1973; Hunter & Smith, 1981; Smith, 1979, 1987).

The contrasting major element composition, notably the degree of silica-saturation, between minette and katungite magmas are attributed to the source mineralogy and nature of the volatile species present during melting. However the spatial distribution of hydrous and carbonated regions within the lithospheric mantle beneath the Colorado Plateau is unknown. The stability fields of phlogopite and carbonate, although not well constrained overlap, a conclusion supported by the presence of carbonate-phlogopite polymineralic inclusions in pyrope xenocrysts derived from the Sub Colorado Plateau mantle lithosphere (Smith, 1987). Xenoliths contained within minette diatremes provide semi-quantative constraints on the location of these source regions beneath the Colorado Plateau. Pressure estimates on xenoliths (Roden et al., 1990; Ehrenberg, 1978, 1982a) from minette diatremes suggest the source region of the latter must be located at approximately 150km depth. Katungites

themselves do not contain xenoliths but the minettes do contain megacrysts, which have been interpreted as precipitates from Fe-Ti rich melts with highly fractionated REE profiles (Ehrenberg, 1982a & b). These yield pressure estimates of approximately 46kb or ≈140km (Roden et al.,1990) and have $^{87}Sr/^{86}Sr$ ratios of ≈0.7037-0.7046 similar to the most isotopically depleted katungites. This suggests that katungites may represent parental magmas to these megacrysts, in which case the source region of katungites must be located at, or greater than, 140km depth. The conclusion based on this rather indirect evidence is that both hydrous and carbonated source regions, although probably patchy, are located within the deep lithospheric mantle of the Colorado Plateau.

As both the minette and katungite 'endmember' source regions are located within the lithospheric mantle it is conceivable that the range of minettes reflect melting of a compositionally variable source. In this scenario carbonate rich regions produce highly silica-undersaturated katungite magmas characterised by within-plate trace element signatures whereas increasingly hydrous regions yield more silica-saturated minette-like magmas with HFS element depletions. The following discussion centres on a possible process that might have given rise to such a compositionally heterogeneous mantle lithosphere.

## 3.3: Lithospheric Mantle Beneath the Colorado Plateau:

Potassic magmas can be broadly divided into high and low Ti varieties (Thompson, 1977; Rogers, 1992). These have been attributed to melting of mantle source regions enriched by asthenosphere-derived melts and fluids/melts derived from subducted sediments respectively (Rogers, 1992; Rogers et al.,1985, 1992). The recognition of both types of primary potassic magma in the NVF implies a complex trace element enrichment history for the lithosphere beneath the Colorado Plateau.

### 3.3.1: Trace element enrichment of the lithosphere:

Although there is a wide range in trace element composition within the NVF there are two distinct endmember magma types, the salient features of which are shown in Table 3.8 and Fig 3.15.

| | Average Katungite | Minette NM-32 |
|---|---|---|
| $SiO_2$ | 34.16 | 54.95 |
| $TiO_2$ | 4.17 | 1.33 |
| $Al_2O_3$ | 6.38 | 10.58 |
| $Fe_2O_3$ | 13.27 | 6.44 |
| MnO | 0.19 | 0.09 |
| MgO | 17.6 | 7.84 |
| CaO | 12.51 | 7.19 |
| $Na_2O$ | 1.37 | 2.01 |
| $K_2O$ | 2.44 | 7.53 |
| $P_2O_5$ | 1.5 | 1.07 |
| Ba | 1902 | 2526 |
| Cr | 588 | 232 |
| Nb | 140 | 33 |
| Ni | 562 | 238 |
| Pb | 17 | 30 |
| Rb | 86 | 210 |
| Sc | 23 | 10 |
| Sr | 2271 | 1380 |
| Ta | 8.75 | 1.82 |
| Th | 19 | 57.9 |
| U | 5.23 | 13 |
| V | 292 | 137 |
| Y | 32 | 35 |
| Zr | 421 | 459 |
| La | 145 | 189 |
| Ce | 295 | 335 |
| Nd | 126 | 166 |
| Sm | 18.9 | 27.6 |
| Eu | 5.08 | 6.45 |
| Tb | 1.70 | 2.02 |
| Yb | 1.82 | 1.77 |
| Lu | 0.22 | 0.26 |
| $^{87}Sr/^{86}Sr$ | 0.705067 | 0.707051 |
| $^{143}Nd/^{144}Nd$ | 0.512743 | 0.512538 |
| $^{206}Pb/^{204}Pb$ | 19.157 | 19.133 |
| $^{207}Pb/^{204}Pb$ | 15.566 | 15.668 |
| $^{208}Pb/^{204}Pb$ | 38.717 | 39.001 |

**Table 3.8.** Composition of extreme endmember magmas from the Navajo volcanic field represented by average katungite and minette NM-32

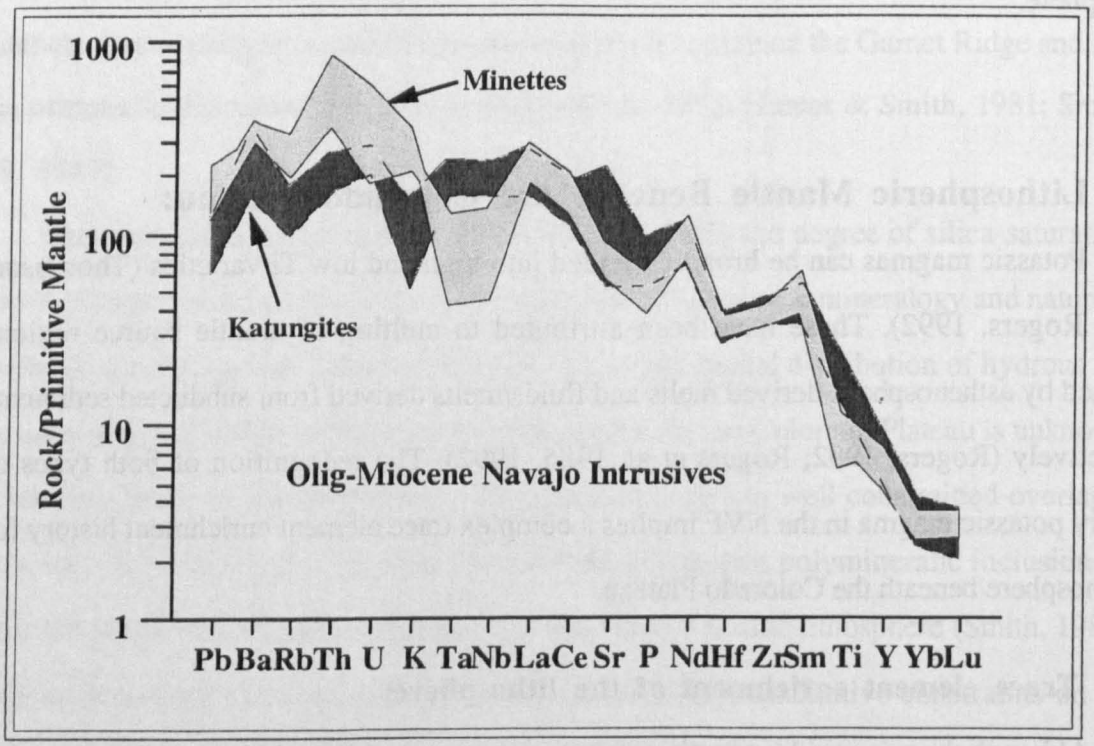


**Figure 3.15.** Mantle normalised trace element profiles of the Navajo minette and katungite endmember magma tpyes.

The Navajo katungites show similar, albeit more extreme, geochemical characteristics to asthenosphere-derived OIB magmas and on a K/Yb vs. Ta/Yb variation diagram shown in Fig 3.16, clearly lie on an extension of the within-plate enrichment trend, defined by the fields for MORB and OIB. Superficially katungites resemble the high-Ti potassic magmas from the Virunga province (Rogers et al.,1992). The absence of negative Nb and Ta depletions in the katungites suggests minimal incorporation of crustal lithologies in their source region. This conclusion is also supported by the low $^{207}Pb/^{204}Pb$ and $^{208}Pb/^{204}Pb$ isotope ratios which lie on the NHRL. Other incompatible trace element ratios of the katungites are also similar to OIB and imply that the katungite source region was enriched in all those elements typically incompatible during melting of the asthenosphere. Thus the metasomatising agent was itself a silicate melt derived from the underlying asthenosphere, similar to the model proposed for the Virunga source region (Rogers et al.,1992). Yet there are differences between the two provinces. The measured Rb/Sr ratios of katungites (0.03-0.06) are less than the Virunga magmas (0.08-0.171) implying either a different enrichment process or a different mineralogical control during melting. The low-$SiO_2$ of the katungites indicates the presence of carbonate during melting as discussed above and it is suggested that the stabilisation of dolomite or even magnesite would preferentially accommodate Sr relative to Rb and so produce low Rb/Sr source ratios. By contrast the Virunga lavas are more $SiO_2$-rich and thus their source region was dominated by a hydrous potassic phase, probably phlogopite, with high Rb/Sr ratios (Rogers et al., 1992). Such different time-integrated Rb/Sr source ratios invoked for the katungite and Virunga mantle source regions are consistent with their measured $^{87}Sr/^{86}Sr$ ratios of 0.704427-0.705768 and 0.705230-0.707094 respectively.

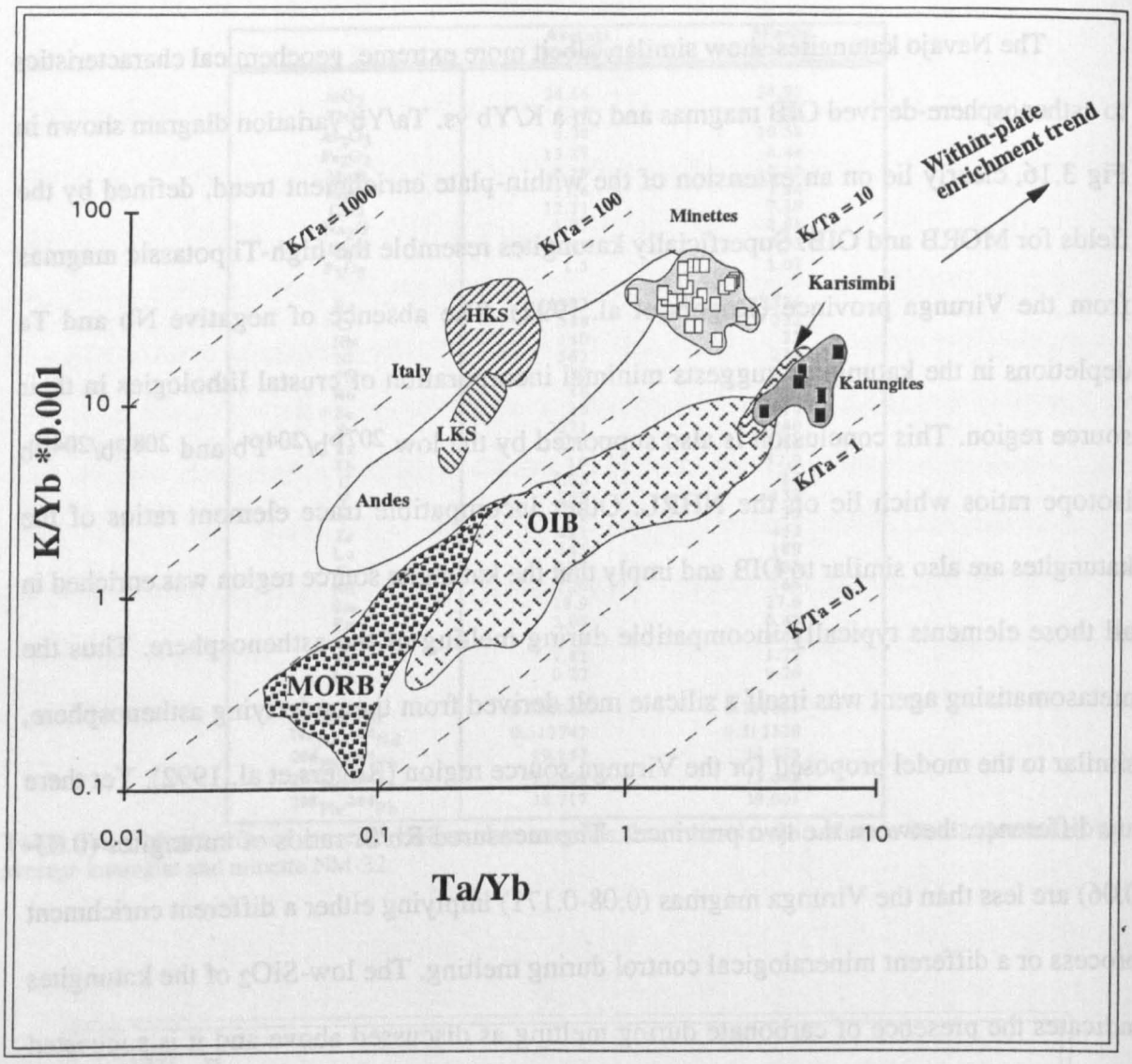


**Figure 3.16.** Variation of K/Yb with Ta/Yb in the mafic potassic -ultrapotassic katungite and minette magmas of the NVF. Also shown for comparison are data for MORB, OIB and the Andes, representative of within-plate oceanic and subduction-related magmatism respectively. Mafic potassic magmas from the low-Ti and High-Ti Italian and Virunga provinces respectively (Roger et al.,1985, 1992) are also shown.

Unlike the katungites, the minettes are clearly displaced above the within-plate trend shown in Fig 3.16. They have K/Ta ratios similar to subduction-related K-rich magmas (eg.Italy; Rogers et al., 1985) but much higher Ta/Yb ratios. Furthermore, in common with the Italian high potassium series magmas (Rogers et al., 1985) the primitive Navajo minettes depart from 'normal' subduction-related magmas in that they have low Sr/Nd ratios that decrease with increasing K/Ta (Fig 3.17).

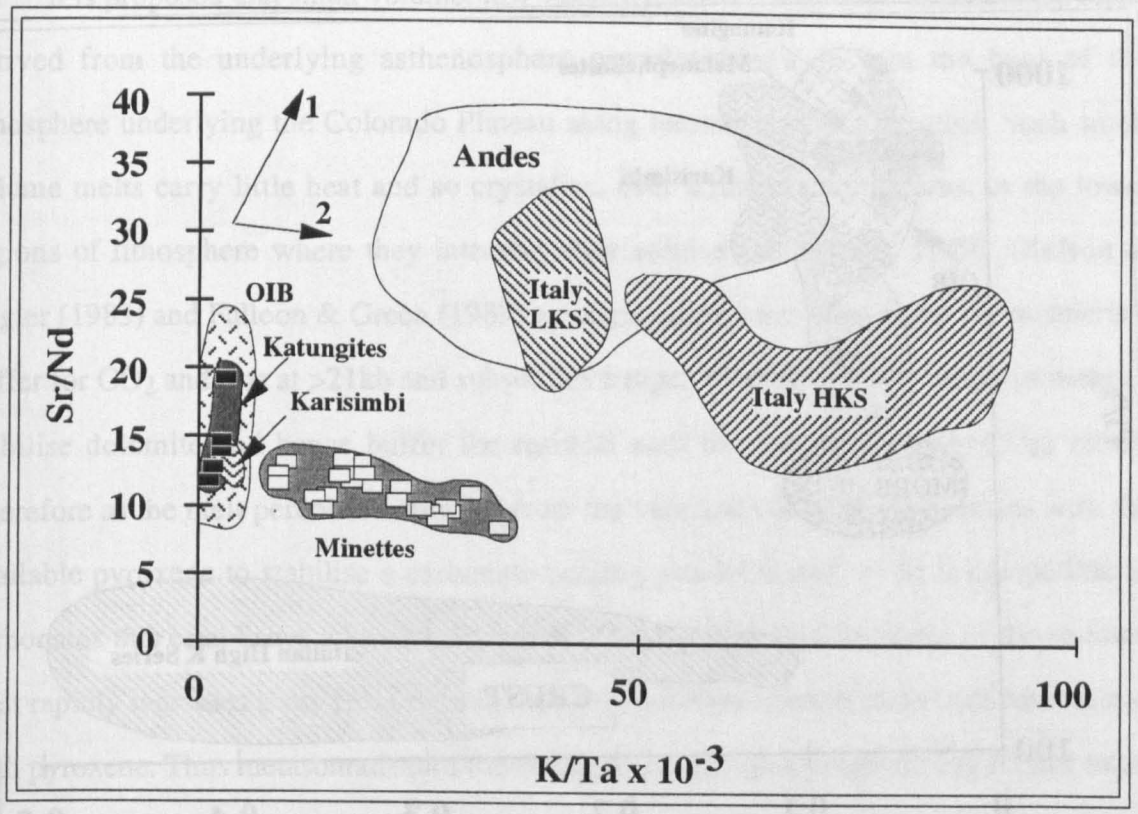


**Figure 3.17.** Variation of Sr/Nd with K/Ta in the Navajo intrusives. Also shown are data for subduction-related magmas from the Andes, Italian potassic volcanics related to the subduction of sediments (Rogers et al., 1985) and within-plate magmas represented by OIB and Karisimbi (Rogers et al., 1992). Vector 1 (top left) represents general direction of fluid-related subduction enrichment whereas vector 2 represents the trend for enrichment related to the subduction of sediments (Rogers et al., 1985).

Such variations in the Italian high potassium series, associated with development of a negative Eu anomaly, have been attributed to the incorporation of sediments in their mantle source (Rogers et al.,1985). Alibert et al (1986) likewise suggested enrichment of the NVF minette source region by the subduction and incorporation of small quantities of pelagic sediments. Eu anomalies are not shown by any of the analyses in this study and although the Pb isotopes are similar to those determined by Alibert et al (1986), certain other aspects of the incompatible trace element variations are also inconsistent with models involving sediment subduction. An example is given in Fig 3.18 which illustrates the variation of Ti/Y with Rb/Ba in the Navajo magmas with the fields for MORB, OIB and crust reservoirs and the potassic magmas from Italy (Rogers et al.,1985) and Karisimbi (Rogers et al.,1992). The Italian high potassium series, derived from a source enriched by subducted sediments, are characterised by low and restricted Ti/Y ratios of 100-200 yet a wide variation in Rb/Ba of 0.1-0.5 producing a sub-horizontal field.

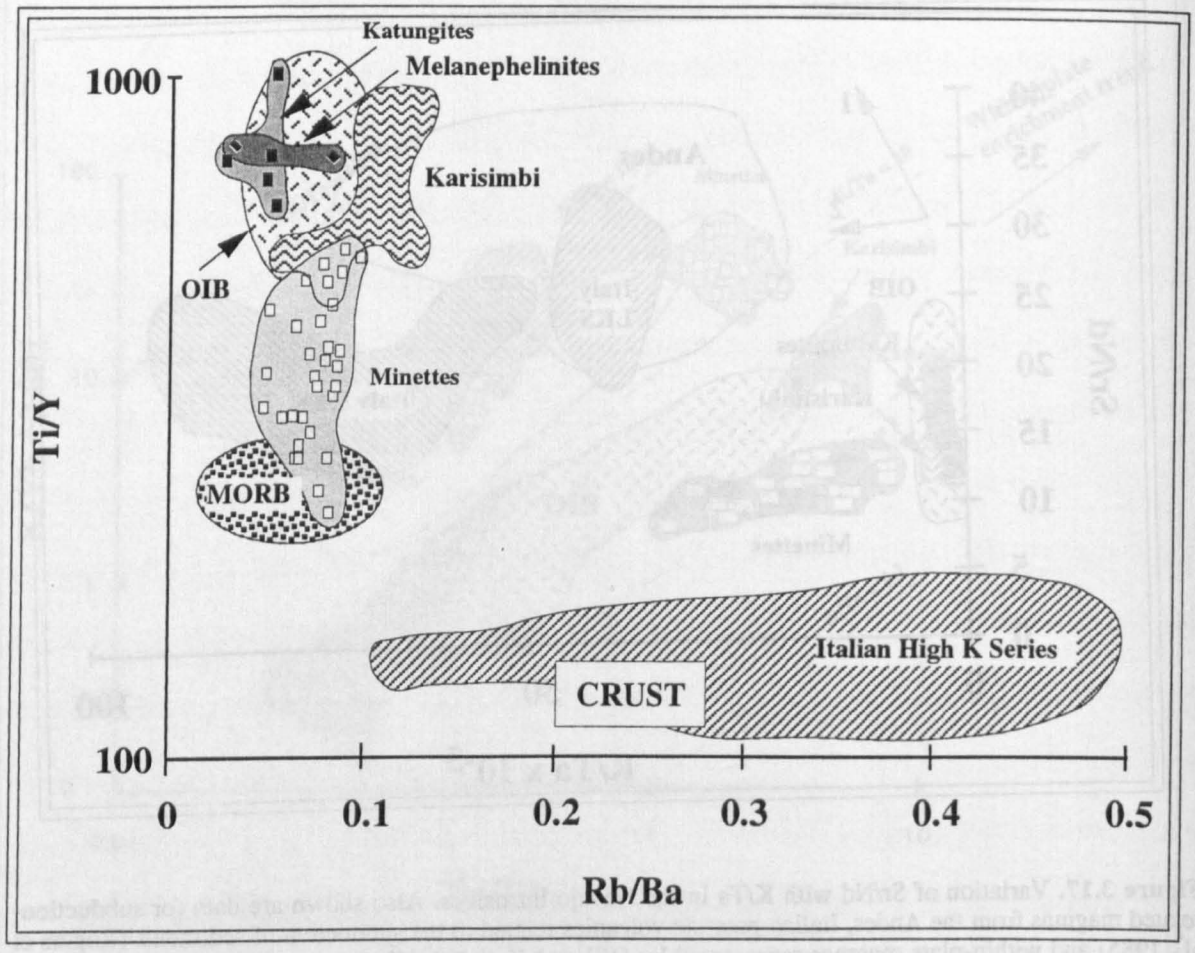


**Figure 3.18.** Variation of Ti/Y with Rb/Ba in the intrusives of the NVF. Also shown are values typical for MORB, OIB and crust. Italian high potassium series volcanics (Rogers et al.,1985) illustrate melts derived from a source enriched by the subduction of sediments whereas the potassic Karisimbi volcanics (Rogers et al., 1992) are derived from a lithospheric mantle source

By contrast the Karisimbi magmas, derived from melt-enriched mantle source are typified by high Ti/Y ratios of 450-950 associated with a low and restricted range in Rb/Ba ratios of 0.05-0.15. The Navajo katungites, like the Karisimbi lavas, are interpreted as products of a melt enriched garnet-bearing lithosphere and have similarly high Ti/Y and low Rb/Ba ratios in keeping with this interpretation. The minettes plot at lower Ti/Y ratios than the katungites but they still have significantly higher values than MORB. Furthermore they also have low and restricted Rb/Ba ratios and define a near vertical trend between MORB and small degree melts. They are therefore interpreted to result from a mafic melt-dominated enrichment process and this process may be related to the enrichment of the katungite source. The following model assumes that the range of NVF intrusives were derived from a common but heterogeneous source region and builds on ideas presented by McKenzie (1989).

It is proposed that small volume, low viscosity, volatile and trace element-rich melts derived from the underlying asthenosphere percolated upward into the base of the lithosphere underlying the Colorado Plateau along narrow conduits or veins. Such small volume melts carry little heat and so crystalise, over a range temperatures, in the lower regions of lithosphere where they intersect their solidus (McKenzie, 1989). Olafson & Eggler (1983) and Falloon & Green (1989) amongst others have shown that the mantle is a buffer for $CO_2$ and that at >21kb and subsolidus temperatures $CO_2$ reacts with pyroxene to stabilise dolomite and hence buffer the residual melt to high $H_2O/(H_2O+CO_2)$ ratios. Therefore as the melt percolates outward from the vein and cools, the $CO_2$ reacts with the available pyroxene to stabilise a carbonate-bearing peridotite and, as Sr is compatible in carbonates this establishes a low Rb/Sr source. The $H_2O/(H_2O+CO_2)$ ratio of the residual melt rapidly increases away from the vein as $CO_2$ continues to undergo subsolidus reaction with pyroxene. Thus metasomatism of the lithospheric wall rock progressively further away from the melt vein is associated with the gradual stabilisation of hydrous, phlogopite-bearing, rather than carbonate-bearing assemblages and consequently is associated with increasing Rb/Sr ratios. The metasomatising agent becomes more fluid-like in nature as it migrates outward and continues to interact with the surrounding mantle and, as the HFS elements Ti, Ta and Nb are less readily transported in fluids than the LIL and LRE elements (Hawkesworth et al., 1984), subsequent enrichment away from the vein is also characterised by the development of LIL/HFS ratios that superficially resemble those of subduction-related magmas. LRE/HRE ratios increase toward the periphery of the enrichment aureole as the LRE's are slightly more mobile than the HRE's in fluids. Such an enrichment process as discussed results in considerable fractionation of Rb/Sr compared to Sm/Nd and over time this source region will develop a wide range in $^{87}Sr/^{86}Sr$ ratios over a relatively restricted range in $^{143}Nd/^{144}Nd$ ratios as is observed for the Navajo magmas. Subsequent melting of this source would yield a range of highly silica-undersaturated to mildly saturated magmas characterised by a range of trace element signatures that resemble within-plate through to subduction-related magmas.

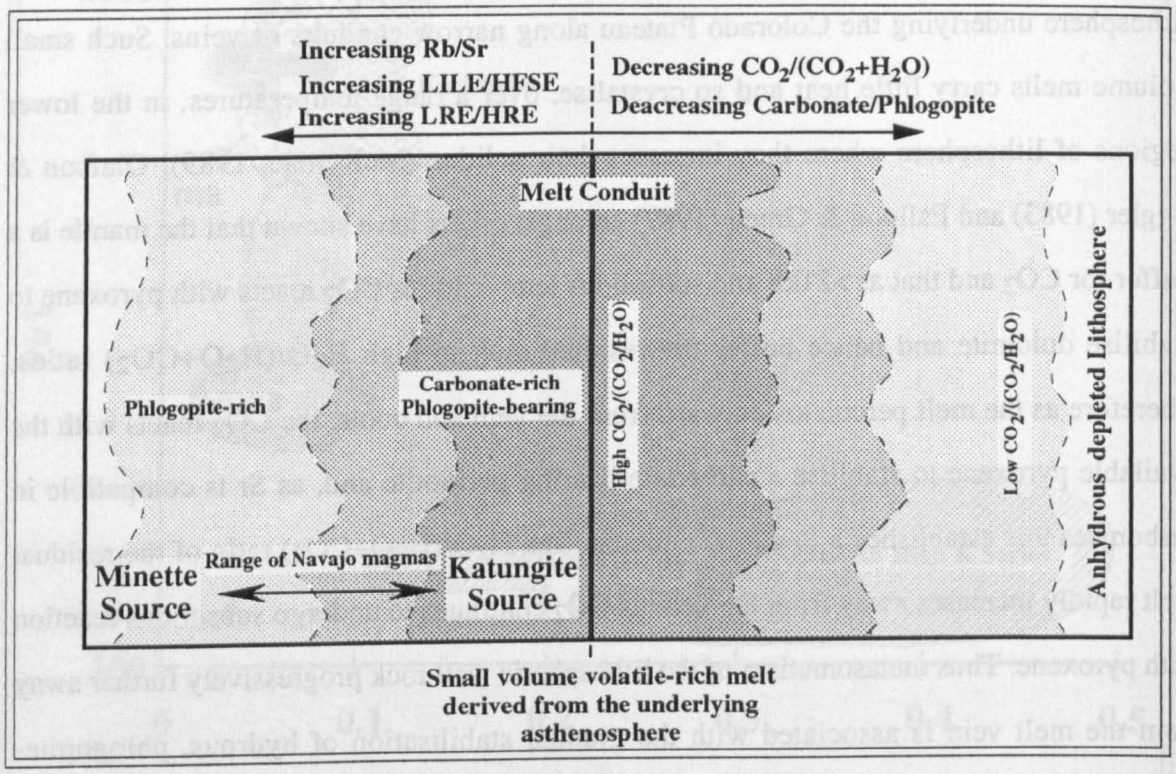


**Figure 3.19.** Proposed enrichment of the mantle beneath the Colorado Plateau resulting from the upward migration of small volume trace element and volatile enriched asthenosphere-derived melts. Crystallisation of a carbonate- and phlogopite-bearing assemblage near the vein yields a source with high CO2/(CO2+H2O), low Rb/Sr and high abundances of the HFS elements. Away from the vein the metasomatic agent gradually becomes more fluid-like with low CO2/(CO2+H2O) ratios and crystallises phlogopite-bearing assemblage with high Rb/Sr and low abundances of the HFS elements. Melting of the carbonate-phlogopite peridotite yields the highly silica undersaturated katungite magmas whereas melting of the increasingly phlogopite-rich peridotite yields more silica-saturated minette magmas.

Fig 3.19 summarises the model discussed above and shows the proposed source regions for the range of Navajo magmas. It is important to note that the 'subduction-trace element signatures' of the minette endmember in this scenario are not related to subduction but to percolation and interaction of asthenosphere-derived melts with lithosphere.

### 3.3.2: Timing of mantle enrichment:

If melt interacted with mantle lithosphere as proposed above, and given the likelihood that this could have occurred as numerous individual events or a quasi-continuous process over a considerable time, the relevance of model ages is questionable. Furthermore during the small degrees of melting invoked for the Navajo magmas Sm/Nd and Rb/Sr in the melts will have been fractionated from their true source ratios. However using a source Sm/Nd

ratio of 0.22, based on the modelling presented in section 3.2.4 and from Bradshaw (1991), yields a range in depleted mantle neodymium model ages ($T_{DM}$) for the Navajo volcanics of 530Ma up to ≈1Ga (see Table 3.9).

| Sample# | Rb | Sr | (87/86)o | Sm | Nd | (143/144)o | $T_{DM}$ Meas | $T_{DM}$ source |
|---|---|---|---|---|---|---|---|---|
| **Minettes** | | | | | | | | |
| 90-NM-5 | 145 | 1232 | 0.706272 | 22.4 | 133 | 0.512664 | 571 | 771 |
| 90-NM-10 | 175 | 1345 | 0.706128 | 21.7 | 126 | 0.512622 | 637 | 843 |
| 90-NM-20B | 188 | 1253 | 0.706785 | 17.5 | 107 | 0.512630 | 600 | 829 |
| 90-NM-21 | 154 | 1234 | 0.706040 | 15.3 | 94.1 | 0.512629 | 598 | 831 |
| 90-NM-22A | 190 | 1278 | 0.706297 | 16.4 | 103 | 0.512705 | 497 | 701 |
| 90-NM-22B | 192 | 1289 | 0.706436 | 15.5 | 102 | 0.512630 | 568 | 829 |
| 90-NM-23 | 199 | 1312 | 0.705978 | 15.9 | 102 | 0.512648 | 557 | 799 |
| 90-NM-25 | 205 | 1373 | 0.705914 | 16.3 | 104 | 0.512660 | 545 | 778 |
| 90-NM-28 | 168 | 1273 | 0.706303 | 17.4 | 113 | 0.512628 | 575 | 833 |
| 90-NM-32 | 210 | 1380 | 0.707051 | 27.6 | 166 | 0.512538 | 723 | 986 |
| 90-NM-34A | 203 | 1587 | 0.706970 | 26 | 164 | 0.512553 | 678 | 961 |
| 09-NM-34B | 202 | 1417 | 0.706971 | 26.2 | 158 | 0.512600 | 644 | 881 |
| 90-NM-35 | 166 | 1195 | 0.706473 | 17.9 | 113 | 0.512594 | 629 | 891 |
| 90-NM-44 | 174 | 1086 | 0.706073 | 32.6 | 209 | 0.512623 | 587 | 841 |
| 90-NM-45B | 140 | 1374 | 0.706200 | 18.4 | 117 | 0.512693 | 506 | 722 |
| 90-NM-46 | 138 | 1544 | 0.706233 | 19.9 | 126 | 0.512675 | 530 | 752 |
| 90-NM-48 | 141 | 1382 | 0.706215 | 19.8 | 123 | 0.512647 | 572 | 800 |
| 90-NM-52 | 126 | 1452 | 0.705746 | 22.3 | 138 | 0.512637 | 586 | 817 |
| 90-NM-53 | 122 | 1418 | 0.705875 | 23.3 | 145 | 0.512624 | 599 | 840 |
| 90-NM-54A | 117 | 1815 | 0.705638 | 24 | 147 | 0.512665 | 556 | 769 |
| 90-NM-55 | 142 | 1742 | 0.705693 | 25.6 | 152 | 0.512674 | 559 | 754 |
| 90-NM-58 | 157 | 1211 | 0.705801 | 14.6 | 99.1 | 0.512661 | 520 | 776 |
| 90-NM-65 | 198 | 1011 | 0.706508 | 17.5 | 104 | 0.512592 | 662 | 894 |
| **Katungites** | | | | | | | | |
| AWL-5-86 | 62.6 | 1118 | 0.704940 | 15.9 | 95.9 | 0.512794 | 401 | 549 |
| BOL-4-84 | 105 | 4373 | 0.705768 | 23.7 | 139 | 0.512728 | 495 | 662 |
| BOL-8-84 | 82.8 | 1492 | 0.704966 | 18.2 | 116 | 0.51273 | 461 | 658 |
| BOL-12-84 | 65.1 | 1598 | 0.704427 | 20.4 | 163 | 0.51272 | 411 | 675 |
| **Melanephelinites** | | | | | | | | |
| 90-NM-1 | 129 | 1040 | 0.705377 | 20.4 | 113 | 0.512791 | 437 | 554 |
| 90-NM-3 | 73 | 1660 | 0.704952 | 21.2 | 124 | 0.512804 | 399 | 532 |

**Table 3.9.** Radiogenic isotope analyses for samples from the Navajo volcanic field on which both Nd and Sr data are available. $T_{DM}$ meas is the model age based on the measured Sm/Nd ratio while $T_{DM}$ source is based on a source Sm/Nd ratio of 0.22 (Bradshaw, 1991).

If enrichment of the lithosphere occurred as a discrete event then the most reliable age is that derived from the minettes as the Sm/Nd used in the model age calculation is taken from a source (Bradshaw, 1991) with trace element characteristics, that is depletions in Nb and Ta, more appropriate for minette rather than katungite magmas. If, however, enrichment was a quasi-continuous event then the model ages must represent minimum ages as the Nd would be partly reset with each event.

Model ages based on Rb/Sr are less reliable than those based on Sm/Nd systematics due to parent-daughter fractionation during melting of a carbonated and phlogopite-bearing source. However it is possible to assess whether the isotopic variation would be consistent with Rb/Sr fractionation between 0.5-1Ga. The variation in $^{87}Rb/^{86}Sr$ and $^{87}Sr/^{86}Sr$ of the

katungites and minettes are presented in Figure 3.20 together with the reference lines corresponding to the range of Nd model ages calculated on the same sample suite.

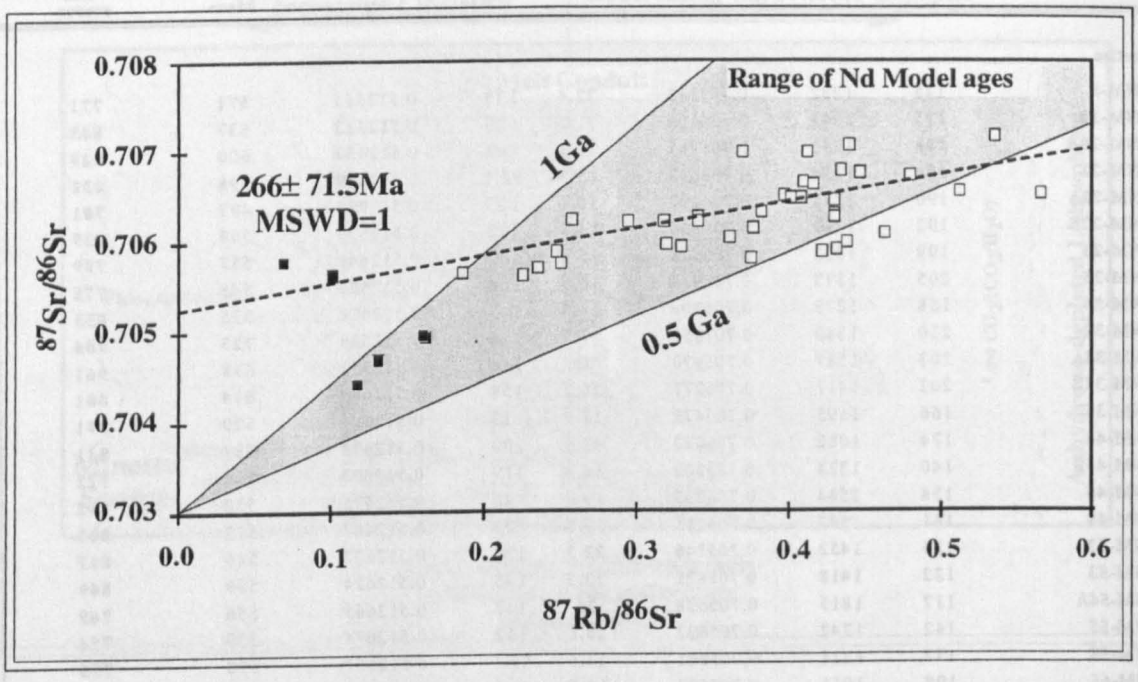


**Figure 3.20.** Variation of $^{87}Sr/^{86}Sr$ with $^{87}Rb/^{86}Sr$ in the magmas of the Navajo volcanic field. The reference line, based on 43 whole-rock analyses, has an age of 266±71.5Ma with an MSWD=1. Also shown for comparison is the range of Nd model ages, based on a source Sm/Nd ratio of 0.22 (used in the REE modelling in Figure 3.7), for the same sample suite, and an initial ratio appropriate for depleted mantle.

The data define a regression-line corresponding to an age of 260±70Ma but this 'age' is inconsistent with the range in Nd model ages. However during partial melting the fractionation of Rb/Sr ratios would have been influenced by the variable proportions of phlogopite and carbonate within the source region. As partial melting of the minette endmember was dominated by the breakdown of phlogopite, Rb/Sr ratios of the melt would be greater than for the source. By contrast melting of the katungite source region was associated with the breakdown of carbonate phases in equilibrium with a phlogopite-bearing restite (section 3.2.5) and in this case Sr would act as an incompatible element while Rb would act compatibly. Hence the katungite magmas probably have lower Rb/Sr ratios than their mantle source region. Fig 3.21 summarises the effects of partial melting of a source with variable modal proportions of phlogopite and carbonate on the Rb/Sr ratio and demonstrates how it could lead to a clockwise rotation of the array and hence younger ages on an isochron diagram.

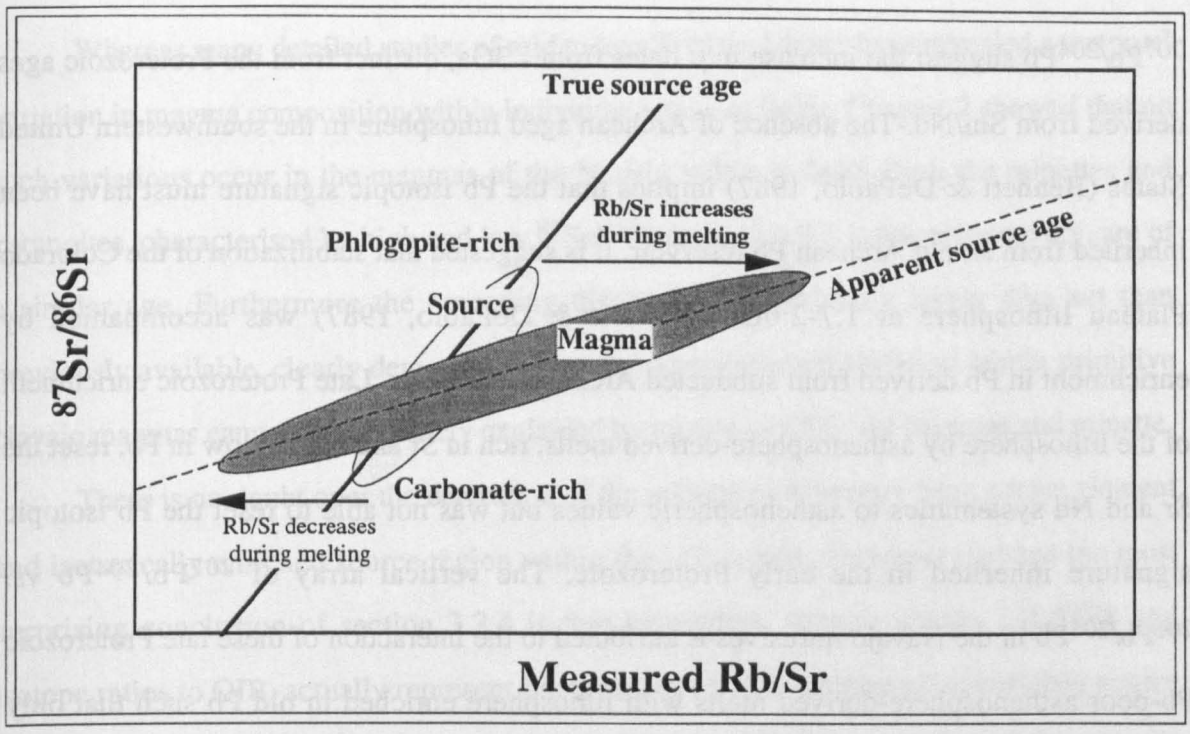


**Figure 3.21.** Apparent versus real Sr isochrons resulting from the differential compatabilities of Rb and Sr during melting of a mineralogically variable source. Where melting is dominated by the breakdown of phlogopite, Rb acts more incompatibly than Sr and the Rb/Sr of the melt exceeds that of the source. However where melting is dominated by the breakdown of carbonate phases in the presence of residual phlogopite, Sr atcs more incompatibly than Rb and hence the Rb/Sr of the melt decreases relative to the source. The range of magmas therefore define an apparent rather than true isochron.

It is suggested therefore that the Sr and Nd isotope systems are consistent with Sm/Nd and Rb/Sr fractionation, and hence trace element enrichment, within the mantle during the late Proterozoic, around 0.5 to 1Ga, significantly pre-dating the Mesozoic and Tertiary subduction episode. Furthermore anticlockwise rotation of the NVF data (about an intermediate point so that the regression line corresponds to the Nd model ages of 0.5-1Ga), yields an initial $^{87}Sr/^{86}Sr$ ratio of 0.7020-0.7035. These ratios are appropriate for asthenospheric mantle and lend further support to the notion that the compositional range of NVF magmas is inherited from a lithospheric source enriched by small volume asthenosphere-derived melts.

In contrast to the coherent Rb/Sr and Sm/Nd fractionation, the vertical $^{207}Pb/^{204}Pb$ vs. $^{206}Pb/^{204}Pb$ array for the Navajo magmas implies a complex history. A similar array for the potassic lavas of the Virunga province have been attributed to mixing (Rogers et al.,1992). The high $^{207}Pb/^{204}Pb$ ratios of the minettes imply either an ancient increase in $\mu$ or the incorporation of old lead in their mantle source region. Pb model ages, based on the composition of present day model depleted mantle, for those minettes with the highest

$^{207}Pb/^{204}Pb$ suggest the increase in μ dates from ~3Ga, distinct from the Proterozoic ages derived from Sm/Nd. The absence of Archean aged lithosphere in the southwestern United States (Bennett & DePaolo, 1987) implies that the Pb isotopic signature must have been inherited from an old Archean Pb reservoir. It is suggested that stabilization of the Colorado Plateau lithosphere at 1.7-2.0Ga (Bennett & DePaolo, 1987) was accompanied by enrichment in Pb derived from subducted Archean sediments. Late Proterozoic enrichment of the lithosphere by asthenosphere-derived melts, rich in Sr and Nd but low in Pb, reset the Sr and Nd systematics to asthenospheric values but was not able to reset the Pb isotopic signature inherited in the early Proterozoic. The vertical array of $^{207}Pb/^{204}Pb$ vs. $^{206}Pb/^{204}Pb$ in the Navajo intrusives is attributed to the interaction of these late Proterozoic Pb-poor asthenosphere-derived melts with lithosphere enriched in old Pb such that only close to the melt vein are the Pb isotopes reset to asthenospheric values.

## 3.4: The temporal transition from lithosphere to asthenosphere derived magmatism on the Colorado Plateau:

In a regional study of basaltic magmatism within the western United States Fitton et al (1991) concluded that prior to 5Ma subduction-modified lithospheric mantle existed beneath the entire region and was the dominant source for magmatism. Post 5Ma magmatism however is characterised by OIB-like compositions and indicates an increasingly dominant role for the asthenosphere. Detailed studies on individual volcanic provinces have revealed that the transition from lithosphere to asthenosphere dominated magmatism in the late-Tertiary was progressive rather than sudden and was characterised by a period of mixing of magmas derived from these distinct mantle sources (Ormerod, 1988; Bradshaw, 1991; Leat et al.,1988; Thompson et al.,1989). Alibert et al (1986) attributed the range of LIL/HFS and isotope ratios of the Navajo minette magmas to a mid-Tertiary phase of mixing between lithosphere and asthenosphere-derived magmas. Similarly Davis (1991) also appealed to mid-Tertiary (≈30Ma) interaction of lithosphere and asthenosphere magmas in the Mogollon Datil volcanic field of the south eastern Colorado Plateau.

Whereas many detailed studies of mid to late-Tertiary basalts have revealed a temporal variation in magma composition within individual volcanic fields, Chapter 2 showed that no such variations occur in the magmas of the Navajo volcanic field. Both the minettes and katungites, characterised by high and low $^{87}Sr/^{86}Sr$ and LIL/HFS ratios respectively, are of a similar age. Furthermore the preceding discussions, based on a larger data set than previously available, clearly demonstrate how the compositional variation within primitive Navajo magmas cannot be adequately explained by mixing of OIB-like magmas and minette.

There is no doubt over the derivation of the minette endmember from a trace element and isotopically enriched source region within the lithosphere. However perhaps the most surprising conclusion of section 3.2.4 is that katungites, despite similar LIL/HFS and isotope ratios to OIB, actually represent the products of «1% melting of an enriched source also located within the lithospheric mantle. Melting of enriched sub-continental lithospheric mantle is therefore interpreted as the source for the Oligo-Miocene magmas of the Navajo volcanic field and that no contribution from asthenosphere-derived magmas was present.

Magmatism on the Colorado Plateau was not confined to the Mid Tertiary, however, the Late Miocene-Early Pliocene Hopi Buttes nephelinites and the Late Pliocene-recent San Francisco Peaks basalts extend its spatial, temporal and compositional range. The Hopi Buttes nephelinites have major and trace element characteristics similar to nephelinites from ocean islands. Their $^{87}Sr/^{86}Sr$ and $^{143}Nd/^{144}Nd$ ratios however are intermediate between values typical of asthenosphere-derived Basin & Range basalts and Katungites. $Al_2O_3$ is also intermediate between the two endmembers and indicates that the Hopi Buttes may be the products of mixing between asthenosphere-derived magmas and lithospheric katungite as illustrated in Fig 3.11. The lack of accurate ages for the Hopi Buttes nephelinites prevents an assessment of the temporal variation in the proportion of the asthenospheric component. A similar contribution of an asthenosphere-derived component in the Pliocene nephelinites of the Wasatch Plateau, central Utah, has been invoked by Tingey (1991).

The San Francisco Peaks basalts have trace element signatures similar to subduction-related magmas (Alibert et al.,1986) albeit at low $^{87}Sr/^{86}Sr$ ratios of 0.70293-0.70448. Section 3.2.4 and Fig 3.7 illustrated that the degree of REE fractionation, La/Yb=15-35, is consistent with these basalts representing the products of melting of an enriched spinel-

bearing mantle source. Unlike the Navajo intrusives and Hopi Buttes nephelinites the major element composition of the San Francisco Peaks basalts have been influenced by crustal-level fractionation processes. However the isotopic variation within those basalts with Ni abundances greater than 120ppm and MgO >7.5% is consistent with mixing of enriched lithospheric magmas with up to 40% of an asthenosphere-derived melt as illustrated in Fig 3.11.

Thus it can be argued that whereas Oligo-Miocene magmas were wholly lithosphere-derived, the later Miocene/Pliocene nephelinites and basalts contain a significant contribution from asthenosphere-derived melts.

The Cenozoic magmatic evolution of the Colorado Plateau as a whole was dominated by melting of enriched lithospheric mantle throughout the Late Oligocene and Early Miocene as represented by the NVF. From the Late Miocene melting of the asthenosphere was taking place and mixing with lithosphere-derived katungite magmas to produce the Hopi Buttes nephelinites. Melting within the lithosphere during the Late Oligocene to Early Pliocene occurred in the garnet stability field but by the Late Pliocene magmas from the southwest periphery of the central plateau were derived from spinel-bearing lithosphere. The temporal evolution of melting enriched lithospheric mantle within the garnet stability field to melting within the shallower spinel field, associated with an increasing input from asthenosphere-derived melts, is also recognised in basalts from the Basin & Range (Bradshaw, 1991). In the Basin & Range province such temporal variations are associated with crustal extension and have been attributed to a thinning of lithosphere and the resultant upwelling and adiabatic melting of asthenosphere. In the case of the Colorado Plateau however, there is no crustal extension and if the temporal variations in magma composition are to be attributed to thinning of the lithosphere an alternative mechanism must be sought.

## 3.5: Summary & Conclusions:

The Oligo-Miocene volcanics of the Navajo volcanic field comprise a series of potassic magmas from highly silica-undersaturated katungites through to mildly silica-undersaturated ultrapotassic minettes. Contrary to the conclusions of Roden (1981) and Roden et al (1990) fractionation has only a minor role in establishing the observed

geochemical variation and is restricted to the development of the felsic minettes with <7.8% MgO. Modelling shows that simple closed system fractional crystallisation of an assemblage consisting of variable proportions of diopside+phlogopite +magnetite+apatite±olivine from several isotopically similar mafic parents can reproduce the compositional variations of the majority of the felsic minettes. However in the case of the Washington Pass volcanic centre increasing SiO2 is accompanied by an increase in Ni abundance which is best modelled in terms of a combination of fractionation of the above assemblage and assimilation of spinel peridotite, present as xenoliths even within the most evolved flows.

The majority of Navajo magmas, despite covering a wide range in composition ($SiO_2$ ≈33-55%), represent primitive melts, the geochemical signatures of which are inherited from their mantle source regions. The range of minette to katungite magmas, despite the latter superficially resembling OIB magmas, are attributed to small degrees of partial melting of heterogeneously enriched lithospheric mantle. A model is proposed whereby the range of within-plate through to 'subduction-like' signatures observed in the Navajo magmas were inherited from deep lithospheric mantle metasomatised by a small volume trace element and volatile enriched melt derived from the underlying asthenosphere during the late Proterozoic. Source variation results from stabilisation of a carbonate-bearing assemblage, with low Rb/Sr and LIL/HFS ratios, close to the melt vein and more hydrous phlogopite-bearing assemblages, with high Rb/Sr and LIL/HFS, progressively further away from the vein. $^{143}Nd/^{144}Nd$ and $^{87}Sr/^{86}Sr$ are consistent with Sm/Nd and Rb/Sr fractionation in a lithospheric mantle source during the Late Proterozoic. In contrast high $^{207}Pb/^{204}Pb$ ratios imply U/Pb fractionation during the Archean. The lack of lithosphere of greater than 2.0 Ga in this region of the southwestern United States suggests this old Pb was inherited from Archean sediments and it is speculated that this dates from the stabilisation of the lithosphere between 1.7 and 2.0Ga (Bennett & DePaolo, 1987).

A direct input to magmatism from the asthenosphere is not apparent in the Oligo-Miocene lithosphere-derived magmas of the NVF. Not until the eruption of the late Miocene to Early-Pliocene (8-4Ma) Hopi Buttes nephelinites is there any contribution from asthenospheric magmas. These are modelled as hybrid magmas produced by mixing of asthenosphere and katungite-like melts (section 3.2.4).

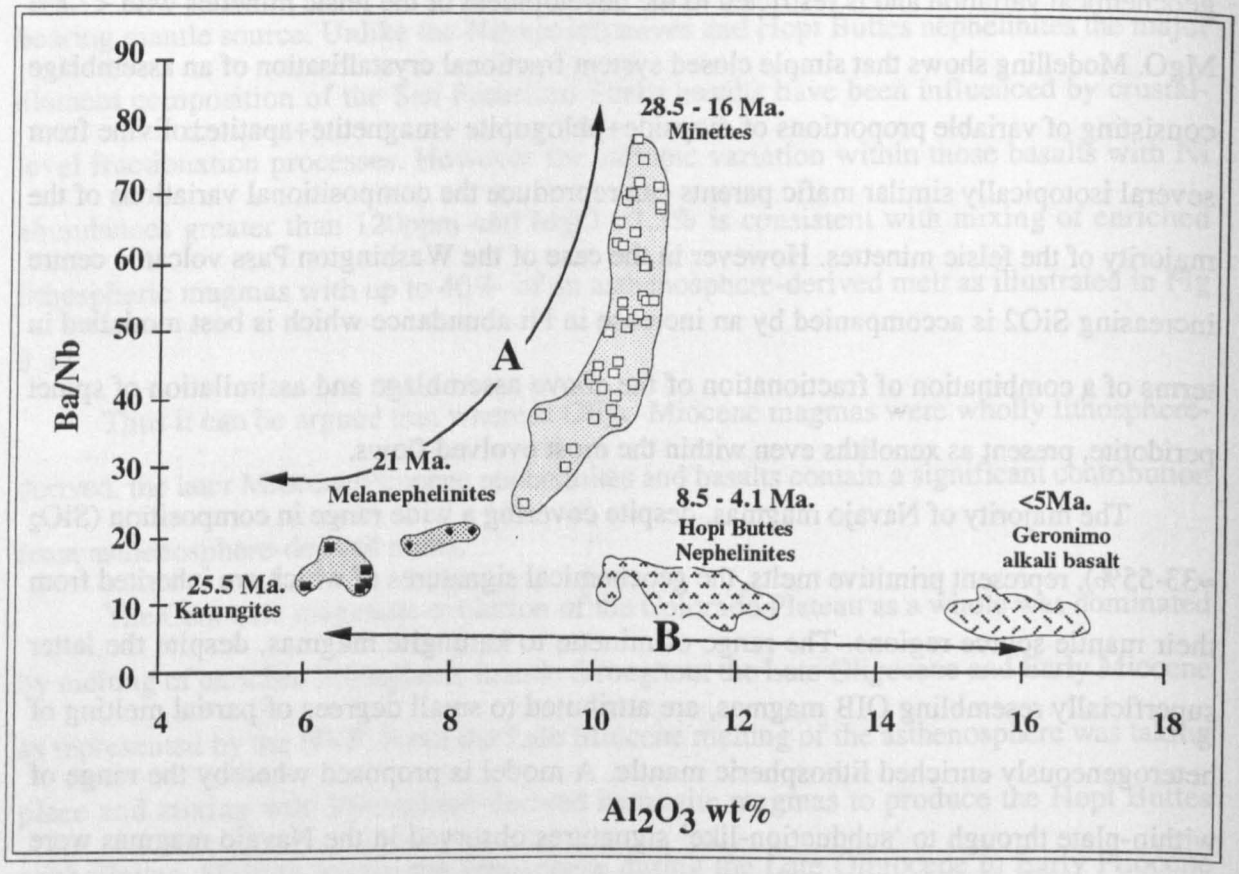


**Figure 3.22.** Summary diagram showing the temporal evolution in composition of magmas from the central Colorado Plateau during the mid to late Tertiary. Arrow A highlights the compositional diversity of the Oligo-Miocene Navajo intrusives which represent melts derived from a compositionally and mineralogically heterogenous mantle beneath the Colorado Plateau. Arrow B shows the late Miocene-early Pliocene mixing of asthenosphere-derived magmas, represented by Geronimo alkali basalts (Kempton et al., 1987; Kempton & Fitton, unpubl data), with katungite-like lithosphere-derived magmas in the generation of the Hopi Buttes nephelinites.

Figure 3.22 summarises the temporal and compositional variations in Colorado Plateau magmatism. The central plateau was dominated by a long period, approximately 11Ma (Chapter 2), of lithosphere-derived magmatism during the late Oligocene-early Miocene. By contrast the last short magmatic pulse in the late Miocene-early Pliocene was characterised by an increasingly dominant role for asthenospheric melting and a decrease in the depth of melting within the lithosphere.

The composition of volcanics from the central Colorado Plateau, in conjunction with the temporal variation from lithosphere to asthenosphere-dominated melting, will be used in Chapter 5 to constrain likely causes of melting within what is essentially a very stable crustal block.

# CHAPTER 4

## Geochemistry and Petrogenesis of Late Cenozoic, Potassic and Alkali-rich Volcanics of the Central Sierra Nevada, California.

## 4.1: Introduction:

The remnant late Cenozoic basaltic flows and hypabyssal intrusives of the San Joaquin-Kings Volcanic Field (SKVF) of the central Sierra Nevada, California, cover a relatively wide range in compositions ($SiO_2$=45.3-59.9wt%) and were erupted over approximately 8-Ma (Dalrymple, 1963; Van Kooten, 1980). Magmatism was volumetrically very limited, temporally sporadic and was restricted to some of the most elevated regions of this subprovince of the Western Cordillera. Furthermore the basalts of the Sierra Nevada are clearly not associated with contemporary extension unlike the volumetrically more significant volcanic fields in the Western Great Basin to the immediate east (Ormerod et al.,1988).

Several aspects of magmatism within the Sierra Nevada, namely the relationship of volumetrically limited volcanics with a region of uplift, the lack of pre-, syn-, or post-magmatic extension, are similar to those identified for the Colorado Plateau in chapters 2 and 3. As with the magmatism on the Colorado Plateau, the SKVF provides an opportunity to constrain further the temporal evolution of magmatism associated with non-extensional elevated regions of the southwestern United States and provides an important comparison study to assess the wider significance of these variations.

The purpose of this chapter is to identify primitive magmas within the basalts of the SKVF and evaluate the relative contributions from asthenospheric and lithospheric mantle sources. A model is then proposed that accounts for the both the temporal and spatial variation in magma composition and the changes in magma source region. The evolution of magmatism within the Sierra Nevada is compared to that of the Colorado Plateau throughout the discussion. In addition this region of the western United States has had a long and complex history of subduction and a major lithospheric boundary between middle Proterozoic North America and late Proterozoic accreted terranes is located in the proximity

of the Sierra Nevada (Kistler & Peterman, 1973; Ormerod, 1988). It is proposed to use the basalts of the SKVF to address the possible nature of this boundary in the central Sierra Nevada.

## 4.2: Background Geology of the western margin of California and the Sierra Nevada:

### 4.2.1: Precambrian-Palaeozoic

The basement of eastern California is thought to have formed at between 2.0-2.3Ga on the basis of Nd model ages, illustrated in Fig 4.1, though this did not form purely from mantle-derived material and involved a substantial amount of older crust (Bennett & DePaolo, 1987).

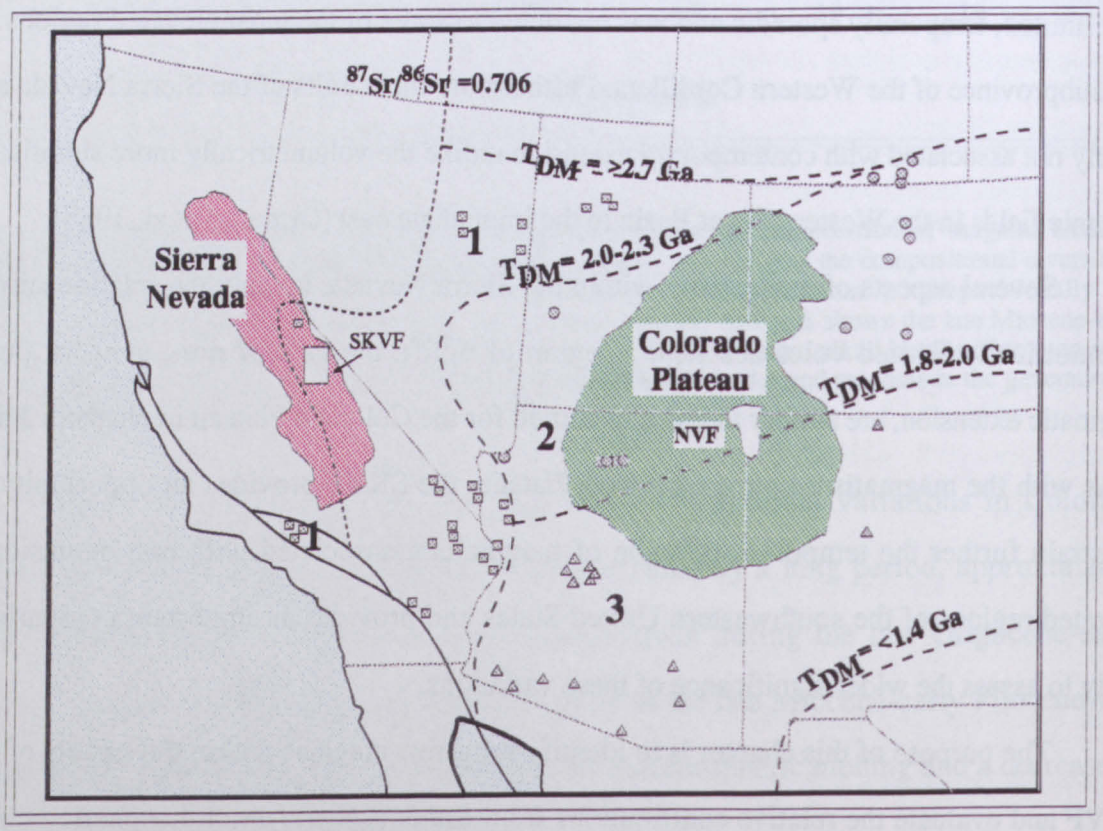


**Figure 4.1.** Crust-formation provinces of the western United States adapted from Bennett & DePaolo (1987). Provinces are distinguished on the basis of regional differences in Nd isotopic evolution paths as determined by measurements of crustal samples of different ages. Squares=province 1 ($T_{DM}$=2.0-2.3Ga), circles=province 2 ($T_{DM}$=1.8-2.0Ga), triangles=province 3 ($T_{DM}$=1.7-1.8Ga). The $^{87}Sr/^{86}Sr_i$ isopleth of Kistler & Peterman (1973) is also shown and is interpreted as the boundary between middle Proterozoic North America and late Proterozoic lithosphere accreted during the Palaeozoic.

During the late Proterozoic a rifting event gave rise to a passive continental margin which accumulated shelf sediments (carbonates and sands) throughout much of the early

Palaeozoic (Stewart & Poole, 1974). Brief periods of convergence and collision in the middle-upper Palaeozoic resulted in the accretion of a series of island-arc and allochthonous assemblages of turbidites, cherts argillites and greenstones (Dickinson, 1977, 1981) onto the western continental margin.

The western edge of the Proterozoic North American continental crust is defined by Kistler & Peterman (1973) on the basis of $^{87}Sr/^{86}Sr$ ratios of Mesozoic granites and is illustrated in Fig 4.1. An isopleth for initial $^{87}Sr/^{86}Sr$ ratios >0.706 encloses all the occurrences of Precambrian sedimentary and metamorphic rocks, although it has become evident that such ratios can occur in regions devoid of Precambrian crust (Stevens et al., 1992). Ormerod (1988) and Ormerod et al (1988) use similar initial $^{87}Sr/^{86}Sr$ ratios of mantle-derived basalts to infer the position of the same boundary as Kistler & Peterman (1973) only at mantle depths. This has considerable significance for the central Sierra Nevada and the San Joaquin-Kings volcanic field as it implies that the crustal boundary lies to the west and the mantle boundary to the immediate east. The implications for this are discussed in section 4.8

### 4.2.2: Mesozoic-Cenozoic

During the latest Triassic to middle Jurassic the passive type margin of the Palaeozoic was replaced by an Andean-type active continental convergent margin that persisted throughout the Mesozoic and consumed all of the Palaeozoic 'Pacific ocean'. All those Palaeozoic terranes to the west of typical passive continental margin sediments were accreted during the Mesozoic phase of convergence (Coney, 1980).

Between 125 and 80Ma (Oldow et al., 1989) a continental arc developed and is now exposed as the Sierra Nevada batholith which comprises numerous distinct granite, granodiorite, diorite and tonalite plutons. Towards the end of the Cretaceous there was a cessation of magmatism in the Sierra Nevada associated with an eastward shift of the locus of magmatism into the central Western Cordillera and Rocky Mtns (Armstrong, 1974), attributed to the progressive shallowing in the angle of subduction of the Farallon plate (Dickinson & Snyder, 1979) as both the age of the Farallon plate decreased and the rate of convergence increased (Engebretson et al., 1985)

At approximately 28Ma the spreading ridge and North American plates intersected resulting in the Mendocino and Rivera triple junctions (Engebretson et al.,1985). The development of a transform margin and the migration of the Mendocino triple junction (MTJ) to the northwest resulted in a gradual northward cessation of subduction. Dickinson & Snyder (1979) postulated that a triangular 'slab window' developed beneath the western United States in response to the time-transgressive cessation of subduction. Many tectonmagmatic events have been attributed to this slab-free region including the onset of Basin & Range extension, uplift of the Colorado Plateau and Sierra Nevada and the north-south temporal variation in magma composition in the western Great Basin (Dickinson & Snyder, 1979; Crough & Thompson, 1977; Ormerod et al., 1988).

Having outlined the general tectonomagmatic evolution of the western margin of North America the following section focuses on the tectonomagmatic development of the Sierra Nevada during the middle Cenozoic to recent.

### 4.2.3: Cenozoic-Recent Uplift of the Sierra Nevada

There is a general consensus regarding the onset of late Cenozoic uplift of the Sierra Nevada range although the ultimate cause of this uplift event remains a subject of much debate (Crough & Thompson, 1977; Huber, 1981; Mavko & Thompson; Unruh, 1991). Chapter 5 presents a more comprehensive assessment of both these issues in the light of the following discussion on the characteristics of magmatism within the Sierra Nevada.

Late Cenozoic uplift of the Sierra Nevada was first recognised by Lindgren (1911) from the preservation of mature river valleys beneath Cenozoic volcanic flows (section 4.2.5).These basalt flows are dated at 9-10Ma and therefore implying that Cenozoic uplift occurred post 9Ma (Dalrymple, 1963; Christensen, 1966; Huber, 1981). In fact approximately 2km of uplift has occurred at the crest of the Sierra Nevada since 9Ma (Huber, 1981). The incision of some 3-4Ma basaltic flows (Christensen, 1966) within the inner gorges of some Sierran rivers suggest that a renewed period of uplift occurred sometime since the eruption of these Pliocene volcanics. Furthermore the influx of clastic debris derived from the Sierra Nevada into the southern California Great Valley from 9Ma onwards led Bartow (1984) to suggest the onset of uplift occurred at this time. Moore and

Dodge (1980) quoting unpublished data of Huber conclude that prior to 10Ma the Sierran drainage divide near latitude 37° 40'N was uplifted to about 38% of its present 3420m elevation; between 10 and 3.6Ma was uplifted a further 34% and finally after 3.6Ma to the present uplift of a further 28% occurred.

The most striking feature of the Sierra Nevada Mtn range is the north-south increase in surface elevation and, although difficult to constrain it may imply that the onset of uplift was a diachronous event beginning in the southern Sierra.

### 4.2.4: Cenozoic-recent Extension in the Sierra Nevada

The Sierra Nevada has experienced little extensional deformation during the Cenozoic despite large scale crustal extension in the Basin & Range and the adjacent western Great Basin. Although the Sierra Nevada is characterised by low measured heatflows, generally 17-50mWm$^{-2}$ (Saltus & Lachenbruch, 1991) some sites have values of 50-91mWm$^{-2}$. These high heat flow sites are restricted to regions within 40km of the Basin & Range and are most common towards the southeastern limit of the Sierra Nevada. This region of elevated heatflow is also a seismically active area. Recent earthquakes in the Durwood Meadows area (35.92°N, 118.32°W) are the result of extensional faulting on N-S striking planes (Jones & Dollar, 1986).The Durwood activity was interpreted by Jones & Dollar (1986) to represent the inception of a new Basin & Range fault in the physiographic Sierra Nevada. It is clear therefore that the thermal and extensional characteristics of the Basin & Range are gradually encroaching on the southeastern Sierra Nevada (Saltus & Lachenbruch, 1991; Jones & Dollar, 1986).

### 4.2.5: Cenozoic Magmatism of the Sierra Nevada

The only Cenozoic lithologies preserved within the predominantly Mesozoic-granitic terrain of the Sierra Nevada are occasional glacial and alluvial deposits, numerous scattered basaltic lava-flow remnants, believed to be near their original sites of eruption, and isolated volcanic necks of 100-600m diameter and rare dykes (Nockolds & Allen, 1954; Peck, 1976; Van Kooten, 1977; 1980; Moore & Dodge, 1977; 1980).

Most late Cenozoic volcanic rocks are alkali-rich, generally sodic although

occasionally potassic, and show a broad range in composition from leucite-basanites, hawaiites and potassic trachybasalts, basaltic trachyandesites through to trachyandesites and occasional rare rhyolite domes. Adjacent flow remnants and volcanic necks are often compositionally distinct and represent numerous localised, small-volume, eruption events.

Although remnant basaltic flows and vents occur throughout the Sierra Nevada range they tend to be concentrated in several discrete volcanic regions. Within the true central Sierra Nevada there are two main regions of volcanism, the Kern and San Joaquin-Kings volcanic fields. The Kern volcanic field is a small area on the Kern Plateau in the southern Sierra Nevada and comprises several olivine basalt flows ($\approx$1km$^3$) and rhyolite domes (1.9km$^3$) dated at 3.6-0.2Ma (Bacon & Duffield, 1980). The San Joaquin-Kings volcanic field, discussed in greater detail below, is the larger of the two volcanic regions. No late Cenozoic volcanics have been found in the 50km span between these two areas. The Coso, Mono-Long Valley and Big Pine volcanic fields are not located in the true Sierra Nevada but in the extensional Western Great Basin province. In general volcanism within the Western Great Basin tends to be younger and volumetrically much greater than the volcanism in the central Sierra Nevada due to the absence of extension in the latter

## 4.3: The San Joaquin-Kings Volcanic Field (SKVF)

The San Joaquin-Kings volcanic field, to use the terminology of Moore & Dodge (1980b), comprises approximately 100 small basalt-flow remnants, several dykes and volcanic necks up to 600m in diameter randomly distributed over an area of $\approx$8500km$^2$ of the western slope of the Sierra Nevada (Fig 4.2).

Dodge & Moore (1980b) divided the volcanics of the SKVF into three groups on the basis of $K_2O$ contents; alkali olivine basalts ($K_2O$<1.8% at 45% $SiO_2$), potassic olivine basalts ($K_2O$=1.8-3.2% at 45% $SiO_2$) and ultrapotassic basalts ($K_2O$>3.2% at 45% $SiO_2$). Overall the distribution of basaltic magmas is random although the ultrapotassic, leucite-bearing, basalts tend to be restricted to the northern and southern margins of the field (Dodge & Moore, 1980b). Adjacent flow remnants and volcanic necks often have distinct compositions and may represent numerous small volume eruptive events. Feeder vents or dykes for the various flows are rarely observed in part due the extensive glacial deposits of

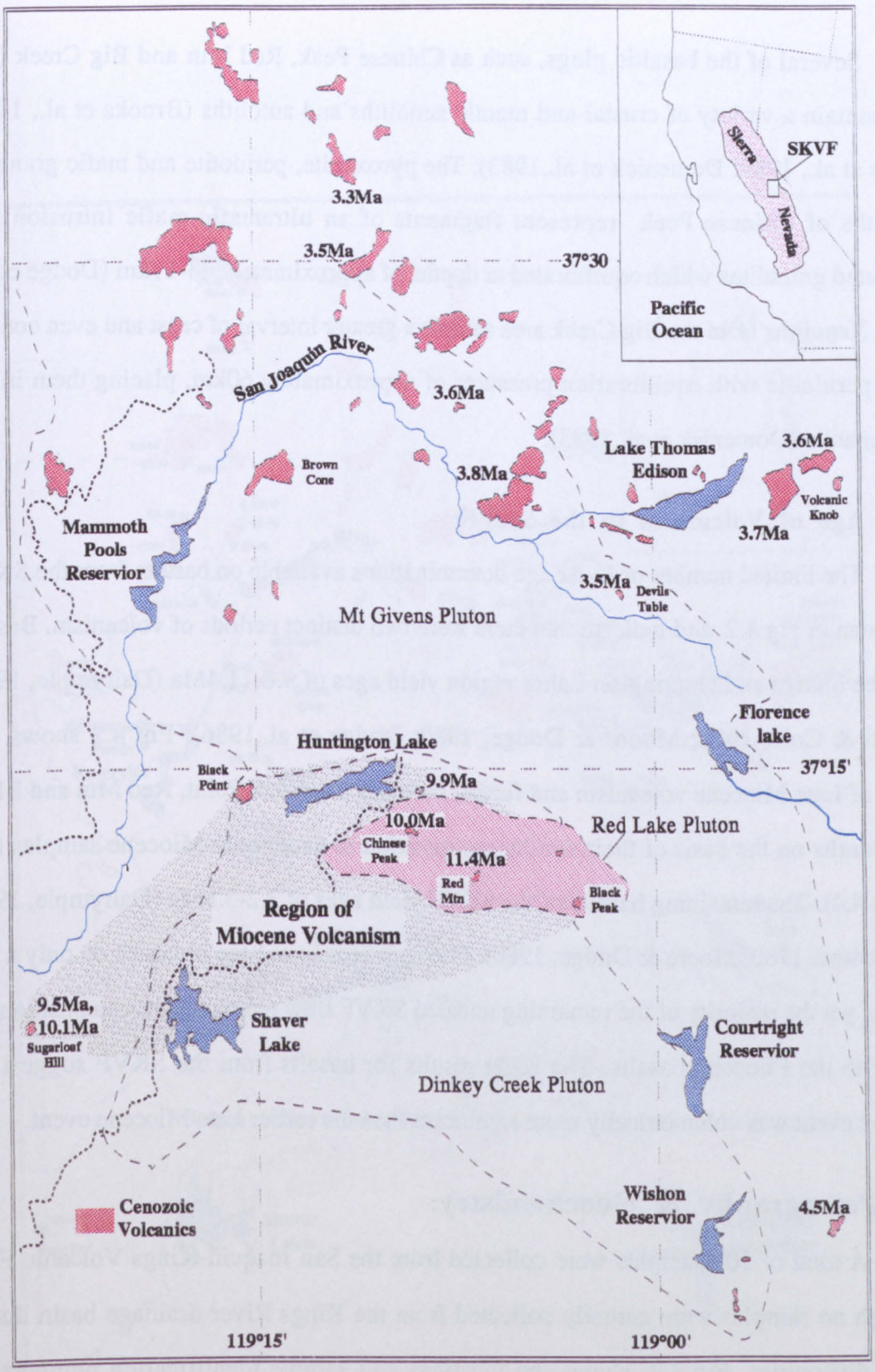


**Figure 4.2**. Distribution of remnant late Cenozoic basalt flows in the San Joaquin-Kings volcanic field, central Sierra Nevada California. Also shown are available K-Ar age determinations from Dalrymple (1963), Dodge et al (1986), Marvin & Cole (1978), and Van Kooten (1980). Region of Late Miocene volcanism is shaded. Approximate outlines of the Dinkey Creek, Red Lake and Mt Givens plutons are also shown.

the area. Moore & Dodge (1980b) estimate the original extruded volumes, adjusted for erosion, of alkali olivine basalt and potassic olivine basalt at ≈3km$^3$ and only 0.03km$^3$ of ultrapotassic basalt .

Several of the basaltic plugs, such as Chinese Peak, Red Mtn and Big Creek (Fig 4.2), contain a variety of crustal and mantle xenoliths and autoliths (Brooks et al., 1980; Dodge et al., 1986; Domenick et al.,1983). The pyroxenite, peridotite and mafic granulite xenoliths of Chinese Peak represent fragments of an ultramafic-mafic intrusion and associated granulites which equilibrated at depths of approximately 43-17km (Dodge et al., 1986). Xenoliths from the Big Creek area sample a greater interval of crust and even contain spinel peridotite with equilibration pressures of approximately 60km, placing them in the upper mantle (Domenick et al.,1983).

### 4.3.1: Age of Volcanism in the SKVF:

The limited number of K-Ar age determinations available on basalts from the SKVF are shown in Fig 4.2. and indicate that there were two distinct periods of volcanism. Basalts from the Shaver and Huntington Lakes region yield ages of 9.8-11.4Ma (Dalrymple, 1963; Marvin & Cole, 1978; Moore & Dodge, 1980; Dodge et al.,1986). Fig 4.2 shows this region of Late Miocene volcanism and further includes the Black Point, Red Mtn and Black Peak basalts on the basis of their similar composition to dated Late Miocene samples (see section 4.4). The remaining basalts of the SKVF yield ages of 3.2-3.8Ma (Dalrymple, 1963; Van Kooten, 1980; Moore & Dodge, 1980). Pliocene ages have been obtained on only a few samples yet the majority of the remaining undated SKVF flow remnants are compositionally similar to the Pliocene basalts. The K-Ar results for basalts from the SKVF suggest the Pliocene event was volumetrically more significant than the earlier Late Miocene event.

## 4.4: Petrography & Geochemistry:

A total of 102 samples were collected from the San Joaquin-Kings Volcanic Field although no samples were actually collected from the Kings River drainage basin due to access difficulties. Fig 4.3. shows the locations and sample identification numbers for material collected during 1990 and 1991.

The number of samples was generally restricted to one or two where the flow remnant was limited in size as within-flow compositional variations have been shown to be rather limited (Moore & Dodge, 1980b; Dodge & Moore, 1980b). The aim of sampling, where possible, was to obtain a suite of basalts spatially representative of the SKVF.

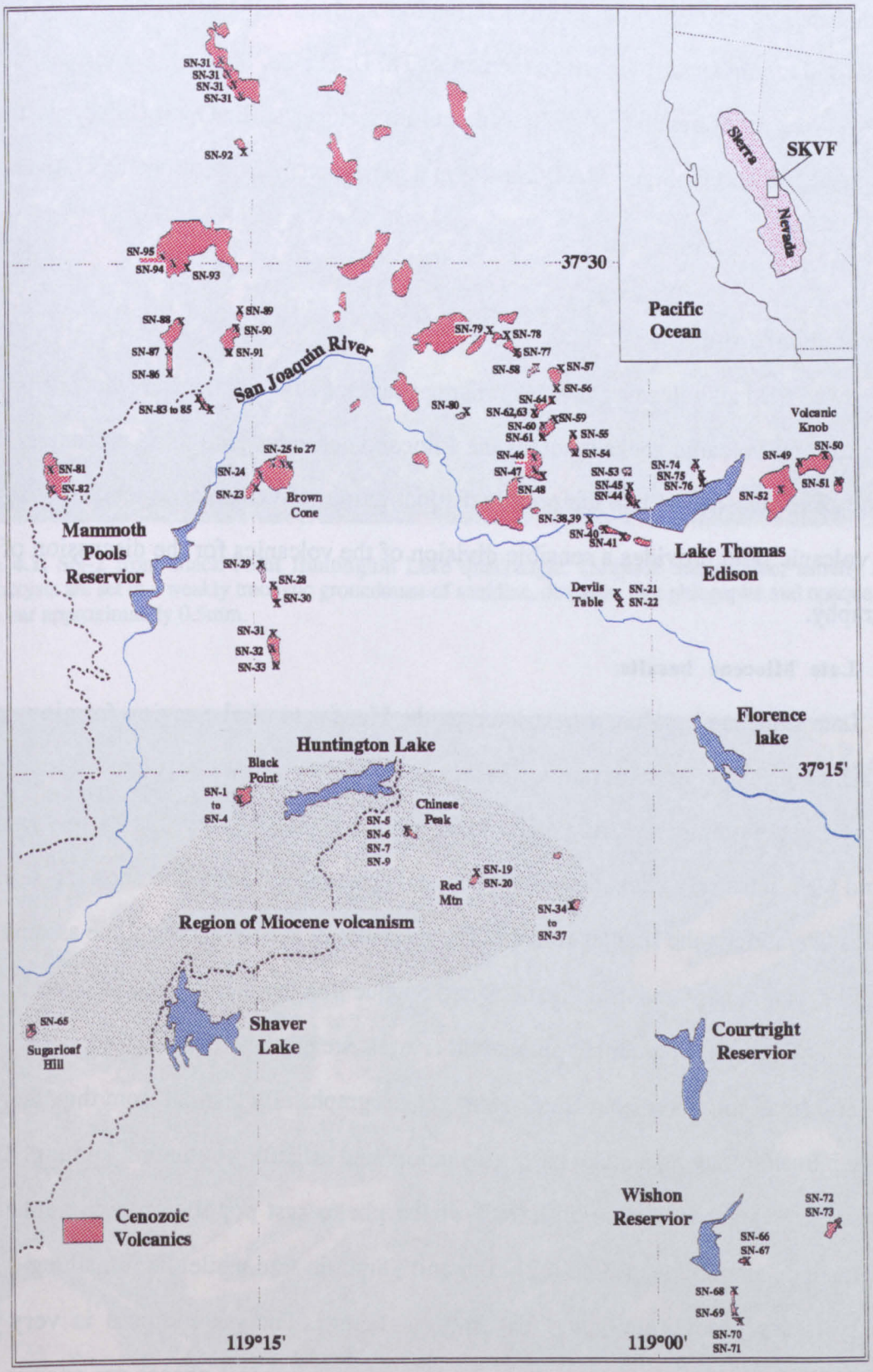


**Figure 4.3.** Map of the San Joaquin-Kings volcanic field showing sampling localities and sample identification numbers. Dotted line highlights region of Late Miocene volcanism.

Major and trace element concentrations were determined on 88 samples using XRF facilities at Nottingham University and The Open University (see Appendix B for analytical information and technique comparison). In addition a representative selection of samples were analysed by instrumental neutron activation analysis for a selection of rare earth elements and a number of other trace elements (Th, U, Hf, Ta, Sc, Co). Samples selected for INAA were further analysed for Sr, Nd, and Pb isotopes at the Open University using VG-Isomass 54E and Finnigan MAT-261 thermal ionization mass spectrometers (Appendix A & B).

### 4.4.1: Petrography:

In the field all volcanics have a similar appearance although the late Miocene basalts in general form volcanic necks whereas the Pliocene volcanics tend to be present as flow remnants. The presence of two temporally distinct groups of volcanics in the San Joaquin-Kings volcanic field provides a sensible division of the volcanics for the discussion of the petrography.

#### 4.4.1a: Late Miocene basalts.

Late Miocene basalts are restricted to the Huntington Lake region forming small peaks reflecting their resistant nature. Typically they are porphyritic (Plate 4.1) with the phenocryst population comprising about 40% subhedral diopside crystals ≥1 to ≤3mm in size, and 60% anhedral to euhedral olivine crystals generally 1-5mm and showing signs of pervasive alteration in the smaller crystals. The groundmass is a microcrystalline assemblage of diopside, plagioclase and sanidine laths and opaque iron oxide minerals. In those basalts with >3% $K_2O$, small groundmass phlogopite crystals are present.

The small intrusion from Black Peak is petrographically distinct from the other late Miocene intrusions having a much paler grey colour and exhibiting columnar jointing. These trachyandesites are porphyritic with 98% of the phenocryst population being euhedral, complex zoned amphiboles (Plate 4.2) ≥0.5 and ≤8mm in size while the remaining 2% of phenocrysts are phlogopite laths ≤0.5mm in length. The groundmass is very fine (microcrystalline to glassy) where the only recognisable mineral phases are opaque iron oxides and very rare «0.2mm sanidine feldspar laths.

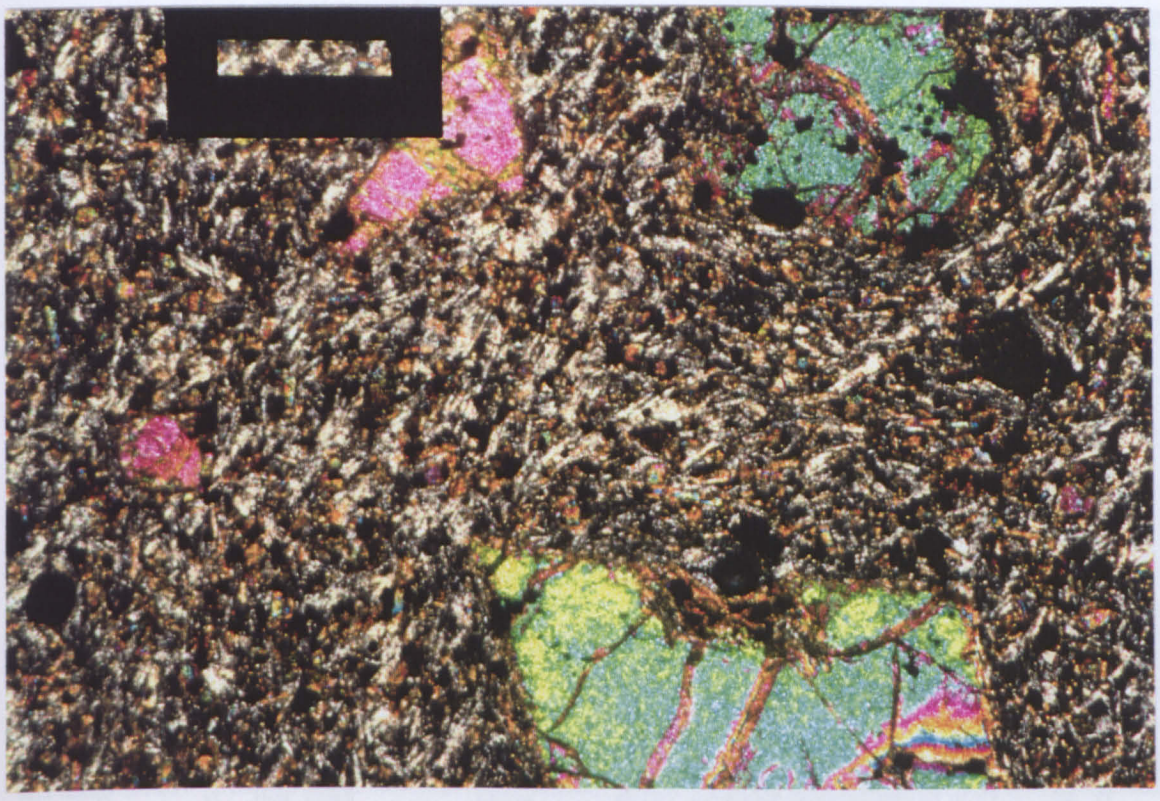

**Plate 4.1.** SN-2 from Black Point Huntington Lake quadrangle. Diopside and olivine, usually altered, phenocrysts are set in a weakly trachytic groundmass of sanidine, diopside, rare phlogopite and opaque oxides. Scale bar approximately 0.5mm.

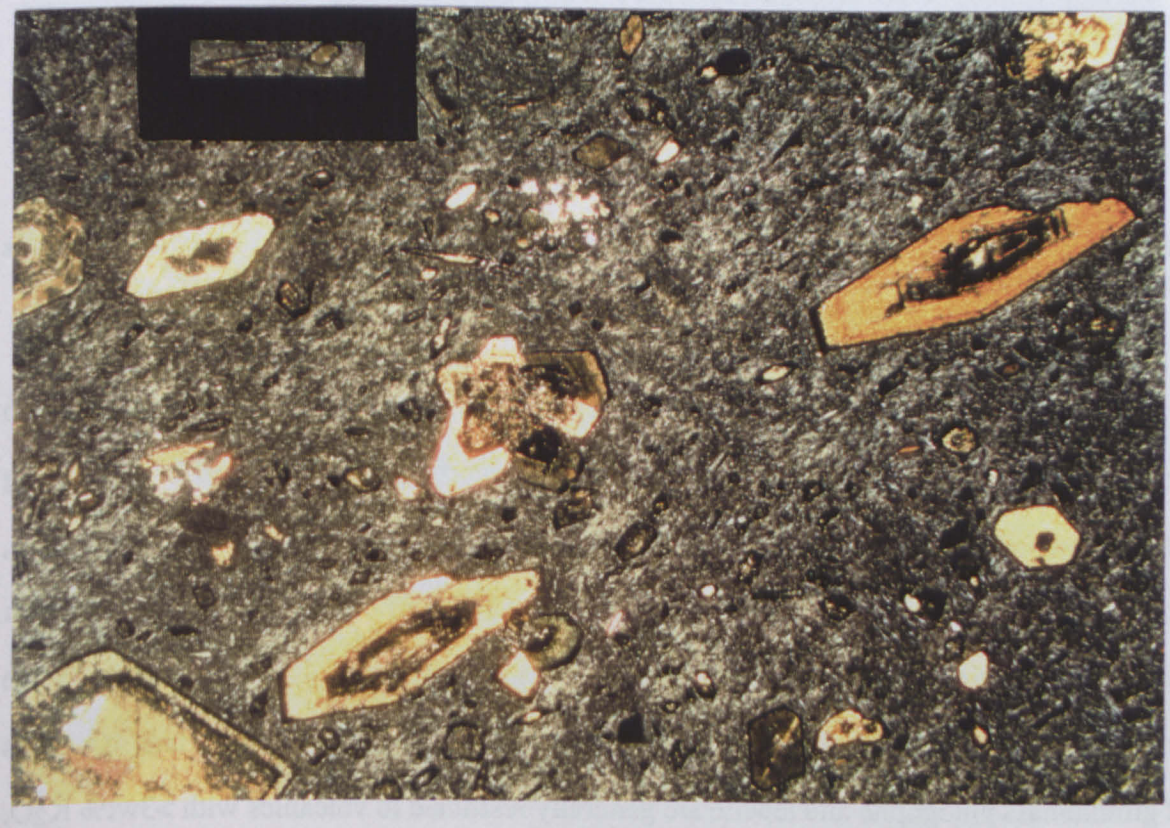

**Plate 4.2.** SN-37C from Black Peak, Dinkey Creek quadrangle. Euhedral well zoned amphibole phenocrysts are set in a trachytic microcrystalline to glassy groundmass where the only recognisable phases are opaque oxides, rare sanidine laths. Scale bar approximately 1mm.

**4.4.1b: Pliocene basalts.**

The petrology of the Pliocene basalts of the SKVF has been discussed in some detail in Moore and Dodge (1980b) and Van Kooten (1980). Both studies identified several systematic mineralogical variations related to the whole-rock abundance of $K_2O$. Figure 4.4. from Van Kooten (1980) summarises the modal mineral variations of the SKVF basalts with $K_2O$.

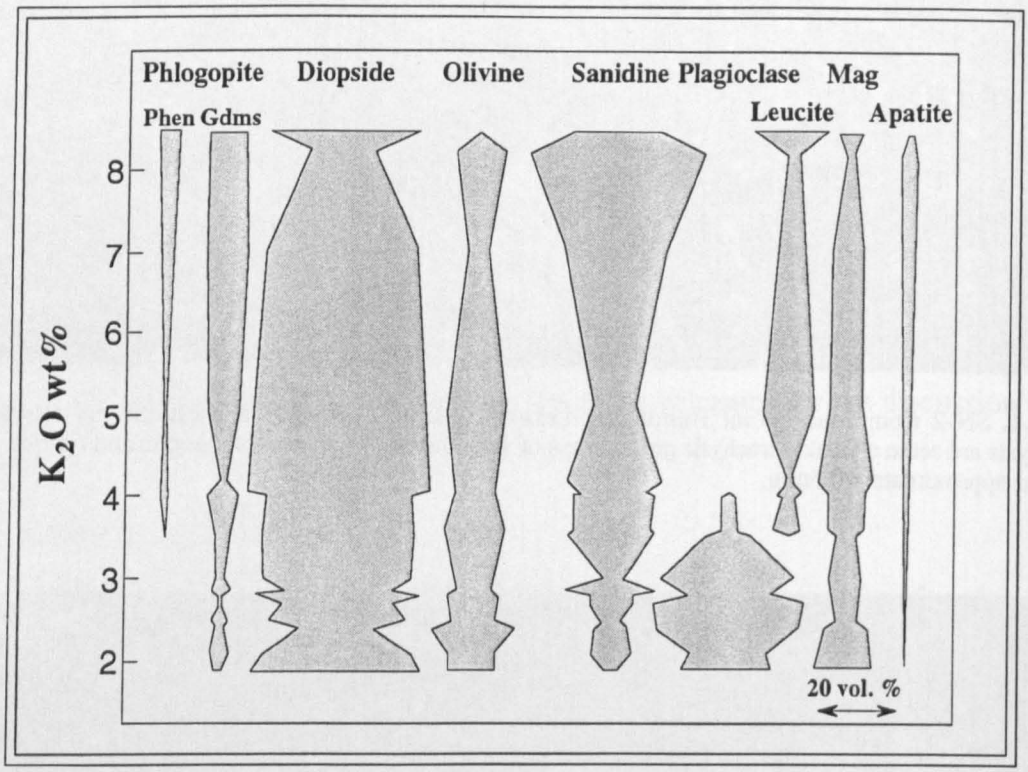


**Figure 4.4.** Modal mineralogy versus $K_2O$ wt% for the Pliocene basalts of the San Joaquin-Kings volcanic field, central Sierra Nevada. Taken from Van Kooten (1980).

While proportions of various minerals vary, this is generally restricted to groundmass phases, all the volcanics are characteristically porphyritic containing phenocrysts of subhedral-euhedral diopside (≥1mm) and anhedral olivine crystals (<1mm), altered along fractures. Furthermore all samples have a fine grained groundmass with trachytic textured sanidine and/or plagioclase feldspar (Plate 4.3). Also present in the groundmass are diopside+olivine+opaque iron oxides+apatite. Minor yet variable amounts of groundmass phlogopite and leucite are generally restricted to volcanics with >3wt% $K_2O$, while phlogopite may form phenocrysts (1-3mm) in samples with $K_2O$ in excess of 5wt%.

**Plate 4.3.** SN-56 shows phenocrysts of diopside set in a fine almost microcrystalline trachytic groundmass of sanidine and plagioclase feldspar laths, diopside and opaque oxides. Scale bar approximately 1mm.

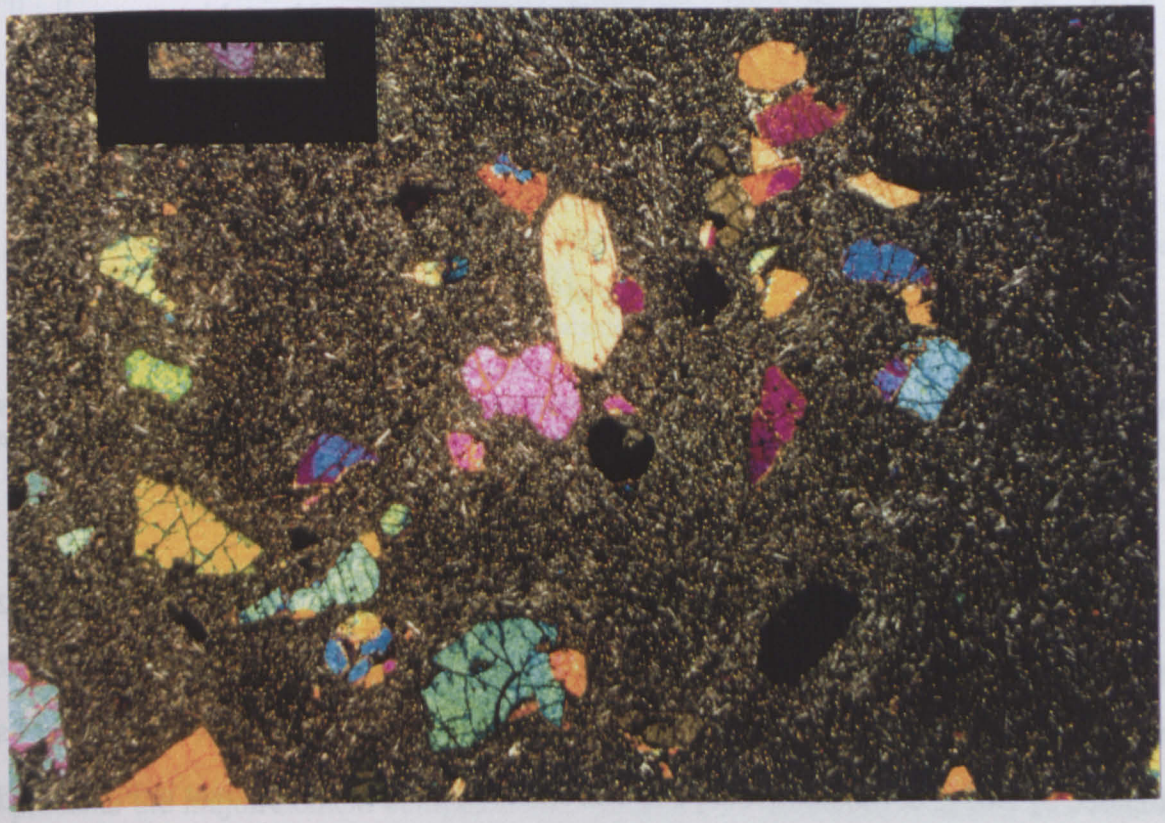

**Plate 4.4.** SN-48 shows two groundmass types with dark oxide-rich groundmass at the lower right of the view. Note also the lighter colour of the groundmass around diopside phenocrysts as illustrated by the crystal in extinction to the lower right of the centre of the field of view. Scale bar approximately 1mm.

Many of the Pliocene samples also show two distinct groundmass types usually one having a much darker appearance reflecting the higher abundances of diopside and opaque iron oxides (Plate 4.4). These samples also tend to have a blotchy appearance where the groundmass surrounding diopside phenocrysts has a low modal abundance of mafic minerals and therefore has a pale colour.

### 4.4.2: Classification.

Dodge & Moore (1980b) and Van Kooten (1980) make no compositional distinction between the two temporal groups of the SKVF and divide the volcanics into three subgroups as outlined in section 4.3.

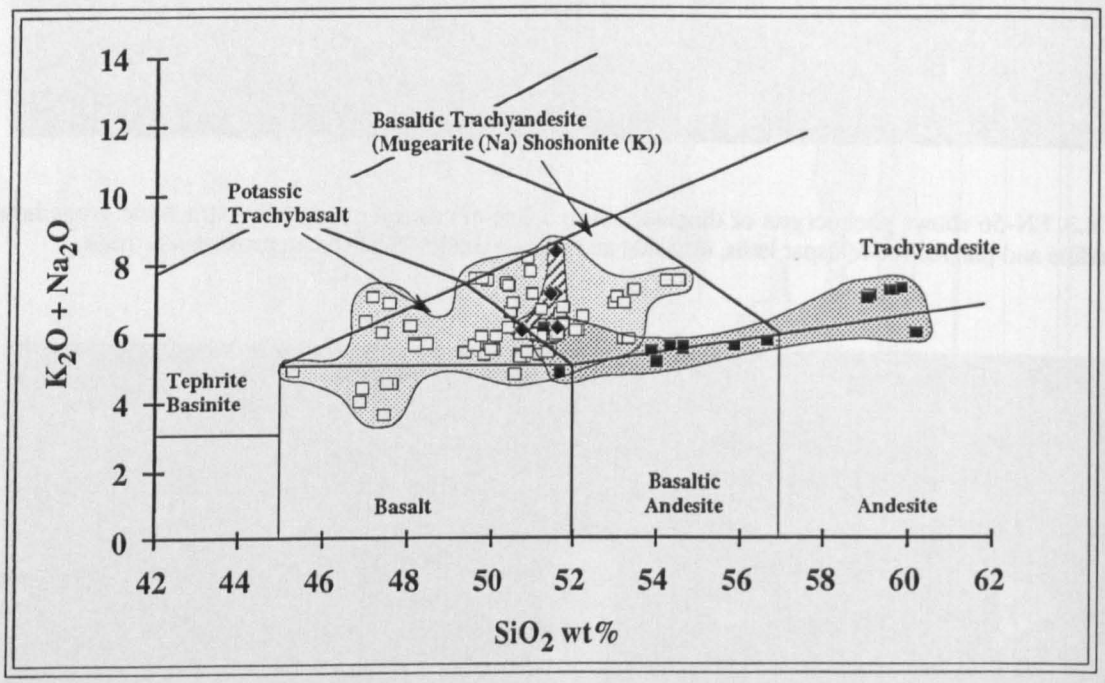


**Figure 4.5.** Total alkali vs. silica for Late Miocene basalts (closed squares), low Rb/Sr Pliocene basalts (open squares) and high Rb/Sr Pliocene basalts (closed diamonds) from the SKVF, central Sierra Nevada. See section 4.4.4. for discrimination between Pliocene basalts.

Fig 4.5 illustrates the variation in abundance of the alkali elements $K_2O$ and $Na_2O$ with $SiO_2$ in volcanics of Late Miocene and Pliocene age along with the IUGS recommended fields for the classification of volcanic rocks (Le Bas, 1986). The three-fold division of volcanics as proposed by Dodge & Moore (1980b) and Van Kooten (1980) is not apparent in Fig 4.5 and is therefore not adopted in the present study. Late Miocene magmatism represents a cogenetic suite of alkali basalts, basaltic trachyandesites and more evolved trachyandesites.

The Pliocene volcanics have generally lower silica, 45-55%, and higher abundances of the alkali elements than their predecessors and from a series of alkali basalts, potassic trachybasalts and shoshonites. As a whole the Pliocene volcanics of the SKVF are characterised by high and variable $K_2O$ contents at a given $SiO_2$ and can be regarded to form a shoshonitic series whereas the late Miocene volcanics form a high-K calcalkaline series as illustrated in Fig 4.6.

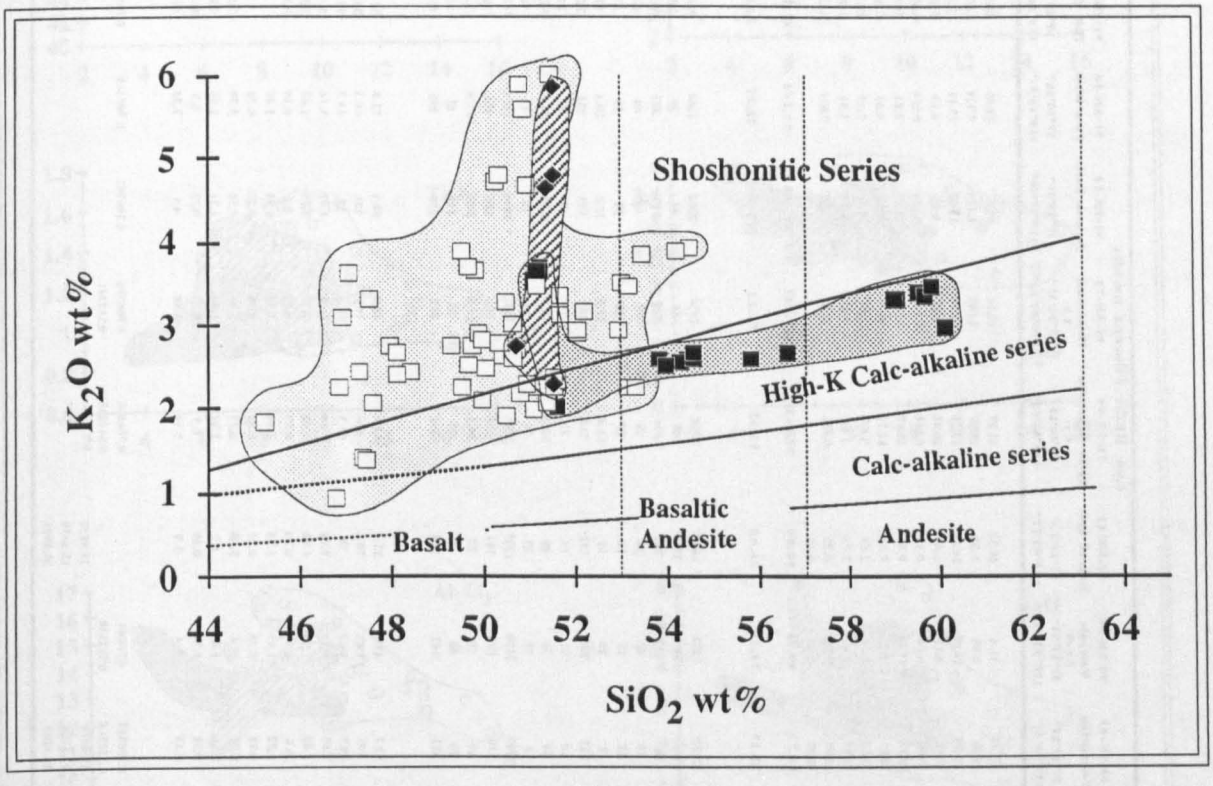


**Figure 4.6.** Variation in $K_2O$ with $SiO_2$ in the Late Miocene and Pliocene basalts from the SKVF, central Sierra Nevada. Calc-alkaline, high-K Calc-alkaline and Shoshonitic series from the Basaltic Volcanism Study Project Fig 1.2.7.1., p.193 (1981).

Hereafter the Cenozoic volcanics of the SKVF are discussed in terms of the two temporally distinct groups identified in section 4.3. and for simplicity will be referred to as basalts.

### 4.4.3: Major element variations.

Geochemical data for a selection of representative samples from the SKVF are presented in Table 4.1 and the complete database presented in Appendix A. Figure 4.7 presents the major element compositional variations of both Late Miocene and Pliocene basalts from the SKVF plotted against MgO. The Pliocene basalts are further divided into two groups on the basis of trace elements as will be discussed in section 4.4.4.

**Table 4.1.** Major and trace element and isotopic composition of representative samples from the three groups identified in the san Joaquin-Kings volcanic field, central Sierra Nevada.

| | Late Miocene basalts | | | Low Rb/Sr Pliocene basalts | | | | | | | | | | High Rb/Sr Pliocene basalts | | | |
|---|---|---|---|---|---|---|---|---|---|---|---|---|---|---|---|---|---|
| *Sample#* | 90-SN-1 | 90-SN-20 | 90-SN-65 | 90-SN-22 | 90-SN-29 | 90-SN-45 | 90-SN-51 | 90-SN-61 | 91-SN-69 | 91-SN-73 | 91-SN-84 | 91-SN-96 | 91-SN-101 | 90-SN-23 | 90-SN-30 | 90-SN-50B | 90-SN-47 |
| *Location* | Black Point | Red Mtn | Sugarloaf Hill | Devils Table | Kaiser Diggings | Vermillion | Volcanic Knob | Hedrick Mdw | Little Rancheria Cr. | Woodchuck Lk. | Jackass Rock | Coco lakes | Fish Camp | Brown Cone | Kaiser Diggings | Volcanic Knob | Coolidge Mdw |
| *Lat* | 37°14'23" | 37°11'54" | 37°07'20" | 37°20'26" | 37°22'47" | 37°23'27" | 37°27'53" | 37°25'23" | 36°58'17" | 37°01'31" | 37°25'56" | 37°35'30" | 37°28'52" | 37°23'57" | 37°20'24" | 37°27'53" | 37°00'03" |
| *Long* | 119°15'26" | 119°06'54" | 119°23'32" | 119°01'38" | 119°14'13" | 119°00'41" | 118°53'22" | 119°03'27" | 118°57'02" | 118°53'22" | 119°17'46" | 119°15'52" | 119°36'59" | 119°14'24" | 119°14'38" | 118°53'22" | 118°56'46" |
| *SiO2* | 51.12 | 56.66 | 51.66 | 52.07 | 50.96 | 53.48 | 51.4 | 49.32 | 45.27 | 48.16 | 47.57 | 53.05 | 50.9 | 51.57 | 51.44 | 51.59 | 51.61 |
| *TiO2* | 1.37 | 0.91 | 0.99 | 0.95 | 1.19 | 1.02 | 0.95 | 1.52 | 1.097 | 1.042 | 1.174 | 0.924 | 1.606 | 1.42 | 1.25 | 1.31 | 0.921 |
| *Al2O3* | 12.46 | 13.18 | 13.79 | 14.36 | 12.84 | 13.99 | 14.07 | 14.18 | 13.26 | 13.57 | 13.02 | 15.11 | 13.51 | 12.98 | 13.09 | 11.19 | 14.67 |
| *Fe2O3* | 9.79 | 7.8 | 9.12 | 7.48 | 7.48 | 7.13 | 8.11 | 8.46 | 10.01 | 8.81 | 9.25 | 6.88 | 7.39 | 7.33 | 7.42 | 7.34 | 7.53 |
| *MnO* | 0.15 | 0.12 | 0.416 | 0.12 | 0.12 | 0.09 | 0.14 | 0.14 | 0.168 | 0.145 | 0.144 | 0.119 | 0.094 | 0.11 | 0.12 | 0.13 | 0.12 |
| *MgO* | 10.26 | 7.47 | 10.61 | 10.16 | 10.47 | 9.32 | 11.21 | 9.85 | 13.15 | 12.69 | 11.64 | 8.81 | 10.5 | 9.05 | 9.49 | 6.2 | 9.18 |
| *CaO* | 8.27 | 7.23 | 8.52 | 7.8 | 8.35 | 6.85 | 8.2 | 8.85 | 11.17 | 9.03 | 8.82 | 6.63 | 5.28 | 7.78 | 8.22 | 9.35 | 8.55 |
| *Na2O* | 2.42 | 3.06 | 2.84 | 3.11 | 2.4 | 3.34 | 3.31 | 2.69 | 3.05 | 2.91 | 3.5 | 3.48 | 2.11 | 2.27 | 2.47 | 2.47 | 3.8 |
| *K2O* | 3.52 | 2.66 | 2 | 2.92 | 4.66 | 3.84 | 2.06 | 2.73 | 1.83 | 2.67 | 3.29 | 3.51 | 5.59 | 4.78 | 4.61 | 5.84 | 2.28 |
| *P2O5* | 0.57 | 0.31 | 0.516 | 0.48 | 0.88 | 0.64 | 0.48 | 0.75 | 0.838 | 0.92 | 1.197 | 0.631 | 1.529 | 1.17 | 0.98 | 0.84 | 0.549 |
| *LOI* | -0.4 | 0.55 | | 0.15 | 0.25 | 0.05 | 0.03 | 0.35 | | | | | | 1.13 | 0.61 | 3.42 | |
| *Total* | 99.53 | 99.95 | 100.462 | 99.6 | 99.6 | 99.75 | 99.96 | 98.84 | 99.843 | 99.947 | 99.605 | 99.144 | 98.509 | 99.59 | 99.7 | 99.68 | 99.21 |
| *Mg#* | 68.73 | 66.76 | 70.93 | 74.02 | 74.59 | 73.27 | 74.35 | 70.95 | 73.37 | 75.13 | 72.52 | 72.87 | 74.87 | 72.14 | 72.84 | 63.92 | 71.88 |
| *XRF* | | | | | | | | | | | | | | | | | |
| *Ba* | 1241 | 973 | 891 | 1834 | 2930 | 2230 | 1232 | 1940 | 2288 | 2436 | 2386 | 2264 | 3638 | 4323 | 3330 | 2066 | 2336 |
| *Co* | 45 | 32 | 45 | 36.7 | 37.5 | 34.4 | 39.6 | 39.7 | 49 | 41 | 44 | 30 | 33 | 41 | 42 | 31 | 32 |
| *Cr* | 570 | 415 | 665 | 338 | 428 | 233 | 417 | 322 | 804 | 742 | 513 | 367 | 532 | 395 | 436 | 159 | 384 |
| *Cu* | 41 | 49 | 59 | 46 | 65 | 44 | 42 | 56 | 79 | 64 | 69 | 49 | 63 | 71 | 82 | 52 | 51 |
| *Ga* | 16 | 18 | 19 | 15 | 18 | 17 | 15 | 16 | 17 | 13 | 16 | 15 | 17 | 18 | 17 | 16 | 18 |
| *Nb* | 15 | 9 | 10.9 | 7 | 9 | 9 | 10 | 15 | 11.4 | 11.9 | 15.8 | 10.4 | 17 | 14 | 12 | 37 | 9.7 |
| *Ni* | 212 | 155 | 212 | 274 | 239 | 272 | 335 | 232 | 314 | 285 | 309 | 251 | 387 | 301 | 233 | 142 | 189 |
| *Pb* | 13 | 15 | 13 | 19 | 17 | 19 | 11 | 14 | 22 | 19 | 17 | 21 | 21 | 30 | 18 | 48 | 24 |
| *Rb* | 121 | 92 | 56.6 | 44 | 76 | 54 | 32 | 80 | 32.2 | 48.7 | 65.3 | 51.8 | 76.4 | 662 | 392 | 152 | 146 |
| *Sc* | 17 | 13 | 22 | 16 | 15 | 8 | 13 | 23 | 24 | 24 | 18 | 15 | 18 | 11 | 11 | 9 | 16 |
| *Sr* | 718 | 769 | 849 | 1467 | 2056 | 1797 | 1110 | 1223 | 1791 | 1532 | 1696 | 1334 | 1489 | 2674 | 2266 | 1323 | 1836 |
| *V* | 160 | 133 | 203 | 147 | 174 | 130 | 136 | 181 | 229 | 181 | 186 | 158 | 209 | 180 | 183 | 146 | 155 |
| *Y* | 20 | 15 | 19.6 | 17 | 17 | 15 | 19 | 22 | 24.4 | 21.8 | 20.5 | 17.6 | 16.6 | 22 | 21 | 27 | 15.8 |
| *Zn* | 88 | 76 | 89 | 69 | 74 | 69 | 68 | 78 | 89 | 73 | 112 | 68 | 82 | 92 | 73 | 93 | 76 |
| *Zr* | 195 | 149 | 151 | 189 | 327 | 232 | 141 | 241 | 202 | 229 | 158 | 289 | 653 | 434 | 358 | 328 | 194 |
| *INAA* | | | | | | | | | | | | | | | | | |
| *La* | 34.6 | 23 | 31.8 | 42.6 | 64.8 | 52.3 | 43.6 | 33.4 | 63.4 | 48.6 | 58.9 | 33.8 | 31.4 | 94.3 | 79.1 | 135 | 50.2 |
| *Ce* | 72.6 | 44.8 | 64.7 | 83.2 | 127 | 105 | 89.4 | 70.6 | 126 | 102 | 121 | 69.5 | 56.7 | 187 | 148 | 244 | 98.4 |
| *Nd* | 46.2 | 25.4 | 33.9 | 32.9 | 64.7 | 49.7 | 36.7 | 38 | 61.5 | 51.4 | 58 | 35.3 | 33.9 | 89.5 | 76.6 | 117 | 47.7 |
| *Sm* | 8.43 | 4.86 | 6.36 | 6.27 | 9.44 | 7.65 | 6.13 | 7.02 | 9.26 | 7.88 | 8.47 | 5.76 | 5.49 | 12.4 | 11.1 | 19.7 | 7.36 |
| *Eu* | 2.24 | 1.41 | 1.89 | 1.62 | 2.25 | 1.89 | 1.62 | 1.97 | 2.42 | 2.25 | 2.25 | 1.62 | 1.54 | 2.94 | 2.6 | 4.58 | 1.98 |
| *Tb* | 0.95 | 0.55 | 0.74 | 0.58 | 0.67 | 0.6 | 0.59 | 0.79 | 0.85 | 0.72 | 0.8 | 0.59 | 0.59 | 0.85 | 0.84 | 1.61 | 0.67 |
| *Yb* | 1.48 | 1.11 | 1.53 | 1.46 | 1.38 | 1.22 | 1.43 | 1.76 | 1.99 | 1.69 | 1.74 | 1.48 | 1.3 | 1.22 | 1.44 | 1.79 | 1.28 |
| *Lu* | 0.21 | 0.14 | 0.24 | 0.24 | 0.21 | 0.18 | 0.23 | 0.25 | 0.33 | 0.26 | 0.27 | 0.24 | 0.2 | 0.16 | 0.22 | | 0.2 |
| *Th* | 12 | 7.31 | 9.87 | 7 | 7.72 | 6.79 | 6.4 | 3.05 | 6.15 | 5.46 | 4.58 | 3.79 | 3.56 | 12.2 | 7.6 | 64.8 | 5.85 |
| *U* | 5.08 | 3.42 | 3.3 | 2.04 | 2.45 | 2.16 | 1.67 | 1.2 | 1.94 | 1.84 | 1.31 | 1.51 | 0.91 | 3.38 | 2.78 | 19.1 | 1.71 |
| *Ta* | 1.05 | 0.71 | 0.6 | 0.5 | 0.56 | 0.58 | 0.56 | 0.89 | 0.5 | 0.57 | 0.73 | 0.5 | 0.73 | 0.69 | 0.63 | 2.35 | 0.41 |
| *Hf* | 5 | 3.99 | 4.17 | 4.38 | 8.28 | 6.18 | 3.4 | 5.9 | 5.14 | 5.98 | 4.1 | 7.38 | 15.6 | 12.1 | 9.56 | 9.11 | 4.97 |
| *ISOTOPES* | | | | | | | | | | | | | | | | | |
| *87/86* | 0.705246 | 0.705295 | 0.704804 | 0.70629 | 0.706687 | 0.706347 | 0.70668 | | 0.706866 | 0.706576 | 0.706761 | 0.706443 | 0.706309 | 0.706301 | 0.706294 | 0.706282 | 0.706706 |
| *143/144* | 0.512609 | 0.512674 | | 0.512421 | 0.512337 | 0.512368 | 0.512338 | | 0.512288 | 0.512341 | | | | 0.512348 | 0.512426 | 0.51265 | |
| *26/204* | 19.1340 | 19.1247 | | 18.9912 | 18.8737 | 18.8474 | | 18.8839 | | | | | | 18.9264 | | 19.1606 | |
| *207/204* | 15.6319 | 15.6234 | | 15.6637 | 15.5986 | 15.5766 | | 15.6439 | | | | | | 15.6643 | | 15.6794 | |
| *208/204* | 38.8127 | 38.7864 | | 38.8767 | 38.6858 | 38.6283 | | 38.8503 | | | | | | 38.9186 | | 39.0426 | |

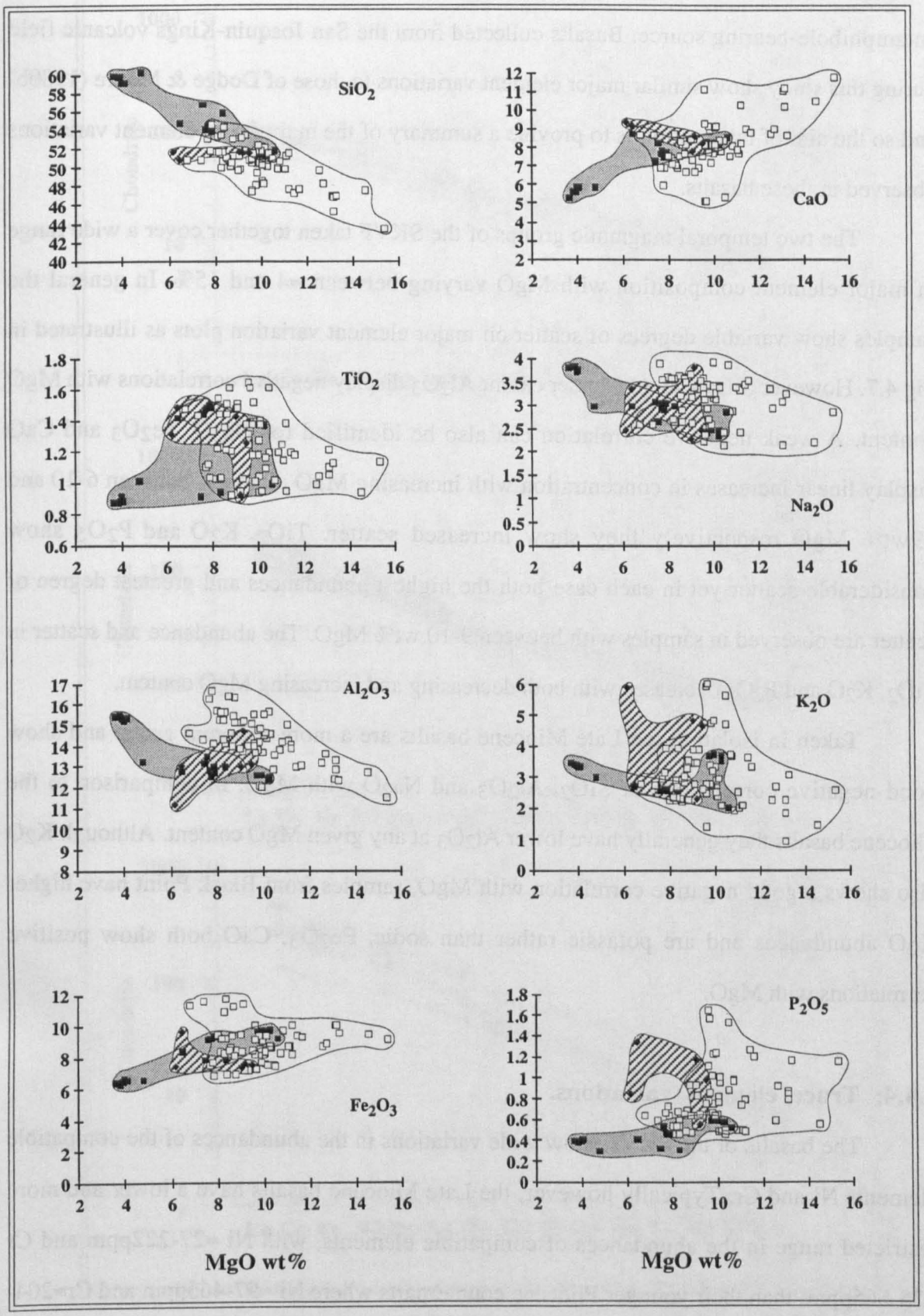


**Figure 4.7.** Major element oxide variations with MgO in late Miocene basalts (closed squares), low Rb/Sr Pliocene basalts (open squares) and high Rb/Sr Pliocene basalts (closed diamonds) from the San Joaquin-Kings volcanic field in the central Sierra Nevada, California. Total Fe expressed as $Fe_2O_3$..

The major and trace element element variations in basalts from the SKVF have already been discussed in detail in Dodge & Moore (1980b) where they argue for melt generation within an amphibole-bearing source. Basalts collected from the San Joaquin-Kings volcanic field during this study show similar major element variations to those of Dodge & Moore (1980b) and so the aim of this section is to provide a summary of the main major element variations observed in these basalts.

The two temporal magmatic groups of the SKVF taken together cover a wide range in major element composition with MgO varying between ≈4 and 15%. In general the samples show variable degrees of scatter on major element variation plots as illustrated in Fig 4.7. However $SiO_2$ and, to a lesser extent $Al_2O_3$ display negative correlations with MgO content. A weak negative correlation can also be identified for $Na_2O$. $Fe_2O_3$ and CaO display linear increases in concentration with increasing MgO although between 6-10 and >9wt% MgO respectively they show increased scatter. $TiO_2$, $K_2O$ and $P_2O_5$ show considerable scatter yet in each case both the highest abundances and greatest degree of scatter are observed in samples with between 9-10 wt% MgO. The abundance and scatter in $TiO_2$, $K_2O$ and $P_2O_5$ decreases with both decreasing and increasing MgO content.

Taken in isolation the Late Miocene basalts are a more coherent group and show good negative correlations of $SiO_2$, $Al_2O_3$ and $Na_2O$ with MgO. In comparison to the Pliocene basalts they generally have lower $Al_2O_3$ at any given MgO content. Although $K_2O$ also shows a good negative correlation with MgO, samples from Black Point have higher $K_2O$ abundances and are potassic rather than sodic. $Fe_2O_3$, CaO both show positive correlations with MgO.

### 4.4.4: Trace element variations.

The basalts of the SKVF show wide variations in the abundances of the compatible elements Ni and Cr. Typically however, the Late Miocene basalts have a lower and more restricted range in the abundances of compatible elements, with Ni ≈27-222ppm and Cr ≈35-665ppm, than their younger Pliocene counterparts where Ni ≈97-465ppm and Cr≈204-1363. These differences might suggest that the Late Miocene basalts are slightly more evolved than the Pliocene basalts.

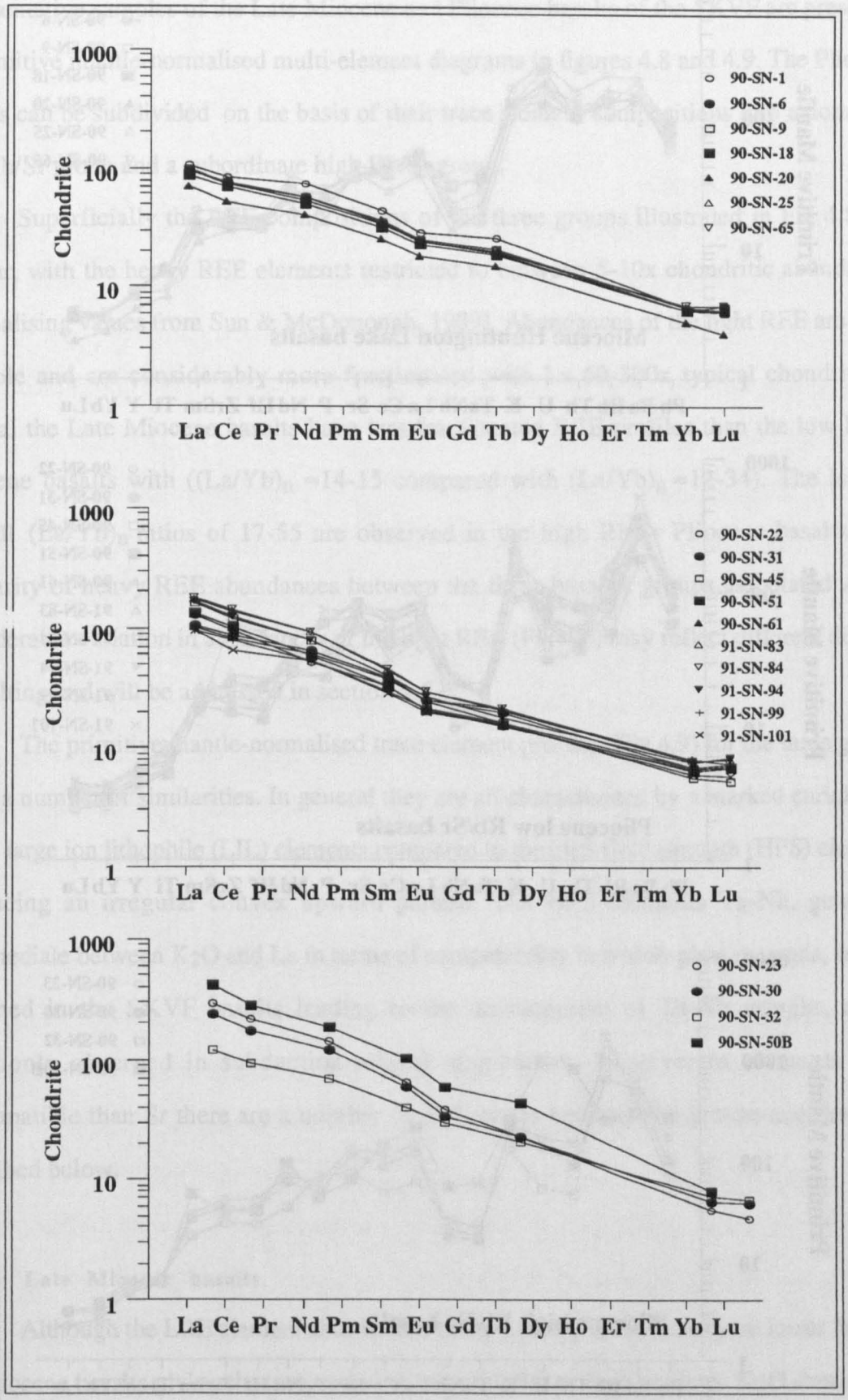


**Figure 4.8.** Rare earth element profiles for Late Miocene and Pliocene basalts of the SKVF. REE normalised to the chondritic abundances of Sun & McDonough (1989).

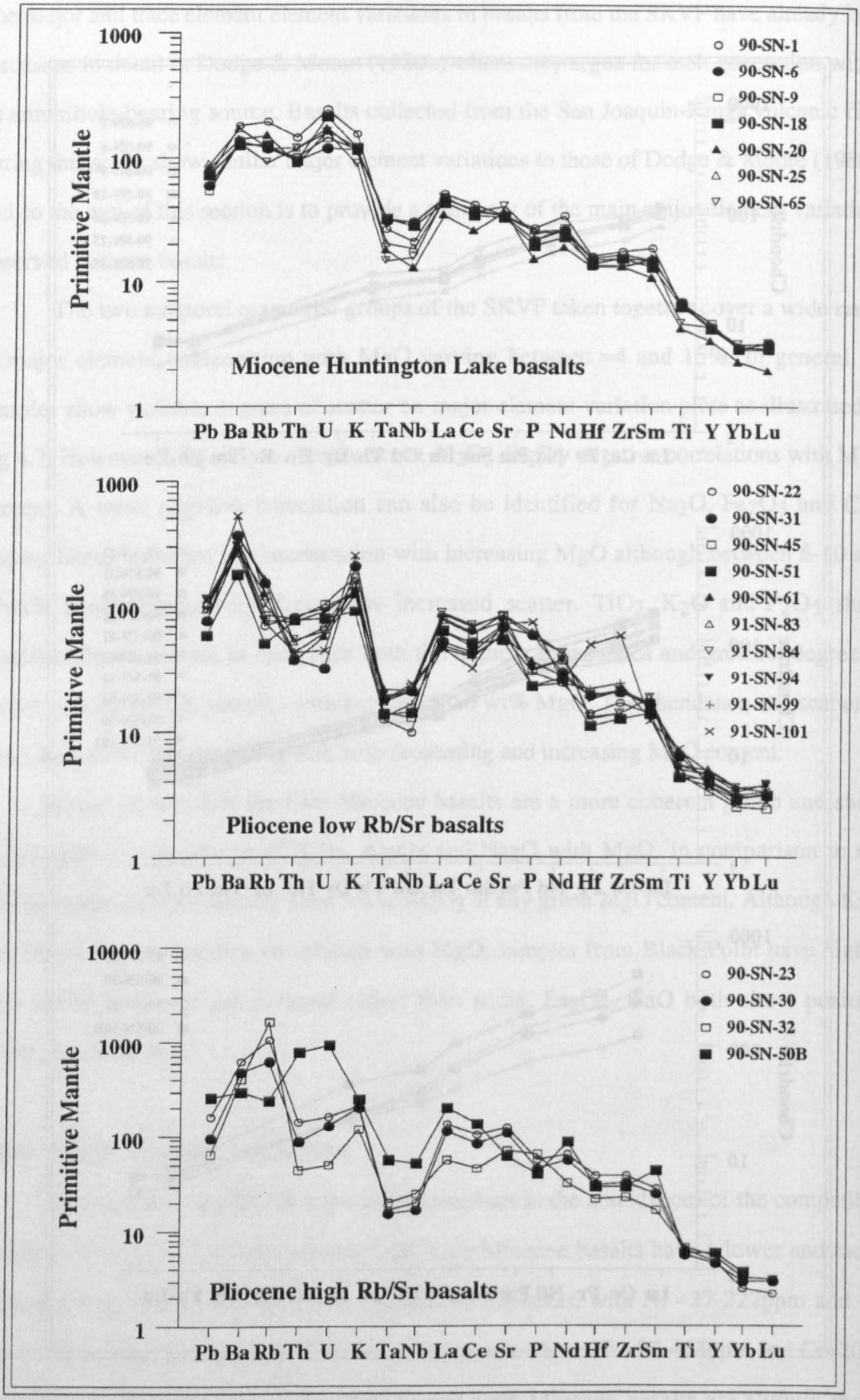


**Figure 4.9**. Incompatible trace element profiles for representative Late Miocene and Pliocene basalts from the SKVF. Trace element abundances are normalised to the primitive mantle abundances of Sun & McDonough (1989).

The rare earth element (REE) and incompatible trace element compositions of representative samples of the Late Miocene and Pliocene basalts of the SKVF are presented as primitive mantle-normalised multi-element diagrams in figures 4.8 and 4.9. The Pliocene basalts can be subdivided on the basis of their trace element compositions into a dominant low Rb/Sr group and a subordinate high Rb/Sr group.

Superficially the REE compositions of the three groups illustrated in Fig 4.8, are similar, with the heavy REE elements restricted to between 5-10x chondritic abundances (normalising values from Sun & McDonough, 1989). Abundances of the light REE are more variable and are considerably more fractionated with La 60-300x typical chondrite. In general the Late Miocene basalts have less fractionated REE profiles than the low Rb/Sr Pliocene basalts with ($(La/Yb)_n \approx 14$-15 compared with $(La/Yb)_n \approx 12$-34). The highest overall $(La/Yb)_n$ ratios of 17-55 are observed in the high Rb/Sr Pliocene basalts. The similarity of heavy REE abundances between the three basaltic groups associated with a considerable variation in abundances of the light REE (Fig 4.8) may reflect different degrees of melting and will be addressed in section 4.5.3.

The primitive mantle-normalised trace element profiles (Fig 4.9) for the three groups share a number of similarities. In general they are all characterised by a marked enrichment of the large ion lithophile (LIL) elements compared to the high field strength (HFS) elements producing an irregular convex upward pattern. The HFS elements Ta-Nb, generally intermediate between $K_2O$ and La in terms of compatability in within-plate magmas, are less enriched in the SKVF basalts leading to the development of Ta-Nb troughs, as are commonly observed in subduction-related magmatism. However in elements more incompatible than Sr there are a number of differences between the groups and these are described below.

#### 4.4.4a: Late Miocene basalts.

Although the LRE element abundances of the Late Miocene basalts are lower than for the Pliocene basalts giving the impression of less significant Ta-Nb trough, $K_2O$ abundances are similar in both groups and on this basis provide a better indication of the extent of the Ta-Nb depletion. The ratio K/Ta, taken as a measure of the Ta-Nb depletion varies from 16-31.

The elements Rb, Th and U in the Late Miocene basalts are generally 100-200x primitive mantle values, similar to Ba and $K_2O$ producing a broad plateau at the extreme left of the trace element profile as shown in Fig 4.9.

#### 4.4.4b: Pliocene basalts.

K/Ta ratios of the Pliocene basalts vary between 18-69 therefore implying the Ta-Nb depletion in these basalts is both greater and more variable than in the Late Miocene basalts. Ba is significantly more enriched than other incompatible elements producing a Ba peak, similar to that observed in many basalts from the western United States (Ormerod, 1988; Gans et al.,1989; Bacon, 1990; Fitton et al., 1991; Bradshaw, 1991; Davis, 1991). Furthermore the abundances of the elements Rb, Th, U are generally between 30-100x primitive mantle forming a broad trough between Ba and $K_2O$ distinct from the 'plateau' observed in the Late Miocene basalts. The Pliocene basalts can be divided into two groups on the basis of their incompatible element compositions as illustrated in Fig 4.9. The main characteristic of the subordinate basalt group is the marked enrichment of Rb (up to 2000x primitive mantle) over the majority of the Pliocene basalts and, as the Sr abundance is similar between the two groups this is associated with higher Rb/Sr ratios. The abundances of Th and U, other than in sample SN-50B, are similar between the two groups.

### 4.4.5: Radiogenic Isotopes.

A total of 39 basalts from the San Joaquin-Kings volcanic field were analysed for $^{87}Sr/^{86}Sr$ and 29 for $^{143}Nd/^{144}Nd$, of these 24 have both Sr and Nd isotope ratios. The isotopic composition of basalts from the SKVF are illustrated in Fig 4.10, a conventional Nd-Sr isotope correlation diagram. Also shown are additional data for basalts from the western Great Basin (Ormerod, 1988) and Geronimo alkali basalts from the southern Basin & Range representative of average post 5Ma asthenosphere-derived alkali basalt (Fitton & Kempton unpubl data; Fitton et al.,1991).

The basalts from the central Sierra Nevada clearly form two groups and these coincide with the temporal groups of section 4.3.1. This may imply melting of different

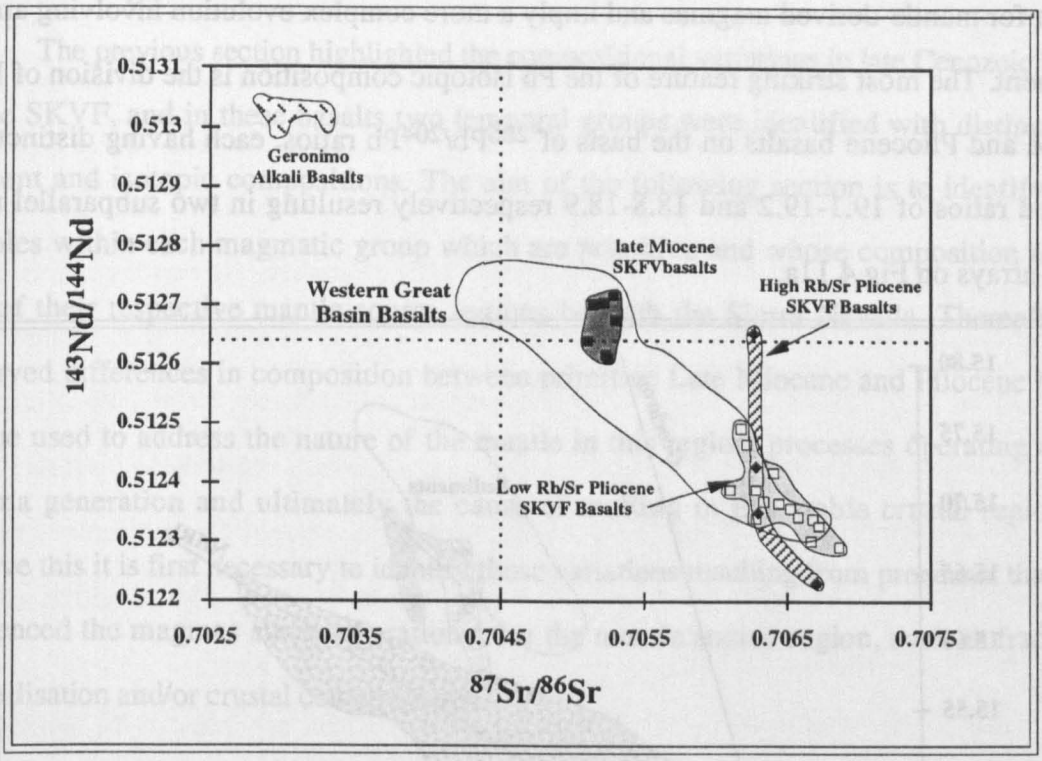


**Figure 4.10**. Variation in $^{143}Nd/^{144}Nd$ with $^{87}Sr/^{86}Sr$ in Late Miocene basalts (closed squares), low Rb/Sr Pliocene basalts (open squares) and high Rb/Sr Pliocene basalts (closed diamonds) from the SKVF, central Sierra Nevada. Shown for comparison is the isotopic variation for basalts from the Western Great Basin (Ormerod, 1988) and alkali basalts from the Geronimo volcanic field, southern Basin & Range (Kempton & Fitton, unpubl data).

mantle source regions at different times. Late Miocene basalts plot to the right of the mantle-array and have a restricted range in $^{87}Sr/^{86}Sr$ ratios of 0.70500-0.70530 and $^{143}Nd/^{144}Nd$ ratios of 0.51260-0.512714, close to bulk earth. The Pliocene basalts however plot to the right of the mantle-array within the enriched quadrant and in general display a broad negative correlation between Nd and Sr isotopes from 0.51249-0.51229 and 0.70613-0.70687 respectively. The high Rb/Sr subgroup, discussed in section 4.4.4, depart from the main Pliocene trend having a very limited range in $^{87}Sr/^{86}Sr$ between 0.70628-0.70671 associated with a large variation in $^{143}Nd/^{144}Nd$ between 0.51223-0.51265 producing an almost vertical array.

The Pb isotopic compositions determined on 6 Late Miocene and 11 Pliocene basalts are shown in Fig4.11 relative to the geochron, northern hemisphere reference line (NHRL) and the fields for Atlantic MORB and ocean sediments from Othman et al (1989). $^{206}Pb/^{204}Pb$ and $^{208}Pb/^{204}Pb$ ratios of 18.8-19.2 and 38.6-39.0 are not particularly extreme and are similar to radiogenic MORB or OIB. However $^{207}Pb/^{204}Pb$ ratios of 15.58-15.69

are high for mantle-derived magmas and imply a more complex evolution involving an old component. The most striking feature of the Pb isotopic composition is the division of Late Miocene and Pliocene basalts on the basis of $^{206}Pb/^{204}Pb$ ratios, each having distinct yet restricted ratios of 19.1-19.2 and 18.8-18.9 respectively resulting in two subparallel near vertical arrays on Fig 4.11a.

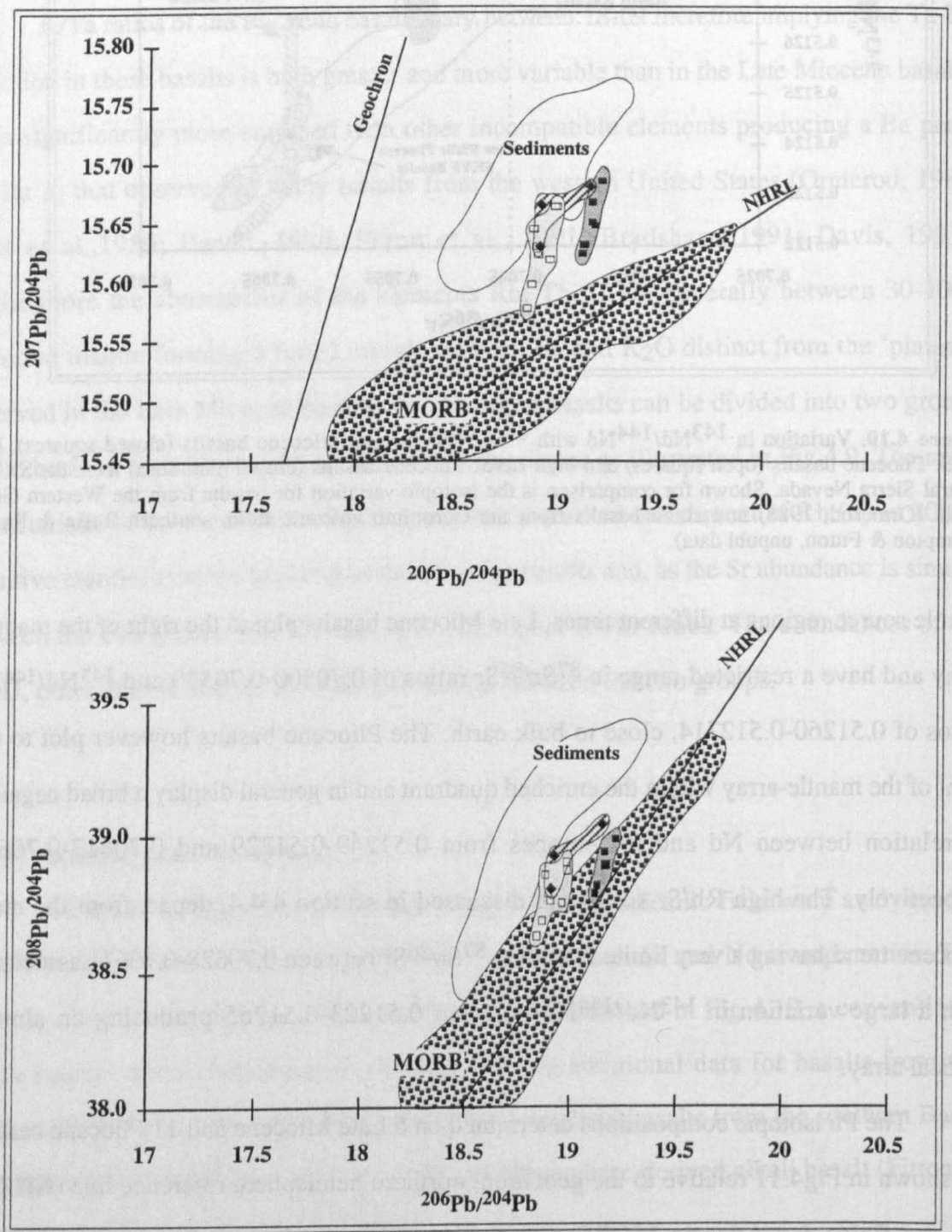


**Figure 4.11.** (A) $^{207}Pb/^{204}Pb$ versus $^{206}Pb/^{204}Pb$ and (B) $^{208}Pb/^{204}Pb$ versus $^{206}Pb/^{204}Pb$ for basalts from the San Joaquin-Kings volcanic field. Also shown for reference are the geochron, northern hemisphere reference line, the field for MORB and for ocean sediments (Othman et al., 1989). Symbols as for Figure 4.7.

## 4.5: Petrogenesis:

The previous section highlighted the compositional variations in late Cenozoic basalts of the SKVF, and in these basalts two temporal groups were identified with distinct trace element and isotopic compositions. The aim of the following section is to identify those samples within each magmatic group which are primitive and whose composition reflects that of their respective mantle source regions beneath the Sierra Nevada. Thereafter the observed differences in composition between primitive Late Miocene and Pliocene basalts can be used to address the nature of the mantle in this region, processes operating during magma generation and ultimately the cause of melting in this stable crustal region. To achieve this it is first necessary to identify those variations resulting from processes that have influenced the magmas since separation from the mantle source region, such as fractional crystallisation and/or crustal contamination.

### 4.5.1: Primitive vs evolved magmas.

Within the basalts from the central Sierra Nevada there is a wide variation in the abundance of the compatible element Ni which is positively correlated with Mg# and MgO content as illustrated in Fig 4.12.

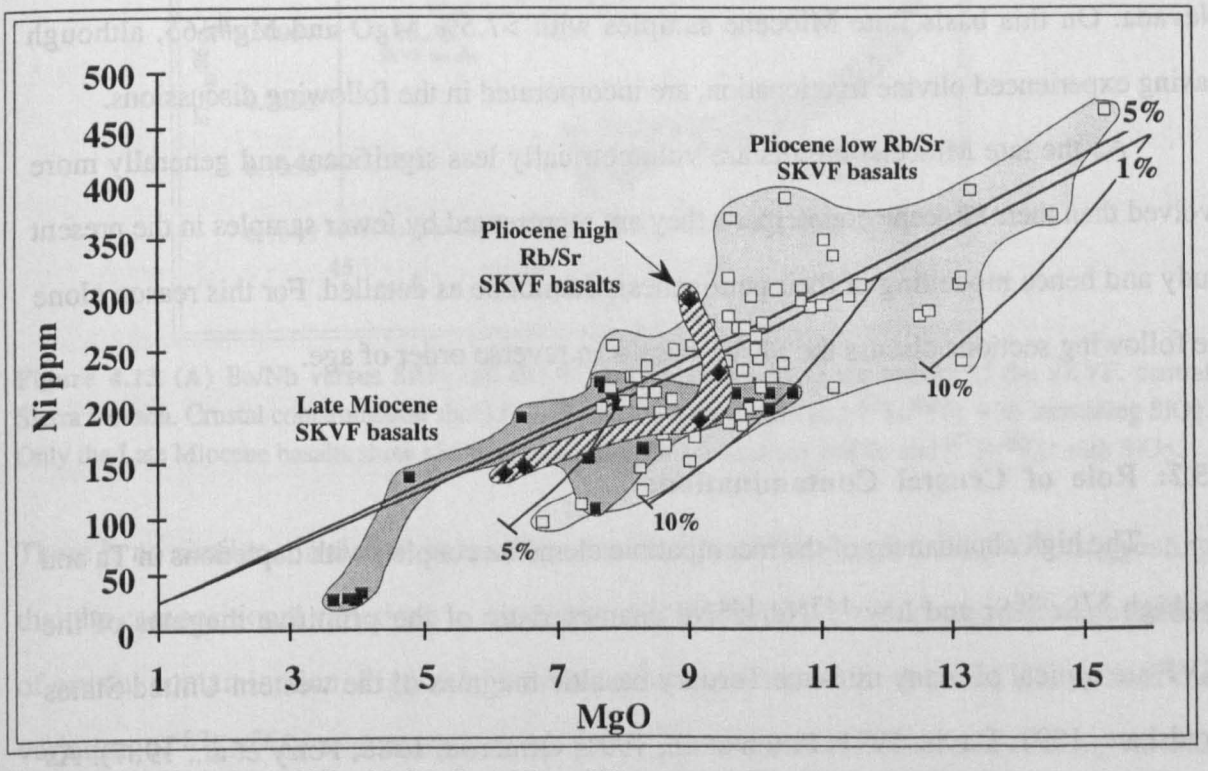


**Figure 4.12.** Variation of Ni with MgO and Late Miocene and Pliocene basalts from the San Joaquin-Kings volcanic field. Melting curves for 1 and 5% melting of a spinel lherzolite and olivine fractionation curves for parental magmas with 8, 12 and 16% MgO, calculated according to the methods presented in Hart & Davis (1978).

In each magmatic group the highest Mg#'s are observed in the most magnesian samples. The higher Mg#'s of ≥70 characteristic of many of the basalts suggest they are primitive melts derived directly from their mantle source region (Frey et al., 1978). Indeed on Fig 4.12 most basalts lie near to the model melting curves for mantle peridotite, calculated according to Hart & Davis (1978), and are therefore consistent with being primitive. However there is some scatter in the data and a number of samples with Mg#'s <70 fall below the modelled melt curves. These samples are consistent with fractionation of between 5 and 10% olivine as illustrated by the model olivine fractionation curves calculated according to Hart & Davis (1978). Those samples that plot above the model melt curves may have experienced minor olivine accumulation. Thus the majority of basalts from the SKVF can be considered to be primary or near primary melts.

Subsequent discussions are based only on those samples with primitive compositions thus avoiding any possible effects of crystal fractionation. In the case of the Pliocene basalts only those samples with Mg#'s >70 are considered as suitably primitive magmas. However of the Late Miocene basalts only one sample, SN-65, has a Mg# >70 and yet these basalts are important in understanding the evolution of magmatism in the Sierra Nevada. On this basis Late Miocene samples with >7.5% MgO and Mg#>65, although having experienced olivine fractionation, are incorporated in the following discussions.

As the late Miocene basalts are volumetrically less significant and generally more evolved than their Pliocene counterparts they are represented by fewer samples in the present study and hence modelling of their petrogenesis cannot be as detailed. For this reason alone the following sections discuss the SKVF basalts in reverse order of age.

### 4.5.2: Role of Crustal Contamination:

The high abundances of the incompatible elements coupled with depletions in Ta and Nb, high $^{87}Sr/^{86}Sr$ and low $^{143}Nd/^{144}Nd$ characteristic of the primitive magmas of the SKVF are typical of many mid-late Tertiary basaltic magmas of the western United States (Bradshaw, 1991; Davis, 1991; Fitton et al., 1991; Ormerod, 1988; Perry et al., 1987). As such, elemental and isotopic compositions are also characteristic of the crust, and several basalt flows and plugs within the SKVF contain granitic xenoliths. This section assesses the

possibility that the range of trace element and isotopic compositions of the SKVF is related to crustal contamination of primitive mantle-derived melts. If this model is correct then increasing contamination should be associated with increasing LIL/HFS, $^{87}Sr/^{86}Sr$ ratios and $SiO_2$ abundances. However, although the SKVF basalts have a large range in LIL/HFS ratios (eg. Ba/Nb =70-325) only the Late Miocene basalts show a systematic increase in Ba/Nb and $^{87}Sr/^{86}Sr$ ratios with $SiO_2$ (Fig 4.13).

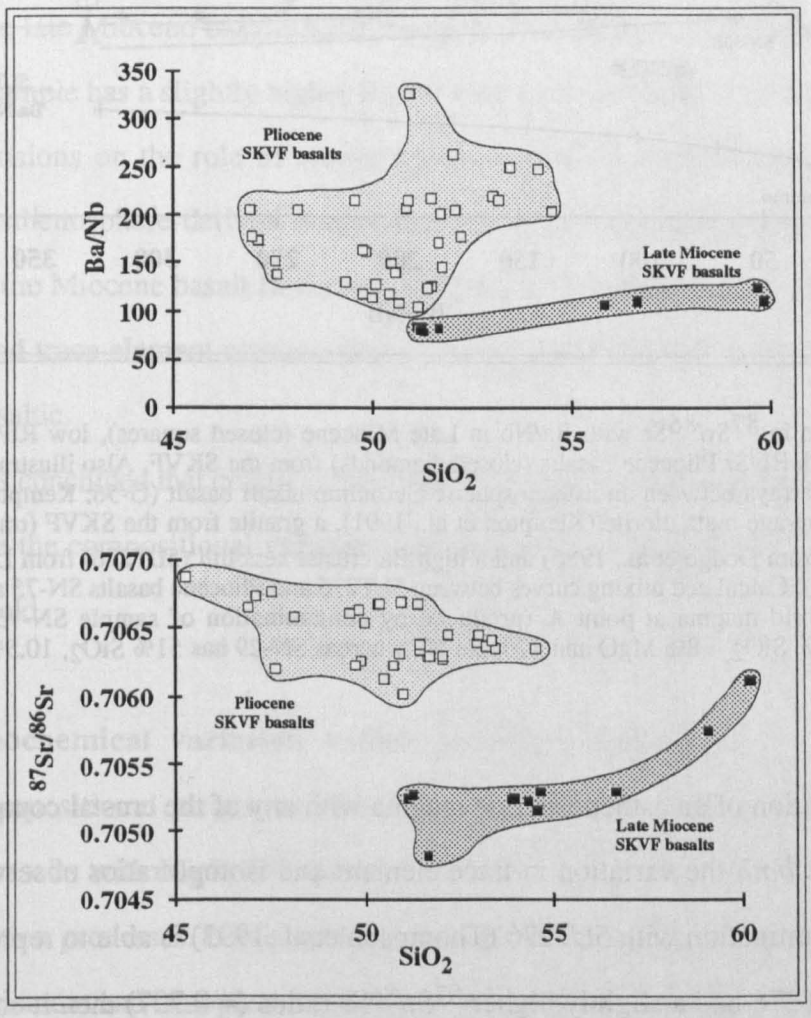


**Figure 4.13.** (A) Ba/Nb versus $SiO_2$ and (B) $^{87}Sr/^{86}Sr$ versus $SiO_2$ for basalts of the SKVF, central Sierra Nevada. Crustal contamination should result in increasing Ba/Nb and $^{87}Sr/^{86}Sr$ with increasing $SiO_2$. Only the Late Miocene basalts show slight positive correlations between Ba/Nb and $^{87}Sr/^{86}Sr$ with $SiO_2$.

There is no similar correlation in the Pliocene basalts, as illustrated in Fig 4.13, suggesting that the compositional variations in these younger basalts do not reflect significant quantities of crustal contamination. Figure 4.14 demonstrates this aspect further and shows both the variation of $^{87}Sr/^{86}Sr$ with Ba/Nb in the SKVF basalts and the effects of mixing various crustal components with a typical western United States asthenosphere-derived magma as represented by Geronimo sample G-56 (Kempton & Fitton, unpubl data).

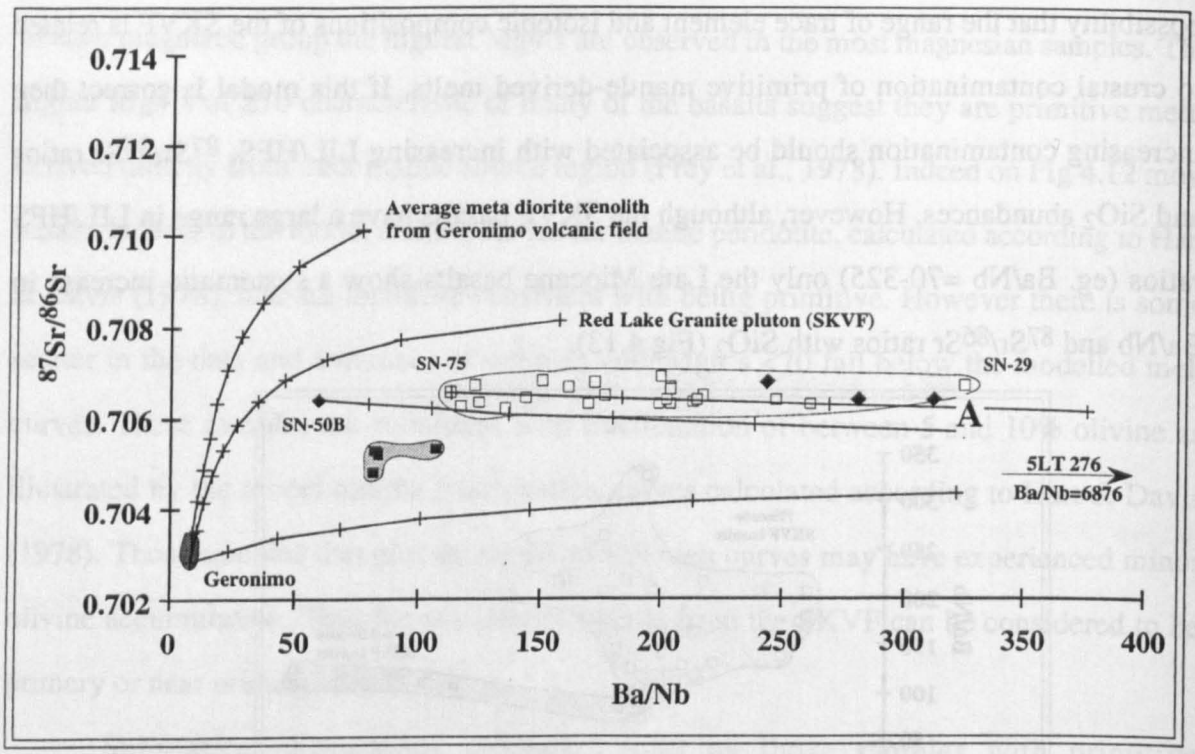


**Figure 4.14**. Variation in $^{87}Sr/^{86}Sr$ with Ba/Nb in Late Miocene (closed squares), low Rb/Sr Pliocene (open squares) and high Rb/Sr Pliocene basalts (closed diamonds) from the SKVF. Also illustrated are bulk crustal contamination arrays between an asthenospheric Geronimo alkali basalt (G-56; Kempton & Fitton unpubl data) and an average meta diorite (Kempton et al., 1991), a granite from the SKVF (trace elements this study, $^{87}Sr/^{86}Sr$ from Dodge et al., 1986) and a high Ba crustal xenolith (5LT276) from Leucite Hills (Thompson et al., 1993). Calculated mixing curves between 5LT276 and Pliocene basalts SN-75 and SN-50B are also shown. A hybrid magma at point **A** (produced by contamination of sample SN-75 with 25% 5LT276) contains ≈52% $SiO_2$, ≈8% MgO and 170ppm Ni, whereas SN-29 has 51% $SiO_2$, 10.5% MgO and 240ppm Ni.

Although contamination of an asthenospheric magma with any of the crustal components is unable to reproduce *both* the variation in trace element and isotope ratios observed in the SKVF basalts, contamination with 5LT276 (Thompson et al.,1993) is able to reproduce the Ba/Nb ratios. If 5LT276 had a slightly higher $^{87}Sr/^{86}Sr$ ratios (≈ 0.707) then it could quite readily reproduce the isotopic and trace element variation of the Miocene and Pliocene basalts. However to reproduce the Ba/Nb ratios of the most enriched of the Pliocene basalts (SN-29) would require 70% addition of 5LT276 resulting in a hybrid magma with $SiO_2$≈55.5wt% in contrast to the 51% $SiO_2$ measured in SN-29.

Contamination of SN-75, the lowest Ba/Nb sample of the main Pliocene basalt group, with the high Ba crustal xenolith from Leucite Hills (5LT276: Thompson et al.,1993) does reproduce the range of trace element and isotope ratios of the Pliocene basalts. To do so requires only 25% addition of 5LT276 (point A on Fig 4.14) which results in a hybrid

magma containing ≈52% $SiO_2$, ≈8% MgO and ≈170ppm Ni. This is relatively similar to the measured abundances in the highest Ba/Nb Pliocene basalt, sample SN-29, with $SiO_2$≈51%, MgO≈10.5% and Ni≈240ppm. However in order to reproduce the high Ba/Nb ratios of the Pliocene basalts an exotic crustal component with an extreme Ba/Nb ratio of 6876 is required which is not typical of crust and certainly not so of the Sierra Nevada region which is dominated by a granitic batholith.

The late Miocene basalts have a very limited range in $^{87}Sr/^{86}Sr$ and Ba/Nb and as only one sample has a slightly higher Ba/Nb than the main group it is inappropriate to draw any conclusions on the role of crustal contamination in these basalts. However mixing between asthenosphere-derived magmas and the Red Lake granite pluton, through which several of the Miocene basalt flows were emplaced, clearly is unable to reproduce both the isotopic and trace element composition of these basalts and still keep the resultant hybrid magma basaltic.

It is concluded that crustal contamination of mafic magmas is not a viable mechanism to generate the compositional variations within primitive basalts of the San Joaquin-Kings volcanic field.

### 4.5.3: Geochemical variation within primitive magmas.

Compositional variations observed in Late Miocene basalts with Mg#≥65 and in Pliocene basalts with Mg#≥70 cannot be reproduced by crystal fractionation and crustal contamination processes. It is concluded that the distinct within-group variations in major and trace element and isotopic compositions of these primitive basalts are inherited from the mantle and reflect either differences in source composition and/or processes operating in the source during magma genesis. The following discussion uses these magmas to determine the processes operating in the mantle during the Late Cenozoic. Incorporated into this discussion are data for alkali basalts from the Geronimo volcanic field, southern Basin & Range (Kempton, 1987), assumed to be typical of Pliocene asthenosphere-derived basalts found across the Basin & Range.

#### 4.5.3 a: Pliocene Basalts:

The variation in degree of REE fractionation (La/Yb ≈20-70) observed in the Pliocene is within the range observed in OIB magmas and can be generated by small degrees of melting of a primitive mantle source in the presence of residual garnet. This suggests that the REE compositions of the Pliocene basalts could be generated by a single stage melting event of an asthenospheric source.

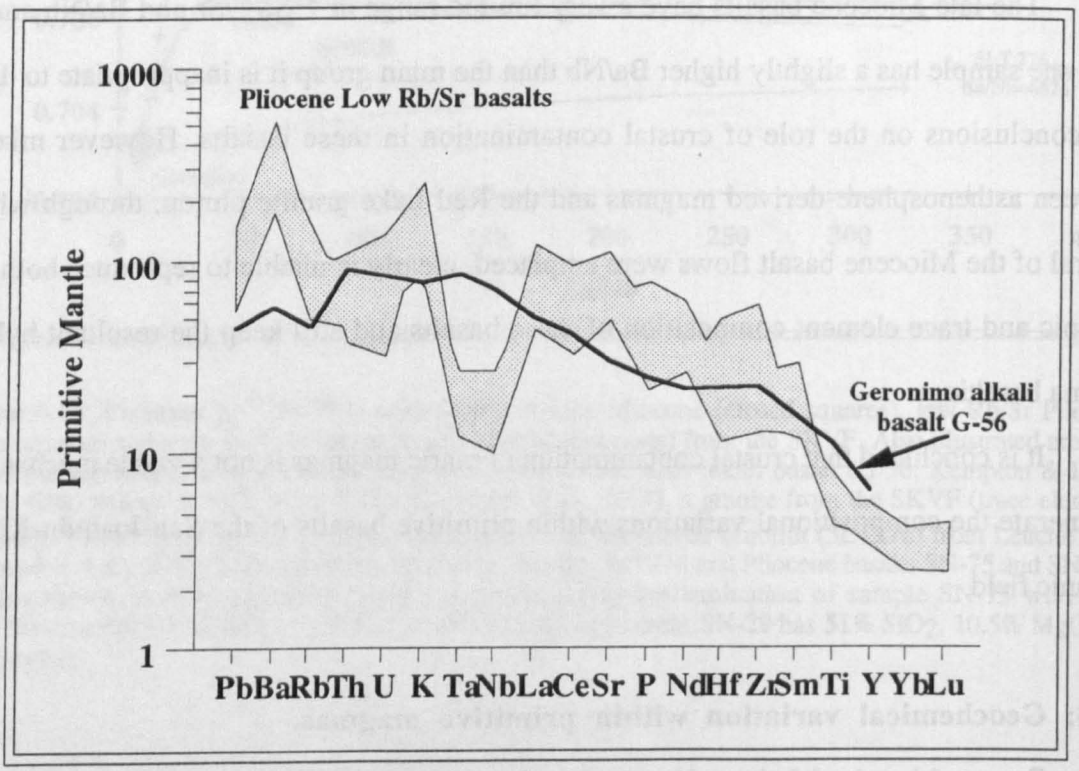


**Figure 4.15.** Comparison of Pliocene basalts from the SKVF with a typical asthenosphere-derived basalt G-56 from the Geronimo volcanic field (Kempton & Fitton, unpubl data).

Figure 4.15 compares the trace element composition of a typical western United States asthensophere-derived magma with the Pliocene basalts. The irregular mantle-normalised trace element profiles of the Pliocene basalts contrast markedly with the smooth profiles typical of the OIB-like asthenosphere-derived basalts implying that they are not derived from an asthenospheric source. High abundances of the LIL elements Ba and K and distinct depletions in the HFS elements Ta and Nb suggest the Pliocene basalts were derived from a trace element enriched source region with HFS element depletions (Ormerod et al., 1991). Furthermore their elevated $^{87}Sr/^{86}Sr$ and low $^{143}Nd/^{144}Nd$ ratios compared to asthenospheric values (Fig 4.10) suggests the source was characterised by a time integrated trace element enrichment. It is therefore suggested that the Pliocene basalts were derived

from melting of an enriched sub-continental lithospheric mantle source beneath the Sierra Nevada.

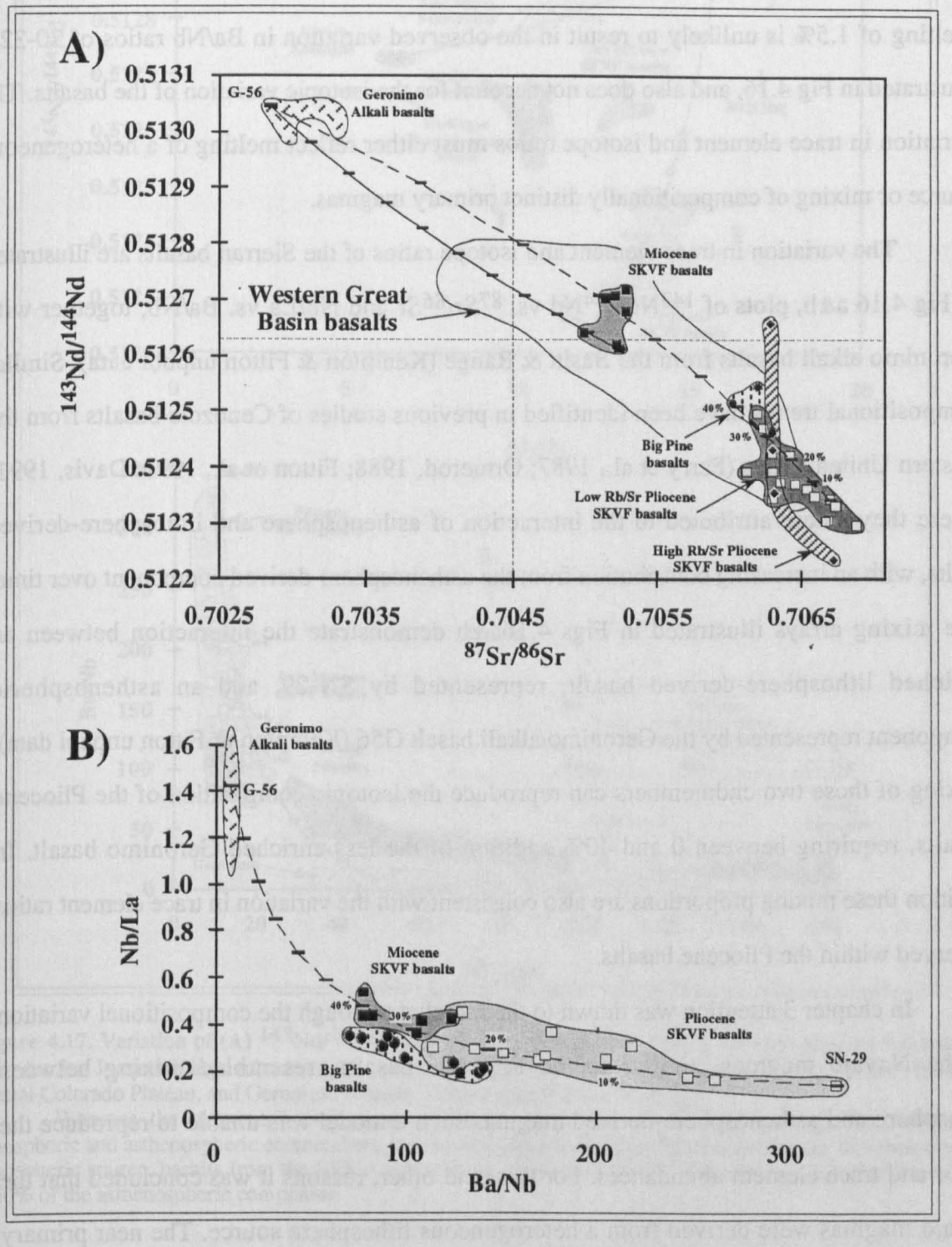


**Figure 4.16**. Variation of (**A**) $^{143}Nd/^{144}Nd$ with $^{87}Sr/^{86}Sr$ and (**B**) Nb/La with Ba/Nb for basaltic volcanics from the San Joaquin-Kings, Big Pine and Geronimo volcanic fields from the central Sierra Nevada, western Great Basin and southern Basin & Range respectively. Also shown is a mixing curve between Geronimo alkali basalt G-56 (Kempton & Fitton unpubl data) and the Pliocene SKVF basalt SN-29. This mixing model is able to reproduce the trace element and isotope ratios of the Sierran basalts by 0-40% addition of the asthenosphere-derived endmember G-56.

Van Kooten (1980, 1981) suggested that the variation in the degree of REE fractionation and trace element abundances can be generated by 1-2.5% melting of a homogeneous phlogopite-bearing garnet peridotite. However a variation in the degree of melting of 1.5% is unlikely to result in the observed variation in Ba/Nb ratios of 70-325, illustrated in Fig 4.16, and also does not account for the isotopic variation of the basalts. The variation in trace element and isotope ratios must either reflect melting of a heterogeneous source or mixing of compositionally distinct primary magmas.

The variation in trace element and isotope ratios of the Sierran basalts are illustrated in Fig 4.16 a&b, plots of $^{143}Nd/^{144}Nd$ vs. $^{87}Sr/^{86}Sr$ and Nb/La vs. Ba/Nb, together with Geronimo alkali basalts from the Basin & Range (Kempton & Fitton unpubl data). Similar compositional trends have been identified in previous studies of Cenozoic basalts from the western United States (Perry et al., 1987; Ormerod, 1988; Fitton et al., 1991; Davis, 1991) where they where attributed to the interaction of asthenosphere and lithosphere-derived melts, with an increasing contribution from the asthenosphere-derived component over time. The mixing arrays illustrated in Figs 4.16a&b demonstrate the interaction between an enriched lithosphere-derived basalt, represented by SN-29, and an asthenospheric component represented by the Geronimo alkali basalt G56 (Kempton & Fitton unpubl data). Mixing of these two endmembers can reproduce the isotopic composition of the Pliocene basalts, requiring between 0 and 40% addition of the less enriched Geronimo basalt. In addition these mixing proportions are also consistent with the variation in trace element ratios observed within the Pliocene basalts.

In chapter 3 attention was drawn to the fact that although the compositional variation of the Navajo magmas, similar to the Pliocene basalts, resembled mixing between lithosphere and asthenosphere-derived magmas such a model was unable to reproduce the major and trace element abundances. For this, and other, reasons it was concluded that the Navajo magmas were derived from a heterogeneous lithosphere source. The near primary Pliocene basalts have not experienced significant fractionation or crustal contamination and therefore the lithosphere-asthenosphere mixing model, presented in Fig 4.16 a&b, can be further assessed in terms of elemental *abundances*.

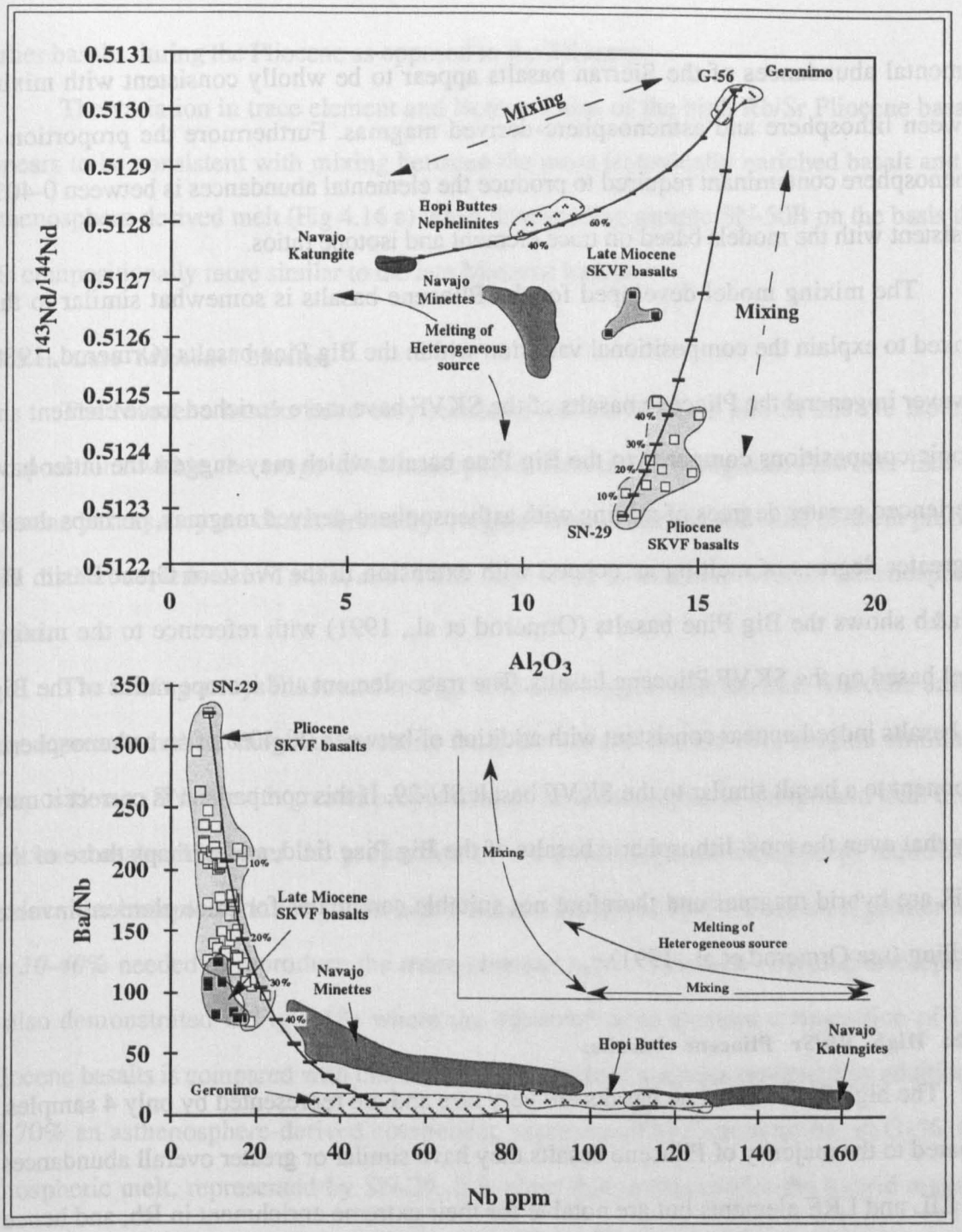


**Figure 4.17.** Variation of **(A)** $^{143}Nd/^{144}Nd$ with $Al_2O_3$ wt% and **(B)** Ba/Nb with Nb ppm for volcanics from the San Joaquin-Kings volcanic field, central Sierra Nevada, the Navajo and Hopi Buttes volcanic fields, central Colorado Plateau, and Geronimo volcanic field, southern Basin & Range.

Whereas the elemental abundances of the Minettes are inconsistent with mixing between lithospheric and asthenospheric endmembers and are attributed to melting of a compositionally heterogeneous lithospheric source, basalts from the SKVF appear to be entirely consistent with mixing, requiring between 0-40% of the asthenospheric component.

Figure 4.17 a&b illustrates the variation of $^{143}Nd/^{144}Nd$ with $Al_2O_3$ and Ba/Nb with Nb respectively. Also shown for reference are analyses for Navajo and Hopi Buttes, a mixing curve between a Navajo Katungite and Geronimo sample G-56 and the mixing model presented in Fig 4.16. Unlike the potassic magmas of the Navajo volcanic field, the

elemental abundances of the Sierran basalts appear to be wholly consistent with mixing between lithosphere and asthenosphere-derived magmas. Furthermore the proportion of asthenosphere contaminant required to produce the elemental abundances is between 0-40%, consistent with the models based on trace element and isotope ratios.

The mixing model developed for the Pliocene basalts is somewhat similar to that invoked to explain the compositional variation within the Big Pine basalts (Ormerod, 1988) However in general the Pliocene basalts of the SKVF have more enriched trace element and isotopic compositions compared to the Big Pine basalts which may suggest the latter have experienced greater degrees of mixing with asthensophere-derived magmas, perhaps due to the greater degrees of melting associated with extension in the Western Great Basin. Fig 4.16a&b shows the Big Pine basalts (Ormerod et al., 1991) with reference to the mixing model based on the SKVF Pliocene basalts. The trace element and isotope ratios of the Big Pine basalts indeed appear consistent with addition of between 20-40% of an asthenospheric component to a basalt similar to the SKVF basalt SN-29. If this comparison is correct it may imply that even the most lithospheric basalts of the Big Pine field, and perhaps those of the SKVF, are hybrid magmas and therefore not suitable candidates for trace element inverse modelling (see Ormerod et al., 1991).

#### 4.5.3.b: High Rb/Sr Pliocene basalts:

The high Rb/Sr Pliocene basalts are very rare and are represented by only 4 samples. Compared to the majority of Pliocene basalts they have similar or greater overall abundances of the LIL and LRE elements but are notable for their extreme enrichment in Rb, and hence high Rb/Sr ratios (Fig 4.9). The degree of REE fractionation is also more extreme than in most Pliocene basalts with La/Yb ≈25-75 which may suggest they may represent smaller degree melts. The similar trace element and isotopic composition to the main Pliocene group suggest they may be derived from a similar lithospheric source to the main Pliocene basalts albeit with slightly different Rb abundances. Sample SN-50B however, despite its Pliocene age (Dalrymple, 1963), is unlike the Pliocene high Rb/Sr basalts and has very similar trace element compositions and Nd and Pb isotope ratios to the Late Miocene basalts (sections 4.4.4 and 4.4.5) which suggests it may have been derived from a similar source to these

earlier basalts during the Pliocene as opposed to the Miocene.

The variation in trace element and isotope ratios of the high Rb/Sr Pliocene basalts appears to be consistent with mixing between the most isotopically enriched basalt and an asthenosphere-derived melt (Fig 4.16 a) when disregarding sample SN-50B on the basis that it is compositionally more similar to the late Miocene basalts.

#### 4.5.3.c: Late Miocene Basalts:

The Miocene basalts have very restricted La/Yb of 21-25 and Sr and Nd isotopic compositions within the range of asthensophere-derived OIB magmas. However like the Pliocene basalts they are characterised by irregular mantle-normalised trace element profiles with distinct depletions in Ta-Nb, and in this respect are inconsistent with an asthenospheric origin.

The mixing arrays illustrated in Figs 4.16 a&b suggest that the Late Miocene basalts may represent hybrid magmas resulting from the contamination of a magma similar in composition to SN-29 with greater proportions of an asthenospheric component than in the Pliocene basalts. However the proportion of the asthenospheric component required to produce the ***isotopic*** variation in the Late Miocene basalts is ***60-70%*** which is greater than the ***30-40%*** needed to reproduce the ***trace element*** ratios. This mass balance discrepancy is also demonstrated in Fig 4.18a where the observed trace element composition of Late Miocene basalts is compared with that calculated for hybrid magmas generated by addition of 30-70% an asthenosphere-derived component, represented by Geronimo basalt G-56, to a lithospheric melt, represented by SN-29. It is clear that in this model the hybrid magmas retain the positive Ba anomaly so characteristic of the Pliocene basalts, have higher overall abundances of all trace elements other than Pb, Rb, Th, and $K_2O$, and lower LIL/HFS ratios because abundances of Ta and Nb are too high. Figure 4.18b, Rb/Ba versus K/Ta, further illustrates the inability of the mixing model presented in Figures 4.16 and 4.17 to reproduce the late Miocene magmas. Whereas the Pliocene basalts are characterised by a large range in K/Ta (18-70) and a very restricted range of Rb/Ba (0.01-0.04), the late Miocene basalts are characterised by more limited K/Ta ratios (18-30) at considerably higher although similarly restricted Rb/Ba ratios (0.06-0.1) than the Pliocene basalts.

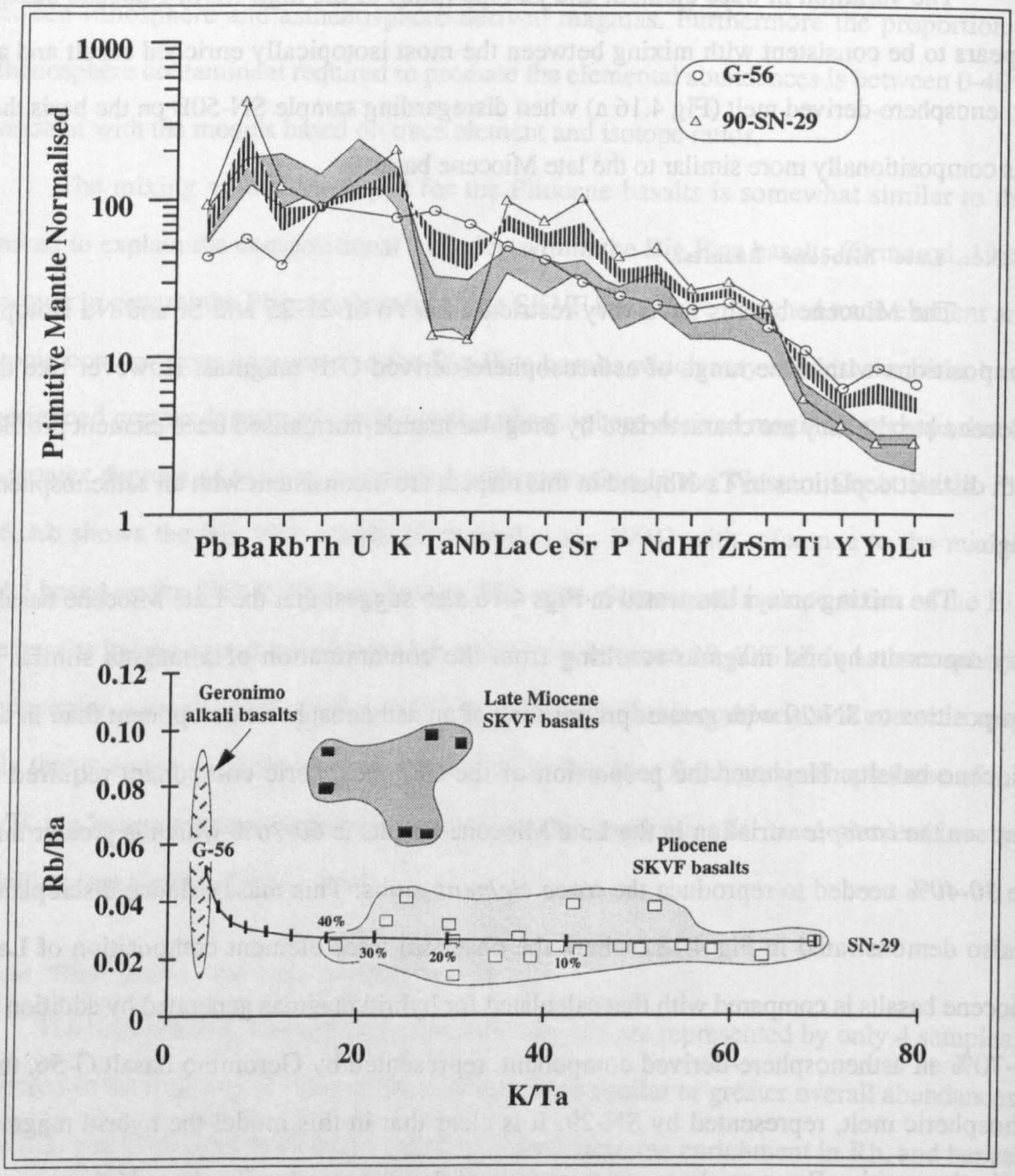


**Figure 4.18.** (**A**) Incompatible trace element profile for Late Miocene basalts (light shading) compared to composition of hybrid magmas (vertical ruling) representing Pliocene basalt SN-29 contaminated with 40-70% of an asthenosphere-derived melt represented by Geronimo alkali basalt G-56 (Kempton & Fitton unpubl). (**B**) Rb/Ba versus K/Ta which demonstrates that the Late Miocene basalts do not lie on a mixing array between asthenosphere and lithosphere as represented by the Pliocene basalts.

The Late Miocene basalts therefore cannot be realistically considered as hybrid magmas generated by the contamination of Pliocene type magmas by asthenospheric melts. If the late Miocene basalts had been reproduced by mixing between SN-29 and an asthenospheric component in the proportions suggested by Fig 4.16 a or b, it would have implied a decreasing material contribution from the asthenosphere with time, the opposite to that

observed for basalts from the adjacent Western Great Basin (Ormerod, 1988). Although this latter point may seem minor, the temporal evolution of magmatism within a given area has important implications for the cause of melt generation, be it a response to extension with a lithosphere to asthenosphere transition, or the presence of a mantle plume with an asthenosphere to lithosphere evolution (Hawkesworth & Gallagher, 1994). It is unlikely for the cause melt generation to vary to such an extent within adjacent and similar aged volcanic provinces.

Although the range in Ba/Nb (Fig 4.16) and the vertical array in $^{207}Pb/^{204}Pb$ vs. $^{206}Pb/^{204}Pb$ (Fig 4.11) may suggest mixing between an enriched component and one resembling an asthenospheric melt, the Late Miocene basalts are otherwise characterised by a very limited range in REE, trace element and Sr and Nd isotopic compositions. Without further samples it is not possible to discriminate convincingly between mixing or melting. Despite this the trace element and isotopic composition of the late Miocene basalts suggest derivation from a time-integrated enriched lithospheric source, albeit one compositionally and isotopically distinct from that of the Pliocene basalts.

The presence of two basaltic groups, each derived from a lithospheric mantle source region with a distinct composition and yet erupted within a spatially restricted area and within only ≈7Ma of one another is not unique to the SKVF. Ormerod (1988) identified two coeval lithospheric endmember magma types, with distinct trace element and isotopic compositions, erupted within the Big Pine volcanic field of the Western Great Basin to the immediate east of the SKVF. Those basalts from the Big Pine volcanic field and the Western Great Basin with Zr/Ba<0.2 and $^{87}Sr/^{86}Sr \geq 0.706$ were interpreted to be derived from middle Proterozoic mantle lithosphere whereas those with Zr/Ba<0.2 and $^{87}Sr/^{86}Sr < 0.706$ were interpreted as melts derived from late Proterozoic mantle lithosphere. Ormerod (1988) therefore constructed a boundary between middle Proterozoic North American subcontinental mantle lithosphere and late Proterozoic lithosphere, accreted during the Palaeozoic, based on initial $^{87}Sr/^{86}Sr$ ratios of 0.706, as used by Kistler and Peterman (1973) to define the crustal boundary and is illustrated in Fig 4.19.

The San Joaquin-Kings volcanic field clearly lies adjacent to this inferred boundary and can be used to constrain further its nature in this region of the Sierra Nevada. To enable this it is first necessary to address the age and location of the source regions for the late Miocene and Pliocene basalts of the SKVF.

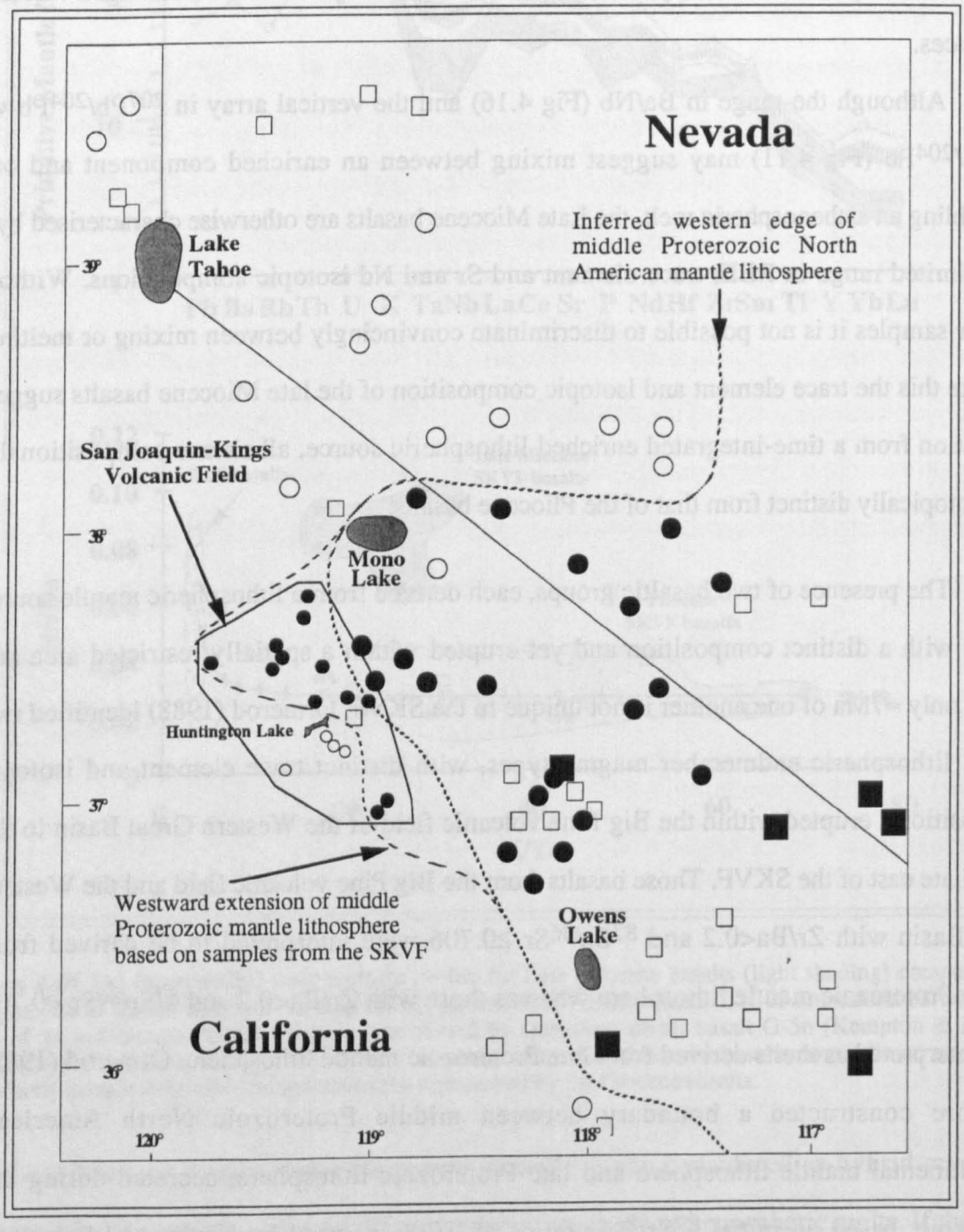


**Figure 4.19**. Spatial distribution of $^{87}Sr/^{86}Sr$ ratios in basalts from the Western Great Basin, taken from Ormerod (1988). Open symbols $^{87}Sr/^{86}Sr \leq 0.706$, closed symbols $^{87}Sr/^{86}Sr > 0.706$; circles have Zr/Ba ≤0.2, square symbols Zr/Ba >0.2. Data from the San Joaquin-Kings volcanic field shown as similar but smaller symbols and taken from this study.

## 4.6: Source age of late Miocene and Pliocene basalts:

The basalts from the SKVF are interpreted as small degree melts and as such the Sm/Nd and Rb/Sr are expected to have fractionated from their true source ratios. However the source Sm/Nd calculated by Ormerod (1988) and Ormerod et al (1991) for the Big Pine basalts can be used to determine the $T_{DM}$ ages of the source regions of Late Miocene and Pliocene basalts. The Miocene basalts yield an average $T_{DM}$ of 0.9Ga whereas the most lithospheric of the Pliocene basalts yield an average $T_{DM}$ age of 1.6Ga. These ages imply that two lithospheric mantle sources of contrasting age are present within a restricted region beneath the Sierra Nevada as represented by the SKVF.

In order to asses whether the Sr isotopic variations are consistent with Rb/Sr fractionation in the source at 0.9 and 1.6Ga the variation of $^{87}Sr/^{86}Sr$ with $^{87}Rb/^{86}Sr$ in the Late Miocene and Pliocene basalts are illustrated in Fig 4.20 together with 0.9 and 1.6Ga reference lines for magmas derived from depleted mantle. The Miocene basalts plot to the right of the 0.9Ga reference line at high $^{87}Rb/^{86}Sr$ ratios though this may in part result from Rb/Sr fractionation associated with melting. The isotopic variations in Miocene basalts therefore appear to be consistent with fractionation of Rb/Sr in their source region at approximately 0.9Ga or younger.

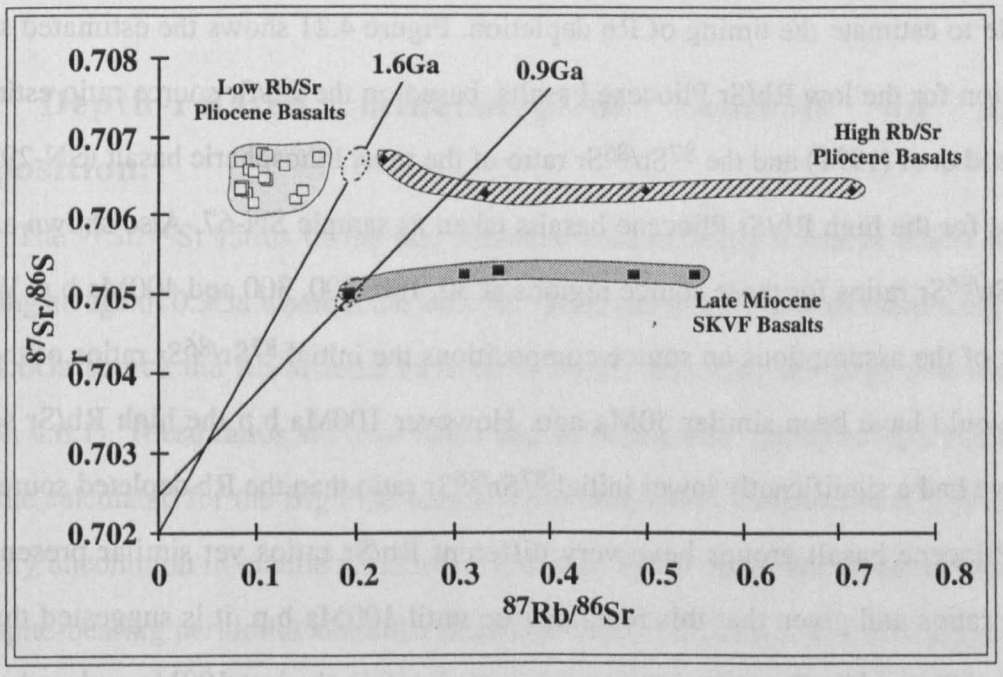


**Figure 4.20**. Variation of $^{87}Sr/^{86}Sr$ with $^{87}Rb/^{86}Sr$ in primitive Late Miocene and Pliocene basalts of the SKVF. The 0.9Ga and 1.6Ga reference lines are calculated for depleted mantle (Faure, 1986) and based on the Nd model ages for the source of the Late Miocene and Pliocene basalts respectively. The light stippled fields show the $^{87}Rb/^{86}Sr$ ratios that would be consistent with Rb/Sr fractionation in the source at 0.9 and 1.6Ga.

In the case of the Pliocene basalts, the majority of samples clearly plot to the left of the 1.6Ga reference line and, as melt Rb/Sr ratios are expected to be greater than those of the source, this would imply that the latter should plot even further from the isochron. This suggests that whereas the Rb/Sr systematics of the source of Miocene basalts has remained closed since the Late Proterozoic, the Mid Proterozoic source of Pliocene basalts has apparently not. A limited number of Pliocene basalts however plot to the right of the 1.6Ga isochron at high $^{87}Rb/^{86}Sr$, obviously constituting the 'high Rb-Sr' group identified in section 4.4. This displacement may in part result from recent Rb/Sr fractionation during melt generation but also reflects high Rb/Sr ratios in the source. These basalts therefore suggest that the Rb/Sr systematics of some portions of the Mid Proterozoic source region of the Pliocene basalts have remained closed.

Similarly elevated $^{87}Sr/^{86}Sr$ ratios, unsupported by the inferred source Rb/Sr ratios have been recognised in many basalts of the western United States (Ormerod, 1988; Davis, 1991). Ormerod et al (1991) attributed the low Rb/Sr ratios in the Big Pine source to a loss of Rb rather than a gain of an exotic Sr component. As the high Rb/Sr Pliocene basalts have $^{87}Sr/^{86}Sr$ ratios similar to the most lithospheric of the low Rb/Sr basalts and assuming they are derived from the same middle Proterozoic source that did not experience Rb depletion it is possible to estimate the timing of Rb depletion. Figure 4.21 shows the estimated source composition for the low Rb/Sr Pliocene basalts, based on the Rb/Sr source ratio estimated by Ormerod et al (1991) and the $^{87}Sr/^{86}Sr$ ratio of the most lithospheric basalt (SN-29), and the source for the high Rb/Sr Pliocene basalts taken as sample SN-67. Also shown are the initial $^{87}Sr/^{86}Sr$ ratios for those source regions at 50, 100, 200, 300 and 400Ma b.p. Within the errors of the assumptions on source compositions the initial $^{87}Sr/^{86}Sr$ ratios of the two sources would have been similar 50Ma ago. However 100Ma b.p the high Rb/Sr source would have had a significantly lower initial $^{87}Sr/^{86}Sr$ ratio than the Rb depleted source. As the two Pliocene basalt groups have very different Rb/Sr ratios yet similar present day $^{87}Sr/^{86}Sr$ ratios and given that this remains true until 100Ma b.p. it is suggested that Rb depletion of the middle Proterozoic source occurred within the last 100Ma and perhaps as recently as 50Ma.

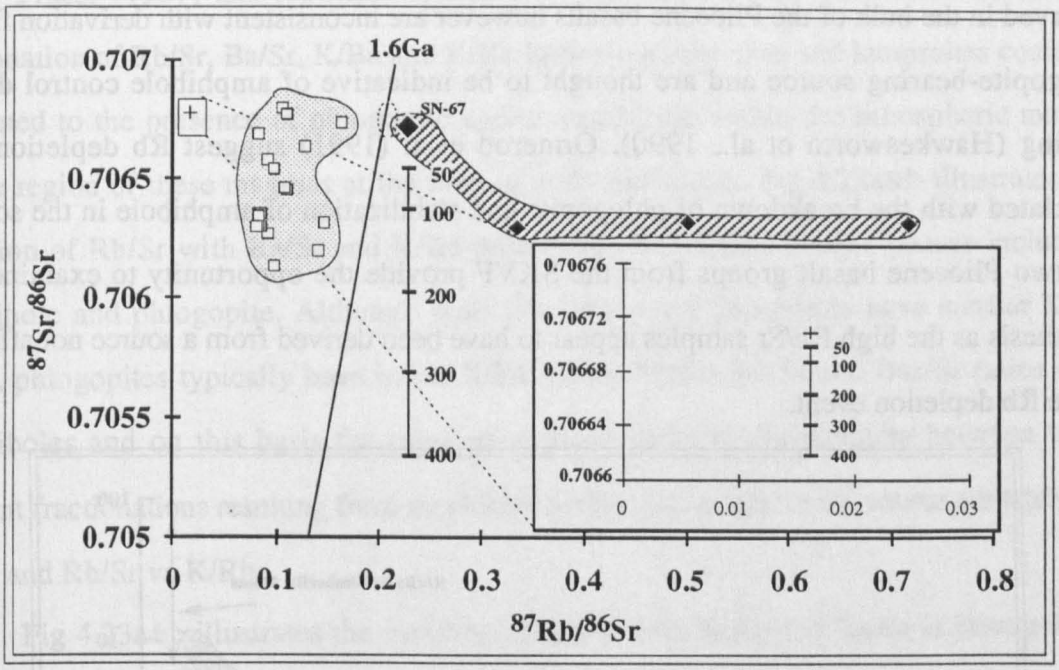


**Figure 4.21**. Initial $^{87}Sr/^{86}Sr$ ratios of the source regions of low and high Rb/Sr Pliocene basalts at 50-400Ma ago; constraints on the date of Rb loss.Rb/Sr ratio of low Rb/Sr source (+) based on inverse modelling of Ormerod et al (1991) and an $^{87}Sr/^{86}Sr$ ratio of the lithospheric endmember SN-29. Source of high Rb/Sr basalts (◆) based on sample SN-67. Inset shows the initial Sr isotope ratios for the low Rb/Sr source. The range of $^{87}Sr/^{86}Sr$ in the Pliocene basalts reflects mixing between the lithospheric endmember SN-29 with depleted asthenosphere rather than source heterogeneity. At 50Ma ago the initial Sr ratios of the two source regions are identical given the assumptions on the source compositions. At 100ma b.p. the initial $^{87}Sr/^{86}Sr$ ratios of the low Rb/Sr source would be ≈0.70669 whereas the high Rb/Sr would be ≈0.7064. Assuming that the low Rb/Sr Pliocene basalts were derived from a source initially similar to that of the high Rb/Sr Pliocene basalts, then the similar present day $^{87}Sr/^{86}Sr$ ratios suggest Rb loss in the source was recent and the results here suggest this occurred within the last 100Ma and perhaps the last 50Ma.

## 4.7: Depth-related mineralogical controls on magma composition.

The $^{87}Sr/^{86}Sr$ ratios of the late Miocene basalts imply a source Rb/Sr of ≈0.08, assuming an age of 0.9Ga whereas the isotopic variations in the Pliocene basalts suggest that for a 1.6Ga source the Rb/Sr must have been ≈0.07, assuming Rb depletion was recent (section 4.6.1). These ratios are over twice that of bulk-earth, approximately fifteen times the value calculated for the Big Pine source (Ormerod, 1988; Ormerod et al.,1991) and are generally uncommon in mantle peridotites. Elevated Rb/Sr ratios are however observed in phlogopite-bearing peridotite xenoliths (Hawkesworth et al.,1990). and it is suggested that the source of the Late Miocene basalts and that of the Pliocene basalts, *prior to Rb depletion*, contained small modal abundances of phlogopite. A similar conclusion was reached by Ormerod et al (1991). The low Rb/Sr ratios associated with high Ba/Sr and K/Rb ratios

observed in the bulk of the Pliocene basalts however are inconsistent with derivation from a phlogopite-bearing source and are thought to be indicative of amphibole control during melting (Hawkesworth et al., 1990). Ormerod et al (1991) suggest Rb depletion was associated with the breakdown of phlogopite and stabilization of amphibole in the source. The two Pliocene basalt groups from the SKVF provide the opportunity to examine this hypothesis as the high Rb/Sr samples appear to have been derived from a source not affected by the Rb depletion event.

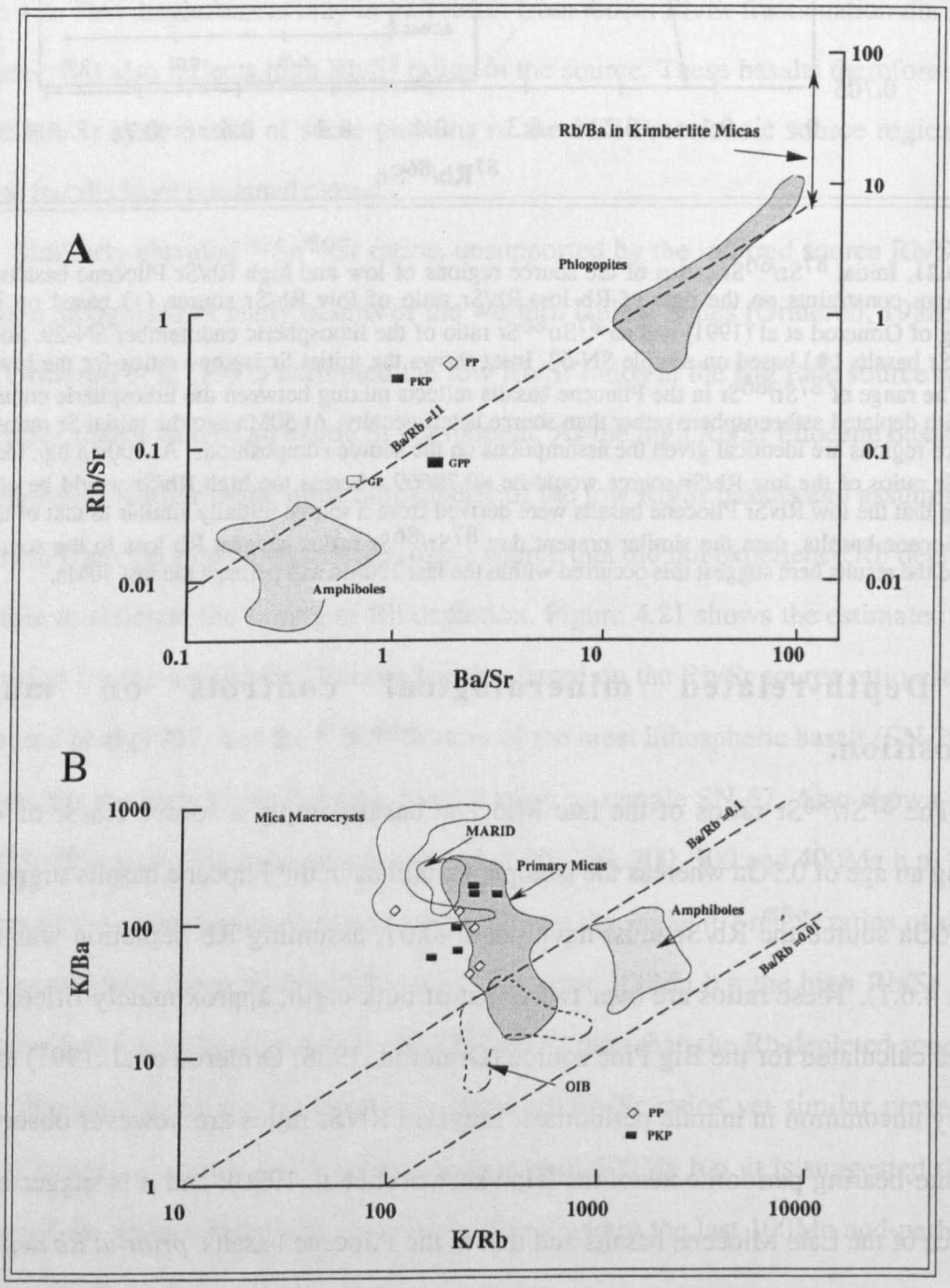


**Figure 4.22.** (A) Rb/Sr vs. Ba/Sr and (B) K/Ba vs. K/Rb for various mantle phases (taken from Hawkesworth et al., 1985 and Fraser, 1988). Fields are shown for selected mineral phases and xenolith data. PKP (phlogopite+K-richterite), PP (Phlogopite), GP (garnet) and GPP (garnet+phlogopite) are whole-rock peridotite averages from the Kimberley area (Erlank et al., 1982).

Fraser (1987) and Hawkesworth et al (1985) argued that the differences in the fractionation of Rb/Sr, Ba/Sr, K/Ba and K/Rb between kimberlites and lamproites could be attributed to the presence of phlogopite and/or amphibole within the lithospheric mantle source region of these magmas at the time of melt generation. Fig 4.22a&b illustrates the variation of Rb/Sr with Ba/Sr and K/Ba with K/Rb for various mantle phases including amphibole and phlogopite. Although both amphibole and phlogopite have similar K/Ba ratios, phlogopites typically have lower K/Rb ratios, higher Rb/Sr and Bas/Sr ratios than amphiboles and on this basis the most appropriate plots to discriminate between trace element fractionations resulting from amphibole and/or phlogopite in the source are Rb/Sr vs Ba/Sr and Rb/Sr vs K/Rb.

Fig 4.23a&b illustrates the variation of Rb/Sr with K/Rb and Ba/Sr in basalts from the SKVF along with minettes from the Navajo volcanic field, for which the role of phlogopite was discussed in chapter 3, and alkali basalts from the Geronimo volcanic field. The high Rb/Sr of the Navajo minettes and Late Miocene SKVF basalts, associated with low K/Rb and moderately low Ba/Sr ratios are consistent with the presence of phlogopite in the source. In contrast the majority of Pliocene basalts have K/Rb ratios of approximately 300 to 650 and although this is within the range of primary peridotite micas (K/Rb= 200-620; Fraser, 1987) it is also at the low end of the range for K-richterite amphiboles from MARID suite nodules. Furthermore Fig 4.23a.shows that the K/Rb ratios of the Pliocene basalts are associated with low Rb/Sr (<0.05) and low Rb/Ba which are inconsistent with the presence of phlogopite in the source. Thus it is suggested that the main group of Pliocene basalts were derived from an amphibole-bearing peridotite. The high Rb/Sr Pliocene basalts not only plot at higher Rb/Sr than the main group of Pliocene basalts they also plot at lower K/Rb ratios and similar Ba/Sr ratios. The low K/Rb and high Rb/Sr is similar to the Navajo minettes and late Miocene Sierran basalts and as such it is suggested that they were also derived from a phlogopite-bearing peridotite. The variation in Rb/Sr, K/Rb and Ba/Sr in the Pliocene basalts of the SKVF suggests that the main group, with low Rb/Sr, were derived from an amphibole-bearing source whereas the subordinate group of high Rb/Sr basalts were generated within a phlogopite-bearing source region. This implies that depletion in Rb within the middle Proterozoic mantle lithosphere, sometime between 50 and 100Ma b.p. was associated with the breakdown of phlogopite and the subsequent stabilization of amphibole.

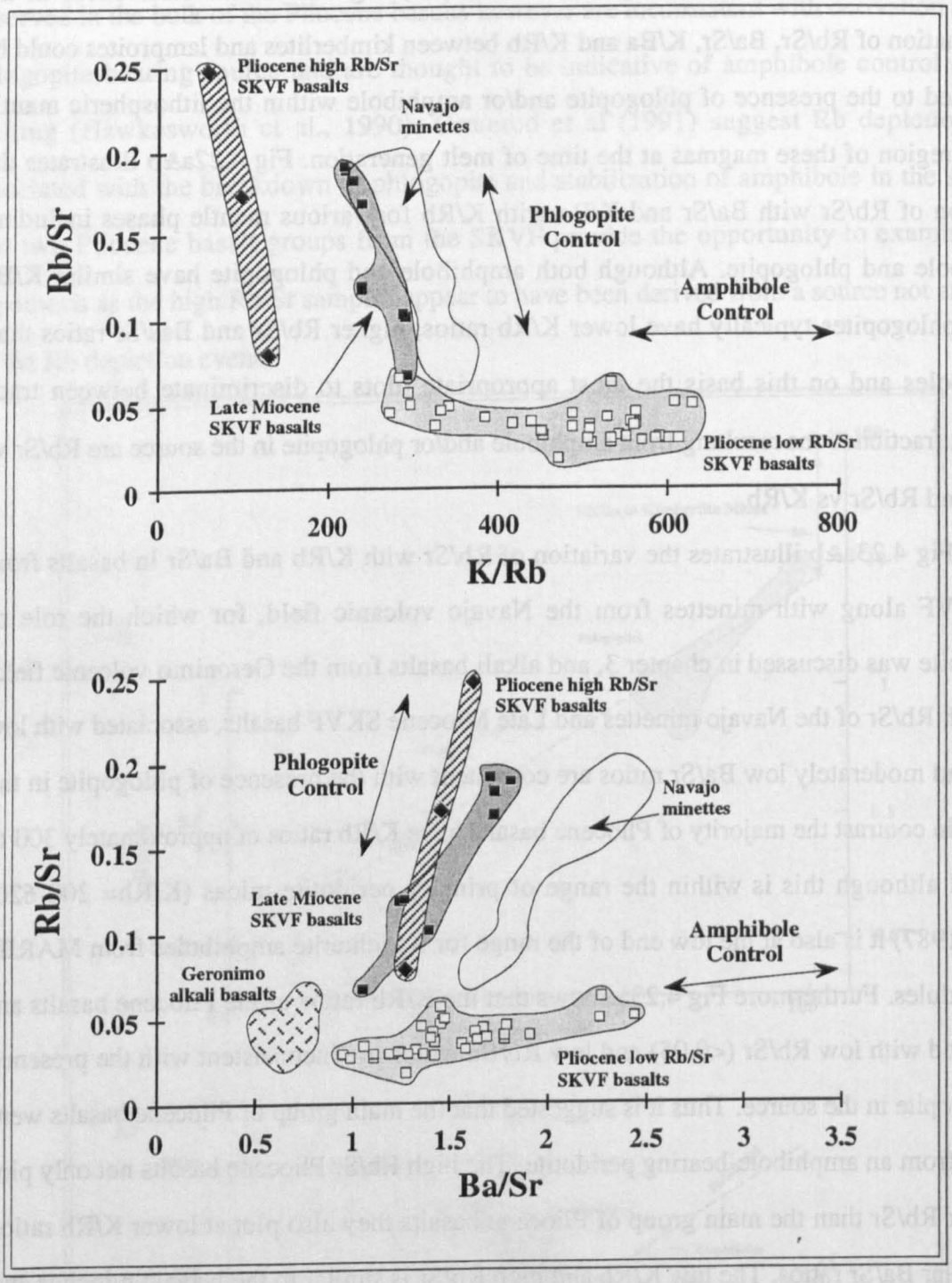


**Figure 4.23.** Variation of Rb/Sr with A) K/Rb and B)Ba/Sr in the late Miocene and Pliocene basalts of the SKVF, minettes from the Navajo volcanic field (this study) and alkali basalts from the Geronimo volcanic field (Kempton & Fitton, unpubl data). The vectors show the trace element fractionations associated with the presence of phlogopite and/or amphibole in the mantle source during partial melting.

The inferred mineralogy of the source regions of late Miocene and Pliocene basalts can be used to estimate qualitatively their relative positions within the lithospheric mantle. Both basaltic groups are derived from garnet-bearing mantle and therefore it is not possible to infer source depth on the basis of the REE compositions. However the source region for

Late Miocene basalts is inferred to have been phlogopite-bearing whereas the Pliocene basalts were derived from an amphibole-bearing peridotite. In the presence of $H_2O$-$CO_2$ vapour, subsolidus amphibole is present only at pressures of less than 30-32kb (Falloon and Green, 1989; Green, 1973; Wyllie, 1979) whereas phlogopite is stable at higher pressures. On this basis it is suggested that the phlogopite-bearing source of the Miocene basalts is located in the deeper lithosphere, possibly in excess of 30kb or 90km, whereas the amphibole-bearing source of the Pliocene basalts is located at shallower levels within the lithosphere, <30kb, but at necessarily greater pressures than the spinel-garnet transition at approximately 18-22kb (Falloon & Green, 1989).

## 4.8: Nature of the sub-Sierran mantle lithosphere: A model for the temporal evolution of magmatism in the SKVF:

The identification of two discrete mantle source regions of middle and late Proterozoic age within a spatially restricted area of the Sierra Nevada and the temporal variation in their contribution to magmatism of the SKVF clearly has important implications for the compositional and/or tectonic structure of the mantle lithosphere in this small region of the western United States. The following discussion uses the magmatic record of the SKVF and the Big Pine volcanic field to construct and propose a model for the mantle beneath the Sierra Nevada.

The inferred western boundary of middle Proterozoic mantle lithosphere at the latitude of the SKVF (Fig 4.19) is defined by those basalts with Zr/Ba <0.2 and $^{87}Sr/^{86}Sr$ ≥0.706, not by the occurrence of basalts with Zr/Ba <0.2 and $^{87}Sr/^{86}Sr$ ≤0.706. The one Big Pine basalt to the west of this boundary has an initial Sr isotopic ratio of <0.706 but its Zr/Ba >0.2 therefore may contain an appreciable asthenospheric component which results in the low $^{87}Sr/^{86}Sr$. Pliocene basalts of the SKVF all have Zr/Ba <0.2 and $^{87}Sr/^{86}Sr$ >0.706 and are derived from middle Proterozoic mantle lithosphere. Therefore basalts from the SKVF enable the inferred western boundary to be shifted further west between the latitudes of 37° and 37° 45'N as shown in Fig 4.19. Additional constraints on the physical nature of the boundary between the two lithospheric mantle source regions can be gained from the

spatial distribution of the Late Miocene and Pliocene basalts and the granite basement through which they were erupted.

In a situation where the boundary between the lithospheric provinces is vertical the initial $^{87}Sr/^{86}Sr$ =0.706 line for crust and mantle should coincide. However where the boundary is inclined to the west with accreted late Proterozoic crust overlying middle Proterozoic mantle then the mantle derived magmas with $^{87}Sr/^{86}Sr$ >0.706 should be emplaced through crust with $^{87}Sr/^{86}Sr$ <0.706 whereas with a boundary inclined to the east the situation would be reversed as illustrated diagrammatically in Fig 4.24.

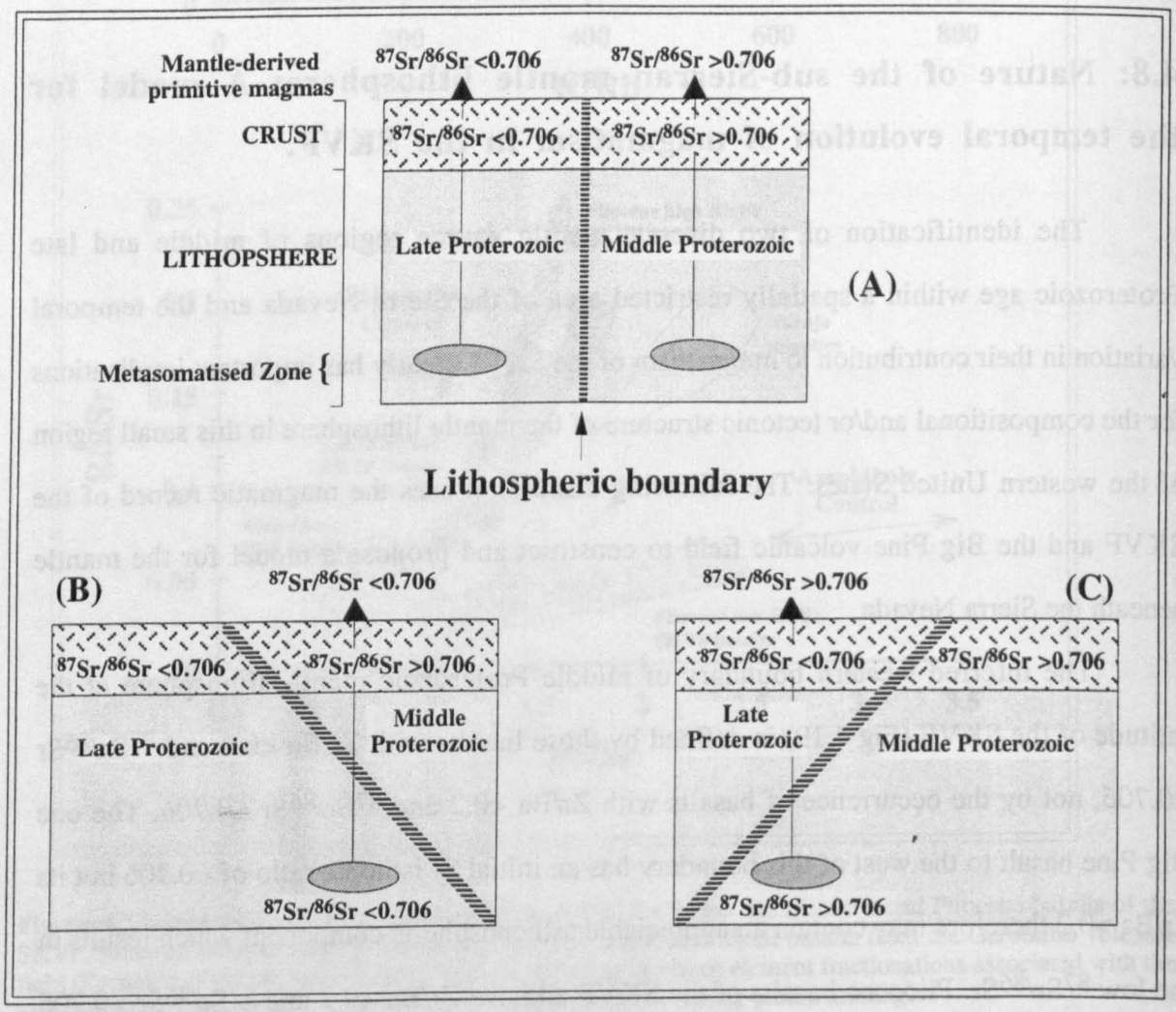


**Figure 4.24.** Relationship between the Sr isotopic composition of primitive lithosphere-derived basalts and the crust through which they are intruded as a function of the inclination of the boundary between middle Proterozoic and late Proterozoic mantle lithosphere. Where the boundary is vertical the mantle and crustal $^{87}Sr/^{86}Sr_i$ 0.706 lines coincide (A). If the boundary is inclined to the east (B) then lithosphere-derived magmas with $^{87}Sr/^{86}Sr_i$ <0.706 may be observed to intrude through crust with $^{87}Sr/^{86}Sr_i$ >0.706 while the opposite would be observed where the boundary is inclined to the west as in C

Figure 4.2. shows the approximate outlines of the Mt.Givens, Eagle Peak, Dinky Creek and Red Lake plutons through which many late Miocene and Pliocene basalts were erupted. These plutons are all characterised by initial $^{87}Sr/^{86}Sr$ ratios of 0.7075-0.7080 (Noyes et al.,1983; Dodge et al.,1986) which suggests they were derived from a Middle Proterozoic protolith. The Pliocene basalts that intrude these plutons all have initial $^{87}Sr/^{86}Sr$ in excess of 0.706, despite containing up to 40% of a low $^{87}Sr/^{86}Sr$ asthenospheric component, and have an average Nd model age of 1.6Ga. This implies that within the bounds of the SKVF the crust is itself underlain by mantle of the same middle Proterozoic age, at least that is mantle down to depths of perhaps 30kb or 90km (section 4.7). Late Miocene basalts although spatially restricted intrude, amongst others, the Dinkey Creek and Red Lake plutons (Fig 4.2) with $^{87}Sr/^{86}Sr$ >0.706. However although these basalts are derived from an enriched lithosphere and do not appear to contain appreciable quantities of an asthenospheric component they have initial $^{87}Sr/^{86}Sr$ ratios of 0.7048-0.7053 and an average Nd model age of 0.9Ga, appropriate for magmas derived from Late Proterozoic accreted lithosphere. As the late Miocene basalts are derived from a source located at depths in excess of the that of the Pliocene basalts the middle Proterozoic upper mantle and crust appears to be underlain by lithospheric mantle of late Proterozoic age. As basalts from a late Proterozoic lithospheric mantle source are emplaced through granites derived from a crustal protolith of middle Proterozoic age it is suggested that the boundary between these two lithospheric provinces is inclined to the east beneath the San Joaquin-Kings and Big Pine volcanic fields at the latitude of 37° to 37° 45'N.

A summary of the structure of the lithosphere beneath the Sierra Nevada is illustrated in Fig 4.25. along with the inferred location of the mantle source regions for Cenozoic basalts and the main tectonomagmatic events of the SKVF discussed above.

Initial magmatism within the SKVF was restricted to the eruption of small volumes of basalt and trachybasalt in the Huntington Lake region during the Miocene (11.4-9.5Ma). Although these magmas have the lowest LIL/HFS ratios and the most depleted Sr and Nd isotopic compositions of the SKVF they show a limited compositional variation and it is suggested that they represent small degree melts of an enriched phlogopite-bearing garnet peridotite located within the lithospheric mantle at depths of approximately 100km+. The degree of REE fractionation further suggests approximately 5% melting.

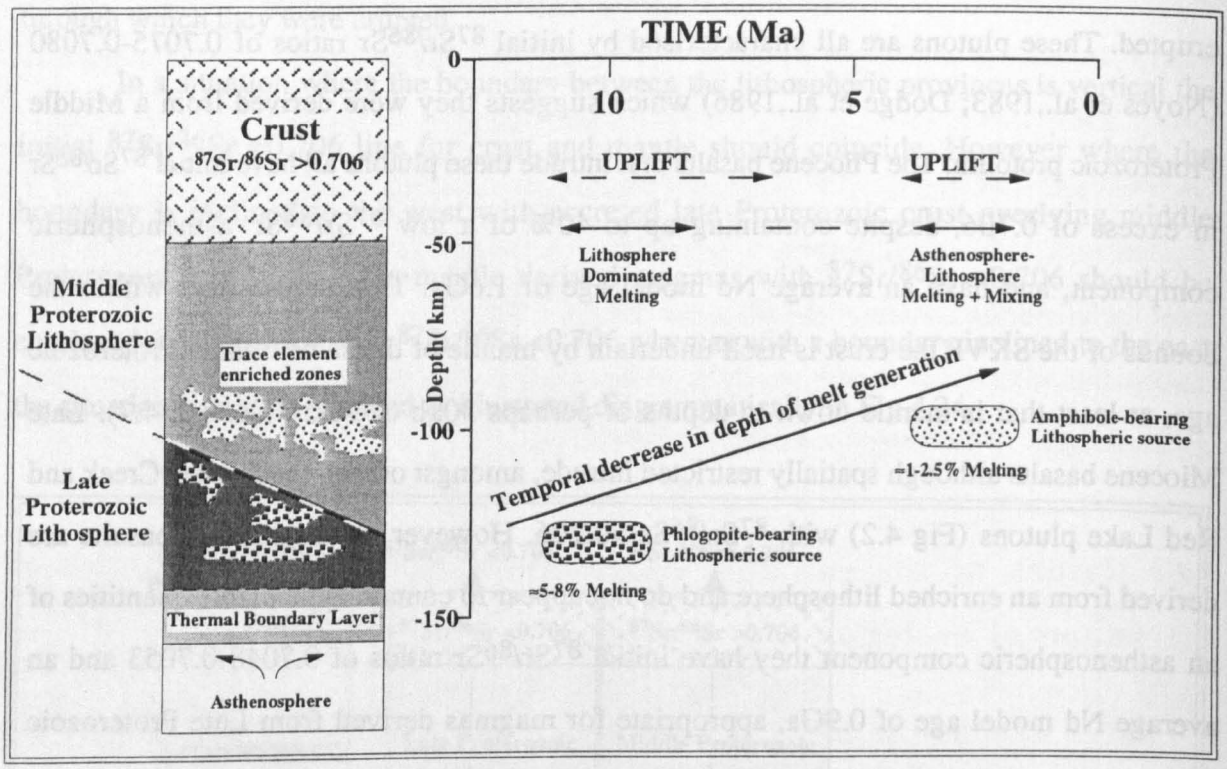


**Figure 4.25.** Summary diagram of the structure of the mantle lithosphere beneath the central Sierra Nevada and the temporal evolution of magmatism within the San Joaquin-Kings volcanic field. The middle Proterozoic crust and upper mantle are underplated by younger late Proterozoic mantle lithosphere, the boundary between the two being inclined to the east.

Initial melt generation occurs exclusively within the lower, late Proterozoic, phlogopite- and garnet-bearing lithospheric mantle during the late Miocene and coincides with the first period of late Cenozoic uplift of the Sierra Nevada. Melt generation in the Pliocene occurs both within the asthenosphere and shallower, middle Proterozoic, amphibole- and garnet-bearing lithospheric mantle and coincides with a second period of uplift.

Important aspects of this model are that with time melt generation occurs at progressively shallower, and older, levels within the lithosphere and by the Pliocene also takes place in anhydrous asthenospheric mantle.

The second and more voluminous magmatic episode during the Pliocene (4.4-3.2Ma) resulted in numerous small volume eruptions of shoshonitic basalts over a more extensive area than the previous Late Miocene event. These Pliocene basalts have a much greater variation in both LIL/HFS and $^{87}Sr/^{86}Sr$ ratios with the highest overall values of SKVF basalts. The variation in composition is attributed to the contamination of small degree melts (≈2%) derived from an amphibole-bearing garnet peridotite, located within lithosphere between 70-100km, with up to 40% of an asthenospheric component.

Cenozoic magmatism within the San Joaquin-Kings volcanic field therefore records a progression from initial melt generation exclusively within the lithosphere during the Late Miocene to a final period of melt generation occurring both within the lithosphere and

asthenosphere in the Pliocene. Although there is a 7Ma period of volcanic quiescence from the late Miocene to the Pliocene, the depth of melt generation within the *lithosphere* in the final stages of magmatism had progressed to shallower levels and was associated with an increase in the age of the mantle source regions from Late Proterozoic (900Ma) to Mid Proterozoic (1600Ma).

A similar temporal decrease in the depth of melting within the lithosphere, associated with an increasing material input from asthenosphere-derived melts, is recognised in basaltic volcanism of the Colorado River Trough, southern Basin & Range, where it is associated with crustal extension and hence lithospheric thinning (Bradshaw, 1991; Daley & DePaolo, 1992). As such, these variations have been attributed to extension of the lithosphere and the resultant upwelling and adiabatic melting of the asthenosphere. However in the central Sierra Nevada, as with the Colorado Plateau, there is no evidence for pre-, syn- or post-magmatic crustal extension. Therefore the temporal variations in magmatism of the Sierra Nevada cannot be attributed to thinning of the lithosphere resulting from extension and an alternative mechanism must be sought. Figure 4.25. shows the approximate timing of two periods of uplift of the Sierra Nevada which appear to coincide with late Miocene and Pliocene magmatism suggesting that these two phenomena are related. Chapter 5 addresses further the spatial and temporal association between uplift and magmatism.

## 4.9: Summary and Conclusions:

1) The Late Miocene and Pliocene basalts of the San Joaquin-Kings volcanic field of the central Sierra Nevada form a high-K calcalkaline and shoshonitic series respectively. Fractionation processes have had only a minor role in establishing the observed geochemical variation in the Sierran basalts and is at most limited to approximately 5-10% fractionation of olivine. The majority of basalts are primitive with Mg#≥70 yet exhibit a wide range in composition most notably in LIL/HFS ratios (Ba/Nb =70-325).

2) Although high LIL/HFS and $^{87}Sr/^{86}Sr$ ratios are observed in silicic crustal lithologies there is no correlation between LIL/HFS and $^{87}Sr/^{86}Sr$ and SiO2 in the Pliocene basalts making crustal contamination unlikely. Furthermore contamination of late Miocene or

Pliocene basalts with crust is unable to reproduce the ratios observed in the Sierran basalts whilst retaining primitive compositions. The range in compositions is attributed to variations in source composition and processes in operation during melt generation.

3) The range of trace element and isotope ratios in the magmas of the SKVF are similar those observed in many basaltic provinces of the western United States (Ormerod, 1988; Leat et al.,1988; Thompson et al.,1989; Perry et al., 1989; Bradshaw, 1991; Fitton et al.,1991; Davis, 1991). In general the initial Late Miocene magmas have less enriched trace element and isotope ratios than the Pliocene basalts which might initially suggest a decreasing contribution from the asthenosphere with time. In detail it becomes apparent that this is not the case and the evolution of magmatism in the SKVF follows a similar pattern of lithosphere to asthenosphere dominated magmatism recognised in the Basin & Range (Bradshaw et al, 1993) and on the Colorado Plateau (Chapter 3).

4) The basalts of the San Joaquin-Kings volcanic field were derived from two compositionally distinct lithospheric mantle source regions.

The Late Miocene basalts represent small degree melts (approximately 5% based on the degree of REE fractionation) of an enriched phlogopite-bearing garnet peridotite source of *Late Proterozoic* (0.9Ga) age located in the lithosphere at depths in excess of 90km. The limited number of samples and hence range in isotopic composition prevents a rigorous assessment of any mixing though it is suggested that there is no input from an asthenospheric component to the Miocene basalts.

The Pliocene basalts are the products of approximately 2% melting of an amphibole-bearing garnet peridotite source of *Middle Proterozoic* (1.6Ga) ages located in the lithosphere at depths between approximately 70-90km. The large variation in LRE/HRE, LIL/HFS and isotopic compositions cannot be attributed to variable degrees of melting and reflect mixing of lithosphere and asthenosphere-derived magmas.

5) The distribution of late Miocene and Pliocene basalts defines the boundary between late Proterozoic lithospheric mantle, accreted during the Palaeozoic, and middle Proterozoic lithospheric mantle that formed part of the North American continent in the

Proterozoic. Furthermore the emplacement of basalts with $^{87}Sr/^{86}Sr_i$ <0.706, derived from late Proterozoic mantle, through granitic plutons with $^{87}Sr/^{86}Sr_i$ ≥0.706, is used to infer that this boundary is inclined toward the east and is located at approximately 70-100km beneath the SKVF.

**6)** The temporal evolution of magmatism within the central Sierra Nevada shares many similarities with that of the Colorado Plateau discussed in Chapter 3. Both volcanic provinces are characterised by small melt volumes and a dominant role for lithosphere-derived melts in the early stages of magmatism. Only in the final short pulse of magmatic activity in each province is there a clearly identifiable role for melt generation within the asthenosphere. Furthermore in neither province is there evidence for crustal extension as the driving mechanism for melt generation as in the Basin & Range and Rio Grande Rift.

The following chapter uses the temporal variation in the composition of basalts from the central Sierra Nevada, and Colorado Plateau, in conjunction with geophysical observations and the inferred geometry of the subducting Farallon plate during the late Cenozoic, to propose a model that accounts for melt generation and uplift within these two provinces.

# CHAPTER 5

## Magmatism and Uplift of the Colorado Plateau and Central Sierra Nevada Provinces: A Case for Oligo-Miocene Convective Thinning of the Mantle Lithosphere Beneath the Western United States.

### 5.1: Introduction:

The Tertiary of the western United States was marked by a change in tectonic regime from one of compression, associated with subduction of the Farallon plate off the western margin of the North American continent, to one of intraplate crustal extension, associated with voluminous magmatism within the Basin & Range and Rio Grande Rift provinces. The cause of Tertiary magmatism and its relationship to changing tectonics has received considerable attention in recent years. Early studies (Lipman et al., 1972; Christiansen & Lipman, 1972) attributed Tertiary calcalkaline magmatism to subduction of the Farallon plate. However recent studies of mid to late Tertiary magmatism (this study; Bradshaw, 1991; Bradshaw et al., 1993; Davis, 1991; Davis et al., in press; Fitton et al.,1988, 1991; Kempton, 1991; Ormerod et al., 1988; Perry et al., 1987; Thompson et al.,1990) have shown that these magmas have signatures inherited from old trace element enriched lithospheric mantle and show little or no contribution from Tertiary subduction.

Magmatism within the Basin & Range shows a closer temporal and spatial relationship to extension than to the configuration of the subducting plate (Gans et al., 1989). This has led many authors to suggest that crustal extension was the driving force of Tertiary magmatism. However Gans et al (1989) and Best & Christiansen (1991) have shown that magmatism and extension are not always spatially associated and where they do coexist magmatism precedes extension by several million years. Nowhere is this more clearly illustrated than the central Colorado Plateau and Sierra Nevada where there is no evidence for extension some 30Ma and 10Ma respectively since the onset of magmatism. Although once initiated extension undoubtedly plays an important role in the magmatic evolution of the Basin & Range it is clear that where it was preceded by magmatism it cannot be the initial cause of melt generation.

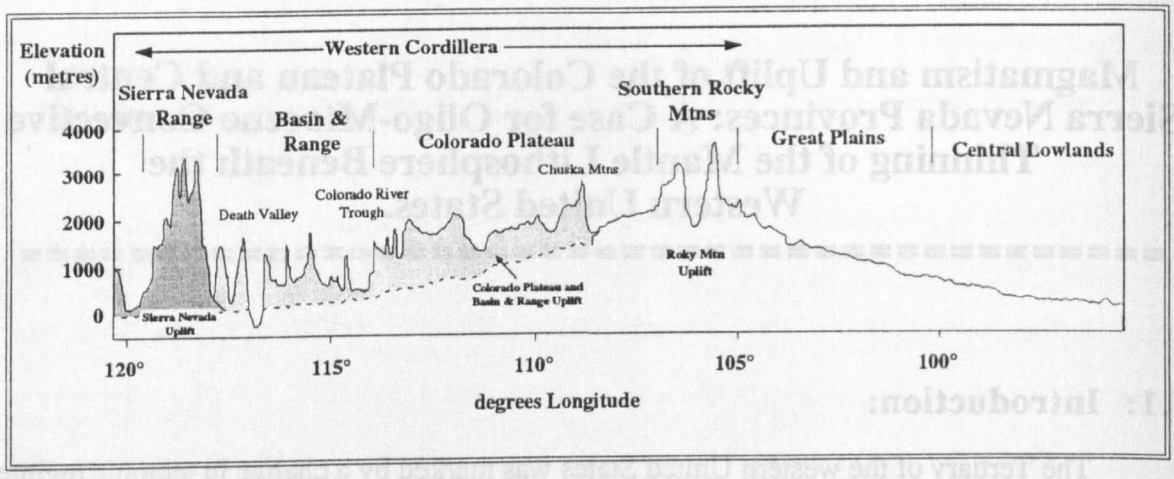


**Figure 5.1.** Topographic profile of the western Cordillera (modified after Eaton 1987) from the Sierra Nevada to the Rocky Mtns. Vertical exaggeration approximately 100:1. Although there is an element of first order bilateral symmetry to uplift of the western United States, most clearly observed on the western and eastern flanks nearest the crest of the Rocky Mtns this cannot account for the total uplift of the western Cordillera. A mirror image of the topography eastern flank of the Rocky Mtns is superimposed on the western limb and clearly illustrates the excess elevation of the Sierra Nevada-Basin & Range-Colorado Plateau over that expected from symmetrical uplift about the Rocky Mtns. This suggests possibly two uplift events, the Colorado Plateau/Basin & Range uplift (section **5.2.1**) and the Sierra Nevada uplift (section **5.4.1**), in addition to the Rocky Mtns uplift (<17Ma: Eaton, 1987) to account for Cenozoic uplift of the western Cordillera.

In addition to extension and magmatism, much of the western United States also experienced considerable uplift during the Eocene-Oligocene (Eaton, 1986), as illustrated in Fig 5.1. Clearly the Colorado Plateau, with an average elevation of 2.0-2.5km (Mayer, 1986) and the Sierra Nevada and southern Rocky Mtns (which both reach elevations of ≈4km) are regions that have undergone considerable uplift during the late Cenozoic (sections 5.2.1 and 5.4.1). What is less obvious however is that the Basin & Range province with an average elevation of 1.5 to 1.8km is also anomalously high, considering its present crustal thickness of 25-35km (Benz et al.,1990; Catchings & Mooney, 1991). The extent, symmetry and rapidity of this uplift (Eaton, 1984), in conjunction with the high heatflow characteristics of the Basin & Range and presence of OIB-like magmas in the western United States, has led Fitton et al (1991) to suggest that magmatism and uplift are consistent with active mantle upwelling beneath the southwestern United States. Bradshaw et al (1993) argue against a role for a mantle plume in magmatism of the southwestern United States, on the basis of the limited volume and low eruption rate and the shift from lithospheric to asthenospheric characteristics observed in basalts from the Colorado River Trough.

Models which appeal to crustal extension as the main cause of Tertiary magmatism do not adequately explain the relationship between magmatism and regional uplift. Conversely, although a mantle plume might result in magmatism and some domal uplift it does not provide a driving force for large scale Tertiary extension of the Basin & Range. A third scenario involving the convective thinning of previously thickened mantle lithosphere has also received attention recently (Houseman et al., 1981; Sandiford & Powell, 1990; etc), partly because it relates uplift, extension and magmatism to a single geodynamic process.

The aim of this chapter is to combine the composition and temporal evolution of magmatism on the Colorado Plateau and in the Sierra Nevada (discussed in chapters 2 through 4) with information on uplift and extension as a means of assessing the competing geodynamic models for the Tertiary evolution of the western United States. The Colorado Plateau and Sierra Nevada provinces represent just a small portion of the Western Cordillera that underwent uplift during the Cenozoic yet, unlike the Basin & Range, they have experienced negligible subsequent extensional deformation. The Colorado Plateau and Sierra Nevada therefore also represent appropriate areas for addressing the nature of Cenozoic uplift and magmatism in the western United States, and indeed provide two different perspectives on this problem. Because of its relatively extensive and uniform average elevation associated with a long punctuated magmatic history from the Oligocene to the present, the Colorado Plateau yields temporal rather than spatial constraints on mantle processes operating in this region. By contrast, within the Sierra Nevada uplift and magmatism are comparatively recent phenomena and although a temporal variation is observed in the magmatism (section 5.3.2) the most striking feature of this mountain range is the decrease in elevation from south to north (Chase & Wallace, 1986; Crough & Thompson, 1977; Unruh, 1991) thus providing both *spatial* and temporal controls on the process responsible for uplift and magmatism.

## 5.2: Uplift and magmatism of the Colorado Plateau.

### 5.2.1: Timing and amount of Colorado Plateau uplift:

A topographic cross-section across the western United States, at the latitude of 36°N, from the Great Valley of California to Tulsa, Oklahoma, illustrated in Fig 5.1, demonstrates the greater elevations of the Colorado Plateau, Basin & Range and Sierra Nevada provinces

in comparison to regions east of the Rocky Mtns. Furthermore if the topography of the eastern flank of the Rocky Mtns is superimposed on the western flank as shown in Fig 5.1., then clearly symmetrical uplift cannot account for the total elevation of regions to the west of the Continental Divide. Strictly speaking therefore Cenozoic uplift of the western United States symmetrical about the southern Rocky Mtns (Eaton, 1984; Fitton et al.,1991) is not wholly correct and it appears that two uplift events are required. The nature and cause of the uplift event that gave rise to the excess elevation of the Colorado Plateau over that expected from symmetrical uplift is the focus of section 5.2.4 though it is first necessary to establish an age for this event. In practice this proves to be both difficult and controversial, in part due to the methods employed to date 'uplift'. Uplift based on the dating of geomorphological features along the boundary between the Colorado Plateau and the extensional Basin & Range may reflect uplift of the former and/or collapse of the latter. Furthermore uplift of the Colorado Plateau is also related to the southern Rocky Mtn event and so distinguishing between the development of the plateau and Rocky Mtns presents problems.

The topographic differentiation between the Colorado Plateau and Basin & Range provinces was sufficient by 26Ma to alter the movements of ash-flow tuffs on the northwestern margin of the plateau (Rowley et al.,1978). Furthermore by 24Ma fanglomerates were also being shed from the southeastern margin of the plateau (Chapin & Seager, 1978). What is not clear from these results is whether the topographic differentiation reflects true uplift of the plateau or extensional collapse of the Basin & Range. Hamblin (1984) agues on the basis of comparing palaeostream profiles, preserved beneath lava flows, with their modern counterparts that the absolute movement along the Colorado Plateau-Basin & Range boundary faults in southern Utah did indeed involve uplift of the plateau alongside an essentially stable Basin & Range. Similar constraints on the direction of absolute movement along the boundary between the Colorado Plateau and surrounding extensional provinces are lacking and it is concluded that 24-26Ma merely reflects the timing of topographic and structural differentiation between the two provinces and ***not*** the initial onset of plateau uplift. It is also plausible that both provinces had already experienced concomitant uplift prior to topographic differentiation.

Sedimentological and palaeo-faunal and floral evidence have been used to try to constrain the timing and amount of uplift of the Tibetan Plateau (Li et al., 1981; Xu Ren, 1981) and this approach may be applied to the timing of uplift of the Colorado Plateau-Basin & Range provinces. During the Cretaceous, shallow marine and coastal deposits demonstrate that the plateau was certainly at sealevel prior to the 70-45Ma Laramide orogeny (Kauffman, 1977). By the late Eocene post-Laramide palaeotopographic relief was as great as 1000m (Hansen, 1984) although palaeo-flora suggest that the absolute elevations of Laramide uplifts were generally <1000m in the southern cordillera (Epis & Chapin, 1975). By contrast fish fauna from lacustrine environments, such as the Green River basin, suggest Laramide basins had much lower average elevations of ≤300m (Hansen, 1985). These studies suggest that by the late Eocene the elevation of the Colorado Plateau region was generally less than 1000m and therefore approximately 2000m must have occurred since to account for the total elevation observed today. However in addition to a dependence on elevation, climates also vary with latitude and have changed on the global-scale throughout geological time (Molnar & England, 1990; England & Molnar, 1990). Estimates of absolute elevation based on the climate regimes of flora and fauna may therefore be erroneous.

Despite the lack of evidence for the temporal variations in absolute elevation of the Colorado Plateau during the late Cenozoic, Oldow et al (1989) suggest that by mid to late Oligocene the Colorado Plateau-Basin & Range province had experienced uplift in the order of 2-3km. Clearly by 26Ma and perhaps as early as 28Ma (Laughlin et al.,1983; 1985) the two provinces had become topographically differentiated due to increased uplift of the Colorado Plateau and/or extensional collapse of the Basin & Range.

Izett (1975) suggests that uplift and erosion continued in the northern Colorado Plateau after 11Ma. Within the last 10Ma the Colorado River has incised its canyon by almost 1km, with 300m of that total in the last 1.5Ma (Larson et al., 1975) suggesting continued uplift. The onset of uplift of the Rocky Mtns dates from 17Ma and accelerated after 12Ma reaching a peak between 7-4Ma (Eaton, 1986, 1987). On this basis the continued uplift of the Colorado Plateau subsequent to 10Ma could simply reflect uplift on the western flank of the Rocky Mtns as illustrated in Fig 5.1. Molnar & England (1990) however warn that renewed incision of river channels or increased sedimentation may be a consequence of global climate change in the late Cenozoic, leading to increased erosion and hence isostatic rebound, rather than actual surface uplift.

If topographic differentiation between the Colorado Plateau and Basin & Range did indeed result from uplift of the former then the onset of uplift occurred at 26Ma and perhaps as early as 28Ma. However if topographic differentiation resulted from extensional collapse of the Basin & Range alongside a stable Colorado Plateau then uplift of both provinces may predate 28Ma, occurring in the late Oligocene. Turner et al (1993) have argued that the onset of uplift of the Tibetan Plateau can be dated by the appearance of magmas derived from the lithospheric mantle.

Magmatism within the central Colorado Plateau is volumetrically limited and is restricted to the laccoliths of southeastern Utah (Nelson & Davidson, 1993) and the minettes of the Wasatch Plateau (Tingey et al., 1991) and the Navajo volcanic field (Chapter 2 & 3). Although the plagioclase-hornblende prophyry laccoliths of southeastern Utah have experienced fractional crystallisation and crustal contamination the trace element abundance patterns suggest they were derived from an incompatible trace element-enriched mantle source (Nelson & Davidson, 1993). The potassic and ultrapotassic minette lamprophyres from the Wasatch Plateau and Navajo volcanic field are undoubtedly derived from incompatible trace element-enriched portions of the subcontinental mantle lithosphere (Tingey et al., 1991; Chapter 3).

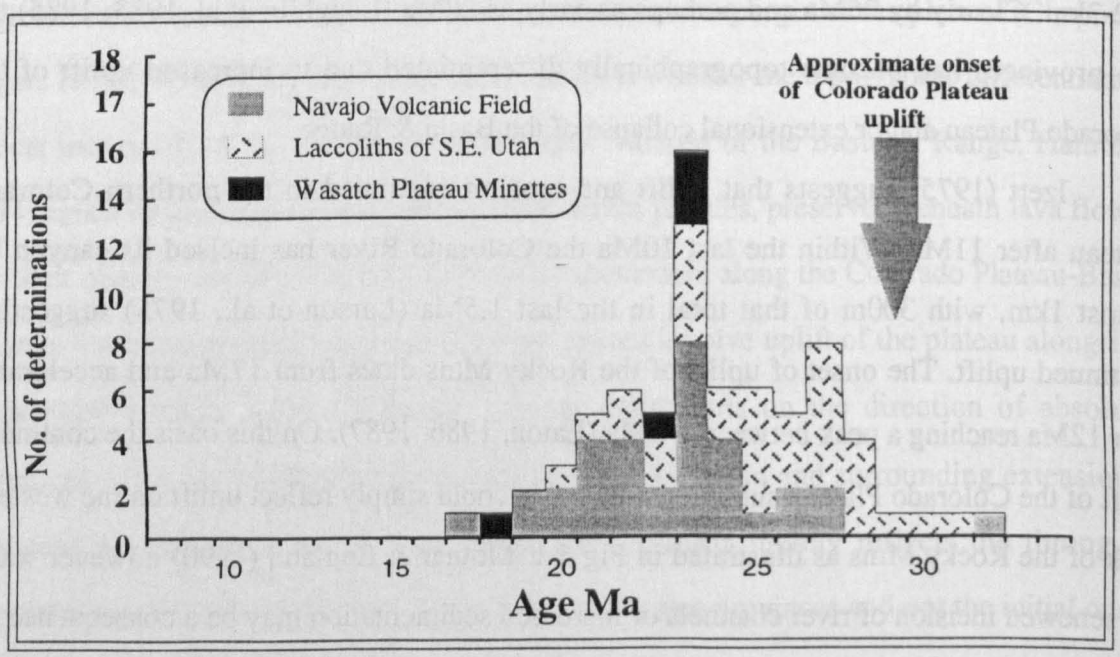


**Figure 5.2.** K-Ar and Ar-Ar age determinations on magmas from the Colorado Plateau with the approximate onset of uplift (Laughlin et al., 1983; Rowley et al., 1978). Navajo volcanic field, this study and Laughlin et al., (1986); Laccoliths from S.E. Utah, Nelson et al., (1992); Wasatch Plateau minettes, Tingey et al., (1991). Note the coincidence of the onset of major volcanism with the approximate onset of uplift.

A histogram of ages for these lithosphere-derived volcanics from the central Colorado Plateau is illustrated in Fig 5.2. along with the approximate age of uplift as determined from geomorphological features along the boundary of the Colorado Plateau. The earliest magmas on the Colorado Plateau date from approximately 32Ma, although this is based on fission-track dating of apatites and therefore may reflect incomplete annealing during magmatism (Roden et al., 1979). The onset of significant lithosphere derived magmatism on the plateau occurred at 28Ma which is very close to the approximate onset of uplift discussed above.

Thus it is concluded that uplift of the Colorado Plateau and the onset of magmatism occurred together at approximately 28-30Ma, strongly suggesting a linked origin. Furthermore as the main phase of uplift of the Rocky Mtns occurred after 12Ma it appears that uplift of the Colorado Plateau and Rocky Mtns were two separate events although the cause may ultimately have been the same.

### 5.2.2: The temporal evolution of Magmatism on the Colorado Plateau:

Magmatic activity on the central Colorado Plateau was confined to two periods, the first, represented by the 28.5-17Ma (Oligo-Miocene) ultrapotassic volcanism of the Navajo volcanic field, was followed some 10Ma later by the 8-4Ma (Pliocene) sodic volcanism of the Hopi Buttes.

Initial magmatism on the Colorado Plateau, as represented by the Navajo lamprophyres was characterised by a wide range in major and trace element and isotopic compositions despite having primitive compositions. It was argued in chapter 3 that mixing does not reproduce the composition of the Navajo lamprophyres and that their isotopic composition and degree of REE fractionation required derivation from an enriched source located within the mantle lithosphere. Therefore the earliest phase of magmatism from 28.5-17Ma records a period entirely dominated by melting within enriched lithospheric mantle.

The Hopi Buttes nephelinites, emplaced between 8.5 and 4.0 Ma represent the youngest phase of magmatic activity on the central plateau. The composition of these magmas were shown, in chapter 3, to be consistent with mixing between lithosphere-derived katungite-like melts and 40-60% of an asthenosphere-derived alkali-basalt.

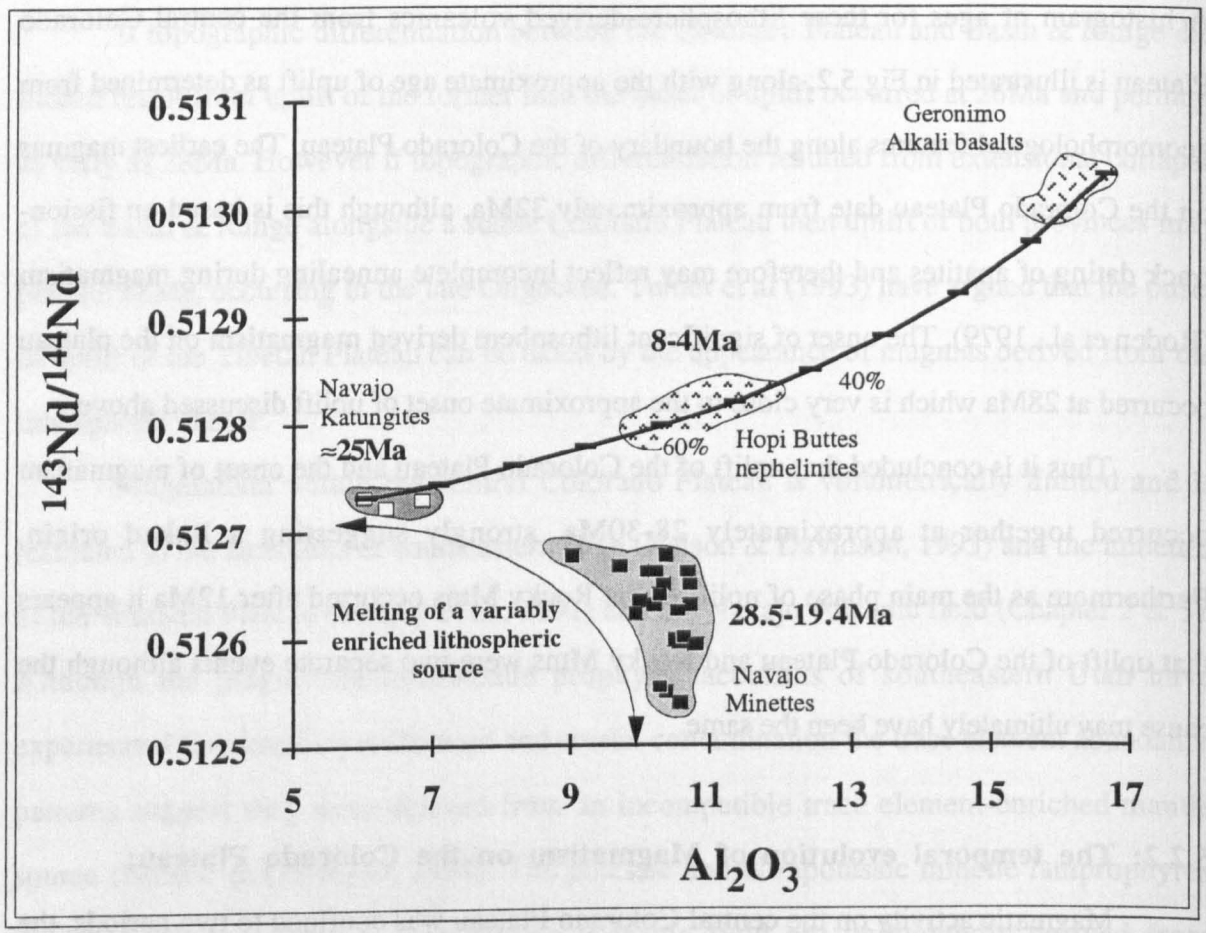


**Figure 5.3.** Variation of $^{143}Nd/^{144}Nd$ with $Al_2O_3$ of magmas from the central Colorado Plateau and from Geronimo (data from Kempton & Fitton unpub). Initial magmatism on the Colorado Plateau as represented by the katungites and minettes of the Navajo volcanic field represent small degree melts derived entirely from within a compositionally and mineralogically variable lithosphere source. The final Hopi Buttes magmatic episode reflects mixing of a katungite-like lithospheric melts with melts derived from the underlying asthenosphere, as represented by Geronimo alkali basalts.

Fig 5.3 illustrates the variation of $^{143}Nd/^{144}Nd$ with $Al_2O_3$ in magmas from the Colorado Plateau and serves as a summary for the temporal evolution of magmatism during the mid-late Cenozoic. The earliest phase of magmatism was dominated by small degrees of melting of lithospheric mantle for approximately 8Ma. Furthermore this earliest phase of lithosphere-dominated magmatism was a plateau wide event and, as illustrated in fig 5.4, was associated with a major period of lithosphere-dominated volcanism in the immediate vicinity of the plateau. Only in the final stages of magmatism on the Colorado Plateau during the late Miocene did melting occur in the asthenospheric mantle and is observed as the ***nephelinites*** of the Hopi Buttes and Wasatch Plateau emplaced between 8-4Ma (Alibert et al.,1986; Tingey, 1991).

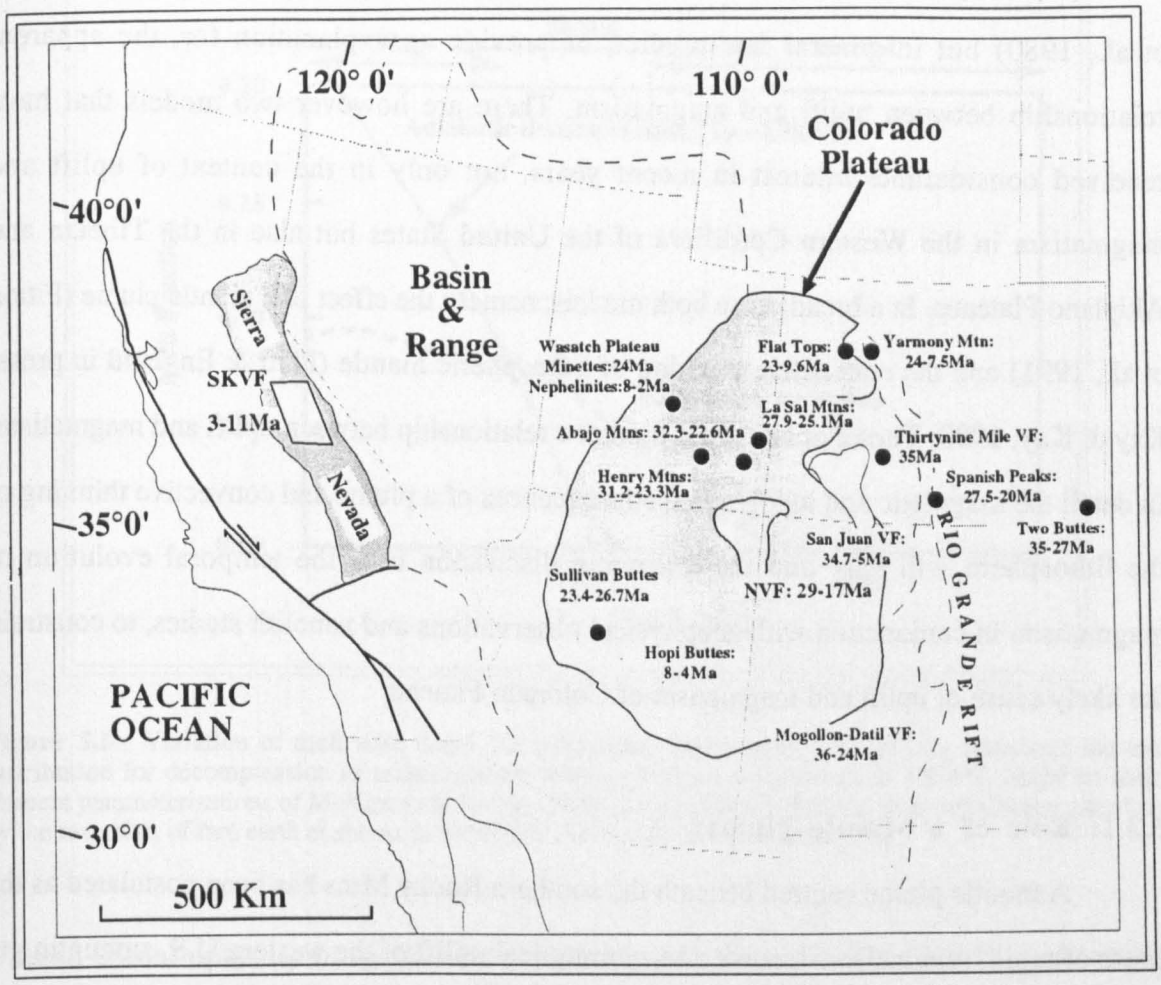


**Figure 5.4.** Age and distribution of magmatism on and immediately surrounding the Colorado Plateau illustrating the major magmatic event at 30±Ma. NVF, this study and Laughlin et al (1986); Sullivan Buttes, Tyner & Smith (1986); Henry, Abajo and La Sal Mtns, Nelson et al (1992); Thirtynine Mile volcanic field, Wobus et al (1990); San Juan volcanic field, Lipman et al (1978); Mogollon-Datil volcanic field, McIntosh, (1989); Yarmony Mtns, Leat et al (1990); Flat Tops, Leat et al (1988); Spanish Peaks and Two Buttes, Gibson et al (1993).

## 5.3: Melt generation beneath the Colorado Plateau:

The temporal evolution from lithosphere to asthenosphere-derived magmatism on the Colorado Plateau has also been documented in basalts from the Colorado River Trough (Bradshaw, 1991; Bradshaw et al.,1993; Hawkesworth & Gallagher, 1994) and the Mogollon-Datil volcanic field (Davis, 1991), adjacent to the plateau, and can be clearly related to crustal extension. However in the case of the central Colorado Plateau there is no evidence for extension either during or subsequent to the onset of magmatism. Instead magmatism appears to be inextricably linked to uplift of the Colorado Plateau in the Oligocene suggesting a common geodynamic origin for both magmatism and uplift

Numerous models have been proposed for uplift of the Colorado Plateau (McGetchin et al., 1980) but in general few predict, or provide an explanation for, the apparent relationship between uplift and magmatism. There are however two models that have received considerable interest in recent years, not only in the context of uplift and magmatism in the Western Cordillera of the United States but also in the Tibetan and Altiplano Plateaus. In a broad sense both models; namely the effect of a mantle plume (Fitton et al., 1991) and the convective thinning of lithospheric mantle (Platt & England in press; Kay & Kay, 1993; Turner et al., 1993) predict a relationship between uplift and magmatism. In detail the magmatic and topographic consequences of a plume and convective thinning of the lithosphere will vary and the following discussion uses the temporal evolution of magmatism, in conjunction with geophysical observations and xenolith studies, to constrain the likely cause of uplift and magmatism of Colorado Plateau.

### 5.3.1: Role of a Mantle Plume:

A mantle plume centred beneath the southern Rocky Mtns has been postulated as the cause of rapid, regionally extensive and symmetrical uplift of the western U.S. amounting to 1-3km since the late Tertiary (≥17Ma) (Fitton et al.,1991; Eaton 1986; 1987). In support of this model Fitton et al.(1988; 1991) noted the eruption of small volumes of OIB-like asthenosphere-derived magmas within the Basin & Range, southern Rio Grande Rift and Colorado Plateau (Hopi Buttes) within the last 8Ma. However the presence of small volume alkali basalts with OIB-like compositions in itself is not proof of the existence of a mantle plume, it may merely reflect small degrees of partial melting in the asthenosphere (Hawkesworth & Gallagher, 1994). Indeed rare-earth element inversions based on Rayleigh melting models (McKenzie & O'Nions, 1991) suggest that asthenospheric mantle of normal potential temperature (Tp=1280°C) can undergo small degrees of melting at depths of approaching 100km as shown in Fig 5.5.

The role of a mantle plume in uplift and magmatism of the Colorado Plateau and other regions of the western United States is even less convincing if both the topography of the S.W.United States and the calculated volumes and eruption-rates of basalts in the Basin & Range extensional province are considered. A mantle plume would be expected to result in

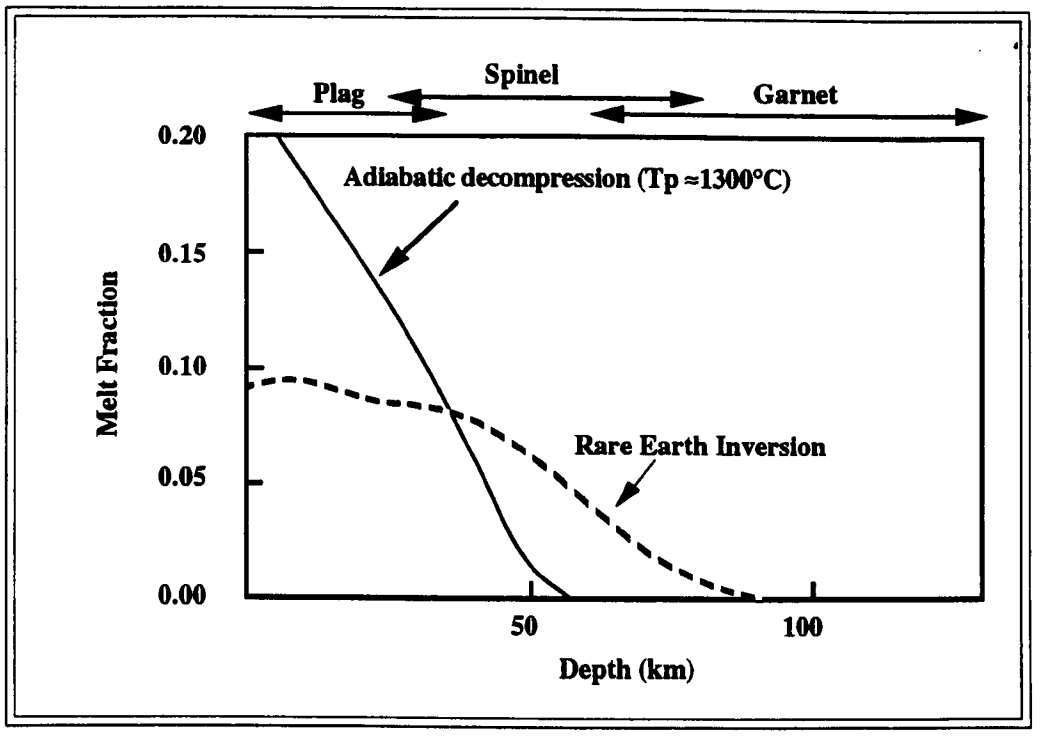


**Figure 5.5.** Variation of melt with depth for anhydrous asthenosphere. Solid line illustrates the melt distribution for decompression of asthenosphere with a potential temperature of 1300°C, based on major element parameterisations of McKenzie & Bickle (1988). Dashed line represents melt distribution calculated by the inversion of rare earth elements in N-MORB (McKenzie & O'Nions, 1991).

a broad domal uplift up of approximately 1000km diameter (White & McKenzie, 1989). However although Fig 5.1 demonstrates that there is an element of symmetrical uplift centred on the southern Rocky Mtns, the Colorado Plateau-Basin & Range-Sierra Nevada provinces clearly have an elevation in excess of that expected for truly symmetrical uplift. Though a mantle plume could account for the symmetrical uplift it is unlikely to produce the observed asymmetry in elevation and this requires some alternative uplift mechanism.

Furthermore the higher potential temperatures associated with a mantle plume (Tp≈1480°C) would also be expected to result in greater degrees of melting and hence volumes of magma and increased eruption rates within extensional provinces, such as the Rio Grande Rift and Basin & Range, yet this is contrary to observations (Bradshaw, 1991; Bradshaw et al 1993; Davis, 1991). In the Colorado River Trough the volumes of magma and eruption rates are estimated at 11600km$^3$ and 0.0023km$^3$yr$^{-1}$ respectively (Bradshaw et al.,1993), far less than for the eruption rates on Hawaii at ≈0.16km$^3$yr$^{-1}$ (Watson & McKenzie, 1991) and for the Deccan at ≈8km$^3$a$^{-1}$ (Richards et al., 1989) where the role of a mantle plume is clear.

Despite the presence of OIB-like magmas in the Basin & Range, Rio Grande Rift and Colorado Plateau provinces, which are interpreted as small degree melts of the asthenosphere, there is no convincing evidence for plume-initiated uplift and magmatism of the Colorado Plateau.

### 5.3.2: Convective Thinning Of Lithospheric mantle:

Although controversial, it has been proposed that rapid regional uplift associated with magmatism and extension (such as observed in the Tibetan Plateau (Turner et al., 1993) and perhaps the western United States (Platt & England, in press; Turner et al., 1992) may be reconciled by a single geodynamic process involving the foundering, or convective removal, of dense, over-thickened, lithospheric mantle into the underlying asthenosphere (Bird,1979; England & Houseman, 1988; Houseman et al.,1981; Sandiford & Powell, 1990; Turner et al.,1992)

In these models it is proposed that during convergent orogenesis both the crust and lithosphere experience homogeneous thickening resulting in both an increase in surface elevation and corresponding downward displacement of cold dense lithosphere into hot and convecting asthenosphere. This produces both a gravitational and thermal instability which Houseman et al (1981) showed could be resolved by the convective removal of part of the thickened mantle lithosphere, although the timing of onset and degree of thinning is in part dependant upon the convective state of the underlying asthenosphere. The isostatic response to this process is a rapid increase in the isostatically supported surface elevation which results in an increase in the outward-directed buoyancy forces (Houseman et al.,1981; England & Houseman, 1988; 1989; Sandiford & Powell, 1990). These in turn may lead to extensional collapse of the orogen if they exceed the compressional boundary forces (Sandiford & Powell, 1990). In addition removal of some portion of cold dense mantle lithosphere also has thermal and therefore magmatic implications (Turner et al., 1992)

The subcontinental mantle lithosphere is inferred to contain a zone enriched in incompatible elements and volatiles formed where small volume metasomatic melts or fluids intersect their solidus (Hawkesworth et al., 1984, 1990; Menzies & Murthy, 1980; Wass & Rogers, 1980). As the enriched zone is therefore likely to be defined by the solidus

temperature of the melts it requires only a small thermal perturbation to result in remobilisation (McKenzie, 1989). Whereas the magmatic response to the emplacement of a mantle plume at the base of the lithosphere is delayed because of the low thermal conductivity of the lithosphere, removal of the base of the lithosphere rapidly juxtaposes hot (Tp ≈1280°C) asthenospheric mantle against cool, possibly enriched, lithosphere. The local rapid increase in the geotherm is sufficient to cause remelting of volatile-rich regions of the *lithosphere* and generate small volume highly trace element enriched, and hence potassic or ultrapotassic magmas shortly after, or concomitant with, uplift. Not only is the magmatic response to convective thinning of the lithosphere ***rapid*** compared to a plume, but once initiated the period of ***lithosphere***-dominated magmatism is expected to span some period of time until the lithosphere is thinned sufficiently for melting of the anhydrous asthenosphere to occur.

The following discussion examines uplift of the Colorado Plateau and the temporal evolution of magmatism in the light of the expected responses to convective thinning of mantle lithosphere.

The present crustal thickness of the Colorado Plateau is 50-51km (Hauser & Lundy, 1989) similar to that of the western Great Plains (Hauser & Lundy, 1989), yet has a greater average elevation than the latter (Fig 5.1). Seismic studies reveal that the base of the mantle lithosphere beneath the Great Plains lies at a depth of approximately 160km whereas beneath the Colorado Plateau it lies at ≈90-100Km (Parker et al.,1984; Thompson & Zoback, 1979). Assuming the two provinces were comparable, it is apparent that the lithosphere beneath the plateau has been thinned although the timing of this event cannot be constrained from this simple observation.

Fortunately mantle-derived xenoliths carried in the Navajo minette diatremes provide a unique opportunity to estimate the thickness of the lithosphere beneath the Colorado Plateau during the Oligocene. Thermobarometric studies on spinel and garnet-bearing peridotite xenoliths, summarised in Fig 5.6, suggest they were derived from lithosphere at depths of between approximately 60 and 150km (Ehrenberg, 1978, 1982; Roden et al.,1990) and that 150km may be regarded as an estimate of the *minimum* thickness of the lithosphere during the Oligocene. This estimate of the thickness of the Colorado Plateau

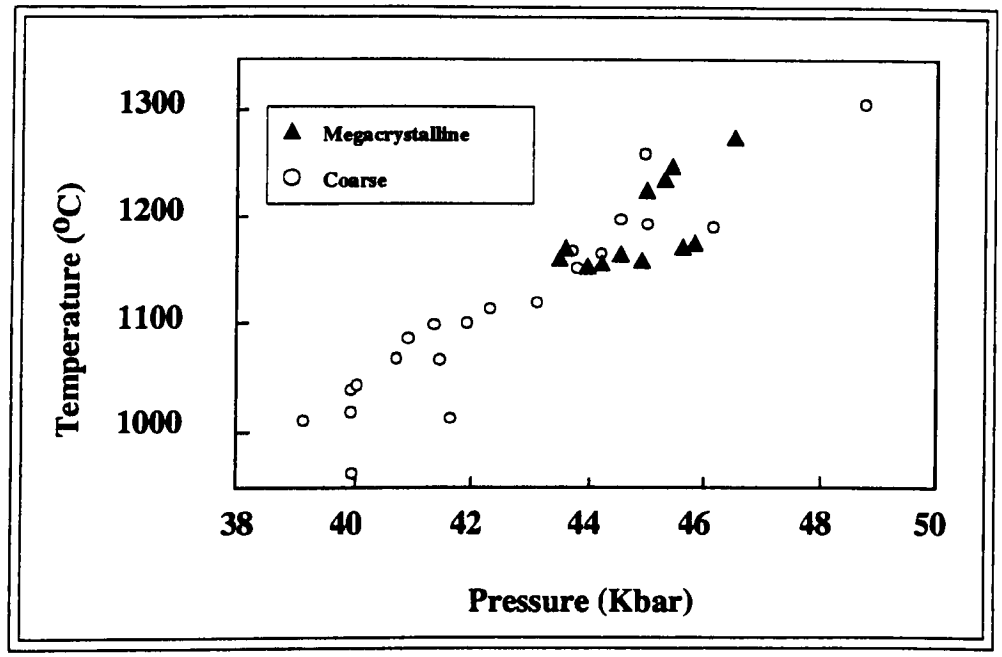


**Figure 5.6.** Calculated temperatures plotted against pressures using the preferred method of Finnerty & Boyd (1987) for garnet peridotites from the Thumb minette diatreme, Navajo volcanic field, central Colorado Plateau. Mineral compositions from Ehrenberg (1978). Taken from Roden et al (1990).

lithosphere during the Oligocene is very similar to the present lithosphere thickness estimated for the Great Plains. As the present, seismically determined, lithospheric thickness is approximately 90-100km, at least 50 and perhaps as much as 60km of lithospheric thinning appears to have occurred over the last 30Ma as illustrated in Fig 5.7 where the present lithospheric thickness, based on seismic studies, is compared to the thickness of the Oligocene lithosphere determined from Navajo xenoliths. Previous studies have attempted to estimate the degree of lithospheric thinning by determining the amount required to produce the observed uplift (Turner et al.,1993). In this study the better constrained degree of lithospheric thinning is used to estimate semi-quantatively the increase in isostatically supported surface elevation consequent on thinning, using the approach of Sandiford & Powell (1990).

In this approach deformation in the lithosphere is described in terms of two parameters: a crustal thickening factor, $f_c$, the ratio of the thickness of deformed crust to initial crust; and a lithospheric thickening factor $f_l$, the ratio of the total thickness of deformed lithosphere (crust and mantle) to initial lithosphere. The assumptions in this model are that the initial lithosphere, prior to thickening, consisted of a 35km thick crust underlain by mantle lithosphere of 100km (Fig 5.8 $\psi$=0.35) and that thickening was homogeneous

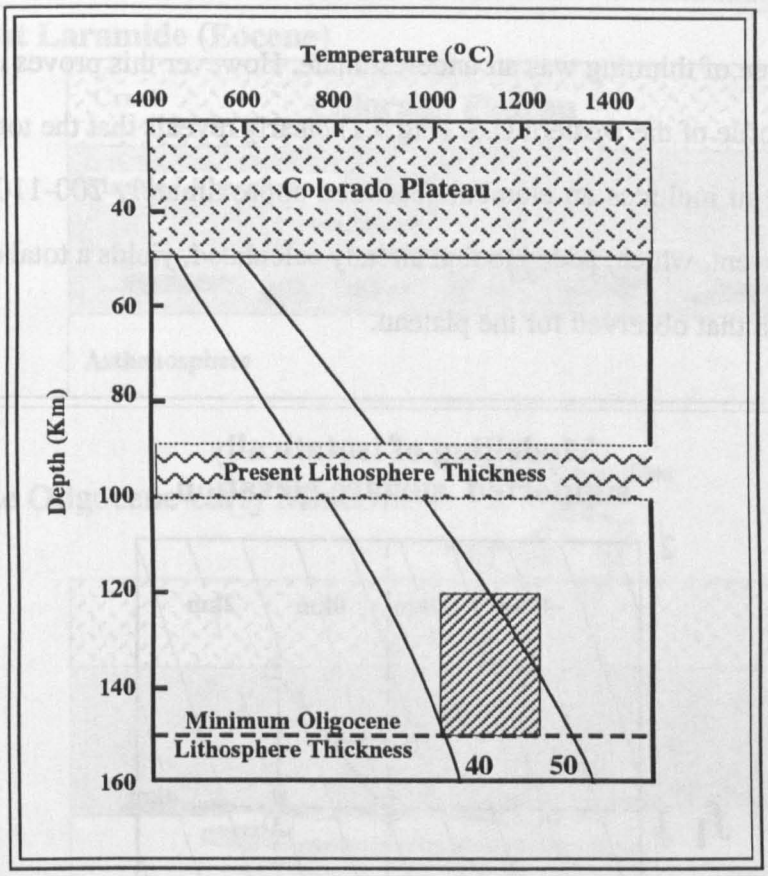


**Figure 5.7.** Comparison of minimum thickness of lithosphere during the Oligocene with the present-day seismically determined thickness illustrating the reduction the overall reduction in lithospheric thickness of the Colorado Plateau by 50-60Km. Base of Oligocene lithosphere defined by the maximum pressure estimates obtained on garnet peridotites from the Navajo minette diatremes (hatched box). Also shown are continental geotherms for heatflows of 40 and 50mw//m2. Modified after Hunter & Smith (1981).

throughout the crust-lithosphere column. Fig 5.8 and 5.9 show the isostatic and magmatic consequences of deformation of the crust and/or lithosphere ($f_c$ and $f_l$) for the Colorado Plateau. Prior to crustal thickening in the Eocene the plateau was at sealevel (Kauffman, 1977). Homogeneous thickening by a factor of ≈1.5 (as illustrated by Fig 5.8) during the Laramide orogeny to produce the present 52km thick crust resulted in an isostatically supported elevation of ≈1-1.2km (② in Fig 5.8). Subsequent thinning of the lithosphere by 50-70km, as determined from xenolith and seismic studies, resulted in further uplift which would be expected to increase surface elevation to ≈1.8-2.1km at approximately 30Ma (③ in Fig 5.8). A calculated elevation of ≈2km is close to the observed 2000m average elevation of the Colorado plateau (Beghoul & Barazangi, 1989) yet falls short of the 2900m elevation of an Oligocene palaeo-surface recognised in the Chuska Mtns (Chapter 2, section 2.3.1) of the NVF. This additional 900m of uplift could be accounted for by the model developed in Fig 5.8 by changing the initial ratio of crust to lithosphere or their relative densities, or indeed if

the calculated degree of thinning was an underestimate. However this proves unnecessary as the topographic profile of the western U.S. (Fig 5.1) clearly reveals that the total elevation of the Colorado Plateau includes an element (between approximately 200-1100m) from the Rocky Mtn uplift event, which, added to that already calculated, yields a total elevation of 2-3km consistent with that observed for the plateau.

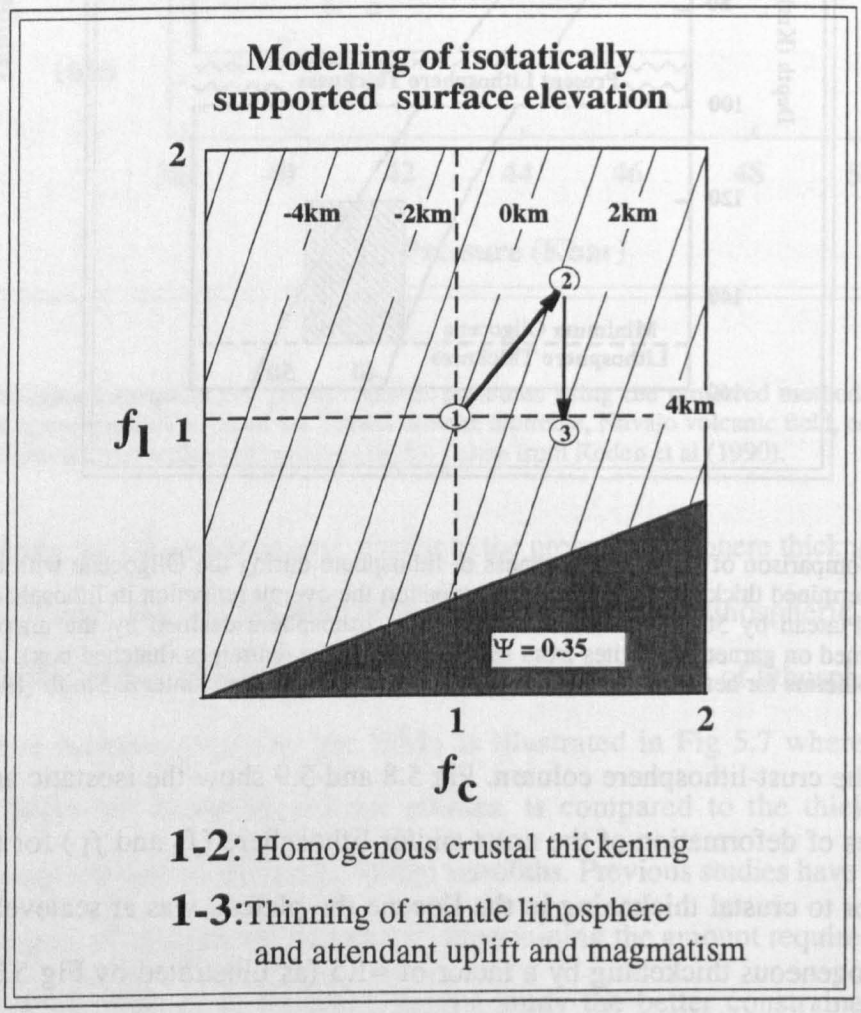


**Figure 5.8.** Isostatic modelling of a three stage evolution for the Colorado Plateau from Laramide crustal thickening (70-40Ma) followed by subsequent thinning of the lithosphere associated with magmatism during the late Oligocene to late Miocene/Pliocene. $f_l$-$f_c$ plane (where $f_c$ is the crustal thickening factor and $f_l$ is the total lithospheric thickening factor, see text and Sandiford & Powell (1990) is contoured for the isostatically compensated surface elevation. Initial crust to lithosphere ratio ($\psi$) = 0.35.

Point ① represent crust of normal thickness at sea level prior to Laramide compression.

Point ② represent homogenous thickening ($f_c$=$f_l$) until crustal thickness reaches its present thickness of 50-51km (Hauser & Lundy, 1989). Total elevation at point ≠ is ≈1km,

From point ② to ③ the mantle lithosphere is thinned from 150km to approximately 90-100km resulting in further 1km of uplift producing a total of 2km, appropriate for the excess elevation of the Colorado Plateau (section **5.2.1**).

The lithosphere is assumed to initially contain a metasomatised K-rich layer defined by it solidus termperature (McKenzie, 1989). Thickening moves all material downwards without melting. Convective thinning of the lithosphere brings asthenospheric mantle of normal potential temperature (≈1280°C) into contact with the metasomatised layer causing melt generation and the eruption of K-rich minettes and basalts. The low thermal conductivity of the lithosphere is such that the K-rich layer will pass through its solidus and hence melt over ≈10Ma plus. The important point is that this model predicts a close temporal relationship between uplift and magmatism.

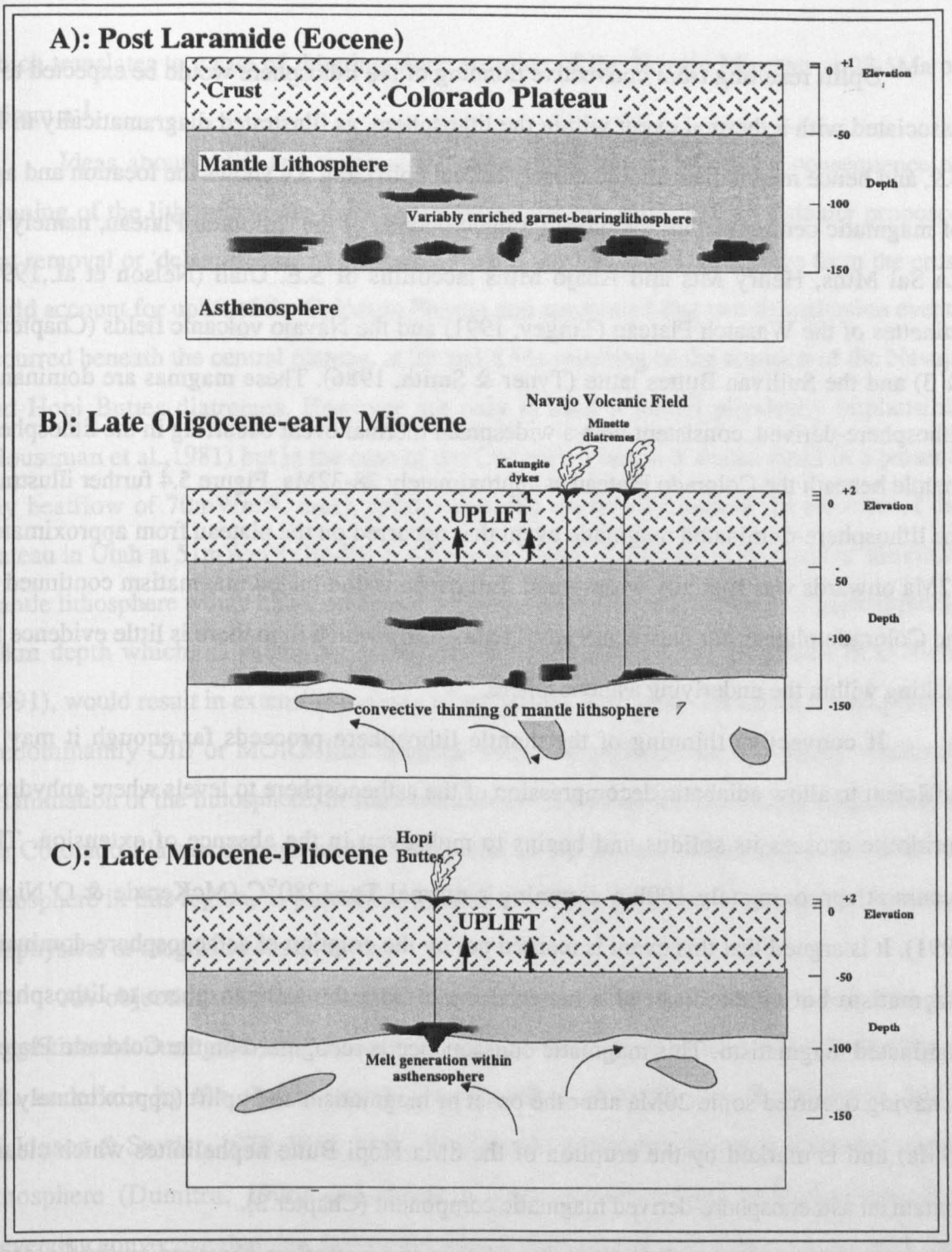


**Figure 5.9**. Tectonomagmatic evolution of the Colorado Plateau from the post Laramide late Eocene to the late Miocene-early Pliocene.

**A**): The post Laramide 'Colorado Plateau' stands at an elevation of 1km. Crustal thickness is approximately 50km (Hauser & Lundy, 1989) and the base of the lithosphere is at 150km depth (Roden et al., 1990). The lower lithosphere contains a variably enriched phlogopite-carbonate bearing zone formed by the percolation of small volume asthenosphere-derived melts into the base of the lithosphere at approximately 1Ga (chapter 3).

**B**): During the late Oligocene to early Miocene the gravitationally unstable overthickened mantle lithosphere begins founder into the underlying asthenosphere which results in renewed uplift of the plateau. The juxtaposition of asthenosphere (Tp≈1280°C) with volatile and trace element enriched lower lithosphere is sufficient to cause melting and results in the eruption of the Navajo minettes and katungites shortly after the onset of uplift. Melting of the asthenosphere is prevented by a sufficiently thick lithospheric mantle.

**C**): In the late Miocene to early Pliocene convective thinning of the lithospheric mantle has resulted in a total uplift of 2km. Furthermore asthenosphere is able to undergo decompression melting at depths of 100km and so contributes to the nephelinitic magmatism of the Hopi Buttes and Wasatch Plateau (Alibert et al., 1986; Tingey, 1991).

Uplift resulting from convective thinning of the lithosphere would be expected to be associated with a thermal event within the lithosphere, as illustrated diagramatically in Fig 5.9, and hence magmatism should closely follow uplift. Fig 5.4 shows the location and ages of magmatic centres within the physiographic bounds of the Colorado Plateau, namely the La Sal Mtns, Henry Mts and Abajo Mtns laccoliths of S.E. Utah (Nelson et al.,1992), minettes of the Wasatch Plateau (Tingey, 1991) and the Navajo volcanic fields (Chapters 2 & 3) and the Sullivan Buttes latite (Tyner & Smith, 1986). These magmas are dominantly lithosphere-derived, consistent with a widespread thermal event occurring in the lithospheric mantle beneath the Colorado Plateau at approximately 28-32Ma. Figure 5.4 further illustrates the lithosphere-dominated magmatic event that occurred on the plateau from approximately 32Ma onwards was spatially widespread. Lithosphere-dominated magmatism continued on the Colorado plateau for between 8 and 11Ma during which time there is little evidence for melting within the underlying asthenosphere.

If convective thinning of the mantle lithosphere proceeds far enough it may be sufficient to allow adiabatic decompression of the asthenosphere to levels where anhydrous peridotite crosses its solidus and begins to melt even in the absence of extension. This occurs at approximately 100km assuming a normal Tp≈1280°C (McKenzie & O'Nions, 1991). It is argued that this event is marked not by the eruption of asthenosphere-dominated magmatism but as the onset of a material input from the asthenosphere to lithosphere-dominated magmatism. This magmatic consequence is recognised on the Colorado Plateau as having occurred some 20Ma after the onset of magmatism and uplift (approximately 28-30Ma) and is marked by the eruption of the 8Ma Hopi Butte nephelinites which clearly contain an asthenosphere-derived magmatic component (Chapter 3).

As with elevation, the temporal evolution of magmatism observed on the Colorado Plateau, from lithosphere-dominated magmatism throughout the Oligocene and early Miocene to only a minor contribution from the asthenosphere in the final stages of magmatism during the Pliocene, is consistent with a model that extensively thins the lithosphere during the late Cenozoic. If this model is correct it is also possible to invoke a rate of lithospheric thinning assuming that the minimum initial lithospheric thickness during the Oligocene, on the basis of xenolith data, was at least 150km and asthenosphere of normal Tp (1280°C) will melt at a depth of around 100km. This being the case eruption of the Hopi Buttes nephelinites at ≈8Ma would imply a lithospheric thickness of ≈100km

which translates to a rate of thinning since eruption of the Navajo Minettes at 28.5Ma of 2.5mm $a^{-1}$.

Ideas about uplift and magmatism of the Colorado Plateau as a consequence of thinning of the lithosphere are not a recent development. Bird (1979) originally proposed that removal or 'delamination' of the *entire* mantle portion of the lithosphere from the crust could account for uplift of the Colorado Plateau and speculated that two delamination events occurred beneath the central plateau, at 29 and 8 Ma resulting in the eruption of the Navajo and Hopi Buttes diatremes. However not only is such a model physically implausible (Houseman et al.,1981) but in the case of the Colorado Plateau it would result in a present-day heatflow of 70mW$m^{-2}$, much greater than the observed heatflow for the core of the plateau in Utah at 51mW$m^{-2}$ (Bodell & Chapman, 1982). Furthermore removal of the entire mantle lithosphere would allow adiabatic decompression of asthenosphere to approximately 50km depth which, as shown by Mckenzie & Bickle (1988) and McKenzie & O'Nions (1991), would result in extensive melting of anhydrous peridotite. Therefore the eruption of predominantly OIB or MORB-like magmas would be expected to accompany wholesale delamination of the lithosphere, in stark contrast to the lithosphere dominated magmatism of the Colorado Plateau throughout the Oligocene to the present. Wholesale removal of the lithosphere in this region, as postulated by Bird (1979), is therefore not supported by either geophysical or magmatic observations.

An objection to the lithosphere thinning model proposed here arises from the suggestion that during the late-Mesozoic to mid-Cenozoic much of the western United States was underlain by the shallow-subducting Farallon plate (Coney & Reynolds, 1977; Dickinson & Snyder, 1978; Bird, 1988). This would refrigerate the sub-continental mantle lithosphere (Dumitru, 1990) and shield it from the underlying asthenosphere, thus preventing convective thinning. Indeed Dumitru (1990) suggest that apatite fission-track data from samples at the base of the Grand Canyon, western Colorado Plateau, which indicate cooling of approximately 40°C from an initial temperature of 130°C at around 70Ma may reflect refrigeration of the lithosphere as a result of Laramide shallow subduction. Furthermore the presence of eclogite xenoliths contained within the Navajo diatremes have been interpreted as fragments of the Farallon plate and cited as supporting evidence for the shallow subduction model (Helmstaedt & Doig, 1975; Helmstaedt & Schulze, 1991). The onset of the Laramide orogeny ca.70Ma was associated with crustal thickening and a certain degree of uplift and it is reasonable to attribute the apatite cooling data to uplift and unroofing

of the Colorado Plateau during this period (Dumitru, 1990). An isotopic and geochemical study on the eclogite xenoliths from the NVF (Wendlandt et al., 1993) suggest that they do not represent fragments of Mesozoic MORB and therefore cannot be interpreted as direct evidence in support of shallow subduction during the Laramide. There is hence no convincing evidence to support shallow subduction of oceanic lithosphere beneath the Colorado Plateau during the Cenozoic and therefore prevent convective thinning of the lithosphere during the Oligocene.

The present tectonomagmatic model for the evolution of the Colorado Plateau, summarised in Fig 5.9, is consistent with geophysical measurements such as heatflow (Bodell & Chapman, 1982) and seismics, and can account for the uplift and associated magmatism. Furthermore convective thinning of the lithosphere predicts the evolution from an initial long period of lithosphere dominated magmatism to later asthenosphere-derived magmatism, consistent with that observed.

## 5.4:Uplift and magmatism within the Sierra Nevada:

### 5.4.1: Timing of uplift of the Sierra Nevada:

Although the timing and magnitude of Cenozoic uplift of the Sierra Nevada range remain a matter of controversy, the situation is even more straightforward than for the Colorado Plateau. Whereas much of the western United States, including the Colorado Plateau, has been influenced by regional uplift centred on the southern Rocky Mtns, (Eaton 1986; 1987) the Sierra Nevada is sufficiently distant from the latter not to have been influenced by this uplift event (Fig 5.1). Accordingly there is no need to separate various uplift events as for the Colorado Plateau. Furthermore the Sierra Nevada is bounded on the west by the comparatively stable California Great Valley which provides a suitable base level reference (Huber, 1981; Unruh, 1991), whereas the Colorado Plateau is surrounded by extensional provinces.

The Sierra Nevada range comprises a large uplifted and westward-tilted fault block, dominated by the Mesozoic Sierra Nevada batholith. Elevations vary along the length of the range with the highest regions in the south (Mt Whitney ≈3.96km) decreasing to an average of 1-2km in the north (Lassen Park ≈1.68km). Most authors agree that uplift occurred during the last 10Ma (Christensen, 1966; Crough and Thompson 1977; Axelrod, 1980;

Huber, 1981; 1990; Bartow, 1984; Chase and Wallace, 1986; Loomis and Burbank, 1988; Unruh, 1991) although the precise onset of uplift and whether it was simultaneous along the length of the range or diachronous is a matter of contention.

Uplift of the Sierra Nevada can be crudely divided into two periods; a late Cretaceous unroofing of the batholith due to arc inflation by intrusion of large magma bodies (Bruce et al., 1989; Dumitru, 1990), followed by a late Cenozoic event, the timing and magnitude of which is the focus of this section. Late Mesozoic early Tertiary uplift and unroofing of the Sierra Nevada ceased before the Eocene, allowing erosion to reduce the range to one of moderate relief (Huber, 1981). Peaks either side of the San Joaquin Canyon, Central Sierra Nevada, rise only 450-750m above the reconstructed Eocene base level. However these same peaks rise 1500-1700m above the 10Ma base level suggesting relief increased substantially between the Eocene and Miocene (Huber, 1981). Late Cenozoic uplift was sufficient by 8-9Ma for the Sierra Nevada to become a sediment source for sedimentary basins in the Californian Great Valley to the west and Basin & Range to the east (Bartow, 1984; Loomis and Burbank,1988).

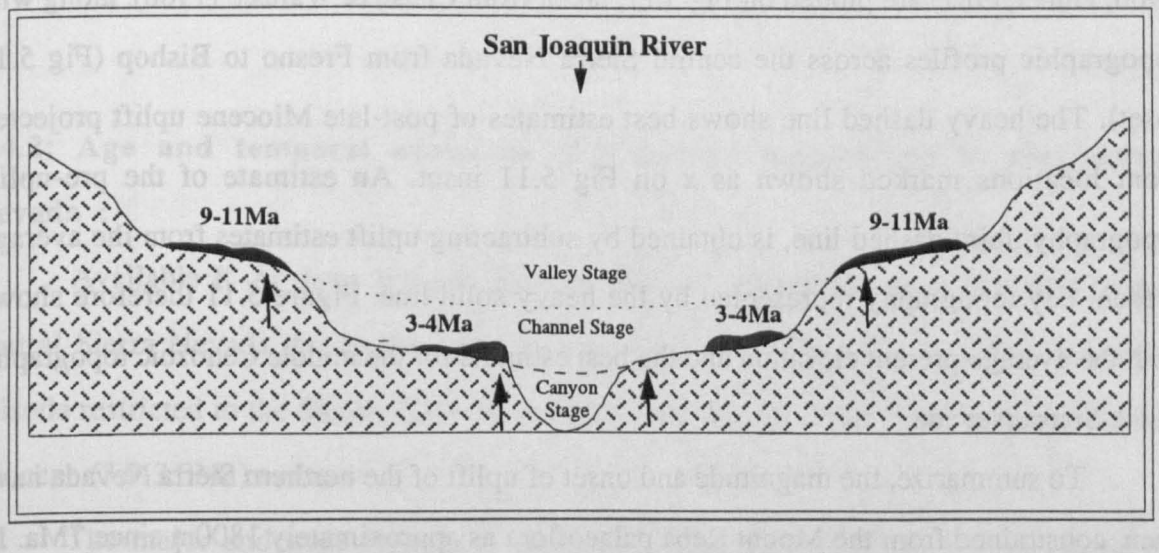


**Figure 5.10**. Diagramatical representation of the San Joaquin River, central Sierra Nevada, illustrating palaeo river channels of varying maturity preserved beneath remnant Cenozoic basalt flows observed along its course (Dalrymple, 1964; Christensen, 1966; Huber, 1981). Subsequent to the eruption of basalts at 9-11Ma the pre 11-Ma San Joaquin river channel is incised suggesting uplift of the Sierra Nevada at or immediately following 11Ma. This new inner channel reaches a degree of maturity prior to the eruption Pliocene basalts at 3-4Ma. Hence between 11Ma and 4Ma the rate of uplift either decreased or uplift ceased altogether, some Pliocene basalts in the southern Sierra Nevada are themselves incised by the latest canyon-cutting phase of the San Joaquin River. This implies a second period of uplift or at least an increase in the rate of uplift shortly after 3-4Ma. The faint dotted line is the pre-11Ma valley profile while the dashed line is the pre-4Ma channel profile. Arrows indicate uplift.

Ancestral river channels of the San Joaquin and Stanislaus, preserved beneath 9-10Ma old Cenozoic basalts (Dalrymple, 1963, 1964; Christensen, 1966; Huber, 1981), contrast with less mature modern channels suggesting that uplift occurred sometime after 9-10Ma. However 3.9Ma basalts (Dalrymple, 1963) outcrop within the *inner* gorges of several larger Sierran rivers, including the San Joaquin, and imply that renewed canyon cutting, and hence uplift, began prior to 3.9Ma (Unruh, 1991). In the southern Sierra Nevada some approximately 3Ma old basalts are occasionally dissected by river canyons and this led Christensen (1966) to conclude that uplift was greater here than in the north and continued after 3Ma. These observations, diagrammatically illustrated in Fig 5.10 on the preceding page, bracket the onset of late Cenozoic uplift of the Sierra Nevada to sometime between 10 and 4 Ma with continued uplift after 3Ma in the southern Sierra Nevada although caution must be applied here in that renewed incision of the San Joaquin River may reflect global climate change (Molnar & England, 1990). Axlerod (1980) provided independent and supporting palaeobotanical evidence for the timing of uplift; the Mount Reba flora, a lowland assemblage, found in 6-7Ma volcaniclastics, is presently exposed at the crest of the *northern* Sierra Nevada indicating that uplift of approximately 1,800m began here sometime after 6-7Ma. Locations where the amount of late Cenozoic uplift have been estimated (Christensen, 1966; Huber,1981) are plotted on Fig 5.11, taken from Chase & Wallace (1986), along with topographic profiles across the central Sierra Nevada from Fresno to Bishop (Fig 5.11 inset). The heavy dashed line shows best estimates of post-late Miocene uplift projected from locations marked shown as x on Fig 5.11 inset. An estimate of the pre-uplift topography, faint dashed line, is obtained by subtracting uplift estimates from the average present-day topography represented by the heavy solid line. Figure 5.11 therefore shows both the average present elevation and the best estimate for the middle Cenozoic topography of the Sierra Nevada.

To summarize, the magnitude and onset of uplift of the northern Sierra Nevada have been constrained from the Mount Reba palaeoflora as approximately 1800m since 7Ma. In the central and southern Sierra Nevada such constraints are lacking and best estimates for the magnitude and timing of uplift, based on dating of volcanic flows in channels of the San Joaquin River (Fig 5.10), are approximately 2km sometime between 10 and 4Ma. The lack of more precise estimates on the uplift of the southern Sierra Nevada prevent an assessment of any diachronous element to uplift. The general consensus is that uplift has occurred in the last 10Ma with 1km or more during the last 3Ma (Huber, 1981).

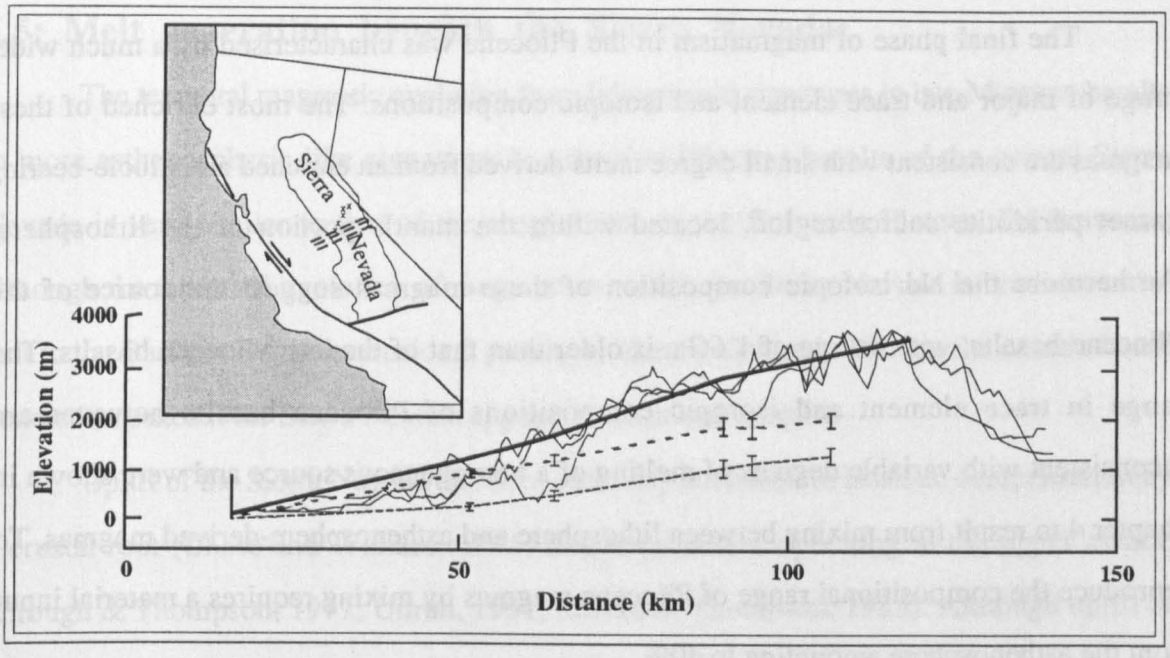


**Figure 5.11**. Present and palaeotopography of the Sierra Nevada modified after Chase & Wallace (1986). Light solid lines represent profiles of present-day topography, the locations of which are shown in the inset map as dashed lines. The heavy solid line is the average present elevation or more precisely the present position of an average surface prior to uplift. Heavy vertical line at 16km shows the crossing point of present and palaeo drainage of the San Joaquin River. Error bars connected by dotted line shows estimates of amount of post-middle Miocene uplift (Christensen, 1966; Huber, 1981). Uplift estimates are projected onto profile from locations shown as x on inset map. Heavy dashed line shows palaeotopography; error bars represent uncertainty in uplift. Palaeotopography is calculated by subtracting uplift (dotted line) from present topography (heavy solid line). Vertical exaggeration approximately 7x.

### 5.4.2: Age and temporal evolution of Cenozoic magmatism in the Sierra Nevada :

Available K-Ar dates indicate that two distinct magmatic events occurred in the central Sierra Nevada during the late Cenozoic, a late Miocene (11.4-9.4Ma) volcanic episode restricted to the Shaver Lake-Huntington Lake region and a more widespread late Pliocene (3.9-3.0Ma) event .

The major and trace element composition of initial, primitive or near primary, magmas of the central Sierra Nevada were shown in chapter 4 to be consistent with small degree melts of an enriched phlogopite-bearing garnet peridotite source located within the lithospheric mantle. Furthermore the isotopic composition of these magmas suggest a source age of 0.9Ga. Although there is only a limited number of primitive late Miocene magmas, it is suggested that the earliest phase of magmatism within the Sierra Nevada, as on the

Colorado Plateau, was dominated by melting within the lithospheric mantle.

The final phase of magmatism in the Pliocene was characterised by a much wider range of major and trace element and isotopic compositions. The most enriched of these magmas are consistent with small degree melts derived from an enriched amphibole-bearing garnet peridotite source region, located within the mantle portion of the lithosphere. Furthermore the Nd isotopic composition of these magmas suggest the source of the Pliocene basalts, with an age of 1.6Ga, is older than that of the late Miocene basalts. The range in trace element and isotopic compositions of Pliocene basalts however are inconsistent with variable degrees of melting of a homogeneous source and were shown in chapter 4 to result from mixing between lithosphere and asthenosphere-derived magmas. To reproduce the compositional range of Pliocene magmas by mixing requires a material input from the asthenosphere amounting to 40%.

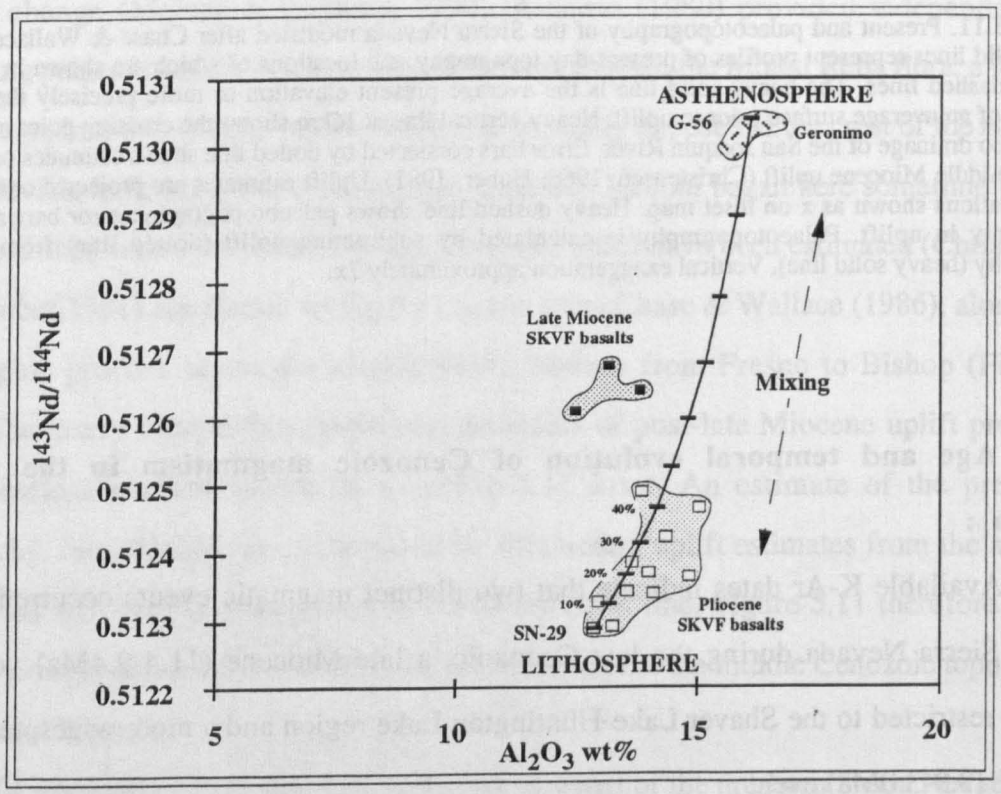


**Figure 5.12.** $^{143}Nd/^{144}Nd$ versus $Al_2O_3$ for basalts from the San Joaquin-Kings volcanic field, central Sierra Nevada, illustrating the temporal evolution of magmatism and the interaction of the Pliocene lithospheric endmember with the asthenosphere endmember G-56 (Kempton & Fitton, unpubl data).

The temporal evolution in composition of primitive basalts from the central Sierra Nevada, illustrated by the variation of $^{143}Nd/^{144}Nd$ with $Al_2O_3$ in Fig 5.12, thus records an evolution from lithosphere dominated magmatism to magmatism in which there is a significant contribution from the asthenosphere. Concomitant with the lithosphere to asthenosphere transition is a decrease in the depth of melting within the lithosphere and in

the apparent age of the source.

## 5.5: Melt generation beneath the Sierra Nevada:

The temporal magmatic evolution from lithospheric signatures in late Miocene basalts to more asthenospheric-like signatures in primitive Pliocene basalts of the central Sierra Nevada is very similar to that of the magmatism on the Colorado Plateau. Furthermore, although the temporal evolution of magmatism within the Sierra Nevada is reminiscent of that in the Basin & Range extensional province, like the Colorado Plateau the cause of melt generation beneath the Sierra Nevada appears to be linked to uplift.

Uplift of the Sierra Nevada has been variously attributed to isostatic compensation by a crustal root (Chase and Wallace, 1986) and to processes operating in the upper mantle (Crough & Thompson, 1977; Unruh, 1991; Mavko & Thompson, 1983). Although uplift of the Sierra Nevada occurred during the last 10Ma (Huber, 1981; Unruh, 1991) the crustal root comprises Mesozoic (Bateman & Eaton, 1967; Schwaeichert & Cowan, 1975) plutons. It is therefore difficult to reconcile late Cenozoic uplift with the formation of this crustal root. To avoid this problem Chase & Wallace (1986) suggest that the buoyancy effects of the Mesozoic root were suppressed by the flexural strength of the lithosphere developed during cooling of the Sierra Nevada batholith. This situation prevailed until Basin & Range extension 'broke' the lithosphere along the eastern front of the Sierra Nevada batholith at around 10Ma allowing westward tilting of the whole block. However, local large-scale Tertiary extension in the western Basin & Range predated the onset of late Cenozoic tilting of the Sierra Nevada by 7-12Ma (Unruh, 1991 and references there in). Jones (1987) also noted that the gravity low over the Sierra Nevada correlates with late Cenozoic topography rather than with the distribution of the Mesozoic batholith which forms the crustal root. Finally a crustal origin for uplift of the Sierra Nevada does not account for the temporal association of uplift and mantle-derived magmas identified in sections 5.4.1 and 5.4.2. It is therefore concluded that the late Cenozoic uplift of the Sierra Nevada is not an isostatic response to a crustal root.

The close temporal and spatial association of mantle-derived magmas and uplift recognised in the Sierra Nevada (section 5.4.1 & 5.4.2; Van Kooten, 1980; Moore & Dodge, 1980) suggest that late Cenozoic uplift of the range has its origins in the upper

mantle rather than the crust and geophysical evidence supports this interpretation (Crough & Thompson, 1977; Mavko & Thompson, 1983; Jones, 1987). The gravity anomaly over the Sierra Nevada is suggested to reflect the presence of low-density mantle beneath the southern Sierra Nevada (Jones, 1987). This low density mantle does not relate to a mantle plume as the Sierra Nevada is a non-symmetrical linear topographic feature rather than the regional domal feature expected of a plume.

Mavko & Thompson (1983) suggest that the increasing delay in P wave arrival times between the northern and southern regions of the Sierra Nevada, may either reflect a horizontal decrease in Pn velocities of 7.9 to 7.6kms$^{-1}$ from north to south or, as shown in Fig 5.13, a gradual decrease in lithospheric thickness toward the southern Sierra Nevada.

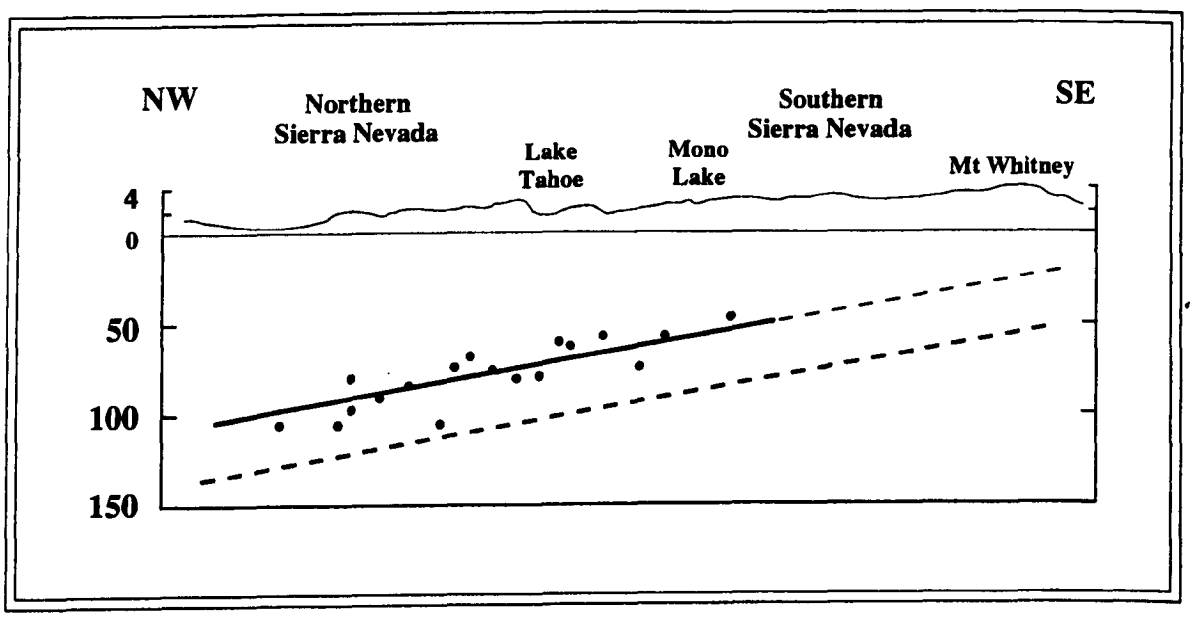


**Figure 5.13.** Profile of lithospheric thickness and elevation along the crest of the Sierra Nevada from Lassen Park in the north to Mt. Whitney in the south. The computed lithospheric thickness sampled by each ray path is marked and a straight line fit to the lithosphere-asthenosphere boundary is drawn (solid line). A second model giving a better lithospheric thickness beneath Mt. Whitney is shown by the dashed line 30km deeper. Modified after Mavko & Thompson, (1983).

Extrapolation of the lithospheric thickness south of Mono lake (Fig 5.13) to beneath the Mt Whitney region yields unrealistic values <25km (Mavko & Thompson, 1983) though there is sufficient flexibility in the interpretation of the teleseismic data to increase the thickness of the lithosphere throughout the section by 30km (dashed line in Fig 5.13) resulting in a *spatial* variation in lithospheric thickness of 140-55km, similar to the *temporal* variation calculated for the Colorado Plateau in section 5.3.2. The north to south decrease in

lithosphere thickness from 110-60km correlates with an increase in surface elevation prompting the suggestion that late Cenozoic uplift of the Sierra Nevada was caused by convective thinning of the mantle lithosphere (Mavko & Thompson, 1983). Although the crust beneath the Sierra Nevada is as much as 55km thick (Pakiser & Brune, 1980) it is uncertain whether this reflects crustal thickening associated with Laramide compression or pre-Laramide crustal growth resulting from magmatic contributions from the arc. As there are few constraints on either the initial crustal structure of the Sierra Nevada or whether crustal thickening was homogeneous, as assumed for the Colorado Plateau, or heterogeneous, it is difficult to model the degree of uplift from the $f_l$-$f_c$ parameterisation of Sandiford & Powell (1990). An alternative approach taken by Mavko & Thompson (1983) was to use a lithosphere-asthenosphere density contrast of 0.085gm/cm$^3$ to estimate the degree lithospheric thinning necessary to balance the topographic mass from Lassen Park (1.68km) to Mt. Whitney (3.96km). The north-south increase in elevation requires approximately 72km of lithospheric thinning which is close to the estimated decrease in lithospheric thickness of 80km based on seismicity (Mavko & Thompson, 1983).

Although seismic and gravity data indicate and are consistent with a shallow thermal anomaly beneath the high Sierra Nevada, this region is characterised by heat flows of <25 to 50mWm$^{-2}$, some of the lowest known on the continents (Saltus & Lachenbruch, 1991). Higher heatflows of up to 91mWm$^{-2}$ are observed, but in general are restricted to sites <40km from the Basin & Range, supporting the view that Basin & Range extensional tectonics and magmatism are encroaching on the eastern Sierra Nevada (Saltus & Lachenbruch, 1991). However Dumitru (1990) and Saltus & Lachenbruch (1991) demonstrated that so long as the conductive lithosphere above the thermal anomaly was at least 50km thick, as shown by Mavko & Thompson (1983), the heatflow data would be consistent with the introduction of a thermal anomaly beneath the Sierra Nevada within the last 15-20Ma.

The onset of late Miocene magmatism in the Huntington Lake region of the central Sierra Nevada (section 5.4.2) indicate the presence of a thermal anomaly in the lower lithosphere at approximately 12Ma, within the 15-20Ma limit set by the heatflow data (Dumitru, 1990; Saltus & Lachenbruch, 1991). As on the Colorado Plateau the composition of this initial magmatism within the central Sierra Nevada (Chapter 4 and section 5.3.2) is

dominated by melting a lithospheric mantle source. Although there are few primitive late Miocene basalts there is no conclusive evidence for a magmatic contribution from the asthenosphere in the early magmas. In the context of section 5.3.2 this suggests that during the Miocene the lithospheric mantle was ≥100km thick in order to prevent the upwelling and melting of anhydrous asthenosphere. This is also consistent with the late Miocene basalts being derived from a phlogopite-bearing garnet peridotite, stable only at depths in excess of 90km (chapter 4; Falloon & Green, 1989).

The final stage of magmatism in the Sierra Nevada during the Pliocene was characterised by a decrease in the depth of melting within the lithosphere, melts being derived from an amphibole-bearing peridotite at depths of less than 90km (chapter 4). The final stages of magmatism also record between 0-40% material input from asthenosphere-derived magmas. 3Ma thus marks the approximate time at which convective thinning of the mantle lithosphere was sufficient to allow upwelling of asthenosphere to depths of ≤100km (McKenzie & O'Nions, 1991).

The preceding discussion illustrates how the uplift and temporal evolution of magmatism within the central Sierra Nevada are consistent with a model which appeals to convective thinning of the mantle-lithosphere during the late Miocene and Pliocene. Simple convective thinning of the mantle lithosphere does not by itself explain the north-south spatial variation in both the degree of uplift and of lithospheric thinning observed in the Sierra Nevada. Evolution of the Sierra Nevada, because of its proximity to the western margin of the North American plate, has been influenced by the subduction of the Farallon plate throughout the Mesozoic and Cenozoic and, in the last 28Ma by the gradual northward migration in the cessation of subduction (Engebretson et al., 1985).

The low measured heatflows of the Sierra Nevada are testimony to shallow and rapid subduction of the Farallon plate between 80 and 40Ma that resulted in the Laramide Orogeny (Dumitru, 1990). At approximately 28Ma the Farallon spreading ridge and Mendocino Fracture Zone arrived at the subduction zone off the western margin of North America resulting in the cessation of subduction and the development of a transform margin (Engebretson et al.,1985). The northern terminus of the developing transform margin, the Mendocino Triple Junction (MTJ), migrated northward throughout the late Cenozoic to its present position at latitude 40°N. The cessation of subduction associated with the northward migration of the MTJ is critically important in understanding the spatial variation of uplift

and the magmatic history of the Sierra Nevada.

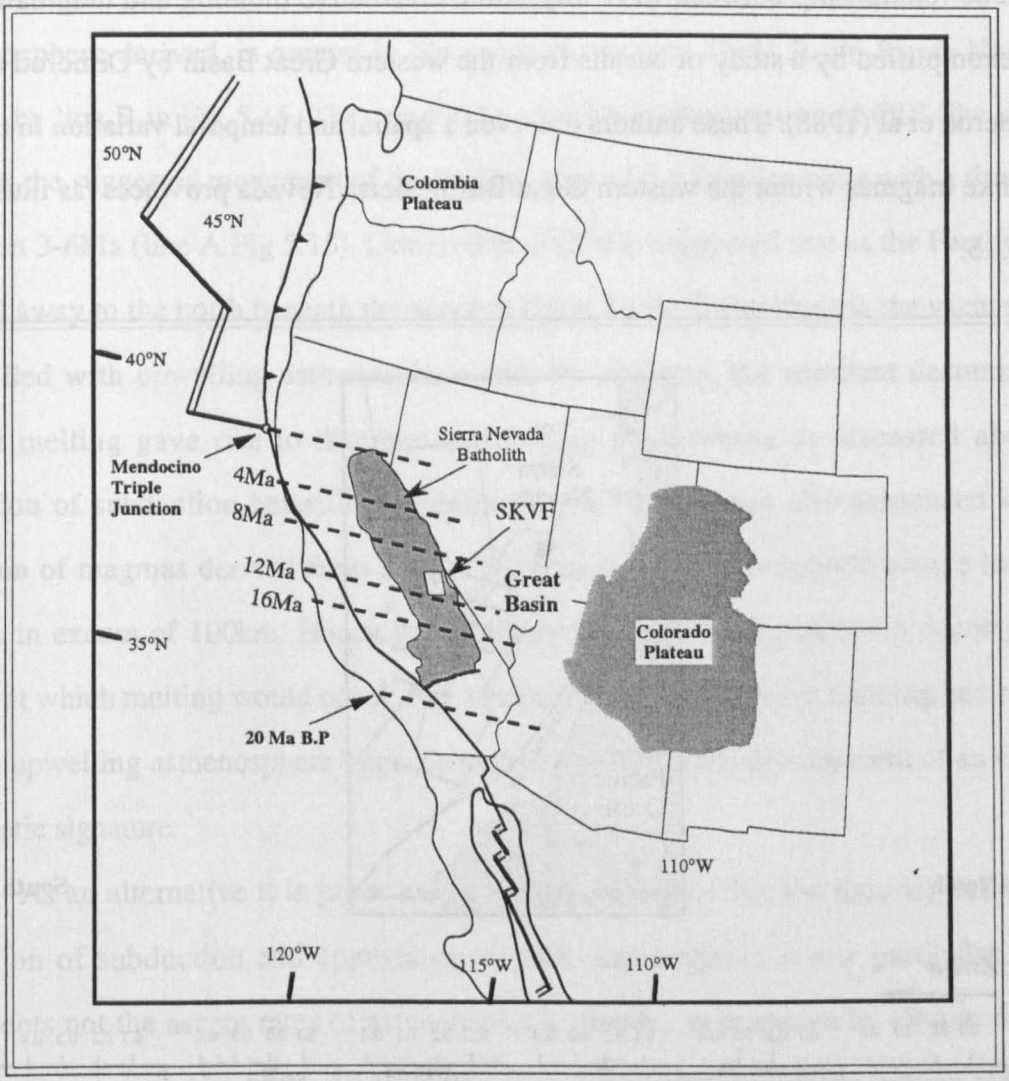


**Figure 5.14**. Northward migration of the Mendocino Triple Junction from 20Ma to the present in 4Ma intervals (Engebretson et al., 1985). Note that the MTJ passes north of the San Joaquin-Kings volcanic field (SKVF) at approximately 10-11Ma.

Crough & Thompson (1977) suggested that, after subduction at any given latitude ceased, the upwelling of asthenosphere would result in convective and thermal thinning of the lithosphere. Figure 5.14 shows how the MTJ has migrated over the range of latitudes covered by the Sierra Nevada over the last 20Ma (Engebretson et al.,1985). Consequently convective thinning of the mantle lithosphere should have been in operation beneath the southern Sierra Nevada for a longer period compared to the north and hence exhibit the highest elevations (Fig 5.13). Furthermore Fig 5.14 shows that the onset of thinning of the lithosphere beneath the San Joaquin-Kings volcanic field, estimated at 11.4Ma from the initiation of Miocene magmatism coincides with the inferred migration of the MTJ north of the SKVF at around 10-11Ma (Engebretson et al.,1985), suggesting that there is indeed a

link between migration of the MTJ, lithospheric thinning, uplift and magmatism.

The relationship between MTJ migration, convective thinning and magmatism is further exemplified by a study of basalts from the western Great Basin by Ormerod (1988) and Ormerod et al (1988). These authors observed a spatial and temporal variation in the age of OIB-like magmas within the western Great Basin-Sierra Nevada provinces as illustrated in Fig 5.15.

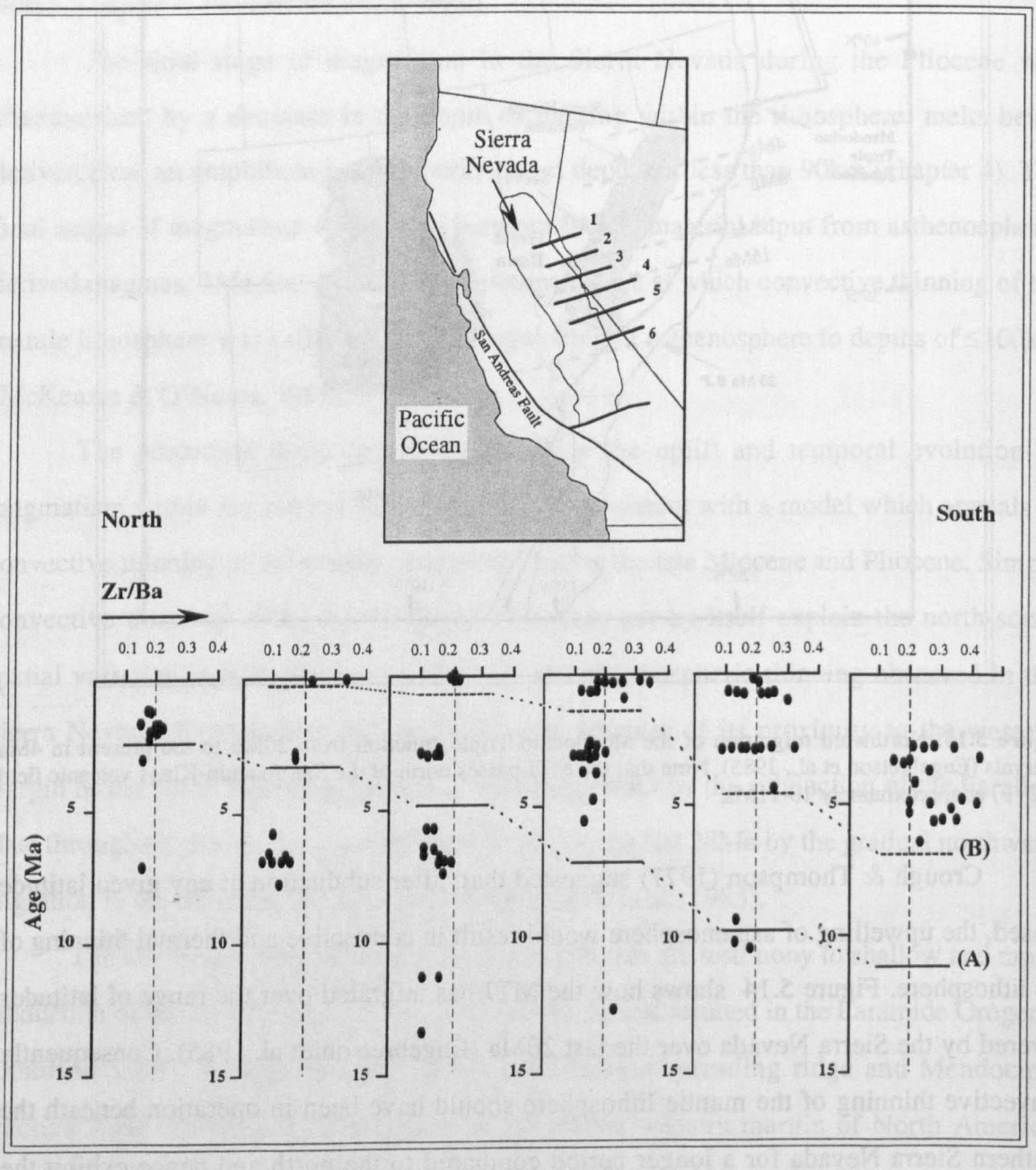


**Figure 5.15**. Temporal evolution of magmatism in the Western Great Basin (modified after Ormerod, 1988). Each section represents 30' latitude and contains all the data from late Cenozoic lavas within broad bands normal to the direction of Subduction as illustrated in insert map and numbered accordingly. Line (**A**) represents the projected time when the trailing edge of subducted lithosphere passes beneath each section approximates the northward migration of the MTJ (Engebretson et al., 1985). Line (**B**) marks the onset of magmatism dominated by an asthenospheric component as indicated by magmas with Zr/Ba>0.2 (Ormerod, 1988).

The maximum age of basaltic magmas with Zr/Ba>0.2, interpreted as being predominantly asthenosphere-derived, is greater in the southern western Great Basin-Sierra Nevada as shown by line B in Fig 5.15. The temporal and northward migration of OIB-like magmas follows the suggested movement of the trailing edge of the Farallon plate with a time-lag of between 3-6Ma (line A Fig 5.15). Ormerod et al (1988) suggested that as the Farallon plate moved away to the north beneath the western Great Basin-Sierra Nevada the vacated space was filled with upwelling asthenosphere and, by inference the resultant decompression partial melting gave rise to discrete mantle diapirs. However as discussed above the cessation of subduction beneath the central Sierra Nevada was also associated with the eruption of magmas derived from a trace element enriched lithospheric source located at depths in excess of 100km. Hence it is unlikely that mantle diapirs could decompress to levels at which melting would occur. Not until sufficient lithospheric thinning had occurred would upwelling asthenosphere begin to melt and result in the development of an OIB-like magmatic signature.

As an alternative it is proposed in the present study that the time-lag between the cessation of subduction and appearance of OIB-like magmas at any particular latitude represents not the ascent rates of asthenospheric diapirs, as proposed by Ormerod (1988), but the time required to thin the lithosphere to approximately 100km where melting of anhydrous peridotite of normal Tp (1280°C) will begin (McKenzie & O'Nions, 1991). In the central Sierra Nevada the time lag between the onset of lithosphere dominated magmatism in the late Miocence, interpreted to reflect the onset of lithospheric thinning, and the first evidence for melt generation within the asthenosphere is approximately 7.5Ma. The initial late Miocene magmas are interpreted to be derived from lithosphere in excess of 90km and perhaps as great as 140km, the present thickness of the lithosphere beneath the northern Sierra Nevada. Assuming an initial lithosphere thickness of 140km the rate of lithospheric thinning beneath the central Sierra Nevada would be around $\approx 5 mma^{-1}$, reasonably close to the $2.5 mma^{-1}$ estimated for the Colorado Plateau. However if the lithosphere was initially only 120km, still consistent with the evidence from magmatism, the rate of thinning would be the same as that estimated for the Colorado Plateau.

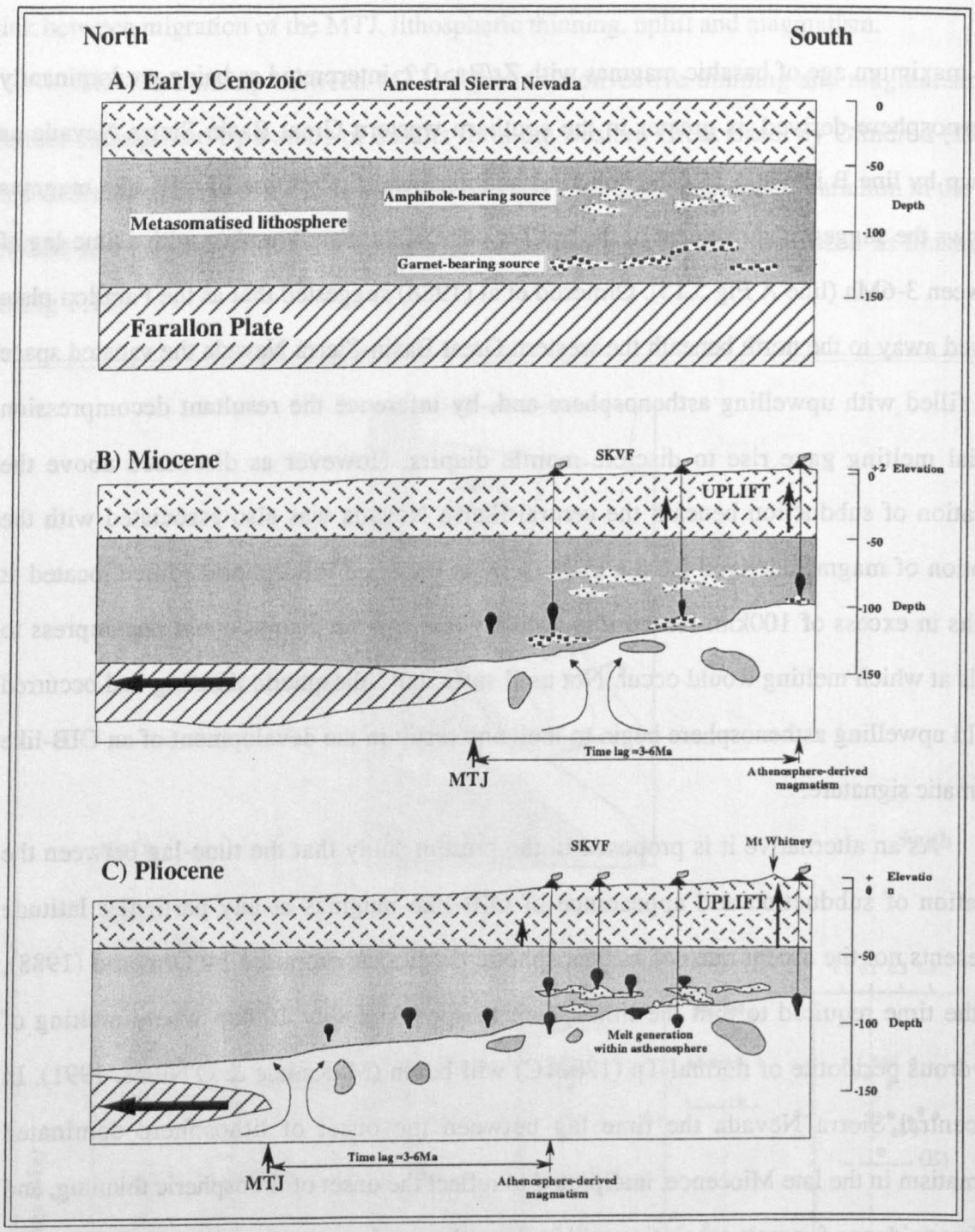


**Figure 5.16**. Tectonomagmatic evolution of the Sierra Nevada from the early Cenozoic to the Pliocene. In all the sections the Farallon plate follows a northward oblique trajectory into the plane of the diagram. During the early Cenozoic the Sierra Nevada was above the subducting Farallon plate resulting in the refrigeration of the lithosphere (Dumitru, 1990).

B) During the late Miocene, approximately 10-11Ma, the southern trailing edge of the Farallon plate, marked by the northward migration of the MTJ, passes beneath the San Joaquin-Kings volcanic field of the central Sierra Nevada. The subsequent upwelling of asthenosphere into the region vacated by the slab causes convective thinning of the lithosphere and hence uplift. The asthenosphere is initially unable to decompress to depths where melting will begin but causes melting of trace element enriched phlogopite-bearing garnet peridotite located in the lower lithosphere.

C) Continued thinning of the lithosphere during the Pliocene leads to further uplift and melting of enriched amphibole-bearing lithosphere at progressively shallower levels. Adiabatic decompression of asthenosphere to ≤100Km results in melting and the eruption of asthenosphere-lithosphere hybrid shoshonites.

Uplift is greatest in the southern Sierra Nevada as lithospheric thinning is initiated earlier than to the north which remains above the Farallon plate and is hence shielded from the asthenosphere. The time lag between the passage of the MTJ and the first asthenosphere contaminated basalts is 3-6Ma and represents the

time required for thinning of the lithosphere from 140 to ≤100km.

Figure 5.16 summarises the late Cenozoic, post Laramide, evolution of the Sierra Nevada illustrating the role of the Farallon plate and changing tectonic regime in controlling the onset of convective thinning of the lithosphere and hence the spatial and temporal variations in uplift and magmatism.

## 5.6: Summary and Conclusions:

The temporal evolution of magmatism on the Colorado Plateau and in the central Sierra Nevada, from initial magmas with strong lithospheric mantle signatures to late magmas with increasingly asthenospheric mantle characteristics is similar to that observed in basalts from the Basin & Range (Bradshaw, 1991; Bradshaw et al.,1993; Fitton et al., 1991). In the Basin & Range these compositional variations have been used to show magmatism was initiated by lithospheric extension (Hawkesworth, submitted). However in the central Colorado Plateau and Sierra Nevada there is no evidence for pre-, syn- or post-magmatic extension and therefore the cause of magmatism cannot be the same as in the Basin & Range. Although magmatism within the Colorado Plateau and Sierra Nevada is associated with late Cenozoic uplift there is no evidence to support a model for plume-related uplift and magmatism of the southwestern United States (Fitton et al., 1991).

A recent model for the mechanics of continental extension in western North America (Harry et al., 1993) attributes the late Cenozoic increase in elevation of the Colorado Plateau and Sierra Nevada, marginal highlands of the Great Basin, to flank uplift associated with extensional collapse of a pre-Great Basin plateau. The model results shown in Figure 5.17, suggest that uplift of the marginal highlands would follow extension and subsidence of the Great Basin within several million years. Two implications of this model, if correct, are that uplift of the Colorado Plateau and Sierra Nevada should be essentially coeval and post date the onset of extension at any particular latitude. However section 5.2.1 argued that the onset of uplift of the Colorado Plateau occurred at ≈28-30Ma which ***predates*** the onset of rapid and large magnitude extension in the Great Basin, at the latitude 36-37°N, by 12-15Ma (Gans et al.,1989). Furthermore section 5.4.1 illustrated that the main phase of uplift of the Sierra Nevada was restricted to the last 10Ma, some 20Ma after the onset of uplift of the

Colorado Plateau. The spatial variations in elevation of the Sierra Nevada suggest that Cenozoic uplift was governed more by subduction and changing tectonics than extensional collapse of the Basin & Range. These observations are inconsistent with uplift of the Colorado Plateau and Sierra Nevada associated with extensional collapse of a pre-Great Basin plateau as proposed by Harry et al. (1993). Furthermore this model does not predict or explain the observed relationship between uplift and magmtism within the 'peripheral highlands' of the Colorado Plateau and Sierra Nevada.

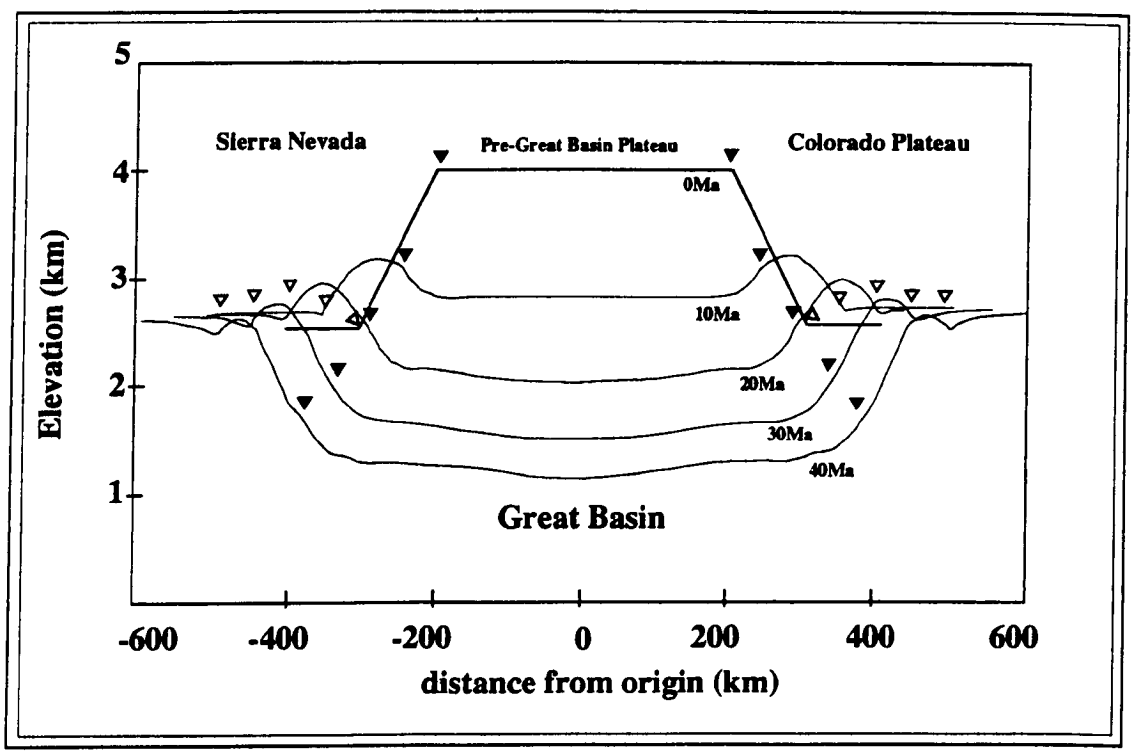


**Figure 5.17.** Finite element model illustrating the temporal evolution of topography between 0-40Ma after extensional collapse of an early Tertiary proto-Great Basin plateau (Harry & Sawyer, 1993). Initial crustal structure consists of a 40km thick quartz-diorite crust overlying a dunitic mantle. A 400km wide plateau with a 50km thick crust in the centre is bounded by 100km wide regions of transitional crust. Constant velocity and temperature boundary conditions apply at the sides and surfaces of the model which floats on an inviscid asthenosphere. Solid triangles indicate the elements which initially bound the thick crust of the continetal Plateau. Open triangles indicate the elements which initially separate normal crust from the transitional crust bounding the plateau.

The Colorado Plateau and Sierra Nevada become topographically elevated with respect to the Great Basin within 10Ma after the onset of extension.

It is suggested here that the cause of melt generation beneath the Colorado Plateau at approximately 28-30Ma was related to the convective removal of 50-60km of mantle lithosphere from the middle Oligocene to the present at a rate of perhaps 2.5mma$^{-1}$. Furthermore the onset and degree uplift of the plateau are entirely consistent with the model

of lithospheric thinning. Likewise magmatism and associated uplift of the Sierra Nevada can be related to a similar process involving convective thinning of the lithosphere. However in the latter case the spatial variations in both the degree of uplift and the composition of magmatism reflect the changing geometry of the subducting Farallon plate during the late Cenozoic and the gradual northward migration of the Mendocino Triple Junction.

The present study of magmatism and uplift of the Colorado Plateau and Sierra Nevada suggests an important role for convective thinning of the lithosphere in the tectonomagmatic evolution of the Western Cordillera. One further consequence of convective thinning of the lithosphere overlooked in this chapter, partly because it is not observed in either study area, is that uplift results in increased potential energy which could provide a driving force for extension, particularly if the compressive boundary forces are reduced. Although much of the Western Cordillera is undergoing extension, it is clear from Fig 5.1 that it is also characterised by anomalous elevations, suggesting that elevation may have been the driving force for the extension. The final chapter addresses the broader implications of convective thinning of lithospheric mantle in the evolution of magmatism and extension in the Basin & Range.

# Chapter 6

## Summary and Conclusions

### 6.1: Introduction:

Although much has already been published about mid to late Tertiary mafic magmatism in the southwestern United States, most of this work concerns volcanism associated with extension and addresses the relationship between magmatism and extension in the Basin & Range and/or Rio Grande Rift provinces. This project has taken an equally extreme approach and examined the compositional evolution of middle and late Cenozoic magmatism within the central Colorado Plateau and Sierra Nevada to address the cause of melt generation within *nonextensional* regions and asses the relationship of uplift and magmatism in the western United States. A model has been proposed whereby melt generation and concomitant uplift of the Colorado Plateau and Sierra Nevada resulted from convective thinning of lithosphere, previously thickened during the Laramide orogeny.

The aim of this chapter is to provide an initial summary of the temporal variation in composition of magmatism associated with convective thinning of the lithosphere beneath the Colorado Plateau and Sierra Nevada. The subsequent section examines the further tectonomagmatic consequences of convective thinning of the lithosphere, not observed within either the Colorado Plateau or Sierra Nevada provinces, but nevertheless extremely important, and integrates these into a general model for the evolution of magmatism and extension in the Basin & Range.

### 6.2: Magmatism within the central Colorado Plateu:

Initial magmatism on the Colorado Plateau, as represented by the Oligo-Miocene ultrapotassic diatremes of the Navajo region, was characterised by a wide range of LIL/HFS, $^{87}Sr/^{86}Sr$ and $^{143}Nd/^{144}Nd$ ratios, but with two compositionally distinct endmember magma-types as illustrated in Fig 6.1. Superficially the compositional range of the Navajo intrusives resembles the temporal variation in composition observed in basaltic volcanics from the surrounding extensional provinces, attributed to mixing of magmas derived from enriched lithospheric and depleted asthenospheric sources. The high

LRE/HRE, LIL/HFS and $^{87}Sr/^{86}Sr$ ratios of the minette endmember are consistent with a melt derived from a trace element enriched phlogopite and garnet-bearing lithospheric mantle source. However the Katungite endmember, which has trace element and isotope ratios similar to many asthensophere-derived magmas, also appears to be derived from a trace element enriched lithospheric source region within the garnet stability field. Therefore the preferred interpretation for the range of Navajo magmas involves melting of a compositionally and mineralogically heterogeneous lithospheric mantle. This explains why magmas covering the entire spectrum of compositions were erupted at the same time.

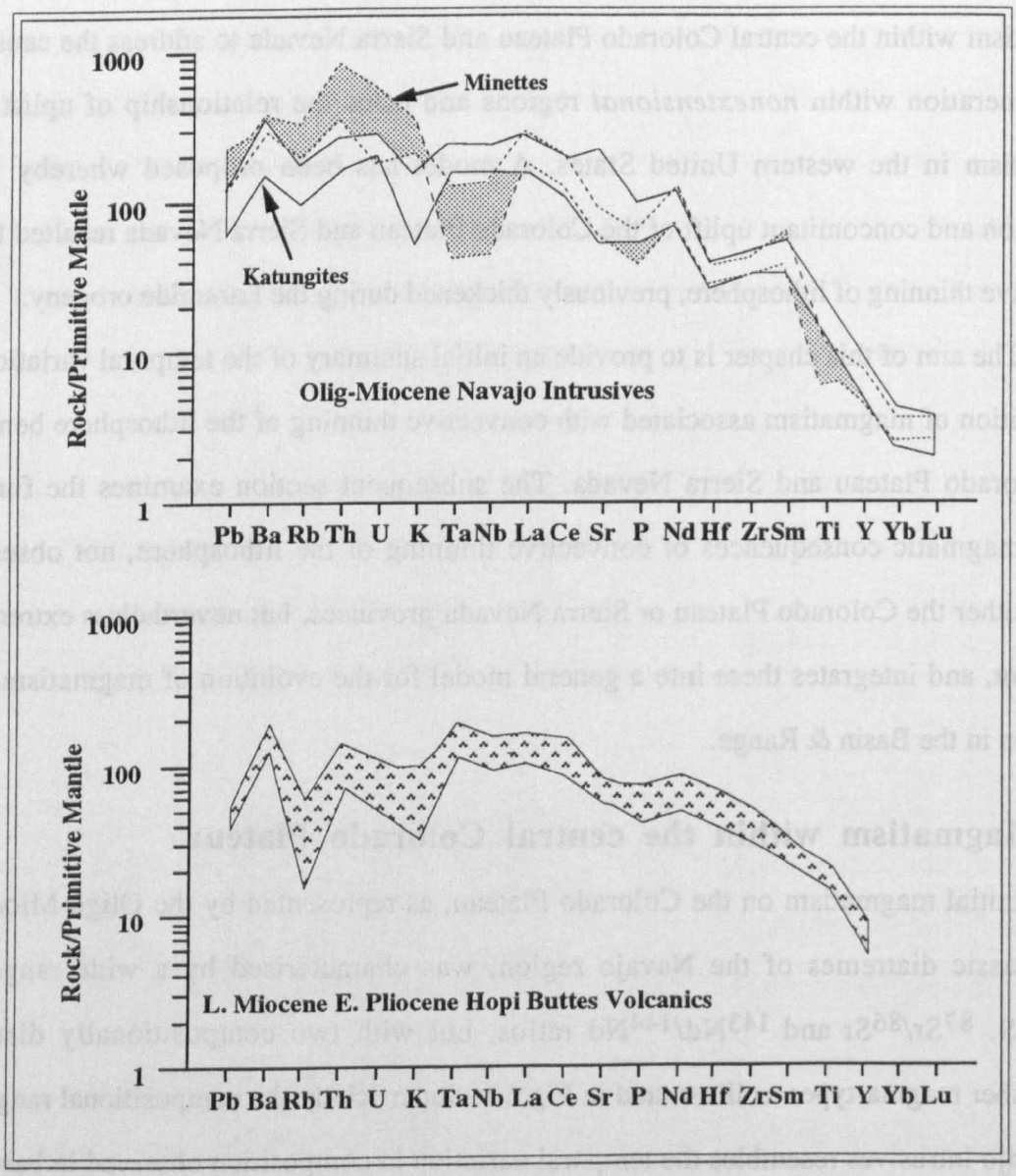


**Figure 6.1.** Trace element compositions of Oligo-Miocene ultrapotassic magmas of the navajo volcanic field and the late Miocene-early Pliocene sodic nephelinites of the Hopi Buttes volcanic field, central Colorado Plateau. Data for the Hopi Buttes from Alibert et al (1986).

From the late Miocene to the Pliocene a second period of magmatism, represented by the Hopi Buttes nephelinite diatremes, occurred within the central plateau and was characterised by low LIL/HFS and $^{87}Sr/^{86}Sr$ ratios, similar to asthenosphere-derived OIB-like magmas from other regions of the western United States (Fitton et al., 1991). However the $^{143}Nd/^{144}Nd$ of these magmas is significantly *lower* than typical post 5Ma asthenosphere-derived OIB-like magmas from the Basin & Range and Rio Grande provinces. Furthermore the major element abundances and $^{143}Nd/^{144}Nd$ ratios of the Hopi Buttes are intermediate between typical asthenosphere-derived OIB-like magmas and the Navajo katungite endmember. Thus the Hopi Butte nephelinites are interpreted as hybrid magmas produced by mixing of a lithosphere-derived katungite-like endmember and an OIB-like melt derived from the asthenospheric mantle.

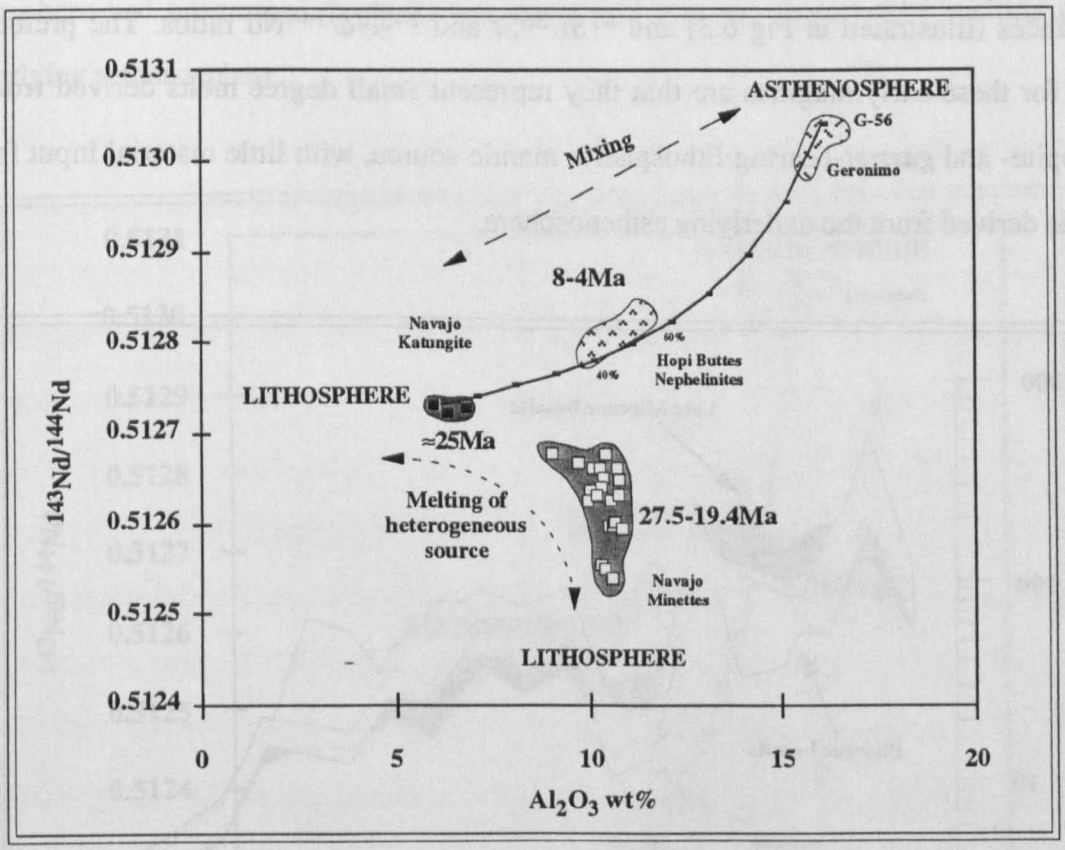


**Figure 6.2.** $^{143}Nd/^{144}Nd$ versus $Al_2O_3$ for magmas of the Navajo and Hopi Buttes volcanic, central Colorado Plateau, showing the temporal evolution of magmatism and the interaction between the katungite lithospheric endmember and asthenospheric component represented by G-65 (Kempton & Fitton, unpubl data).

The temporal evolution of magmatism on the Colorado Plateau and the interaction of the three endmembers throughout the late Cenozoic is summarised in Fig 6.2, a plot of $^{143}Nd/^{144}Nd$ versus $Al_2O_3$. This shows how the earliest magmatism on the Colorado

Plateau was dominated by melting entirely within enriched lithospheric mantle (in the presence of garnet) for approximately 8Ma. After approximately 10Ma of volcanic quiescence the final stages of magmatism record a contribution from asthenosphere-derived melts (associated with a decreased role for lithosphere-derived magmas). Whether the proportion of the asthenospheric endmember increases throughout the final period of magmatism cannot be assessed due to the lack of age determinations for the Hopi Buttes.

## 6.3: Magmatism within the central Sierra Nevada:

Two periods of magmatism occurred in the central Sierra Nevada during the late Cenozoic. The initial period of magmatism during the late Miocene was spatially restricted, volumetrically limited, and was characterised by a rather limited range of trace element abundances (illustrated in Fig 6.3) and $^{87}Sr/^{86}Sr$ and $^{143}Nd/^{144}Nd$ ratios. The preferred model for these early magmas are that they represent small degree melts derived from a phlogopite- and ***garnet***-bearing lithospheric mantle source, with little material input from magmas derived from the underlying asthenosphere.

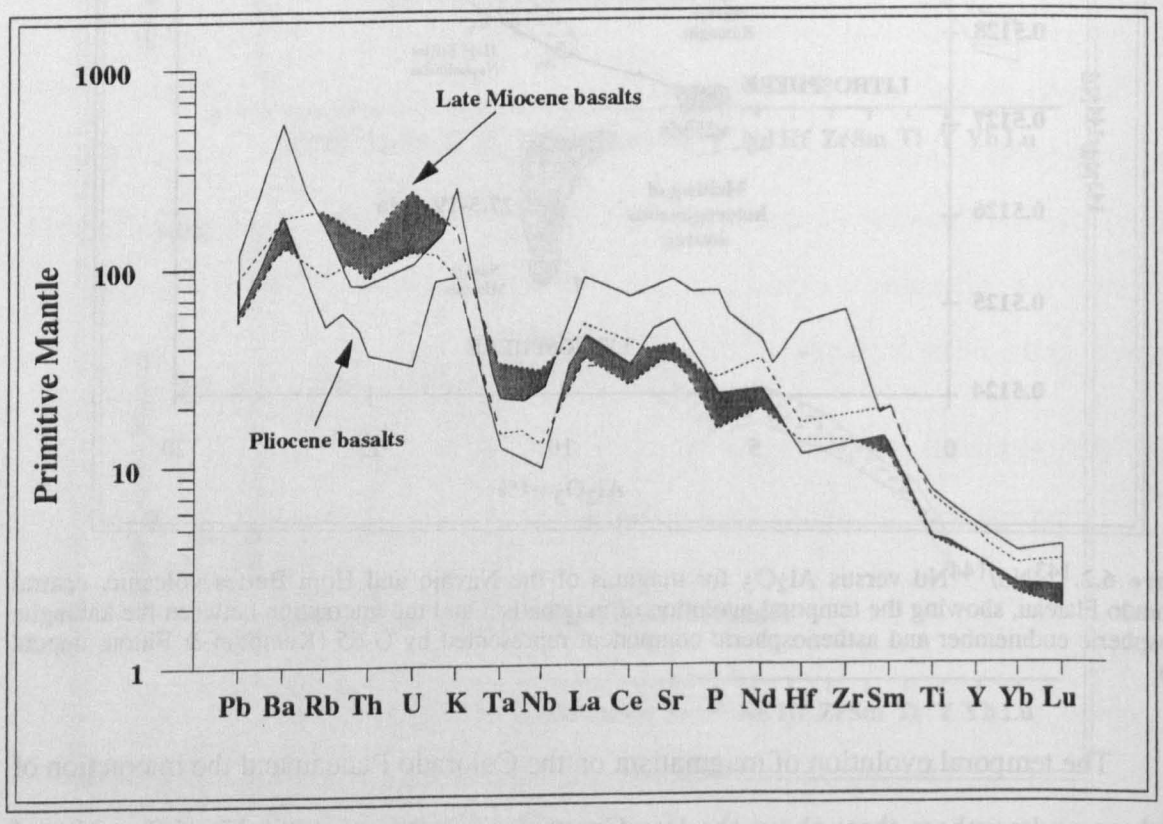


**Figure 6.3.** Trace element composition of the Late Miocene and Pliocene basalts from the San Joaquin-Kings volcanic field, central Sierra Nevada. Normalisation values from the Sun & McDonough (1989).

The second period of magmatism, during the Pliocene, was spatially more extensive and not restricted to the San Joaquin-Kings volcanic field. Compositionally these later magmas are more variable than the late Miocene magmatism (Fig 6.3) but typically they have higher LIL/HFS and $^{87}Sr/^{86}Sr$ ratios. The compositional variation of the Pliocene basalts is interpreted as a result of mixing of small degree melts derived from a trace element enriched, amphibole- and ***garnet***-bearing, lithospheric source with up to 40% of an asthensophere-derived component.

Figure 6.4 summarises the evolution of Cenozoic magmatism within the central Sierra Nevada and shows the interaction of lithospheric and asthenospheric magmas. The earliest phase of magmatism was dominated by melt generation within a deep lithospheric mantle source whereas in the final short period of magmatism, melt generation within the lithosphere had progressed to shallower levels and was accompanied by melting of the underlying asthenosphere.

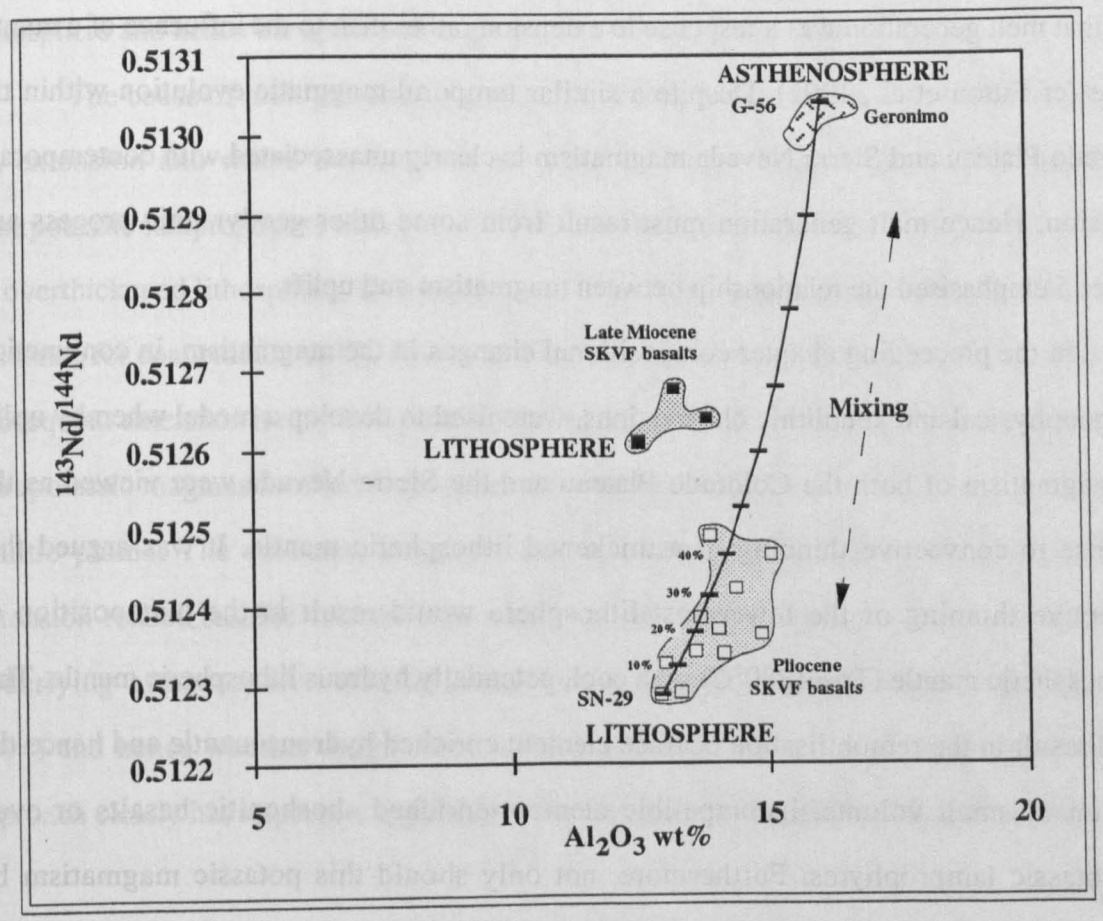


**Figure 6.4.** $^{143}Nd/^{144}Nd$ versus $Al_2O_3$ for basalts from the San Joaquin-Kings volcanic field, central Sierra nevada, illustrating the temporal evolution of magmatism and the interaction of the Pliocene lithospheric endmember with the asthenospheric endmember G-56 (Kempton & Fitton, unpubl data).

## 6.4: A model for uplift-related magmatism:

The temporal evolution of magmatism within the central Colorado Plateau and Sierra Nevada share a number of similarities. In both regions the earliest phase of magmatism was clearly dominated by melting of a trace element-enriched lithospheric mantle source, while later magmatism, also dominated by an enriched lithospheric mantle signature, has a noticeable asthenospheric contribution. Associated with this shift from predominantly lithospheric to more asthensopheric characteristics is a decrease in the depth of melt generation within the lithosphere, most clearly observed in the Sierran basalts initially derived from a phlogopite-bearing source and subsequently an amphibole-bearing source.

A similar lithosphere to asthenosphere transition associated with a progressive decrease in the depth of melt generation within the lithosphere has been inferred for the Colorado River Trough magmatism (Bradshaw, 1991; Bradshaw et al., 1993; Daley & DePaolo, 1992). Within this region magmatism is clearly related to major crustal extension and Hawkesworth & Gallagher (1994) use the temporal variation in magma composition to infer that melt generation was a response to extension rather than to the influence of a mantle plume (cf Fitton et al., 1991). Despite a similar temporal magmatic evolution within the Colorado Plateau and Sierra Nevada magmatism is clearly unassociated with contemporary extension. Hence melt generation must result from some other geodynamic process and chapter 5 emphasised the relationship between magmatism and uplift.

In the preceeding chapter compositional changes in the magmatism, in conjunction with geophysical and xenolithic observations, were used to develop a model whereby uplift and magmatism of both the Colorado Plateau and the Sierra Nevada were viewed as the response to convective thinning of a thickened lithospheric mantle. It was argued that convective thinning of the lowermost lithosphere would result in the juxtaposition of asthenospheric mantle (Tp ≈1280°C) with cool, potentially hydrous lithospheric mantle. This would result in the remobilisation of trace element enriched hydrous mantle and hence the eruption of small volume, incompatible element-enriched shoshonitic basalts or even ultrapotassic lamprophyres. Furthermore, not only should this potassic magmatism be spatially and temporally related to uplift but, as the process of convective thinning only occurrs in regions of overthickened lithosphere, magmatism may be expected to show REE

fractionations consistent with melt generation with the deeper ***garnet*** stability field rather than the spinel field. If magmatism within a particular area continued for a long enough period then a temporal transition toward more asthenospheric compositions may be observed as the lithosphere is gradually thinned to the extent where asthensophere intersects its solidus and begins to melt. Highly trace element enriched potassic magmas with REE fractionations consistent with melt generation in the garnet stability field and which are related to uplift are not restricted to only the western United States. Turner et al. (1993) use just such magmas on the Tibetan Plateau not only to date uplift of the plateau but also to invoke convective removal of mantle lithosphere as the cause of melt generation.

Similar compositional variations however may be expected in magmatism associated with a mantle plume impinging on the base of a thickened lithosphere. However although uplift resulting from a plume may be rapid, the magmatic response would be delayed as the lithosphere is characterised by a low thermal coductivity. In the case of convective thinning of the lithosphere, asthenosphere is rapidly juxtaposed against cool posibly enriched lithosphere and hence the uplift and magmatic response should be concomitant.

The cause of melt generation in regions where magmatism occurs without, or prior to, extension and where the magmas are small volume potassic shoshonitic basalts or ultrapotassic lamprophyres with garnet REE signatures, may be due to convective thinning of overthickened lithosphere. This interpretation is clearly strengthened where there is direct evidence for concomitant uplift. However even if evidence for uplift has been overprinted by subsequent extension it may still possible to identify regions where small volume potassic to ultrapotassic magmas resulted from convective thinning of lithospheric mantle rather than a mantle plume. The volumes, eruption rates and temporal variations in composition of extension-related basaltic volcanism provide constraints on the potential temperatures of the underlying asthensopheric mantle (Bradshaw et al., 1993; Hawkesworth & Gallagher, 1994) and hence whether magmatism is related to the presence of a mantle plume. This approach clearly has important applications for the Basin & Range extensional province.

## 6.5: Convective thinning of the lithosphere: A tectonomagmatic model for the Basin & Range:

The Colorado Plateau and Sierra Nevada comprise only part of the Western Cordillera, all of which experienced uplift during the late Cenozoic (Oldow et al., 1989). This section summarises the evolution of magmatism and extension in the Basin & Range and discusses the evidence for the role of post-Laramide convective thinning of the lithosphere as the driving force for Cordilleran-wide Cenozoic uplift, magmatism and extension.

The temporal and spatial evolution of extension and magmatism within the Great Basin-Basin & Range remains controversial (Best & Christiansen, 1991; Gans et al.,1989; Armstrong & Ward, 1991) although extension appears to have developed in two main phases, beginning in the late Eocene-early Oligocene (Best & Chrsitiansen, 1991; Harry & Sawyer, 1993). Mid-Tertiary extension, contemporaneous with subduction of the Farallon plate, occurred randomly throughout the Great Basin and southern Basin & Range and was characterised by major low angle detachment faults that exhumed midcrustal lithologies forming metamorphic core complexes (Armstrong & Ward, 1991). This initial period of extension was accompanied by voluminous silicic volcanism and pyroclastic activity (Gans et al., 1989; Armstrong & Ward, 1991). In contrast the late-Tertiary was marked by a change in the mode of extension from one of core complex to wide rift extension (Buck, 1991), and was associated with a transition to bimodal volcanism within the Basin & Range (Gans et al., 1989; Wernicke et al.,1987; Harry & Sawyer, 1993). In the northern Basin & Range the onset of Cenozoic extension and magmatism migrated southward (Armstrong, 1970; Best & Christiansen, 1991; Lipman et al., 1972) and was mirrored by a northward migration in the southern Basin & Range as shown in Fig 6.5 (Gans et al.,1989; Glazner & Bartley, 1984). These spatial and temporal patterns are somewhat complicated by the additional outward migration of extension and magmatism from the interior of the Basin & Range towards the peripheral highlands of the Colorado Plateau and the Sierra Nevada (Best & Brimhall, 1974; Eaton, 1980; Gans et al.,1989; Saltus & Lachenbruch, 1991; Tanaka et al., 1986).

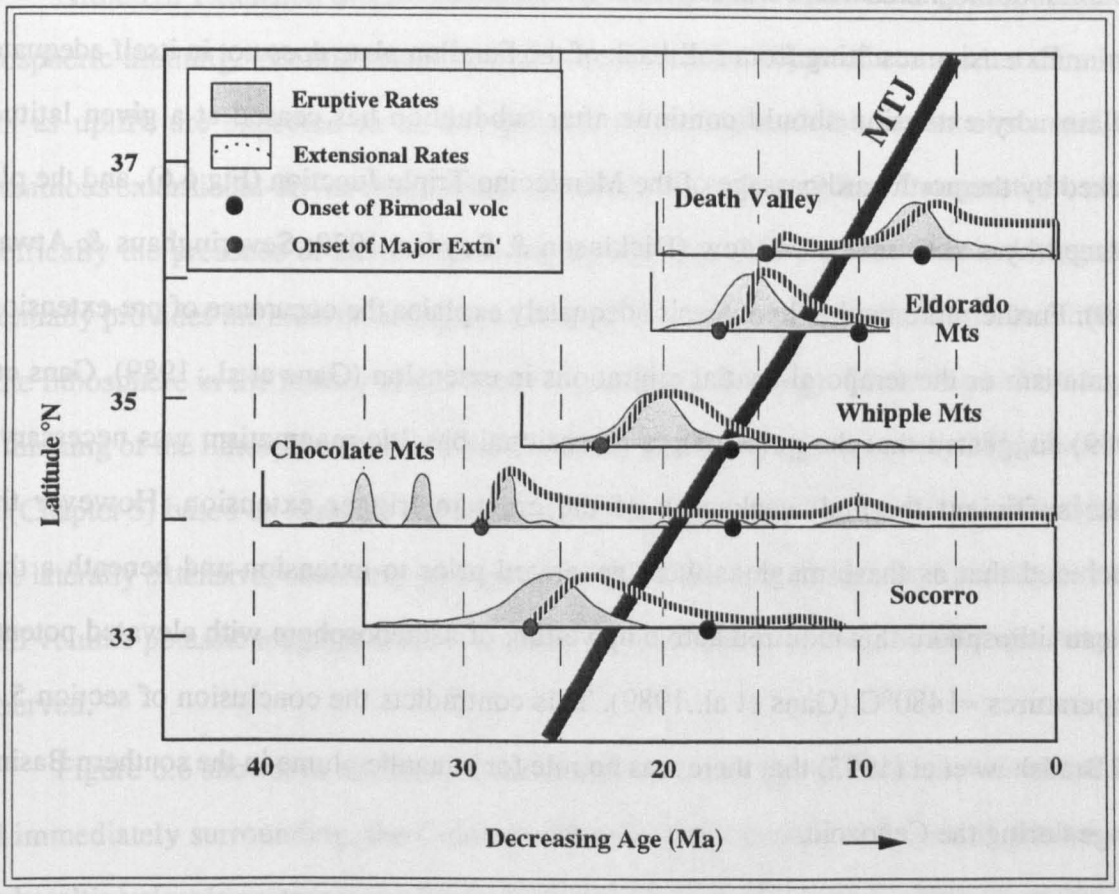


**Figure 6.5.** Eruptive rates (shaded) and extensional strain rates (vertical ruled lines) from selected regions of the southern Basin & Range, plotted as function of age and latitude. Curves are highly generalised and vertical axes for each region are probably logarithmic, maximum straun rates and eruptive rates are approximately $10^{-14}s^{-1}$ and $1000km^3Ma^{-1}$. Grey circles mark the onset of rapid large magnitude extension; black circles represent the approximate onset of basaltic or bimodal volcanism. Position of the MTJ as a function of age from Engebretson et al (1985). Taken from Gans et al (1989).

Two main hypotheses have been advanced to explain the cause or driving force for mid-late Cenozoic extension and magmatism in the Great Basin-Basin & Range provinces. One model attributes tectonics and magmatism to plate interactions along the west coast of North America involving the reduction in the rate of convergence between North American and the Farallon plates and hence roll-back of the Farallon plate and the development of a back-arc extensional regime (Coney & Reynolds, 1977; Coney, 1979; Best & Christiansen, 1991). The alternative model invokes thermal relaxation and gravitational spreading of crust thickened during the Laramide orogeny as the driving force for extension and hence magmatism (Glazner & Bartley, 1985; Wernicke et al.,1987; Molnar & Chen, 1983; Harry & Sawyer, 1993). Although these processes are not mutually exclusive and it is probable

that they both had role in extension, neither adequately explain certain aspects of the evolution of magmatism and extension within the Basin & Range.

Extension resulting from roll-back of the Farallon plate does not in itself adequately explain why extension should continue after subduction has ceased at a given latitude, marked by the northward passage of the Mendocino Triple Junction (Fig 6.6), and the plate replaced by a slab absent window (Dickinson & Snyder, 1979; Severinghaus & Atwater 1989). Furthermore neither hypothesis adequately explains the occurence of pre-extensional magmatism or the temporal-spatial migrations in extension (Gans et al., 1989). Gans et al (1989) suggested that the pulse of pre-extensional basaltic magmatism was necessary to cause sufficient thermal weakening of the crust to trigger extension. However they concluded that as these magmas were generated prior to extension and beneath a thick plateau lithosphere this required active upwelling of asthenosphere with elevated potential temperatures ≈1480°C (Gans et al.,1989). This contradicts the conclusion of section 5.4.1 and Bradshaw et al (1993) that there was no role for a mantle plume in the southern Basin & Range during the Cenozoic.

One consequence of the convective removal of lithosphere not observed in either the Colorado Plateau or Sierra Nevada, and hence not discussed in chapter 5, is the increased potential for extensional collapse of the orogen (England & Houseman, 1988; Sandiford & Powell, 1990; Zhou & Sandiford, 1992). Uplift associated with the removal of dense mantle lithosphere results in gains in gravitational potential energy producing outward-directed bouyancy forces. Tensile stresses arising from the increased gravitational potential of an uplifted plateau may exceed convergent driving forces and lead to extensional collapse of an orogen despite ongoing convergence. This is the case for the Tibetan Plateau (Houseman et al 1981; England & Houseman, 1988; Turner et al.,1993). However if the extensional forces do not exceed the convergent forces then the orogen will not necessarily collapse but is ***primed*** for later extensional collapse consequent upon a reduction in the convergent forces. Lithospheric thickening occurred throughout the Western Cordillera during the Laramide orogeny (70-40Ma) as a response to both a shallowing and an increase in the rate of subduction of the Farallon plate (Engbretson et al.,1985). This increased the potential for

convective removal of part of the thickened lithosphere.

Although extension within the Basin & Range may itself be a consequence of lithospheric thinning, tectonic criteria which would date the *onset* of convective thinning, such as uplift, are expected to be overprinted by extensional fabrics or obscurred by voluminous extensional-driven magmatism. However the earliest phase of magmatism, more specifically the presence of small degree highly incompatible element enriched magmas, potentially provides the most enduring evidence for the onset and role of convective thinning of the lithosphere in the history of the Great Basin-Basin & Range. There is good evidence for thinning of the lithosphere beneath the Colorado Plateau at approximately 28Ma±several Ma (Chapter 5) based on xenolith and seismic data (see section 5.4.1). If this event had been more laterally extensive, occurring perhaps beneath the Basin & Range, then pre-extensional small volume potassic magmas similar to those on the plateau, and of a similar age, may be preserved.

Figure 6.6 shows, in addition to the distribution and age of potassic volcanism on, and immediately surrounding, the Colorado Plateau, the locations and ages of potassium-rich basaltic volcanic centres in the Basin & Range. The age of potassic volcanism within the Basin & Range falls between 30 and 38Ma, similar to that observed on the Colorado Plateau. It is suggested that these pre-extensional potassic magmas resulted from melt generation in response to convective thinning of the lithosphere between 38 to 30Ma and the juxtaposition of asthenosphere of normal Tp≈1280°C against cooler, volatile-enriched, lithospheric mantle as proposed for the small volume potassic melts of the Navajo volcanic field (Fig 5.10).

With convective thinning of the lithospheric mantle, uplift of the Basin & Range would be expected to be coeval with the phase of Eocene-Oligocene potassic magmatism yet Unruh (1991), and references therein, date uplift as late-Miocene-early Pliocene. However drainage and ash-flow directions indicate that prior to approximately 26-24Ma (section 5.2.1) the Basin & Range was elevated with respect to the Colorado Plateau, despite magmatism suggesting that uplift of the latter was underway by 28-30Ma (Elston & Young, 1991; Hendricks & Plescia, 1991; Sherrod & Tosdal, 1991).

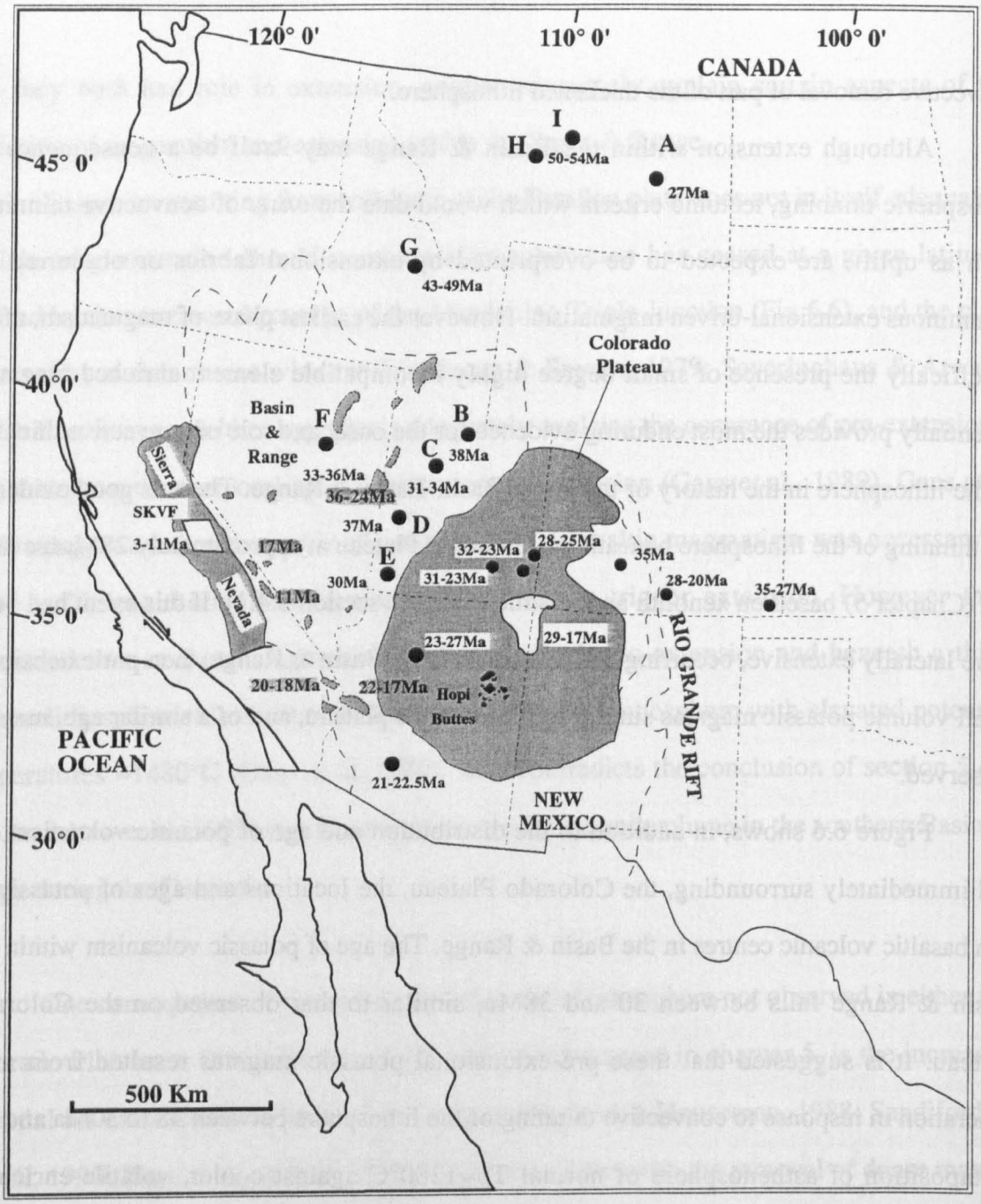


**Figure 6.6.** Spatial and temporal distribution of potassic mafic volcanism in the western United States (adapted from Rowell & Edgar, 1983). Radiometric ages from Lipman (1972), Barker (1974), Keith (1978) and references cited below for each locality. A, Smokey Butte (Mitchell et al., 1987); B, Moon Canyon (Best et al.,1968); C, Black Hills (Sharwood, 1911; Noble, 1948); D, Little Drum Mtns (Leedom, 1974); E, Marysville (Callaghan, 1939, Best et al.,1980); F, Eureka (Blake et al.,1975); G, Challis volcanic field (Seims & Jones, 1977); H & I, Highwood and Bearpaw Mtns (Marvin et al.,1980). References for potassic volcanism on, and immediately surrounding, the Colorado Plateau as for Fig 5.5. Dark shaded regions within the Basin & Range which are outlined by a dashed line represent metamorphic core complexes. Approximate ages of core complex formation (Armstrong & Ward, 1991; and references therein) are shown without white backgrounds.

Such a scenario necessitates some form of uplift of the Basin & Range prior to and concomitant with the Colorado Plateau during the late Eocene-early Oligocene. The young inferred uplift ages of around 10-5Ma (Unruh, 1991) most likely reflect later uplift associated with the Rocky Mtns event (Fig 5.2) not the initial Basin & Range uplift event. The greater age of potassic magmatism in the Basin & Range compared to the Colorado

Plateau would be consistent with uplift of the Basin & Range prior to that of the Colorado Plateau.

It is suggested that the presence of small volume potassium-rich magmas within the Basin & Range province, the general onset of basaltic magmatism prior to extension (Fig 6.5) and the excess elevation (see Fig 5.2) resulted from the convective thinning of the lithosphere during the late Eocene-early Oligocene, prior to and concomitant with the Colorado Plateau thinning event.

The model suggested here, and summarised in Fig 6.7, integrates convective thinning of the lithosphere with previous models which invoke an important role for plate tectonics and the configuration of the North American transform/subduction margin and the models for extension proposed by Harry & Sawyer (1993) and Buck (1991). The pulse of melt generation within the mantle prior to extension was a direct consequence of convectively thinning a gravitationally unstable thickened lithosphere beneath the pre-extensional plateau during the Oligocene (see above). Lithospheric thinning also resulted in an increase in the isostatically supported elevation and hence the horizontal buoyancy force (Sandiford & Powell, 1989) which, combined with the thermal weakening of the crust caused by ponding of basaltic magmas compounded the likelihood of gravitational collapse of the plateau region. Two factors facilitated the eventual collapse of the plateau. First, at approximately 40Ma, a reduction in the rate of convergence from 150mm/a to 40mm/a and hence compressive boundary forces, between the Farallon and North American plates (Engebretson et al.,1985). Secondly at about 28Ma subduction ceased and was replaced by a transform margin resulting in a reduction of the compressive boundary forces yet further. The initial decrease in compressive boundary forces in the Eocene was probably sufficient to allow spatially limited synsubduction, core-complex, extension. The random occurrence of regions of core complex extension in the late Eocene-early Oligocene (Fig 6.6) may simply be attributable to variations in the crustal thickness and thermal structure of the pre-extensional plateau and the degree to which the lithosphere was thinned in any particular region. In order to allow the rapid lower crustal flow necessary for core complex formation moho and lower crustal temperatures must be high and it is suggested that this would be consistent with a *thin lithosphere* (Buck, 1991). However as the lithosphere was thickened

during the Laramide orogeny the onset of core complex extension would thus require an earlier phase of convective thinning of the lithosphere. If the eruption of potassic volcanics mark the onset of convective thinning of the lithosphere, as argued above, then core complex development should post-date such magmas in any particular region. Although there are core complexes that predate potassic magmatism within the Basin & Range, such as the Wood Hills complex at ≈56-47Ma, Fig 6.6 shows that several for which dates are available just post-date the phase of potassic volcanism. Furthermore in the southern Basin & Range where the age of potassic volcanism, at 27-21 Ma, is slightly younger than the 30-38Ma of the central and northern regions the apprximate timming of core complex extension also appears to mirror this decrease in age (Armstrong & Ward, 1991). During this initial phase of extension exhumation of high temperature middle-lower crustal lithologies could also result in sufficient decompression melting of lower crustal lithologies to generate the observed coeval and extensive silicic volcanism (Buck, 1991). As extension proceeds, crustal thinning leads to enhanced heat loss through conduction and the rate of increase in the temperature of the mantle lithosphere decelerates. Decreasing lithosphere temperatures prevent rapid lower crustal flow and wide rift extension thereafter replaces core complex extension as is observed throughout the Basin & Range (Buck, 1991; Harry & Sawyer, 1993).

The cessation of subduction, and hence decrease in compressive boundary forces, migrated northward with the MTJ during the middle to late Cenozoic. This decrease in compressive boundary forces resulted in further extensional collapse of the proto-Basin & Range plateau and was associated with major, extensional driven, magmatism (Fig 6.5; Gans et al.,1989; Glazner & Bartley, 1984). Furthermore as the cessation of subduction migrated northward so did the onset of extension and bimodal volcanism in the southern Basin & Range (Gans et al., 1989; Glazner & Bartley, 1985). Crustal extension gradually reduced the elevation and hence the gravitational potential, resulting in a decrease in strain rates and the formation of the relatively stable present crustal thickness of 25-35Km (Gans et al.,1989; Harry & Sawyer, 1993).

Meanwhile the thick insulative crust of the Colorado Plateau and Sierra Nevada allowed Moho temperatures to rise as the geothermal gradient reequilabrated to a thinner

lithosphere, further weakening the crust in the peripheral regions and allowing ductile flow of the lower crust. Therefore extension and the locus of magmatism gradually migrated outward from the Basin & Range into the weakened crust of the peripheral highlands. This is observed in the elevated heatflows of the transition zones between the Colorado Plateau and Sierra Nevada with the Basin & Range (Bodell & Chapman, 1982; Saltus & Lachenbruch , 1991), and reflected in the great volumes of late-Cenozoic lithosphere-derived magmatism restricted to the peripheries of the Great Basin-Basin & Range (Luedke & Smith, 1984; Fitton et al.,1991) and the migration of magmatism into the Colorado Plateau (Tanaka et al., 1986).

The last magmatic event within the extensional provinces was the eruption of small volumes of OIB-like magmas throughout the Basin & Range since approximately 5Ma. A recent model presented in Bradshaw et al (1993) suggests that melting within lithosphere, overlying asthenosphere with a Tp≈1280°C, will cease altogether if if is less than 60km and, if ß≥1.5 melting of asthenosphere will dominate. Hence the dominance of OIB-like asthenosphere-derived melts erupted after 5Ma may reflect extensional-driven thinning of the lithosphere to less than 60km and perhaps as low as 35-50km.

The model presented above can explain the evolution and migration of extension in the southern Basin & Range but does not account for the north to south migration of extension in the northern Basin & Range. This may indicate that the crust was weaker in the northern Basin & Range and once the compressive boundary forces were reduced at the end of the Laramide orogeny it was less able to support the high elevations resulting from convective removal of the lower mantle lithosphere. It may also be possible that the Yellowstone plume had a role in thermally weaking the crust in this region of the Basin & Range. An earlier phase of convective thinning of the lithosphere north of the Basin & Range may also account for the north-south migration in extension. Indeed small volume ultrapotassic magmas are found just to the north of the Basin & Range in central Idaho (Fig 6.6) at 43-49Ma (Siems & Jones, 1977) predate the main phase of Basin & Range potassic volcamism. Potassic volcamism of the Bearpaw and Highwood Mtns of Montana is even older at 50-54 and 45-53Ma respectively (Marvin et al., 1980). In the context of the model presented in section 6.4. this magmatism may reflect melt generation resulting from the convective thinning of the underlying lithosphere.

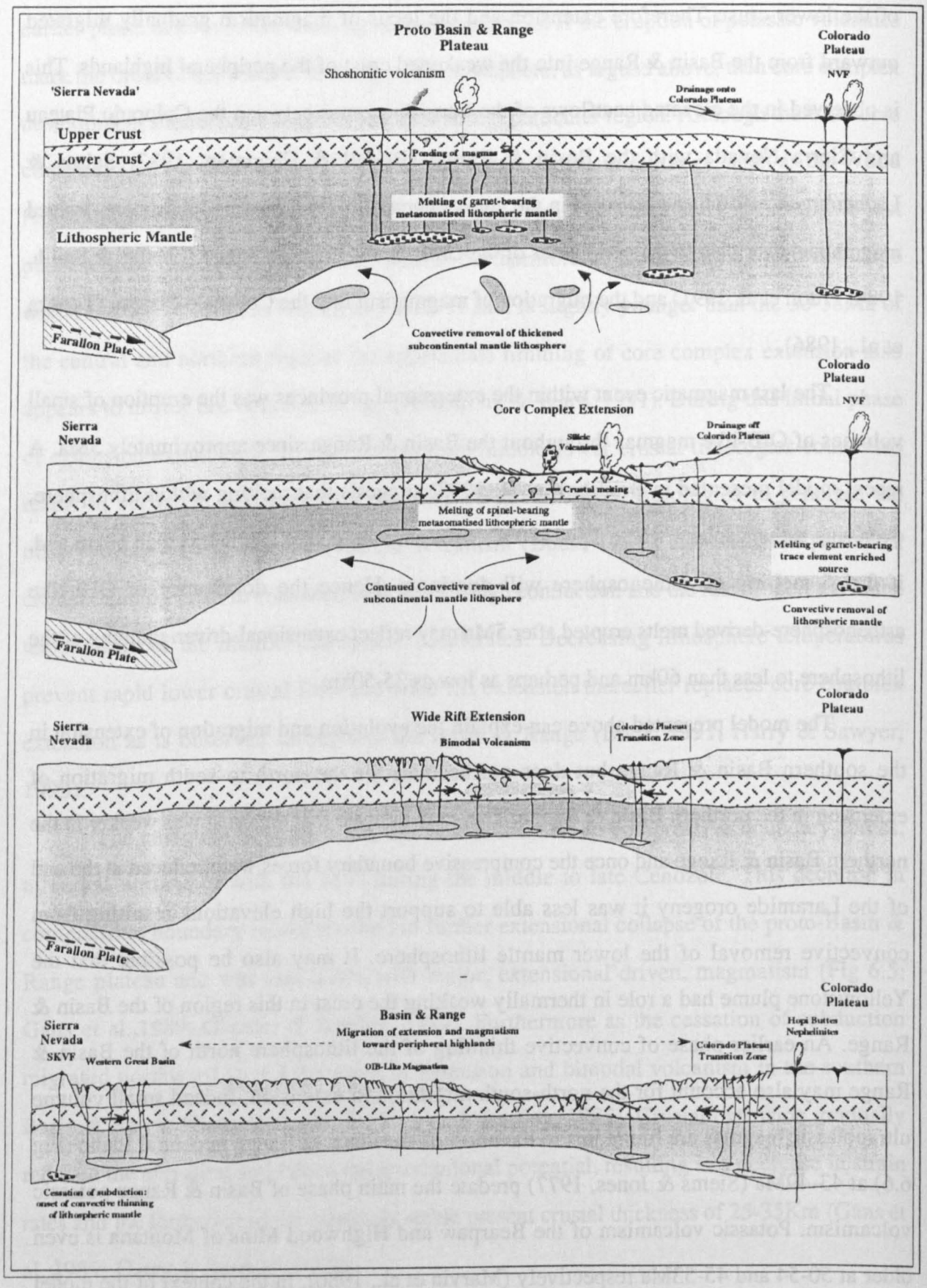


**Fig 6.7.** Late Eocene-Recent evolution of the western United States showing the role of convective thinning of the lithospheric mantle in the western Cordillera during the late Eocene. Descriptions for each stage in the evolution are on the adjacent page.

## Stage 1 (Late Eocene-Early Oligocene):

Rapid convective thinning of the lithosphere beneath the proto Basin & Range ca. 38-30Ma leads to uplift of a plateau region. Resultant melting of metasomatised enclaves within the **garnet** stability field of the lithosphere yields ***small volume*** trace element-enriched lamprophyric and/or potassic shoshonitic basaltic magmas which may pond within the lower crust or occasionally erupt. Thermal weaking of the lower crust in response to the ponding of magmas, in conjunction with the increased gravitational potential of the plateau, compound the likelihood for later extensional collapse. Uplift of the Basin & Range plateau outpaces uplift of the 'Colorado Plateau' during this stage and hence drainage of the latter is internal.

## Stage 2 (Late Oligocene-Early Miocene):

Horizontal bouancy forces of the plateau exceed the compressional boundary forces following a decrease in the rate of convergence between the Farallon and North American plates allowing the initiation of exensional collapse of the plateau. High temperatures within the lower crust resulting from the ponding of magmas and thermal reequilibration after initial lithosphere thinning allow ductile flow of the lower crust and the development of core complex extension. Associated with this phase of extension is the eruption of large volumes of silicic volcanism (the 'Ignimbrite Flareup') due to adiabatic decompression melting of the lower crust. Convective thinning of the lithosphere beneath the Colorado Plateau ca.28-30Ma results in uplift and the eruption of small volume lamprophyric magmas. Concomitant uplift of the Colorado Plateau and collapse and of the Basin & Range is reflected by a reversal of drainage direction across the boundary.

## Stage 3 (Middle Miocene):

Crustal thinning within the central Basin & Range enhances conductive heat loss and the rate of increase in temperature within the upper mantle-lower crust decelerates. Ductile flow of the lower crust can therefore no longer keep pace with the strain rates and wide rift extension soon replaces the earlier period of core complex extension. Silicic volcanism also wanes, as the lower crustal temperatures gradually decrease, and is replaced by bimodal volcanism. Basaltic volcanism is derived from spinel-bearing trace element enriched enclaves suggesting the continued thinning of the lithosphere associated with extension.

## Stage 4 (Late Miocene-Recent):

Continued extension and crustal thinning strengthen the crust of the Basin & Range. Meanwhile the thick crust of the peripheral Sierra Nevada and Colorado Plateau prevent conductive cooling and the upper mantle-lower crust within these regions weaken relative to the Basin & Range. Extension and magmatism migrate outward to the weaker peripheral highlands represented by the transition zone of the Colorado Plateau and western Great Basin adjacent to the Sierra Nevada. Crustal thinning within the transition zones stabilize mantle temperatures and extension continues to encroach on the 'stable' highlands. OIB-Like magmas are erupted within the central Basin & Range as melting no longer occurs within the thin mantle lithosphere beneath this region. The eruption of the Hopi Buttes nephelinites ca.8-4Ma, interpreted as asthenospheric magmas contaminated with lithosphere, suggest that the lithosphere beneath the Colorado Plateau has been thinned to approximately 100km. Cessation of subduction off western North America and the gradual removal of the Farallon plate beneath the Sierra Nevada between 16 and 8Ma leads to uplift and magmatism as a result of convective thinning of lithosphere.

One feature immediately apparent in this model is that the Colorado Plateau and Sierra Nevada have not behaved in a similar manner to the Basin & Range which has undergone massive extensional collapse. The Sierra Nevada experienced major uplift within the last 10Ma as a result of convective thinning of the lithosphere and this is probably too short a period for major extensional collapse to begin, although it is clear that extension has now begun in some regions (Jones & Dollar, 1986). Convective thinning of the lithosphere and uplift of the Colorado Plateau is inferred to have occurred 30Ma ago and yet has experienced negligible subsequent extension. The high lower-crustal Pn velocities and high proportion of mafic xenoliths collected from the laccoliths of southern Utah (Nelson et al, 1992) suggest that the crust of the Colorado Plateau is probably mafic. As mafic rocks have high strengths relative to quartz-rich lithologies it suggested that the Laramide crustal shortening was accommodated in the surrounding terranes rather than the Colorado Plateau. It is also suggested that extension resulting from the convective thinning of the lithosphere was concentrated in those regions were major contractional shortening had provided numerous crustal weaknesses. Hence the Colorado Plateau because of its rheological properties remained an elevated plateau-region while surrounding provinces underwent extensional collapse.

## 6.6: Concluding Remarks:

The principle conclusion of this thesis is that the evolution from lithosphere- to asthenosphere-dominated magmatism within the central Colorado Plateau and Sierra Nevada was associated with concomitant uplift and resulted from the convective thinning of mantle lithosphere thickened during the Laramide Orogeny. Convective thinning of the lithosphere beneath the Colorado Plateau occurred at approximately 30Ma, based on the age of magmatism, whereas in the case of the Sierra Nevada the presence of the shallow Farallon plate beneath the lithosphere during the middle to late Cenozoic delayed this process until the trailing edge of the plate migrated northward with the MTJ. This occurred at approximately 12Ma at the latitude of the San Joaquin-Kings volcanic field.

The excess elevation of the Basin & Range, given its present crustal thickness, and the presence of pre-extensional potassic magmas are consistent with convective thinning of

the lithosphere beneath a much larger region of the Western Cordillera during the Oligocene. Uplift resulting from the convective thinning of lithosphere beneath the Basin & Range provided the driving force for later extension while the geometry of the plate margin off California had an important controlling influence on the temporal and spatial evolution of extension and related magmatism in the southern Basin & Range.

Magmatism provides some of the most enduring evidence for convective thinning of the lithosphere (Kay & Kay, 1993) and the model presented in chapter 5 and above would be greatly improved with more detailed and integrated geochemical and geochronological studies on the potassic basalts from the Basin & Range and peripheral regions.

# References


Alibert, C., Michard, A. & Albarede, F. (1986). Isotope and trace element geochemistry of Colorado Plateau volcanics, *Geochim. et Cosmochim. Acta,* **50**, 2735-2750.

Allegre, C.J. & Minster, J.F. (1978). Quantitative models of trace element behaviour in magmatic processes, *EPSL*, **38**, 1-25.

Armstrong, R.L. & Ward, P. (1991). Evolving Geographic Patterns of Cenozoic Magmatism in the North American Cordillera: The Temporal and Spatial Association of Magmatism and Metamorphic Core Complexes, *J. Geophys. Res.*, **96**, No B8, 13,201-13,224.

Armstrong, R.L. (1969). K-Ar dating of laccolithic centres of the Colorado Plateau and vicinity, *Geol. Soc. Am. Bull.,* **80**, 2081-2086.

Armstrong, R.L. (1970). Geochronology of Tertiary igneous rocks, eastern Basin and Range province, western Utah, eastern Nevada, and vicinity, U.S.A., *Geochim. Cosmochim. Acta*, **34**, 203-232.

Armstrong, R.L. (1974). Magmatism, orogenic timing and orogenic diachronism in the Cordillera from Mexico to Canada, *Nature*, **247**, 348-351.

Axelrod, D.I. (1980). Contributions to the Neogene paleobotany of central California, *University of California Publications in Geological Sciences*, **121**, 212.

Bacon, C.R. & Duffield, W.A. (1980). Late Cenozoic rhyolites from the Kern Plateau, southern Sierra Nevada, California: *American Journal of Science*

Bacon, C.R. (1990). Calk-alkaline, shoshonitic, and primitive tholeiitic lavas from monogenetic volcanoes near Crater Lake, Oregon, *J. Petrol.,* **31,** 135-166.

Bartow, J.A. (1984). Geologic map and cross sections of the southeastern margin of the San Joaquin Valley, California, *U. S. Geol. Surv. Misc. Invest. Ser. Map, I-1496*, 2 sheets.

Bateman, P.C. & Eaton, J.P. (1967). Sierra Nevada batholith, *Science*, **158**, 1407-1417.

Beghoul, W.S. & Barazangi, M. (1989). Mapping high Pn velocity beneath the Colorado Plateau constrains uplift models, *J. Geophys. Res.*, **94**, 7083-7104.

Bennett, V.C. & DePaolo, D.J. (1987). Proterozoic crustal history of the western United States as determined by neodymium isotopic mapping, *Geol. Soc. Am. Bull.*, **99**, 674-685.

Benz, H.M., Smith, R.B. & Mooney, W.D. (1990). Crustal structure of the northwestern Basin and Range province from the 1986 Program for Array Seismic Studies of the Continental Lithosphere seismic experiment, *J. Geophys. Res.*, **95**, 21,823-21,842.

Best, M.G. & Brimhall, W.H. (1974). Late Cenozoic alkalic basalt magmas in the Western Colorado Plateaus and the Basin and Range Transition Zone, USA, and their bearing on mantle dynamics, *Geol. Soc. Am. Bull.*, **85**, 1667-1690.

Best, M.G. & Christiansen, E.H. (1991). Limited Extension During Peak Tertiary Volcanism, Great Basin of Nevada and Utah, *J. Geophys. Res.*, **96**, B8, 13,509-13,528.

Best, M.G., Henage, L.F. & Adams, J.A.S. (1968). Mica peridotite, wyomingite, and associated potassic igneous rocks in northeastern Utah, *Am. Mineral*, **53**, 1041-1048.

Best, M.G., McKie, E.H. & Damon, P.E. (1980). Space, time, composition patterns of Late Cenozoic mafic volcanism, southwestern Utah and ajoining areas, *Am. Journ. Sci.*, **280**, 1035-1050.

Bird, P. (1979). Continental delamination and the Colorado Plateau *J. Geophys. Res.*, **84** 7561-7571.

Bird, P. (1984). Laramide crustal thickening event in the Rocky Mountains foreland and Great Plains *Tectonics* , **3** 741-758.

Bird, P. (1988). Formation of the Rocky Mountains, western United States: a continuum computer model, *Science*, **239**, 1501-1507.

Blake, M.C., McKie, E.H., Marrion, R.F., Sillerman, M.L. & Nolan, T.B. (1975). The Arizona volcanic crater at Eureka, Nevada, *Journ. Res. U.S. Geol. Survey*, **3**, 605-612.

Bodell, J.M. & Chapman, J.M. (1982). Heat flow in the north-central Colorado Plateau, *J. Geophys. Res.*, **87**, 2869-2884.

Bradshaw, T.K. (1991). Tectonics and Magmatism in the Basin and Range Province of the Western United States.

Bradshaw, T.K., Hawkesworth, C.J. & Gallagher, K. (1993). Basaltic volcanism in the Southern Basin and Range: no role for a mantle plume, *EPSL*, **116**, 45-62.

Brey, G. & Green, D.H. (1975). The Role of $CO_2$ in the Genesis of Olivine Melilitite, *Contrib. Mineral. Petrol.*, **49**, 93-103.

Brey, G. & Green, D.H. (1977). Systematic Study of Liquidus Phase Relations in Olivine Melilitite + $H_2O$ + $CO_2$ at High Pressures and Petrogenesis of an Olivine Melilitite Magma, *Contrib. Mineral. Petrol.*, **61**, 141-162.

Brooks, P.K., Dodge, F.C.W. & Kistiler, R.W. (1980). Inclusions from late cenozoic volcanic rocks, Sierra Nevada batholith and adjacent areas, California, *Geol. Soc. Amer. Abstracts with Programs*, **12**, 99.

Bruce, R,M., Nelson, E.P. & Weaver, S.G. (1989). Effects of synchronous uplift and intrusion during magmatic arc construction, *Tectonophysics*, **161**, 317-329.

Buck, W.R. (1991). Modes of Continental Lithospheric Extension, *J. Geophys. Res.*, **96**, B12, 20,161-20,178.

Callaghan, E. (1939). Volcanic sequence in the Marysville region in southwest-central Utah, *Trans. Am. Geophys. Un. 24th Ann. Mtg*, 243-249.

Catchings, R.D. & Mooney, W.D. (1991). Basin and Range crustal and upper mantle structure, northwest to central Nevada, *J. Geophys. Res.*, **96**, 6247-6268.

Chapin, C.E. & Seager, W.R. (1975). Evolution of the Rio Grande rift in the Socorro and Las Cruces areas, *New Mexico Geol. Soc. Guidebook, 26th Field Conf*, 297-321.

Chapman,D., Pollack, H.N. (1977). Regional geotherms and lithospheric thickness, *Nature.*,**5**, 265-268.

Chase, C.G. & Wallace, T.C. (1986). Uplift of the Sierra Nevada of California, *Geology*, **14**, 730-733.

Christensen, M.N. (1966). Late Cenozoic crustal movements in the Sierra Nevada of California, *Geol. Soc. Am. Bull.*, **77**, 163-182.

Christiansen, R.L. & Lipman, P.W. (1972). Cenozoic volcanism and plate-tectonic evolution of the Western United States. II Late Cenozoic, *Phil. Trans. R. Soc. Lond.*, **A271**, 249-284.

Condie, K. (1982). A plate tectonics model for Proterozoic continental accretion in the southwestern United States, *Geology* , **10**, 37-42.

Condie, K.C. (1986). Geochemistry and tectonic setting of early Proterozoic supra-crustal rocks in the Southwestern United States, *J. Geol.*, **94**, 845-864.

Coney, P.J. & Reynolds, S.J. (1977). Cordilleran Benioff zones, *Nature*, **270**, 403-406.

Coney, P.J., Jones, D.L. & Monger, J.W.H. (1980). Cordilleran suspect terranes, *Nature*, **288**.

Cox, K.G., Duncan, A.R., Bristow, J.W., Taylor, S.R. & Erlank, A.J. (1984). Petrogenesis of the basic rocks of the Lebombo, *Spec. Publ. Geol. Soc. S.Africa*, **13**, 149-169.

Crough, S.T. & Thompson G.A. (1977). Upper mantle origin of Sierra Nevada uplift, *Geology*, **5**, 396-399.

Daley, E.E. & DePaolo, D.J. (1992). Isotopic evidence for lithospheric thinning during extension, southeastern Great Basin, *Geology*, **20**, 104.

Dalrymple, G.B. (1963). Potassium-Argon Dates of Some Cenozoic Volcanic Rocks of the Sierra Nevada, *Geol. Soc. Am. Bull.*, **74**, 379-390.

Dalrymple, G.B. (1964). Cenozoic chronology of the Sierra Nevada, California, *Univ. Calif. Publ. Geol. Sci.*, **47**, 41pp.

Davis, J. & Hawkesworth, C., Early calc alkaline magmatism in the Mogollon-Datil volcanic field, New Mexico, USA, Submitted to the Geol. Soc. Lond.

Davis, J. M. (1991). The geochemical evolution of basic and intermediate mid- to late Tertiary volcanism of the Mogollon-Datil volcanic field, southwestern New Mexico, USA, PhD *thesis. The Open University* 270.

Davis, J.M. (1991). The geochemical evolution of basis and intermediate mid- to late Tertiary volcanism from the Mogollon-Datil volcanic field, southwestern New Mexico, USA, *Dept of Earth Sciences, The Open University, Milton Keynes.*

Dickinson, W.R. & Snyder, W.S. (1978). Plate tectonics of the Laramide orogeny, *Geol. Soc. Am. Mem.*, **151**, 370pp.

Dickinson, W.R. & Synder, W.S. (1978). Geometry of subducted slabs related to San Andreas transform, *J. Geol.*, **87**, 609-628.

Dickinson, W.R. (1977). in Paleozoic Paleogeography of the Western United States (eds Stewart, J.H., Stevens, C.H. & Fritsche, A.E.) *Pacific Coast Paleogeography Symp* No 1.

Dickinson, W.R. (1981). Plate tectonics and the continental margin. In The *geotectonic development of California (Rubey Volume I)* (ed. W.G. Ernst), pp. 1-28. Prentice Hall, Inc., New Jersey.

Dickinson, W.R., Klute, M.A., Hayes, M.J., Janecke, S.U., Lundin, E.R., McKittrick, M.A. & Olivares, M.D. (1988). Paleogeographic and paleotectonic setting of Laramide sedimentary basins in the central Rocky Mountain region, *Geol. Soc. Am. Bull*, **100**, 1023-1039.

Dickinson, W.R., Klute, M.A., Hayes, M.J., Janecke, S.U., Lundin, E.R., McKittrick, M.A. & Olivares, M.D. (1988). Paleogeographic and paleotectonic setting of Laramide sedimentary basins in the central Rocky Mountain region, *Geol. Soc. Am. Bull.*, **100**, 1023-1039.

Dodge, F.C.W. & Bateman, P.C. (1988). Nature and origin of the root of the Sierra Nevada, *Am. J. Sci .*, **288A**, 341-357.

Dodge, F.C.W. & Moore, J.G. (1981). Part I., Late Cenozoic volcanic rocks of the southern Sierra Nevada, California: II. Geochemistry: Summary, *Geol. Soc. Am. Bull.*, **92**, 912-914.

Dodge, F.C.W. & Moore, J.G. (1981). Part II., Late Cenozoic volcanic rocks of the southern Sierra Nevada, California: II. Geochemistry, *Geol. Soc. Am. Bull.*, **92**, 1670-1761.

Dodge, F.C.W., Calk,L.C. & Kistler, R.W. (1986). Lower crustal xenoliths, Chinese Peak lava flow, central Sierra Nevada, *J. Petrol.*, **27**, Part 6, 1277-1304.

Domenick, M.A., Kistler, R.W., Dodge, F.C.W. & Tatsumoto, M. (1983). Nd and Sr isotopic study of crustal and mantle inclusions from the Sierra Nevada and implications for batholith petrogenesis, *Geol. Soc. Am. Bull.*, **94**, 713-719.

Dumitru, T.A. (1990). Subnormal Cenozoic Geothermal Gradients in the Extinct Sierra Nevada Magmatic Arc: Consequences of Laramide and Post-Laramide Shallow-Angle Subduction, *J. Geophys. Res.*, **95**, B4, 4925-4941.

Dumitru, T.A. (1990). Subnormal Cenozoic geothermal gradients in the extinct Sierra Nevada magmatic arc: Consequences of Laramide and post-Laramide shallow-angle subduction, *J. Geophys. Res*, **95**, No B4, 4925-4941.

Duncan, R.A. & Green, D.H. (1987). The genesis of refractory melts in the formation of oceanic crust, *Contrib. Mineral. Petrol.*, **96**, 326-342.

Eaton, G.P. (1980). Geophysical and geological characteristics of the crust of the Basin and Range province, in *Continental Tectonics, Stud. Geophys*, 96-113, U.S. National Academy of Sciences, Washington, D.C.

Eaton, G.P. (1986). A tectonic redefinition of the southern Rocky Mountains, *Tectonophysics*, **91**, 163-193.

Eaton, G.P. (1987). Topography and origin of the southern Rocky Mountains and Alverado ridge, in *Continental Extensional Tectonics*, Coward, M.P., Dewey, J.F. & Hancock, P.L. (eds.), Geol. Soc. Spec. Publ, **28**, 355-369.

Ehrenberg, S.N. (1977). The Washington Pass volcanic center: Evolution, and eruption of minette magmas of the Navajo volcanic field (abstract), in Extended Abstracts, 2nd International Kimberlite Conference, *2nd International Kimberlie Conference Santa Fe, New Mexico.*

Ehrenberg, S.N. (1978). Petrology of potassic volcanic rocks and ultramafic xenoliths from the Navajo volcanic field, New Mexico and Arizona, *Unpub. Ph.D. dissertation, Univ. California, Los Angeles.*

Ehrenberg, S.N. (1979). Garnetiferous ultramafic inclusions in minette from the Navajo volcanic field, in *The Mantle Sample: Inclusions in kimberlites and other volcanics*, edited by Boyd, F.R. & Meyer, H.O.A., 330-344.

Ehrenberg, S.N. (1982a). Petrogenesis of Garnet Lherzolite and Megacrystalline Nodules from the Thumb, Navajo Volcanic Field, *J. Petrol.*, **23**, Part 4, 507-547pp.

Ehrenberg, S.N. (1982b). Rare earth element geochemistry of garnet lherzolite and megacrystalline nodules from minette of the Colorado Plateau province *EPSL*, **57** 191-210.

Elston, D.P. & Young, R.A. (1991). Cretaceous-Eocene (Laramide) landscape development and Oligocene-Pliocene drainage reorganization of transition zone and Colorado Plateau, Arizona, *J. Geophys. Res.*, **96**, 12,389-12,406.

Elston, W.E. (1984b). Mid-Tertiary ash flow tuff cauldrons, southwestern New Mexico, *J. Geophys. Res.*, **89**, 8733-8757.

Engebretson, D.C., Cox, A, & Gordon, R.G. (1985). Relative motions between oceanic and continental plates in the Pacific basin, *Geol. Soc. Am. Spec Pap.*, **206**, 64pp.

England, P. & Houseman, G. (1988). The mechanics of the Tibetan Plateau, in Shackleton, R.M., Dewey, J.F. & Windley, B.F., eds, Tectonic evolution of the Himalayas and Tibet, *Royal Society of London Philosophical Transactions, Ser. A.*, **326**, 301-320.

England, P. & Molnar, P. (1990). Surface uplift, uplift of rocks, and exhumation of rocks, *Geology*, **18**, 1173-1177.

Epis, R.C. & Chapin, C.E. (1975). Geomorphic and tectonic implications of the post-Laramide, late Eocene erosion surface in the southern Rocky Mountains, in Cenozoic history of the Southern Rocky Mountains, *Geol. Soc. Am. Mem.*, **144**, 45-74.

Ericksen, M.C. & Slingerland, R. (1990). Numerical simulations of tidal and wind-driven circulation in the Cretaceous interior seaway of North America, *Geol. Soc. Am. Bull.*, **102**, 1499-1516.

Evernden, J.F., Savage, D.E. & Curtis, G.H. (1964). Potassium-argon dates and the Cenozoic mammalian chronology of North America, *Amer. J. Sci.*, **262**, 145-198.

Falloon, T.J. & Green, D.H. (1989). The solidus of carbonated, fertile peridotite, *EPSL* , **94**, 364-370.

Faure, G. (1986). Principals of isotope geology. 2nd edition *J Wiley & Sons Publishers*, **589**.

Finnerty, A.A. & Boyd, F.R. (1987). Thermobarometry for garnet peridotite xenoliths: A basis for mantle stratigraphy, in *Mantle Xenoliths*, edited by *P H Nixon*, pp 381-402, John Wiley, New York.

Fitton, J.G., James D. & Leeman W.P. (1991). Basic magmatism associated with late Cenozoic extension in the western United States: compositional variations in space and time *J. Geophys. Res.*

Fitton, J.G., James, D. & Leeman, W.P. (1991). Basic Magmatism Associated with Late Cenozoic Extension in the Western United States: Compositional Variations in Space and Time, *J. Geophys. Res.*, **96**, 13693-13711.

Fitton, J.G., James, D., Kempton, P.D., Ormerod, D.S. & Leeman, W.P. (1988). The role of lithospheric mantle in the generation of late Cenozoic basic magmas in the S.W. United States, "Oceanic and Continental Lithosphere: Similarities and Differences", *J Petrol.*, **29**, *Spec. Lithosphere Issue.*, (Eds M.A. Menzies & K.G. Cox ) 331-350.

Fraser, K.J. (1987). Petrogenesis of Kimberlites from South Africa and lamproites from Western Australia and North America, PhD *thesis. The Open University* 270.

Frey, F.A., Green, D.H. & Roy, S.D. (1978). Integrate models of basalt petrogenesis; A study of quartz tholeiites to olivine melilitites from south eastern Australia utilising geochemical and experimental petrological data, *J. Petrol.*, **19**, 463-513.

Gans, P.B., Mahood, G.A. & Schermer, E. (1989). Synextensional magmatism in the Basin and Range Province; a case study from the eastern Great Basin, *Geol. Soc. Am. Spec. Pap.*, **233**, 53.

Gibson, S.A., Thompson, R.N., Leat, P.T., Morrison, M.A., Hendry, G.L., Dickin, A.P. & Mitchell, J.G. (1993). Ultrapottassic magmas along the flanks of the oligo-miocene Rio Grande Rift, U.S.A.: Monitors of the zone of lithospheric mantle extension and thinning beneath a continental rift, *J. Petrol*, .....

Gill, J.B. (1991). Orogenic andesites and plate tectonics, Springer-Verlag, Berlin.

Glazner, A.F, Bartley, J.M. (1985). Evolution of lithospheric strength after thrusting. *Geology*, **13**, 42-45.

Glazner, A.F. & Bartley, J.M. (1984). Timing and tectonic setting of Tertiary low-angle normal faulting and associated magmatism in the southwestern United States, *Tectonics*, **3**, 385-396.

Green, D.H. (1973). Experimental melting studies on a model upper mantle composition at high pressure under water-saturated and water-undersaturated conditions, *EPSL*, **19**, 37-53.

Gregory, H.E. (1917). Geology of the Navajo country. A reconnaissance of parts of Arizona, New Mexico, and Utah, *U.S. Geol. Survey. Prof*, **93**, 161.

Hagen, E.S., Schuster, M.W., Furlong, K.P.(1985).Tectonic loading and subsidence of intermontane basins, Wyoming foreland province, *Geology*, **13**, 529-532.

Hamblin, W.K. (1984). Direction of absolute movement along the boundary faults of the Basin and Range-Colorado Plateau margin, *Geology*, **12**, 116-119.

Hamblin, W.K., Damon, P.E. & Bull, W.B. (1981). Estimates of vertical crustal strain rates along the western margins of the Colorado Plateau, *Geology*, **9**, 293-298.

Hansen, W.R. (1984). Post-Laramide tectonic history of the eastern Uinta Mountains, Utah, colorado, and Wyoming: *Mountain Geologist*, **21**, 5-29.

Hansen, W.R. (1985). Drainage development of the Green River basin in southwestern Wyoming and its bearing on fish biogeography , neotectonics, and paleoclimates: *Mountain Geologist*, **22**, 192-204.

Harry, D.L., Sawyer, D.S. & Leeman, W.P. (1993). The mechanics of continental extension in western North America: implications for the magmatic and structural evolution of the Great Basin, *EPSL*, **117**, 59-71.

Hart, S.R. & Davis, K.E. (1978). Nickel Partitioning between Olivine and Silicate Melt, *EPSL*, **40**, 203-219.

Hart, S.R. (1984). The DUPAL anomaly: a large-scale isotopic anomaly in the southern hemisphere, *Nature*, **309**, 753-6.

Hauser, E.C. & Lundy, J. (1989). Cocorp Deep Reflections: Moho at 50 KM (16 S) beneath the Colorado Plateau, *J. Geophys. Res.*, **94**, B6, 7071-7081.

Hawkesworth, C.J., Erlank, A.J., Kempton, P.D. & Waters, F.G. (1990). Mantle metasomatism: Isotope and trace-element trends in xenoliths from Kimberley, South Africa, *Chemical Geology*, **85**, 19-34.

Hawkesworth, C.J., Fraser, K.J., Rogers, N.W. (1985). Kimberlites and lamproites: Extreme products of mantle enrichment processes, *Trans. Soc. S. Afr.*, **88**, 439-447.

Hawkesworth, C.J., Kempton, P.D., Rogers, N.W., Ellam, R.M. & van Calsteren, P.W. (1990). Continental mantle lithosphere, and shallow level enrichment processes in the Earth's manle, *EPSL*, **96**, 256-268.

Hawkesworth, C.J., Rogers, N.W., van Calsteren, P. & Menzies, M. (1984). Mantle enrichment processes, *Nature*, **311**, 331-335.

Hawkesworth,.C.J., & Gallagher,.K.(1993). Mantle hotspots, plumes and regional tectonics as causes of intraplate magmatism, *Terra Nova* , **5**, 552-559.

Hay, E. A. (1976). Cenozoic uplifting of the Sierra Nevada in isostatic response to North American and Pacific plate interactions, *Geology*, **4**, 763-766.

Hay, E.A. (1976). Cenozoic uplifting of the Sierra Nevada in isostatic response to North American and Pacific plate interactions, *Geology*, **4**, 763-766.

Helmstaedt, H. & Doig, R. (1975). Eclogitic nodules from Kimberlite pipes of the Colorado Plateau: Samples of subducted Franciscan-type oceanic lithosphere, *Phys. Chem. Earth*, **9**, 95-111.

Helmstaedt, H.H. & Schulze, D.J. (1991). Early to mid-tertiary inverted metamorphic gradient under the Colorado Plateau: Evidence from ecclogite xenoliths in ultramafic microbreccias, Navajo volcanic field, *J. Geophys. Res.*, **96**, No B8, 13,225-13,235.

Hendricks, J.D. & Plescia, J.B. (1991). A review of the regional geophysics of the transition zone, *J. Geophys. Res.*, **96**, 12,351-12,374.

Holmes, A. (1937). The petrology of a katungite, *Geol. Mag.*,**74**, 200-219.

Houseman, G.A., McKenzie, D.P. & Molnar, P. (1981). Convective instability of a thickened boundary layer and its relevance for the thermal evolution of continental convergent belts. *J. Geophys. Res.*, **86**, 6135-6155.

Huber, N.K. (1981). Amount and timing of late Cenozoic uplift and tilt of the central Sierra Nevada, California-Evidence from the upper San Joaquin River basis, *US. Geol. Surv. Prof. Pap.*, **1197**, 28pp.

Huber, N.K. (1990). The late Cenozoic evolution of the Tuolumne river, central Sierra Nevada, California, *Geol. Soc. Am. Bull.*, **102**, 102-115.

Hunter, W.C. & Smith, D. (1981). Garnet Peridotite from Colorado Plateau Ultramafic Diatremes: Hydrates, Carbonates, and Comparative Geothermometry, *Mineral Petrol*, **76**, 312-320.

Izett, G.A. (1975). Late Cenozoic sedimentation and deformation in northern Colorado and adjacent areas, *Mem. Geol. Soc. Am.*, **144**, 179-209.

Jaques, A.L., Webb, A.W., Fanning, C.M., Black, L.P., Pidgeon, R.T., Ferguson, J., Smith, C.B. & Gregory, G.P. (1984). The age of the diamond-bearing pipes and associated leucite lamproites of the West Kimberley Region, Australia, Bur. Miner. Resour. Aust. Geol, *Geophys*, **9**, 1-7.

Jijun, L., Bingyuan, L., Fubao, W., Qingsong, Z., Shixuan, W. & Benxing, Z. (1981). The process of the uplift of the Qinghai-Xizang Plateau. In: *Geological and Ecological studies of Qinghai-Xizang Plateau*, **1**, 111-118, Beijing: Science Press.

Jones, C.H. (1987). Is Extension in Death Valley accommodated by thinning of the mantle lithosphere beneath the Sierra Nevada, California?, *Tectonics*, **6**, No 4, 449-473.

Jones, C.H. (1987). Is extension in Death Valley accomodated by thinning of the mantle lithosphere beneath the Sierra Nevada, California, *Tectonics,* **6,** 449-473.

Jones, L.M., Dollar, R.S. (1986). Evidence of Basin-and-Range extensional tectonics in the Sierra Nevada: The Durrwood Meadows swarm, Tulare County, California (1983-1984), *Bull. Seismol. Soc. Am.*, **76**, 439-461.

Kauffman, E.G. (1977). Geological and biological overview: Western Interior Cretaceous basin, *The Mountain Geologist*, **14**, 75-99.

Kay, R.W. & Mahlburg-Kay, S. (1993). Delamination and delamination magmatism, *Tectonophysics* , **219**, 177-189.

Keller, G.R., Braile, L.W. & Morgan, P. (1979). Crustal structure, geophysical models and contemporary tectonism of the Colorado Plateau, *Tectonophysics*, **61**, 131-147.

Kempton, P.D. Dungan, M.A. & Blancard, D.P. (1987). Petrology and geochemistry of xenolith-bearing alkalic basalts from the Geronimo Volcanic Field, southeast Arizona; Evidence for polybaric fractionation and implications for mantle heterogeneity, *Geol. Soc. Am. Spec. Pap.*, **215**, 347-370.

Kempton, P.D., Fitton, J.G., Hawkesworth, C.J. & Ormerod, D.S. (1991). Isotopic and trace element constraints on the composition and evolution of the lithosphere beneath the southwestern United States, *J. Geophys. Res.*, **96**, B8, 13,713-13,735.

Kempton, P.D., Harmon, R.S., Hawkesworth, C.J. & Moorbath, S. (1990). Petrology and geochemistry of lower crustal granulites from the Geronimo volcanic field, southeastern Arizona, *Geochim. et Cosmochim. Acta*, **54**, 3401-3426.

Kistler, R.W. & Peterman, Z.E. (1973). Variations in Sr, Rb, K, Na, and initial $^{87}Sr/^{86}Sr$ in Mesozoic granitic rocks and intruded wall rocks in Central California, *Bull. Geol. Soc. Am.*, **84**, 3489.

Kistler, R.W. & Peterman, Z.E. (1978). Reconstruction of crustal blocks of California on the basis of initial strontium isotopic compositions of Mesozoic grantic rocks, US *Geol. Surv. Prof. Pap.*, **1071**, 17pp.

Kushiro, I. (1975). On the nature of silicate melt and its significance in magma genesis: Regularities in the shift of the liquidus boundaries involving Olivine, Pyroxene and Silica Minerials, *American Journal of Science*, **275**, 411-431.

Langmuir, C.H., Vocke, Jr. R.D., Hanson, G.N. & Hart, S.R. (1978). A general mixing equation with applications to Icelandic basalts, *EPSL*, **37**, 380-392.

Larson, E.E., Ozima, M. & Bradley, W.C. (1975). Late Cenozoic volcanism in northwestern Colorado and its implications concerning tectonism and the origin of the Colorado River system, *Mem. Geol. Soc. Am.*, **144**, 155-178.

Laughlin, A.W., Aldrich Jr, M.J., Squafiqullah, M. & Husler, J. (1986). Tectonic implications of the age, composition, and orientation of lamprophyre dykes, Navajo volcanic field, Arizona, *EPSL.*, **76,** 361-374.

Laughlin, A.W., Aldrich, M.J. & Vaniman, D.T. (1983). Tectonic implications of mid-Tertiary dikes in west-central New Mexico, *Geology*, **11**, 45-48.

Le Bas, M.J., Le Maitre, R.W., Streckeisen, A. & Zanettin, B. (1986). A chemical classification of volcanic rocks based on the total alkali-silica diagram, *J. Petrol.*, **27**, 745-750.

Leat, P.T., Thompson, R.N., Dickin. A.P., Morrison, M.A. & Hendry, G.L. (1989). Quaternary volcanism in northwestern Colorado: Implications for the roles of asthenosphere and lithosphere in the genesis of continental basalts, *Journal of Volcanology and Geothermal Research*, **37**, 291-310.

Leat, P.T., Thompson, R.N., Morrison, M.A. Hendry, G.L. & Dickin, A.P. (1988). Compositionally diverse Miocene-Recent rift-related magmatism in NW Colorado: partial melting and mixing of mafic magmas from 3 different asthenospheric and lithosphereic mantle sources, in, *"Oceanic and Continental Lithosphere: Similarities and Differences"*, J. Petrol., 29, Spec. Lithosphere Issue, (eds M.A. Menzies & K. G. Cox) 351-378.

Leat, P.T., Thompson, R.N., Morrison, M.A., Hendry, G.L. & Dickin, A.P. (1990). Geochemistry of mafic lavas in the early Rio Grande Rift Yarmony Mountain, Colorado, USA, *Chem Geol* , **81**, 23-43.

Leat, P.T., Thompson, R.N., Morrison, M.A., Hendry, G.L. & Dickin, A.P. (1991). Alkaline hybrid mafic magmas of the Yampa area, NW Colorado, and their relationship to the Yellowstone mantle plume and lithospheric mantle domains, *Contrib. Mineral. Petrol.*, **107**, 310-327.

Leedom, S.H, (1974). Little Drum mountain, an early Tertiary shoshonitic volcanic center in Millard County, *Utah, Brigham Young Univ. Geology Studies*, **21**, 73-108.

Lindgren, W. & Loughlin, G.J. (1919). Geology and ore deposits of the Tintic mining district, Utah, *U.S. Geol. Surv. Prof. Paper*, **107**, 282.

Lindgren, W. (1911). The Tertiary gravels of the Sierra Nevada of California: *US Geological Survey Professional Paper*, **73**, 226p.

Lipman, P.W., Doe, B.R., Hedge, C.E. & Steven, T.A. (1978). Petrologic evolution of the San Juan volcanic field; Pb and Sr isotope evidence, *Geol. Soc. Am. Bull.*, **89**, 59-82.

Lipman, P.W., Prostka, H.J. & Christiansen, R.L. (1972). Cenozoic volcanism and plate-tectonic evolution of the western United States. I. Early and Middle Cenozoic, *Phil. Trans. R. Soc. Lond.*, **A271**, 217-248.

Loomis, D.P., Burbank, D.W. (1988). The stratigraphic evolution of the El Paso Basin, southern California: Implications for the Miocene development of the Garlock fault and the uplift of the Sierra Nevada, *Geol. Soc. Am. Bull.*, **100**, 12-28.

Luedke, R.G. & Smith, R.L. (1984). Map showing distribution, composition, and age of late Cenozoic volcanic centers in the western conterminous United States, *U.S. Geol. Surv. Misc. Inv. Series, Maps*, I-1523.

Marvin, R.F. & Cole, J.C. (1978). Radiometric ages. Compilation A. *Isocron/West*, **22**, 3-14.

Mavko, B.B. & Thompson, G.A. (1983). Crustal and upper mantle structure of the northern and central Sierra Nevada, *J. Geophys. Res.*, **88**, No B7, 5874-5892.

Mayer, L. (1986). Topographic constraints on models of lithospheric stretching of the Basin and Range province, western United States, in: Extensional Tectonics of the Southwestern United States: A Perspective on Processes and Kinematics, L. Mayer, ed., *Geol. Soc. Am. Spec. Pap.*, **208**, 5-14.

McDowell, F.W., Roden, M.F. & Smith, D. (1986). Comments on "Tectonic implications of the age, composition, and orientation of lamprophyre dikes, Navajo volcanic field, Arizona", by A.W. Laughlin, M.J. Aldrich, Jr., M. Shafiqullah & J. Husler, *EPSL*, **80**, 415-417.

McGetchin, T .R. (1968). The Moses Rock dike: Geology, Petrology, and mode of emplacement of a kimberlite-bearing breccia dike, San Juan County, Utah, PhD thesis, *Calf. Inst. of Technol., Pasadena*, 405pp.

McGetchin, T.R. & Besancon, J.R. (1973). Carbonate inclusions in mantle-derived pyropes, *EPSL*, **18**, 408-410.

McGetchin, T.R. & Silver, L.T. (1970). Compositional relations in minerals from kimberlite and related rocks in the Moses Rock dike, San Juan County, Utah, *Am. Mineral.*, **55**, 1738-1771.

McGetchin, T.R., Burke, K.C., Thompson, G.A. & Young, R.A. (1980). Mode and mechanisms of plateau uplifts, in *Dynamics of Plate Interiors*, edited by A.W. Bally, P.L. Bender, T.R. McGetchin and R.I. Walcott, *Am. Geophys. Union Geodynamics*, Series **1**, 99-110.

McIntosh, W.C. (1989). Timing and distribution of ignimbrite volcanism in the Eocene-Miocene, Mogollon-Datil volcanic field, *New Mexico Bureau of Mines and Mineral Resources*, Memoir, **46**, 58-59.

McKenzie, D. & O'Nions, R.K. (1991). Partial melt distributions from Inversion of Rare Earth Element Concentrations, *J. Petrol.*, **32**, 1021-1091.

McKenzie, D. (1989). Some remarks on the movement of small melt fraction in the mantle , *Ibid.*, **95**, 53-72.

McKenzie, D.P. & Bickle M.J. (1988). The volume and composition of melt generated by extension of the lithosphere *J. Petrol.* , **29** 625-679.

Menzies, M.A. & Murphy, V.R. (1980). Enriched mantle: Nd and Sr isotopes in diopsides from kimberlite nodules, *Nature*, **283**, 634-636.

Merrihue, C., & Turner, G. (1966). Potassium-argon dating by activation with fast neutrons, *J.Geophys. Res.*,**71**, 2852-2857.

Molnar, P. & Chen, W.P. (1983). Focal depths and fault plane solutions of earthquakes under the Tibetan plateau, *J. Geophys. Res.*, **88**, 1180-1196.

Molnar, P. & England, P. (1990). Late Cenozoic uplift of mountain ranges and global climate change: chicken or egg?, *Nature*, **346**.

Moore, J.G. & Dodge, F.C.W. (1977). Late Cenozoic basaltic and phonolitic lavas of the Sierra Nevada (abstract). *EOS Trans. Am. Geophys. Un.*, **58**, 1246.

Moore, J.G. & Dodge, F.C.W. (1980). Late Cenozoic volcanic rocks of the southern Sierra Nevada, California: I. Geology and petrology: Summary, *Geol. Soc. Am. Bull*, Part I, **91**, 515-518.

Naeser, G.W. (1971). Geochronology of the Navajo-Hopi diatremes, Four Corners area, *J. Geophys. Res*, **76**, 4978-4985.

Nelson, S.T. & Davidson, J.P. (1993). Interactions Between Mantle-Derived Magmas and Mafic Crust, Henry Mountains, Utah, *J. Geophys. Res.*, **98**, No B2, 1837-1852.

Nelson, S.T., Sullivan, K.R. & Davidson, J.P. (1992). New age determinations of central Colorado Plateau laccoliths, Utah: Recognizing disturbed K-Ar systematics and re-evaluating tectonomagmatic relationships, *Geol. Soc. Am. Bull.*, **104**, 1547-1560.

Nicholls, J. (1969). Studies of the volcanic petrology of the Navajo-Hopi area, Arizona, *Unpub PhD thesis*, U. Calif Berkeley, **107**.

Nielson, J.E., Lux, D.R., Dalrymple, G.B & Glazner, A.F. (1990). Age of the Peach Springs Tuff, S.E. California and W. Arizona,*J. Petrol.*, **95**, 571-580.

Nockolds, S.R. & Allen, R. (1954). The geochemistry of some igneous rock series, part 2: *Geochimica et Cosmochimica Acta*, **5**, 245-285.

Noyes, H.J., Frey, F.A. & Wones, D.R. (1983). A tale of two plutons: Geochemical evidence bearing on the origin and differentiation of the Red Lake and Eagle Peak plutons, Central Sierra Nevada, California, *J. Geol.*, **91**, 487-509.

Olafsson, M. & Eggler, D.H. (1983). Phase relations of amphibole, amphibole-carbonate, and phlogopite-carbonate peridotite: petrologic constraints on the asthenosphere, *EPSL*, **64**, 305-315.

Oldow, J.S., Bally A.W., Ave Lallemant H.G. & Leeman W.P. (1989). Phanerozoic evolution of the North American Cordillera; United States and Canada in: *The Geology of North America - An overview. Geol. Soc. Am. Volume* A 139-232. Editors: Bally A.W. & Palmer A.R.

Oltham, D Ben, White, W.M. & Patchett, J (1989). The geochemistry of marine sediments, island arc magma genesis, and crust-mantle recycling, *EPSL*, **94**, pg 1-21.

Ormerod, D.S. (1988). Late- to post subduction magmatic transitions in the western Great Basin, USA., Unpublished PhD Thesis, The Open University, Milton Keynes, UK., 313.

Ormerod, D.S., Hawkesworth, C.J., Rogers, N.W., Leeman, W.P. & Menzies, M.A. (1988) . Tectonic and magmatic transitions in the Western Great Basin, *Nature*, **333**, 349-353.

Ormerod, D.S., Rogers, N.W. & Hawkeswortth, C.J. (1991). Melting in the lithospheric mantle. Inverse modelling of alkali olivine basalt from the Big Pine volcanic field, California, *Contrib. Mineral. Petrol.*, **108**, 305-317.

Othman, D.B., White, W.M. & Patchett, J. (1989). The geochemistry of marine sediments, island arc magma genesis, and crust-mantle recycling, *EPSL*, **94**, 1-21.

Pakiser, L.C. & Brune, J.N. (1980). Seismic models of the root of the Sierra Nevada, *Science*, **210**, 1088-1094.

Parker, E.C., Davis, P.M., Evans, J.R., Iyer, H.M. & Olsen, K.H. (1984). Upwarp of anomalous asthenosphere beneath the Rio Grande rift, *Nature*, **312**, 354-356.

Peck, D.L. (1976), Mafic phonolites in the Sierra Nevada, California, *Geol. Surv. Research: Prof. Paper U.S. geol. Surv.*, **1000**, 173.

Perry, F.V., Baldridge W.S. & DePaolo D.J. (1987). Role of asthenosphere and lithosphere in the genesis of late Cenozoic basaltic rocks from the Rio Grande Rift

and adjacent regions of the southwestern United States *J. Geophys. Res.*, **92** 9193-9213.

Platt, J.P. & England, P.C.: Convective removal of lithosphere beneath mountain belts: Thermal and mechanical consequences, *J. Struct. Geology* (submitted).

Potts, P.J., Thorpe, O.W. & Watson, J.S, (1981). Determination of rare earth element abundances in 29 international rock standards by instrumental neutron activation analysis: a critical appraisal of calibration errors, *Chem Geol.*, **34**, 331-352.

Potts, P.J.,Thorpe, O.W., Isaacs, M.C. & Wright, D.W. (1985). High precision neutron activation analysis of geological samples employing simultaneous counting with both planar and coaxial detectors, *Chem Geol.*,**48**, 145-155.

Ren, X. (1981). Vegetational changes in the past and uplift of Qinghai-Xizang plateau. In: *Geological and Ecological studies of Qinghai-Xizang Plateau*, **1**, 139-144, Beijing: Science Press.

Richards, M.A., Duncan, R.A. & Courtillot, V.E. (1989). Flood basalts and hot spot tracks: plume heads and tails, *Science*, **246**, 103-107.

Rock, N.M.S. (1984). Nature and origin of calc-alkaline lamprophyres: minettes, vogesites, kersantites and spessartites, *Transactions of the Royal Society of Edinburgh: Earth Sciences*, **74**, 193-227.

Roden, M.F. & Smith, D. (1979). Field geology, chemistry, and petrology of Buell Park minette diatreme, Apache county, Arizona, *Proc, 2nd. Int. Kimb. Conf.*, 364-381.

Roden, M.F. (1977). Field geology and petrology of the minette diatreme at Buell Park, Apache county, Arizona, paper presented at *2nd. Int. Kimb. Conf,* AGU Santa Fe, N.M.

Roden, M.F. (1981). Origin of coexisting minette and ultramafic breccia, Navajo volcanic field, *Contrib. Mineral. Petrol .*, **77** 195-206.

Roden, M.F., Smith D. & McDowell F.W. (1979). Age and extent of potassic volcanism on the Colorado Plateau *EPSL* **43** 279-284.

Roden, M.F., Smith, D. & Murthy, V.R. (1990). Geochemical constraints on lithosphere composition and evolution beneath the Colorado Plateau, *J. Geophys. Res*, **95**, 2811-2831.

Rogers, N.W. (1992). Potassic magmatism as a key to trace element enrichment processes in the upper mantle, *J. Volc. Geoth. Res.*, **50**, 85-99

Rogers, N.W., De Mulder, M. & Hawkesworth, C.J. (1992). An enriched mantle source for potassic basanites: evidence from Karisimbi volcano, Virunga volcanic province, Rwanda, *Contrib. Mineral Petrol.*, **111**, 543-556.

Rowell, W.F. & Edgar, A.D. (1983). Cenozoic potassium-rich mafic volcanism in the western U.S.A.: Its relationship to deep subduction,*Geology*, **91**, 338-341.

Rowley, P.D., Anderson, J.J., Williams, P.L. & Fleck, R.J. (1978). Age of structural differentiation between the Colorado Plateaus and Basin and Range provinces in southwestern Utah, *Geology*, **6**, 51-55.

Ruddiman, W.F., Prell, W.L. & Raymo, M.E. (1989). Late Cenozoic uplift in southern Asia and the american west: Rationale for general circulation modelling experiements, *J. Geophys. Res.*, **94**, No D15, 18,379, 18,391.

Saltus, R.W. & Lachenbruch, A.H. (1991). Thermal evolution of the Sierra Nevada; Tectonic implications of new heat flow data, *Tectonics*, **10**, No 2, 325-344.

Sandiford, M. & Powell, R. (1990). Some isostatic and thermal consequences of the vertical strain geometry in convergent orogens, *EPSL*, **98**, 154-165.

Schweichert, R.A. & Cowan, D.S. (1975). Early Mesozoic tectonic evolution of the western Sierra Nevada, California, *Geol. Soc. Am. Bull.*, **86**, 1329-1336.

Severinghaus, J. & Atwater, T. (1990). Cenozoic geometry and thermal state of the subducting slabs beneath western North America, *Geol. Soc. Am.*, **176**, 1-22.

Sherrod, D.R. & Tosdal, R.M. (1991). Geological setting and Tertiary structural evolution of southwestern Arizona and southeastern California, *J. Geophys. Res.*, **96**, 12,351-12,374.

Shoemaker, E.M. (1956). Occurrence of uranium in diatremes on the Navajo and Hopi reservation, Arizona, New Mexico and Utah, in *Contributions to the Geology of Uranium*, compiled by L.R. Page et al., *U.S. Geol. Surv. Prof. Pap*, **300**, 179

Siems, P.L. & Jones, R.W. (1977). The Challis Volcanic Field, a review: *Geol. Soc. America, Abs. with Prog.*, **9**, 762-763.

Smith, D. & Ehrenberg, S.N. (1984). Zoned minerals in garnet peridotite nodules from the Colorado Plateau: Implications for mantle metasomatism and kinetics, *Contrib, Mineral. Petrol.*, **86**, 275-285.

Smith, D. & Levy, S. (1976). Petrology of the green knobs diatreme and implications for the upper mantle below the Colorado Plateau, *EPSL*, **29**, 107-125.

Smith, D. (1977). The origin and interpretation of spinel-pyroxene clusters in peridotite, *J. Geology*, **85**, 476-482.

Smith, D. (1979). Hydrous minerals and carbonates in periditite inclusions from the Green Knobs and Buell Park kimberlitic diatremes on the Colorado Plateau, in *The Mantle Sample: Inclusions in Kimberlites and Other Volcanics*, edited by Boyd, F.R. & Meyer, H.O.A., 345-356.

Smith, D. (1987). Genesis of carbonate in pyrope from ultramafic diatremes on the Colorado Plateau, southwestern United States, *Contrib. Mineral. Petrol.*, **97**, 389-396.

Snyder, W.S., Dickinson, W.R. & Silberman, M.L. (1976). Tectonic implications of space-time patterns of Cenozoic magmatism in the western US, *EPSL*, **32**, 91-106.

Stevens, C.H., Stone, P. & Kistler, R.W. A speculative reconstruction of the middle paleozoic continental margin of southwestern North America, *Tectonics*, **11**, No 2, 405-419.

Stewart, J.H. & Poole, F.G. (1974). in Tectonics and sedimentation (ed. Dickinson, W.R.) 57, *Society of Economists Paleontologists and Mineralogists Spec. Pub.*, 22.

Sullivan, K.R., Kowallis, B.J. & Mehnert, H.H. (1991). Isotopic ages of igneous intrusions in southeastern Evidence for a mid-Cenozoic Reno-San Juan magmatic zone: *Brigham Young University Geology Studies*, 139-144.

Sun, S.-s. & McDonough, W.F. (1989). Chemical and isotopic systematics of oceanic basalts; implications for mantle composition and processes, *Magmatism in the Ocean Basins*, Geol. Soc. Spec. Pub., **42**, (Saunders, A.D. & Norry, M.J. eds) 313-345.

Sun, S.S. (1980). Lead isotopic study of young volcanic rocks from mid-ocean ridges, ocean islands and island arcs, *Phil. Trans. R. Soc. Lond.*, **A297**, 409-45

Tanaka, K.L., Shoemaker, E.M., Ulrich, G.E. & Wolfe, E.W. (1986). Migration of Volcanism in the San Francisco Volcanic Field, Arizona, *Geol. Soc. Am. Bull.*, **97**, 129-141.

Taylor, S.R. & McLennan, S.M. (1985). The Continental Crust: It's composition and evolution. An examination of the geochemical record preserved in sedimentary rocks, Blackwell, Oxford.

Thompson, G.A. & Zoback, M.L. (1979). Regional geophysics of the Colorado Plateau, *Tectonophysics*, **61**, 149-181.

Thompson, R.N. (1977). Primary basalts and magma genesis: III Alban Hills, Roman comagmatic Province, Central Italy, *Contrib. Mineral.Petrol.*, **60**, 91-108

Thompson, R.N. Gibson, S.A., Leat, P.T., Mitchell, J.G., Morrison, M.A., Hendry, G.L. & Dickin, A.P. (1993). Early Miocene continental extension-related basaltic magmatism at Walton Peak, northwest Colorado: further evidence on continental basalt genesis, *J. Geol. Soc. London*, **150**, 277-292.

Thompson, R.N., Leat, P.T., Dickin, A.P., Morrison, M.A., Hendry, G.L. & Gibson, S.A. (1989). Strongly potassic mafic magmas from lithospheric mantle sources during continental extension and heating: evidence from Miocene minettes of northwest Colorado, U.S.A., *EPSL*, **98**, 139-153.

Thompson, R.N., Leat, P.T., Dickin, A.P., Morrison, M.A., Hendry, G.L. & Gibson, S.A. (1990). Strongly potassic lavas from lithospheric mantle sources during continental extensions and heating: evidence from Miocene minettes of northwest California, USA., *EPSL*, **98**, 139-153.

Tingey, D.G., Christiansen, E.H., Best, M.G., Ruiz, J. & Lux, D.R. (1991). Tertiary minette and melanephelinite dikes, Wasatch Plateau, Utah: Records of mantle heterogeneities and changing tectonics, *J. Geophys. Res.*, **96**, No B8, 13,529-13,544.

Trimble, D.E. (1980). Cenozoic tectonic history of the Great Plains contrasted with that of the southern Rocky Mountains: A synthesis: *Mountain geologist*, **17**, 59-69.

Turner, S., Hawkesworth, C., Liu, J., Rogers, N., Kelley, S. & Van Calsteren, P. (1993). Timing of Tibetan uplift constrained by analysis of volcanic rocks, *Nature*, **364**.

Turner, S., Sandiford, M. & Foden, J. (1992). Some geodynamic and compositional constraints on "postorogenic" magmatism, *Geology*, **20**, 931-934.

Tyner, G.N. & Smith, D. (1986). Peridotite xenoliths in silica-rich, potassic latite from the transition zone of the Colorado Plateau in north-central Arizona, *Contrib. Mineral. Petrol.*, **94**, 63-71.

Unruh, J.R. (1991). The uplift of the Sierra Nevada and implications for late Cenozoic epeirogeny in the western Cordillera, *Geol. Soc. Am. Bull.*, **103**, 1395-1404.

Van Kooten, G. (1980). Mineralogy, petrology and geochemistry of an ultrapotassic basaltic suite, Central Sierra Nevada, California, USA *J. Petrol.*, **21** 651-684.

Van Kooten, G.K. & Peck, D.L. (1977). Highly potassic phonolite of Pliocene age near Merced Peak, central Sierra Nevada, California (abstract). *Abstr. Progrm. geol. Soc. Am.*, **10**, 1208-9.

Van Kooten, G.K. (1981). Pb and Sr systematics of ultrapotassic and basaltic rocks from the Central Sierra Nevada, California, *Contrib Mineral Petrol.*, **76**, 378-385.

Wass, S.Y. & Rogers, N.W. (1980). Mantle metasomatism - precursor to continental alkaline volcanism, *Geochim. Cosmochim. Acta.*, **44**, 1811-1823.

Watson, S. & McKenzie, D. (1991). Melt generation by plumes: A study of Hawaiian Volcanism, *J. Petrol.*, **32**, 501-537.

Wenrich, K.J. (1989). Third-day field trip: Hopi Buttes volcanic field. Field excursions to volcanic terranes in the western United States, Volume 1: Southern Rocky Mountain Region, (Edited by Charles E. Chapim and Jim Zidek, *New Mexico Bureau of Mines and Mineral resources memoir*, No. **46**.

Wernicke, B.P., Christiansen, R.L., England, P.C. & Sondar, L.J. (1987). Tectonomagmatic evolution of Cenozoic extension in the North American Cordillera, in Continental Extensional Tectonics, (eds. Coward, M.P., Dewey, J.F. & Hancock, P.L.), *Geol. Soc. Spec. Pub.*, **28**, 203-221.

Williams, H. (1936). Pliocene volcanoes of the Navajo-Hopi country, *Geol. Soc. Am. Bull.*, **47**, 111-172.

Wobus, R.A., Mochel, D.W., Mertzman, S.A., Eide, E.A., Rothwarf, M.T., Loeffler, B.M., Johnson, D.A., Keating, G.N., Sultze, K., Benjamin, A.E., Venzke, E.A.

& Filson, T. (1990). Geochemistry of high-potassium rocks from the mid-Tertiary Guffey volcanic center, Thirtynine Mile volcanic field, central Colorado, *Geology*, **18**, 642-645.

Wright, T.L. & Doherty, P.C. (1970). A linear programming and least squares computer method for solving petrologic mixing problems, *Geol. Soc. Am. Bull.*, **81**, 1995-2008.

Young, R.A. & Brennan, W.J. (1974). The Peach Springs Tuff - Its bearing on structural evolution of the Colorado Plateau and development of Cenozoic drainage in Mohave County, Arizona, *Geol. Soc. Am. Bull.*, **85**, 83-90.

Young, R.A. (1979). Laramide deformation, erosion and plutonism along the southwestern margin of the Colorado Plateau, *Tectonophysics*, **61**, 25-47.

Zhou, S. & Sandiford, M.J. (1992). On the stability of isostatically compensated mountain belts, *J.Geophys. Res.*,**97**, 14207-14223.

Ziony, J.I. (1966). Analysis of systematic jointing in part of the Monument upwarp, southeastern Utah, *Ph.D. Thesis, University of California, Los Angeles*, 112p

# Appendix A

## Whole Rock Geochemical Data

The following Tables present the major, trace and rare earth element and isotopic analyses of the intrusives and volcanics from the Navajo and San Joaquin-Kings Volcanic Fields respectively. Data for the intrusives of the Navajo volcanic field are divided into the four main petrographic and compositional groups, mafic minettes, felsic minettes, katungites and melanephelinites, and within each group are listed as the individual diatremes or volcanic centres. The acronym for each diatreme are as follows:

| | |
|---|---|
| BenP | Bennet Peak. |
| BarP | Barber Peak. |
| SRSD | Ship Rock southern Dyke. |
| SRNEP | Ship Rock Northeastern plug. |
| ON | Outlet Neck. |
| TB | The Beast. |
| CRED | Church Rock eastern Dyke. |
| CRNED | Church Rock northeastern Dyke. |
| CRND | Church Rock northern Dyke. |
| PbC | Plug by Chiastla Butte. |
| CN-SD | Chiastla North-South Dyke. |
| CE-WD | Chiastla East-West Dyke. |
| S.MH | South of Mexican Hat. |
| WP | Washington Pass volcanic centre. |
| WL | Wheatfields Lake. |
| BR | Black Rock. |
| PD | Porass Dykes. |
| Chil | Chilchinbito. |
| Black P | Black Peak. |
| Luk Mtn | Lukachukai Mountain. |

Within each petrographic group despite there being a wide range in composition there is little mineralogical variation therefore rather than list petrographic descriptions of each sample the following descriptions summarise the main petrographic features of the four groups into which the Navajo intrusives are divided.

**Mafic Minette:**

Seriate-textured diopside and phlogopite in a glassy or microcrystalline, commonly trachytic, groundmass comprising sanidine, diopside, phlogopite, oxides and small modal quantities of olivine.

**Felsic Minette:**

Petrographically felsic minettes are similar to the mafic minettes in terms of phenocryst phases present. However the groundmass consists of higher proportions of sanidine, lesser quantities of diopside and phlogopite and is notable for the presence of quartz at the expense olivine.

**Katungite:**

Notable for the considerable variation in mineral phases present (see Table 2.1) despite a similar major element composition. Typically samples exhibit seriate-texured olivine and phlogopite in a coarse groundmass of anhedral olivine, phlogopite, melilite, perovskite, clinopyroxene and apatite.

**Melanephelinite:**

Seriate-textured olivine, diopside and phlogopite is set in a micro-crystalline often glassy matrix of olivine, diopside, phlogopite, nepheline and minor quantities of perovskite and melilite. Phenocryst and groundmass olivine is extensively altered to chlorite and is usually rimmed by phlogopite. Where olivine was originally the dominant phenocryst phases the prefix olivine is used whereas where phlogopite was dominant the prefix phlogopite is used.

Samples from the San Joaquin-Kings volcanic field are divided into the Late Miocene and Pliocene groups (Dalrymple, 1963, Van Kooten, 1980) and the Pliocene samples are themselves further subdivided into the low Rb/Sr and high Rb/Sr types identified in section 4.4.4. General sample locations are not abbreviated for the Sierran samples.

Petrographic variations between samples is limited and the rock type listed is based on the TAS classification of Le Bas (1986).

For the major element XRF analyses the total iron content is expressed as $Fe_2O_3$.

Loss on ignition (LOI) and Mg number (Mg#) are also presented. Mg# is calculated as follows and assumes FeO =0.85*Total Fe.

$$Mg\# = \frac{\frac{MgO}{40.304}}{\left\{\frac{MgO}{40.304} + \frac{Fe2O3}{159.677}\right\}} \times 100$$

Trace elements are expressed in parts per million (ppm) and are divided into XRF and INAA determinations (see appendix ? for techniques). U, Th, La, Ce and Nd were determined by XRF for all samples, however where INAA daterminations are available these data are quoted in preference to the XRF data because of its greater precision.

**Addtional Note:**

Samples AWL-5-86, BOL-4-84, BOL-8-84, BOL-12-84 and BOL-13-84 were kindly provided by A.W.Laughlin (see Laughlin et al., 1986; 1989).

| *Sample#* | 90-NM-6 | 90-NM-7 | 90-NM-8 | 90-NM-9 | 90-NM-10 | 90-NM-11 | 90-NM-65 |
|---|---|---|---|---|---|---|---|
| *Location* | Ben P | Ben P | Ben P | Ben P | D SE Bar P | D SE Bar P | SE. Bar P |
| *Rock Type* | Mafic Minette | Mafic Minette | Mafic Minette | Mafic Minette | Mafic Minette | Mafic Minette | Mafic Minette |
| *Lat* | 36°22'28" | 36°22'23" | 36°22'23" | 36°22'23" | 36°34'16" | 36°34'13" | 36°32'39" |
| *Long* | 108°44'09" | 108°44'16" | 108°44'16" | 108°44'16" | 108°41'25" | 108°41'17" | 108°39'45" |
| *SiO2* | 55.02 | 54.83 | 55.13 | 55.44 | 50.88 | 48.89 | 54.76 |
| *TiO2* | 1.45 | 1.44 | 1.44 | 1.34 | 2.08 | 2.28 | 1.62 |
| *Al2O3* | 10.45 | 10.55 | 10.51 | 10.6 | 9.93 | 9.25 | 10.82 |
| *Fe2O3* | 6.6 | 6.57 | 6.55 | 6.25 | 8.28 | 8.74 | 7 |
| *MnO* | 0.1 | 0.11 | 0.09 | 0.08 | 0.12 | 0.13 | 0.1 |
| *MgO* | 8.77 | 8.68 | 8.71 | 8.5 | 9.71 | 10.28 | 8.09 |
| *CaO* | 6.87 | 6.88 | 6.78 | 6.71 | 8.14 | 9.21 | 6.98 |
| *Na2O* | 2.36 | 2.37 | 2.38 | 2.44 | 2 | 2.31 | 2.03 |
| *K2O* | 6.75 | 6.6 | 6.71 | 6.71 | 6.11 | 5.09 | 6.95 |
| *P2O5* | 0.88 | 0.9 | 0.9 | 0.9 | 1.17 | 1.2 | 0.85 |
| *LOI* | 0.51 | 0.75 | 0.65 | 0.76 | 1.56 | 2.18 | 0.45 |
| *Total* | 99.76 | 99.68 | 99.85 | 99.73 | 99.98 | 99.56 | 99.65 |
| *Mg#* | **73.59** | **73.48** | **73.61** | **74.04** | **71.09** | **71.15** | **70.79** |
| *XRF* | | | | | | | |
| *Ba* | 2230 | 2214 | 2264 | 2488 | 2491 | 2690 | 1809 |
| *Co* | 33 | 27 | 42 | 30 | 44 | 48 | 32 |
| *Cr* | 299 | 278 | 287 | 257 | 320 | 354 | 250 |
| *Cu* | 48 | 44 | 48 | 44 | 55 | 56 | 45 |
| *Ga* | 20 | 18 | 18 | 17 | 18 | 19 | 18 |
| *Nb* | 33 | 35 | 33 | 29 | 60 | 73 | 34 |
| *Ni* | 285 | 278 | 280 | 273 | 268 | 306 | 234 |
| *Pb* | 36 | 39 | 35 | 35 | 17 | 23 | 20 |
| *Rb* | 192 | 186 | 193 | 186 | 175 | 133 | 198 |
| *Sc* | 9 | 9 | 8 | 8 | 14 | 10 | 9 |
| *Sr* | 1082 | 1145 | 1088 | 1273 | 1345 | 1696 | 1011 |
| *Th* | | | | | | | |
| *U* | | | | | | | |
| *V* | 138 | 142 | 140 | 127 | 193 | 208 | 143 |
| *Y* | 22 | 25 | 23 | 23 | 32 | 30 | 26 |
| *Zn* | 95 | 91 | 85 | 83 | 94 | 99 | 83 |
| *Zr* | 390 | 397 | 391 | 379 | 432 | 417 | 410 |
| *La* | | | | | | | |
| *Ce* | | | | | | | |
| *Nd* | | | | | | | |
| *INAA* | | | | | | | |
| *La* | 129 | 129 | 129 | 134 | 143 | 147 | 105 |
| *Ce* | 239 | 239 | 238 | 247 | 259 | 285 | 199 |
| *Nd* | 113 | 115 | 114 | 117 | 126 | 130 | 104 |
| *Sm* | 17 | 17.3 | 17 | 17.8 | 21.7 | 21.6 | 17.5 |
| *Eu* | 4.18 | 4.23 | 4.13 | 4.24 | 4.93 | 5.34 | 4.17 |
| *Tb* | 1.04 | 1.12 | 1.05 | 1.19 | 1.59 | 1.72 | 1.35 |
| *Yb* | 1.1 | 1.05 | 1.07 | 1.11 | 1.55 | 1.51 | 1.39 |
| *Lu* | 0.16 | 0.17 | 0.17 | 0.18 | 0.25 | 0.21 | 0.18 |
| *Th* | 52.6 | 53.3 | 52.7 | 52.9 | 29.1 | 28.2 | 25.6 |
| *U* | 14.3 | 13.1 | 14.7 | 15.6 | 7.58 | 6.47 | 7.19 |
| *Ta* | 1.96 | 1.96 | 2.11 | 1.8 | 3.46 | 4.2 | 2.26 |
| *Hf* | 9.79 | 9.82 | 9.7 | 9.72 | 10.2 | 10.1 | 10.3 |
| *ISOTOPES* | | | | | | | |
| *87Sr/86Sr* | 0.706535 | | | | 0.706128 | 0.705619 | 0.706508 |
| *143Nd/144Nd* | | | 0.512597 | 0.512595 | 0.512622 | | 0.512592 |
| *206Pb/204Pb* | | | | | 19.1671 | | |
| *207Pb/204 Pb* | | | | | 15.7494 | | |
| *208Pb/204Pb* | | | | | 39.1810 | | |

| *Sample#* | 90-NM-13A | 90-NM-13B | 90-NM-13C | 90-NM-16 | 90-NM-32 | 90-NM-33 | 90-NM-34A |
|---|---|---|---|---|---|---|---|
| *Location* | SRSD | SRSD | SRSD | SRNEP | ON | TB | TB |
| *Rock Type* | Mafic Minette | Mafic Minette | Mafic Minette | Mafic Minette | Mafic Minette | Mafic Minette | Mafic Minette |
| *Lat* | 36°38'32" | 36°38'50" | 36°39'27" | 36°41'41" | 35°54'47" | 35°54'32" | 35°54'32" |
| *Long* | 108°49'41" | 108°49'47" | 108°50'01" | 108°49'49" | 109°02'32" | 109°01'36" | 109°01'36" |
| *SiO2* | 53.72 | 54.21 | 53.81 | 53.18 | 54.95 | 54.87 | 53.81 |
| *TiO2* | 1.74 | 1.79 | 1.76 | 1.95 | 1.33 | 1.38 | 1.5 |
| *Al2O3* | 10.35 | 10.7 | 10.52 | 10.39 | 10.58 | 10.6 | 10.3 |
| *Fe2O3* | 7.41 | 7.24 | 7.43 | 7.89 | 6.44 | 6.56 | 7.01 |
| *MnO* | 0.1 | 0.11 | 0.11 | 0.11 | 0.09 | 0.09 | 0.09 |
| *MgO* | 8.73 | 7.86 | 8.21 | 8.36 | 7.84 | 8.13 | 8.61 |
| *CaO* | 7.11 | 6.99 | 7.36 | 7.58 | 7.19 | 7.27 | 7.72 |
| *Na2O* | 2.19 | 2.25 | 2.31 | 2.59 | 2.01 | 2.01 | 1.8 |
| *K2O* | 6.65 | 7.01 | 6.59 | 6.49 | 7.53 | 7.41 | 7.14 |
| *P2O5* | 0.93 | 0.96 | 0.9 | 0.97 | 1.07 | 1 | 1.07 |
| *LOI* | 0.83 | 0.73 | 0.78 | 0.35 | 0.63 | 0.45 | 0.8 |
| *Total* | 99.76 | 99.85 | 99.78 | 99.86 | 99.66 | 99.77 | 99.85 |
| *Mg#* | **71.19** | **69.48** | **69.86** | **68.96** | **71.86** | **72.22** | **72.03** |
| *XRF* | | | | | | | |
| *Ba* | 2634 | 2316 | 2427 | 2406 | 2526 | 2534 | 2519 |
| *Co* | 38 | 32 | 31 | 34 | 33 | 30 | 33 |
| *Cr* | 247 | 231 | 244 | 249 | 232 | 241 | 256 |
| *Cu* | 48 | 44 | 49 | 49 | 46 | 43 | 48 |
| *Ga* | 18 | 19 | 17 | 18 | 17 | 16 | 17 |
| *Nb* | 41 | 46 | 48 | 47 | 33 | 36 | 41 |
| *Ni* | 231 | 217 | 226 | 220 | 238 | 241 | 240 |
| *Pb* | 23 | 24 | 26 | 24 | 30 | 29 | 30 |
| *Rb* | 180 | 193 | 178 | 189 | 210 | 206 | 203 |
| *Sc* | 11 | 11 | 6 | 10 | 10 | 10 | 10 |
| *Sr* | 1252 | 1263 | 1298 | 1341 | 1380 | 1370 | 1587 |
| *Th* | | 61 | 42 | 46 | | 62 | |
| *U* | | 10 | 8 | 9 | | 10 | |
| *V* | 171 | 157 | 159 | 171 | 137 | 133 | 145 |
| *Y* | 33 | 32 | 29 | 31 | 35 | 37 | 33 |
| *Zn* | 88 | 89 | 94 | 97 | 100 | 98 | 104 |
| *Zr* | 376 | 429 | 405 | 394 | 459 | 438 | 443 |
| *La* | | 147 | 157 | 147 | | 189 | |
| *Ce* | | 291 | 290 | 270 | | 348 | |
| *Nd* | | 127 | 134 | 110 | | 157 | |
| *INAA* | | | | | | | |
| *La* | 142 | | | | 189 | | 177 |
| *Ce* | 276 | | | | 335 | | 332 |
| *Nd* | 121 | | | | 166 | | 164 |
| *Sm* | 19.8 | | | | 27.6 | | 26 |
| *Eu* | 4.73 | | | | 6.45 | | 6.28 |
| *Tb* | 1.57 | | | | 2.02 | | 1.94 |
| *Yb* | 1.79 | | | | 1.77 | | 1.7 |
| *Lu* | 0.25 | | | | 0.26 | | 0.25 |
| *Th* | 41.4 | | | | 57.9 | | 51.1 |
| *U* | 9.87 | | | | 13 | | 12.2 |
| *Ta* | 2.42 | | | | 1.82 | | 2.37 |
| *Hf* | 9.22 | | | | 10.8 | | 10.6 |
| *ISOTOPES* | | | | | | | |
| *87Sr/86Sr* | 0.706609 | | 0.70649 | 0.706476 | 0.707051 | | 0.70708 |
| *143Nd/144Nd* | | | | 0.512549 | 0.512538 | | 0.512553 |
| *206Pb/204Pb* | 19.2007 | | | | 19.1328 | | 19.0925 |
| *207Pb/204 Pb* | 15.6994 | | | | 15.6678 | | 15.6378 |
| *208Pb/204Pb* | 39.0143 | | | | 39.0014 | | 38.8990 |

| *Sample#* | 90-NM-34B | 90-NM-46 | 90-NM-47 | 90-NM-48 | 90-NM-49 | 90-NM-52 | 90-NM-53 |
|---|---|---|---|---|---|---|---|
| *Location* | TB | CRED | CRNED | CRND | PbC | CN-SD | CE-WD |
| M M | Mafic Minette | Mafic Minette | Mafic Minette | Mafic Minette | Mafic Minette | Mafic Minette | Mafic Minette |
| *Lat* | 35°54'32" | 36°44'15" | 36°44'16" | 36°44'19" | 36°46'09" | 36°46'55" | 36°47'01" |
| *Long* | 109°01'36" | 110°06'53" | 110°06'59" | 110°07'05" | 110°13'15" | 110°12'20" | 110°12'20" |
| *SiO2* | 54.54 | 52.1 | 53.59 | 53.41 | 50.08 | 50.86 | 51.14 |
| *TiO2* | 1.39 | 1.29 | 1.27 | 1.27 | 1.72 | 1.62 | 1.63 |
| *Al2O3* | 10.65 | 10.38 | 10.69 | 10.72 | 10.32 | 10.3 | 10.55 |
| *Fe2O3* | 6.58 | 7.52 | 7.62 | 7.27 | 8.62 | 8.26 | 8.36 |
| *MnO* | 0.08 | 0.12 | 0.11 | 0.12 | 0.13 | 0.12 | 0.14 |
| *MgO* | 8.05 | 9.05 | 8.46 | 8.8 | 9.27 | 9.8 | 9.21 |
| *CaO* | 7.2 | 8.53 | 7.89 | 7.67 | 9.12 | 8.9 | 8.65 |
| *Na2O* | 1.9 | 2.45 | 2.6 | 2.64 | 2.34 | 2.39 | 2.33 |
| *K2O* | 7.49 | 5.45 | 5.36 | 5.49 | 5.06 | 5.22 | 5.33 |
| *P2O5* | 1.09 | 0.9 | 0.86 | 0.88 | 1.05 | 0.97 | 1.01 |
| *LOI* | 0.65 | 1.99 | 1.28 | 1.56 | 2.07 | 1.2 | 1.26 |
| *Total* | 99.62 | 99.78 | 99.73 | 99.83 | 99.78 | 99.64 | 99.61 |
| *Mg#* | **71.96** | **71.62** | **69.96** | **71.74** | **69.28** | **71.33** | **69.79** |
| *XRF* | | | | | | | |
| *Ba* | 2658 | 2094 | 2232 | 2135 | 2329 | 1998 | 2171 |
| *Co* | 33 | 40 | 28 | 35 | 42 | 40 | 37 |
| *Cr* | 237 | 281 | 261 | 268 | 316 | 359 | 331 |
| *Cu* | 47 | 46 | 25 | 50 | 51 | 55 | 55 |
| *Ga* | 19 | 18 | 17 | 15 | 15 | 16 | 18 |
| *Nb* | 36 | 41 | 38 | 40 | 59 | 56 | 53 |
| *Ni* | 235 | 302 | 249 | 268 | 246 | 297 | 272 |
| *Pb* | 29 | 37 | 43 | 38 | 33 | 35 | 41 |
| *Rb* | 202 | 138 | 141 | 141 | 135 | 126 | 122 |
| *Sc* | 8 | 8 | 13 | 10 | 12 | 12 | 12 |
| *Sr* | 1417 | 1544 | 1405 | 1382 | 1050 | 1452 | 1418 |
| *Th* | | | 67 | | 71 | | |
| *U* | | | 11 | | 12 | | |
| *V* | 128 | 156 | 153 | 162 | 173 | 173 | 171 |
| *Y* | 34 | 27 | 28 | 28 | 32 | 31 | 31 |
| *Zn* | 107 | 89 | 93 | 86 | 96 | 102 | 103 |
| *Zr* | 464 | 339 | 326 | 335 | 344 | 355 | 359 |
| *La* | | | 137 | | 178 | | |
| *Ce* | | | 264 | | 330 | | |
| *Nd* | | | 117 | | 137 | | |
| *INAA* | | | | | | | |
| *La* | 176 | 137 | | 137 | | 163 | 168 |
| *Ce* | 318 | 260 | | 256 | | 292 | 304 |
| *Nd* | 158 | 126 | | 123 | | 138 | 145 |
| *Sm* | 26.2 | 19.9 | | 19.9 | | 22.3 | 23.3 |
| *Eu* | 6.45 | 4.91 | | 4.83 | | 5.34 | 5.85 |
| *Tb* | 2.05 | 1.61 | | 1.64 | | 1.72 | 1.88 |
| *Yb* | 1.7 | 1.47 | | 1.56 | | 1.76 | 1.76 |
| *Lu* | 0.23 | 0.24 | | 0.25 | | 0.28 | 0.24 |
| *Th* | 49.9 | 59.4 | | 58.9 | | 62.5 | 63.9 |
| *U* | 11.9 | 10.6 | | 11.9 | | 15.6 | 16.9 |
| *Ta* | 2.29 | 2.41 | | 2.32 | | 3.28 | 3.08 |
| *Hf* | 10.3 | 7.83 | | 8.06 | | 8.49 | 8.45 |
| *ISOTOPES* | | | | | | | |
| *87Sr/86Sr* | 0.706971 | 0.706233 | | 0.706215 | | 0.705746 | 0.705875 |
| *143Nd/144Nd* | 0.5126 | 0.512675 | | 0.512647 | | 0.512637 | 0.512624 |
| *206Pb/204Pb* | 19.0957 | 19.1364 | | | | 19.1345 | 19.1199 |
| *207Pb/204 Pb* | 15.6891 | 15.6562 | | | | 15.6335 | 15.6264 |
| *208Pb/204Pb* | 38.7389 | 38.9363 | | | | 39.1614 | 38.9106 |

| *Sample#* | 90-NM-54A | 90-NM-54B | 90-NM-55 | 90-NM-21 | 90-NM-23 | 90-NM-24 | 90-NM-25 |
|---|---|---|---|---|---|---|---|
| *Location* | SMH | SMH | SMH | WP | WP | WP | WP |
| M M | Mafic Minette | Mafic Minette | Mafic Minette | Mafic Minette | Mafic Minette | Mafic Minette | Mafic Minette |
| *Lat* | | | | 36°05'28" | 36°05'19" | 36°05'19" | 36°05'19" |
| *Long* | | | | 108°51'35" | 108°52'24" | 108°52'24" | 108°52'24" |
| *SiO2* | 48.05 | 47.95 | 47.99 | 53.86 | 52.93 | 54.6 | 53.23 |
| *TiO2* | 1.9 | 2.01 | 2.38 | 1.75 | 1.93 | 1.6 | 1.96 |
| *Al2O3* | 9.71 | 9.61 | 9.01 | 10.18 | 10.33 | 10.66 | 10.11 |
| *Fe2O3* | 9.2 | 9.69 | 8.9 | 7.5 | 7.5 | 6.88 | 7.62 |
| *MnO* | 0.15 | 0.15 | 0.11 | 0.11 | 0.1 | 0.1 | 0.09 |
| *MgO* | 10.61 | 10.41 | 10.52 | 9.13 | 9.14 | 8.8 | 9.46 |
| *CaO* | 10.22 | 10.58 | 10.12 | 6.94 | 7.25 | 6.48 | 7.34 |
| *Na2O* | 2.1 | 1.99 | 1.45 | 2.23 | 2.18 | 2.42 | 1.99 |
| *K2O* | 4.84 | 4.58 | 5.43 | 6.3 | 6.33 | 6.33 | 6.57 |
| *P2O5* | 1.19 | 1.13 | 1.27 | 0.74 | 0.76 | 0.77 | 0.75 |
| *LOI* | 1.64 | 1.54 | 2.73 | 0.9 | 1.36 | 0.9 | 0.78 |
| *Total* | 99.61 | 99.64 | 99.91 | 99.64 | 99.81 | 99.54 | 99.9 |
| *Mg#* | **70.75** | **69.26** | **71.26** | **71.85** | **71.88** | **72.84** | **72.25** |
| *XRF* | | | | | | | |
| *Ba* | 2442 | 2234 | 2229 | 2278 | 2255 | 2268 | 2136 |
| *Co* | 44 | 46 | 42 | 41 | 37 | 40 | 38 |
| *Cr* | 357 | 338 | 435 | 288 | 301 | 303 | 345 |
| *Cu* | 61 | 64 | 61 | 58 | 51 | 53 | 53 |
| *Ga* | 15 | 16 | 15 | 17 | 16 | 21 | 18 |
| *Nb* | 77 | 76 | 94 | 47 | 51 | 42 | 53 |
| *Ni* | 288 | 277 | 312 | 299 | 273 | 272 | 275 |
| *Pb* | 27 | 23 | 25 | 32 | 32 | 43 | 36 |
| *Rb* | 117 | 106 | 142 | 154 | 199 | 184 | 205 |
| *Sc* | 14 | 10 | 16 | 9 | 7 | 10 | 10 |
| *Sr* | 1815 | 1619 | 1742 | 1234 | 1312 | 1237 | 1373 |
| *Th* | | 45 | | | | 75 | |
| *U* | | 9 | | | | 14 | |
| *V* | 201 | 216 | 226 | 167 | 172 | 169 | 177 |
| *Y* | 35 | 33 | 33 | 21 | 21 | 24 | 22 |
| *Zn* | 103 | 108 | 109 | 84 | 76 | 77 | 78 |
| *Zr* | 366 | 365 | 430 | 376 | 402 | 419 | 409 |
| *La* | | 163 | | | | 144 | |
| *Ce* | | 327 | | | | 250 | |
| *Nd* | | 138 | | | | 96 | |
| *INAA* | | | | | | | |
| *La* | 163 | | 172 | 120 | 128 | | 128 |
| *Ce* | 300 | | 316 | 214 | 232 | | 239 |
| *Nd* | 147 | | 152 | 94.1 | 102 | | 104 |
| *Sm* | 24 | | 25.6 | 15.3 | 15.9 | | 16.3 |
| *Eu* | 5.88 | | 6.1 | 3.51 | 3.71 | | 3.84 |
| *Tb* | 1.95 | | 1.91 | 1.21 | 1.23 | | 1.35 |
| *Yb* | 1.9 | | 1.63 | 1.45 | 1.21 | | 1.29 |
| *Lu* | 0.3 | | 0.25 | 0.23 | 0.22 | | 0.21 |
| *Th* | 49.8 | | 49.6 | 52.2 | 54.9 | | 55.5 |
| *U* | 12.8 | | 10.1 | 13.2 | 13.5 | | 15 |
| *Ta* | 4.3 | | 5.02 | 2.84 | 3.14 | | 3.28 |
| *Hf* | 8.53 | | 9.83 | 9.03 | 9.98 | | 9.91 |
| *ISOTOPES* | | | | | | | |
| *87Sr/86Sr* | 0.705638 | | 0.705693 | 0.70604 | 0.705978 | 0.70627 | 0.705914 |
| *143Nd/144Nd* | 0.512665 | | 0.512674 | 0.512629 | 0.512648 | 0.512659 | 0.51266 |
| *206Pb/204Pb* | 19.2112 | | 19.2401 | 19.1571 | | | 19.1454 |
| *207Pb/204 Pb* | 15.7076 | | 15.6437 | 15.7072 | | | 15.6615 |
| *208Pb/204Pb* | 39.1614 | | 38.9758 | 39.0776 | | | 38.9862 |

| *Sample#* | 90-NM-26 | 90-NM-28 | 90-NM-29 | 90-NM-58 | 90-NM-60 | 90-NM-62 |
|---|---|---|---|---|---|---|
| *Location* | WP | WP | WP | WP | WP | WP |
| M M | Mafic Minette | Mafic Minette | Mafic Minette | Mafic Minette | Mafic Minette | Mafic Minette |
| *Lat* | 36°05'19" | 36°05'18" | 36°05'18" | 36°05'18" | 36°05'33" | 36°05'48" |
| *Long* | 108°52'24" | 108°52'29" | 108°52'29" | 108°52'43" | 108°52'24" | 108°51'22" |
| | | | | | | |
| *SiO2* | 53.2 | 55.17 | 53.62 | 53 | 53.97 | 53.09 |
| *TiO2* | 1.96 | 1.67 | 1.77 | 2.04 | 1.82 | 2.06 |
| *Al2O3* | 10.01 | 10.72 | 10.27 | 10.22 | 10.45 | 9.99 |
| *Fe2O3* | 7.6 | 7.06 | 7.45 | 7.71 | 7.6 | 7.87 |
| *MnO* | 0.11 | 0.09 | 0.1 | 0.11 | 0.12 | 0.12 |
| *MgO* | 9.59 | 8.28 | 9.33 | 9.44 | 8.89 | 9.91 |
| *CaO* | 7.46 | 6.53 | 6.97 | 7.29 | 7 | 7.28 |
| *Na2O* | 1.85 | 2.41 | 2.22 | 1.62 | 2.08 | 1.64 |
| *K2O* | 6.47 | 6.22 | 6.14 | 6.24 | 6.13 | 6.41 |
| *P2O5* | 0.81 | 0.83 | 0.73 | 0.73 | 0.74 | 0.75 |
| *LOI* | 0.91 | 0.85 | 1.3 | 1.31 | 0.85 | 0.6 |
| *Total* | 99.97 | 99.83 | 99.9 | 99.71 | 99.65 | 99.72 |
| *Mg#* | **72.58** | **71.09** | **72.42** | **71.97** | **71.04** | **72.53** |
| | | | | | | |
| *XRF* | | | | | | |
| *Ba* | 2153 | 2209 | 2167 | 2023 | 2399 | 2017 |
| *Co* | 37 | 36 | 41 | 37 | 44 | 39 |
| *Cr* | 326 | 247 | 266 | 502 | 290 | 304 |
| *Cu* | 56 | 49 | 58 | 56 | 55 | 56 |
| *Ga* | 18 | 19 | 18 | 16 | 17 | 16 |
| *Nb* | 51 | 38 | 51 | 54 | 49 | 56 |
| *Ni* | 276 | 240 | 296 | 301 | 290 | 322 |
| *Pb* | 31 | 42 | 36 | 33 | 33 | 32 |
| *Rb* | 186 | 168 | 176 | 157 | 191 | 224 |
| *Sc* | 8 | 3 | 8 | 8 | 10 | 11 |
| *Sr* | 1274 | 1273 | 1207 | 1211 | 1228 | 1197 |
| *Th* | 67 | | 67 | | 58 | |
| *U* | 12 | | 10 | | 10 | |
| *V* | 189 | 157 | 160 | 179 | 160 | 184 |
| *Y* | 23 | 23 | 23 | 23 | 22 | 22 |
| *Zn* | 77 | 89 | 84 | 80 | 83 | 76 |
| *Zr* | 361 | 381 | 387 | 415 | 371 | 412 |
| *La* | 130 | | 132 | | 138 | |
| *Ce* | 249 | | 232 | | 222 | |
| *Nd* | 97 | | 102 | | 99 | |
| | | | | | | |
| *INAA* | | | | | | |
| *La* | | 132 | | 126 | | 118 |
| *Ce* | | 243 | | 222 | | 215 |
| *Nd* | | 113 | | 99.1 | | 98.5 |
| *Sm* | | 17.4 | | 14.6 | | 14.5 |
| *Eu* | | 4.2 | | 3.69 | | 3.62 |
| *Tb* | | 1.4 | | 1.24 | | 1.18 |
| *Yb* | | 1.29 | | 1.3 | | 1.31 |
| *Lu* | | 0.2 | | 0.19 | | 0.2 |
| *Th* | | 57.1 | | 55.5 | | 49.9 |
| *U* | | 12.6 | | 12.7 | | 12 |
| *Ta* | | 2.23 | | 3.12 | | 3.27 |
| *Hf* | | 9.24 | | 10.2 | | 10 |
| | | | | | | |
| *ISOTOPES* | | | | | | |
| *87Sr/86Sr* | 0.705866 | 0.706303 | | 0.705801 | | |
| *143Nd/144Nd* | | 0.512628 | | 0.512661 | | 0.512634 |
| *206Pb/204Pb* | | 19.0399 | | | | 19.1120 |
| *207Pb/204 Pb* | | 15.6173 | | | | 15.6240 |
| *208Pb/204Pb* | | 38.7656 | | | | 38.8611 |

| *Sample#* | *90-NM-57* | *90-NM-27* | *90-NM-59* | *90-NM-61* | *90-NM-64* | *90-NM-20A* |
|---|---|---|---|---|---|---|
| *Location* | *WL* | *WP* | *WP* | *WP* | *WP* | *WP[4]* |
| *Rock Type* | *Felsic Minette* | *Felsic Minette* | *Felsic Minette* | *Felsic Minette* | *Felsic Minette* | *Felsic Minette* |
| *Lat* | *36°11'50"* | *36°05'18"* | *36°05'33"* | *36°05'33"* | *36°05'48"* | *36°05'28"* |
| *Long* | *109°04'16"* | *108°52'29"* | *108°52'24"* | *108°52'24"* | *108°51'22"* | *108°51'35"* |
| *SiO2* | 54.93 | 56.96 | 56.09 | 55.82 | 55.53 | 58.02 |
| *TiO2* | 1.67 | 1.67 | 1.58 | 1.63 | 1.69 | 1.36 |
| *Al2O3* | 10.69 | 10.61 | 10.88 | 10.91 | 10.69 | 11.04 |
| *Fe2O3* | 6.63 | 6.93 | 6.75 | 6.88 | 6.98 | 5.57 |
| *MnO* | 0.1 | 0.11 | 0.11 | 0.13 | 0.1 | 0.06 |
| *MgO* | 7.34 | 6.71 | 7.43 | 7.3 | 7.41 | 7.24 |
| *CaO* | 7.44 | 6.28 | 6.24 | 6.54 | 6.74 | 5.52 |
| *Na2O* | 2.18 | 2.23 | 1.95 | 2.17 | 2.23 | 2.3 |
| *K2O* | 6.11 | 6.47 | 6.82 | 6.37 | 6.36 | 7.27 |
| *P2O5* | 0.74 | 0.84 | 0.78 | 0.77 | 0.82 | 0.71 |
| *LOI* | 1.81 | 1.24 | 1.28 | 1.13 | 1.21 | 0.68 |
| *Total* | 99.64 | 100.05 | 99.91 | 99.65 | 99.76 | 99.77 |
| *Mg** | **69.9** | **67** | **69.77** | **68.99** | **69.01** | **73.16** |
| *XRF* | | | | | | |
| *Ba* | 1924 | 2281 | 2297 | 2419 | 2205 | 2266 |
| *Co* | 35 | 37 | 32 | 39 | 34 | 25 |
| *Cr* | 261 | 252 | 269 | 271 | 254 | 236 |
| *Cu* | 49 | 50 | 47 | 42 | 50 | 40 |
| *Ga* | 19 | 19 | 16 | 18 | 17 | 22 |
| *Nb* | 45 | 38 | 33 | 36 | 38 | 35 |
| *Ni* | 245 | 274 | 257 | 244 | 233 | 243 |
| *Cr* | 261 | 252 | 269 | 271 | 254 | 236 |
| *Pb* | 22 | 31 | 38 | 34 | 33 | 35 |
| *Rb* | 131 | 140 | 177 | 179 | 206 | 186 |
| *Sc* | 7 | 6 | 11 | 6 | 10 | 6 |
| *Sr* | 1104 | 1282 | 1259 | 1252 | 1228 | 1291 |
| *Th* | 43 | 63 | 70 | 58 | 56 | 73 |
| *U* | 4 | 12 | 11 | 11 | 10 | 7 |
| *V* | 154 | 146 | 155 | 148 | 145 | 141 |
| *Y* | 22 | 26 | 22 | 23 | 23 | 23 |
| *Zn* | 76 | 91 | 94 | 94 | 93 | 78 |
| *Zr* | 413 | 374 | 386 | 389 | 373 | 411 |
| *La* | 112 | 138 | 151 | 127 | 149 | 127 |
| *Ce* | 209 | 238 | 243 | 242 | 245 | 233 |
| *Nd* | | | | | | |
| *INAA* | | | | | | |
| *La* | | | | | | |
| *Ce* | | - | | | | |
| *Nd* | | | | | | |
| *Sm* | | | | | | |
| *Eu* | | | | | | |
| *Tb* | | | | | | |
| *Yb* | | | | | | |
| *Lu* | | | | | | |
| *Th* | | | | | | |
| *U* | | | | | | |
| *Ta* | | | | | | |
| *Hf* | | | | | | |
| *ISOTOPES* | | | | | | |
| *87/86* | | | | 0.706189 | | |
| *143/144* | | 0.512633 | | | | |
| *206Pb/204Pb* | | | | | | |
| *207Pb/204Pb* | | | | | | |
| *208Pb/204Pb* | | | | | | |

| *Sample#* | *90-NM-22A* | *90-NM-22B* | *90-NM-40* | *90-NM-41* | *90-NM-42* | *90-NM-50* |
|---|---|---|---|---|---|---|
| *Location* | *WP* | *WP* | *Chil* | *Chil* | *Chil* | *PD* |
| *Rock Type* | *Felsic Minette* | *Felsic Minette* | *Felsic Minette* | *Felsic Minette* | *Felsic Minette* | *Felsic Minette* |
| *Lat* | *36°05'19"* | *36°05'19"* | *36°35'33"* | *36°35'11"* | *36°34'53"* | *36°46'39"* |
| *Long* | *108°51'37"* | *108°51'37"* | *110°05'11"* | *110°04'56"* | *110°04'37"* | *110°09'52"* |
| *SiO2* | 58.18 | 58.43 | 54.06 | 54.16 | 53.39 | 51.52 |
| *TiO2* | 1.28 | 1.2 | 1.47 | 1.4 | 1.45 | 1.31 |
| *Al2O3* | 10.94 | 11.03 | 11.35 | 11.56 | 11.27 | 11.44 |
| *Fe2O3* | 5.45 | 5.25 | 7.75 | 7.51 | 7.6 | 7.51 |
| *MnO* | 0.05 | 0.07 | 0.2 | 0.16 | 0.14 | 0.13 |
| *MgO* | 7.4 | 7.35 | 6.64 | 6.4 | 6.41 | 5.85 |
| *CaO* | 5.51 | 5.27 | 7.91 | 7.97 | 8.37 | 9.56 |
| *Na2O* | 2.26 | 2.42 | 2.27 | 2.24 | 2.2 | 2.65 |
| *K2O* | 7.25 | 7.28 | 6.43 | 6.81 | 6.97 | 5.87 |
| *P2O5* | 0.71 | 0.71 | 1.04 | 0.96 | 1 | 0.86 |
| *LOI* | 0.65 | 0.78 | 0.88 | 0.58 | 1.06 | 3.2 |
| *Total* | 99.68 | 99.79 | 100 | 99.75 | 99.86 | 99.9 |
| *Mg** | **74.01** | **74.59** | **64.25** | **64.12** | **63.88** | **62.03** |
| *XRF* | | | | | | |
| *Ba* | 2271 | 2337 | 2312 | 2641 | 2777 | 1995 |
| *Co* | 26 | 28 | 30 | 34 | 30 | 32 |
| *Cr* | 252 | 268 | 161 | 143 | 146 | 167 |
| *Cu* | 40 | 41 | 33 | 43 | 41 | 47 |
| *Ga* | 18 | 19 | 18 | 17 | 15 | 17 |
| *Nb* | 33 | 26 | 44 | 44 | 44 | 41 |
| *Ni* | 265 | 272 | 146 | 136 | 139 | 141 |
| *Cr* | 252 | 268 | 161 | 143 | 146 | 167 |
| *Pb* | 39 | 42 | 46 | 46 | 45 | 46 |
| *Rb* | 190 | 192 | 181 | 151 | 159 | 152 |
| *Sc* | 5 | 10 | 9 | 9 | 9 | 9 |
| *Sr* | 1278 | 1289 | 1591 | 1339 | 1437 | 1382 |
| *Th* | 72 | 76 | 80 | 80 | 79 | 65 |
| *U* | 9 | 9 | 10 | 13 | 11 | 7 |
| *V* | 132 | 120 | 157 | 153 | 154 | 144 |
| *Y* | 22 | 19 | 32 | 30 | 29 | 27 |
| *Zn* | 78 | 76 | 95 | 90 | 89 | 90 |
| *Zr* | 413 | 397 | 373 | 356 | 363 | 340 |
| *La* | | | 175 | 152 | 161 | 135 |
| *Ce* | | | 318 | 273 | 275 | 247 |
| *Nd* | | | | | | |
| *INAA* | | | | | | |
| *La* | 136 | 134 | | | | |
| *Ce* | 241 | 221 | - | | | |
| *Nd* | 103 | 102 | | | | |
| *Sm* | 16.4 | 15.5 | | | | |
| *Eu* | 3.71 | 3.56 | | | | |
| *Tb* | 1.28 | 1.24 | | | | |
| *Yb* | 1.15 | 1.15 | | | | |
| *Lu* | 0.16 | 0.16 | | | | |
| *Th* | 63 | 60.4 | | | | |
| *U* | 9.94 | 9.84 | | | | |
| *Ta* | 1.89 | 1.63 | | | | |
| *Hf* | 9.97 | 9.45 | | | | |
| *ISOTOPES* | | | | | | |
| *87/86* | 0.706297 | 0.706443 | 0.705937 | | 0.705953 | 0.70568 |
| *143/144* | 0.512705 | 0.51263 | | | | |
| *206Pb/204Pb* | | | | | | |
| *207Pb/204Pb* | | | | | | |
| *208Pb/204Pb* | | | | | | |

| *Sample#* | *90-NM-51* | *90-NM-19* | *90-NM-38* | *90-NM-39* |
|---|---|---|---|---|
| *Location* | *PD* | *Luk Mtn* | *Black P* | *Black P* |
| *Rock Type* | *Felsic Minette* | *Felsic Minette* | *Felsic Minette* | *Felsic Minette* |
| *Lat* | *36°46'19"* | | *36°15'04"* | *36°15'04"* |
| *Long* | *110°09'52"* | | *109°09'16"* | *109°09'16"* |
| | | | | |
| *SiO2* | 52.64 | 56.68 | 57.16 | 57.88 |
| *TiO2* | 1.33 | 1.66 | 1.22 | 1.26 |
| *Al2O3* | 11.51 | 10.9 | 11.37 | 11.76 |
| *Fe2O3* | 7.55 | 6.79 | 5.66 | 5.81 |
| *MnO* | 0.13 | 0.09 | 0.06 | 0.08 |
| *MgO* | 6.2 | 6.12 | 6.18 | 6.21 |
| *CaO* | 8.53 | 6.61 | 6.41 | 5.84 |
| *Na2O* | 2.54 | 2.38 | 2.46 | 2.69 |
| *K2O* | 5.97 | 6.97 | 7.27 | 6.82 |
| *P2O5* | 0.85 | 0.98 | 0.83 | 0.83 |
| *LOI* | 2.36 | 0.68 | 1.08 | 0.55 |
| *Total* | 99.61 | 99.86 | 99.7 | 99.73 |
| *Mg** | **63.26** | **65.4** | **69.6** | **69.15** |
| | | | | |
| *XRF* | | | | |
| *Ba* | 2173 | 2251 | 2299 | 2354 |
| *Co* | 30 | 31 | 21 | 25 |
| *Cr* | 159 | 167 | 164 | 186 |
| *Cu* | 49 | 40 | 44 | 46 |
| *Ga* | 18 | 18 | 19 | 20 |
| *Nb* | 39 | 34 | 28 | 26 |
| *Ni* | 142 | 149 | 176 | 194 |
| *Cr* | 159 | 167 | 164 | 186 |
| *Pb* | 45 | 22 | 31 | 100 |
| *Rb* | 151 | 204 | 211 | 209 |
| *Sc* | 9 | 9 | 7 | 2 |
| *Sr* | 1357 | 1228 | 1106 | 1127 |
| *Th* | 75 | 35 | 65 | 72 |
| *U* | 10 | 6 | 10 | 10 |
| *V* | 201 | 136 | 126 | 119 |
| *Y* | 30 | 29 | 25 | 26 |
| *Zn* | 93 | 89 | 85 | 106 |
| *Zr* | 344 | 429 | 413 | 418 |
| *La* | 140 | 138 | 144 | 144 |
| *Ce* | 256 | 262 | 259 | 266 |
| *Nd* | | | | |
| | | | | |
| *INAA* | | | | |
| *La* | | | | |
| *Ce* | | - | | |
| *Nd* | | | | |
| *Sm* | | | | |
| *Eu* | | | | |
| *Tb* | | | | |
| *Yb* | | | | |
| *Lu* | | | | |
| *Th* | | | | |
| *U* | | | | |
| *Ta* | | | | |
| *Hf* | | | | |
| | | | | |
| *ISOTOPES* | | | | |
| *87/86* | | 0.706641 | | 0.707151 |
| *143/144* | | | | |
| *206Pb/204Pb* | | | | |
| *207Pb/204Pb* | | | | |
| *208Pb/204Pb* | | | | |

| *Sample#* | AWL-35-83 | BOL-4-84 | BOL-8-84 | BOL-12-84 | BOL-13-84 | AWL-5-86 |
|---|---|---|---|---|---|---|
| *Location* | Hasbidito Ck | Hasbidito Ck | Hasbidito Ck | Hasbidito Ck | Hasbidito Ck | Hasbidito Ck |
| *Rock type* | | | | | | |
| *Lat* | ? | ? | ? | ? | ? | ? |
| *Long* | ? | ? | ? | ? | ? | ? |
| | | | | | | |
| *SiO2* | 33.58 | 33.82 | 34.81 | 32.66 | 33.16 | 36.94 |
| *TiO2* | 4.74 | 4.267 | 4.338 | 4.124 | 4.283 | 3.295 |
| *Al2O3* | 6.84 | 6.85 | 6.01 | 6.34 | 6.76 | 5.45 |
| *Fe2O3* | 12.96 | 13.57 | 12.91 | 12.91 | 14.06 | 13.22 |
| *MnO* | 0.2 | 0.2 | 0.178 | 0.186 | 0.211 | 0.185 |
| *MgO* | 16.14 | 16.61 | 18.45 | 16.09 | 15.72 | 22.59 |
| *CaO* | 14.25 | 13.5 | 11.21 | 12.42 | 14.37 | 9.28 |
| *Na2O* | 1.45 | 1.22 | 1.17 | 1.49 | 1.57 | 1.33 |
| *K2O* | 2.87 | 2.95 | 2.56 | 1.85 | 3.13 | 1.26 |
| *P2O5* | 1.6 | 1.701 | 1.185 | 1.478 | 1.918 | 1.103 |
| *LOI* | 5.37 | 5.312 | 7.179 | 10.452 | 4.818 | 5.347 |
| *Total* | 100 | 100 | 100 | 100 | 100 | 100 |
| *Mg#* | **72.31** | **72.53** | **75.14** | **72.96** | **72.09** | **79.53** |
| | | | | | | |
| *XRF* | | | | | | |
| *Ba* | 1960 | 2197 | 1607 | 2504 | 1928 | 1221 |
| *Co* | | | | | | |
| *Cr* | 560 | 526 | 602 | 548 | 487 | 806 |
| *Cu* | | | | | | |
| *Ga* | | | | | | |
| *Nb* | 155 | 152 | 128 | 139 | 161 | 110 |
| *Ni* | 510 | 481 | 641 | 501 | 405 | 834 |
| *Pb* | | 21 | 15 | 15 | 22 | 12 |
| *Rb* | 95 | 105 | 82.8 | 65.1 | 103 | 62.6 |
| *Sc* | 24.6 | 25.7 | 19.8 | 21.9 | 25 | 19.2 |
| *Sr* | 2090 | 4373 | 1492 | 1598 | 2958 | 1118 |
| *Th* | | | | | | |
| *U* | | | | | | |
| *V* | | 314 | 293 | 277 | 302 | 276 |
| *Y* | | 36 | 25.8 | 32.7 | 40.1 | 26.2 |
| *Zn* | | 130 | 106 | 117 | 136 | 115 |
| *Zr* | 450 | 441 | 376 | 387 | 497 | 376 |
| *La* | | | | | | |
| *Ce* | | | | | | |
| *Nd* | | | | | | |
| | | | | | | |
| *INAA* | | | | | | |
| *La* | 164 | 157 | 117 | 142 | 180 | 107 |
| *Ce* | 335 | 301 | 226 | 278 | 346 | 206 |
| *Nd* | 151 | 131 | 101 | 125 | 154 | 95.9 |
| *Sm* | 15.6 | 20.2 | 15.4 | 19 | 23.2 | 15.9 |
| *Eu* | 4.99 | 5.64 | 4.24 | 5.31 | 6.38 | 4.27 |
| *Tb* | 2.28 | 1.69 | 1.26 | 1.58 | 1.92 | 1.31 |
| *Yb* | 2.66 | 1.95 | 1.23 | 1.5 | 2 | 1.22 |
| *Lu* | 0.282 | 0.26 | 0.15 | 0.19 | 0.25 | 0.16 |
| *Ta* | 9.2 | 9.21 | 8.38 | 8.91 | 9.79 | 7.03 |
| *Th* | 20.2 | 20.9 | 16.4 | 19.9 | 22.6 | 14.6 |
| *U* | 5.56 | 5.58 | 4.42 | 5.46 | 5.87 | 4.49 |
| *Hf* | 11 | 10.5 | 8.94 | 9.09 | 11.3 | 8.36 |
| | | | | | | |
| *ISOTOPES* | | | | | | |
| *87Sr/86Sr* | 0.704676 | 0.705768 | 0.704966 | 0.704427 | 0.705623 | 0.70494 |
| *143Nd/144Nd* | | 0.512728 | 0.51273 | 0.51272 | | 0.512794 |
| *206Pb/204Pb* | | 19.1860 | 19.2020 | 19.1640 | 19.0960 | 19.2520 |
| *207Pb/204Pb* | | 15.6260 | 15.5790 | 15.6090 | 15.5610 | 15.5840 |
| *208Pb/204Pb* | | 38.9350 | 38.7640 | 38.7980 | 38.6720 | 38.8720 |

| *Sample* | 90-NM-1 | 90-NM-3 | 90-NM-4 |
|---|---|---|---|
| *Location* | Newcombe | Newcombe | Newcombe |
| *Rock type* | Mica Melanephelinite | Olivine Melanephelinite | Olivine Melanephelinite |
| *Lat* | 36°16'49" | 36°20'43" | 36°20'43" |
| *Long* | 108°42'10" | 108°38'29" | 108°41'21" |
| | | | |
| *SiO2* | 45.97 | 42.02 | 41.83 |
| *TiO2* | 3.23 | 3.65 | 3.41 |
| *Al2O3* | 8.02 | 8.33 | 7.48 |
| *Fe2O3* | 9.57 | 11.94 | 11.68 |
| *MnO* | 0.1 | 0.15 | 0.18 |
| *MgO* | 13.22 | 12.62 | 13.99 |
| *CaO* | 9.32 | 12.31 | 12.44 |
| *Na2O* | 0.87 | 2.51 | 2.42 |
| *K2O* | 5.26 | 1.59 | 1.65 |
| *P2O5* | 1.16 | 1.41 | 1.33 |
| *LOI* | 2.81 | 3.36 | 3.5 |
| *Total* | 99.53 | 99.89 | 99.91 |
| *Mg#* | **74.34** | **68.91** | **71.53** |
| | | | |
| *XRF* | | | |
| *Ba* | 1537 | 2437 | 2040 |
| *Co* | 55 | 63 | 57 |
| *Cr* | 339 | 454 | 489 |
| *Cu* | 75 | 83 | 77 |
| *Ga* | 18 | 14 | 12 |
| *Nb* | 77 | 122 | 115 |
| *Ni* | 381 | 263 | 382 |
| *Pb* | 14 | 21 | 15 |
| *Rb* | 129 | 73 | 63 |
| *Sc* | 9 | 12 | 19 |
| *Sr* | 1040 | 1660 | 1513 |
| *Th* | | | |
| *U* | | | |
| *V* | 258 | 354 | 287 |
| *Y* | 26 | 28 | 26 |
| *Zn* | 75 | 114 | 100 |
| *Zr* | 438 | 435 | 384 |
| *La* | | | |
| *Ce* | | | |
| *Nd* | | | |
| | | | |
| *INAA* | | | |
| *La* | 114 | 140 | 135 |
| *Ce* | 236 | 277 | 267 |
| *Nd* | 113 | 124 | 121 |
| *Sm* | 20.4 | 21.2 | 20.9 |
| *Eu* | 5.08 | 5.58 | 5.46 |
| *Tb* | 1.5 | 1.69 | 1.68 |
| *Yb* | 1.22 | 1.45 | 1.4 |
| *Lu* | 0.14 | 0.21 | 0.2 |
| *Th* | 23.8 | 28.8 | 27.3 |
| *U* | 7.38 | 8.44 | 7.49 |
| *Ta* | 5.37 | 7.2 | 6.97 |
| *Hf* | 11.1 | 10.1 | 9 |
| | | | |
| *ISOTOPES* | | | |
| *87Sr/86Sr* | 0.705377 | 0.705203 | 0.70514 |
| *143Nd/144Nd* | 0.512791 | 0.512804 | |
| *206Pb/204Pb* | | 19.192 | 19.183 |
| *207Pb/204Pb* | | 15.651 | 15.656 |
| *208Pb/204Pb* | | 39.009 | 39.039 |

| *Sample* | 90-SN-1 | 90-SN-2 | 90-SN-3 | 90-SN-4 | 90-SN-5 | 90-SN-6 |
|---|---|---|---|---|---|---|
| *Location* | Black Point | Black Point | Black Point | Black Point | Chinese peak | Chinese peak |
| *Rock Type* | Shoshonite | Shoshonite | Shoshonite | Shoshonit | Mugearite | Mugearite |
| *Lat* | 37°14'23" | 37°14'23" | 37°14'23" | 37°14'23" | 37°13'13" | 37°13'13" |
| *Long* | 119°15'26" | 119°15'26" | 119°15'26" | 119°15'26" | 119°09'13" | 119°09'13" |
| *SiO2* | 51.12 | 51.28 | 51.26 | 51.18 | 54.46 | 54.34 |
| *TiO2* | 1.37 | 1.38 | 1.39 | 1.36 | 1.47 | 1.48 |
| *Al2O3* | 12.46 | 12.56 | 12.56 | 12.36 | 12.8 | 12.68 |
| *Fe2O3* | 9.79 | 9.69 | 9.71 | 9.69 | 9.17 | 9.25 |
| *MnO* | 0.15 | 0.14 | 0.15 | 0.14 | 0.14 | 0.14 |
| *MgO* | 10.26 | 9.95 | 9.73 | 10.25 | 7.67 | 7.93 |
| *CaO* | 8.27 | 8.22 | 8.28 | 8.14 | 7.68 | 7.74 |
| *Na2O* | 2.42 | 2.45 | 2.4 | 2.31 | 3.02 | 3.02 |
| *K2O* | 3.52 | 3.67 | 3.66 | 3.66 | 2.57 | 2.55 |
| *P2O5* | 0.57 | 0.58 | 0.58 | 0.57 | 0.47 | 0.45 |
| *LOI* | -0.4 | -0.18 | -0.05 | 0 | 0.38 | 0.2 |
| *Total* | 99.53 | 99.74 | 99.67 | 99.66 | 99.83 | 99.78 |
| *Mg#* | **68.73** | **68.29** | **67.76** | **68.93** | **63.69** | **64.26** |
| *XRF* | | | | | | |
| *Ba* | 1241 | 1328 | 1243 | 1251 | 1024 | 916 |
| *Co* | 45 | 39 | 45 | 46 | 41 | 43 |
| *Cr* | 570 | 531 | 573 | 556 | 386 | 378 |
| *Cu* | 41 | 43 | 43 | 38 | 43 | 43 |
| *Ga* | 16 | 19 | 1 | 19 | 17 | 18 |
| *Nb* | 15 | 17 | 15 | 16 | 20 | 21 |
| *Ni* | 212 | 203 | 213 | 199 | 222 | 201 |
| *Pb* | 13 | 14 | 14 | 11 | 10 | 11 |
| *Rb* | 121 | 138 | 139 | 132 | 74 | 73 |
| *Sc* | 17 | 15 | 17 | 15 | 15 | 14 |
| *Sr* | 718 | 734 | 730 | 722 | 734 | 720 |
| *Th* | | 8 | 18 | 12 | 7 | |
| *U* | | 3 | 4 | 6 | 3 | |
| *V* | 160 | 166 | 168 | 164 | 169 | 153 |
| *Y* | 20 | 21 | 22 | 20 | 21 | 19 |
| *Zn* | 88 | 91 | 92 | 93 | 90 | 86 |
| *Zr* | 195 | 200 | 200 | 191 | 179 | 174 |
| *La* | | 39 | 35 | 30 | 30 | |
| *Ce* | | 106 | 67 | 91 | 68 | |
| *Nd* | | 43 | 43 | 44 | 35 | |
| *INAA* | | | | | | |
| *La* | 34.6 | | | | | 31 |
| *Ce* | 72.6 | | - | | | 65.8 |
| *Nd* | 46.2 | | | | | 35.3 |
| *Sm* | 8.43 | | | | | 6.65 |
| *Eu* | 2.24 | | | | | 1.89 |
| *Tb* | 0.95 | | | | | 0.72 |
| *Yb* | 1.48 | | | | | 1.43 |
| *Lu* | 0.21 | | | | | 0.24 |
| *Th* | 12 | | | | | 7.89 |
| *U* | 5.08 | | | | | 2.47 |
| *Ta* | 1.05 | | | | | 1.26 |
| *Hf* | 5 | | | | | 4.59 |
| *ISOTOPES* | | | | | | |
| $^{87}Sr/^{86}Sr$ | 0.705246 | | 0.705253 | | | 0.705217 |
| $^{143}Nd/^{144}Nd$ | 0.512609 | | | | | 0.512703 |
| $^{206}Pb/^{204}Pb$ | 19.1340 | | | | | 19.2147 |
| $^{207}Pb/^{204}Pb$ | 15.6319 | | | | | 15.6867 |
| $^{208}Pb/^{204}Pb$ | 38.8127 | | | | | 38.9882 |

| *Sample* | 90-SN-7 | 90-SN-9 | 90-SN-17 | 90-SN-18 | 90-SN-19 | 90-SN-20 |
|---|---|---|---|---|---|---|
| *Location* | Chinese Peak | Chinese peak | Big Creek | Big Creek | Red Mtn | Red Mtn |
| *Rock Type* | Mugearite | Mugearite | Andestite | Mugearite | Mugearite | Basaltic Andestite |
| *Lat* | 37°13'13" | 37°13'13" | 37°14'10" | 37°14'10" | 37°11'54" | 37°11'54" |
| *Long* | 119°09'13" | 119°09'13" | 119°08'06" | 119°08'06" | 119°06'54" | 119°06'54" |
| *SiO2* | 53.89 | 54.61 | 60.2 | 54.64 | 55.85 | 56.66 |
| *TiO2* | 1.5 | 1.48 | 1.01 | 1.41 | 0.94 | 0.91 |
| *Al2O3* | 12.93 | 12.5 | 13.21 | 12.74 | 12.99 | 13.18 |
| *Fe2O3* | 9.36 | 9.14 | 6.56 | 8.29 | 7.8 | 7.8 |
| *MnO* | 0.13 | 0.14 | 0.11 | 0.16 | 0.12 | 0.12 |
| *MgO* | 7.85 | 7.73 | 4.8 | 6.47 | 8.33 | 7.47 |
| *CaO* | 7.47 | 7.79 | 5.84 | 8.68 | 7.3 | 7.23 |
| *Na2O* | 2.89 | 2.93 | 2.97 | 2.96 | 2.97 | 3.06 |
| *K2O* | 2.58 | 2.58 | 2.98 | 2.65 | 2.59 | 2.66 |
| *P2O5* | 0.45 | 0.45 | 0.29 | 0.41 | 0.3 | 0.31 |
| *LOI* | 0.58 | 0.3 | 1.54 | 1.56 | 0.46 | 0.55 |
| *Total* | 99.63 | 99.65 | 99.51 | 99.97 | 99.65 | 99.95 |
| *Mg#* | **63.75** | **63.95** | **60.54** | **62.07** | **69.13** | **66.76** |
| *XRF* | | | | | | |
| *Ba* | 929 | 934 | 998 | 862 | 946 | 973 |
| *Co* | 41 | 45 | 25 | 40 | 38 | 32 |
| *Cr* | 404 | 395 | 243 | 372 | 432 | 415 |
| *Cu* | 45 | 49 | 30 | 35 | 41 | 49 |
| *Ga* | 20 | 18 | 19 | 17 | 19 | 18 |
| *Nb* | 21 | 21 | 16 | 20 | 9 | 9 |
| *Ni* | 211 | 217 | 137 | 190 | 162 | 155 |
| *Pb* | 10 | 10 | 10 | 13 | 15 | 15 |
| *Rb* | 76 | 74 | 143 | 79 | 90 | 92 |
| *Sc* | 15 | 17 | 12 | 9 | 13 | 13 |
| *Sr* | 704 | 714 | 612 | 692 | 761 | 769 |
| *Th* | 2 | | 8 | | 7 | |
| *U* | 5 | | 4 | | 2 | |
| *V* | 169 | 163 | 109 | 178 | 135 | 133 |
| *Y* | 20 | 21 | 17 | 19 | 15 | 15 |
| *Zn* | 93 | 85 | 74 | 82 | 80 | 76 |
| *Zr* | 190 | 182 | 164 | 173 | 150 | 149 |
| *La* | 27 | | 33 | | 25 | |
| *Ce* | 52 | | 41 | | 50 | |
| *Nd* | 34 | | 27 | | 34 | |
| *INAA* | | | | | | |
| *La* | | 32.1 | | 29 | | 23 |
| *Ce* | | 64.7 | | 60.6 | | 44.8 |
| *Nd* | | 36 | | 31 | | 25.4 |
| *Sm* | | 6.6 | | 5.92 | | 4.86 |
| *Eu* | | 1.94 | | 1.74 | | 1.41 |
| *Tb* | | 0.76 | | 0.69 | | 0.55 |
| *Yb* | | 1.4 | | 1.43 | | 1.11 |
| *Lu* | | 0.21 | | 0.22 | | 0.14 |
| *Th* | | 8.28 | | 7.77 | | 7.31 |
| *U* | | 3.01 | | 4.34 | | 3.42 |
| *Ta* | | 1.28 | | 1.3 | | 0.71 |
| *Hf* | | 4.74 | | 4.34 | | 3.99 |
| *ISOTOPES* | | | | | | |
| $^{87}Sr/^{86}Sr$ | 0.70523 | 0.705149 | 0.706114 | 0.70529 | | 0.705295 |
| $^{143}Nd/^{144}Nd$ | 0.512616 | 0.512698 | 0.512546 | 0.512714 | | 0.512674 |
| $^{206}Pb/^{204}Pb$ | | 19.1692 | | 19.1765 | | 19.1247 |
| $^{207}Pb/^{204}Pb$ | | 15.6499 | | 15.6481 | | 15.6234 |
| $^{208}Pb/^{204}Pb$ | | 38.8894 | | 38.8886 | | 38.7864 |

| *Sample* | 90-SN-25 | 90-SN-34A | 90-SN-34B | 90-SN-34C | 90-SN-36A | 90-SN-37C | 90-SN-65 |
|---|---|---|---|---|---|---|---|
| *Location* | Brown Cone | Black Peak | Black Peak | Black Peak | Black Peak | Black Peak | Sugarloaf Hill |
| *Rock Type* | Mugearite | Trachy andestite | Trachy andestite | Trachy andestite | Trachy andestite | Trachy andesite | Basalt |
| *Lat* | 37°24'26" | 37°11'01" | 37°11'01" | 37°11'01" | 37°11'01" | 37°11'01" | 37°07'20" |
| *Long* | 119°13'53" | 119°03'01" | 119°03'01" | 119°03'01" | 119°03'01" | 119°03'01" | 119°23'32" |
| *SiO2* | 53.99 | 59.13 | 59.59 | 59.04 | 59.71 | 59.87 | 51.66 |
| *TiO2* | 1.44 | 0.88 | 0.87 | 0.91 | 0.89 | 0.87 | 0.99 |
| *Al2O3* | 13.44 | 15.32 | 15.46 | 15.22 | 15.33 | 15.37 | 13.79 |
| *Fe2O3* | 9.09 | 6.52 | 6.29 | 6.63 | 6.42 | 6.32 | 9.12 |
| *MnO* | 0.13 | 0.1 | 0.09 | 0.1 | 0.1 | 0.1 | 0.416 |
| *MgO* | 7.59 | 4.07 | 3.84 | 4 | 3.95 | 3.65 | 10.61 |
| *CaO* | 8.2 | 5.82 | 5.6 | 5.78 | 5.59 | 5.27 | 8.52 |
| *Na2O* | 2.64 | 3.74 | 3.81 | 3.7 | 3.83 | 3.8 | 2.84 |
| *K2O* | 2.52 | 3.32 | 3.38 | 3.31 | 3.35 | 3.44 | 2 |
| *P2O5* | 0.53 | 0.4 | 0.38 | 0.39 | 0.39 | 0.39 | 0.516 |
| *LOI* | 0.23 | 0.35 | 0.35 | 0.56 | 0.33 | 0.73 | 0.09 |
| *Total* | 99.8 | 99.65 | 99.66 | 99.64 | 99.89 | 99.81 | 100.462 |
| *Mg#* | **63.65** | **56.69** | **56.15** | **55.86** | **56.34** | **54.78** | **70.93** |
| *XRF* | | | | | | | |
| *Ba* | 1170 | 1286 | 1292 | 1309 | 1361 | 1299 | 891 |
| *Co* | 37 | 16 | 25 | 19 | 20 | 24 | 45 |
| *Cr* | 316 | 76 | 71 | 69 | 35 | 67 | 665 |
| *Cu* | 34 | 23 | 24 | 23 | 23 | 23 | 59 |
| *Ga* | 19 | 21 | 21 | 21 | 23 | 24 | 19 |
| *Nb* | 13 | 12 | 13 | 12 | 11 | 12 | 10.9 |
| *Ni* | 108 | 32 | 29 | 28 | 27 | 27 | 212 |
| *Pb* | 16 | 21 | 20 | 18 | 15 | 21 | 13 |
| *Rb* | 75 | 95 | 95 | 97 | 100 | 108 | 56.6 |
| *Sc* | 12 | 11 | 10 | 14 | 11 | 12 | 22 |
| *Sr* | 707 | 1040 | 1066 | 1037 | 1041 | 1055 | 849 |
| *Th* | | 8 | 8 | 6 | 10 | 13 | |
| *U* | | 5 | 6 | 6 | 3 | 3 | |
| *V* | 181 | 117 | 116 | 115 | 101 | 111 | 203 |
| *Y* | 20 | 15 | 15 | 15 | 14 | 15 | 19.6 |
| *Zn* | 84 | 84 | 86 | 83 | 77 | 80 | 89 |
| *Zr* | 147 | 189 | 191 | 185 | 185 | 181 | 151 |
| *La* | | 25 | 24 | 27 | 26 | 29 | |
| *Ce* | | | | | | | |
| *Nd* | | 31 | 37 | 30 | 30 | 34 | |
| *INAA* | | | | | | | |
| *La* | 31.6 | | | | | | 31.8 |
| *Ce* | 66.3 | | | | | | 64.7 |
| *Nd* | 35.6 | | | | | | 33.9 |
| *Sm* | 6.91 | | | | | | 6.36 |
| *Eu* | 1.93 | | | | | | 1.89 |
| *Tb* | 0.77 | | | | | | 0.74 |
| *Yb* | 1.49 | | | | | | 1.53 |
| *Lu* | 0.22 | | | | | | 0.24 |
| *Th* | 10 | | | | | | 9.87 |
| *U* | 3.48 | | | | | | 3.3 |
| *Ta* | 0.83 | | | | | | 0.6 |
| *Hf* | 4.02 | | | | | | 4.17 |
| *ISOTOPES* | | | | | | | |
| $^{87}Sr/^{86}Sr$ | 0.705241 | 0.705734 | | | | | 0.704804 |
| $^{143}Nd/^{144}Nd$ | | | | | | | |
| $^{206}Pb/^{204}Pb$ | 19.1692 | | | | | | |
| $^{207}Pb/^{204}Pb$ | 15.6662 | | | | | | |
| $^{208}Pb/^{204}Pb$ | 38.9355 | | | | | | |

| *Sample#* | 90-SN-21 | 90-SN-22 | 90-SN-29 | 90-SN-31 | 90-SN-33 |
|---|---|---|---|---|---|
| *Location* | Devils Table | Devils Table | Kaiser Diggings | West Kaiser | West Kaiser |
| *Rock Type* | Mugearite | Mugearite | Shoshonite | Shoshonite | Shoshonite |
| *Lat* | 37°20'26" | 37°20'26" | 37°22'47" | 37°20'39" | 37°20'39" |
| *Long* | 119°01'38" | 119°01'38" | 119°14'13" | 119°14'30" | 119°14'30" |
| *SiO2* | 52.1 | 52.07 | 50.96 | 50.35 | 50.4 |
| *TiO2* | 0.94 | 0.95 | 1.19 | 1.39 | 1.39 |
| *Al2O3* | 14.44 | 14.36 | 12.84 | 12.09 | 11.99 |
| *Fe2O3* | 7.51 | 7.48 | 7.48 | 9.06 | 9.02 |
| *MnO* | 0.11 | 0.12 | 0.12 | 0.13 | 0.14 |
| *MgO* | 10.04 | 10.16 | 10.47 | 9.85 | 9.93 |
| *CaO* | 7.83 | 7.8 | 8.35 | 8.1 | 8.15 |
| *Na2O* | 3.14 | 3.11 | 2.4 | 2.66 | 2.56 |
| *K2O* | 2.88 | 2.92 | 4.66 | 4.72 | 4.79 |
| *P2O5* | 0.48 | 0.48 | 0.88 | 1.22 | 1.23 |
| *LOI* | 0.15 | 0.15 | 0.25 | 0.13 | 0.03 |
| *Total* | 99.62 | 99.6 | 99.6 | 99.7 | 99.63 |
| *Mg#* | **73.71** | **74.02** | **74.59** | **69.51** | **69.78** |
| *XRF* | | | | | |
| *Ba* | 1842 | 1834 | 2930 | 2521 | 2624 |
| *Co* | 38 | 36.7 | 37.5 | 40.3 | 43 |
| *Cr* | 314 | 338 | 428 | 536 | 537 |
| *Cu* | 47 | 46 | 65 | 64 | 64 |
| *Ga* | 14 | 15 | 18 | 15 | 16 |
| *Nb* | 9 | 7 | 9 | 15 | 15 |
| *Ni* | 263 | 274 | 239 | 183 | 198 |
| *Pb* | 18 | 19 | 17 | 14 | 14 |
| *Rb* | 44 | 44 | 76 | 97 | 96 |
| *Sc* | 10 | 16 | 15 | 12 | 15 |
| *Sr* | 1387 | 1467 | 2056 | 1392 | 1370 |
| *Th* | 1 | | | | 1 |
| *U* | 3 | | | | <1 |
| *V* | 146 | 147 | 174 | 181 | 178 |
| *Y* | 15 | 17 | 17 | 18 | 18 |
| *Zn* | 64 | 69 | 74 | 90 | 96 |
| *Zr* | 181 | 189 | 327 | 230 | 232 |
| *Lu* | 44 | | | | 37 |
| *Ce* | 80 | | | | 75 |
| *Nd* | 42 | | | | 36 |
| *INAA* | | | | | |
| *La* | | 42.6 | 64.8 | 35 | |
| *Ce* | | 83.2 | 127 | 74.2 | |
| *Nd* | | 32.9 | 64.7 | 40.6 | |
| *Sm* | | 6.27 | 9.44 | 7.39 | |
| *Eu* | | 1.62 | 2.25 | 1.97 | |
| *Tb* | | 0.58 | 0.67 | 0.74 | |
| *Yb* | | 1.46 | 1.38 | 1.49 | |
| *Lu* | | 0.24 | 0.21 | 0.23 | |
| *Th* | | 7 | 7.72 | 3.2 | |
| *U* | | 2.04 | 2.45 | 0.66 | |
| *Ta* | | 0.5 | 0.56 | 0.75 | |
| *Hf* | | 4.38 | 8.28 | 6.08 | |
| *ISOTOPES* | | | | | |
| $^{87}Sr/^{86}Sr$ | 0.706263 | 0.70629 | 0.706687 | 0.706668 | 0.706672 |
| $^{143}Nd/^{144}Nd$ | | 0.512421 | 0.512337 | 0.512299 | |
| $^{206}Pb/^{204}Pb$ | | 18.9912 | 18.8737 | 18.9089 | |
| $^{207}Pb/^{204}Pb$ | | 15.6637 | 15.5986 | 15.6229 | |
| $^{208}Pb/^{204}Pb$ | | 38.8767 | 38.6858 | 38.7585 | |

| *Sample#* | 90-SN-39A | 90-SN-40 | 90-SN-42 | 90-SN-43 | 90-SN-44 | 90-SN-45 |
|---|---|---|---|---|---|---|
| *Location* | Warm Creek Mdw | Warm Creek Mdw | Vermillion | Vermillion | Vermillion | Vermillion |
| *Rock Type* | Mugearite | Basalt | Shoshonite | Shoshonite | Shoshonite | Shoshonite |
| *Lat* | 37°22'44" | 37°22'44" | 37°23'24" | 37°23'25" | 37°23'26" | 37°23'27" |
| *Long* | 119°01'33" | 119°01'33" | 119°00'41" | 119°00'41" | 119°00'41" | 119°00'41" |
| *SiO2* | 50.48 | 46.93 | 51.69 | 51.73 | 54.54 | 53.48 |
| *TiO2* | 1.04 | 1.05 | 1.18 | 1.18 | 1.03 | 1.02 |
| *Al2O3* | 14.52 | 12.39 | 13.63 | 13.81 | 14.13 | 13.99 |
| *Fe2O3* | 8.19 | 10.02 | 8.13 | 8.13 | 6.79 | 7.13 |
| *MnO* | 0.14 | 0.17 | 0.11 | 0.13 | 0.1 | 0.09 |
| *MgO* | 10.07 | 13.11 | 9.98 | 9.78 | 7.86 | 9.32 |
| *CaO* | 8.22 | 11.02 | 7.68 | 7.71 | 6.84 | 6.85 |
| *Na2O* | 3.89 | 2.12 | 3.22 | 2.91 | 3.54 | 3.34 |
| *K2O* | 2.64 | 2.23 | 3.29 | 3.33 | 3.91 | 3.84 |
| *P2O5* | 0.81 | 0.87 | 0.65 | 0.66 | 0.63 | 0.64 |
| *LOI* | -0.03 | -0.25 | 0.05 | 0.53 | 0.28 | 0.05 |
| *Total* | 99.97 | 99.66 | 99.61 | 99.9 | 99.65 | 99.75 |
| *Mg#* | **72.06** | **73.29** | **72.02** | **71.61** | **70.83** | **73.27** |
| *XRF* | | | | | | |
| *Ba* | 1791 | 2043 | 2046 | 2199 | 2227 | 2230 |
| *Co* | 38 | 52 | 38.9 | 37 | 33 | 34.4 |
| *Cr* | 280 | 860 | 367 | 344 | 231 | 233 |
| *Cu* | 33 | 74 | 54 | 55 | 37 | 44 |
| *Ga* | 15 | 13 | 15 | 16 | 16 | 17 |
| *Nb* | 12 | 10 | 12 | 11 | 11 | 9 |
| *Ni* | 242 | 308 | 299 | 270 | 254 | 272 |
| *Pb* | 18 | 10 | 14 | 12 | 21 | 19 |
| *Rb* | 43 | 42 | 46 | 46 | 53 | 54 |
| *Sc* | 13 | 23 | 12 | 15 | 11 | 8 |
| *Sr* | 1609 | 1069 | 1582 | 1603 | 1837 | 1797 |
| *Th* | 7 | 1 | | 1 | 2 | |
| *U* | 3 | 1 | | 2 | 2 | |
| *V* | 149 | 194 | 155 | 156 | 135 | 130 |
| *Y* | 18 | 22 | 17 | 16 | 16 | 15 |
| *Zn* | 65 | 69 | 78 | 76 | 69 | 69 |
| *Zr* | 187 | 226 | 219 | 221 | 236 | 232 |
| *La* | 73 | 38 | | 50 | 55 | |
| *Ce* | 158 | 62 | | 103 | 103 | |
| *Nd* | 58 | 39 | | 57 | 49 | |
| *INAA* | | | | | | |
| *La* | | | 48.1 | | | 52.3 |
| *Ce* | | | 96.3 | | | 105 |
| *Nd* | | | 48.5 | | | 49.7 |
| *Sm* | | | 7.23 | | | 7.65 |
| *Eu* | | | 1.83 | | | 1.89 |
| *Tb* | | | 0.65 | | | 0.6 |
| *Yb* | | | 1.4 | | | 1.22 |
| *Lu* | | | 0.19 | | | 0.18 |
| *Th* | | | 6.08 | | | 6.79 |
| *U* | | | 1.75 | | | 2.16 |
| *Ta* | | | 0.62 | | | 0.58 |
| *Hf* | | | 5.52 | | | 6.18 |
| *ISOTOPES* | | | | | | |
| $^{87}Sr/^{86}Sr$ | | 0.706642 | 0.706293 | 0.706293 | 0.706347 | 0.706347 |
| $^{143}Nd/^{144}Nd$ | | | 0.512385 | | | 0.512368 |
| $^{206}Pb/^{204}Pb$ | | | 18.9002 | | | 18.8474 |
| $^{207}Pb/^{204}Pb$ | | | 15.6300 | | | 15.5766 |
| $^{208}Pb/^{204}Pb$ | | | 38.7866 | | | 38.6283 |

| *Sample#* | 90-SN-46 | 90-SN-47 | 90-SN-48 | 90-SN-49 | 90-SN-50A |
|---|---|---|---|---|---|
| *Location* | Onion-Spring Mdw | Onion-Spring Mdw | Onion-Spring Mdw | Volcanic Knob | Volcanic Knob |
| *Rock Type* | Mugearite | Mugearite | Basalt | Potassic Trachybasalt | Potassic Trachybasalt |
| *Lat* | 37°24'30" | 37°24'30" | 37°24'30" | 37°27'53" | 37°27'53" |
| *Long* | 119°04'24" | 119°04'24" | 119°04'24" | 118°53'22" | 118°53'22" |
| *SiO2* | 53.23 | 53.36 | 50.57 | 51.46 | 51.14 |
| *TiO2* | 1.02 | 1.02 | 1.19 | 1.16 | 1.14 |
| *Al2O3* | 15.25 | 15.25 | 14.17 | 14.53 | 14.22 |
| *Fe2O3* | 8.33 | 8.25 | 9.66 | 8.54 | 8.66 |
| *MnO* | 0.13 | 0.13 | 0.15 | 0.13 | 0.13 |
| *MgO* | 8.15 | 8.31 | 10.86 | 10.35 | 11.09 |
| *CaO* | 7.42 | 7.24 | 8.11 | 7.78 | 7.64 |
| *Na2O* | 3.54 | 3.53 | 2.86 | 3.38 | 3.36 |
| *K2O* | 2.24 | 2.24 | 1.9 | 2.07 | 1.99 |
| *P2O5* | 0.46 | 0.46 | 0.49 | 0.5 | 0.49 |
| *LOI* | -0.08 | -0.2 | -0.38 | -0.2 | -0.2 |
| *Total* | 99.69 | 99.59 | 99.58 | 99.7 | 99.66 |
| *Mg#* | **67.23** | **67.87** | **70.22** | **71.76** | **72.87** |
| *XRF* | | | | | |
| *Ba* | 1552 | 1543 | 1396 | 1128 | 1127 |
| *Co* | 40 | 34.2 | 46 | 33 | 39 |
| *Cr* | 248 | 235 | 400 | 318 | 341 |
| *Cu* | 47 | 56 | 49 | 33 | 36 |
| *Ga* | 14 | 16 | 15 | 18 | 15 |
| *Nb* | 9 | 9 | 10 | 9 | 11 |
| *Ni* | 226 | 203 | 288 | 304 | 348 |
| *Pb* | 13 | 10 | 8 | 6 | 7 |
| *Rb* | 30 | 31 | 31 | 34 | 31 |
| *Sc* | 15 | 13 | 17 | 15 | 11 |
| *Sr* | 1167 | 1163 | 891 | 1178 | 1135 |
| *Th* | 1 | | 2 | 1 | 4 |
| *U* | 3 | | 2 | 2 | <1 |
| *V* | 137 | 137 | 145 | 136 | 145 |
| *Y* | 20 | 20 | 22 | 17 | 17 |
| *Zn* | 75 | 77 | 76 | 66 | 73 |
| *Zr* | 165 | 169 | 175 | 149 | 142 |
| *La* | 28 | | 20 | 30 | 43 |
| *Ce* | 55 | | 61 | 59 | 65 |
| *Nd* | 34 | | 27 | 34 | 43 |
| *INAA* | | | | | |
| *La* | | 30.2 | | | |
| *Ce* | | 62.8 | | | |
| *Nd* | | 28 | | | |
| *Sm* | | 5.91 | | | |
| *Eu* | | 1.62 | | | |
| *Tb* | | 0.59 | | | |
| *Yb* | | 1.78 | | | |
| *Lu* | | 0.25 | | | |
| *Th* | | 3.87 | | | |
| *U* | | 1.46 | | | |
| *Ta* | | 0.53 | | | |
| *Hf* | | 4.25 | | | |
| *ISOTOPES* | | | | | |
| $^{87}Sr/^{86}Sr$ | 0.70637 | 0.706407 | | 0.706337 | |
| $^{143}Nd/^{144}Nd$ | | 0.512414 | | | |
| $^{206}Pb/^{204}Pb$ | | 18.9641 | | | |
| $^{207}Pb/^{204}Pb$ | | 15.6184 | | | |
| $^{208}Pb/^{204}Pb$ | | 38.7496 | | | |

| *Sample#* | 90-SN-51 | 90-SN-52 | 90-SN-53 | 90-SN-54 | 90-SN-55 | 90-SN-56 |
|---|---|---|---|---|---|---|
| *Location* | Volcanic Knob | SW Volcanic Knob | Vermillion | S. Saddle Mtn | S. Saddle Mtn | Saddle Mtn peak |
| *Rock Type* | Potassic Trachybasalt | Basalt | Shoshonite | Potassic Trachybasalt | Potassic Trachybasalt | Potassic Trachybasalt |
| *Lat* | 37°27'53" | 37°23'30" | 37°23'40" | 37°25'15" | 37°25'15" | 37°26'17" |
| *Long* | 118°53'22" | 118°53'42" | 119°00"42" | 119°02'25" | 119°02'25" | 119°02'30" |
| *SiO2* | 51.4 | 47.63 | 54.21 | 50.71 | 50.79 | 49.78 |
| *TiO2* | 0.95 | 1.38 | 1.03 | 1.47 | 1.43 | 1.51 |
| *Al2O3* | 14.07 | 13.86 | 14.24 | 14.62 | 14.28 | 13.7 |
| *Fe2O3* | 8.11 | 10.05 | 6.87 | 11.27 | 11.52 | 11.38 |
| *MnO* | 0.14 | 0.17 | 0.11 | 0.14 | 0.14 | 0.15 |
| *MgO* | 11.21 | 11.23 | 8.39 | 6.78 | 7.38 | 9.11 |
| *CaO* | 8.2 | 10.26 | 6.86 | 8.67 | 8.66 | 8.4 |
| *Na2O* | 3.31 | 2.41 | 3.56 | 2.58 | 2.56 | 2.61 |
| *K2O* | 2.06 | 2.07 | 3.88 | 2.75 | 2.71 | 2.75 |
| *P2O5* | 0.48 | 0.79 | 0.65 | 0.64 | 0.59 | 0.64 |
| *LOI* | 0.03 | -0.08 | -0.05 | -0.05 | -0.48 | -0.5 |
| *Total* | 99.96 | 99.77 | 99.75 | 99.58 | 99.58 | 99.53 |
| *Mg#* | **74.35** | **70.09** | **71.92** | **55.78** | **57.33** | **62.67** |
| *XRF* | | | | | | |
| *Ba* | 1232 | 1495 | 2220 | 1682 | 1767 | 1870 |
| *Co* | 39.6 | 44 | 37 | 42 | 40 | 50 |
| *Cr* | 417 | 469 | 240 | 204 | 216 | 329 |
| *Cu* | 42 | 57 | 47 | 82 | 78 | 107 |
| *Ga* | 15 | 15 | 16 | 19 | 18 | 17 |
| *Nb* | 10 | 11 | 9 | 8 | 6 | 9 |
| *Ni* | 335 | 217 | 237 | 97 | 112 | 172 |
| *Pb* | 11 | 10 | 18 | 13 | 10 | 13 |
| *Rb* | 32 | 50 | 55 | 36 | 38 | 44 |
| *Sc* | 13 | 18 | 12 | 18 | 18 | 18 |
| *Sr* | 1110 | 1020 | 1863 | 861 | 855 | 914 |
| *Th* | | | 1 | 1 | 1 | 1 |
| *U* | | | <1 | <1 | <1 | 2 |
| *V* | 136 | 185 | 135 | 197 | 201 | 181 |
| *Y* | 19 | 24 | 15 | 21 | 20 | 17 |
| *Zn* | 68 | 74 | 69 | 89 | 90 | 84 |
| *Zr* | 141 | 208 | 231 | 221 | 204 | 214 |
| *La* | | | 43 | 21 | 13 | 15 |
| *Ce* | | | 108 | 67 | 29 | 44 |
| *Nd* | | | 53 | 34 | 23 | 31 |
| *INAA* | | | | | | |
| *La* | 43.6 | 38.3 | | | | |
| *Ce* | 89.4 | 78.8 | | | | |
| *Nd* | 36.7 | 45 | - | | | |
| *Sm* | 6.13 | 7.46 | | | | |
| *Eu* | 1.62 | 2.05 | | | | |
| *Tb* | 0.59 | 0.8 | | | | |
| *Yb* | 1.43 | 2.03 | | | | |
| *Lu* | 0.23 | 0.32 | | | | |
| *Th* | 6.4 | 4.57 | | | | |
| *U* | 1.67 | 1.12 | | | | |
| *Ta* | 0.56 | 0.74 | | | | |
| *Hf* | 3.4 | 5.04 | | | | |
| *ISOTOPES* | | | | | | |
| $^{87}Sr/^{86}Sr$ | 0.70668 | 0.706187 | | | 0.706223 | |
| $^{143}Nd/^{144}Nd$ | 0.512338 | 0.512489 | | | | |
| $^{206}Pb/^{204}Pb$ | | 18.9853 | | | | |
| $^{207}Pb/^{204}Pb$ | | 15.6638 | | | | |
| $^{208}Pb/^{204}Pb$ | | 38.8969 | | | | |

| *Sample#* | 90-SN-57 | 90-SN-58 | 90-SN-59 | 90-SN-60 | 90-SN-61 | 90-SN-62 |
|---|---|---|---|---|---|---|
| *Location* | Saddle Mtn peak | Saddle Mtn peak | Hedrick Mdw | Hedrick Mdw | Hedrick Mdw | Hedrick Mdw |
| *Rock Type* | Potassic Trachybasalt | Potassic Trachybasalt | Potassic Trachybasalt | Potassic Trachybasalt | Potassic Trachybasalt | Potassic Trachybasalt |
| *Lat* | 37°26'17" | 37°26'17" | 37°25'23" | 37°25'23" | 37°25'23" | 37°25'56" |
| *Long* | 119°02'30" | 119°02'30" | 119°03'27" | 119°03'27" | 119°03'27" | 119°03'12" |
| *SiO2* | 50.66 | 49.91 | 50.04 | 50.69 | 49.32 | 48.43 |
| *TiO2* | 1.44 | 1.54 | 1.51 | 1.44 | 1.52 | 1.4 |
| *Al2O3* | 14.1 | 14.32 | 13.95 | 14.63 | 14.18 | 14.64 |
| *Fe2O3* | 11.7 | 10.86 | 11.17 | 9.32 | 8.46 | 9.33 |
| *MnO* | 0.16 | 0.15 | 0.14 | 0.13 | 0.14 | 0.16 |
| *MgO* | 8.32 | 8.27 | 8.66 | 8.64 | 9.85 | 10.08 |
| *CaO* | 8.57 | 8.68 | 8.45 | 8.18 | 8.85 | 9.1 |
| *Na2O* | 2.62 | 2.69 | 2.62 | 2.89 | 2.69 | 3.26 |
| *K2O* | 2.65 | 2.87 | 2.81 | 3 | 2.73 | 2.42 |
| *P2O5* | 0.59 | 0.67 | 0.64 | 0.69 | 0.75 | 0.95 |
| *LOI* | -0.23 | -0.3 | -0.4 | 0.05 | 0.35 | 0.05 |
| *Total* | 100.58 | 99.66 | 99.59 | 99.66 | 98.84 | 99.82 |
| *Mg#* | **59.86** | **61.49** | **61.92** | **66.03** | **70.95** | **69.38** |
| *XRF* | | | | | | |
| *Ba* | 1767 | 1892 | 1777 | 1976 | 1940 | 1999 |
| *Co* | 46 | 47 | 42 | 38 | 39.7 | 42 |
| *Cr* | 277 | 279 | 320 | 280 | 322 | 268 |
| *Cu* | 160 | 80 | 56 | 53 | 56 | 46 |
| *Ga* | 18 | 18 | 18 | 18 | 16 | 14 |
| *Nb* | 8 | 8 | 8 | 14 | 15 | 19 |
| *Ni* | 125 | 145 | 165 | 175 | 232 | 201 |
| *Pb* | 9 | 15 | 7 | 12 | 14 | 16 |
| *Rb* | 37 | 46 | 44 | 45 | 80 | 51 |
| *Sc* | 13 | 17 | 17 | 17 | 23 | 19 |
| *Sr* | 847 | 957 | 898 | 1132 | 1223 | 1572 |
| *Th* | 1 | 2 | 1 | 1 | | 8 |
| *U* | <1 | <1 | <1 | <1 | | 2 |
| *V* | 182 | 191 | 194 | 169 | 181 | 168 |
| *Y* | 21 | 19 | 19 | 21 | 22 | 25 |
| *Zn* | 25 | 84 | 91 | 72 | 78 | 67 |
| *Zr* | 204 | 214 | 214 | 246 | 241 | 278 |
| *La* | 20 | 22 | 18 | 37 | | 63 |
| *Ce* | 69 | 55 | 24 | 71 | | 131 |
| *Nd* | 35 | 33 | 25 | 37 | | 58 |
| *INAA* | | | | | | |
| *La* | | | | | 33.4 | |
| *Ce* | | | | | 70.6 | |
| *Nd* | | - | | | 38 | |
| *Sm* | | | | | 7.02 | |
| *Eu* | | | | | 1.97 | |
| *Tb* | | | | | 0.79 | |
| *Yb* | | | | | 1.76 | |
| *Lu* | | | | | 0.25 | |
| *Th* | | | | | 3.05 | |
| *U* | | | | | 1.2 | |
| *Ta* | | | | | 0.89 | |
| *Hf* | | | | | 5.9 | |
| *ISOTOPES* | | | | | | |
| $^{87}Sr/^{86}Sr$ | | 0.706253 | | | | |
| $^{143}Nd/^{144}Nd$ | | | | | | |
| $^{206}Pb/^{204}Pb$ | | | | | 18.8839 | |
| $^{207}Pb/^{204}Pb$ | | | | | 15.6439 | |
| $^{208}Pb/^{204}Pb$ | | | | | 38.8503 | |

| *Sample#* | 90-SN-63 | 90-SN-64 | 91-SN-66 | 91-SN-68 | 91-SN-69 |
|---|---|---|---|---|---|
| *Location* | Hedrick Mdw | Hedrick Mdw | Coolidge Mdw | Hoffman Mtn | Lt. Rancheria Cr. |
| *Rock Type* | Potassic Trachybasalt | Potassic Trachybasalt | Potassic Trachybasalt | Basalt | Basalt |
| *Lat* | 37°25'56" | 37°25'56" | 37°00'02" | 36°59'31" | 36°58'17" |
| *Long* | 119°03'12" | 119°03'12" | 118°56'38" | 118°56'42" | 118°57'02" |
| *SiO2* | 48.01 | 48.15 | 49.57 | 47.42 | 45.27 |
| *TiO2* | 1.37 | 1.37 | 0.986 | 0.938 | 1.097 |
| *Al2O3* | 14.77 | 14.6 | 13.13 | 12.72 | 13.26 |
| *Fe2O3* | 9.31 | 9.34 | 8.65 | 9.38 | 10.01 |
| *MnO* | 0.16 | 0.15 | 0.141 | 0.15 | 0.168 |
| *MgO* | 9.79 | 10.1 | 12.55 | 14.55 | 13.15 |
| *CaO* | 9.14 | 9.17 | 8.69 | 10.5 | 11.17 |
| *Na2O* | 3.41 | 3.24 | 3.35 | 2.18 | 3.05 |
| *K2O* | 2.74 | 2.39 | 2.24 | 1.42 | 1.83 |
| *P2O5* | 1.02 | 1.01 | 0.578 | 0.551 | 0.838 |
| *LOI* | 0.08 | 0.15 | 0.21 | -0.07 | -0.006 |
| *Total* | 99.8 | 99.67 | 99.885 | 99.809 | 99.843 |
| *Mg#* | **68.80** | **69.40** | **75.26** | **76.49** | **73.37** |
| *XRF* | | | | | |
| *Ba* | 2085 | 2073 | 2054 | 1742 | 2288 |
| *Co* | 41 | 39 | 44 | 48 | 49 |
| *Cr* | 259 | 270 | 685 | 1363 | 804 |
| *Cu* | 41 | 45 | 59 | 70 | 79 |
| *Ga* | 14 | 15 | 17 | 14 | 17 |
| *Nb* | 17 | 19 | 9.6 | 8.2 | 11.4 |
| *Ni* | 193 | 216 | 280 | 371 | 314 |
| *Pb* | 15 | 11 | 17 | 10 | 22 |
| *Rb* | 40 | 67 | 67.9 | 35.9 | 32.2 |
| *Sc* | 19 | 18 | 19 | 30 | 24 |
| *Sr* | 1641 | 1634 | 1516 | 976 | 1791 |
| *Th* | 8 | 2 | 5 | 3 | |
| *U* | <1 | 3 | 0 | 0 | |
| *V* | 186 | 187 | 214 | 199 | 229 |
| *Y* | 26 | 27 | 16.1 | 19.4 | 24.4 |
| *Zn* | 70 | 67 | 58 | 72 | 89 |
| *Zr* | 288 | 285 | 204 | 136 | 202 |
| *La* | 73 | 65 | | | |
| *Ce* | 135 | 143 | | | |
| *Nd* | 57 | 56 | | | |
| *INAA* | | | | | |
| *La* | | | | | 63.4 |
| *Ce* | | | | | 126 |
| *Nd* | | | - | | 61.5 |
| *Sm* | | | | | 9.26 |
| *Eu* | | | | | 2.42 |
| *Tb* | | | | | 0.85 |
| *Yb* | | | | | 1.99 |
| *Lu* | | | | | 0.33 |
| *Th* | | | | | 6.15 |
| *U* | | | | | 1.94 |
| *Ta* | | | | | 0.5 |
| *Hf* | | | | | 5.14 |
| *ISOTOPES* | | | | | |
| $^{87}Sr/^{86}Sr$ | | | | | 0.706866 |
| $^{143}Nd/^{144}Nd$ | | | | | 0.512288 |
| $^{206}Pb/^{204}Pb$ | | | | | |
| $^{207}Pb/^{204}Pb$ | | | | | |
| $^{208}Pb/^{204}Pb$ | | | | | |

| *Sample#* | 91-SN-70 | 91-SN-71 | 91-SN-73 | 91-SN-74 | 91-SN-75 |
|---|---|---|---|---|---|
| *Location* | Lt. Rancheria Cr. | Lt. Rancheria Cr. | Woodchuck Lk. | Lk.Thomas Edison | Lk.Thomas Edison |
| *Rock Type* | Basalt | Basalt | Potassic Trachybasalt | Potassic Trachybasalt | Potassic Trachybasalt |
| *Lat* | 36°58'12" | 36°58'09" | 37°01'31" | 37°24'26" | 37°24'09" |
| *Long* | 118°57'28" | 118°57'25" | 118°53'22" | 118°57'40" | 118°57'40" |
| *SiO2* | 47.5 | 46.83 | 48.16 | 51.23 | 50 |
| *TiO2* | 1.331 | 1.209 | 1.042 | 1.202 | 1.093 |
| *Al2O3* | 14.11 | 12.8 | 13.57 | 16.31 | 15.61 |
| *Fe2O3* | 10.01 | 10.04 | 8.81 | 8.43 | 8.65 |
| *MnO* | 0.161 | 0.16 | 0.145 | 0.132 | 0.135 |
| *MgO* | 9.64 | 13.15 | 12.69 | 8.81 | 10.3 |
| *CaO* | 11.14 | 10.21 | 9.03 | 8.15 | 8.34 |
| *Na2O* | 3.11 | 3.04 | 2.91 | 3.58 | 3.37 |
| *K2O* | 1.39 | 0.93 | 2.67 | 2.25 | 2.09 |
| *P2O5* | 0.856 | 0.789 | 0.92 | 0.472 | 0.45 |
| *LOI* | 0.01 | 0.03 | 0.006 | 0.02 | 0.44 |
| *Total* | 99.248 | 99.158 | 99.947 | 100.566 | 100.038 |
| *Mg#* | **66.88** | **73.31** | **75.13** | **68.67** | **71.41** |
| *XRF* | | | | | |
| *Ba* | 2549 | 2351 | 2436 | 1214 | 1205 |
| *Co* | 49 | 49 | 41 | 36 | 40 |
| *Cr* | 804 | 1011 | 742 | 334 | 421 |
| *Cu* | 79 | 69 | 64 | 37 | 69 |
| *Ga* | 17 | 17 | 13 | 18 | 16 |
| *Nb* | 10.9 | 11.6 | 11.9 | 13.1 | 10.6 |
| *Ni* | 314 | 240 | 285 | 183 | 227 |
| *Pb* | 22 | 19 | 19 | 13 | 15 |
| *Rb* | 62.2 | 63.1 | 48.7 | 38.8 | 38.4 |
| *Sc* | 24 | 27 | 24 | 19 | 23 |
| *Sr* | 1729 | 1540 | 1532 | 1139 | 1130 |
| *Th* | 6 | 8 | | 5 | |
| *U* | 0 | 0 | | 0 | |
| *V* | 229 | 237 | 181 | 186 | 182 |
| *Y* | 22.8 | 20.9 | 21.8 | 20.5 | 19.3 |
| *Zn* | 89 | 85 | 73 | 75 | 77 |
| *Zr* | 195 | 192 | 229 | 158 | 145 |
| *La* | | | | | |
| *Ce* | | | | | |
| *Nd* | | | | | |
| *INAA* | | | | | |
| *La* | | | 48.6 | | 36 |
| *Ce* | | | 102 | | 75.5 |
| *Nd* | | | 51.4 | | 35.7 |
| *Sm* | | | 7.88 | | 5.58 |
| *Eu* | | | 2.25 | | 1.65 |
| *Tb* | | | 0.72 | | 0.64 |
| *Yb* | | | 1.69 | | 1.62 |
| *Lu* | | | 0.26 | | 0.25 |
| *Th* | | | 5.46 | | 5.07 |
| *U* | | | 1.84 | | 1.64 |
| *Ta* | | | 0.57 | | 0.58 |
| *Hf* | | | 5.98 | | 3.6 |
| *ISOTOPES* | | | | | |
| $^{87}Sr/^{86}Sr$ | | | 0.706576 | | 0.706532 |
| $^{143}Nd/^{144}Nd$ | | | 0.512341 | | 0.512352 |
| $^{206}Pb/^{204}Pb$ | | | | | |
| $^{207}Pb/^{204}Pb$ | | | | | |
| $^{208}Pb/^{204}Pb$ | | | | | |

| *Sample#* | 91-SN-76 | 91-SN-77 | 91-SN-78 | 91-SN-79 | 91-SN-80 |
|---|---|---|---|---|---|
| *Location* | Lk.Thomas Edison | S. Frog Lake | NW. Frog Lake | NW.Rock Creek Lk. | Fawn Mdw |
| *Rock Type* | Potassic Trachybasalt | Potassic Trachybasalt | Potassic Trachybasalt | Potassic Trachybasalt | Basalt |
| *Lat* | 37°23'40" | 37°26'58" | 37°23'43" | 37°28'25" | 37°25'56" |
| *Long* | 118°57'40" | 119°03'32" | 119°04'24" | 119°05'00" | 119°06'54" |
| *SiO2* | 50.84 | 50.41 | 50.11 | 49.76 | 47.36 |
| *TiO2* | 1.214 | 1.242 | 1.269 | 1.241 | 1.309 |
| *Al2O3* | 16.41 | 15.51 | 15.52 | 15.01 | 15.53 |
| *Fe2O3* | 8.53 | 8.18 | 8.29 | 8.61 | 9.08 |
| *MnO* | 0.132 | 0.13 | 0.132 | 0.136 | 0.154 |
| *MgO* | 8.58 | 9.61 | 10.05 | 11.03 | 9.62 |
| *CuO* | 8.29 | 8.15 | 8.13 | 7.88 | 9.25 |
| *Na2O* | 3.2 | 3.37 | 3.38 | 3.37 | 3.56 |
| *K2O* | 2.18 | 2.76 | 2.48 | 2.49 | 2.44 |
| *P2O5* | 0.479 | 0.772 | 0.756 | 0.742 | 1.108 |
| *LOI* | 0.59 | 0.07 | 0.17 | 0.06 | 0.02 |
| *Total* | 99.855 | 100.134 | 100.117 | 100.269 | 99.411 |
| *Mg#* | **67.84** | **71.13** | **71.77** | **72.88** | **68.96** |
| *XRF* | | | | | |
| *Ba* | 1259 | 1858 | 1932 | 1824 | 2150 |
| *Co* | 36 | 35 | 38 | 39 | 38 |
| *Cr* | 344 | 353 | 350 | 377 | 308 |
| *Cu* | 43 | 45 | 48 | 46 | 47 |
| *Ga* | 18 | 16 | 16 | 15 | 16 |
| *Nb* | 12.9 | 15.9 | 15.2 | 15.5 | 17.5 |
| *Ni* | 194 | 241 | 250 | 291 | 185 |
| *Pb* | 14 | 16 | 16 | 15 | 20 |
| *Rb* | 35.4 | 47 | 61.8 | 53.6 | 40.9 |
| *Sc* | 23 | 21 | 23 | 17 | 25 |
| *Sr* | 1157 | 1298 | 1328 | 1288 | 1794 |
| *Th* | 3 | 3 | 5 | 5 | 8 |
| *U* | 0 | 0 | 0 | 0 | 0 |
| *V* | 181 | 173 | 179 | 176 | 210 |
| *Y* | 21.1 | 20.4 | 21.6 | 21.5 | 27 |
| *Zn* | 80 | 67 | 70 | 71 | 76 |
| *Zr* | 160 | 251 | 255 | 248 | 305 |
| *La* | | | | | |
| *Ce* | | | | | |
| *Nd* | | | | | |
| *INAA* | | | | | |
| *La* | | | | | |
| *Ce* | | | | | |
| *Nd* | | | | | |
| *Sm* | | | | | |
| *Eu* | | | | | |
| *Tb* | | | | | |
| *Yb* | | | | | |
| *Lu* | | | | | |
| *Th* | | | | | |
| *U* | | | | | |
| *Ta* | | | | | |
| *Hf* | | | | | |
| *ISOTOPES* | | | | | |
| $^{87}Sr/^{86}Sr$ | | | | 0.706226 | |
| $^{143}Nd/^{144}Nd$ | | | | 0.512464 | |
| $^{206}Pb/^{204}Pb$ | | | | | |
| $^{207}Pb/^{204}Pb$ | | | | | |
| $^{208}Pb/^{204}Pb$ | | | | | |

| *Sample#* | 91-SN-81 | 91-SN-83 | 91-SN-83A | 91-SN-84 | 91-SN-86 | 91-SN-87 |
|---|---|---|---|---|---|---|
| *Location* | Soda Springs | Jackass Rock | Jackass Rock | Jackass Rock | Graveyard Cr. | Graveyard Cr. |
| *Rock Type* | Mugearite | Potassic Trachybasalt | Potassic Trachybasalt | Potassic Trachybasalt | Mugearite | Mugearite |
| *Lat* | 37°23'40" | 37°25'56" | 37°25'56" | 37°25'56" | 37°26'42" | 37°27'19" |
| *Long* | 119°22'51" | 119°17'40" | 119°17'40" | 119°17'40" | 119°18'12" | 119°18'14" |
| *SiO2* | 51.01 | 47.16 | 46.97 | 47.57 | 51.59 | 51.62 |
| *TiO2* | 1.354 | 1.191 | 1.127 | 1.174 | 1.327 | 1.224 |
| *Al2O3* | 16.39 | 12.96 | 12.33 | 13.02 | 15.67 | 15.61 |
| *Fe2O3* | 8.37 | 9.35 | 9.51 | 9.25 | 9.4 | 9.19 |
| *MnO* | 0.128 | 0.144 | 0.15 | 0.144 | 0.135 | 0.135 |
| *MgO* | 8.52 | 11.47 | 13.28 | 11.64 | 8.04 | 8.33 |
| *CaO* | 7.51 | 9 | 8.64 | 8.82 | 7.54 | 7.03 |
| *Na2O* | 3.63 | 3.42 | 3.21 | 3.5 | 3.6 | 3.56 |
| *K2O* | 2.29 | 3.59 | 3.06 | 3.29 | 2.24 | 2.33 |
| *P2O5* | 0.644 | 1.261 | 1.162 | 1.197 | 0.533 | 0.537 |
| *LOI* | 0.5 | 0.34 | 0.52 | 0.59 | 0.4 | 0.65 |
| *Total* | 99.846 | 99.546 | 99.439 | 99.605 | 100.075 | 99.566 |
| *Mg#* | 68.10 | 72.01 | 74.55 | 72.52 | 64.21 | 65.53 |
| *XRF* | | | | | | |
| *Ba* | 1387 | 2578 | 2520 | 2386 | 1627 | 1725 |
| *Co* | 35 | 43 | 49 | 44 | 41 | 37 |
| *Cr* | 299 | 513 | 540 | 513 | 312 | 339 |
| *Cu* | 42 | 72 | 68 | 69 | 48 | 46 |
| *Ga* | 18 | 13 | 15 | 16 | 19 | 19 |
| *Nb* | 18.6 | 14.9 | 14.3 | 15.8 | 12.4 | 13.1 |
| *Ni* | 212 | 298 | 393 | 309 | 204 | 213 |
| *Pb* | 12 | 17 | 18 | 17 | 13 | 13 |
| *Rb* | 33.9 | 101 | 85.3 | 65.3 | 35.7 | 38 |
| *Sc* | 16 | 22 | 23 | 18 | 17 | 19 |
| *Sr* | 1276 | 1771 | 1708 | 1696 | 1283 | 1228 |
| *Th* | | | 5 | 5 | 5 | 2 |
| *U* | | | 0 | 0 | 0 | 0 |
| *V* | 155 | 220 | 193 | 186 | 163 | 152 |
| *Y* | 23.2 | 22.1 | 19.8 | 20.5 | 22.9 | 29.6 |
| *Zn* | 72 | 111 | 110 | 112 | 81 | 80 |
| *Zr* | 212 | 159 | 152 | 158 | 191 | 196 |
| *La* | | | | | | |
| *Ce* | | | | | | |
| *Nd* | | | | | | |
| *INAA* | | | | | | |
| *La* | 48.2 | 57.2 | | 58.9 | | |
| *Ce* | 90.6 | 119 | | 121 | | |
| *Nd* | 42.5 | 57.8 | | 58 | | |
| *Sm* | 6.32 | 8.37 | | 8.47 | | |
| *Eu* | 1.88 | 2.28 | | 2.25 | | |
| *Tb* | 0.69 | 0.77 | | 0.8 | | |
| *Yb* | 1.83 | 1.74 | | 1.74 | | |
| *Lu* | 0.29 | 0.27 | | 0.27 | | |
| *Th* | 5.74 | 4.45 | | 4.58 | | |
| *U* | 1.79 | 1.41 | | 1.31 | | |
| *Ta* | 1.06 | 0.69 | | 0.73 | | |
| *Hf* | 4.6 | 3.92 | | 4.1 | | |
| *ISOTOPES* | | | | | | |
| $^{87}Sr/^{86}Sr$ | 0.706008 | 0.70673 | | 0.706761 | | |
| $^{143}Nd/^{144}Nd$ | 0.512385 | 0.512326 | | | | |
| $^{206}Pb/^{204}Pb$ | | | | | | |
| $^{207}Pb/^{204}Pb$ | | | | | | |
| $^{208}Pb/^{204}Pb$ | | | | | | |

| *Sample#* | 91-SN-87A | 91-SN-88 | 91-SN-89 | 91-SN-91 | 91-SN-91A | 91-SN-92 |
|---|---|---|---|---|---|---|
| *Location* | Graveyard Cr. | Graveyard Mdw | Squaw Dome | Squaw Dome | Squaw Dome | Granite Cr. |
| *Rock Type* | Mugearite | Mugearite | Shoshonite | Mugearite | Mugearite | Mugearite |
| *Lat* | 37°27'19" | 37°27'48" | 37°28'46" | 37°28'29" | 37°28'29" | 37°31'58" |
| *Long* | 119°18'14" | 119°17'46" | 119°15'41" | 119°15'38" | 119°15'38" | 119°16'02" |
| *SiO2* | 51.6 | 50.68 | 49.59 | 49.85 | 49.74 | 50.52 |
| *TiO2* | 1.22 | 1.375 | 1.47 | 1.014 | 1.016 | 1.606 |
| *Al2O3* | 15.61 | 15.09 | 13.85 | 13.76 | 13.76 | 15.47 |
| *Fe2O3* | 9.13 | 8.41 | 9.42 | 8.23 | 8.26 | 8.04 |
| *MnO* | 0.14 | 0.14 | 0.138 | 0.123 | 0.12 | 0.123 |
| *MgO* | 8.2 | 9.49 | 9.03 | 10.74 | 10.73 | 8.76 |
| *CaO* | 7.05 | 7.53 | 8.45 | 7.48 | 7.48 | 7.63 |
| *Na2O* | 3.55 | 3.51 | 3.66 | 3.84 | 3.86 | 3.57 |
| *K2O* | 2.34 | 2.57 | 3.87 | 3.64 | 3.69 | 3.26 |
| *P2O5* | 0.537 | 0.746 | 0.931 | 0.973 | 0.971 | 0.93 |
| *LOI* | 0.62 | 0.44 | 0.89 | 0.15 | 0..14 | 0.18 |
| *Total* | 99.377 | 99.541 | 100.409 | 99.65 | 99.627 | 99.909 |
| *Mg#* | **65.32** | **70.30** | **66.78** | **73.24** | **73.15** | **69.56** |
| *XRF* | | | | | | |
| *Ba* | 1697 | 1929 | 2597 | 2328 | 2262 | 2171 |
| *Co* | 39 | 37 | 39 | 37 | 38 | 33 |
| *Cr* | 349 | 420 | 400 | 458 | 468 | 303 |
| *Cu* | 47 | 54 | 72 | 58 | 59 | 52 |
| *Ga* | 19 | 16 | 15 | 15 | 16 | 18 |
| *Nb* | 13 | 17.9 | 14.6 | 14.4 | 13.9 | 22.7 |
| *Ni* | 227 | 234 | 151 | 307 | 295 | 206 |
| *Pb* | 16 | 16 | 15 | 17 | 17 | 17 |
| *Rb* | 38.9 | 37.4 | 61.4 | 61.8 | 57.9 | 56.4 |
| *Sc* | 16 | 18 | 22 | 18 | 17 | 17 |
| *Sr* | 1251 | 1348 | 1273 | 1387 | 1386 | 1661 |
| *Th* | 5 | 4 | | 6 | 4 | 6 |
| *U* | 0 | 0 | | 0 | 0 | 0 |
| *V* | 162 | 181 | 223 | 171 | 180 | 171 |
| *Y* | 34.1 | 23 | 19.6 | 17.6 | 17.5 | 21.1 |
| *Zn* | 83 | 83 | 109 | 97 | 97 | 75 |
| *Zr* | 200 | 240 | 180 | 164 | 163 | 329 |
| *La* | | | | | | |
| *Ce* | | | | | | |
| *Nd* | | | | | | |
| *INAA* | | | | | | |
| *La* | | | 42.1 | | | |
| *Ce* | | | 91.3 | | | |
| *Nd* | | | 48.2 | | | |
| *Sm* | | | 7.58 | | | |
| *Eu* | | | 2.06 | | | |
| *Tb* | | | 0.78 | | | |
| *Yb* | | | 1.63 | | | |
| *Lu* | | | 0.25 | | | |
| *Th* | | | 4.23 | | | |
| *U* | | | 1.29 | | | |
| *Ta* | | | 0.77 | | | |
| *Hf* | | | 4.84 | | | |
| *ISOTOPES* | | | | | | |
| $^{87}Sr/^{86}Sr$ | | | 0.706604 | 0.706626 | | 0.706128 |
| $^{143}Nd/^{144}Nd$ | | | | | | |
| $^{206}Pb/^{204}Pb$ | | | | | | |
| $^{207}Pb/^{204}Pb$ | | | | | | |
| $^{208}Pb/^{204}Pb$ | | | | | | |

| *Sample#* | 91-SN-94 | 91-SN-95 | 91-SN-96 | 91-SN-97 | 91-SN-98 | 91-SN-99 |
|---|---|---|---|---|---|---|
| *Location* | Bowler Camp | Bowler Camp | Cora lakes | Cora lakes | Cora lakes | Cora lakes |
| *Rock Type* | Mugearite | Mugearite | Shoshonite | Shoshonite | Shoshonite | Mugearite |
| *Lat* | 37°30'41" | 37°30'41" | 37°35'30" | 37°35'30" | 37°35'22" | 37°35'22" |
| *Long* | 119°18'11" | 119°18'32" | 119°15'52" | 119°15'50" | 119°15'50" | 119°15'50" |
| *SiO2* | 52.98 | 51.76 | 53.05 | 51.23 | 53.19 | 52.23 |
| *TiO2* | 1.1 | 1.116 | 0.924 | 1.479 | 0.944 | 1.005 |
| *Al2O3* | 16.25 | 16.67 | 15.11 | 15.14 | 15.16 | 14.83 |
| *Fe2O3* | 7.47 | 7.66 | 6.88 | 8.34 | 7.13 | 7.64 |
| *MnO* | 0.119 | 0.122 | 0.119 | 0.128 | 0.12 | 0.121 |
| *MgO* | 7.69 | 7.82 | 8.81 | 9.08 | 9.19 | 9.88 |
| *CaO* | 6.84 | 5.96 | 6.63 | 7.33 | 6.66 | 7.19 |
| *Na2O* | 3.88 | 3.54 | 3.48 | 3.16 | 3.37 | 3.26 |
| *K2O* | 2.92 | 3.12 | 3.51 | 3.44 | 3.45 | 3.17 |
| *P2O5* | 0.658 | 0.727 | 0.631 | 0.821 | 0.646 | 0.63 |
| *LOI* | 0.19 | 1.7 | 0.29 | 0.09 | 0.51 | -0.1 |
| *Total* | 99.907 | 98.495 | 99.144 | 100.148 | 99.86 | 99.956 |
| *Mg#* | **68.34** | **68.16** | **72.87** | **69.54** | **73.00** | **73.06** |
| *XRF* | | | | | | |
| *Ba* | 2100 | 2212 | 2264 | 2017 | 2306 | 2052 |
| *Co* | 30 | 30 | 30 | 36 | 32 | 34 |
| *Cr* | 259 | 292 | 367 | 327 | 382 | 376 |
| *Cu* | 30 | 94 | 49 | 50 | 50 | 40 |
| *Ga* | 18 | 16 | 15 | 16 | 16 | 16 |
| *Nb* | 14.5 | 15.2 | 10.4 | 15.8 | 10.8 | 11.6 |
| *Ni* | 198 | 216 | 251 | 254 | 279 | 270 |
| *Pb* | 21 | 22 | 21 | 16 | 23 | 18 |
| *Rb* | 48.2 | 48.6 | 51.8 | 50.7 | 51.5 | 46.9 |
| *Sc* | 12 | 14 | 15 | 20 | 15 | 17 |
| *Sr* | 1562 | 1504 | 1334 | 1128 | 1292 | 1244 |
| *Th* | | 8 | | 4 | 5 | |
| *U* | | 0 | | 0 | 0 | |
| *V* | 153 | 155 | 158 | 181 | 149 | 154 |
| *Y* | 20.1 | 21.7 | 17.6 | 21.9 | 17.7 | 18.4 |
| *Zn* | 79 | 72 | 68 | 75 | 71 | 69 |
| *Zr* | 239 | 249 | 289 | 326 | 288 | 270 |
| *La* | | | | | | |
| *Ce* | | | | | | |
| *Nd* | | | | | | |
| *INAA* | | | | | | |
| *La* | 54.5 | | 33.8 | | | 31.6 |
| *Ce* | 107 | | 69.5 | | | 67.7 |
| *Nd* | 50.2 | | 35.3 | | | 33.4 |
| *Sm* | 7.52 | | 5.76 | | | 5.66 |
| *Eu* | 2.1 | | 1.62 | | | 1.64 |
| *Tb* | 0.68 | | 0.59 | | | 0.61 |
| *Yb* | 1.66 | | 1.48 | | | 1.52 |
| *Lu* | 0.28 | | 0.24 | | | 0.25 |
| *Th* | 6.33 | | 3.79 | | | 3.58 |
| *U* | 1.87 | | 1.51 | | | 1.28 |
| *Ta* | 0.8 | | 0.5 | | | 0.52 |
| *Hf* | 5.67 | | 7.38 | | | 6.74 |
| *ISOTOPES* | | | | | | |
| $^{87}Sr/^{86}Sr$ | 0.706387 | | 0.706443 | | | 0.706449 |
| $^{143}Nd/^{144}Nd$ | | | | | | 0.512364 |
| $^{206}Pb/^{204}Pb$ | | | | | | |
| $^{207}Pb/^{204}Pb$ | | | | | | |
| $^{208}Pb/^{204}Pb$ | | | | | | |

| *Sample#* | 91-SN-100 | 91-SN-101 | 91-SN-102 |
|---|---|---|---|
| *Location* | Fish Camp | Fish Camp | Fish Camp |
| *Rock Type* | Shoshonite | Shoshonite | Shoshonite |
| *Lat* | 37°28'54" | 37°28'52" | 37°28'55" |
| *Long* | 119°37'14" | 119°36'59" | 119°36'38" |
| | | | |
| *SiO2* | 50.85 | 50.9 | 51.49 |
| *TiO2* | 1.644 | 1.606 | 1.613 |
| *Al2O3* | 14.01 | 13.51 | 13.65 |
| *Fe2O3* | 7.31 | 7.39 | 7.22 |
| *MnO* | 0.098 | 0.094 | 0.098 |
| *MgO* | 9.62 | 10.5 | 9.67 |
| *CaO* | 5.12 | 5.28 | 5.1 |
| *Na2O* | 2.2 | 2.11 | 2.35 |
| *K2O* | 5.88 | 5.59 | 6 |
| *P2O5* | 1.636 | 1.529 | 1.567 |
| *LOI* | 1.83 | 1.71 | 1.53 |
| *Total* | 98.368 | 98.509 | 98.758 |
| *Mg#* | 73.40 | 74.87 | 73.75 |
| | | | |
| *XRF* | | | |
| *Ba* | 3501 | 3638 | 3403 |
| *Co* | 30 | 33 | 31 |
| *Cr* | 477 | 532 | 517 |
| *Cu* | 56 | 63 | 58 |
| *Ga* | 19 | 17 | 17 |
| *Nb* | 17 | 17 | 15.8 |
| *Ni* | 281 | 387 | 368 |
| *Pb* | 23 | 21 | 21 |
| *Rb* | 77.7 | 76.4 | 93.5 |
| *Sc* | 18 | 18 | 14 |
| *Sr* | 1547 | 1489 | 1492 |
| *Th* | 5 | | 4 |
| *U* | 0 | | 0 |
| *V* | 219 | 209 | 208 |
| *Y* | 15.3 | 16.6 | 15.3 |
| *Zn* | 83 | 82 | 77 |
| *Zr* | 662 | 653 | 648 |
| *La* | | | |
| *Ce* | | | |
| *Nd* | | | |
| | | | |
| *INAA* | | | |
| *La* | | 31.4 | |
| *Ce* | | 56.7 | |
| *Nd* | | 33.9 | |
| *Sm* | | 5.49 | - |
| *Eu* | | 1.54 | |
| *Tb* | | 0.59 | |
| *Yb* | | 1.3 | |
| *Lu* | | 0.2 | |
| *Th* | | 3.56 | |
| *U* | | 0.91 | |
| *Ta* | | 0.73 | |
| *Hf* | | 15.6 | |
| | | | |
| *ISOTOPES* | | | |
| $^{87}Sr/^{86}Sr$ | | 0.706309 | 0.706374 |
| $^{143}Nd/^{144}Nd$ | | | |
| $^{206}Pb/^{204}Pb$ | | | |
| $^{207}Pb/^{204}Pb$ | | | |
| $^{208}Pb/^{204}Pb$ | | | |

| *Sample* | 90-SN-23 | 90-SN-30 | 90-SN-32 | 90-SN-50B | 90-SN-67 |
|---|---|---|---|---|---|
| *Location* | Brown Cone | Kaiser Diggings | West kaiser | Volcanic Knob | Coolidge Mdw |
| *Rock Type* | Shoshonite | Shoshonite | Potassic Trachybasalt | Shoshonite | Mugearite |
| *Lat* | 37°23'57" | 37°20'26" | 37°20'39" | 37°27'53" | 37°00'03" |
| *Long* | 119°14'24" | 119°14'38" | 119°14'30" | 118°53'22" | 118°56'40" |
| *SiO2* | 51.57 | 51.44 | 50.77 | 51.59 | 51.61 |
| *TiO2* | 1.42 | 1.25 | 1.48 | 1.31 | 0.921 |
| *Al2O3* | 12.98 | 13.09 | 13.02 | 11.19 | 14.67 |
| *Fe2O3* | 7.33 | 7.42 | 9.6 | 7.34 | 7.53 |
| *MnO* | 0.11 | 0.12 | 0.14 | 0.13 | 0.12 |
| *MgO* | 9.05 | 9.49 | 6.49 | 6.2 | 9.18 |
| *CaO* | 7.78 | 8.22 | 9.17 | 9.35 | 8.55 |
| *Na2O* | 2.27 | 2.47 | 3.34 | 2.47 | 3.8 |
| *K2O* | 4.78 | 4.61 | 2.73 | 5.84 | 2.28 |
| *P2O5* | 1.17 | 0.98 | 1.34 | 0.84 | 0.549 |
| *LOI* | 1.13 | 0.61 | 1.54 | 3.42 | |
| *Total* | 99.59 | 99.7 | 99.62 | 99.68 | 99.21 |
| *Mg#* | **72.14** | **72.84** | **58.64** | **63.92** | **71.88** |
| *XRF* | | | | | |
| *Ba* | 4323 | 3330 | 2820 | 2066 | 2336 |
| *Co* | 41 | 42 | 49 | 31 | 32 |
| *Cr* | 395 | 436 | 591 | 159 | 384 |
| *Cu* | 71 | 82 | 63 | 52 | 51 |
| *Ga* | 18 | 17 | 16 | 16 | 18 |
| *Nb* | 14 | 12 | 18 | 37 | 9.7 |
| *Ni* | 301 | 233 | 149 | 142 | 189 |
| *Pb* | 30 | 18 | 12 | 48 | 24 |
| *Rb* | 662 | 392 | 1029 | 152 | 146 |
| *Sc* | 11 | 11 | 15 | 9 | 16 |
| *Sr* | 2674 | 2266 | 1505 | 1323 | 1836 |
| *Th* | | | | | |
| *U* | | | | | |
| *V* | 180 | 183 | 168 | 146 | 155 |
| *Y* | 22 | 21 | 25 | 27 | 15.8 |
| *Zn* | 92 | 73 | 110 | 93 | 76 |
| *Zr* | 434 | 358 | 251 | 328 | 194 |
| *La* | | | | | |
| *Ce* | | | | | |
| *Nd* | | | | | |
| *INAA* | | | | | |
| *La* | 94.3 | 79.1 | 39 | 135 | 50.2 |
| *Ce* | 187 | 148 | 80 | 244 | 98.4 |
| *Nd* | 89.5 | 76.6 | 44.2 | 117 | 47.7 |
| *Sm* | 12.4 | 11.1 | 7.52 | 19.7 | 7.36 |
| *Eu* | 2.94 | 2.6 | 2.28 | 4.58 | 1.98 |
| *Tb* | 0.85 | 0.84 | 0.76 | 1.61 | 0.67 |
| *Yb* | 1.22 | 1.44 | 1.59 | 1.79 | 1.28 |
| *Lu* | 0.16 | 0.22 | 0.23 | | 0.2 |
| *Th* | 12.2 | 7.6 | 3.67 | 64.8 | 5.85 |
| *U* | 3.38 | 2.78 | 1.04 | 19.1 | 1.71 |
| *Ta* | 0.69 | 0.63 | 0.82 | 2.35 | 0.41 |
| *Hf* | 12.1 | 9.56 | 6.62 | 9.11 | 4.97 |
| *ISOTOPES* | | | | | |
| $^{87}Sr/^{86}Sr$ | 0.706301 | 0.706294 | | 0.706282 | 0.706706 |
| $^{143}Nd/^{144}Nd$ | 0.512348 | 0.512426 | | 0.51265 | |
| $^{206}Pb/^{204}Pb$ | 18.9264 | | 18.9169 | 19.1606 | |
| $^{207}Pb/^{204}Pb$ | 15.6643 | | 15.6295 | 15.6794 | |
| $^{208}Pb/^{204}Pb$ | 38.9186 | | 38.7993 | 39.0426 | |

# Appendix B

## Analytical Techniques

### B.1: Sample Preparation.

Approximately 1-2kg of fresh sample material was collected from the field. A fraction of each sample was retained for archive material while the remainder was cut into 40mm thick slabs which were trimmed to remove any altered material or weathered surfaces. The clean slabs were then split into 20mm cubes using a hydraulic splitter and finally reduced into chips <5mm using a hardened steel jaw crusher. A representative sample, obtained by the 'cone and quartering' technique, was powdered in an agate tema for approximately 30 minutes or until all mica flakes were themselves powdered.

### B.2: X-Ray Fluorescence (XRF) Analysis.

#### B.2.1: Sample Preparation.

Sample powders were dried overnight at 110°C to eliminate moisture. For trace element analyses approximately 7g of powder were mixed with 6 drops of 'Moviol' binding agent and formed formed in to a 3cm diameter pellet using a hydraulic press. These pellets were then dried again overnight at 110°C.

Glass discs for major element analyses were formed by adding a 6:1 ratio of fluxing agent (Spectraflux 100B) with 0.4g of dried sample powder in a platinum crucible. These mixtures were then mixed before being placed in a furnace at 1100°C and fused for 15 minutes. The melt was thoroughly mixed before being poured onto a heated 3cm diameter brass mould to form a glass disc. The glass disc was allowed to cool slowly to avoid cracking. Loss on ignition (LOI) was calculated by heating the sample at 1000°C for 20 minutes and measuring the percentage mass loss.

#### B.2.2: Major element analysis:

Samples from the Navajo and San Joaquin-Kings volcanic fields collected during the 1990 field season were analysed for major elements at Nottingham University on a wavelength dispersive XRF spectrometer (WDXRF). Glass beads were counted in duplicate

for 500secs at 10Kv, 0.2mA with no primary beam filter. Instrument drift was monitored by analysis of USGS AGV-1. Detection limits for the major elements are generally 0.05wt% except for the light elements Na, Mg, Al and Si for which the detection limits are between 0.2wt% (Si) and 0.96wt% (Na). Precision is better the 1% (at 2 sigma certainty level) except for Al (25), Mg (3%), and Na (10%).

Samples collected from the San Joaquin-Kings volcanic field, central Sierra Nevada, during the 1991 field season were analysed for major elements at the Open University using an ARL 8420+ XRF.

### B.2.3: Trace element analysis:

Samples from the Navajo and San Joaquin-Kings volcanic fields collected during the 1990 field season were analysed for trace elements at Nottingham University on a Phillips PW1400 WDXRF using pellets prepared at The Open University. A detailed account of the technique is given by Harvey and Atkin (1981). Trace element detection limits 6ppm for Rb, Sr, Y, Nb and Ni, 15ppm for Zr, and 31ppm for Ba. Precision for all trace elements is about 2% at 100ppm level.

Samples from the San Joaquin-Kings volcanic fields collected during the 1991 field season were analysed for trace elements at The Open University on an ARL 8420+ XRF.

Several samples from the Navajo and San Joaquin-Kings volcanic fields, collected during the 1990 field season and analysed at Nottingham University were also run as duplicates at the Open University for comparison purposes. The major and trace element analyses of these reference samples are presented below:

| | COLORADO PLATEAU INTRUSIVES | | | | | |
|---|---|---|---|---|---|---|
| *Sample#* | OU 90-NM-3 | OU 90-NM-5 | OU 90-NM-45A | NOT 90-NM-3 | NOT 90-NM-5 | NOT 90-NM-45A |
| $SiO_2$ | 40.54 | 35.62 | 38.47 | 42.02 | 38.02 | 40.15 |
| $TiO_2$ | 3.686 | 2.11 | 1.067 | 3.65 | 2.04 | 1.01 |
| $Al_2O_3$ | 9.22 | 11.04 | 8.89 | 8.33 | 10.17 | 8.14 |
| $Fe_2O_3$ | 11.98 | 7.11 | 5.41 | 11.94 | 7.11 | 5.39 |
| *MnO* | 0.141 | 0.483 | 0.161 | 0.15 | 0.45 | 0.15 |
| *MgO* | 12.28 | 3.31 | 6.58 | 12.62 | 3.35 | 6.67 |
| *CaO* | 12.08 | 15.99 | 18.91 | 12.31 | 16.07 | 18.83 |
| $Na_2O$ | 2.74 | 1.05 | 2.02 | 2.51 | 1.01 | 1.88 |
| $K_2O$ | 1.48 | 6.89 | 4.13 | 1.59 | 7.63 | 4.56 |
| $P_2O_5$ | 1.33 | 1.262 | 0.695 | 1.41 | 1.25 | 0.7 |
| *LOI* | 4.26 | 13.36 | 12.5 | 3.36 | 13.07 | 12.18 |
| *Total* | 99.74 | 98.23 | 98.83 | 99.89 | 100.16 | 99.65 |
| *Ba* | 2466 | 2281 | 1357 | 2437 | 2238 | 1382 |
| *Co* | 57 | 31 | 22 | 63 | 34 | 30 |
| *Cr* | 505 | 366 | 331 | 454 | 334 | 295 |
| *Cu* | 96 | 59 | 43 | 83 | 53 | 34 |
| *Ga* | 14 | 19 | 13 | 14 | 19 | 13 |
| *Nb* | 115 | 58.6 | 34.9 | 122 | 61 | 38 |
| *Ni* | 257 | 235 | 272 | 263 | 248 | 273 |
| *Pb* | 26 | 34 | 40 | 21 | 28 | 39 |
| *Rb* | 74.7 | 149 | 120 | 73 | 145 | 118 |
| *Sc* | 20 | 21 | 20 | 12 | 13 | 17 |
| *Sr* | 1659 | 1235 | 1137 | 1660 | 1232 | 1152 |
| *Th* | 30 | 47 | 53 | 28 | 46 | 58 |
| *U* | 4 | 7 | 10 | 6 | 9 | 11 |
| *V* | 333 | 183 | 137 | 354 | 185 | 124 |
| *Y* | 31.6 | 31.3 | 21.7 | 28 | 29 | 20 |
| *Zn* | 127 | 103 | 76 | 114 | 94 | 65 |
| *Zr* | 469 | 462 | 276 | 435 | 433 | 270 |

| | SIERRA NEVADA BASALTS | | | | | |
|---|---|---|---|---|---|---|
| *Sample#* | OU 90-SN-2 | OU 90-SN-31 | OU 90-SN-50B | NOT 90-SN-2 | NOT 90-SN-31 | NOT 90-SN-50B |
| $SiO_2$ | 50.83 | 49.6 | 50.43 | 51.28 | 50.35 | 51.59 |
| $TiO_2$ | 1.384 | 1.42 | 1.309 | 1.38 | 1.39 | 1.31 |
| $Al_2O_3$ | 13.23 | 12.89 | 11.83 | 12.56 | 12.09 | 11.19 |
| $Fe_2O_3$ | 9.63 | 8.96 | 7.3 | 9.69 | 9.06 | 7.34 |
| *MnO* | 0.143 | 0.133 | 0.125 | 0.14 | 0.13 | 0.13 |
| *MgO* | 9.86 | 9.84 | 6.18 | 9.95 | 9.85 | 6.2 |
| *CaO* | 8.29 | 8.14 | 9.41 | 8.22 | 8.1 | 9.35 |
| $Na_2O$ | 2.66 | 2.93 | 2.67 | 2.45 | 2.66 | 2.47 |
| $K_2O$ | 3.5 | 4.5 | 5.52 | 3.67 | 4.72 | 5.84 |
| $P_2O_5$ | 0.581 | 1.23 | 0.857 | 0.58 | 1.22 | 0.84 |
| *LOI* | -0.1 | 0.29 | 3.7 | -0.18 | 0.13 | 3.42 |
| *Total* | 100.01 | 99.93 | 99.33 | 99.74 | 99.7 | 99.68 |
| *Ba* | 1265 | 2374 | 1943 | 1328 | 2521 | 2066 |
| *Co* | 40 | 37 | 29 | 39 | 40.3 | 31 |
| *Cr* | 619 | 622 | 191 | 531 | 536 | 159 |
| *Cu* | 46 | 74 | 55 | 43 | 64 | 52 |
| *Ga* | 19 | 16 | 16 | 19 | 15 | 16 |
| *Nb* | 16.6 | 15.2 | 36.9 | 17 | 15 | 37 |
| *Ni* | 194 | 178 | 135 | 203 | 183 | 142 |
| *Pb* | 15 | 18 | 48 | 14 | 14 | 48 |
| *Rb* | 142 | 97.3 | 156 | 138 | 97 | 152 |
| *Sc* | 23 | 17 | 16 | 15 | 12 | 9 |
| *Sr* | 733 | 1392 | 1312 | 734 | 1392 | 1323 |
| *Th* | 12 | 5 | 68 | 8 | <1 | 73 |
| *U* | 2 | 0 | 10 | 3 | <1 | 12 |
| *V* | 194 | 196 | 165 | 166 | 181 | 146 |
| *Y* | 21.2 | 18.2 | 26.8 | 21 | 18 | 27 |
| *Zn* | 101 | 100 | 97 | 91 | 90 | 93 |
| *Zr* | 204 | 234 | 342 | 200 | 230 | 328 |

**Table B.1** comparison of the composition of selected samples run on both the XRF facilities at Nottingham University and The Open University.

## B.3: Instrumental Neutron Activation Analysis.

REE, U, Th, Ta, Rb, Cs, Co, Sc, Cr, and W were determined using Instrumental Neutron Activation Analysis (INAA) at the Open University. Full details of the analytical techniques are described in Potts et al (1981; 1985).

0.3g of rock powder was weighed into a polythene vial and then sealed. Nine samples and two standards were placed in a cylinder, each separated by a pre-weighed iron foil laquered to a polythene disc. The iron foils were used to monitor the neutron flux along the length of the cylinder during irradiation at the Imperial College Reactor Centre near Ascot, in a thermal neutron flux of $5x10^{12}ncm^2sec^{-1}$ for 24-30 hours. The two standards used in each cylinder were an irradiation standard AC-2 (Ailsa Craig microgranite) and a sample from the Whin Sill (WS) which was used as an internal standard.

After cooling for one week to allow short lived radio-nucleides to decay, samples were counted at the Open University. Two detectors were used in tandom on either side of the sample vial: a coaxial Ge(Li) detector and a planar low-energy photon spectrometer (LEPS). Two sets of counting were performed on each sample over a one month period. Initial counting ('Short Counts') lasted for 800secs was followed, two to four weeks after irradiation, by counting for 6-10 hours ('Long Counts') to detect the longer lived isotopes.

Table B.2 shows the average composition of the Whin Sill standard, analysed with each batch of samples, with the standard deviation and approximate detection limits.

| | Average | St.Dev | CV% | Detection Limit |
|---|---|---|---|---|
| La | 25.6 | 0.28 | 1.09 | 0.5 |
| Ce | 56.7 | 1.18 | 2.18 | 0.5 |
| Nd | 31.5 | 1.11 | 3.52 | 1 |
| Sm | 7.04 | 0.14 | 2.02 | 0.02 |
| Eu | 2.17 | 0.06 | 2.54 | 0.02 |
| Tb | 1.08 | 0.03 | 2.63 | 0.1 |
| Yb | 2.41 | 0.07 | 2.81 | 0.1 |
| Lu | 0.37 | 0.01 | 3.21 | 0.05 |
| Th | 2.94 | 0.07 | 2.37 | 0.3 |
| U | 0.75 | 0.13 | 17 | 0.3 |
| Ta | 1.16 | 0.06 | 5.59 | 0.05 |
| Hf | 4.85 | 0.12 | 2.41 | 0.1 |
| Cs | 1.08 | 0.08 | 7.57 | 0.3 |
| Rb | 35 | 3.46 | 9.89 | 20 |
| Zn | 109 | 5.8 | 5.31 | 10 |
| Na2O | 2.73 | 0.06 | 2.29 | 0 |
| W | 52 | 2.16 | 4.12 | 10 |

**Table B.2.** Average composition of Whin Sill standard with standard deviation and approximate detection limits.

## B.3: Radiogenic Isotope Analysis:

All of the radiogenic isotope analyses were prepared and carried out in clean-air laboratories at The Open University. All reagents used were teflon distiled (TD) or twice quartz distiled (QD). Solutions were made with Milli-Q reverse osmosis purified water ($RoH_2O$).

Beakers were cleaned by leaving them overnight in cold QD 1.5M HNO3. They were then washed in $RoH_2O$ and placed in warm 15M $HNO_3$ for at least 24 hours. They were then washed in $RoH_2O$ and left in warm $RoH_2O$ overnight. After another rinse with $RoH_2O$ a few mls of QD 6M HCl were placed in the beakers which were then placed under the evaporating hoods for approximately one hour. After a final rinse with $RoH_2O$ the beakers were left to dry inverted on tissue paper.

### B.3.1: Sr and Nd Sample Preparation:

150-200mg of sample powder was placed in cleaned teflon beaker. A couple of drops of TD 15M $HNO_3$ were added to wet the powder, followed by ~2mls of of TD 40% HF. The beaker was then left overnight on a hot plate in a laminar flow fume cupboard. Once the powder was dissolved the solution was gently evaporated under heat lamps and in a compressed air supply until it attained a colloidal consistency. At this stage a further 2mls of TD 15M $HNO_3$ were added. This solution was evaporated to dryness before adding a second 2ml aliquot of TD 15M $HNO_3$. Upon evaporation of this solution 6mls of TD 6M HCl were added and evaporated to dryness. If the sample is not completely dissolved at this stage then a succession of the TD 15M $HNO_3$ followed by TD 6M HCl stages were repeated until the sample was completely dissolved.

The samples were re-dissolved in 2mls of QD 2.5M HCl, transferred to clean centrifuge tubes, and centrifuged for 5 minutes to remove any undissolved residue. 1ml of the centrifuged solution was carefully added to preconditioned ion exchange resin (200-400 mesh AG 50W-X8) for Sr separation. Once the sample had sunk to the top of the resin bed it was washed with two 1ml aliquots of QD 2.5M HCl. 48mls of QD 2.5M HCl were eluted through the column in order to remove the Rb fraction. The Sr was collected in the following 14mls of QD 2.5M HCl which was evaporated to dryness in preparation for loading onto

filaments for the mass spectrometer.

For Nd, 32mls of QD 3M $HNO_3$ were eluted through the column after Sr collection and a further 22mls of QD 3M $HNO_3$ were collected. This fraction, which contained Nd and other REEs, was then evaporated to dryness and transferred to a set of reverse chromatography columns used for separating the REEs. Before loading, the fraction containing Nd was re-dissolved in 0.5mls QD 0.25M HCl. The column bed is composed of 1g of teflon powder coated with 100mg of di-(2-ethylhexyl) phosphate (DEHP). The sample was carefully loaded onto the top of the column bed and was washed down by two aliquots of 0.5ml QD 0.25M HCl. 14mls QD 0.25M HCl were eluted and a further 5ml QD 0.25M HCl, containing the Nd fraction were collected.

**B.3.2: Pb Preparation:**

Prior to use the beakers used for Pb preparation went through the normal set of cleaning procedures outlined above, but with the additional stage of placing several mls of QD 6M HCl in the Sevalex bombs overnight, and then the following day with 2mls of 1M HBr. The bomb was then rinsed out with 2xTD $RoH_2O$ and left to dry inverted on tissue paper. One cleaned 100mg of sample powders were weighed into the Sevalex beakers to which 1ml 2xTD 15M $HNO_3$ and then 3ml 2xTD 48% HF were added. The bombs were sealed and left to stand cold overnight and then evaporated as for the Sr and Nd preparation. 2mls of 2xTD 15M $HNO_3$ where added, and evaporated to incipient dryness. A further 2mls of 2xTD 15M $HNO_3$ where added and evaporated to dryness. 2mls 2xTD 6M HCl were added and evaporated to dryness. At this stage the sample should have completely dissolved in the 6M HCl. 1ml of 1M HBr was added, and the sample was left standing cold overnight.

Micro ion exchange columns were made from 1ml polypropylene pipette tips which were left overnight in warm $RoH_2O$, with a small teflon frit at the tip. 3-4 drops of Dowex 200-400 mesh anionic resin were added to the tips and were preconditioned with 1 volume column (CV) 2xTD 6M HCl, 1CV 2xTD $RoH_2O$, 1CV 2xTD 6M HCl, 1CV 2xTD $RoH_2O$ and finally 0.5CV 1M HBr. 1ml of sample solution was loaded onto the columns. This was

washed down with 0.5ml 1M HBr, and then 1ml 1M HBr. Pb is collected with 2ml 2xTD 6M HCl. 3-4 drops of 2xTD $HNO_3$ are added to the Pb fraction in order to remove the bromine. This mixture is then evaporated to dryness. The above procedure is then repeated, although the Pb fraction is now collected in 2.5mls 2xTD 6M HCl. In addition to the 3-4 drops of 2xTD $HNO_3$, 1µl of phosphoric acid was also added to the collected Pb fraction.

**B.3.3: Mass Spectrometry:**

All isotopes were determined on a Finnigan MAT261 multi-collector mass spectrometer at the Open University running software developed by D.W.Wright and P.W.C. van Calsteren.

For Sr isotopic analysis samples were loaded onto outgassed single Ta filaments, onto which a drop (1µl) of phosphoric acid had been placed. A current of ~1.5A was allowed to pass through the filament until the sample was dry at which point the current was increased to ~2A in order to burn off the $H_3PO_4$.

For Nd analysis the sample was re-dissolved in ~2ml dil.$HNO_3$, and loaded onto a side of a Ta-Re double filament. The Re filament was used for ionization. ~1.5-2A was passed through the filament until the sample was dry.

For Pb analysis, the samples in their drops of $H_3PO_4$ were placed on to a single Re filament preconditioned with a drop of silica gel and $H_3PO_4$ to help secure the Pb. The current passing though the filament was increased to 0.9A until the sample was dry at which point the current was increased to 1.7-1.9A to fumme off the $H_3PO_4$.

Total procedure blanks for Sr, Nd and Pb were determined on a VG-Isomass 54E mass spectrometer. Throughout the course of this study the blanks were below 3ng for Sr and 2ng for both Pb and Nd. Though these values are not particularly low they are sufficiently low considering the highly trace element enriched nature of the potassic-ultrapotassic volcanics and intrusives that constitute this study.

Sr ratios were corrected for mass fractionation within a run to $^{87}Sr/^{86}Sr$ =0.1194. Repeat analyses of the Sr standard NBS 987 gave a mean of $^{87}Sr/^{86}Sr$ =0.710242 ±0.000015 (2σ standard deviation on 21 analyses).

Nd isotope ratios were corrected for mass fractionation within each run to

$^{146}Nd/^{144}Nd$ =0.72190. Repeat analyses of the Nd standard J+M gave a mean $^{143}Nd/^{144}Nd$ =0.511824 ±0.000018 (2σ standard deviation on 15 analyses).

Pb isotope fractionation corrections were made using mass discrimination coefficients calculated from the mean value of the standard NBS 981 for each run, and assuming this standard to have $^{206}Pb/^{204}Pb$ =16.937, $^{207}Pb/^{204}Pb$ =15.491 and $^{208}Pb/^{204}Pb$ =36.702.

Samples which run with a beam intensity on the $^{208}Pb$ peak of <2pA were rejected as intensities less than this result in large errors on the $^{204}Pb$ peak measurement relative to $^{206}Pb$, $^{207}Pb$ and $^{208}Pb$. The NBS 981 207Pb/204Pb and 206Pb/204Pb ratios measured throughout the period of this project are shown in Fig B.1 along with the preferred values for this standard.

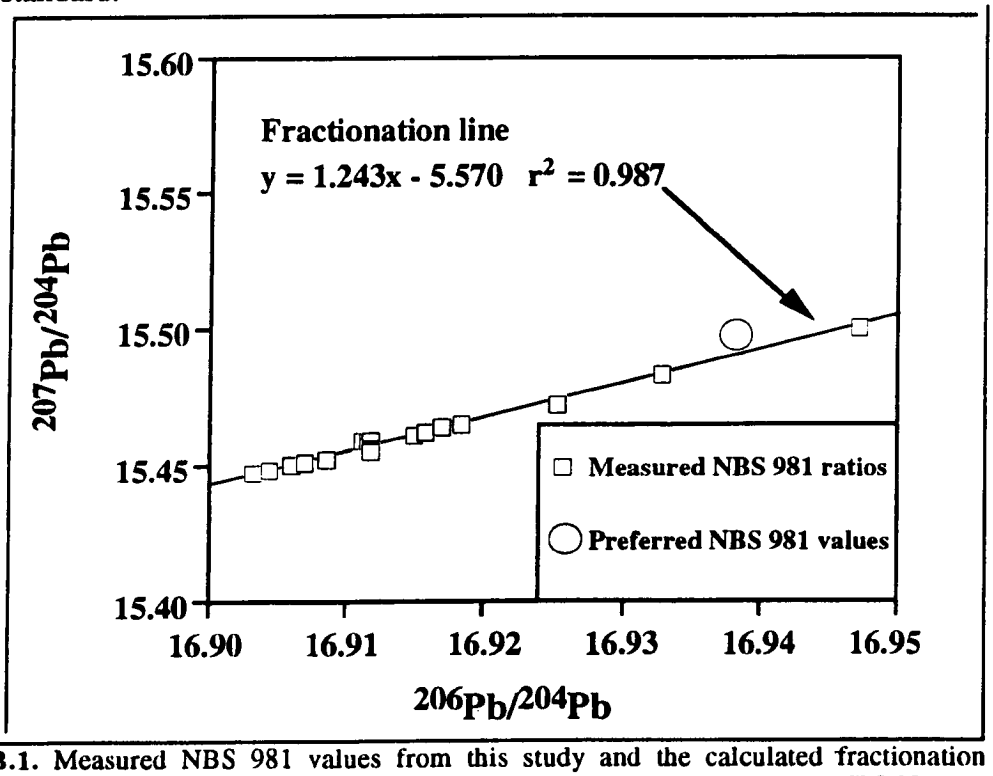


**Figure B.1.** Measured NBS 981 values from this study and the calculated fractionation line for 207Pb/204Pb versus 206Pb/204Pb. samples were corrected to the preferred values for NBS 981.

### B.3.4. Age correction.

Age correction of the measured 87Sr/86Sr and 143Nd/144Nd were performed assuming an age of 25Ma for all the Navajo samples, 10Ma for 'late Miocene' Sierran basalts and 3Ma for the 'Pliocene' basalts. The natural abundances of $^{87}Rb$, $^{86}Sr$, $^{147}Sm$ and $^{144}Nd$ were used to calculate $^{87}Rb/^{86}Sr$ and $^{147}Sm/^{144}Nd$ for each sample from the elemental ratios measured by XRF (Rb, Sr) or INAA (SM, Nd);

$87Rb/86Sr = 2.891 * Rb/Sr$

$147Sm/144Nd = 0.602 * Sm/Nd$

$$(^{87}Sr/^{86}Sr)_{measured} = (^{87}Sr/^{86}Sr)_{initial} + ^{87}Rb/^{86}Sr\ (e^{\lambda 1 t} - 1)$$

$$(^{143}Nd/^{144}Nd)_{measured} = (^{143}Nd/^{144}Nd)_{initial} + ^{147}Sm/^{144}Nd(e^{\lambda 2 t} - 1)$$

where $\lambda 1 = 1.42 \times 10^{-11}\ a^{-1}$ and $\lambda 2 = 6.54 \times 10^{-12}\ a^{-1}$

Pb isotope data were corrected for U and Th decay using

$$(^{206}Pb/^{204}Pb)_{measured} = (^{206}Pb/^{204}Pb)_{initial} + ^{238}U/^{204}Pb(e^{\lambda 3 t} - 1)$$

$$(^{207}Pb/^{204}Pb)_{measured} = (^{207}Pb/^{204}Pb)_{initial} + ^{235}U/^{204}Pb(e^{\lambda 4 t} - 1)$$

$$(^{208}Pb/^{204}Pb)_{measured} = (^{208}Pb/^{204}Pb)_{initial} + ^{232}Th/^{204}Pb(e^{\lambda 5 t} - 1)$$

Where $\lambda 3 = 1.55125 \times 10^{-10}\ a^{-1}$, $\lambda 4 = 9.8485 \times 10^{-10}\ a^{-1}$ and $\lambda 5 = 4.9475 \times 10^{-11}\ a^{-1}$

238U/204Pb, 235U/204Pb and 232Th/204Pb were calculated from:

$$^{238}U/^{204}Pb = U/Pb \times (\text{atomic weight Pb}/238.08) \times (99.27/\%^{204}Pb)$$

where 238.08 is the atomic weight of U and 99.27 is the percentage of $^{238}U$;

$$^{235}U/^{204}Pb = (^{238}U/^{204}Pb)/137.88$$

$^{232}Th/^{204}Pb = Th/Pb \times (\text{atomic weight Pb}/232.038) \times (100/\%^{204}Pb)$ where 232.038 is the atomic weight of Th and 100 is the percentage of $^{232}Th$. The atomic weight of Pb, and the concentration of $^{204}Pb$ was calculated separately for each sample.

## B.4: Ar-Ar mass spectrometry.

Phlogopite separates from Navajo minette dykes were irradiated at the Ascott reactor, Imperial College, in a central cadmium-lined tube for five days. They received 1016 fast neutrons cm-1 where the ratio between fast and thermal neutrons was 10:1. The J value of 0.00007±0.0000007 for the irradiation was calculated using the flux monitor BERN4B whose known age is 17.3±0.2Ma at 1σ. Argon was extracted from individual phlogopite crystals by firing short pulses of a continuous Nd YAG laser beam (TEMoo, wavelength

1064nm) through a modified petrological microscope and focussed to a spot size of 25μm, resulting in a pit size of approximately 100μm. A typical power of 2W was used, with pulse lengths of 500-2000ms. The argon was purified using a SAES GP10 getter at 400°C for 5 minutes, and the isotopic analysis carried out using a Mass Analyser Products 215 mass spectrometer with an electron multiplier detector. Seven masses were analysed; 25, 36, 37, 38, 39, 40 and 41. Measurement of mass 41 was made in order to assess the levels of hydrocarbon, and 35 in order to monitor the presence of Cl background in the mass spectrometer. At the end of each run, peaks were regressed to the inlet time. Each sample analysis was followed by a blank run. Corrections were applied for mass spectrometer fractionation, background levels of Ar (monitored from analysis of blanks) and interfering nuclear reactions involving K; $(^{40}Ar/^{39}Ar)_K = 0.031 \pm 0.008$.

The argon isotopic composition for each phlogopite analysis is presented in Table B.3. opposite.

| Sample | 40Ar | +- | 39Ar | +- | 38Ar | +- | 37Ar | +- | 36Ar | +- | 40Ar*/39Ar | +- | Age (Ma) | +- | Mean | +- |
|---|---|---|---|---|---|---|---|---|---|---|---|---|---|---|---|---|
| 5 | 3.13265 | 0.00589 | 0.01361 | 0.00019 | 0.00028 | 0.00027 | -0.00187 | 0.00202 | 0.00150 | 0.00016 | 197.55960 | 4.46577 | 24.78 | 0.61 | 24.48 | 0.35 |
| 5 | 13.86059 | 0.02254 | 0.06149 | 0.00089 | 0.00264 | 0.00027 | 0.00010 | 0.00205 | 0.00654 | 0.00012 | 193.99920 | 2.89720 | 24.33 | 0.43 | | |
| 3 | 7.40930 | 0.01262 | 0.03362 | 0.00052 | 0.00220 | 0.00028 | 0.00137 | 0.00202 | 0.00508 | 0.00014 | 175.75530 | 3.01750 | 22.06 | 0.44 | 21.75 | 0.35 |
| 3 | 4.11803 | 0.00548 | 0.02242 | 0.00056 | 0.00088 | 0.00027 | 0.00305 | 0.00203 | 0.00116 | 0.00013 | 168.41150 | 4.52968 | 21.14 | 0.60 | | |
| 1 | 21.18894 | 0.02028 | 0.04402 | 0.00044 | 0.00975 | 0.00034 | -0.00141 | 0.00203 | 0.04546 | 0.00076 | 176.17350 | 5.43271 | 22.11 | 0.71 | 22.02 | 0.53 |
| 1 | 14.64397 | 0.02323 | 0.03189 | 0.00054 | 0.00755 | 0.00030 | 0.00060 | 0.00202 | 0.03072 | 0.00057 | 174.52160 | 6.04678 | 21.91 | 0.79 | | |
| 4 | 4.45543 | 0.00801 | 0.02027 | 0.00055 | 0.00290 | 0.00027 | 0.00191 | 0.00204 | 0.00298 | 0.00018 | 176.38160 | 5.44347 | 22.14 | 0.71 | 21.82 | 0.66 |
| 4 | 2.08957 | 0.00357 | 0.00723 | 0.00048 | 0.00302 | 0.00032 | 0.00283 | 0.00204 | 0.00322 | 0.00024 | 157.32010 | 14.41049 | 19.76 | 1.81 | | |
| 34 | 12.28724 | 0.00934 | 0.02355 | 0.00074 | 0.00726 | 0.00027 | 0.00139 | 0.00203 | 0.02552 | 0.00030 | 201.50360 | 7.36073 | 25.27 | 0.95 | 24.21 | 0.50 |
| 34 | 4.12264 | 0.00421 | 0.01753 | 0.00035 | 0.00129 | 0.00029 | 0.00183 | 0.00203 | 0.00270 | 0.00013 | 189.71500 | 4.32080 | 23.80 | 0.59 | | |
| 24 | 8.33434 | 0.01058 | 0.01590 | 0.00043 | 0.00357 | 0.00029 | -0.00231 | 0.00202 | 0.01652 | 0.00030 | 217.16920 | 8.10869 | 27.22 | 1.04 | 27.49 | 0.56 |
| 24 | 6.77196 | 0.01060 | 0.01532 | 0.00024 | 0.00207 | 0.00028 | -0.00279 | 0.00202 | 0.01150 | 0.00018 | 220.27920 | 4.90602 | 27.61 | 0.67 | | |
| 64 | 8.36210 | 0.01697 | 0.02752 | 0.00039 | 0.00248 | 0.00029 | -0.00163 | 0.00203 | 0.01020 | 0.00018 | 194.36620 | 3.42908 | 24.38 | 0.49 | 24.31 | 0.33 |
| 64 | 9.98903 | 0.01482 | 0.04231 | 0.00048 | 0.00191 | 0.00029 | -0.00032 | 0.00202 | 0.00612 | 0.00027 | 193.35320 | 2.89982 | 24.25 | 0.43 | | |
| 50 | 9.18929 | 0.01413 | 0.02970 | 0.00031 | 0.00320 | 0.00032 | 0.00022 | 0.00205 | 0.01422 | 0.00019 | 167.94870 | 2.60307 | 21.09 | 0.39 | 21.15 | 0.32 |
| 50 | 6.40328 | 0.00797 | 0.02361 | 0.00046 | 0.00220 | 0.00032 | 0.00125 | 0.00205 | 0.00812 | 0.00022 | 169.56180 | 4.31917 | 21.29 | 0.58 | | |
| 10 | 1.84899 | 0.00385 | 0.00620 | 0.00017 | 0.00038 | 0.00028 | 0.00086 | 0.00202 | 0.00110 | 0.00008 | 245.76580 | 7.90863 | 30.77 | 1.03 | 28.93 | 0.38 |
| 10 | 5.44883 | 0.01225 | 0.01325 | 0.00029 | 0.00076 | 0.00027 | 0.00165 | 0.00203 | 0.00264 | 0.00023 | 352.37660 | 9.36244 | 43.96 | 1.23 | | |
| 10 | 6.41528 | 0.01017 | 0.02787 | 0.00031 | 0.00050 | 0.00028 | -0.00247 | 0.00202 | 0.00158 | 0.00013 | 213.40790 | 2.74757 | 26.75 | 0.43 | | |
| 46 | 8.45990 | 0.01112 | 0.02242 | 0.00020 | 0.00349 | 0.00029 | 0.00189 | 0.00203 | 0.01474 | 0.00038 | 183.07730 | 5.25787 | 22.97 | 0.69 | 23.12 | 0.61 |
| 46 | 1.90603 | 0.00426 | 0.00610 | 0.00026 | 0.00094 | 0.00027 | 0.00151 | 0.00203 | 0.00256 | 0.00013 | 188.32090 | 10.35715 | 23.63 | 1.31 | | |
| 44 | 20.83449 | 0.03273 | 0.05237 | 0.00056 | 0.00940 | 0.00032 | 0.00227 | 0.00202 | 0.04124 | 0.00046 | 165.13440 | 3.21428 | 20.73 | 0.45 | 20.55 | 0.31 |
| 44 | 15.51597 | 0.02026 | 0.04861 | 0.00077 | 0.00676 | 0.00028 | 0.00281 | 0.00203 | 0.02580 | 0.00025 | 162.36940 | 3.01772 | 20.39 | 0.43 | | |
| 6 | 4.84310 | 0.00717 | 0.01589 | 0.00034 | 0.00151 | 0.00028 | -0.00239 | 0.00203 | 0.00626 | 0.00022 | 188.42190 | 5.83386 | 23.64 | 0.76 | 24.51 | 0.38 |
| 6 | 6.60013 | 0.00952 | 0.02627 | 0.00033 | 0.00157 | 0.00027 | -0.00121 | 0.00202 | 0.00476 | 0.00013 | 197.70460 | 2.90608 | 24.80 | 0.44 | | |
| 48 | 6.98114 | 0.01362 | 0.03011 | 0.00054 | 0.00240 | 0.00027 | 0.00042 | 0.00203 | 0.00532 | 0.00016 | 179.63620 | 3.58891 | 22.54 | 0.50 | 22.52 | 0.37 |
| 48 | 11.79986 | 0.01116 | 0.04229 | 0.00058 | 0.00480 | 0.00029 | 0.00195 | 0.00203 | 0.01428 | 0.00043 | 179.24440 | 3.88668 | 22.50 | 0.53 | | |
| 47 | 27.85704 | 0.08452 | 0.06404 | 0.00123 | 0.01322 | 0.00030 | 0.00303 | 0.00203 | 0.05348 | 0.00048 | 188.21570 | 4.45397 | 23.61 | 0.60 | 22.48 | 0.41 |
| 47 | 7.55181 | 0.01952 | 0.02148 | 0.00035 | 0.00385 | 0.00029 | 0.00233 | 0.00202 | 0.01312 | 0.00022 | 171.10760 | 4.17965 | 21.48 | 0.56 | | |
| 14 | 0.70342 | 0.00296 | 0.00381 | 0.00023 | 0.00042 | 0.00026 | 0.00187 | 0.00203 | 0.00060 | 0.00010 | 138.21950 | 11.61710 | 17.37 | 1.46 | 17.06 | 0.68 |
| 14 | 0.81241 | 0.00279 | 0.00447 | 0.00023 | 0.00038 | 0.00027 | 0.00105 | 0.00207 | 0.00052 | 0.00016 | 147.54130 | 12.75493 | 18.54 | 1.60 | | |
| 14 | 1.14880 | 0.00339 | 0.00798 | 0.00031 | 0.00062 | 0.00029 | 0.00103 | 0.00203 | 0.00034 | 0.00013 | 131.31420 | 6.92601 | 16.51 | 0.88 | | |

**Tabel B.3.** Argon isotopic composition for individual analyses on phlogopite separates from minette dykes from the Navajo Volcanic Field, central Colorado Plateau.

# Appendix C

## Distribution Coefficients, Normalising Values and Equations

==========

## C.1. Distribution Coefficients.

The following list is a compilation of crystal/liquid distribution coefficients for trace elements used in geochemical modelling in chapters 3 and 4. References: Cox et al (1984); Feigenson et al (1983); Henderson (1986); Irving & Frey (1984, 1987); Irving (1978); Leeman (1976, and references therein); Pearce & Norry (1979); Ulmer (1988)

| | OL | OPX | CPX | GT | SP | PHLOG | MAG | APAT |
|---|---|---|---|---|---|---|---|---|
| La | 0.0002 | 0.002 | 0.069 | 0.01 | 0.01 | 0.03 | | 9.4 |
| Y | 0.001 | 0.04 | 0.3 | 2 | 0.02 | 0.03 | | |
| Nd | 0.001 | 0.0065 | 0.18 | 0.08 | 0.07 | 0.017 | | 12 |
| Sm | 0.0013 | 0.013 | 0.26 | 0.217 | 0.05 | 0.03 | | 13 |
| Nb | 0.001 | 0.15 | 0.1 | 0.1 | | 1.2 | | |
| Zr | 0.001 | 0.03 | 0.1 | 0.3 | | 0.6 | | |
| Tb | 0.0015 | 0.02 | 0.3 | 0.7 | 0.007 | 0.03 | | |
| $TiO_2$ | 0.02 | 0.1 | 0.3 | 0.3 | | 0.9 | | |
| Yb | 0.0015 | 0.049 | 0.28 | 7 | 0.007 | 0.042 | | 4.1 |
| Ce | 0.0005 | 0.003 | 0.098 | 0.021 | 0.08 | 0.03 | | 17 |
| Rb | 0.0001 | 0.001 | 0.05 | 0.01 | 0.01 | 3.1 | | |
| Ba | 0.0001 | 0.001 | 0.05 | 0.01 | 0.01 | 1.1 | | 0.001 |
| Th | 0.001 | 0.01 | 0.1 | 0.02 | | 0.052 | | |
| $K_2O$ | 0.007 | 0.015 | 0.03 | | | 4 | | |
| Ta | 0.001 | 0.15 | 0.07 | 0.1 | | 0.33 | | |
| Sr | 0.001 | 0.01 | 0.1 | 0.01 | 0.004 | 0.08 | | 2 |
| $P_2O_5$ | 0.001 | 0.008 | 0.14 | 0.09 | | | | |
| Hf | 0.001 | 0.04 | 0.31 | 0.3 | | | | |
| Lu | 0.001 | 0.11 | 0.8 | 10 | | 0.04 | | |
| Sc | 0.22 | 1.1 | 2.7 | 4 | | | 1 | 3.3 |
| Ni | 14 | 5 | 3 | | | 3 | 20 | |
| Cr | 2.1 | 2 | 10 | | | 3 | 100 | |

**Table C.1.** Mineral/liquid distribution coefficients used in this study

## C.2. Normalising Values:

Normalising values for primitive mantle and chondrite used in chapters 2 through 4 were taken from Sun & McDonough (1989) and are reproduced below:

| | | | | | | | |
|---|---|---|---|---|---|---|---|
| Pb | 0.185 | K | 250 | Sr | 21.1 | Sm | 0.444 |
| Ba | 6.989 | Ta | 0.041 | P | 95 | T | 1300 |
| Rb | 0.635 | Nb | 0.713 | Nd | 1.354 | Y | 4.55 |
| Th | 0.085 | La | 0.687 | Hf | 0.309 | Yb | 0.493 |
| U | 0.021 | Ce | 1.775 | Zr | 11.2 | Lu | 0.074 |

**Table C.2.** Primitve mantle normalisation values of Sun & McDonough (1989).

| | | | | | | | |
|---|---|---|---|---|---|---|---|
| La | 0.237 | Nd | 0.467 | Eu | 0.058 | Yb | 0.170 |
| Ce | 0.612 | Sm | 0.153 | Tb | 0.0374 | Lu | 0.0254 |

**Table C.3.** Chondrite normalisation values of Sun & McDonough (1989).

## C.3. Epsilon Nd and Sr Calculations:

$$\varepsilon^{t}_{CHUR} = \left[ \frac{(^{143}Nd/^{144}Nd)_i}{I^{t}_{CHUR}} - 1 \right] * 10^4$$

Where:

$\varepsilon^{t}_{CHUR}$ = the difference between the initial 143Nd/144Nd of a rock and the value of this ratio in the 'chondritic uniform reservoir' (*CHUR*) at that time;

$I^{t}_{CHUR}$ = $^{143}Nd/^{144}Nd$ of *CHUR* at time t;

$(^{143}Nd/^{144}Nd)_i$ = initial $^{143}Nd/^{144}Nd$ ratio of the rock;

$I^{t}_{CHUR}$ is calculated by;

$$I^{t}_{CHUR} = I^{0}_{CHUR} - \left(\frac{^{147}Sm}{^{144}Nd}\right)^{0}_{CHUR} (e^{\lambda t} - 1)$$

Where:

$I^0_{CHUR}$ $=^{143}Nd/^{144}Nd$ ratios of *CHUR* at the present time;

$\left(\frac{^{147}Sm}{^{144}Nd}\right)^0_{CHUR}$ =present value of $^{147}Sm/^{144}Nd$ in *CHUR*

Similar equations are used to calculate $\varepsilon Sr$. Ratios and constants used in the calculations are taken from Faure (1986) and are as follows:

For $\varepsilon Nd$

$I^0_{CHUR}$ =0.512638

$\left(\frac{^{147}Sm}{^{144}Nd}\right)^0_{CHUR}$ =0.1967

$\lambda = 6.54*10^{12}\ a^{-1}$

For $\varepsilon Sr$

$I^0_{UR}$ =0.7045

$\left(\frac{^{87}Rb}{^{86}Sr}\right)^0_{UR}$ =0.0.0816

$\lambda = 1.42*10^{-11}\ a^{-1}$ $\left(\frac{^{147}Sm}{^{144}Nd}\right)^0_{CHUR}$ =0.1967

## C.4. Nd Model Age.

$$T_{Nd} = \frac{1}{\lambda} \ln\left[\frac{(^{143}Nd/^{144}Nd)m - I^0_{CHUR}}{(^{147}Sm/^{144}Nd)m - (^{147}Sm/^{144}Nd)CHUR} + 1\right]$$

Where:

$(^{143}Nd/^{144}Nd)_m$ and $(^{147}Sm/^{144}Nd)_m$ are measured ratios of the rock.